

IMPACT DAMAGE MECHANISMS IN SEVERAL LAMINATED MATERIAL SYSTEMS

by

Edward Wolf

B.S. Mechanical Engineering, Rutgers University (1989)

Submitted to the Department of Aeronautics and Astronautics in Partial
Fulfillment of the Requirements for the Degree of

MASTER OF SCIENCE

at the

MASSACHUSETTS INSTITUTE OF TECHNOLOGY

June 1992

Copyright © Massachusetts Institute of Technology, 1992. All rights reserved.

Signature of Author _____

Department of Aeronautics and Astronautics
March 19, 1992

Certified by _____

Professor Paul A. Lagace
Thesis Supervisor

Accepted by _____

Professor Harold Y. Wachenman
Chairman, Department Graduate Committee

ARCHIVES
MASSACHUSETTS INSTITUTE
OF TECHNOLOGY

JUN 05 1992

LIBRARIES

IMPACT DAMAGE MECHANISMS IN SEVERAL LAMINATED MATERIAL SYSTEMS

by
Edward Wolf

Submitted to the Department of Aeronautics and Astronautics on March 19, 1992
in partial fulfillment of the requirements for the Degree of Master of Science.

ABSTRACT

The impact behavior of several laminated material systems was investigated experimentally. The effect of layup, material system and damage state on the impact force-time signature and the resulting damage modes were investigated for laminates of Hercules AS4/3501-6 and IM7G/X8553-50 ("toughened" matrix) tape prepregs, Hercules A370-5H/3501-6S fabric prepreg, and a wet layup of woven fiberglass plies and epoxy. Twelve-ply laminates were constructed of AS4/3501-6 and IM7G/X8553-50 in a $[\pm\theta_2/0_2]_s$ layup with θ taking on the values of 15° , 45° , 60° and 90° . Two quasi-isotropic 16-ply laminates, one with double effective ply thickness and one with single effective ply thickness, were constructed of AS4/3501-6 for comparison with a $(45_2/0_2)_s$ layup of A370-5H/3501-6S. Contact force data were obtained from the impact tests. The damage in the graphite/epoxy laminates was evaluated using X-ray and deply methods, and the glass/epoxy specimens were inspected visually for damage. The occurrence of incipient damage could not be detected in the force-time signature of these impacts whereas penetration was clearly indicated. The force-time signature, in terms of peak force and duration, was not significantly affected by the layup angle θ , or material system in the $[\pm\theta_2/0_2]_s$ laminates. Thus, the major extensional and bending stiffnesses of the laminate (A_{1111} and D_{1111}) do not appear to be the factors controlling the shape of the signature. The impact force history can be integrated to obtain the deflection history, and the deflections in this study were typically 5 to 10 laminate thicknesses, indicating that membrane stretching is significant. The incipient damage mode in the 12-ply laminates was matrix cracking of the rearmost plies, regardless of layup or material system. This matrix cracking was followed by delamination at the rearmost interface at higher impact velocities. Ply grouping changed the incipient damage mode and lowered the incipient damage force in the 16-ply laminates. The incipient damage force was higher for the graphite/epoxy fabric laminate than for the 16-ply tape simulations likely due to the ability of the fabric plies to inhibit long matrix cracks. Fiber damage was preceded by delamination in the tape laminates, while fiber damage occurred without the presence of interlaminar damage in the graphite/epoxy fabric laminate. It appears that the dissipation of energy through delamination may act to prevent fiber damage. Higher contact forces were required to cause incipient damage to the laminates of IM7G/X8553-50 because of the higher transverse tensile ply failure strain of this material system as compared to AS4/3501-6. Thus, the use of contact force as a parameter for comparing the impact damage resistance of laminates is suggested.

Thesis Supervisor: Paul A. Lagace
Title: Associate Professor, Department of Aeronautics and
Astronautics, Massachusetts Institute of Technology

ACKNOWLEDGMENTS

STARRING	FRED (as himself)
DIRECTOR	Paul Lagace
TECHNICAL ASSISTANCE	Tsang Associates
MAN BEHIND CURTAIN	Al Supple
GAME WARDENS	Deborah Bowser, Barbara Pierce
STUNT DRIVER	M. J. Graves
MAN ON BICYCLE	Narendra Bhat
THE PROFESSOR	Professor John Dugundji
TOUR GUIDES	Claudia Ranniger, Kerry Forbes
TOURIST	Luca Marmorini
USED CAR SALESMAN #1	James Williamson
USED CAR SALESMAN #2	Ken Bonello
SURGICAL IMPLANT TEAM	Laura Kozel, Wai Tuck Chow
PAPERBOY	Peter Dunn
HELICOPTER REPAIRMAN	Adam Sawicki
ASSISTANT	Vera Martinovich
FIREMAN	Tom Wilson
BARTENDER	Matt Fox
BAR FLY	Rich Pemberton
FRIENDLY ANDROID	Stuart Pekowsky
CONVERTIBLE DRIVER	Ricardo Zemella
VOLLEYBALL PLAYERS ON BEACH	Teresa Guy, Randy Notestine, Mary Mahler
CURIOUS ONLOOKERS	Darryl Pines, Aaron Bent, Jeff Farmer
PINBALL WIZARD	Adam Matteo
WOMAN IN RED	Elana Lehman
SPECIAL EFFECTS	Beaumont Industries
COSTUME DESIGN	Malee Lucas, Chantell Wyland
LIGHTING	Elizabeth Smith
LIBRARY STAFF	Chantal Moore, Shannan Moynihan
CINEMATOGRAPHY	Yew-Poh Mak
LOCATIONS COORDINATOR	McManus World of Travel
COMPUTER GRAPHICS	Matsuhashi Video
LEGAL AFFAIRS	Thomas, Thomas, Budiman and Priest
PRODUCTION COORDINATORS	Liz Zotos, Ping Lee

A James Mar Production filmed in TELAColor with special thanks
to Dr. Doug Cairns at the Hercules Aerospace Company.

FOREWORD

This investigation was conducted in the Technology Laboratory for Advanced Composites (TELAC) of the Department of Aeronautics and Astronautics at the Massachusetts Institute of Technology. This work was sponsored by the FAA under Navy Contract N00019-89-C-0058.

TABLE OF CONTENTS

<u>CHAPTER</u>		<u>PAGE</u>
1	INTRODUCTION	17
2	PREVIOUS WORK	21
	2.1 Overview	21
	2.2 Experimental Studies	21
	2.3 Analyses	25
3	EXPERIMENTAL PROCEDURES	29
	3.1 Test Matrix and Specimen Description	29
	3.2 Manufacturing Procedures	35
	3.2.1 Graphite/Epoxy Prepreg Layup	35
	3.2.2 Glass/Epoxy Wet Layup	36
	3.2.3 AS4/3501-6 and A370-5H/3501-6S Cure	37
	3.2.4 IM7G/X8553-50 Cure	42
	3.2.5 Glass/Epoxy Cure	46
	3.2.6 Final Preparation	46
	3.3 Impact Test Procedures	50
	3.4 Damage Evaluation	56
4	EXPERIMENTAL RESULTS	63
	4.1 Overview	63
	4.2 Force-Time Data	63
	4.2.1 AS4/3501-6 Material System	63
	4.2.2 IM7G/X8553-50 Material System	73
	4.2.3 A370-5H/3501-6S Material System	79
	4.2.4 Glass/Epoxy Material System	82
	4.2.5 General Characteristics	88
	4.3 Damage Characteristics	90
	4.3.1 AS4/3501-6 Material System	91
	4.3.2 IM7G/X8553-50 Material System	107
	4.3.3 A370-5H/3501-6S Material System	118
	4.3.4 Glass/Epoxy Material System	121
	4.3.5 General Characteristics	129

TABLE OF CONTENTS (continued)

<u>CHAPTER</u>		<u>PAGE</u>
5	DISCUSSION	132
5.1	Force-Time Signatures	132
5.1.1	Effect of Layup	132
5.1.2	Effect of Material System	141
5.1.3	Effect of Damage	153
5.1.4	Effect of Impact Velocity	160
5.2	Incipient Damage Characteristics	164
5.2.1	Effect of Layup	166
5.2.2	Effect of Material System	169
5.3	General Damage Characteristics	172
5.3.1	Effect of Layup	173
5.3.2	Effect of Material System	177
6	CONCLUSIONS AND RECOMMENDATIONS	181
	REFERENCES	187
	APPENDIX A	190

LIST OF FIGURES

FIGURE		PAGE
3.1	Impact specimen geometry.	34
3.2	Schematic of glass/epoxy cure layup.	38
3.3	Schematic of AS4/3501-6 and A370-5H/3501-6S cure layup.	39
3.4	Illustration of cure plate (top view).	41
3.5	AS4/3501-6 and A370-5H/3501-6S cure cycle.	43
3.6	Schematic of IM7G/X8553-50 cure layup.	44
3.7	IM7G/X8553-50 cure cycle.	45
3.8	Glass/epoxy cure cycle.	47
3.9	Coupon measurement locations.	48
3.10	Specimen holding jig measurements.	51
3.11	Illustration of jig support stand for impact testing.	52
3.12	Illustration of Free Rolling Energy Device (FRED) for impact.	53
3.13	Illustration of impactor rod and light gates.	55
3.14	Example of typical X-ray photographs.	57
3.15	Example of typical photographs of glass/epoxy specimens impacted at 3.0 and 5.0 m/s.	59
3.16	Example of typical deply transcription of impacted graphite/epoxy specimen.	62
4.1	Force-time signatures of AS4/3501-6 [$\pm 15_2/0_2$] _s laminate impacted at 1.0 m/s (undamaged) , 3.0 m/s, and 5.0 m/s (penetrated).	65
4.2	Force-time signatures of AS4/3501-6 [$\pm 45_2/0_2$] _s laminate impacted at 1.0 m/s (undamaged), 3.0 m/s, and 5.0 m/s (penetrated).	66
4.3	Force-time signatures of AS4/3501-6 [$\pm 60_2/0_2$] _s laminate impacted at 0.72 m/s (undamaged), 3.0 m/s, and 5.0 m/s (penetrated).	67

LIST OF FIGURES (continued)

FIGURE		PAGE
4.4	Force-time signatures of AS4/3501-6 $[90_4/0_2]_s$ laminate impacted at 0.75 m/s (undamaged), 3.0 m/s, and 5.0 m/s (penetrated).	68
4.5	Force-time signatures of AS4/3501-6 $[\pm 45_2/0_2/90_2]_s$ laminate impacted at 2.0 m/s (undamaged), 3.0 m/s, and 5.0 m/s.	71
4.6	Force-time signatures of AS4/3501-6 $[(\pm 45)_2/(0/90)_2]_s$ laminate impacted at 2.8 m/s (undamaged), 3.0 m/s, 5.0 m/s.	72
4.7	Force-time signatures of IM7G/X8553-50 $[\pm 15_2/0_2]_s$ laminate impacted at 1.0 m/s (undamaged), 3.0 m/s, and 5.0 m/s.	74
4.8	Force-time signatures of IM7G/X8553-50 $[\pm 45_2/0_2]_s$ laminate impacted at 2.2 m/s (undamaged), 3.0 m/s, and 5.0 m/s.	75
4.9	Force-time signatures of IM7G/X8553-50 $[\pm 60_2/0_2]_s$ laminate impacted at 2.0 m/s (undamaged), 3.0 m/s, and 5.0 m/s.	76
4.10	Force-time signatures of IM7G/X8553-50 $[90_4/0_2]_s$ laminate impacted at 1.0 m/s (undamaged), 3.0 m/s, and 5.0 m/s.	77
4.11	Force-time signature of A370-5H/3501-6S $(45_2/0_2)_s$ laminate impacted at 4.0 m/s (undamaged).	80
4.12	Force-time signature of A370-5H/3501-6S $(45_2/0_2)_s$ laminate impacted at 5.0 m/s.	81
4.13	Force-time signatures of glass/epoxy $(45_2/0_2)_s$ laminate impacted at 1.2 m/s (undamaged), 3.0 m/s, and 5.0 m/s.	83
4.14	Force-time signatures of glass/epoxy $(90_2/0_2)_s$ laminate impacted at 1.0 m/s (undamaged), 3.0 m/s, and 5.0 m/s.	84
4.15	Force-time signatures of glass/epoxy $(0_2/45_2)_s$ laminate impacted at 1.0 m/s (undamaged), 3.0 m/s, and 5.0 m/s.	85
4.16	Force-time signature of glass/epoxy $(45/0)_{2s}$ laminate impacted at 1.0 m/s (undamaged), and 3.0 m/s.	86
4.17	Force-time signatures of glass/epoxy $(0/45)_{2s}$ laminate impacted at 1.0 m/s (undamaged), 3.0 m/s, and 5.0 m/s.	87

LIST OF FIGURES (continued)

FIGURE		PAGE
4.18	X-ray photographs of AS4/3601-6 [$\pm 15_2/0_2$] _s specimens for impact velocities of (top) 1.1 m/s (incipient), (middle) 1.3 m/s, and (bottom) 3.0 m/s .	92
4.19	Depty transcription of AS4/3501-6 [$\pm 15_2/0_2$] _s specimen impacted at 3.0 m/s.	93
4.20	X-ray photographs of AS4/3501-6 [$\pm 45_2/0_2$] _s specimens for impact velocities of (top) 1.2 m/s (incipient), (middle) 2.0 m/s, and (bottom) 3.0 m/s.	95
4.21	Depty transcription of AS4/3501-6 [$\pm 45_2/0_2$] _s specimen impacted at 3.0 m/s.	96
4.22	X-ray photographs of AS4/3501-6 [$\pm 60_2/0_2$] _s specimens for impact velocities of (top) 0.9 m/s (incipient), (middle) 1.5 m/s, and (bottom) 3.0 m/s.	97
4.23	Depty transcription of AS4/3501-6 [$\pm 60_2/0_2$] _s specimen impacted at 3.0 m/s.	98
4.24	X-ray photographs of AS4/3501-6 [$90_4/0_2$] _s specimens for impact velocities of (top) 0.9 m/s (incipient), (middle) 2.0 m/s, and (bottom) 3.0 m/s.	100
4.25	Depty transcription of AS4/3501-6 [$90_4/0_2$] _s specimen impacted at 3.0 m/s.	101
4.26	X-ray photographs of AS4/3501-6 [$\pm 45_2/0_2/90_2$] _s specimens for impact velocities of (top) 2.3 m/s (incipient), (middle) 2.6 m/s, and (bottom) 5.0 m/s.	102
4.27	Depty transcription of AS4/3501-6 [$\pm 45_2/0_2/90_2$] _s specimen impacted at 5.0 m/s.	103
4.28	X-ray photographs of AS4/3501-6 [$(\pm 45)_2/(0/90)_2$] _s specimens for impact velocities of (top) 3.0 m/s (incipient), (middle) 3.6 m/s, and (bottom) 5.0 m/s.	105
4.29	Depty transcription of AS4/3501-6 [$(\pm 45)_2/(0/90)_2$] _s specimen impacted at 5.0 m/s.	106

LIST OF FIGURES (continued)

FIGURE		PAGE
4.30	X-ray photographs of IM7G/X8553-50 $[\pm 15_2/0_2]_s$ specimens for impact velocities of (top) 1.5 m/s (incipient), (middle) 4.0 m/s, and (bottom) 5.0 m/s.	108
4.31	Depty transcription of IM7G/X8553-50 $[\pm 15_2/0_2]_s$ specimen impacted at 5.0 m/s.	109
4.32	X-ray photographs of IM7G/X8553-50 $[\pm 45_2/0_2]_s$ specimens for impact velocities of (top) 2.5 m/s (incipient), (middle) 4.0 m/s, and (bottom) 5.0 m/s.	111
4.33	Depty transcription of IM7G/X8553-50 $[\pm 45_2/0_2]_s$ specimen impacted at 5.0 m/s.	112
4.34	X-ray photographs of IM7G/X8553-50 $[\pm 60_2/0_2]_s$ specimens for impact velocities of (top) 2.2 m/s (incipient), (middle) 4.0 m/s, and (bottom) 5.0 m/s.	113
4.35	Depty transcription of IM7G/X8553-50 $[\pm 60_2/0_2]_s$ specimen impacted at 5.0 m/s.	114
4.36	X-ray photographs of IM7G/X8553-50 $[90_4/0_2]_s$ specimens for impact velocities of (top) 1.5 m/s (incipient), (middle) 4.0 m/s, and (bottom) 5.0 m/s.	116
4.37	Depty transcription of IM7G/X8553-50 $[90_4/0_2]_s$ specimen impacted at 3.0 m/s.	117
4.38	X-ray photographs of A370-5H/3501-6S $(45_2/0_2)_s$ specimens for impact velocities of (top) 4.1 m/s (incipient), (middle) 4.5 m/s, and (bottom) 5.0 m/s.	119
4.39	Depty transcription of A370-5H/3501-6S $(45_2/0_2)_s$ specimen impacted at 5.0 m/s.	120
4.40	Illustration of cross-section of glass/epoxy $(45/0)_{2s}$ specimen impacted at 5.0 m/s.	122
4.41	Photographs of glass/epoxy $(45_2/0_2)_s$ specimens impacted at (top) 3.0 m/s and (bottom) 5.0 m/s.	123
4.42	Photographs of glass/epoxy $(90_2/0_2)_s$ specimens impacted at (top) 3.0 m/s and (bottom) 5.0 m/s.	124

LIST OF FIGURES (continued)

FIGURE		PAGE
4.43	Photographs of glass/epoxy $(0_2/45_2)_s$ specimens impacted at (top) 3.0 m/s and (bottom) 5.0 m/s.	125
4.44	Photograph of glass/epoxy $(45/0)_{2s}$ specimen impacted at 3.0 m/s.	126
4.45	Photographs of glass/epoxy $(0/45)_{2s}$ specimens impacted at (top) 3.0 m/s and (bottom) 5.0 m/s.	127
5.1	Peak force versus impact velocity for the 12-ply AS4/3501-6 layups.	133
5.2	Peak force versus impact velocity for the 12-ply IM7G/X8553-50 layups.	134
5.3	Impact duration versus impact velocity for the 12-ply AS4/3501-6 layups.	136
5.4	Impact duration versus impact velocity for the 12-ply IM7G/X8553-50 layups.	137
5.5	Comparison of 3.0 m/s signatures of $[\pm 15_2/0_2]_s$ and $[90_4/0_2]_s$ layups of AS4/3501-6 impacted at 3.0 m/s.	139
5.6	Signatures of AS4/3501-6 $[\pm 45_2/0_2/90_2]_s$ and $[(\pm 45)_2/(0/90)_2]_s$ laminates impacted at 5.0 m/s.	140
5.7	Signatures of AS4/3501-6 $[\pm 45_2/0_2/90_2]_s$ and $[\pm 15_2/0_2]_s$ laminates impacted at 3.0 m/s.	143
5.8	Force-time signatures of glass/epoxy $(45_2/0_2)_s$ and $(90_2/0_2)_s$ laminates impacted at 3.0 m/s.	144
5.9	Signatures of $[\pm 15_2/0_2]_s$ laminates of AS4/3501-6 and IM7G/X8553-50 impacted at 3.0 m/s.	145
5.10	Signatures of $[\pm 45_2/0_2]_s$ laminates of AS4/3501-6 and IM7G/X8553-50 impacted at 3.0 m/s.	146
5.11	Signatures of $[\pm 60_2/0_2]_s$ laminates of AS4/3501-6 and IM7G/X8553-50 impacted at 3.0 m/s.	147
5.12	Signatures of $[90_4/0_2]_s$ laminates of AS4/3501-6 and IM7G/X8553-50 impacted at 3.0 m/s.	148

LIST OF FIGURES (continued)

FIGURE		PAGE
5.13	Signatures of $[\pm 60_2/0_2]_s$ laminates of AS4/3501-6 and IM7G/X8553-50 impacted at 5.0 m/s.	151
5.14	Signatures of AS4/3501-6 $[(\pm 45)_2/(0/90)_2]_s$ and A370-5H/3501-6S $(45_2/0_2)_s$ laminates impacted at 5.0 m/s.	152
5.15	Signatures of A370-5H/3501-6S and glass/epoxy $(45_2/0_2)_s$ laminates impacted at 5.0 m/s.	154
5.16	Signatures of AS4/3501-6 $[\pm 45_2/0_2]_s$ and glass/epoxy $(45_2/0_2)_s$ laminates impacted at 3.0 m/s.	155
5.17	Signatures of IM7G/X8553-50 $[\pm 60_2/0_2]_s$ laminates for impact velocities of 2.0 m/s (undamaged) and 3.0 m/s (damaged).	157
5.18	Signatures of $[\pm 45_2/0_2]_s$ laminates of AS4/3501-6 and IM7G/X8553-50 impacted at 3.0 m/s.	158
5.19	X-ray photographs of $[\pm 45_2/0_2]_s$ laminates of (upper) AS4/3501-6 and (lower) IM7G/X8553-50 impacted at 3.0 m/s.	159
5.20	Signatures of $[90_4/0_2]_s$ laminates of AS4/3501-6 (penetrated) and IM7G/X8553-50 (no penetration) impacted at 5.0 m/s.	161
5.21	Force-time signatures of IM7G/X8553-50 $[\pm 60_2/0_2]_s$ laminate impacted at 2.0 m/s (undamaged), 3.0 m/s, and 5.0 m/s.	162
5.22	Derived center deflection curves (normalized by thickness) for AS4/3501-6 $[\pm 15_2/0_2]_s$ laminates impacted at 1.0 and 3.0 m/s.	165
5.23	Incipient damage force versus layup angle for 12-ply laminates of AS4/3501-6 and IM7G/X8553-50.	167
5.24	Penetration force versus layup angle for the 12-ply laminates of AS4/3501-6.	175
A.1-A.10	Force versus time and X-ray photographs for AS4/3501-6 $[\pm 15_2/0_2]_s$ specimens.	192-201
A.11-A.20	Force versus time and X-ray photographs for AS4/3501-6 $[\pm 45_2/0_2]_s$ specimens.	202-211

LIST OF FIGURES (continued)

FIGURE		PAGE
A.21-A.31	Force versus time and X-ray photographs for AS4/3501-6 [$\pm 60_2/0_2$] _s specimens.	212-222
A.32-A.42	Force versus time and X-ray photographs for AS4/3501-6 [$90_4/0_2$] _s specimens.	223-233
A.43-A.52	Force versus time and X-ray photographs for AS4/3501-6 [$\pm 45_2/0_2/90_2$] _s specimens.	234-243
A.53-A.61	Force versus time and X-ray photographs for AS4/3501-6 [$(\pm 45)_2/(0/90)_2$] _s specimens.	244-252
A.62-A.74	Force versus time and X-ray photographs for IM7G/X8553-50 [$\pm 15_2/0_2$] _s specimens.	253-265
A.75-A.84	Force versus time and X-ray photographs for IM7G/X8553-50 [$\pm 45_2/0_2$] _s specimens.	266-275
A.85-A.94	Force versus time and X-ray photographs for IM7G/X8553-50 [$\pm 60_2/0_2$] _s specimens.	276-285
A.95-A.104	Force versus time and X-ray photographs for IM7G/X8553-50 [$90_4/0_2$] _s specimens.	286-295
A.105-A.113	Force versus time and X-ray photographs for A370-5H/3501-6S ($45_2/0_2$) _s specimens.	296-304
A.114-A.121	Force versus time and damage photographs for glass/epoxy ($45_2/0_2$) _s specimens.	305-312
A.122-A.127	Force versus time and damage photographs for glass/epoxy ($90_2/0_2$) _s specimens.	313-318
A.128-A.133	Force versus time and damage photographs for glass/epoxy ($0_2/45_2$) _s specimens.	319-324
A.134-A.138	Force versus time and damage photographs for glass/epoxy ($45/0$) _{2s} specimens.	325-329
A.139-A.144	Force versus time and damage photographs for glass/epoxy ($0/45$) _{2s} specimens.	330-335

LIST OF TABLES

<u>TABLE</u>		<u>PAGE</u>
3.1	Impact Velocities for Graphite/Epoxy Tape Systems	31
3.2	Impact Velocities for Fabric Systems	32
3.3	Measured and Nominal Ply Thicknesses	49
4.1	Summary of Incipient Damage Forces and Velocities	130
5.1	Laminate Properties of the $[\pm\theta_2/0_2]_s$ Layups of AS4/3501-6 and IM7G/X8553-50	138
5.2	Laminate Properties of the 16-Ply AS4/3501-6 Laminates and 8-Ply Fabric Laminates of A370-5H/3501-6S and Glass/Epoxy	142
5.3	Ply (Elastic) Properties of the Material Systems	149
5.4	Ply Failure Strains for AS4/3501-6 and IM7G/X8553-50	170
A.1	Appendix Contents	191

NOMENCLATURE

A370-5H/3501-6S	fabric prepreg manufactured by Hercules
AS4/3501-6	tape prepreg manufactured by Hercules
°C	degrees Celsius
E_L	longitudinal modulus
E_T	transverse modulus
F_{ft}	force at the force transducer
F_{tot}	contact force of the impactor
g	grams
glass/epoxy	Interglas 92125 fabric in Rutapox L20/SL resin
Hg	mercury
IM7G/X8553-50	tape prepreg manufactured by Hercules
kg	kilogram
kHz	kiloHertz
m	meters
ml	milliliters
mm	millimeters
MPa	MegaPascals
mR	milliRad
ms	milliseconds
M_{ft}	mass of the force transducer
M_{rod}	mass of the impactor rod
M_{tup}	mass of the tup
N	Newtons
rpm	revolutions per minute
s	seconds

NOMENCLATURE (continued)

sec	seconds
t	time
x_1	coupon length direction
x_2	coupon width direction
ν_{LT}	major Poisson's ratio
θ	lamination angle

Chapter 1

INTRODUCTION

The desire for high stiffness and strength at a reduced weight has driven the aerospace industry toward composite materials for primary and secondary structural applications. Laminated material systems of fibers, such as graphite or glass, in resin matrices are replacing aluminum and other metals in wing skins, control surfaces, and even entire airframes. Upgrades to the McDonnell Douglas F/A 18 have incorporated graphite/epoxy panels into the vertical stabilizers and speed brake, and graphite/epoxy is used extensively in the Airbus A320. The Beechcraft Starship I has a nearly all-composite airframe. Current plans for the Boeing 777 call for a composite empennage on this large commercial airplane.

Of concern to those who design composite structures is the impact response of these relatively new material systems. Unlike metal parts which tend to exhibit impact damage on the surface, laminated composite materials have the unique capability to become damaged internally while showing no visible damage externally. The laminated nature of these materials gives rise to the possibility of delamination and very complicated damage states which do not occur in homogeneous metals. The current understanding of the impact behavior of composite materials lags far behind that for metals.

The topic of impact behavior has been subdivided into two separate areas in recent years: *damage resistance* and *damage tolerance*. The first area, damage resistance, deals with the damage state brought about by an impact event. The physical changes in the laminate, such as broken fibers, delamination and matrix cracks resulting from an impact event are of interest

here. The second area, damage tolerance, concerns the changes in the laminate performance and material properties due to a damage state. The focus is on residual strengths and the ability of a part to perform its intended function with damage present. In order to perform a damage tolerance assessment correctly, the damage state must first be accurately defined. Thus, the proper handling of damage tolerance relies upon a clear understanding of damage resistance.

There is therefore a need to understand the way in which laminated composite materials are damaged from impact. This knowledge is essential in order to determine the subsequent performance of the structure (i.e. damage tolerance). This combined knowledge will lead engineers in learning how to design for impact resistance and subsequent performance. Material system, ply stacking sequence, laminate thickness and ply angles can then be tailored to create the optimum configuration for damage resistance. Also, such knowledge can alleviate the need for conservative designs, allowing the full potential of composite materials to be realized. In the design of composite parts, compensations are often made to take into account unknowns such as impact resistance. Taking some of the mystery out of impact resistance will allow the use of more efficient structures.

Recently, new composite material systems with "toughened" resins have emerged as a possible answer to some of the problems posed by impact. Selected matrix properties have been improved in an effort to prevent damage from occurring due to impact, but the overall impact resistance of these materials needs to be compared to that of conventional composite systems. The impact behavior of a laminated plate is not merely a material property, but a complicated interaction of global structural response and local material response. At the point of contact between the impactor and the laminate, a

localized phenomenon occurs as the impacting object indents the plate. Simultaneously, the plate experiences a global structural vibration caused by the impacting mass. Factors such as laminate bending stiffnesses, plate dimensions and boundary conditions govern the global response, while the local response is dominated by material properties and the geometry of the impactor. The interplay between these two responses can thoroughly mask the contributions of individual material properties toward the damage resistance of an impacted laminate. Thus, impact tests of identical coupons of different material systems cannot be relied upon to characterize all of the aspects of impact resistance of those materials. For a fair comparison between systems, global (i.e. structural) and local (i.e. material) responses need to be separated. This clearly presents some very difficult problems to the experimenter.

Ideally, an analytical technique would be able to predict the damage due to an impact event and, ultimately, the residual strength. The first task of the analysis would be to approximate the local force-displacement behavior between the impactor and the laminate. This local contact relation is necessary in order to model correctly the global structural behavior. The dynamics of the structural response combine with the specifics of the local contact event to dictate the contact force history at the impact site. From the forces, the damage state can be obtained. To do this, stresses and strains need to be calculated in the laminate near the point of contact, and a failure criterion must be employed. It is this area that needs particular attention. It is felt that experimental data relating contact forces and damage states will be of aid in understanding the damage process in an impact event.

The purpose of this investigation is to explore the ways in which several laminated material systems become damaged due to impact and the relationship between contact force and damage states. A direct comparison of

impact behavior is made between various material systems. The types of impact of interest are those that would occur due to nonballistic events such as tool drop or runway kickup. A laminated part could be subjected to this type of impact during manufacture, in service, or during aircraft maintenance. It is known that reductions in strengths and stiffnesses often occur due to impacts that do not create visible surface damage. Therefore, it is a practical concern to investigate the ways in which damage occurs as a means toward understanding the overall effects of damage on laminated structures.

The five chapters that follow are titled Previous Work, Experimental Procedures, Experimental Results, Discussion, and Conclusions and Recommendations. In Chapter 2, the work previously done on impact resistance of composite structures is summarized and the need for understanding damage mechanisms is established. In Chapter 3, the techniques used for manufacturing, impacting and evaluating specimens are shown. This includes the test matrices, specimen description, and method of data acquisition. In Chapter 4, the results from experiments are presented. A discussion of the experimental results is found in Chapter 5. Conclusions and recommendations for further research appear in Chapter 6. The force-time data from all of the impact experiments along with X-ray photographs of damaged specimens can be found in Appendix A.

Chapter 2

PREVIOUS WORK

2.1 Overview

The problem of foreign object impact of composite laminates has received considerable attention over the past two decades. An extensive review of the work done on impact of laminates has been conducted by Abrate [1]. Numerous investigations have addressed the issues of dynamic response, local contact behavior and impact damage. Of these issues, the area of impact damage is of direct interest here. Many experimental and analytical investigations have been performed in an effort to understand this phenomenon. Analytical methods have been proposed for predicting damage, while experiments have been performed in an effort to understand damage mechanisms, compare material systems, or suppress the formation of damage.

2.2 Experimental Studies

A number of purely experimental investigations of impact damage have been performed and they can be categorized as damage resistance comparisons between different material systems, explorations of damage mechanisms, or attempts at suppressing damage from impact.

New material systems have emerged as a possible means to address problems due to impact. Matrix resins and fibers with higher failure strains than their first-generation counterparts are available. In order to assess the damage resistance capabilities of these systems, impact experiments have been performed [2-7,10], usually including an earlier graphite/epoxy system for comparison. But, a standardized impact test does not exist, and there is not

a common parameter for measuring and comparing the "impact resistance" of different materials.

Experimental impact studies on geometrically identical specimens of different material systems have been used to compare the relative merits of different systems. Gause and Buckley [3] compared the impact resistance of nine graphite/epoxy systems, including one first-generation system. They collected force data from impact tests and identified as important the parameters of load at incipient damage, energy absorbed at incipient damage, maximum load before penetration, energy absorbed at maximum load, and total energy absorbed for through-penetration. They found that the ranking of the material systems depended on the parameter used. They mention that the design requirements for a part, in terms of which kind of damage is critical, are necessary in order to rank the damage resistance of different material systems. One material system may effectively prevent delamination, while another may be more resistant to fiber damage, for example.

Researchers have also tried to correlate laminate "impact resistance" to a variety of different material properties. Bowles [4] attempted to relate material properties of the matrix to the "impact resistance" of a laminate. Load at damage initiation and maximum load before penetration were both proposed as measures of laminate "impact resistance". A common graphite fiber was used in conjunction with four different matrix resins to create impact specimens. Several strengths and moduli of the neat resins were obtained and it was hoped that a correlation could be drawn between one of these properties of the matrix and laminate "impact resistance" as defined above. A direct relationship between the matrix properties and either of the chosen "impact resistance" parameters was not established. It was found that different failure modes occurred in the laminates with different matrix resins, making comparisons of the data very difficult.

The importance of impact force data has been recognized by others, as well. Sjoblom, Hartness and Cordell [5] asserted that an understanding of damage mechanisms should be the ultimate goal of research, but for now, low-velocity impact testing should be used as a comparative technique. They state a case for the development of a standardized test of impact resistance, and for the instrumentation of such a test to provide force data. They assert that the force history of the impact event is more revealing than a single parameter such as total impact energy, which indicates nothing about the dynamics of the impact event.

A standardized impact test and common parameters for material comparison have been suggested. Reed and Turner [6] proposed a standardized impact test for composites. They recommended that an impact test currently used to evaluate isotropic thermoplastics be used with instrumentation to compare the impact resistance of fibrous composites. Maximum force before penetration or energy absorbed before penetration were suggested as parameters for comparing material systems. Thus, penetration of the laminate was considered to be the critical failure from impact.

But, penetration is a culmination of damage modes, and it is the understanding of damage mechanisms prior to penetration that is currently absent. Several researchers have looked at damage mechanisms in experimental studies [2,5,7,9,10] and damage modes have been shown to be complicated. Also, the lack of standardized damage metrics is obvious.

For lack of a better damage metric, Lee and Zahuta [7] measured the lengths and widths of delaminations from C-scan images of impacted and statically tested specimens. They found that similar damage extents resulted from impact and quasi-static indentation tests. The indentation force used was that of the peak force encountered during impact. Their results are based on a two-dimensional representation of the damage state, which may or may

not be sufficient to describe the damage. They concluded that the damage growth process during impact can be visualized by a sequence of static indentation tests of various force levels. A similar conclusion was drawn by Elber [8] based on X-ray images of damage states. It was pointed out that low velocity impacts excite mostly first mode, or static mode, bending deflections so that static testing can be used to simulate impact damage.

Experiments have shown that damage modes can be affected by the geometry of an impact specimen. Cantwell and Morton [9] found different modes of damage initiation in specimens with different dimensions. They identified contact failure at the impacted surface for short thick targets and flexural failure at the back surface for long thin targets.

Also, different material systems have been shown to exhibit different damage modes. Boll et al [10] used microscopy to investigate the damage mechanisms in toughened and conventional composite material systems. They found a network of matrix cracks and delaminations under and around the point of impact for the conventional system. Matrix cracking was also observed in the "toughened matrix" system, but with much less delamination. Damage was contained in a smaller area with the toughened system, but fiber breakage was observed, which had not occurred in the first-generation system. They concluded that as the fracture energy of the matrix is increased, fiber strength will become more important because the damage mode will change.

From detailed three-dimensional investigations of damage states [25-28], it is known that certain interfaces of specific laminates are prone to delaminate from impact loading. Suggestions have been made for preventing or limiting the extent of such occurrences. Kumar and Rai [11] investigated kevlar/epoxy laminates and the effect of replacing unidirectional surface plies with glass/epoxy fabric plies. They used cross-sectioning for damage evaluation and found the glass fabric plies to effectively reduce the size of the

delaminations within the laminate and curb the spalling of the plies at the back surface. Sun and Rechak [12] used adhesive layers as a means of suppressing delamination in graphite/epoxy laminates. They observed reductions in matrix cracking with the adhesive layers and were able to effectively control delamination. They also noted, however, that fiber breakage became more prominent with the addition of the adhesive. Works of this type are interesting, but contribute little to the understanding of damage mechanisms. They have a limited scope of application since they deal with specific layup configurations with known damage modes.

In summary, the term "impact resistance" has yet to be quantitatively defined. Several damage modes are possible due to impact, and depending on the application, different modes are considered critical. Hence, a standardized test of "impact resistance" for composite materials does not exist. Also lacking are standardized metrics for quantifying damage states. Damage modes have been shown to depend on specimen geometry and material properties. Some observations of damage mechanisms have been made from experiments, and possible remedies have been suggested. Such remedies were found to suppress certain types of damage, but also could cause a change in the damage mode. Experiments have also shown that static testing can be used to simulate damage states from impact in certain situations.

2.3 Analyses

Because of the nearly infinite number of possible combinations of material system, layup, specimen geometry, and impactor mass and velocity, relying solely on experiments for impact characterization should be avoided if at all possible. An accurate analysis methodology capable of predicting impact damage would be very valuable. Several schemes for such analysis have been proposed.

Some of the early work in predicting stresses in an impacted laminate was done by Greszczuk [13]. A two-dimensional finite element model was used to calculate the local distribution of stresses near the point of contact. The global bending deformation was neglected and the laminate was assumed to be supported on a rigid foundation. Subsurface shear failure was predicted as the initial damage mode using a stress-based failure criterion.

High shear stresses due to impact were also calculated by other researchers [14-16]. Two-dimensional finite element models have been used to predict global response as well as local stresses [14,15]. High shear stresses were calculated in laminates near the impact site, and it was postulated that these could initiate delamination, although no failure criteria were applied.

Predicted stresses have been shown to relate to experimental impact damage states. Ross et al [16] used a three-dimensional finite element formulation to model the stresses within an impacted glass/epoxy plate. The global dynamic response was not modeled. Instead, a loading function was approximated from experimental data. High shear stresses were calculated within the plate in locations that agreed qualitatively with delamination areas observed in experiments.

Predicting damage, on a quantitative basis, requires the additional step of applying a failure criterion. Wu and Springer [17] used a three-dimensional finite element model to predict the global response and local stresses and strains for impacted plates. A total of five failure criteria, including those of Humphreys and Goering [18] and Ramkumar and Chen [19], were invoked in an effort to predict delamination. When none of these criteria successfully predicted the delaminations observed from experiment, a new criterion based on dimensional analysis was proposed and was shown to predict delamination size and location with limited success.

In a different approach to the same problem, Cairns and Lagace [20] modeled the global response and local stresses without using finite elements. A Rayleigh-Ritz energy formulation was used to predict the global response of impacted kevlar/epoxy and graphite/epoxy plates [21], and the local stresses were calculated using an axisymmetric Fourier-Bessel series expansion [22]. A maximum strain ply failure criterion was applied to predict matrix cracking, delamination, and fiber damage. Comparisons with X-rays of damage from experiment showed that overall damage area (i.e. integrated through the thickness) of an impacted laminate was predicted with reasonable success.

However, the work of Chang, Choi and Wang [23] indicated that in order to correctly predict delamination in all cases, stresses may have to be recalculated once matrix cracking occurs. A dynamic finite element analysis was used along with a Hashin failure criterion to predict matrix cracking in impacted thin beams. The analysis was shown to successfully predict matrix cracking observed in experiments. The analysis was also used to recalculate stresses in the vicinity of the matrix cracks, and it was found that the presence of the cracks created a large out-of-plane stress, or peel stress, which could initiate the delaminations which were often observed near the matrix cracks.

Another proposed method of predicting the locations of delaminations and matrix cracks is the K-rule. Gosse and Mori [24] developed this simplistic procedure to predict matrix cracks and associated delaminations from impact. From the strain state due to an impact, tensile principal strains are calculated in each ply on a plane perpendicular to the fibers. Matrix cracking is assumed to occur if the tensile principal strain exceeds the transverse ultimate strain of the ply. Transverse cracks in neighboring plies are connected by delaminations, such that the delamination between the plies is bounded by the matrix cracks in those plies. General agreement was found with

experimental damage states assessed by ultrasound and cross-sectioning techniques.

It is indicated from the literature that the progressive nature of impact damage requires more attention. Analysis techniques which predict damage may have to include the changes in the material state as damage occurs. Also, since it has been shown that certain damage changes the state of stress within a laminate, analyses may need to recalculate laminate stresses as damage occurs. Therefore, it would be beneficial to have experimental examples of incipient failure modes in laminates and their development into advanced damage states from impact. This data would be useful in verifying analytical methods, and also would aid in the development of new material systems to resist impact damage.

Chapter 3

EXPERIMENTAL PROCEDURES

3.1 Test Matrix and Specimen Description

Four material systems were investigated here: Hercules AS4/3501-6 tape prepreg, Hercules A370-5H/3501-6S fabric prepreg, Hercules IM7G/X8553-50 tape prepreg, and a woven fabric fiberglass/epoxy wet layup. The first material system, AS4/3501-6, is unidirectional and has a first generation "brittle" (low strain-to-failure) 3501-6 matrix and is currently widely used in the aerospace industry. It was chosen to provide a base for comparison. The IM7G/X8553-50 unidirectional prepreg material system has IM7 fibers in an experimental "toughened" (high strain-to-failure) matrix and was chosen as a representative "toughened matrix" system. The third material system, A370-5H/3501-6S is the same as the AS4/3501-6, except the fibers are woven in a five-harness arrangement. This allows a comparison of the relative merits of tape and fabric layups in resisting damage. The glass/epoxy system is comprised of Interglas 92125 dry woven fiberglass prepared in a wet layup with Rutapox L20/SL resin. This system is being used in the aircraft industry, and is used here to provide a direct comparison with the graphite/epoxy fabric system.

In addition to identifying the incipient damage type, the general damage characteristics of these laminates are also of interest. In order to observe the progressive stages of damage, impact tests were performed at various velocities while holding constant the impactor mass (1.53 kg), tup diameter (12.7 mm), specimen geometry, and boundary conditions (two sides clamped). The impact velocities used ranged from those causing incipient damage to

those causing penetration of the specimen, when possible. Due to limitations of the impact device, all layups of all material systems used could not be penetrated.

Impact velocities were determined for each layup based on the results of preliminary impact tests. Several trial impacts were performed on specimens of each type of laminate to determine an approximate velocity range in which damage occurred. Using this information, an initial impact velocity was chosen for each laminate such that a level of damage would exist that could be detected easily via X-ray, or visually in the case of the glass/epoxy system. Subsequent impacts were performed at slower velocities, in 0.5 m/s intervals, until no damage was detected, either visually or by X-ray. In addition, the laminates were generally impacted at a common velocity of 5.0 m/s to provide a damage resistance comparison between all layups and material systems. Any remaining specimens were used to isolate further the incipient damage velocity for each layup. This was done by impacting specimens at 0.1 m/s increments in the velocity range where incipient damage was determined to occur. The actual impact velocities used for the tape and fabric layups are listed in Tables 3.1 and 3.2, respectively.

A direct comparison between the AS4/3501-6 and IM7G/X8553-50 material systems was provided by the specimens summarized in Table 3.1. The first four layups consist of 12 plies in a $[\pm\theta_2/0_2]_g$ configuration, with θ taking on the values 15, 45, 60, and 90 degrees. These layups were chosen because they are orthotropic and incorporate varying degrees of bending-twisting coupling. A broad range of ply angles was desired to show the effect of ply angle mismatch and change in structural parameters on impact damage. Also, all plies were repeated twice to limit the number of ply interfaces where delamination could occur and to make matrix cracks more apparent. This

Table 3.1 Impact Velocities^a for Graphite/Epoxy Tape Systems

Laminate	Material System	
	AS4/3501-6	IM7G/X8553-50
[±15 ₂ /0 ₂] _s	1.00, 1.11, 1.14, 1.28, 1.28, 1.52, 2.07, 2.59, 3.01, 5.05	0.96, 0.99, 1.30, 1.50, 1.52, 2.04, 2.51, 3.04, 3.43, 4.03, 4.51, 4.87, 5.46
[±45 ₂ /0 ₂] _s	1.01, 1.21, 1.26, 1.30, 1.38, 1.53, 2.01, 2.60, 3.00, 5.10	2.20, 2.21, 2.55, 2.98, 3.47, 3.97, 4.05, 4.42, 4.96, 5.50
[±60 ₂ /0 ₂] _s	0.57, 0.72, 0.72, 0.88, 0.89, 1.01, 1.54, 2.00, 2.61, 2.96, 5.06	2.06, 2.22, 2.22, 2.45, 2.97, 3.26, 3.83, 4.52, 5.02, 5.45
[90 ₄ /0 ₂] _s	0.58, 0.73, 0.75, 0.87, 0.88, 1.00, 1.53, 2.08, 2.58, 2.98, 5.09	0.99, 1.54, 2.04, 2.46, 3.01, 3.47, 3.95, 4.50, 4.90, 5.46
[±45 ₂ /0 ₂ /90 ₂] _s	2.05, 2.07, 2.11, 2.12, 2.26, 2.28, 2.50, 2.59, 2.96, 5.00	--
[(±45) ₂ /(0/90) ₂] _s	2.60, 2.65, 2.75, 2.77, 2.78, 3.00, 3.04, 3.59, 5.09	--

^aAll velocities in m/s.

Table 3.2 Impact Velocities^a for Fabric Systems

Laminate	Material System	
	Glass/Epoxy	A370-5H/3501-6S
$(45_2/0_2)_s$	1.01, 1.22, 1.22, 1.53, 2.03, 2.72, 2.96, 4.72	4.03, 4.10, 4.13, 4.21, 4.25, 4.36, 4.39, 4.51, 5.10
$(90_2/0_2)_s$	1.02, 1.54, 2.00, 2.62, 2.96, 5.14	--
$(0_2/45_2)_s$	1.03, 1.48, 2.00, 2.64, 2.98, 4.80	--
$(45/0)_{2s}$	1.02, 1.43, 2.02, 2.53, 2.96	--
$(0/45)_{2s}$	1.05, 1.43, 2.00, 2.57, 2.98, 5.08	--

^aAll velocities in m/s.

was done to simplify the detection and recording of damage states. Delamination does not occur between two plies of the same angle [29], and in this way, two neighboring plies of the same angle become one "effective" ply of double thickness.

The last two layups in Table 3.1 exhibit two different stacking sequences for the same 16 plies. These quasi-isotropic layups were intended to mimic, as closely as possible, the fabric layup $(45_2/0_2)_8$ of A.370-5H/3501-6S. This was done so that a comparison of damage resistance could be made between fabric and tape layups with nearly the same laminate (i.e. structural) properties. (Laminate bending stiffnesses are summarized in Chapter 5) Double "effective" plies are used in the first tape layup, while the ply angle in the second tape layup alternates more frequently. Of these two tape layups intended to simulate the fabric layup, the second tape layup imitates more closely the fiber arrangement of the fabric.

All the fabric layups used and the impact velocities are listed in Table 3.2. The glass/epoxy layups were chosen for comparison to graphite/epoxy systems and to demonstrate any change in damage characteristics with stacking sequence.

The geometry of the impact specimens used is the same as that used by Ryan [30]. The specimens are 89 mm wide and 330 mm in length, as can be seen in Figure 3.1. Specimens of this width were used so that damage from impact could progress without the interference of edge effects of the coupon. Three specimens were obtained from each standard TELAC laminate of dimensions 304 mm by 356 mm. When clamped in the impact holding jig, the span of the specimen is 252 mm. All impacts were targeted at the center of the specimen.

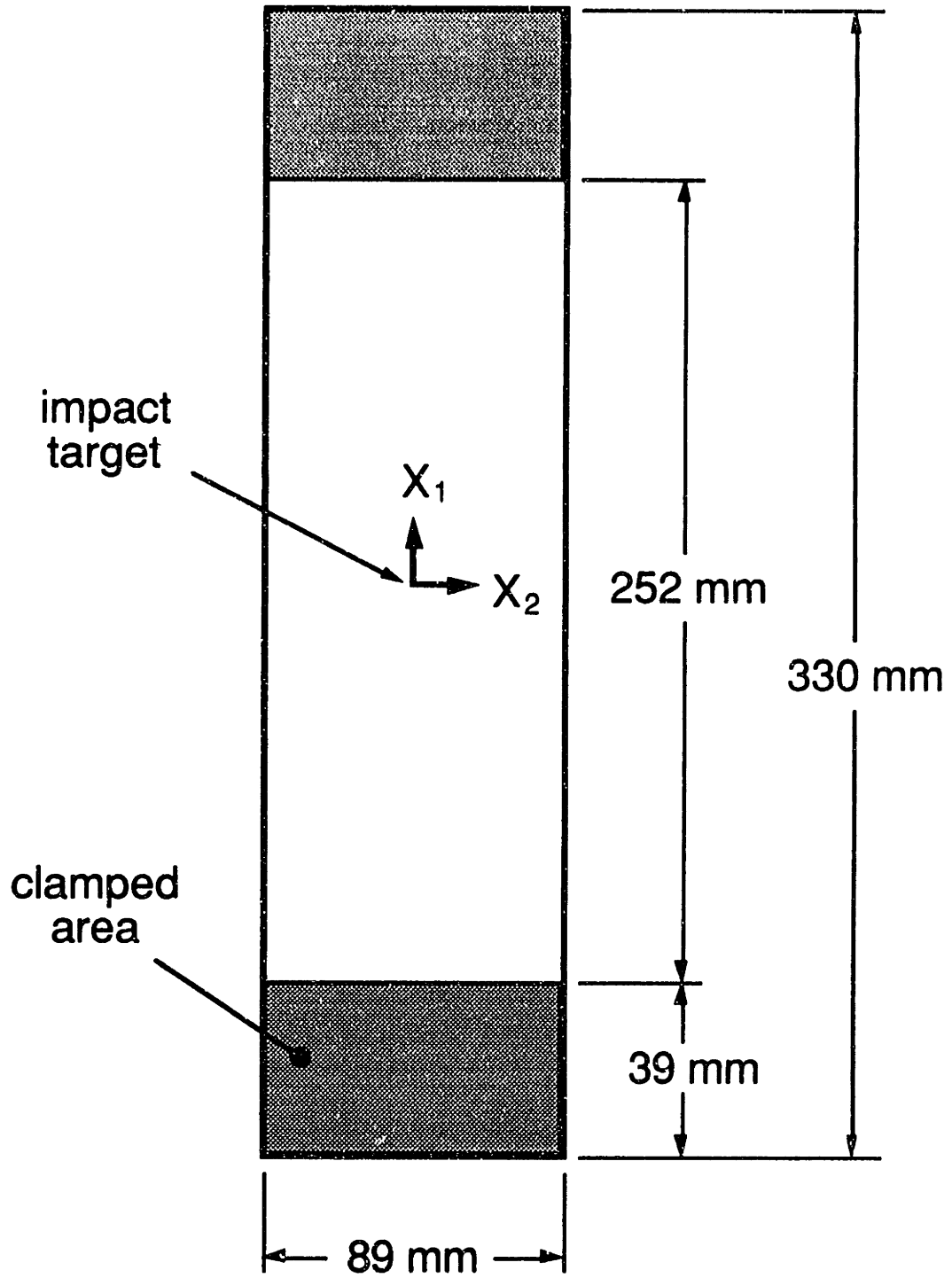


Figure 3.1 Impact specimen geometry.

3.2 Manufacturing Procedures

The manufacturing procedures used for the AS4/3501-6 and A370-5H/3501-6S laminates are standard [31] and are summarized here. Procedures for manufacturing the IM7G/X8553-50 and glass/epoxy laminates were provided by each material's supplier and appear here as well.

Two different layup techniques were followed in this investigation: a prepreg layup for the graphite/epoxy material systems and a wet layup for the glass/epoxy system. Latex gloves were worn whenever the prepreg materials were handled directly, and care was taken to avoid unnecessary contact with the laminates at all times.

3.2.1 Graphite/Epoxy Prepreg Layup

The layup procedures were identical for the AS4/3501-6 and IM7G/X8553-50 material systems. The graphite/epoxy prepreg tape came in the form of rolls 305 mm wide. The rolls of prepreg were stored in sealed bags in a freezer below -18°C . In preparation for layup, the prepreg was taken out of the freezer and allowed to sit at room temperature in the sealed bag for approximately 30 minutes, or until the material was no longer cold to the touch. Had the bag been opened while the material was still cold, unwanted moisture could have condensed on it. The prepreg was then unrolled and the appropriate plies were cut using teflon-coated aluminum patterns and a sharp utility knife. The plies were cut in such a way that any seams within a ply were parallel to the fiber direction. The individual plies were stacked in the proper sequence using an L-shaped aluminum jig to aid in alignment. The corner of the laminate which was situated directly in the corner of the aluminum jig was assumed to have the most accurate ply stacking and was

marked for future reference. The laminate was trimmed with a sharp utility knife and an aluminum pattern to its nominal 304 mm wide by 356 mm long size, and peel-ply was placed on both the top and bottom surfaces. If the laminates were to be cured within 24 hours, they were sealed in a vacuum bag and left out at room temperature. Otherwise, they were sealed in a bag and put into the freezer.

The graphite/epoxy fabric prepreg (A370-5H/3501-6S) was prepared in a similar way. The roll of prepreg was taken from the freezer and allowed to warm up to room temperature before opening it. The plies were cut from the 1245 mm wide roll with a 304 mm by 356 mm rectangular template and a utility knife. The angle plies were cut by placing the template at the desired angle and cutting out the ply, such that no seams existed in any of the fabric plies. The plies were then stacked in the same fashion as the tape prepreg plies, and peel-ply was placed on the top and bottom surfaces.

3.2.2 Glass/Epoxy Wet Layup

The glass/epoxy system requires a wet layup procedure. The raw materials used in preparation of this system were a 1.0 meter wide roll of Interglas 92125 woven fiberglass, a drum of Rutapox L20 epoxy resin and another smaller container of liquid "SL" hardener for the resin. The resin and hardener must be mixed in the correct proportion. This mixture is then added to the dry fabric plies, producing a layup ready to be cured in the autoclave under vacuum.

The wet layup is performed in the following manner. First, the necessary plies of glass fabric are cut from the roll with scissors. The glass plies are then carefully weighed. The appropriate mass of liquid matrix is prepared by mixing the resin and hardener in a 100 to 34 mass ratio to give a

total mass of matrix equal to the total mass of the fabric plies. The layup calls for the combining of equal masses of matrix and fibers.

In preparation for the wet layup and cure, the cure plate is sprayed with Mold Wiz® release agent and covered with a sheet of nonporous teflon. On top of this, three layers of cork dam are used to make a 304 by 356 mm rectangular vessel for the laminate. A sheet of nonporous teflon is placed in the bottom of the vessel, followed by a sheet of peel-ply and then the layers of dry fabric. After the last ply of fabric is placed in the vessel, the matrix is introduced on top and allowed to soak into the plies. The matrix is applied with a one-half inch acid brush starting at the center of the laminate and working outward radially toward the edges. By working from the center outward, the amount of trapped air in the laminate is minimized. Care is taken not to disturb the alignment of the fibers while adding the matrix with the brush. When wetted, the layup changes appearance from white in color to transparent. When no areas of white are visible, any remaining matrix is spread evenly over the laminate and a sheet of peel-ply is smoothed on top. The aluminum top plate, wrapped in nonporous teflon, comes next. Sheets of bleeder paper are rolled into dams and added between the cork vessel and the vacuum ports to prevent liquid matrix from flowing into the vacuum system. The assembly is then covered with a single sheet of porous teflon, a layer of glass breather, and finally, the vacuum bag. The cure plate is then ready for the autoclave. Figure 3.2 is a schematic of the cure layup.

3.2.3 AS4/3501-6 and A370-5H/3501-6S Cure

The AS4/3501-6 and A370-5H/3501-6S materials were cured according to the standard TELAC procedure. The packaging arrangement for the cure is shown in Figure 3.3. The laminate is placed on top of the sheets of nonporous

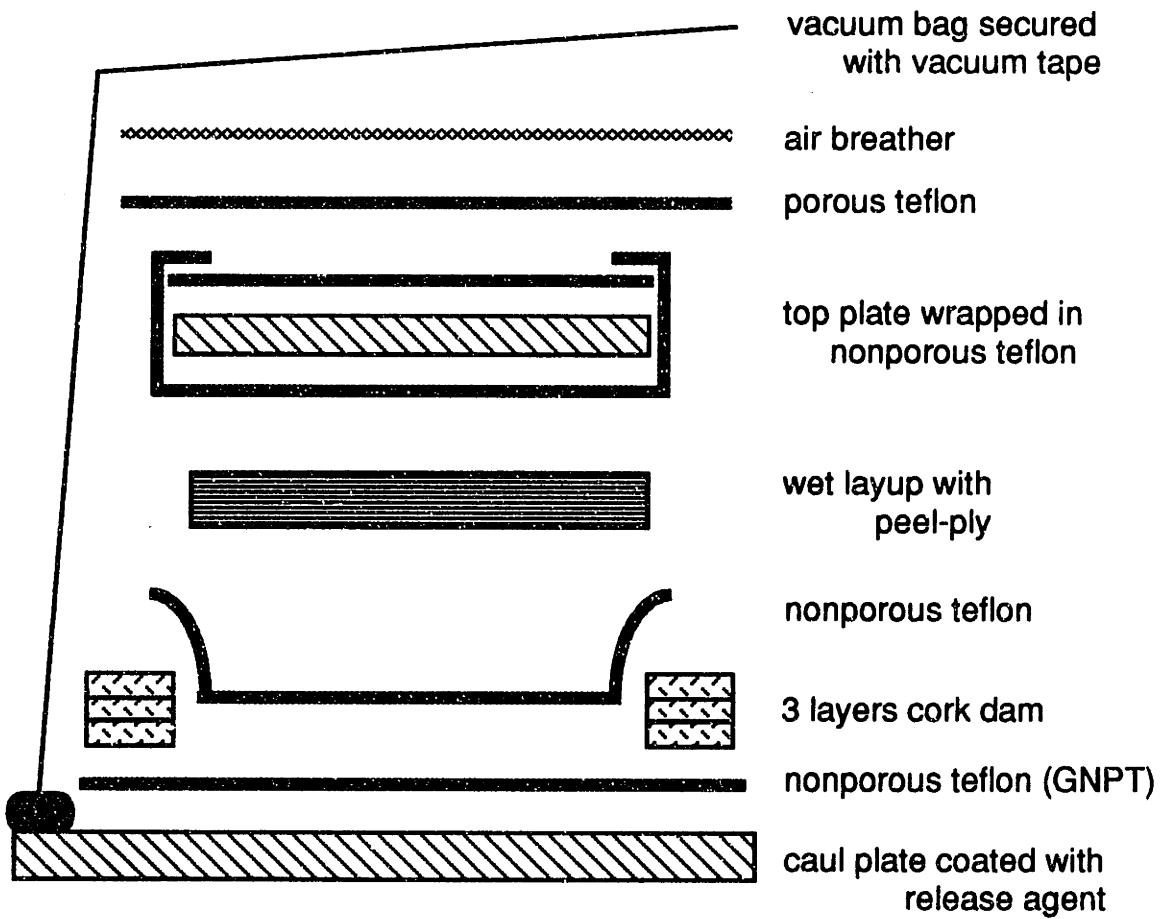


Figure 3.2 Schematic of glass/epoxy cure layup.

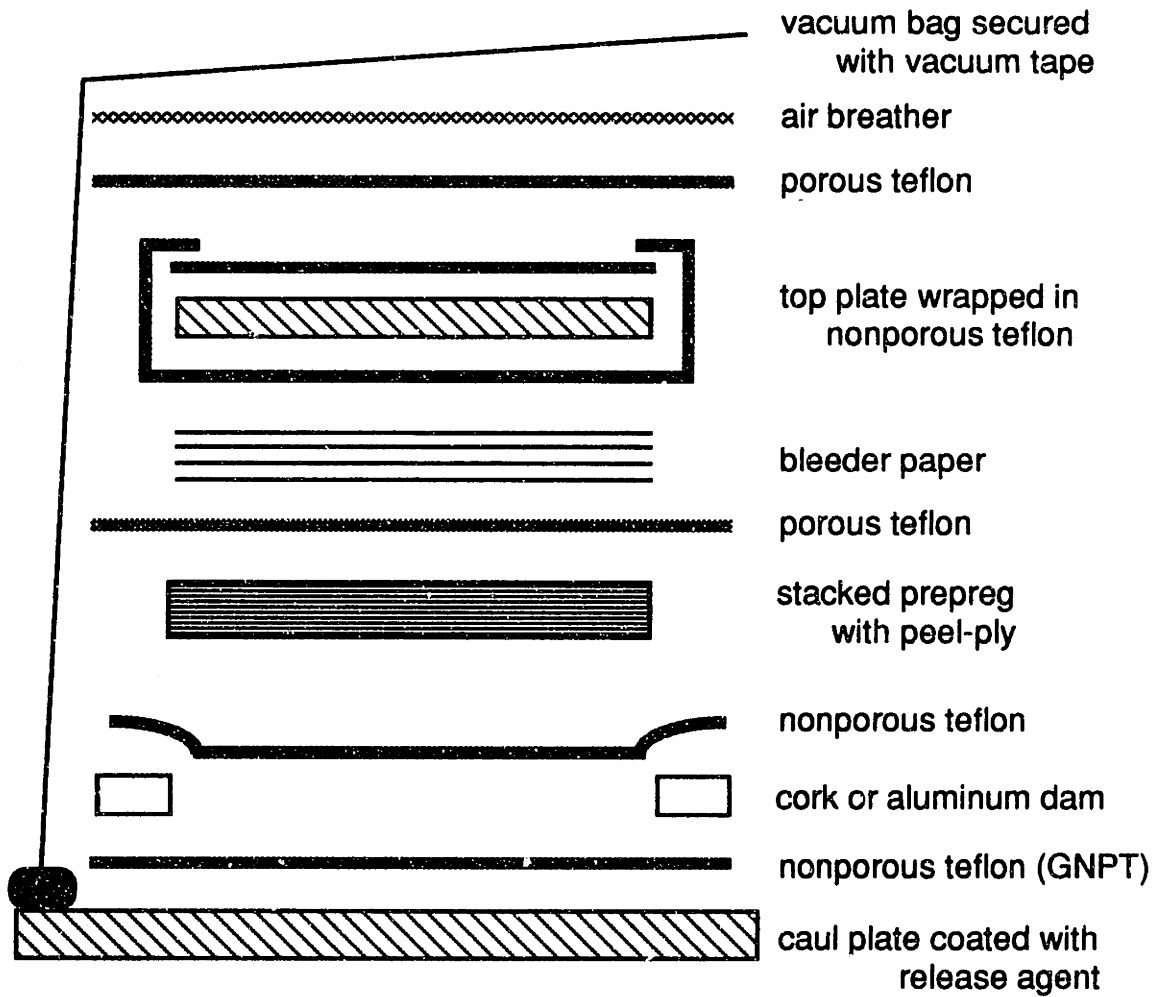


Figure 3.3 Schematic of AS4/3501-6 and A370-5H/3501-6S cure layup.

teflon and confined by the dam material. One sheet of porous teflon is placed on top of the laminate, followed by sheets of bleeder paper, the aluminum top plate, a sheet of porous teflon and a layer of fiberglass air breather. A vacuum bag is placed over this assembly and vacuum tape is used to create a seal between the bag and the aluminum caul plate.

The sheets of guaranteed nonporous teflon (GNPT) are used to keep the resin from contacting the aluminum caul plates, which are sprayed with a release agent to prevent resin from adhering to them. Peel-ply is a nylon-like fabric which is used to give a fine surface texture to the specimen. The peel-ply is removed from the laminates after the postcure. The purpose of the bleeder paper is to soak up resin that is expelled from the laminate. For the tape prepreg, one ply of bleeder paper is used for every two plies of prepreg in the laminate. For the fabric prepreg, one ply of bleeder paper is used for each ply of fabric in the laminate. The fiberglass air breather is used so that the vacuum can be applied evenly over the entire cure plate.

Six laminates are cured at one time in the autoclave. The position of the laminates on the cure plate is illustrated in Figure 3.4. T-shaped aluminum dams, as well as cork dams, are used to hold the laminates in place during the cure. The reference corner of each laminate, which was marked previously during layup, is always placed into the corner of an aluminum T-dam on the cure plate. Thus, each laminate had two sides bordered by aluminum dams and two sides bordered by cork dams.

A vacuum check is performed on the cure plate before it is rolled into the autoclave. This is done by applying a vacuum of 760 mm Hg and then shutting off the vacuum source. The vacuum seal is considered satisfactory if less than 130 mm Hg has been lost after five minutes elapsed time. Otherwise, attempts are made at trying to find and repair leaks in the vacuum bag, or the entire

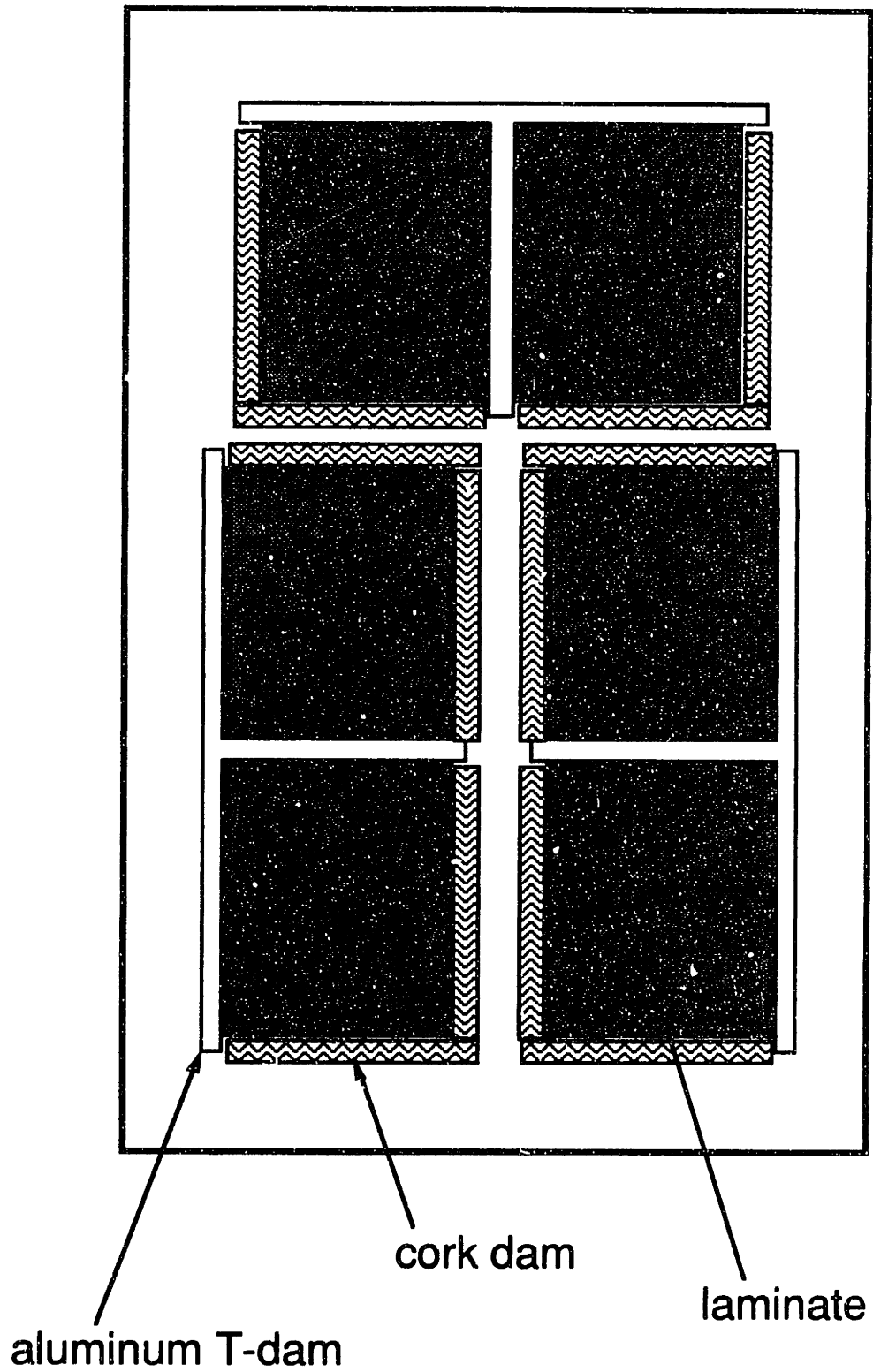


Figure 3.4 Illustration of cure plate (top view).

bag is replaced. Once a successful vacuum check is performed, the cure plate is rolled into the autoclave and the vacuum check repeated.

In the autoclave, a vacuum of 760 mm Hg is applied to the cure plate. The autoclave pressure is raised to a gage pressure of 0.59 MPa and held. Once this pressure is achieved, the autoclave temperature is raised at a rate of 1-3°C per minute until 116°C is reached. After one full hour at 116°C, the temperature is again raised at the same rate to 177°C and held for two hours. Finally the temperature is decreased at 3-5°C per minute to 80°C and the pressure released. The temperature, pressure and vacuum cycles are shown in Figure 3.5. The laminates were postcured in an oven at 177°C for 8 hours with no applied pressure or vacuum.

3.2.4 IM7G/X8553-50 Cure

A similar cure was performed for the IM7G/X8553-50 material system. The cure packaging used for these laminates can be seen in Figure 3.6. As this was a net resin cure, no bleeder paper was used. Otherwise, the cure packaging is very similar to that used for the AS4/3501-6 material. Again, six laminates are cured at one time in the autoclave and the cure plate is arranged in the same way as previously shown.

The temperature, pressure and vacuum cycles can be seen in Figure 3.7. After successful vacuum checks, a vacuum of 760 mm Hg is applied to the cure plate and the temperature ramped up to 116°C at a rate of 3-5°C per minute. After 30 minutes at 116°C, the autoclave pressurization begins. A pressure of 0.69 MPa is reached after approximately 30 minutes, and held for the duration of the cure. At this point, the temperature has been at 116°C for one full hour. The temperature is then ramped up to 177°C at 3-5°C per minute. This temperature is held for two hours, after which time

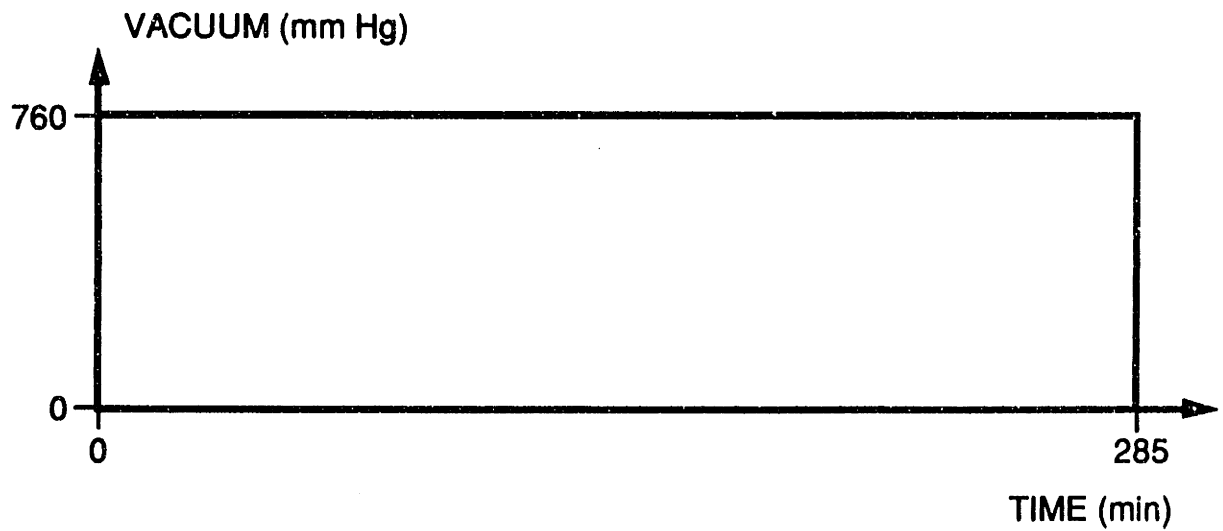
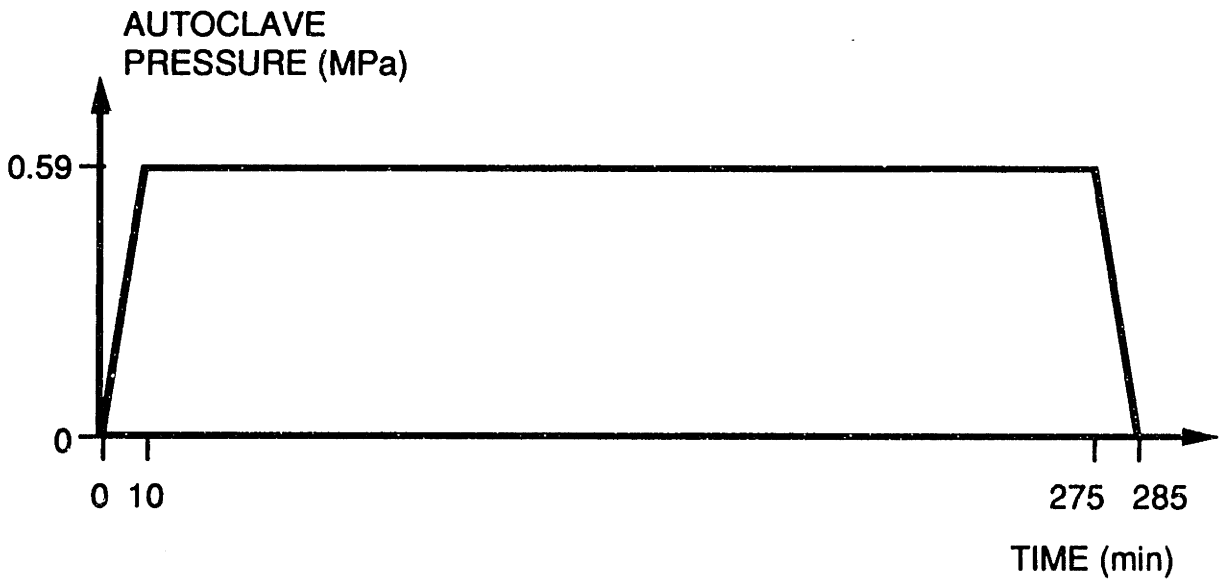
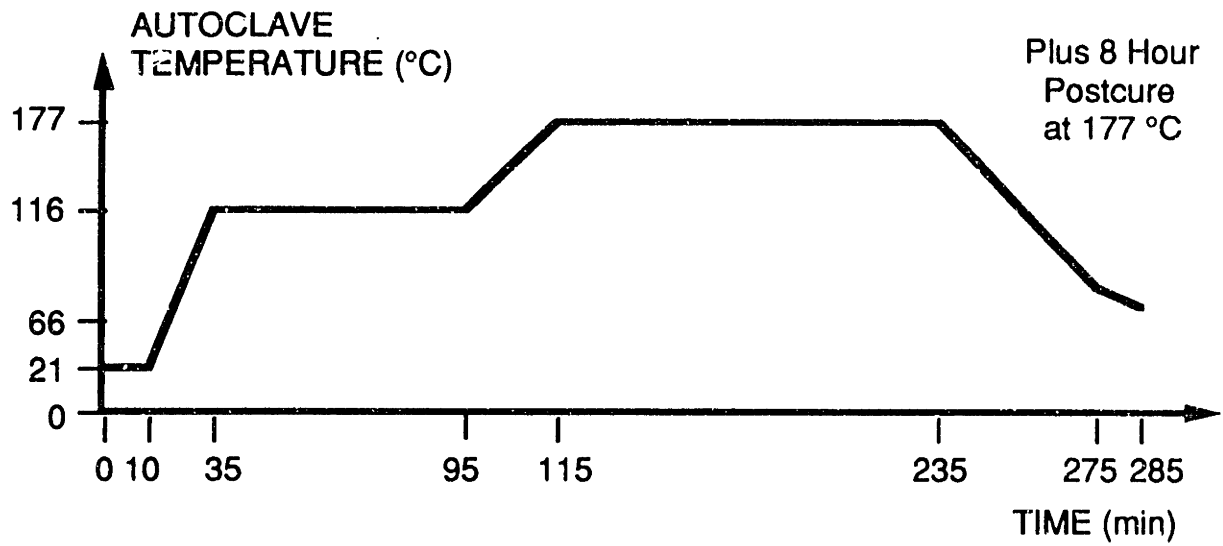


Figure 3.5 AS4/3501-6 and A370-5H/3501-6S cure cycle.

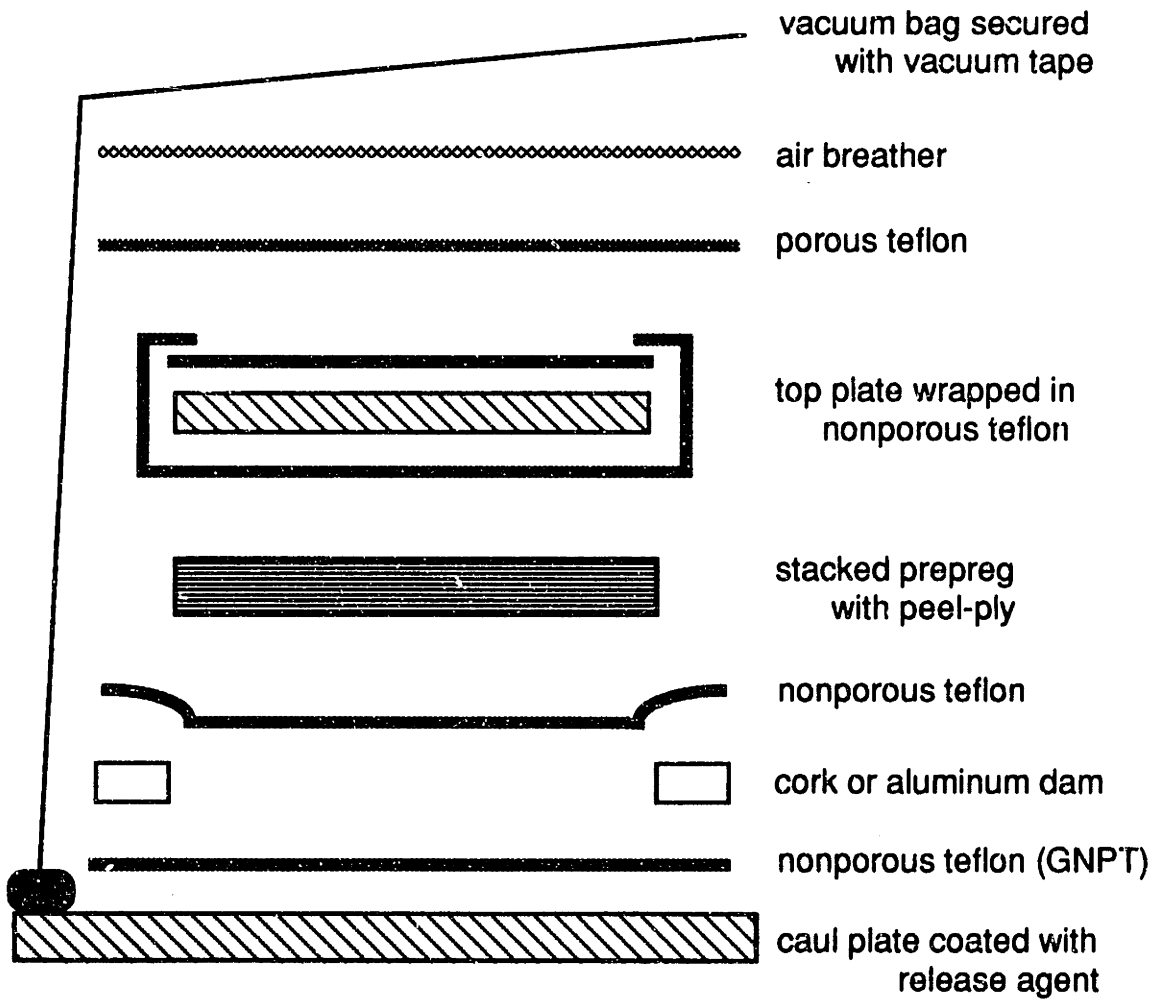


Figure 3.6 Schematic of IM7G/X8553-50 cure layup.

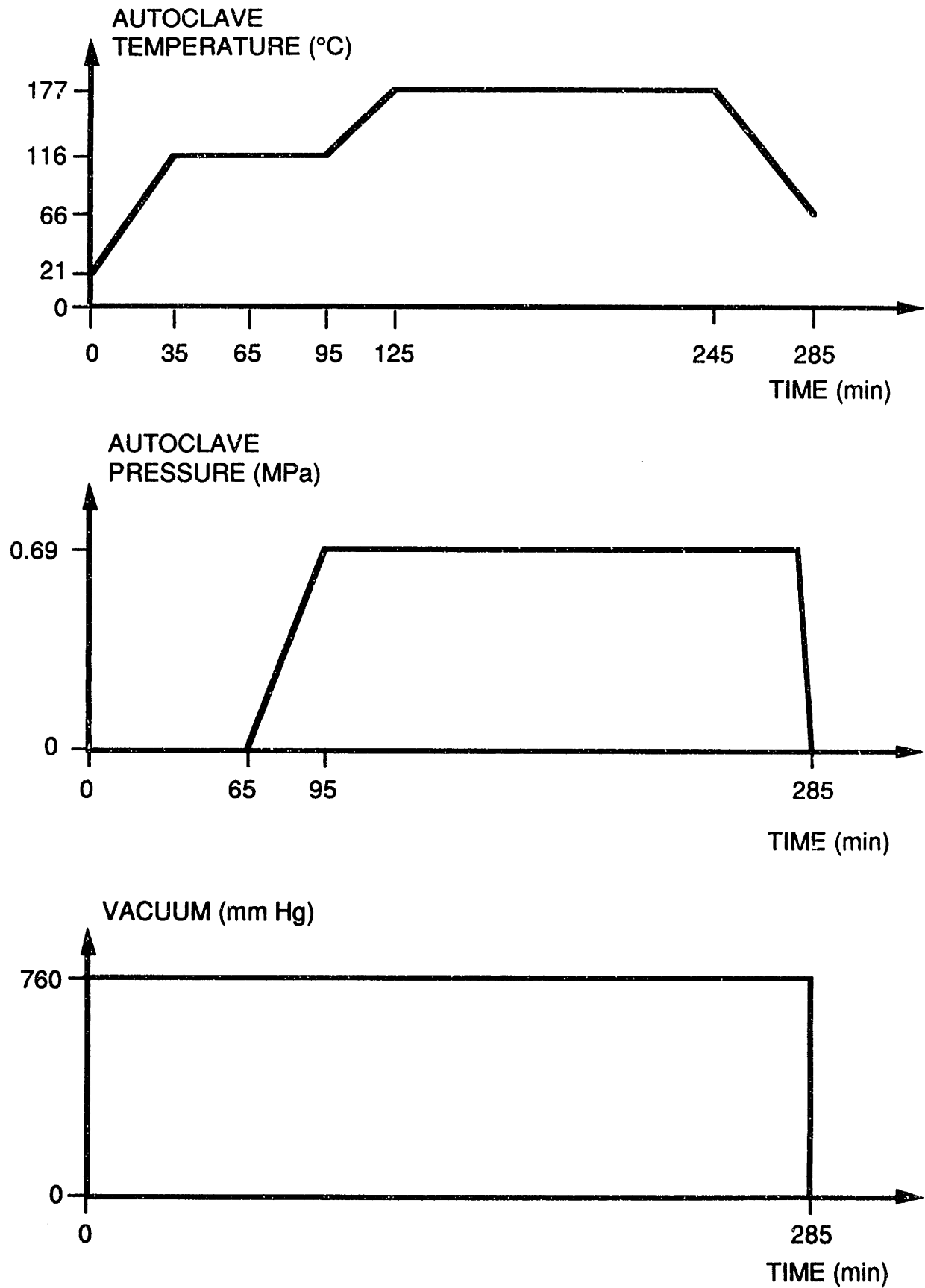


Figure 3.7 IM7G/X8553-50 cure cycle.

the temperature is lowered at 3-5°C per minute and the pressure released. These laminates were not postcured.

3.2.5 Glass/Epoxy Cure

The glass/epoxy required an 8-hour cure cycle with vacuum applied, but no pressure, as shown in Figure 3.8. Only two glass/epoxy laminates were cured in the autoclave at one time. After a successful vacuum check, a vacuum of 760 mm Hg is applied to the cure plate in the autoclave and the temperature raised to 60°C at a rate of 5-6°C per minute. This temperature is held for 8 hours, after which time the vacuum is released and the laminates removed from the autoclave. The laminates were then postcured in an oven for 15 hours at 80°C with no applied vacuum or pressure.

3.2.6 Final Preparation

All laminates were milled into coupons with a water-cooled 220 grit diamond cutting wheel. The diameter of the cutting wheel is 254 mm and a spindle rate of 1100 rpm was used. The milling table feed rate was 279 mm per minute. First, the edges of the laminate were cleaned up by trimming approximately 5 mm from each side. Then, three 89 mm wide specimens were cut from each laminate. For the graphite/epoxy material systems, the coupons were cut from the laminate starting with the edge adjacent to the reference corner previously marked.

The manufacturing consistency of each coupon was then checked. Nine thicknesses, three widths, and the length of each coupon were measured at the locations shown in Figure 3.9. A comparison of the nominal and average measured ply thicknesses for all four material systems can be seen in Table 3.3.

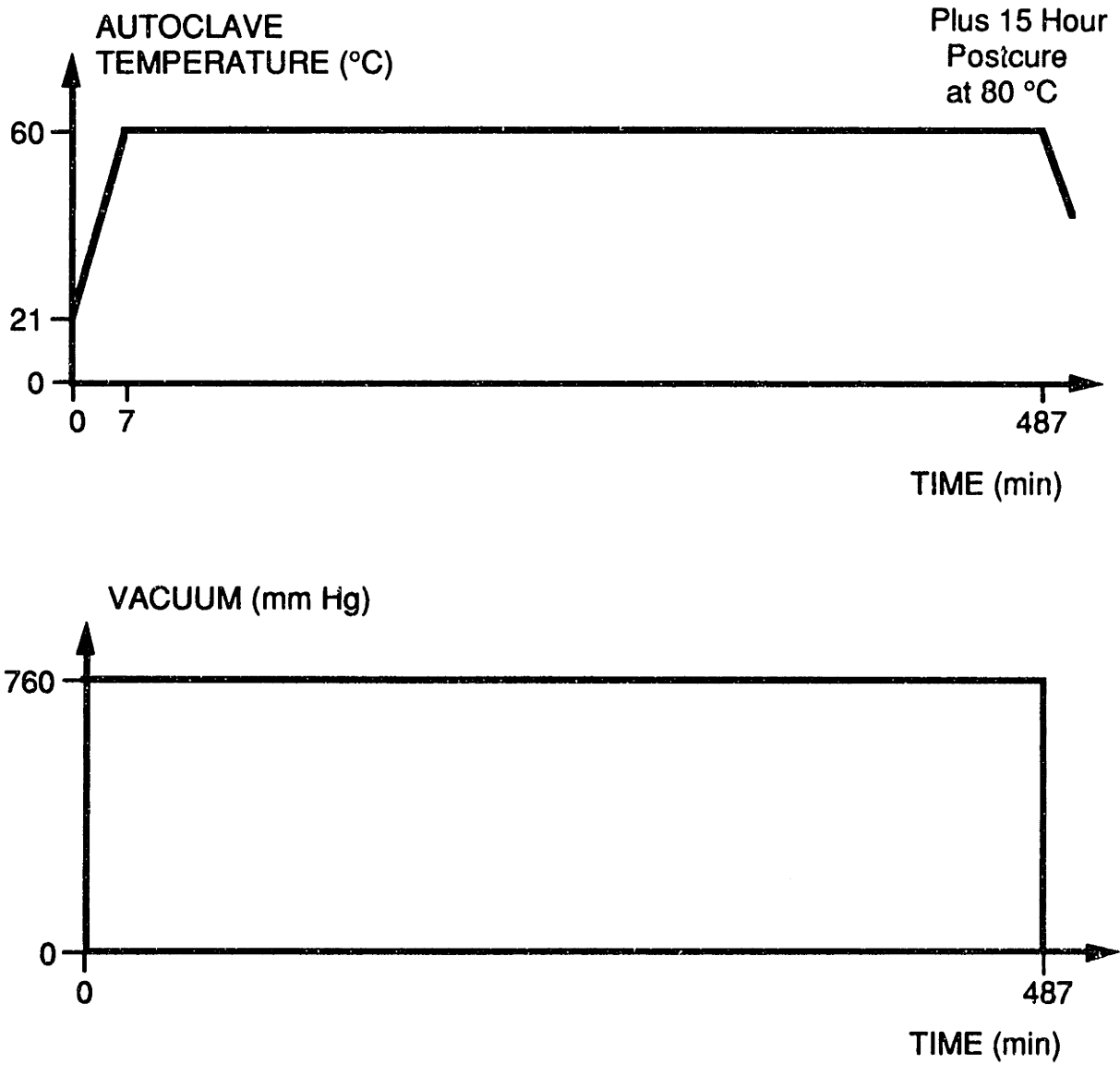


Figure 3.8 Glass/epoxy cure cycle.

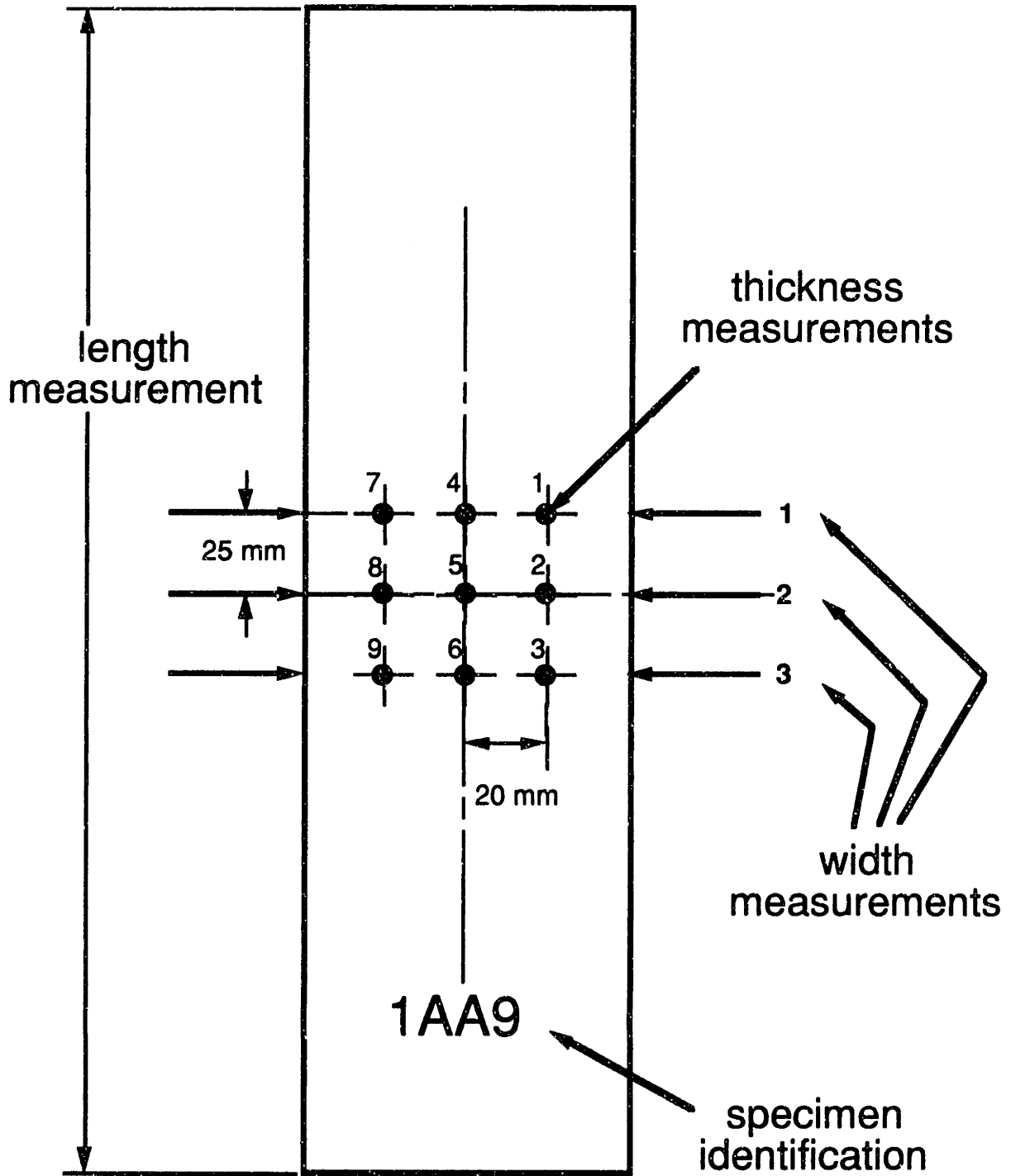


Figure 3.9 Coupon measurement locations.

Table 3.3 Measured and Nominal Ply Thicknesses

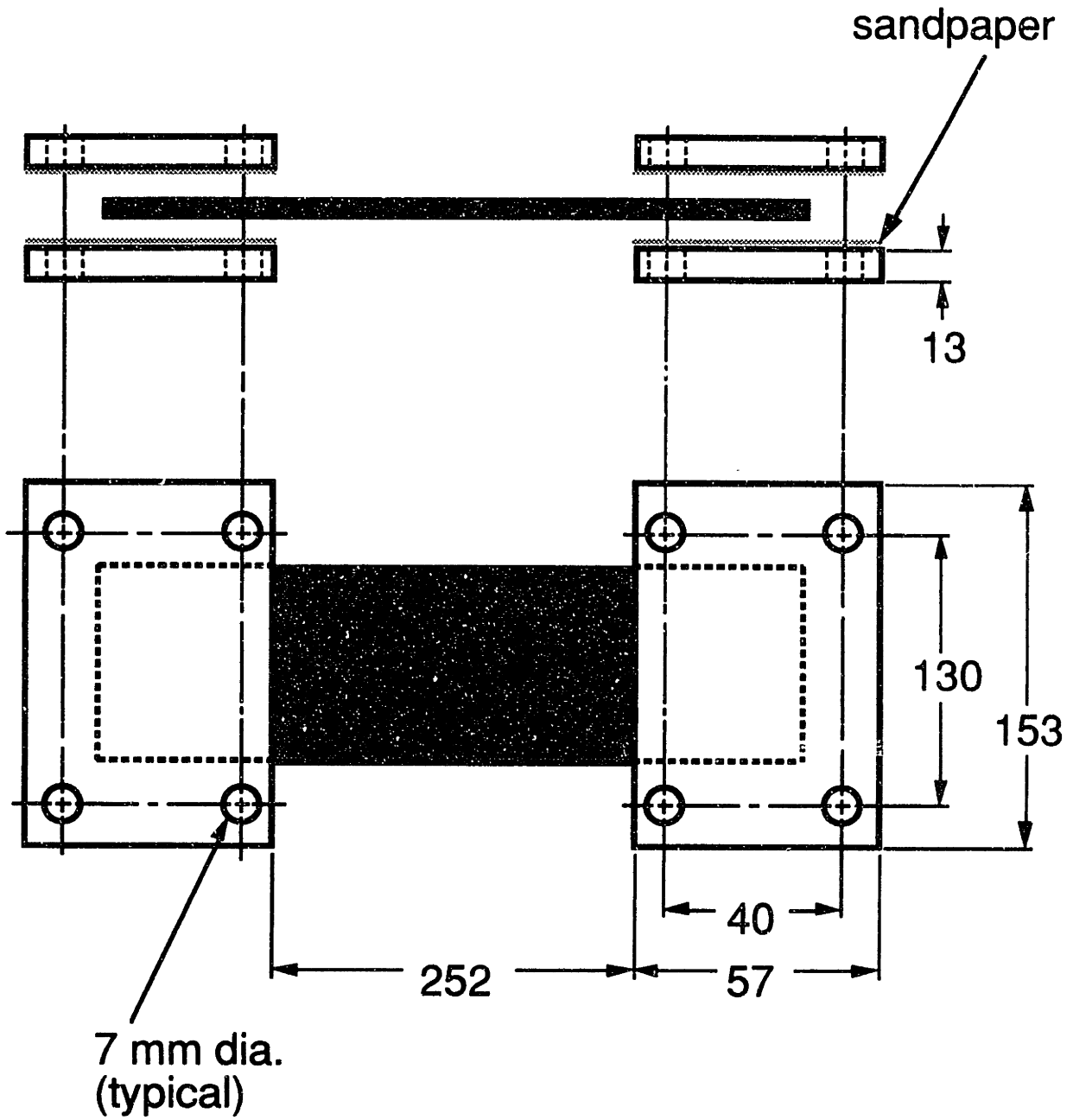
Material System	Nominal Ply Thickness (mm)	Average Measured Per Ply Thickness (mm)
AS4/3501-6	0.134	0.132
IM7G/X8553-50	0.144	0.145
A370-5H/3501-6S	0.350	0.336
Glass/Epoxy	0.260	0.265

3.3 Impact Test Procedures

All specimens were impacted using the Free Rolling Energy Device (FRED) developed at TELAC. These impacts simulate nonballistic events such as tool drops. The test apparatus consists of the specimen holding jig, the striker unit, the impactor unit, and the data acquisition system.

The specimen holding jig shown in Figure 3.10 provides clamped boundary conditions on two sides of the specimen. The specimen is held firmly between the aluminum blocks by 8 bolts, each lubricated with SAE 20 weight oil and torqued to 10 Newton-meters. Sandpaper of 80 grit roughness is glued to the blocks to help prevent slippage of the laminate during impact. All impacts were targeted at the center of the specimen. The specimen holding jig is supported by a drill press stand adopted for this function. This assembly is illustrated in Figure 3.11.

The striker and impactor units of the Free Rolling Energy Device (FRED) are shown in Figure 3.12. The striker unit consists primarily of an electromagnet, a winch and a large spring. The magnet is energized and the winch is used to draw back the striker rod, compressing the spring. Upon release of the magnet, the rod is free from the winch and is propelled toward the impactor unit by the spring. The impactor unit holds the impactor rod via two sets of linear motion bearings, and also houses the light gates and the anti-rebound lever. The anti-rebound lever prevents multiple impacts by restraining the impactor rod after impact. During the initial forward motion of the impactor rod, the plastic doughnut flips the anti-rebound lever into a position to catch the rod after impact. This forward motion triggers the computer to begin taking data.



NOTE: 1. all dimensions in mm.
2. drawing not to scale.

Figure 3.10 Specimen holding jig measurements.

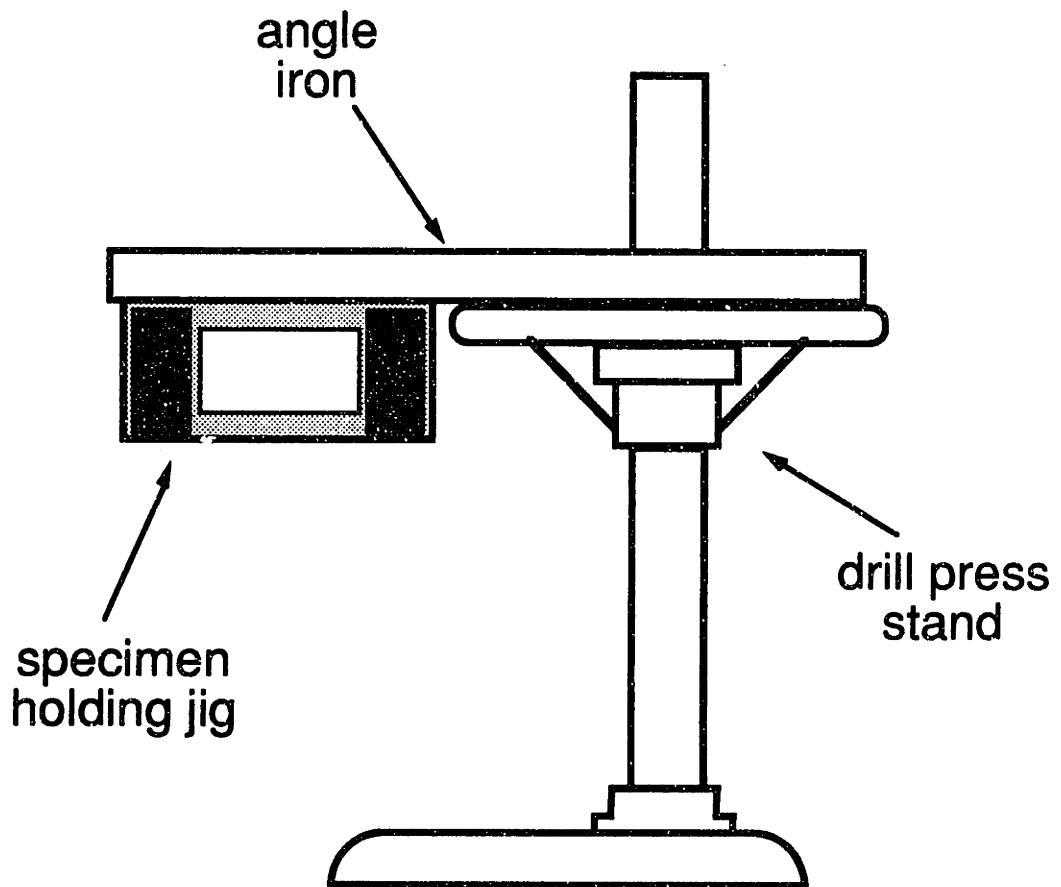


Figure 3.11 Illustration of jig support stand for impact testing.

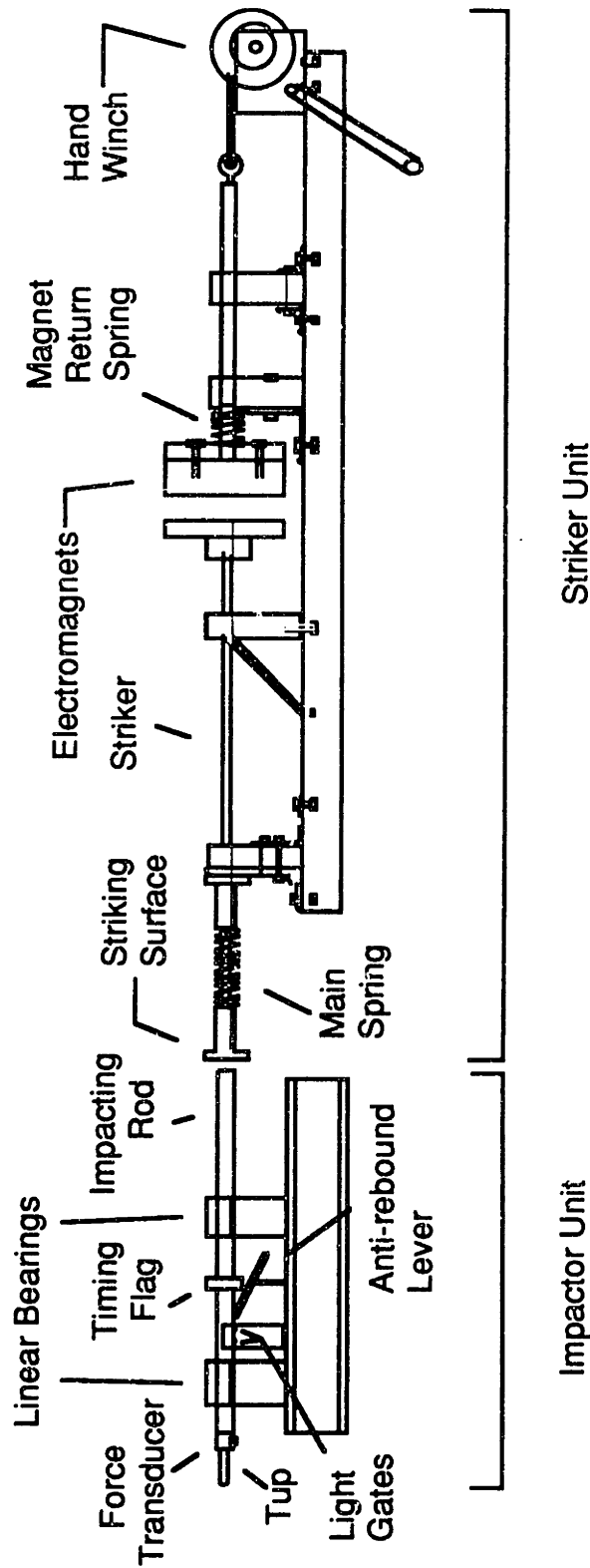


Figure 3.12 Illustration of Free Rolling Energy Device (FRED) for impact.

The light gates are used for impact velocity determination. As the impactor rod approaches the specimen, but before actual contact is made, a plastic "doughnut" on the impactor rod passes through two light beams in sequence. This is shown in Figure 3.13. An electronic timer, in this case a Fluke 1953 A Counter Timer, records the difference in time between the interruption of the first and second beam. The distance between the two beams being known, the impactor rod velocity can be determined.

The force transducer, a PCB Model 208 A05, is mounted behind the tup on the impactor rod. The voltage output of the force transducer is fed into a PCB Signal Conditioner Model 484B. The amplified voltage then goes to a GW Instruments MacADIOS II analog/digital converter connected to a Macintosh IIx computer. Voltages are sampled at 50 kHz and are converted to force units using the conversion factor of 4157 Newtons per volt.

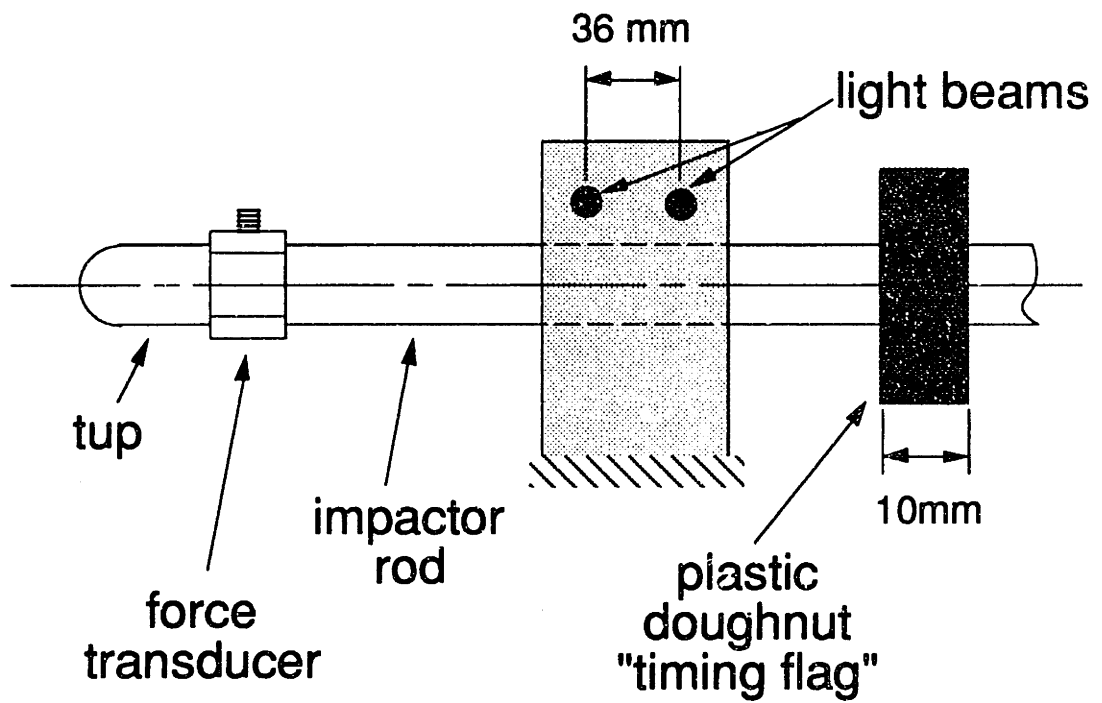
The force experienced by the specimen is calculated using the derivation shown by Ryan [30] and repeated here:

$$F_{tot} = \left(\frac{M_{tup} + M_{ft} + M_{rod}}{M_{rod} + \frac{M_{ft}}{2}} \right) F_{ft} \quad (3.1)$$

where:

- F_{tot} is the total contact force experienced by the specimen,
- F_{ft} is the force exerted on the force transducer,
- M_{tup} is the mass of the tup (47 g),
- M_{ft} is the mass of the force transducer (25 g),
- M_{rod} is the mass of the impactor rod (1458 g),

This conversion is required because the force transducer is not at the point of contact between the specimen and the tup, but is sandwiched between two masses as can be seen in Figure 3.13. The force at the point of contact between



(total impacting mass = 1.53 kg)

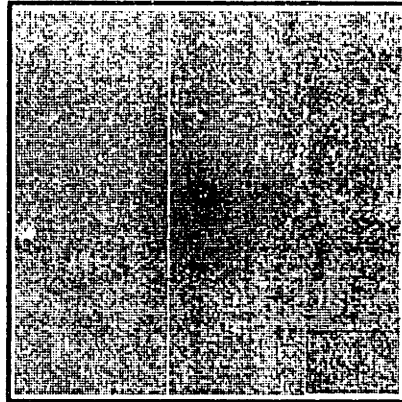
Figure 3.13 Illustration of impactor rod and light gates.

the tup and the specimen is slightly higher than the force experienced by the transducer. In this case, the force applied to the specimen was 1.040 times the force exerted on the force transducer.

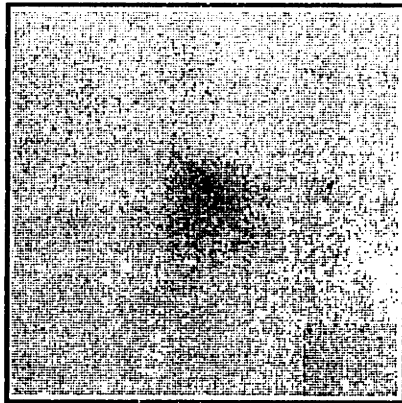
3.4 Damage Evaluation

Three methods were used for damage evaluation: visual inspection, X-ray, and deply. After impact, all graphite/epoxy specimens were X-rayed to determine the damage state. This was performed in the following way. First, a small hole 0.74 mm in diameter was drilled with a Dremel® tool through the specimen at the center of the impact. A piece of blue flash tape was placed over the hole on the back surface (opposite the impact surface) of the laminate. Then the specimen was placed flat on a table with the impacted surface facing upward and 1,4-Diiodobutane (DiB) penetrating dye was injected into the hole with a syringe until a small bubble of dye formed over the hole. The dye seeps into cracks and delaminations and is opaque to X-rays, thus showing up as dark areas in an X-ray photograph. The specimen was then left for 45 minutes to allow the dye to penetrate into the damaged areas, and additional dye was added intermittently to maintain the small bubble of excess dye on the surface. After the 45 minutes, any remaining dye was absorbed with a paper towel and the tape was removed from the back surface. The specimen was then evaluated with a Scanray® Torrex 150D X-ray Inspection System. The specimen was exposed to 240 mR using the "TIMERAD" control and 50 kilovolts potential. An X-ray image of the specimen was obtained on Polaroid Type 52 PolaPan film.

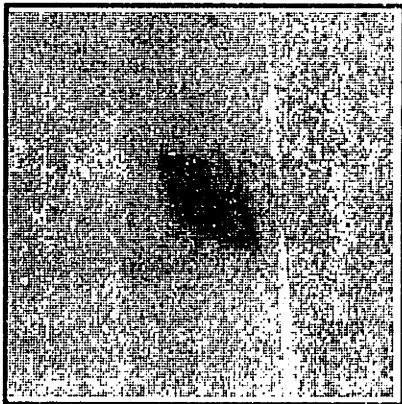
An example of a typical X-ray photograph can be seen in Figure 3.14. The orientation of the specimen in the X-ray is such that the x_1 direction of the



velocity = 2.5 m/s



velocity = 4.0 m/s



velocity = 5.0 m/s



1 cm

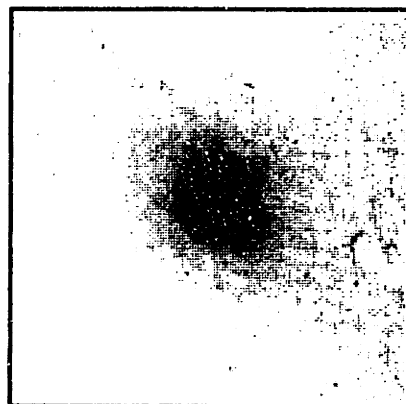
Figure 3.14 Example of typical X-ray photographs.

specimen (see Figure 3.1) is aligned with the vertical axis of the page. Positive ply angles are measured counter-clockwise from vertical.

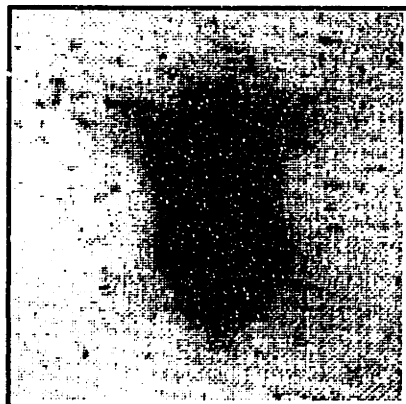
It was found that the dye did not penetrate well into the damage in the glass/epoxy specimens. Thus, these specimens were not X-rayed but were inspected visually for damage. This was possible due to their translucent appearance. Photographs were taken of specimens that exhibited visible damage. The specimens were illuminated from behind with a 100-watt incandescent bulb, and 35 mm black and white film was used to produce the photographs. A sample photograph is shown in Figure 3.15.

The deply evaluation is a destructive examination technique in which the epoxy portion of the composite is "burned off" in an oven, leaving behind only the fibers and traces of an enhancing agent, in this case gold chloride. This method was used successfully with all three graphite/epoxy material systems, but was found to give unsatisfactory results with the glass/epoxy system. The gold chloride did not penetrate into the damage in the glass/epoxy specimens.

The specimens to be evaluated were trimmed into rectangles containing the damaged region, as determined from X-ray, plus approximately 2 cm on either side of the damage. The laminates were trimmed from their original size to reduce the amount of epoxy which needed to be "burned off". Pieces of tape were placed on both the front and back surfaces of the specimen to cover the hole previously drilled for X-ray purposes. This was done to keep dirt and water away from the damage area while milling with the water-cooled diamond grit cutting wheel previously mentioned. The specimens were milled into rectangles typically 80 mm long by their original 89 mm width. The gold chloride, supplied by the Sigma Chemical Company, was suspended in a carrier of isopropyl alcohol. A solution composed of 10 g of gold chloride in 100



velocity = 3.0 m/s



velocity = 5.0 m/s


1 cm

Figure 3.15 Example of typical photographs of glass/epoxy specimens impacted at 3.0 and 5.0 m/s.

ml of isopropyl alcohol was used. Since all specimens had previously been X-rayed, a small hole already existed in the center of the impacted area. As before, tape was placed over the hole on the back surface of the laminate, and a syringe was used to fill the hole with the gold chloride solution and form a bubble of excess on the surface. The solution was allowed 45 minutes to seep into the damaged areas, and the bubble of excess was maintained by periodically adding more gold chloride solution. After the 45 minutes, excess gold chloride was wiped from the surface of the laminate with a paper towel and the tape was removed from the back surface.

The coupon was placed on a stainless steel wire mesh inside a Lindberg Furnace Type 51442. The furnace was preheated to 420°C and a positive pressure of 0.02 MPa of nitrogen was fed into the furnace to avoid the potentially harmful effects of a fire inside the oven. The 12-ply laminates were left in the oven for 15 minutes, the 16-ply laminates required 20 minutes, and the graphite/epoxy fabric specimens required 25 minutes before the plies could be separated. It was discovered that durations longer than these produced a large amount of thermal discoloration of the plies, making detection of the gold chloride very difficult.

Once removed from the oven, the laminates were allowed approximately 5 minutes to cool before the plies of the laminate were separated. It was found that blowing ambient air over the laminate during this cooling period often caused the plies to separate very easily. Starting at the impacted surface, the plies were worked free from each other by gently pulling them apart. Sketches were made by hand of any traces of gold chloride on the ply interfaces. The outlines of the delaminations were very faint, and thus were not easily photographed. It was not possible, nor desired, to separate neighboring plies of the same angle. Adjacent plies of the same orientation become one "effective

ply" of double thickness during the cure, and it was assumed that delamination would not occur between them, as the results did show.

A typical deply transcription is shown in Figure 3.16. The interfaces for each laminate are defined by the layup diagram. Only interfaces where the ply angle changes are numbered, and interface 1 is closest to the impact surface. The small circle seen at the center of each interface represents the hole drilled through the laminate at the center of the impact site, as previously mentioned. The deply technique provided information on delamination and fiber breakage. Delaminations are depicted as shaded areas, and regions of fiber fracture are shown as heavy lines. The regions of fiber fracture generally ran transversely to the fiber direction of the ply. All interfaces are shown as viewed from the impacted side of the laminate, with the x_1 direction of the specimen aligned with the vertical axis of the page. Positive ply angles are measured counter-clockwise from vertical. In several cases, fiber damage in the top ply became visible once the top ply was separated from the rest of the laminate. For such cases, an illustration of the top ply is included in the transcription.

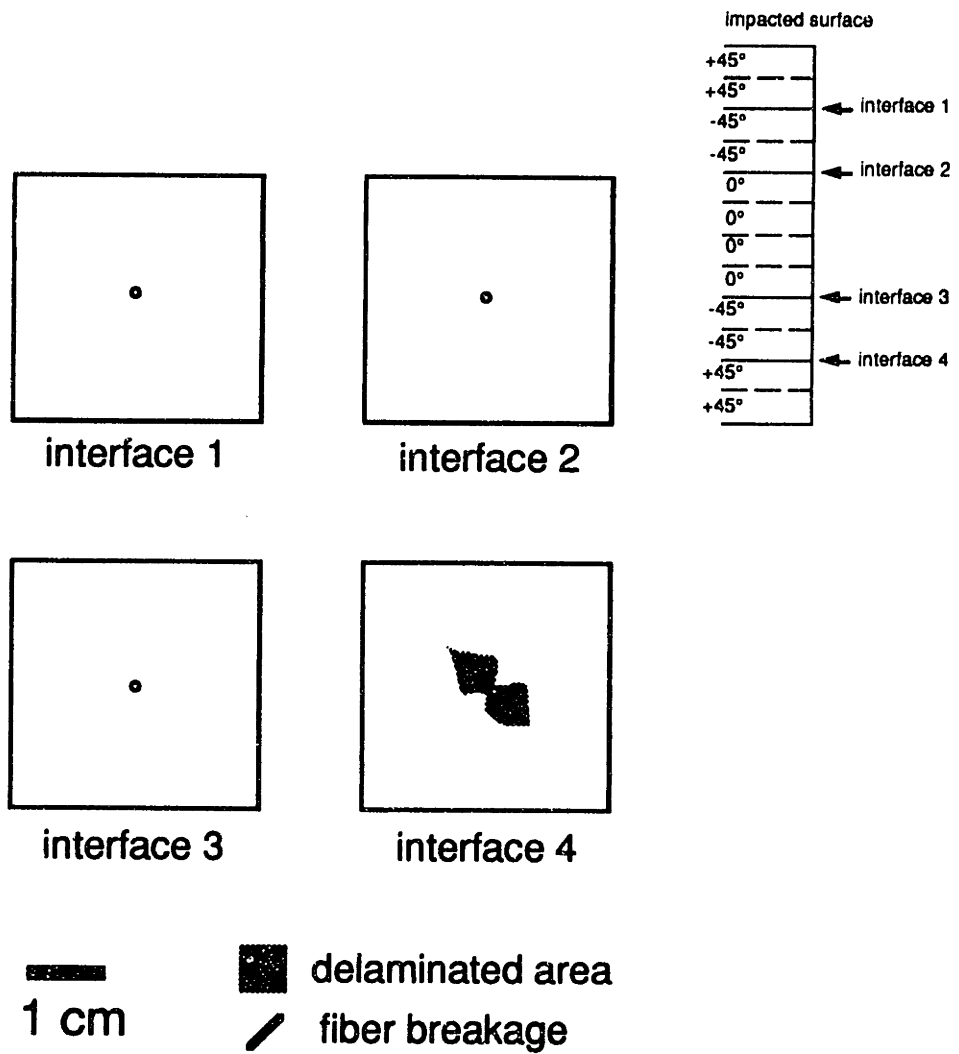


Figure 3.16 Example of typical delamination of impacted graphite/epoxy specimen.

Chapter 4

EXPERIMENTAL RESULTS

4.1 Overview

The experimental results include contact force data taken during the impact event, and X-ray photographs, deply transcriptions and photographs made of the specimens after impact in order to determine the damage state. The force-time data are first presented for all four material systems used in this study. Within each material system, the data are presented by layup. The force history, or signature, of each layup is presented for several different impact velocities, including one velocity which did not cause damage to occur. Next, the data on damage characteristics are presented. Again, the data are presented by material system, and by layup within each material system.

4.2 Force-Time Data

Several representative force-time signatures are presented for each type of laminate used in this investigation. Typically, three force-time histories are shown for each laminate: one in which no damage occurred, one in which moderate damage occurred (generally 3.0 m/s), and one in which heavier damage occurred (generally 5.0 m/s). All of the force-time histories obtained in this investigation can be found in Appendix A.

4.2.1 AS4/3501-6 Material System

Three force-time signatures are shown for each layup of AS4/3501-6 used in this investigation. One signature is from an impact that did not cause damage to the specimen. This is the highest impact velocity used in which

damage did not occur. The other two signatures are those of 3.0 and 5.0 m/s impacts. Generally, moderate damage was caused in the specimens from the 3.0 m/s impact, and heavier damage occurred from the 5.0 m/s impacts.

Signatures for the 12-ply layups of the AS4/3501-6 material system can be seen in Figures 4.1 through 4.4. All of these 12-ply specimens were penetrated by 5.0 m/s impacts. Other than these penetrated specimens, no specimens exhibited visible damage from any of the impacts. The force histories (or signatures) for the $[\pm 15_2/0_2]_s$ of AS4/3501-6 layup are presented in Figure 4.1. The 1.0 m/s impact did not damage the specimen, the 3.0 m/s impact caused matrix cracking and delamination, and the 5.0 m/s impact penetrated the specimen. The overall shape of each force history is approximately half of a sine wave, with oscillations of higher frequency superimposed upon it. For the 1.0 m/s impact, the primary wave reaches a peak (approximately 400 N) at about 8 ms, and the peaks of the secondary oscillations occur approximately 1.5 ms apart. The secondary peaks are again 1.5 ms apart in the 3.0 m/s impact, but the primary wave reaches its peak (of approximately 1400 N) sooner at 5.5 ms. In the 5.0 m/s impact, the peaks of the secondary oscillations again occur every 1.5 ms, but the time-to-peak of the primary wave is obscured by the introduction of further higher frequency oscillations approximately 4 ms into the impact. This higher frequency oscillation is visible in the signature as the force reaches a peak of approximately 2400 N and then drops significantly at about 5.5 ms, presumably as the impactor rod penetrates the specimen.

Signatures for the $[\pm 45_2/0_2]_s$ layup of AS4/3501-6 are presented in Figure 4.2. The 1.0 m/s impact did not damage the specimen, the 3.0 m/s impact caused matrix cracking and delamination, and the 5.0 m/s impact penetrated the specimen. The point of penetration is clearly indicated in the 5.0 m/s impact as a large drop in the contact force after 5.5 ms. Higher frequency

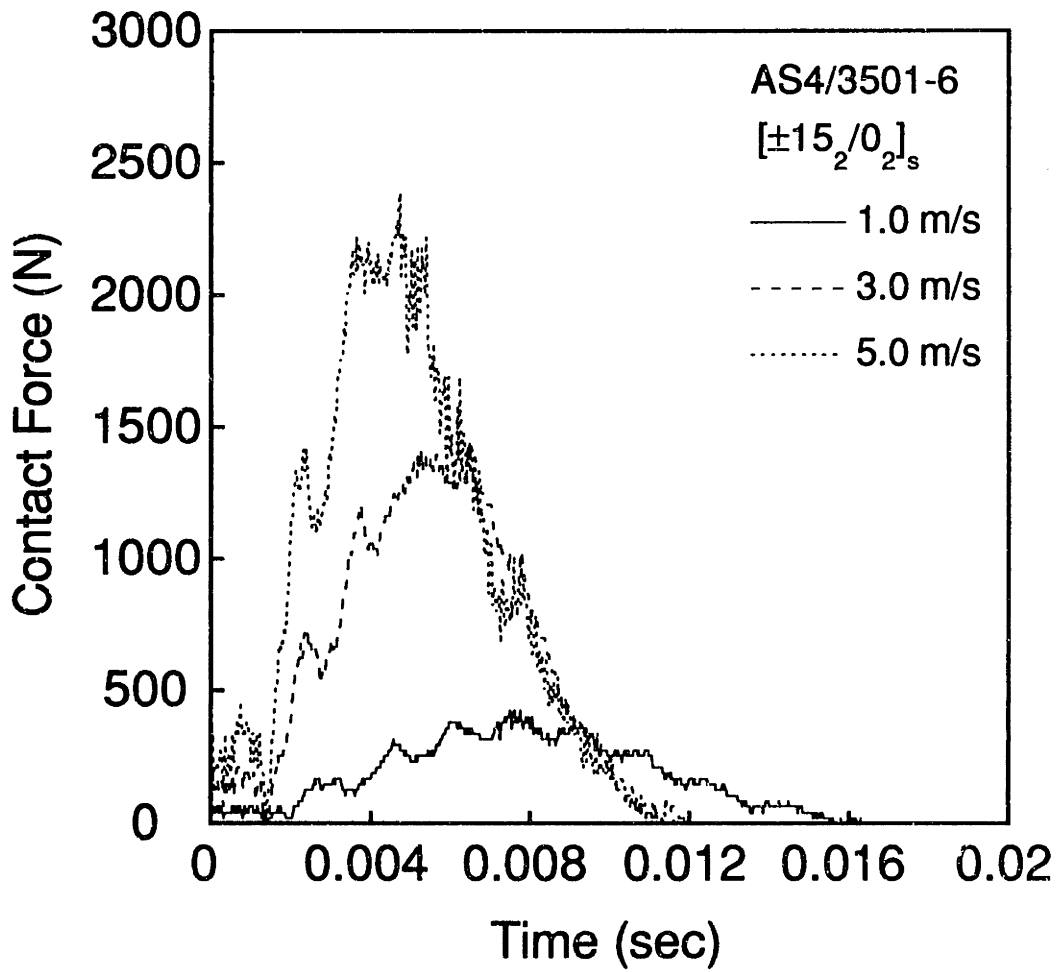


Figure 4.1 Force-time signatures of AS4/3501-6 $[\pm 15_2/0_2]_s$ laminate impacted at 1.0 m/s (undamaged) , 3.0 m/s, and 5.0 m/s (penetrated).

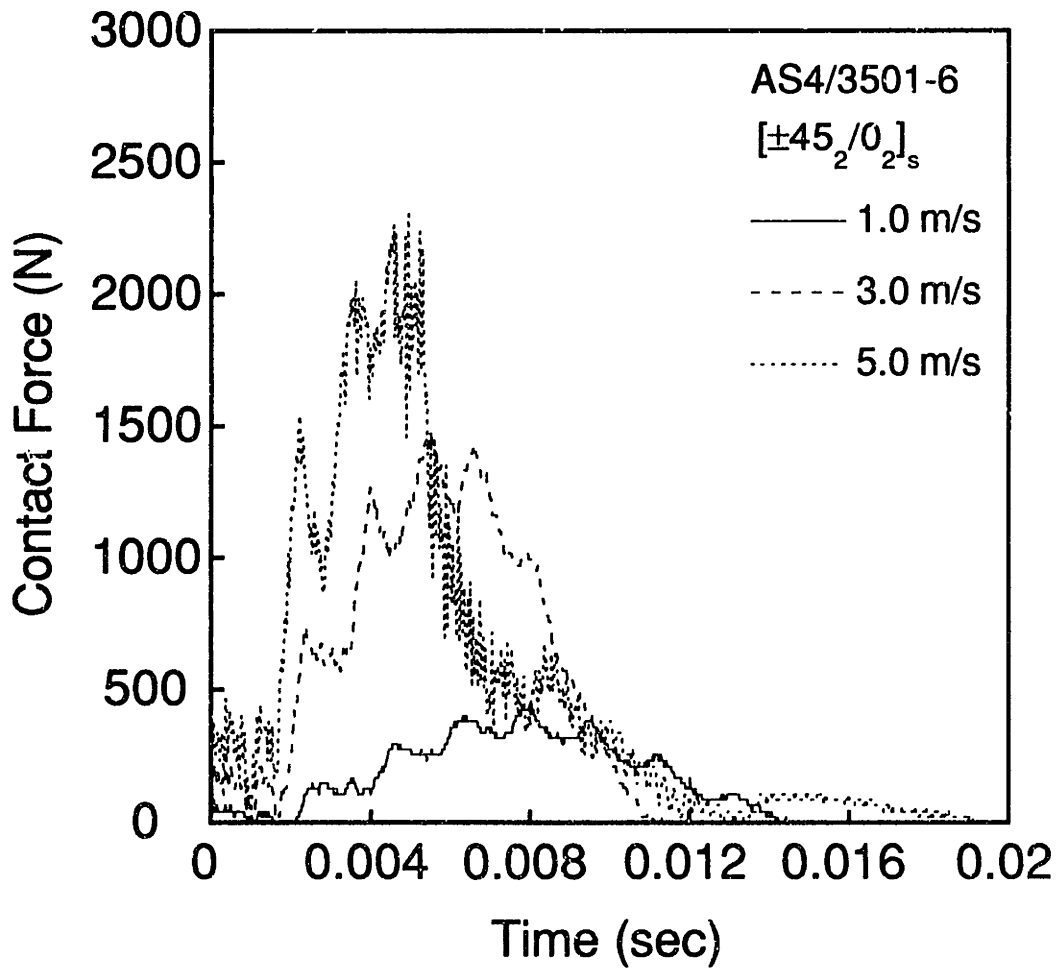


Figure 4.2 Force-time signatures of AS4/3501-6 [$\pm 45_2/0_2$]_s laminate impacted at 1.0 m/s (undamaged), 3.0 m/s, and 5.0 m/s (penetrated).

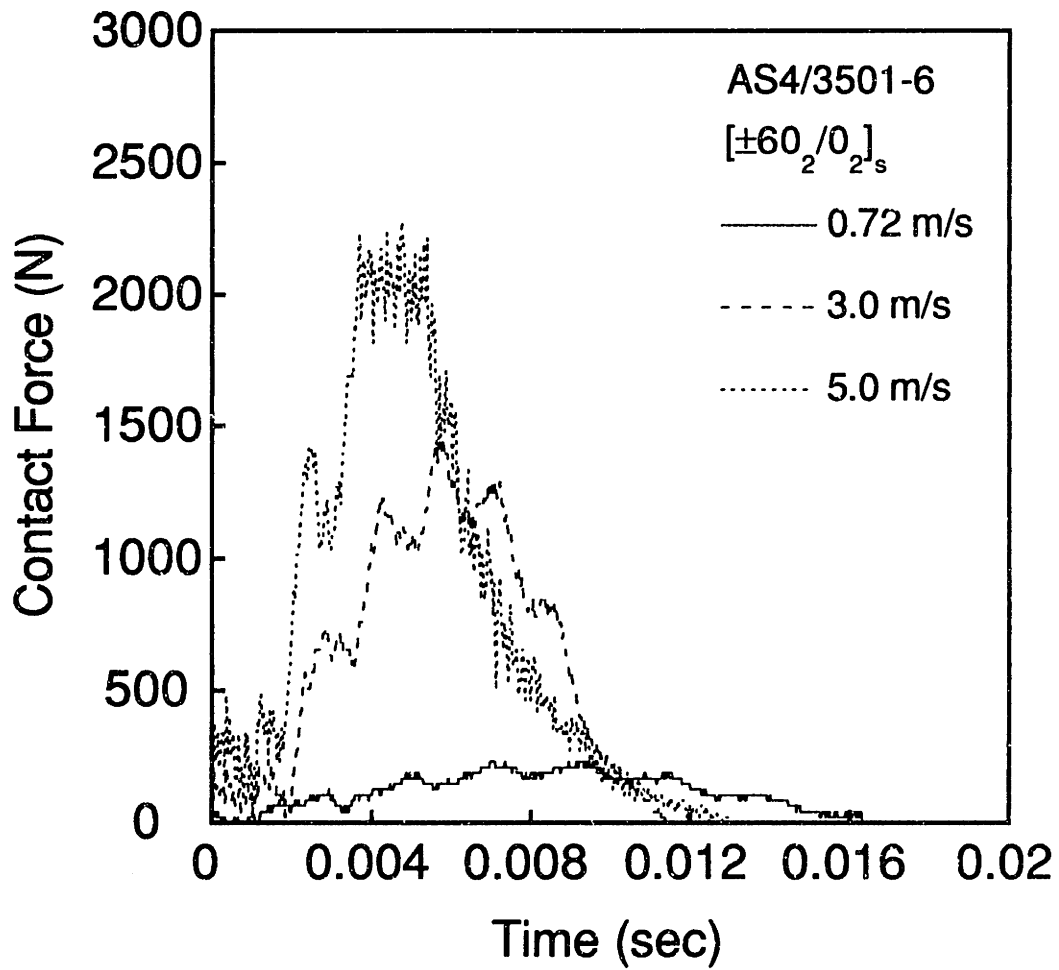


Figure 4.3 Force-time signatures of AS4/3501-6 $[\pm 60_2/0_2]_s$ laminate impacted at 0.72 m/s (undamaged), 3.0 m/s, and 5.0 m/s (penetrated).

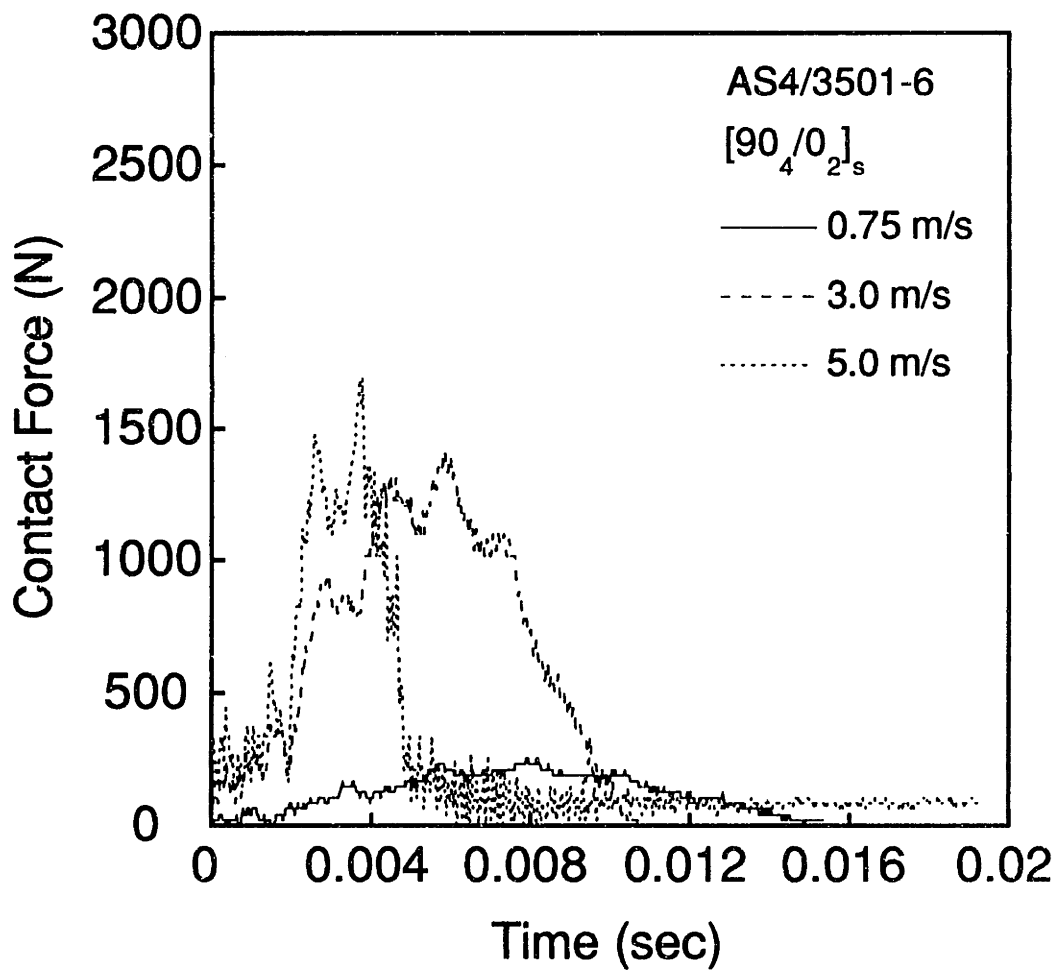


Figure 4.4 Force-time signatures of AS4/3501-6 $[90_4/0_2]_s$ laminate impacted at 0.75 m/s (undamaged), 3.0 m/s, and 5.0 m/s (penetrated).

oscillations can be seen in the vicinity of penetration, and the specimen sustained a peak force of approximately 2300 N before the impactor penetrated it. The primary wave in the 1.0 m/s impact reaches a peak of approximately 400 N at about 8 ms, as with the previous layup. Although the 3.0 m/s impact caused damage to the specimen, there is no distinguishable drop in the contact force which can be attributed to the damage. The signature of the 3.0 m/s impact reaches a peak of approximately 1500 N at about 5.5 ms. The peaks of the secondary oscillation occur approximately 1.5 ms apart, as was also observed with the $[\pm 15_2/0_2]_s$ layup.

Signatures for the $[\pm 60_2/0_2]_s$ layup of AS4/3501-6 are presented in Figure 4.3. The 0.72 m/s impact did not damage the specimen, the 3.0 m/s impact caused matrix cracking and delamination, and the 5.0 m/s impact penetrated the specimen. It can be seen that penetration in the 5.0 m/s impact was accompanied by a high frequency oscillation and large drop in the contact force after 5.5 ms. The specimen sustained a peak force of approximately 2250 N before the impactor penetrated it. The peak force of the 3.0 m/s impact is approximately 1400 N and the duration is about 11 ms. The secondary peaks occur approximately 1.5 ms apart, as was observed for the previous two layups. The peak and duration of the primary wave is nearly the same as that of the previous layup.

Signatures for the $[90_4/0_2]_s$ layup of AS4/3501-6 are presented in Figure 4.4. The 0.75 m/s impact did not cause damage to the specimen, the 3.0 m/s impact caused matrix cracking and delamination, and the 5.0 m/s impact penetrated the specimen. In terms of peak force before penetration, this layup was the most easily penetrated of the 12-ply layups of this material system. It can be seen that after reaching a peak force (at about 4 ms) of approximately 1700 N, the contact force falls dramatically and a higher frequency oscillation

occurs in the signature. The primary wave in the 3.0 m/s impact has nearly the same peak (1500 N) and duration (11 ms) as the previous layup. However, slight differences in the secondary oscillations can be observed.

Signatures of the two 16-ply quasi-isotropic layups of AS4/3501-6 are presented in Figures 4.5 and 4.6. Signatures can be seen for impact velocities of 2.0, 3.0 and 5.0 m/s for the $[\pm 45_2/0_2/90_2]_s$ layup in Figure 4.5. No damage resulted from the 2.0 m/s impact, while the 3.0 and 5.0 m/s impacts both created internal damage to the specimens. In the 5.0 m/s impact, this laminate was able to sustain a contact force of approximately 2600 N without any visible surface damage. Secondary oscillations are visible in the 5.0 m/s signature before the peak force is reached (at approximately 5 ms). After the peak force, higher frequency oscillations are observed, and the amplitudes of the secondary oscillations are smaller. Like the signatures of the 12-ply laminates, the shape of the signatures of the 16-ply laminates is a half sine wave with oscillations of higher frequency superimposed on it. From the 3.0 m/s impact, it can be seen that the peak force and duration are not significantly different from those of the 12-ply laminates.

Signatures for impact velocities of 2.8, 3.0 and 5.0 m/s impacts for the $[(\pm 45)_2/(0/90)_2]_s$ layup of AS4/3501-6 are presented in Figure 4.6. These signatures have more high frequency oscillations than was observed with the $[\pm 45_2/0_2/90_2]_s$ layup. No damage resulted from the 2.8 m/s impact, while the 3.0 and 5.0 m/s impacts created internal damage to the specimens. In the 5.0 m/s impact, this layup withstood a force of approximately 2700 N without visible surface damage. After the peak force (at approximately 5 ms), the secondary oscillation can no longer be seen, as was the case with the previous layup. The amplitudes of the secondary oscillations were greater with this

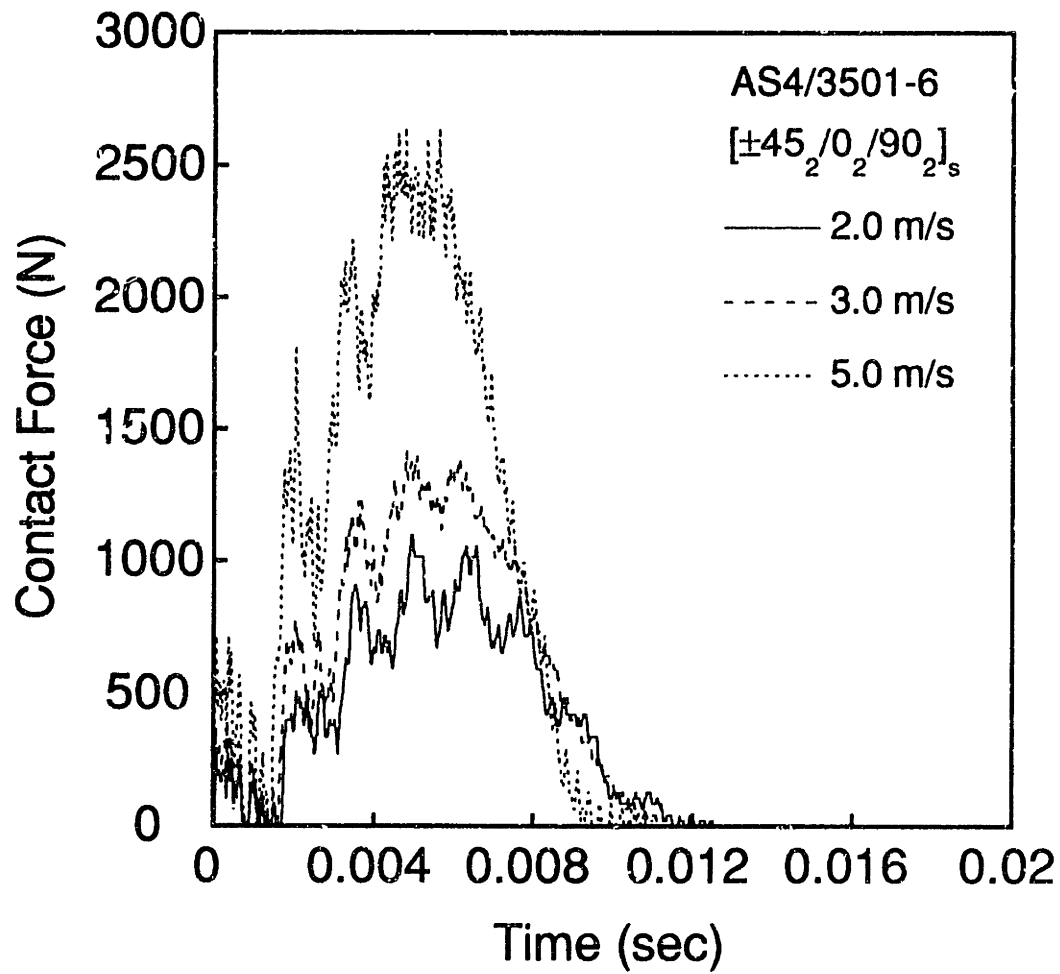


Figure 4.5 Force-time signatures of AS4/3501-6 $[\pm 45_2/0_2/90_2]_s$ laminate impacted at 2.0 m/s (undamaged), 3.0 m/s, and 5.0 m/s.

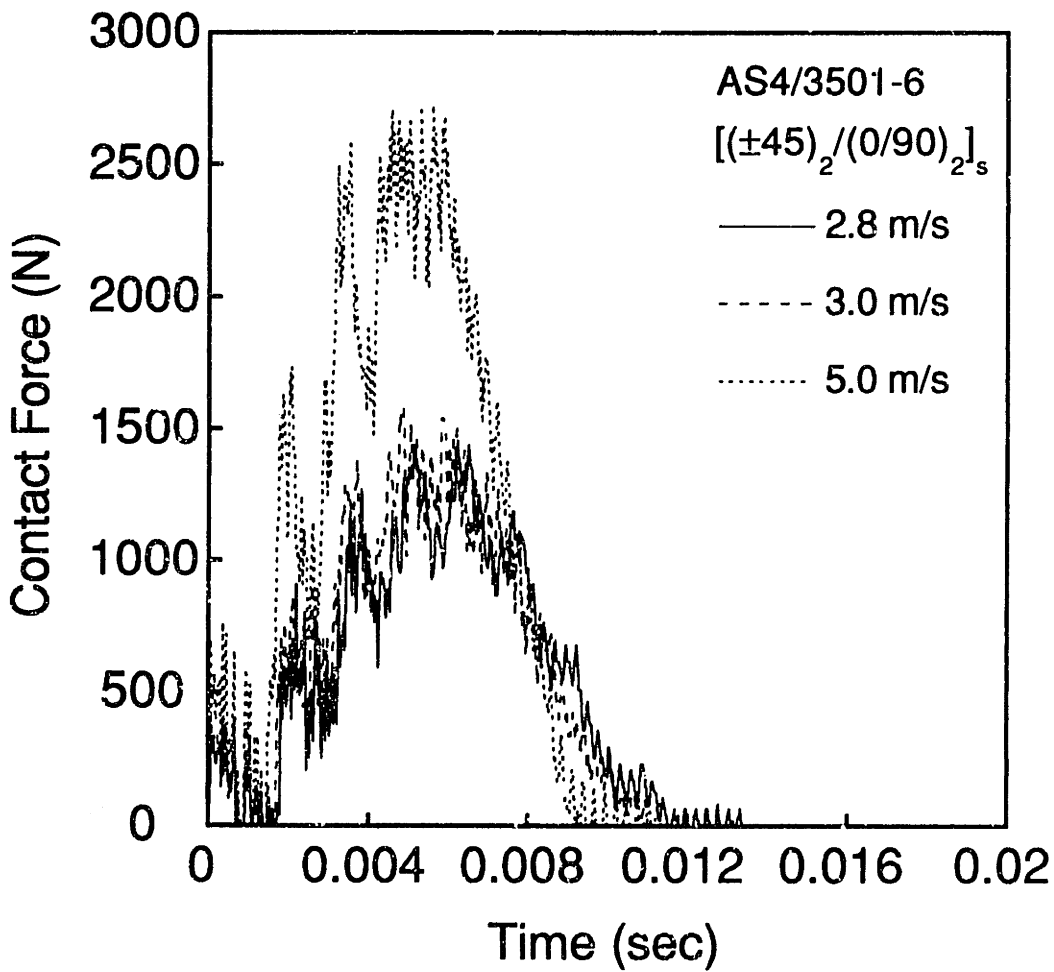


Figure 4.6 Force-time signatures of AS4/3501-6 $[(\pm 45)_2 / (0/90)_2]_s$ laminate impacted at 2.8 m/s (undamaged), 3.0 m/s, 5.0 m/s.

layup than with the $[\pm 45_2/0_2/90_2]_s$ layup, as can be seen clearly from the 3.0 m/s signatures.

4.2.2 IM7G/X8553-50 Material System

The force-time data for layups of the IM7G/X8553-50 material system are shown in Figures 4.7 through 4.10. It is noteworthy that none of the impacted specimens of the IM7G/X8553-50 material system exhibited visible damage.

Signatures for impact velocities of 1.0, 3.0, and 5.0 m/s for the $[\pm 15_2/0_2]_s$ layup of IM7G/X8553-50 are presented in Figure 4.7. The 1.0 m/s impact did not cause damage to the specimen, while the 3.0 and 5.0 m/s impacts caused internal damage. As was the case with the AS4/3501-6 laminates, the shape of these signatures is half of a sine wave with oscillations of higher frequency superimposed on it. As was the case with the AS4/3501-6 laminates, it is observed here that a higher impact velocity causes an impact of shorter duration. The duration of the 1.0 m/s impact is greater than 16 ms, while the duration of the 3.0 m/s impact is about 12 ms and that of the 5.0 m/s impact is less than 10 ms. The peak force of the 5.0 m/s impact is approximately 2550 N, as compared to 2400 N with the same layup of AS4/3501-6, in which penetration occurred. In the 5.0 m/s signature, secondary oscillations can be seen before the peak force is reached (approximately 4.5 ms), but the force falls sharply after 6 ms and the secondary oscillations do not appear on this "downward" side of the signature. This specimen was not penetrated in this impact. A similar behavior can be seen in the 3.0 m/s signature. The secondary peaks are more pronounced on the "upward" side of the signature than on the "downward" side. The signature of the 3.0 m/s impact of this laminate is nearly identical to that of the same layup of AS4/3501-6.

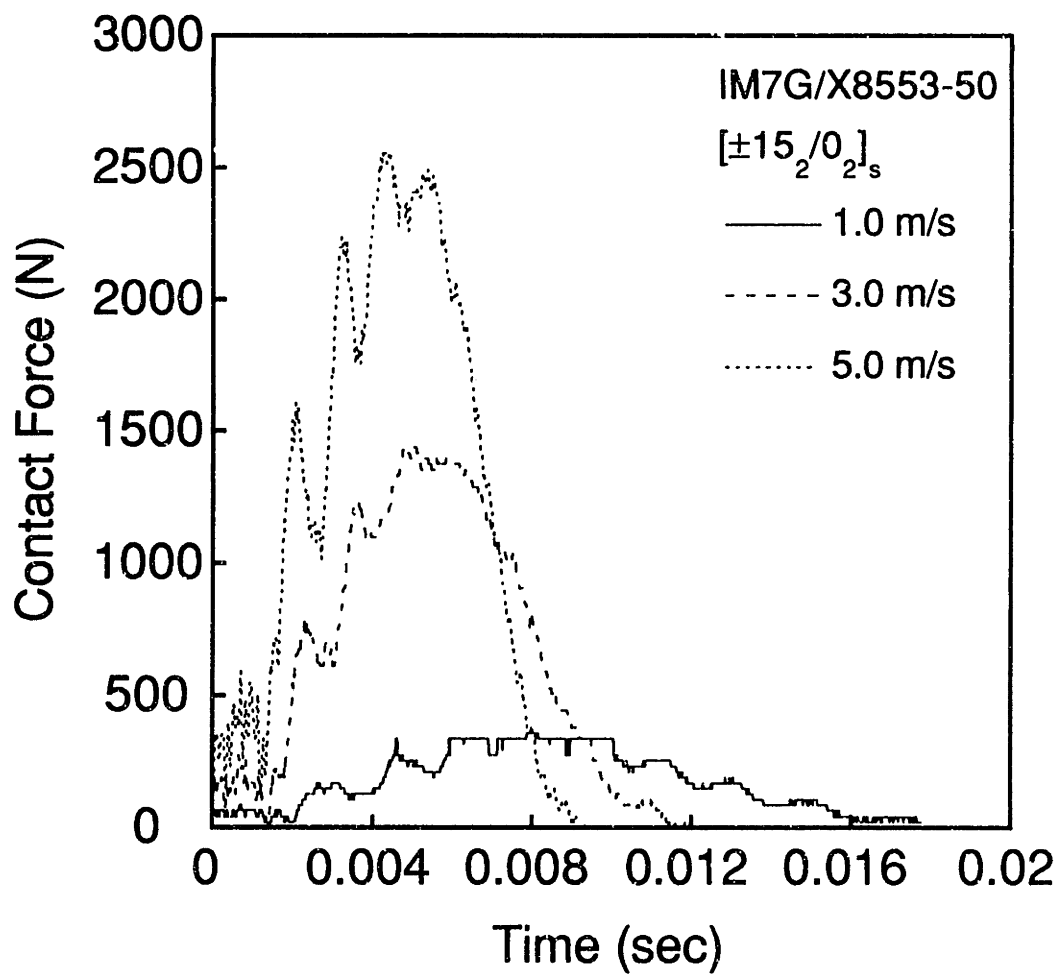


Figure 4.7 Force-time signatures of IM7G/X8553-50 $[\pm 15_2/0_2]_s$ laminate impacted at 1.0 m/s (undamaged), 3.0 m/s, and 5.0 m/s.

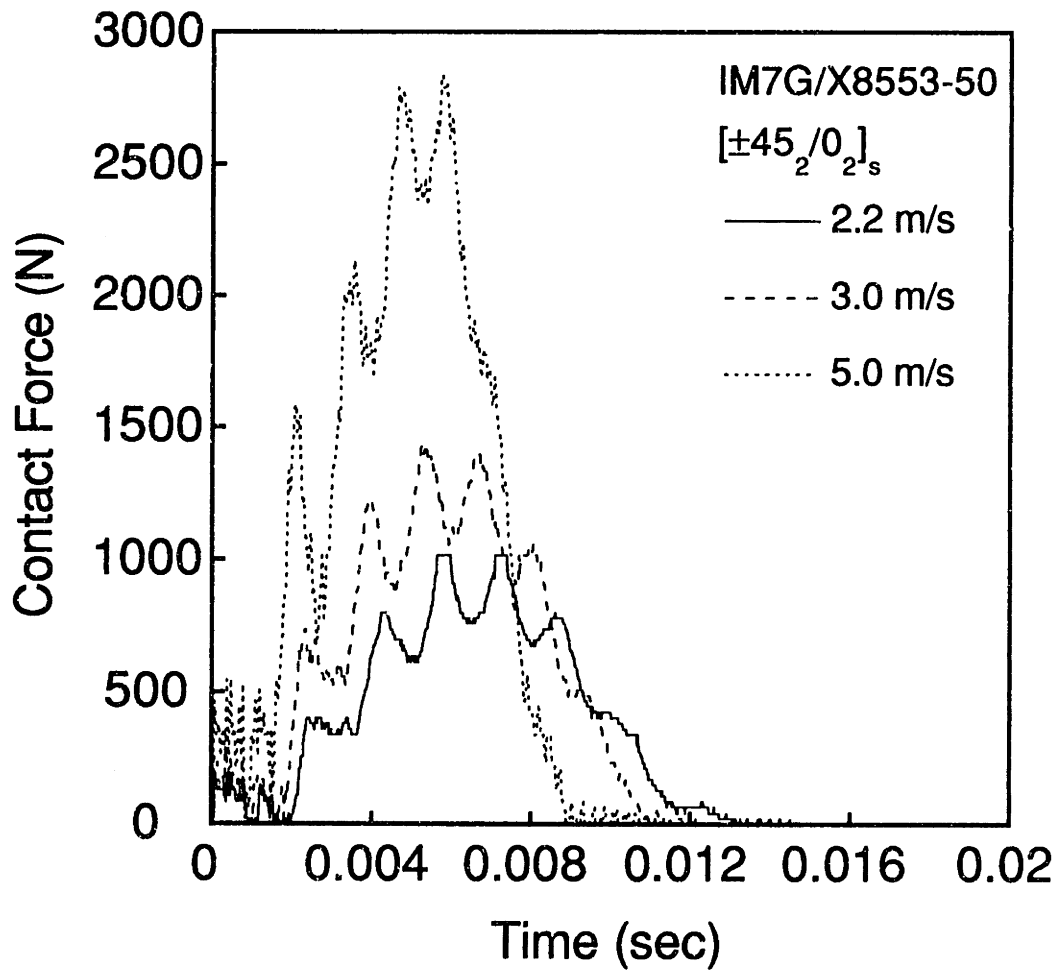


Figure 4.8 Force-time signatures of IM7G/X8553-50 $[\pm 45_2/0_2]_s$ laminate impacted at 2.2 m/s (undamaged), 3.0 m/s, and 5.0 m/s.

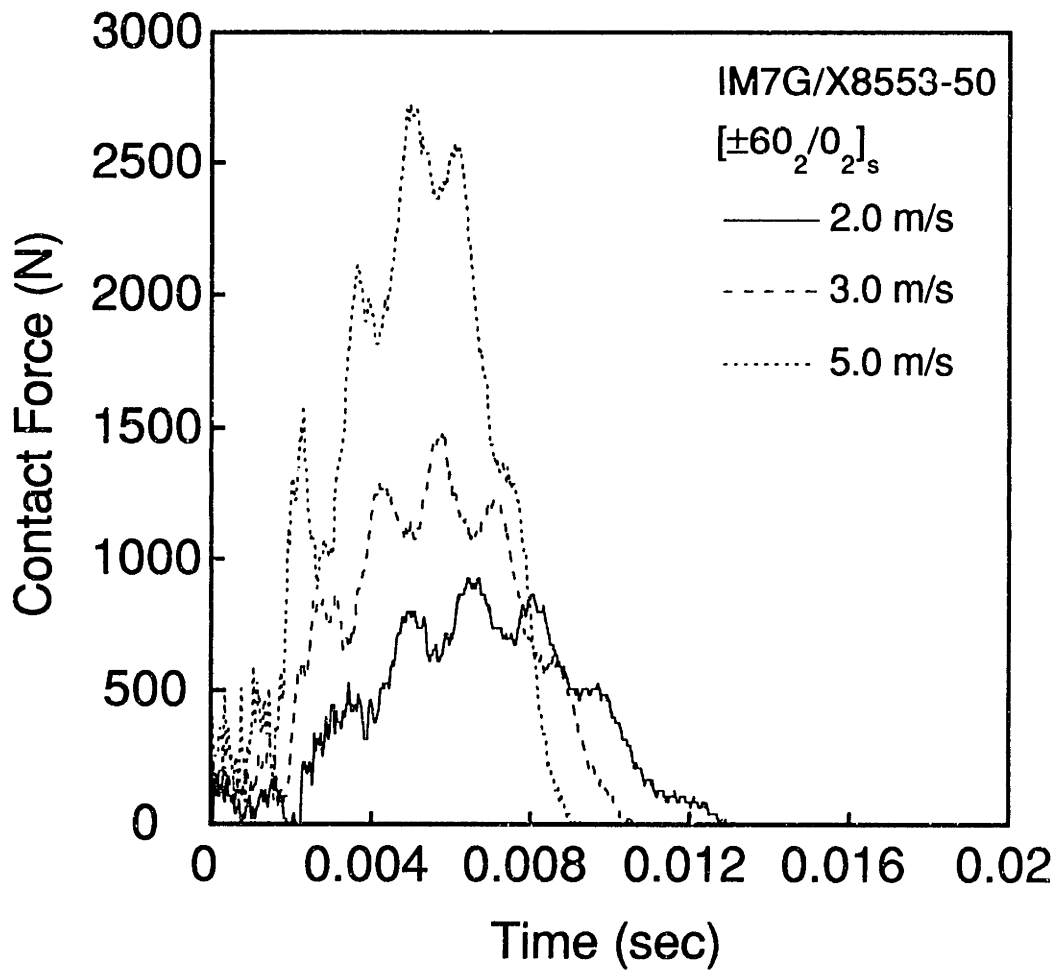


Figure 4.9 Force-time signatures of IM7G/X8553-50 $[\pm 60_2/0_2]_s$ laminate impacted at 2.0 m/s (undamaged), 3.0 m/s, and 5.0 m/s.

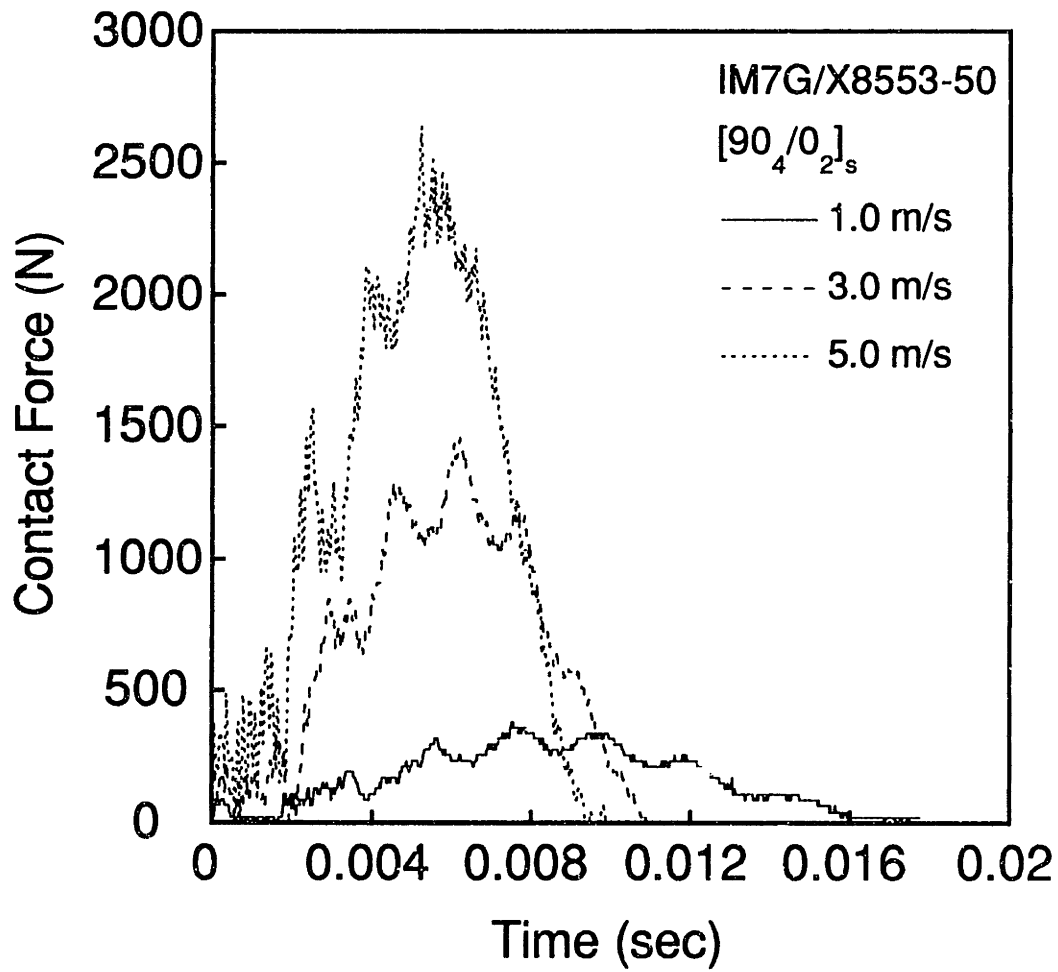


Figure 4.10 Force-time signatures of IM7G/X8553-50 $[90_4/0_2]_s$ laminate impacted at 1.0 m/s (undamaged), 3.0 m/s, and 5.0 m/s.

Signatures for the $[\pm 45_2/0_2]_s$ layup impacted at 2.2, 3.0 and 5.0 m/s are presented in Figure 4.8. The 2.2 m/s impact caused no damage to the specimen, while the 3.0 and 5.0 m/s impacts caused internal damage. As with the previous layups, a shorter impact duration is observed here for a higher impact velocity. The peak force of the 5.0 m/s impact is approximately 2800 N and occurs after 6 ms. The 5.0 m/s impact on the same layup of AS4/3501-6 attained a peak force of only 2250 N, which caused penetration of the specimen. As noted in the 5.0 m/s signature of the $[\pm 15_2/0_2]_s$ layup of IM7G/X8553-50, the force falls sharply on the "downward" side of the signature with little evidence of a secondary oscillation, and this is not due to penetration. The 3.0 m/s signature of this laminate is nearly identical to that of the same layup of AS4/3501-6.

Signatures for the $[\pm 60_2/0_2]_s$ layup of IM7G/X8553-50 impacted at 2.0, 3.0, and 5.0 m/s are presented in Figure 4.9. The 2.0 m/s impact caused no damage, while the 3.0 and 5.0 m/s impacts caused internal damage only. As before, the secondary oscillations are more pronounced on the "upward" side of the 5.0 m/s signature than on the "downward" side. The peak force in this impact is approximately 2700 N, as compared to 2250 N at which the same layup of AS4/3501-6 was penetrated. In the 3.0 m/s signature, the peak force and the spacing of the secondary peaks are virtually identical to those of the same layup of AS4/3501-6. However, there are differences between these two signatures. There is a difference in the height of the last secondary peak on the "downward" side of the signature. This small peak on the signature of the AS4/3501-6 laminate is 200 N higher than its counterpart in the IM7G/X8553-50 signature, and the duration of the impact is about 1 ms longer for the AS4/3501-6 laminate (11.5 ms) than it is for the IM7G/X8553-50 laminate (10.5 ms).

Signatures for the $[90_4/C_2]_s$ layup of IM7G/X8553-50 impacted at 1.0, 3.0 and 5.0 m/s are presented in Figure 4.10. The 1.0 m/s impact did not cause damage to the specimen, while the 3.0 and 5.0 m/s impacts caused internal damage. Secondary oscillations are again more apparent on the "upward" side of the 5.0 m/s signature than on the "downward" side. A peak force of 2600 N is reached after approximately 5.0 ms, as compared to 1700 N at which the same layup of AS4/3501-6 was penetrated. The 3.0 m/s signature has nearly the same peak force and duration as the 3.0 m/s signature of the AS4/3501-6 $[90_4/0_2]_s$ laminate.

4.2.3 A370-5H/3501-6S Material System

Signatures of the fabric graphite/epoxy system impacted at 4.0 and 5.0 m/s are presented in Figures 4.11 and 4.12, respectively. The 4.0 m/s impact did not cause damage to the specimen, while the 5.0 m/s impact caused internal damage. The presence of high frequency oscillations is obvious in these signatures. Also, it can be seen that the amplitudes of the superimposed waves are higher on the "upward" side of the signatures than on the "downward" side. In the 5.0 m/s signature, the location of the secondary peaks is nearly the same as with the 16-ply tape laminates. The duration of the impact is the same (9 ms) but the peak force is higher with the fabric laminate (approximately 3000 N) than with the tape simulations (approximately 2700 N). It is clear that the secondary oscillations are much more pronounced on the "upward" side than on the "downward" side of the signatures for these laminates, but oscillations of higher frequency can be seen on the "downward" side. On the "upward" side, the amplitudes of the secondary oscillations are greater for the fabric laminate.

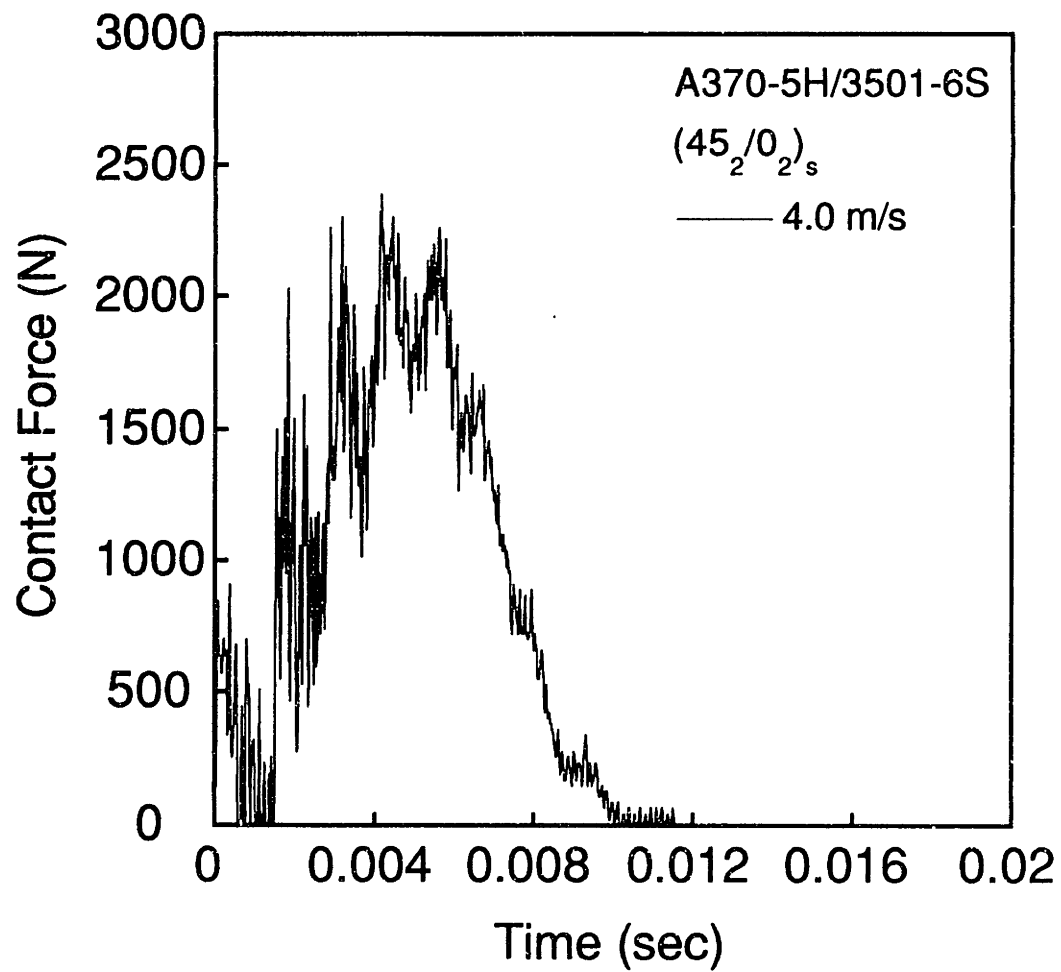


Figure 4.11 Force-time signature of A370-5H/3501-6S $(45_2/0_2)_s$ laminate impacted at 4.0 m/s (undamaged).

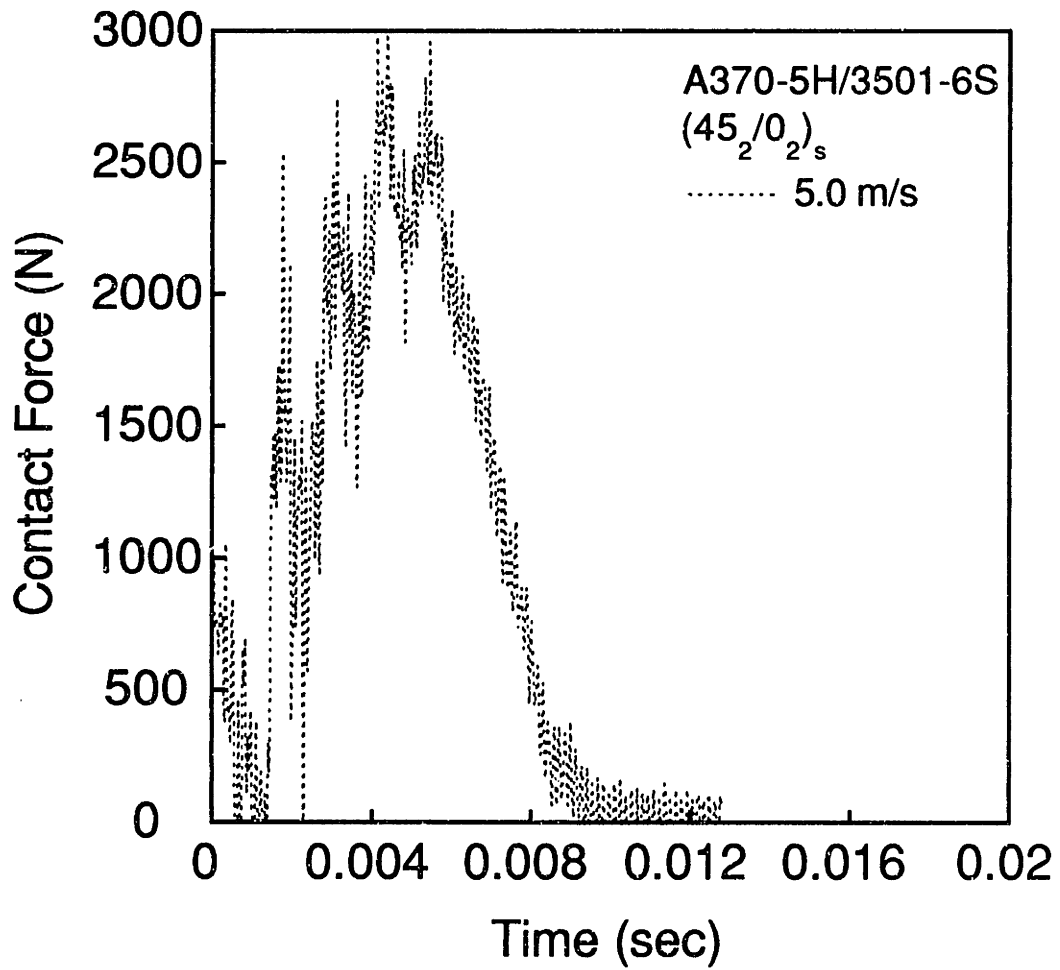


Figure 4.12 Force-time signature of A370-5H/3501-6S (45₂/0₂)_s laminate impacted at 5.0 m/s.

4.2.4 Glass/Epoxy Material System

The signatures for the various layups of glass/epoxy are presented in Figures 4.13 through 4.17. Signatures for the $(45_2/0_2)_s$ layup impacted at 1.2, 3.0, and 5.0 m/s are presented in Figure 4.13. No damage occurred from the 1.2 m/s impact, while visible damage was caused by the 3.0 and 5.0 m/s impacts, but penetration did not occur. The shape of the signatures is a half sine wave with oscillations of higher frequency superimposed on it, as was the case with the signatures of the graphite/epoxy laminates. The peak force of the 3.0 m/s signature is nearly identical to those of the graphite/epoxy specimens (1500 N). Although the locations of the peaks of the secondary oscillations differ somewhat, the peak force of the impact is virtually identical. The duration of the 3.0 m/s impact of the glass/epoxy laminate is approximately 12 ms, which is only 1 ms longer than the typical duration of the same impact on the 12-ply graphite/epoxy laminates. The peak force from the 5.0 m/s impact is approximately 2350 N, which is significantly lower than the peak force of 3000 N experienced by the graphite/epoxy $(45_2/0_2)_s$ laminate. The duration of the glass/epoxy impact (10 ms) is approximately 1 ms longer than that of the impact on the graphite/epoxy, and the peak forces of both impacts occur at nearly the same time (5 ms). The amplitude of the secondary oscillations of the graphite/epoxy laminate are several times larger than those of the glass/epoxy laminate. It can be seen, however, that the secondary oscillations are more apparent on the "upward" side of both signatures than on the "downward" side.

Signatures for the $(90_2/0_2)_s$ layup impacted at 1.0, 3.0, and 5.0 m/s are presented in Figure 4.14. No damage occurred from the 1.0 m/s impact, while visible damage was caused by the 3.0 and 5.0 m/s impacts, again, without penetration.

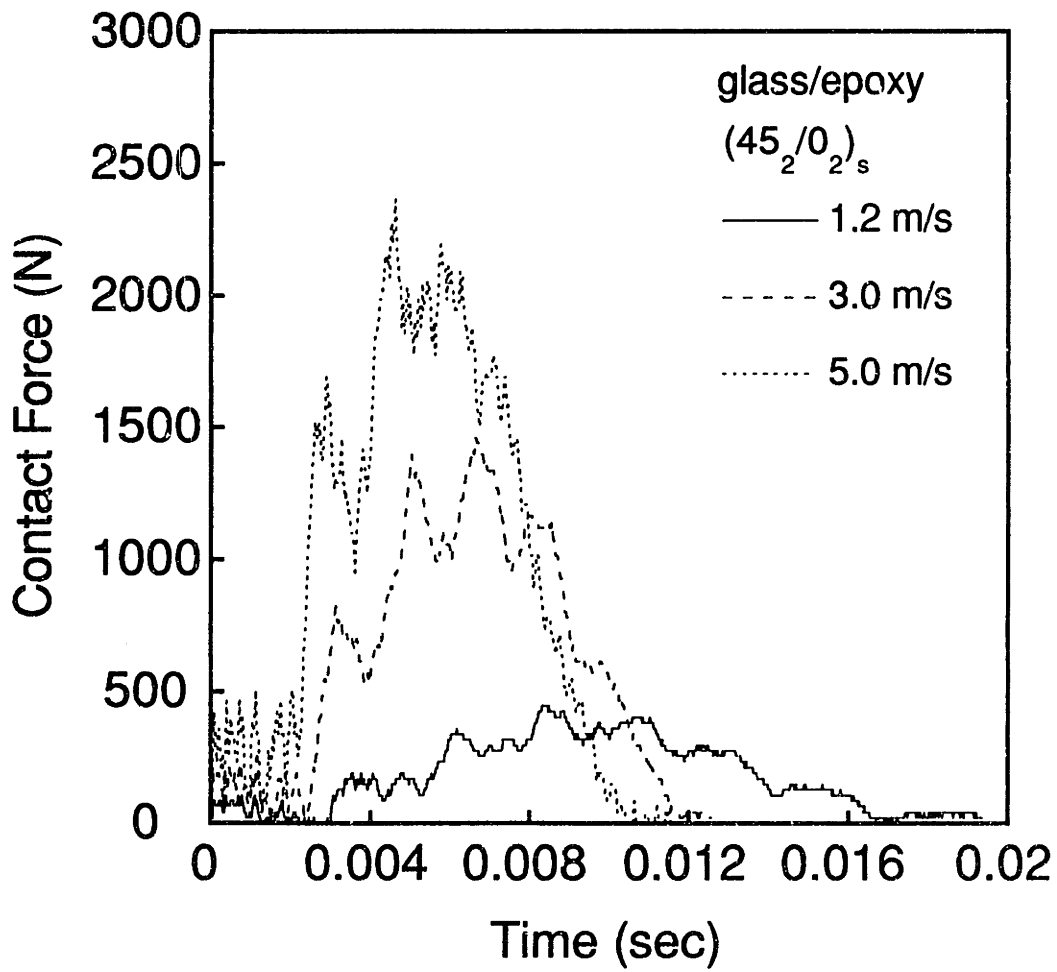


Figure 4.13 Force-time signatures of glass/epoxy $(45_2/0_2)_s$ laminate impacted at 1.2 m/s (undamaged), 3.0 m/s, and 5.0 m/s.

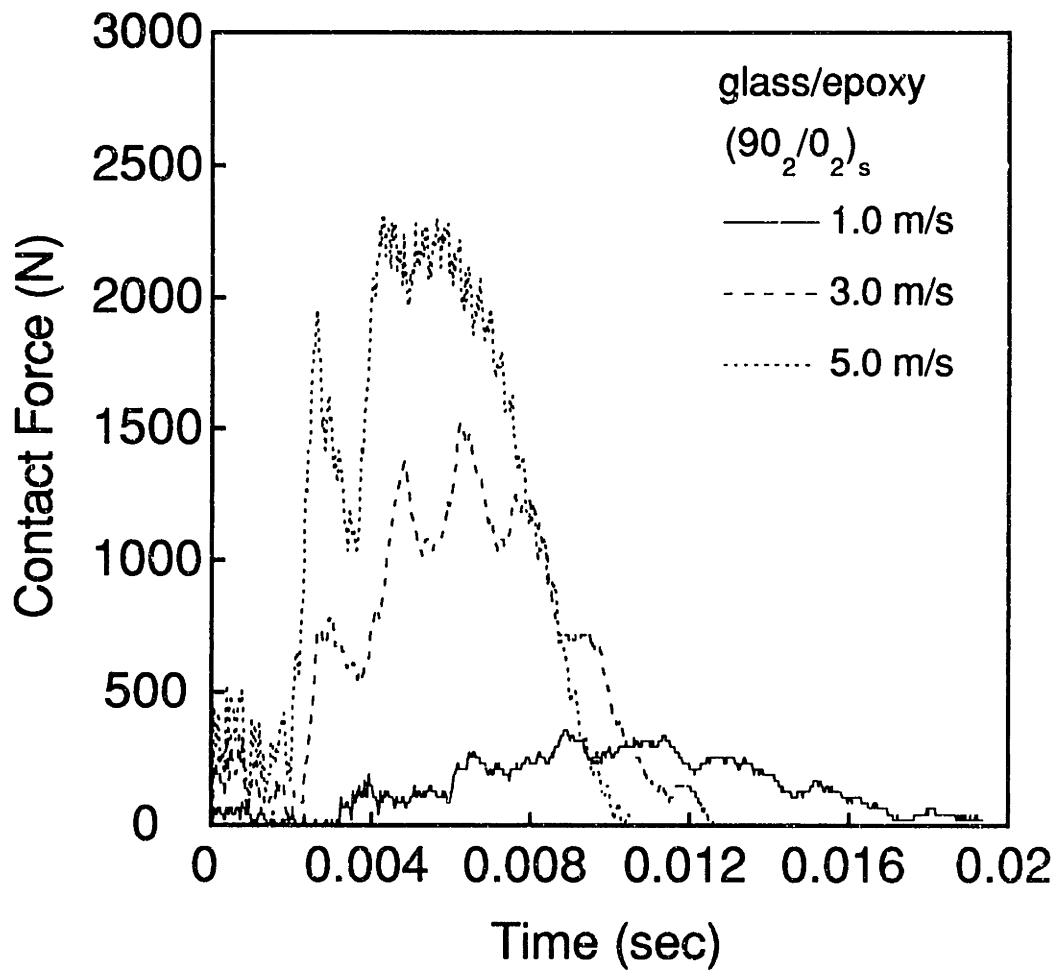


Figure 4.14 Force-time signatures of glass/epoxy (90₂/0₂)_s laminate impacted at 1.0 m/s (undamaged), 3.0 m/s, and 5.0 m/s.

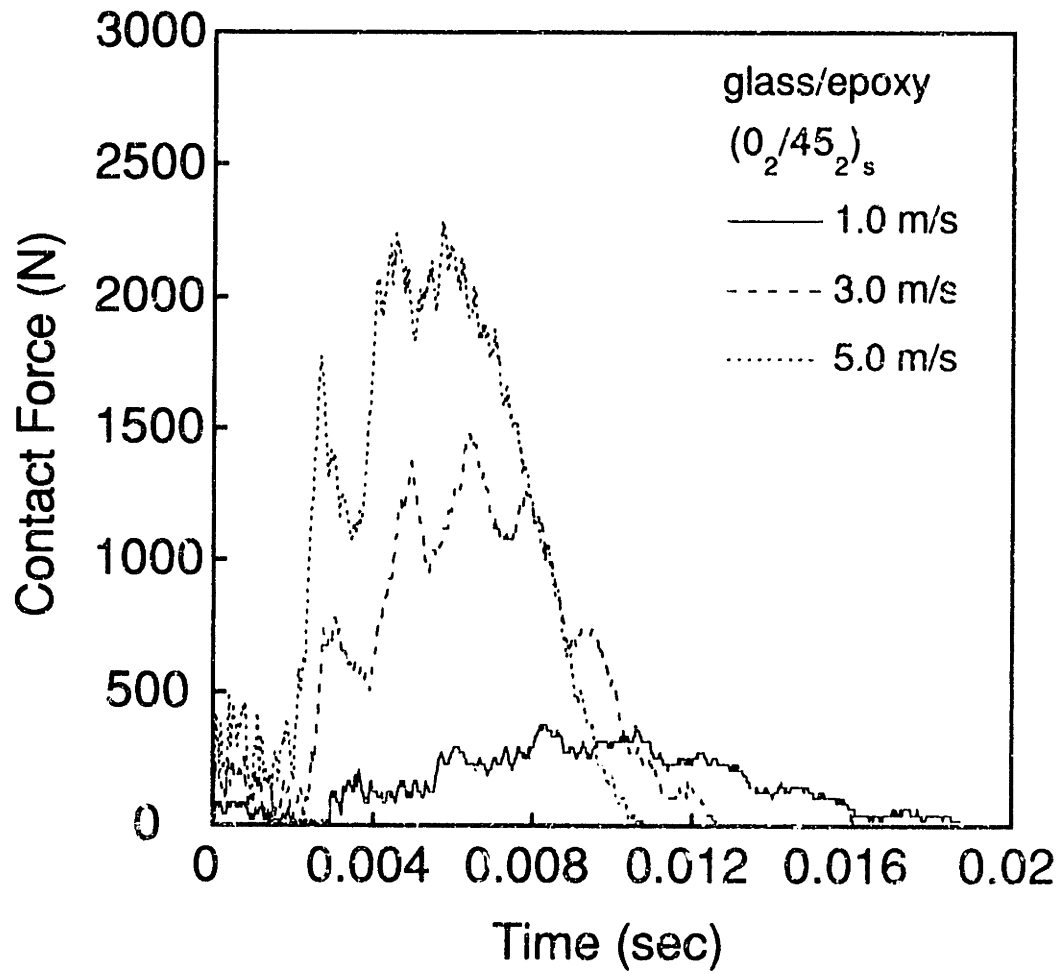


Figure 4.15 Force-time signatures of glass/epoxy (0₂/45₂)_s laminate impacted at 1.0 m/s (undamaged), 3.0 m/s, and 5.0 m/s.

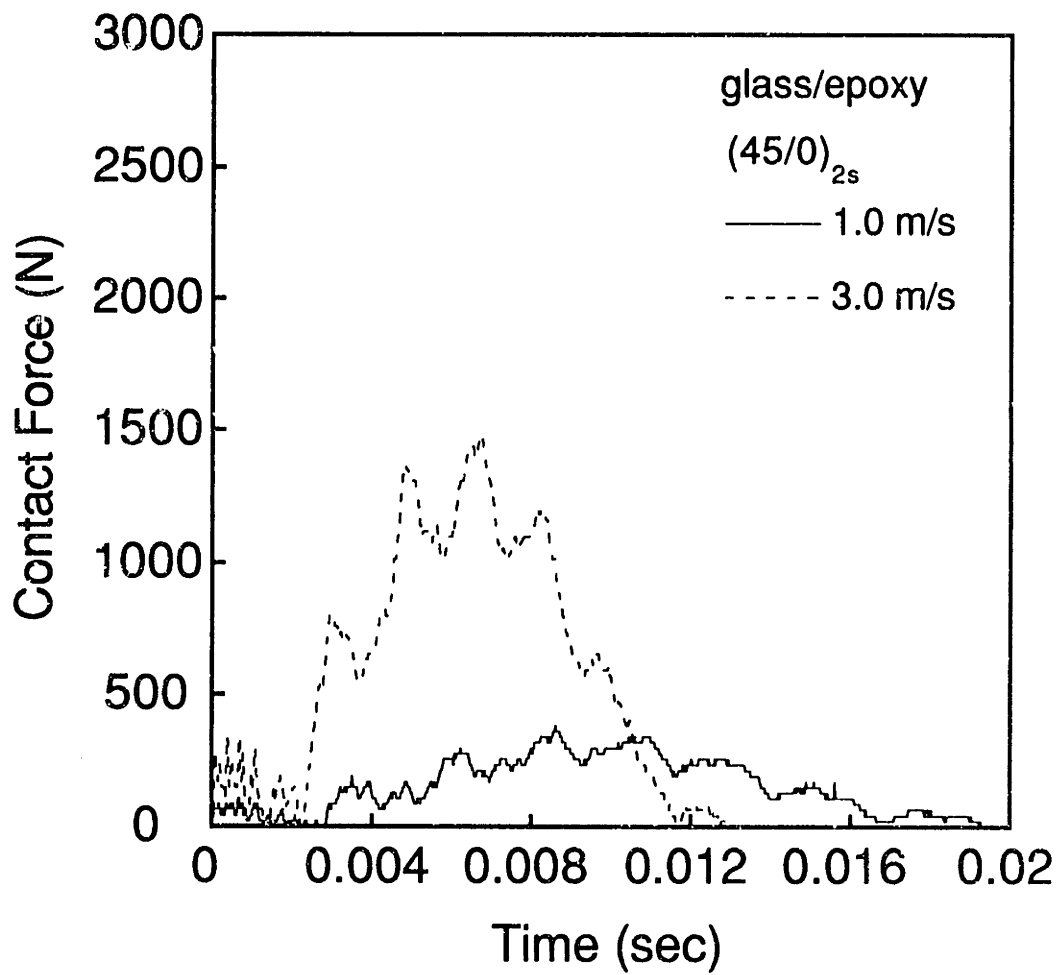


Figure 4.16 Force-time signature of glass/epoxy (45/0)_{2s} laminate impacted at 1.0 m/s (undamaged), and 3.0 m/s.

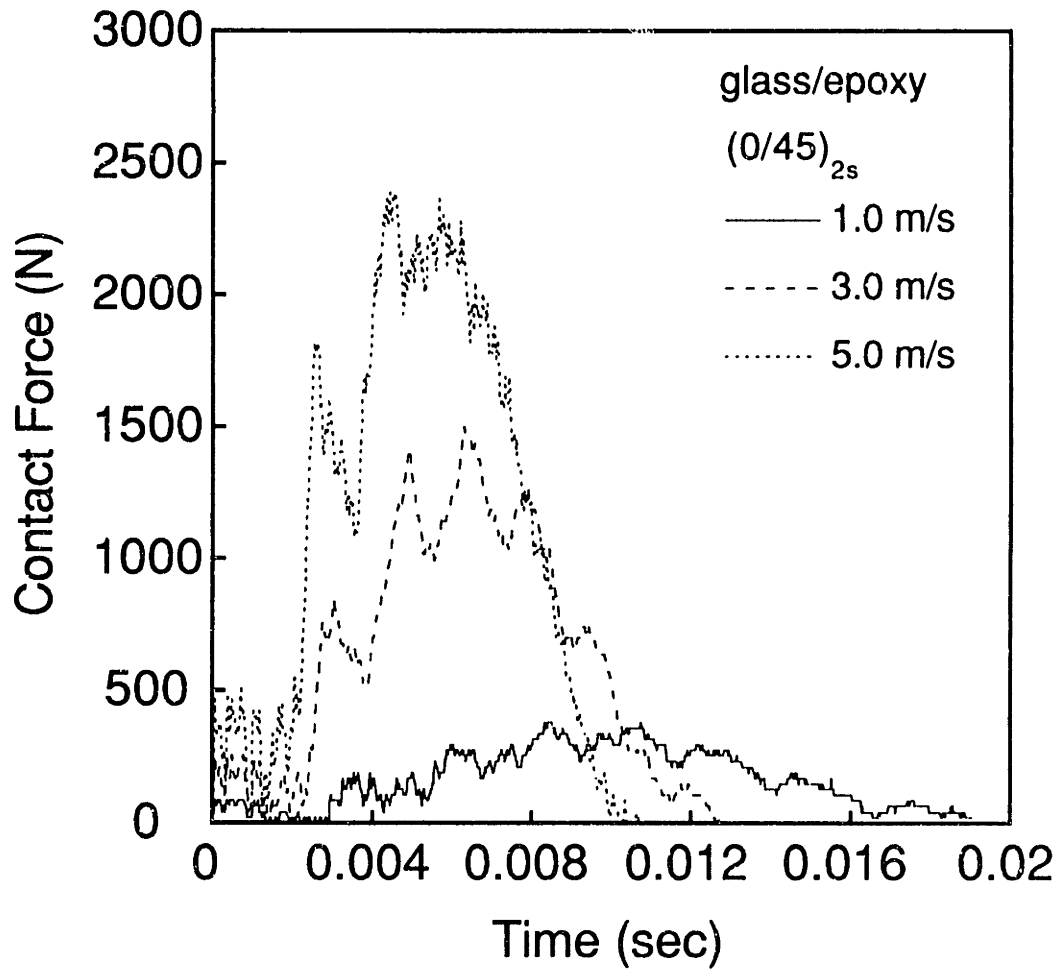


Figure 4.17 Force-time signatures of glass/epoxy (0/45)_{2s} laminate impacted at 1.0 m/s (undamaged), 3.0 m/s, and 5.0 m/s.

Signatures for the $(0_2/45_2)_s$ layup impacted at 1.0, 3.0 and 5.0 m/s are presented in Figure 4.15. No damage occurred from the 1.0 m/s impact, while visible damage was caused by the 3.0 and 5.0 m/s impacts, again, without penetration.

Signatures for the $(45/0)_{2s}$ layup impacted at 1.0 and 3.0 m/s are presented in Figure 4.16. A specimen of this layup was not impacted at 5.0 m/s. The specimen was undamaged from the 1.0 m/s impact, but visible damage occurred from the 3.0 m/s impact.

Signatures for the $(0/45)_{2s}$ layup impacted at 1.0, 3.0 and 5.0 m/s are presented in Figure 4.17. No damage occurred from the 1.0 m/s impact, while visible damage was caused by the 3.0 and 5.0 m/s impacts, but penetration did not occur.

In this material system, the layup does not seem to affect the shape of the signatures. This can be observed most easily from the shapes of the 3.0 m/s signatures, which are virtually identical among these five layups. The peak force is approximately 1500 N, the impact duration is approximately 12 ms, and the locations and amplitudes of the secondary peaks coincide in all of the 3.0 m/s signatures. The impact duration appears to decrease with increasing impact velocity. Impacts of approximately 1.0 m/s have durations typically of 18 ms, while the 5.0 m/s impacts have durations of approximately 10 ms.

4.2.5 General Characteristics

The force-time signatures of all impacts generally had the same shape: a half sine wave with oscillations of higher frequency superimposed on it. Also, the durations of the impacts tended to decrease as the impact velocity increased for all material systems. The signatures of each of the 12-ply layups of AS4/3501-6 had distinguishing features, particularly in the locations and

amplitudes of the peaks of the secondary oscillations, but the peak force and duration for the 3.0 m/s impacts were similar, regardless of layup. This can most easily be seen with the 3.0 m/s impacts, which commonly had peak forces near 1500 N and durations of about 12 ms. The laminates of IM7G/X8553-50 had nearly identical signatures to laminates of AS4/3501-6 with the same layup at non-penetrating velocities.

For all material systems, it was noted from the 5.0 m/s signatures that the secondary oscillations are more pronounced on the "upward" side of the signature (before the peak force is reached) than on the "downward" side (after the peak force). The 5.0 m/s impacts caused penetration in all of the 12-ply AS4/3501-6 laminates, but not in the IM7G/X8553-50 laminates with the same layups. Penetration was observed in the signature as a large load drop and high frequency oscillations could be noticed as penetration occurred. The IM7G/X8553-50 laminates were not penetrated, and thus, were able to attain a higher peak force from the 5.0 m/s impacts than their AS4/3501-6 counterparts.

The signatures of the two 16-ply quasi-isotropic laminates of AS4/3501-6 have similar signatures, in that the peaks of the secondary oscillations of the signatures occur at the same location. However, the amplitudes of the secondary oscillations are greater for the $[(\pm 45)_2/(0/90)_2]_s$ layup than for the $[\pm 45_2/0_2/90_2]_s$ layup. In terms of the locations of the peaks in the secondary oscillations, the signature of the fabric A370-5H/3501-6S laminate is similar to those of the 16-ply tape laminates, but the amplitudes of the secondary oscillations with the fabric laminate are much greater. In addition, the signature of the fabric laminate contains superimposed waves of high frequency which were also noted with the $[(\pm 45)_2/(0/90)_2]_s$ laminate, but not with the $[\pm 45_2/0_2/90_2]_s$ layup.

The signatures of the glass/epoxy laminates were not appreciably affected by layup. This can be seen most clearly between the 3.0 m/s signatures of the different layups. The shapes of the 3.0 m/s signatures are nearly identical, as are the peak forces and durations. The 3.0 m/s signatures of these laminates have virtually the same peak force and impact duration as the 12-ply laminates of AS4/3501-6 and IM7G/X8553-50. Comparing the 5.0 m/s signatures of the $(45_2/0_2)_s$ layup of glass/epoxy and A370-5H/3501-6S, it is noticed that the peak force is substantially higher with the graphite/epoxy system, as are the amplitudes of the secondary oscillations. The 5.0 m/s signature of the glass/epoxy laminates did not contain the high frequency oscillation that was observed with the A370-5H/3501-6S laminate.

4.3 Damage Characteristics

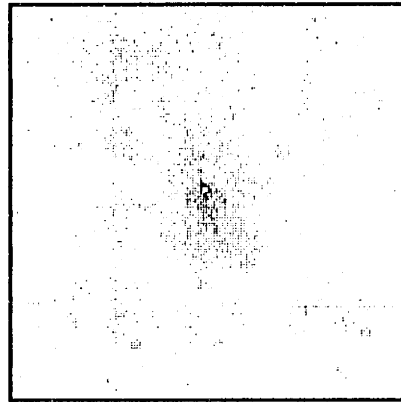
For the graphite/epoxy laminates, X-ray photographs and a deply transcription are shown for each laminate. The deply technique was performed on several specimens of each layup: an incipient damage specimen (specimen impacted at the lowest velocity which showed damage via the X-ray), a specimen impacted at 3.0 m/s, and a specimen impacted at 5.0 m/s. The incipient damage mode was typically matrix cracking and the deply of such specimens did not give any reportable results since only delamination and fiber damage are observable through the deply technique. The deply technique was useful in determining the location (through thickness) of delaminations which could be seen in the X-ray photographs. However, the X-ray photographs provide a more accurate representation of the extent of the delaminations than the hand sketches from the deply. Also, the deply method did not lend any appreciable information with the penetrated specimens, which were dominated by heavy fiber damage in all plies. This fiber damage

was recorded more accurately by the X-ray photograph than by the sketches from the deply. Each deply transcription shown here corresponds to one of the specimens shown in the X-ray photographs, specifically, the one shown with the highest impact velocity.

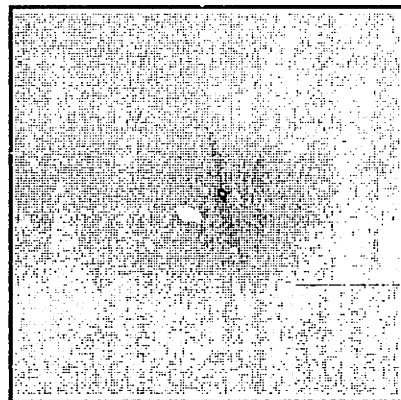
The deply and X-ray techniques were found to give unsatisfactory results with the glass/epoxy system, since neither the X-ray dye nor the gold chloride was found to penetrate into the damaged regions. Therefore, the deply and X-ray techniques were not used with the glass/epoxy system. Instead, photographs were taken of the damaged specimens in order to depict the damage state. Photographs are presented of specimens impacted at 3.0 m/s and also 5.0 m/s where the data was available.

4.3.1 AS4/3501-6 Material System

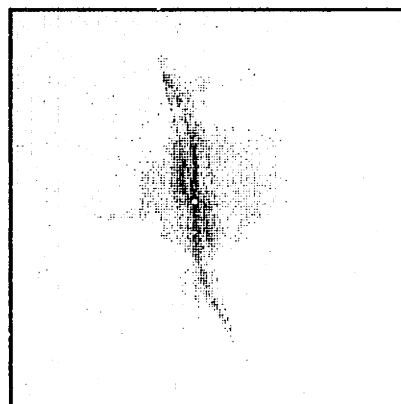
Three X-ray photographs are shown which depict the progression of damage from incipience to a more advanced state in the $[\pm 15_2/0_2]_s$ layup in Figure 4.18. The incipient damage mode is matrix cracking in the $+15^\circ$ plies and this first occurred at an impact velocity of 1.1 m/s. Due to the reproduction technique (X-ray photographs electronically scanned) used in this document, the matrix crack is barely visible in the figure. However, the matrix crack is apparent in the original X-ray photograph and extends approximately 8 mm on either side of the hole at the impact center. At an impact velocity of 1.3 m/s, the matrix crack is larger, extending 12 mm on either side. The 3.0 m/s impact caused delaminations in addition to the matrix crack. The $+15^\circ$ matrix crack extends 20 mm on either side, and delaminations border on this crack. The delaminations are slender half ellipses, and are anti-symmetric about the center of impact. The interface locations of the delaminations in the 3.0 m/s impact specimen are shown in Figure 4.19. The largest delamination appears



velocity = 1.1 m/s



velocity = 1.3 m/s



velocity = 3.0 m/s

1 cm

Figure 4.18 X-ray photographs of AS4/3601-6 $[\pm 15_2/0_2]_s$ specimens for impact velocities of (top) 1.1 m/s (incipient), (middle) 1.3 m/s, and (bottom) 3.0 m/s .

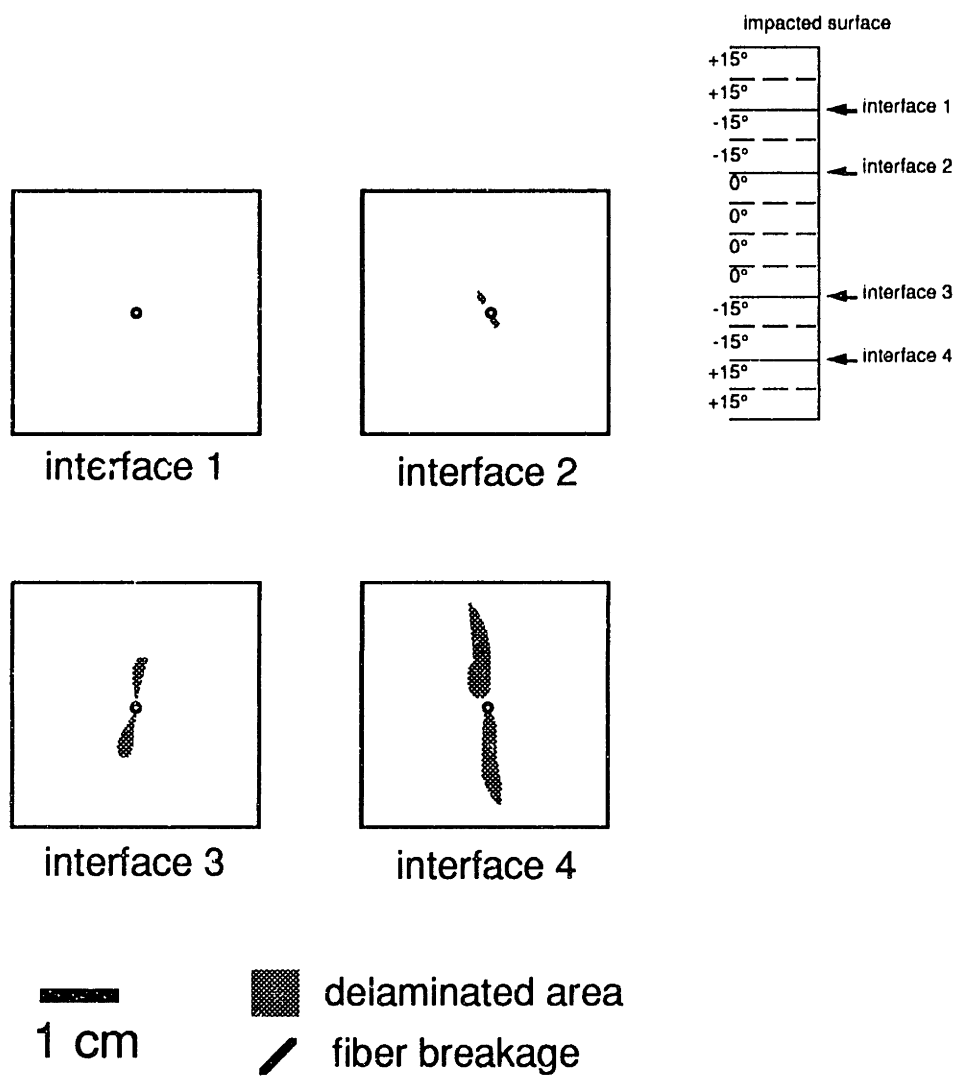
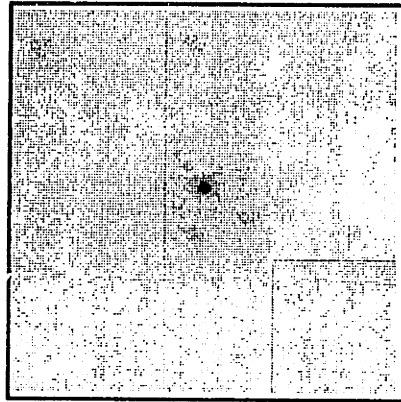


Figure 4.19 Deply transcription of AS4/3501-6 $[\pm 15_2/0_2]_s$ specimen impacted at 3.0 m/s.

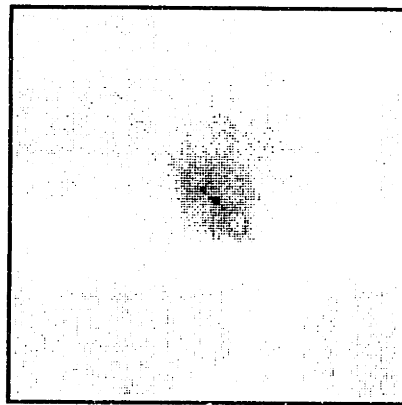
at the interface closest to the back surface of the laminate. It can be inferred from the shape of the delamination that the $+15^\circ$ matrix cracks observed in the X-rays occur in the rearmost plies of the laminate, since the delamination is bounded by a $+15^\circ$ crack and the delamination occurs at the rearmost interface. Other smaller delaminations occur as well, with the size of the delaminations increasing with distance from the impacted surface. The delamination at interface 3 (between the 0° and -15° plies) appears bounded by the 0° and -15° directions.

A similar progression of damage can be seen for the $[\pm 45_2/0_2]_s$ layup in Figure 4.20. A matrix crack 20 mm in total length in the $+45^\circ$ direction can be seen from an impact velocity of 1.2 m/s, and delamination is observed at higher impact velocities. An impact velocity of 2.0 m/s causes a $+45^\circ$ matrix crack 20 mm in total length which bisects two nearly circular delaminations on either side of center. The delaminations have a diameter of approximately 2 mm and their centers are about 4 mm away from the impact center. Larger delaminations of the same variety and also bisected by a $+45^\circ$ crack are visible from the 3.0 m/s impact. The largest delamination occurs at the rearmost interface, as shown in the deply transcription in Figure 4.21. The delamination is symmetric about a line in the $+45^\circ$ direction. Other smaller delaminations occur at interfaces 2 and 3. The major axis of each delamination is aligned with the fiber direction of the ply directly below the interface.

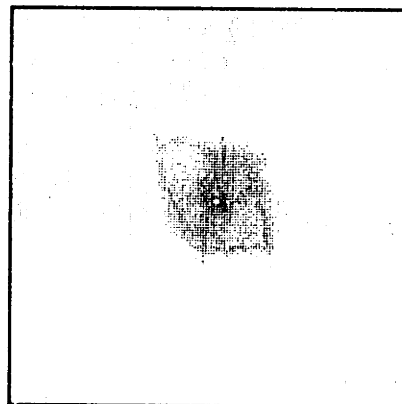
Matrix cracking of the $+60^\circ$ plies is the incipient damage mode for the $[\pm 60_2/0_2]_s$ layup, as shown in Figure 4.22. A crack 35 mm in total length occurred in the $+60^\circ$ direction from an impact of 0.9 m/s, and a 3.0 m/s impact caused significant delamination aligned with a $+60^\circ$ crack 35 mm in total length. In certain places, the edge of the delamination is defined by matrix



velocity = 1.2 m/s



velocity = 2.0 m/s



velocity = 3.0 m/s



1 cm

Figure 4.20 X-ray photographs of AS4/3501-6 $[\pm 45_2/0_2]_s$ specimens for impact velocities of (*top*) 1.2 m/s (incipient), (*middle*) 2.0 m/s, and (*bottom*) 3.0 m/s.

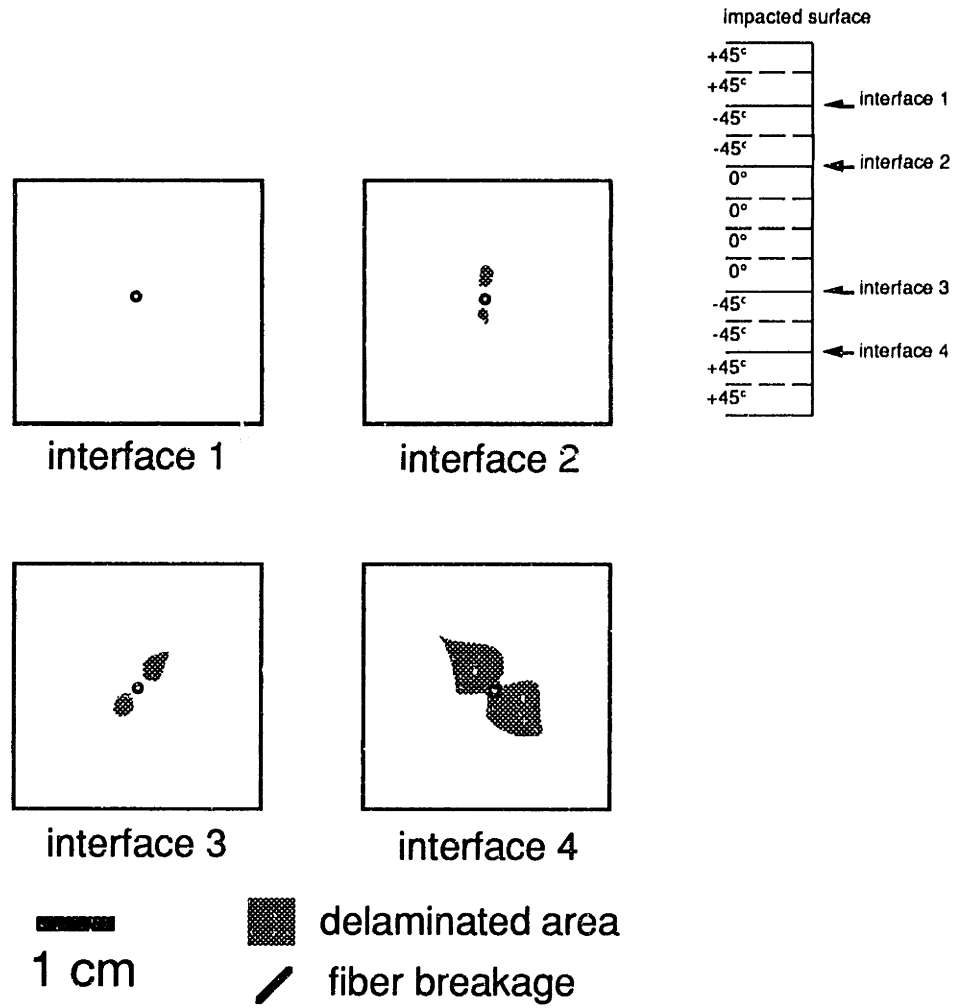
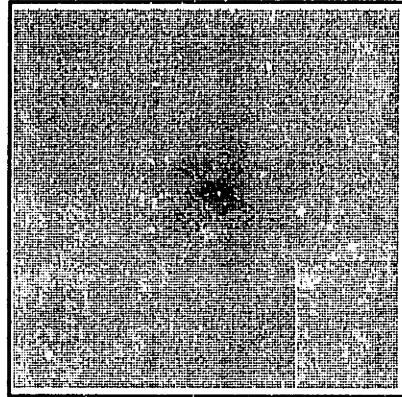
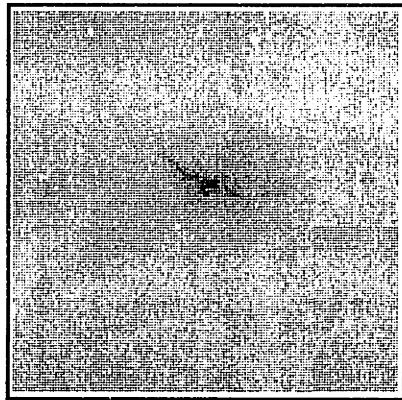


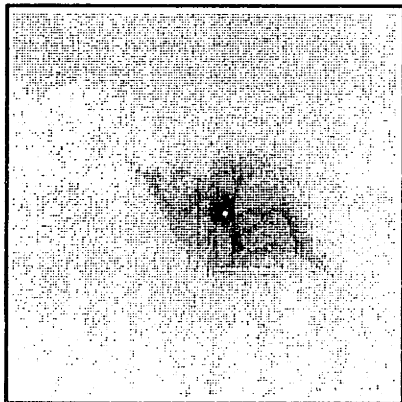
Figure 4.21 Deply transcription of AS4/3501-6 $[\pm 45_2/0_2]_s$ specimen impacted at 3.0 m/s.



velocity = 0.9 m/s



velocity = 1.5 m/s



velocity = 3.0 m/s


1 cm

Figure 4.22 X-ray photographs of AS4/3501-6 $[\pm 60_2/0_2]_s$ specimens for impact velocities of (top) 0.9 m/s (incipient), (middle) 1.5 m/s, and (bottom) 3.0 m/s.

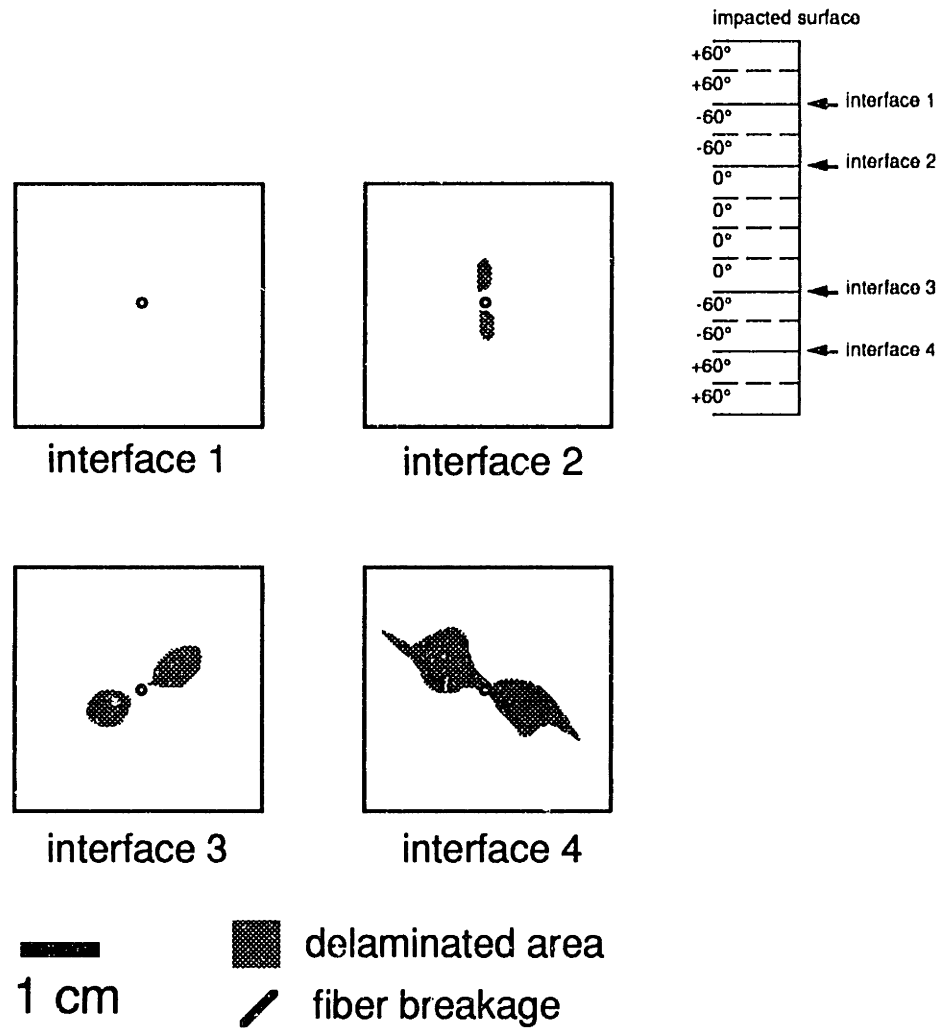
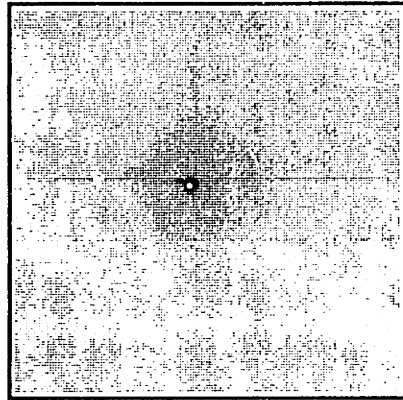


Figure 4.23 Deply transcription of AS4/3501-6 [$\pm 60_2/0_2$]_s specimen impacted at 3.0 m/s.

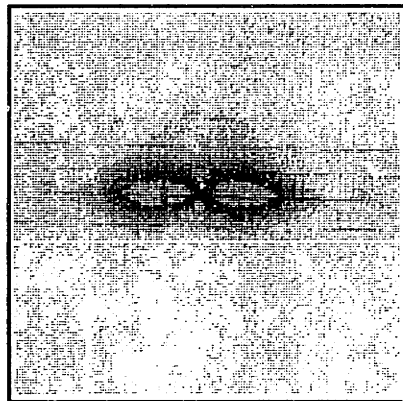
cracks in the $+60^\circ$ direction. The largest delamination occurred at the rearmost interface and the major axis of this delamination followed the fiber direction of the $+60^\circ$ plies below it, as shown in Figure 4.23. This delamination was anti-symmetric about the impact center. Other smaller delaminations occurred at interfaces 2 and 3 and the major axes of these delaminations also followed the fiber directions of the lower ply of the interface.

The damage progression of the $[90_4/0_2]_s$ layup is depicted in Figure 4.24. The incipient damage mode was a matrix crack in the 90° direction. A 90° crack across the entire width (89 mm) of the specimen occurred at an impact velocity of 0.9 m/s. Higher impact velocities caused more 90° matrix cracks and delaminations shaped like a "figure 8" with their longitudinal axes in the 90° direction. A large delamination of approximately 40 mm in overall length is visible in the X-ray image of the specimen impacted at 3.0 m/s and this delamination is bisected by a crack in the 90° direction. As visible from the deply transcription of Figure 4.25, the 3.0 m/s impact caused delaminations at both interfaces of this laminate, but the larger delamination occurred at the interface closer to the back surface of the laminate. The smaller delamination at the upper interface of the laminate is also shaped like a "figure 8" but its longitudinal axis is oriented in the 0° direction. This smaller delamination is approximately 12 mm in its longest dimension. Again, the major axes of the delaminations follow the fiber direction of the lower ply at the interface.

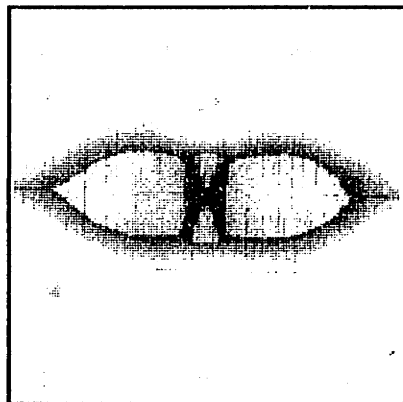
The incipient damage mode in the $[\pm 45_2/0_2/90_2]_s$ layup is matrix cracking in the $+45^\circ$ plies. A matrix crack in the $+45^\circ$ direction and approximately 20 mm in total length was caused from a 2.1 m/s impact, as shown in Figure 4.26. It can be inferred from the shapes of delaminations at higher impact velocities, that the incipient matrix cracks occur in the plies at the back surface of the laminate. Matrix cracks in the 0° and 90° directions as



velocity = 0.9 m/s



velocity = 2.0 m/s



velocity = 3.0 m/s



1 cm

Figure 4.24 X-ray photographs of AS4/3501-6 $[90_4/0_2]_s$ specimens for impact velocities of (top) 0.9 m/s (incipient), (middle) 2.0 m/s, and (bottom) 3.0 m/s.

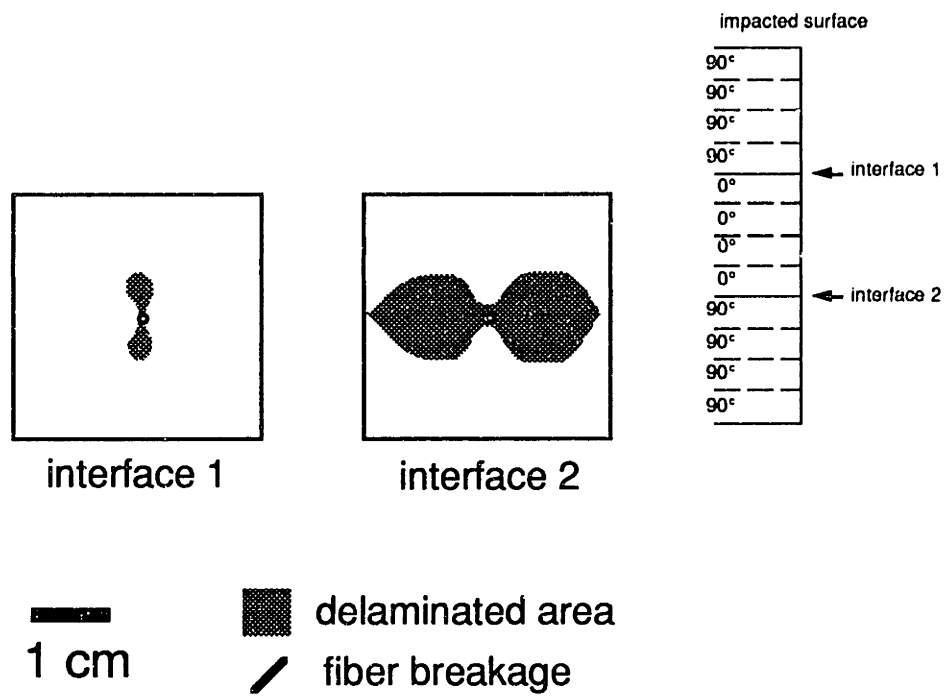
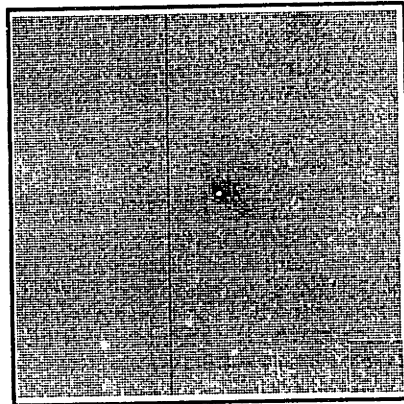
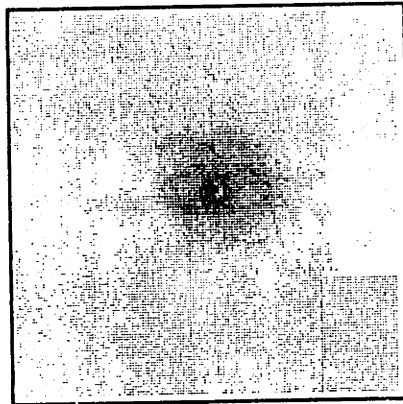


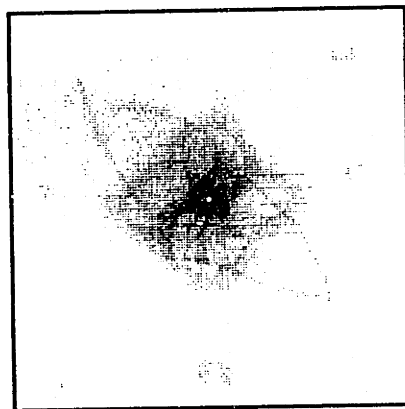
Figure 4.25 Deply transcription of AS4/3501-6 $[90_4/0_2]_s$ specimen impacted at 3.0 m/s.



velocity = 2.1 m/s



velocity = 2.6 m/s



velocity = 5.0 m/s

1 cm

Figure 4.26 X-ray photographs of AS4/3501-6 $[\pm 45_2/0_2/90_2]_s$ specimens for impact velocities of (*top*) 2.3 m/s (incipient), (*middle*) 2.6 m/s, and (*bottom*) 5.0 m/s.

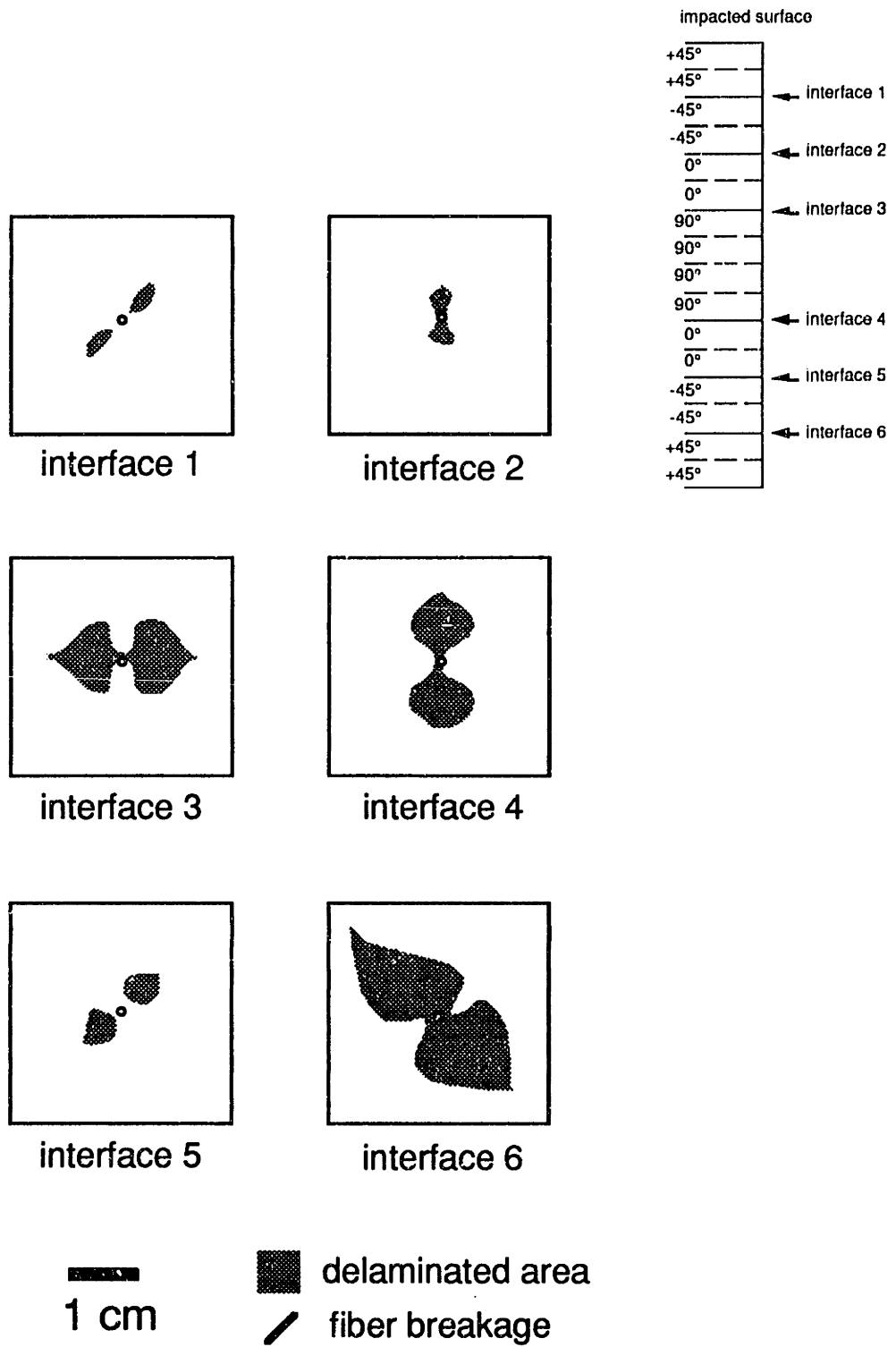
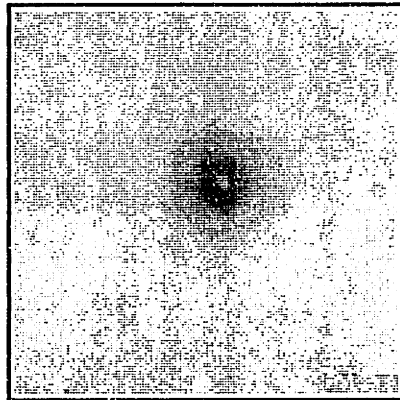


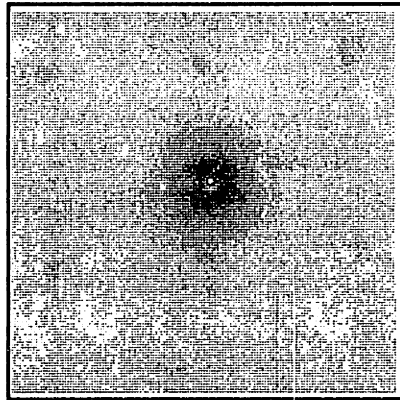
Figure 4.27 Deply transcription of AS4/3501-6 $[\pm 45_2/0_2/90_2]_s$ specimen impacted at 5.0 m/s.

well as delaminations were caused from impacts of higher velocity. The 2.6 m/s impact caused intense matrix cracking in the 0° and 90° direction in addition to several matrix cracks in the $+45^\circ$ direction, and multiple delaminations are observed. The major axis of the largest delamination is aligned with the $+45^\circ$ direction. This delamination appears to have an elliptical shape and its longest dimension is approximately 20 mm. Very extensive matrix cracking in the 0° and 90° directions are also observed from the 5.0 m/s impact. Multiple delaminations are observed, and the largest delamination is again aligned with the $+45^\circ$ direction and has an elliptical shape. The major axis of this delamination is 42 mm and it is bounded by a matrix crack at one end where the edge of the delamination is defined by a $+45^\circ$ matrix crack for approximately 5 mm. The 5.0 m/s impact caused delaminations at all interfaces of the specimen, as can be seen in Figure 4.27. All delaminations have a "figure 8" shape with the longitudinal axis of each delamination aligned with the fiber direction of the lower ply at the interface. The largest delamination occurs at the rearmost interface, and is oriented in the $+45^\circ$ direction.

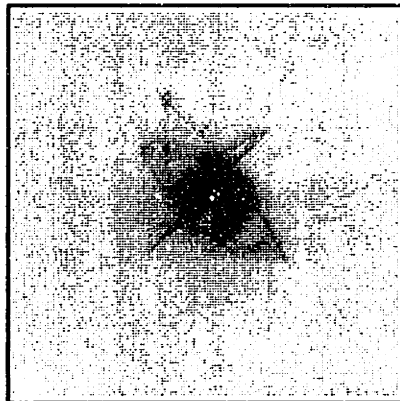
X-ray photographs of impacted specimens of the $[(\pm 45)_2/(0/90)_2]_s$ layup are shown in Figure 4.28. The incipient damage velocity was determined to be 3.0 m/s, but a single incipient damage mode is not easily described. What appears to be a combination of matrix cracking and delamination resulted from the 3.0 m/s impact. A circular area of intense matrix cracking in the 0° and 90° directions can be seen near the impact center, and this damage area has a diameter of approximately 9 mm. This area of intense matrix cracking is surrounded by a circular "halo" of delamination of diameter 12 mm. Virtually the same damage state is observed from the 3.6 m/s impact. The 5.0 m/s impact caused elliptical delaminations of approximately 20 mm in length



velocity = 3.0 m/s



velocity = 3.6 m/s



velocity = 5.0 m/s



1 cm

Figure 4.28 X-ray photographs of AS4/3501-6 $[(\pm 45)_2/(0/90)_2]_s$ specimens for impact velocities of (top) 3.0 m/s (incipient), (middle) 3.6 m/s, and (bottom) 5.0 m/s.

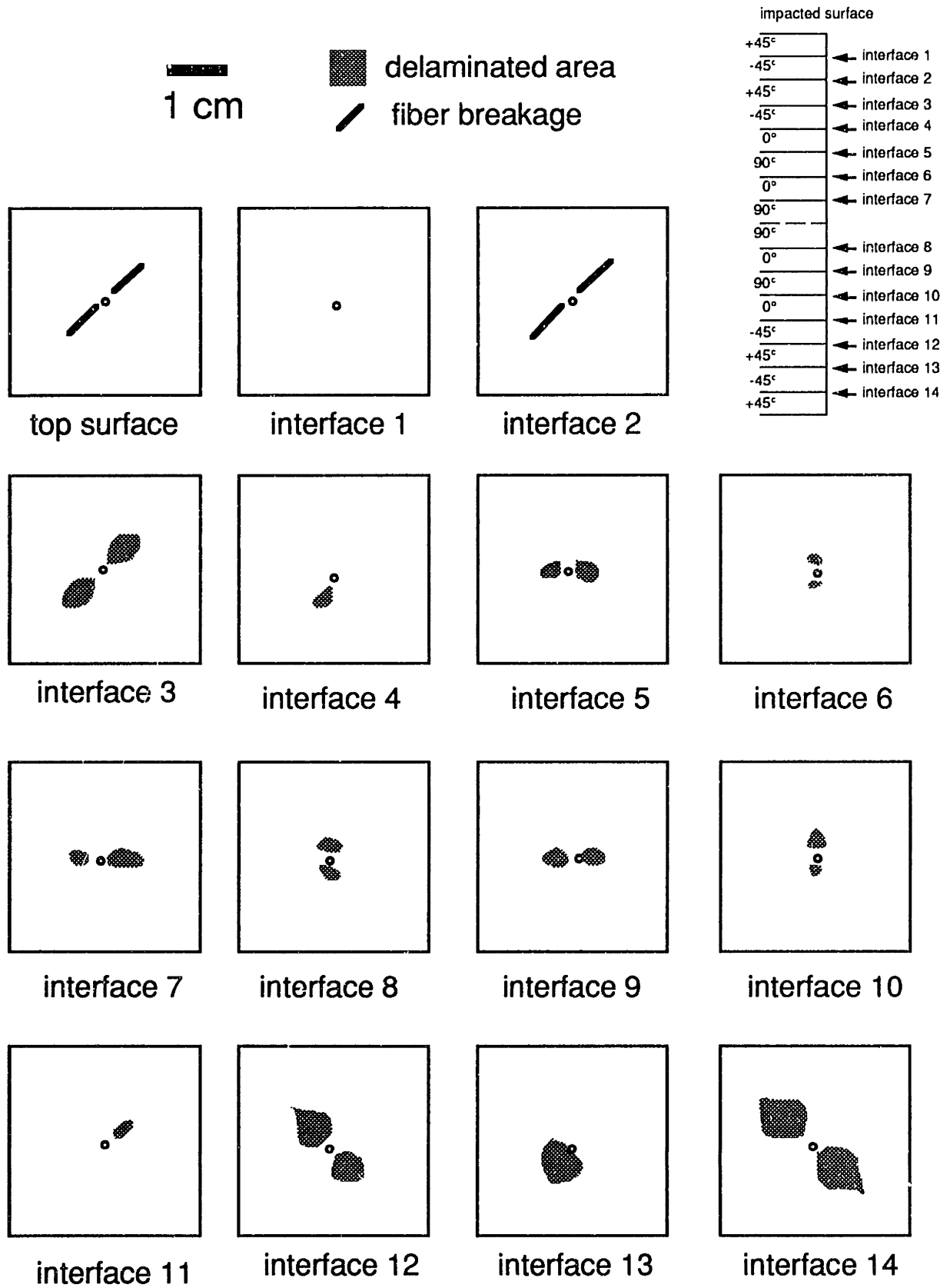
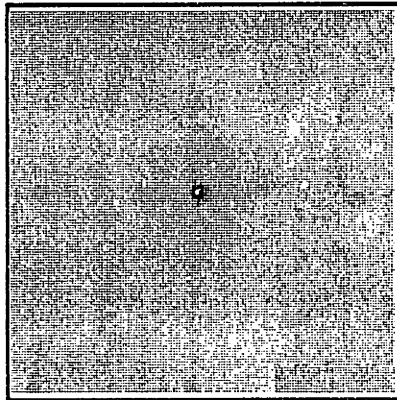


Figure 4.29 Deply transcription of AS4/3501-6 $[(\pm 45)_2 / (0/90)_2]_s$ specimen impacted at 5.0 m/s.

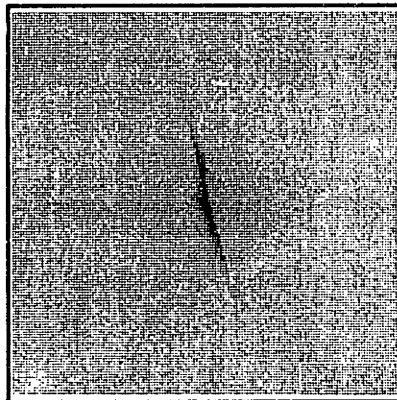
aligned with the +45° direction. These delaminations are noticeably smaller than those observed in the previous laminate impacted at the same velocity. A dark line in the -45° direction can be seen in the X-ray, and this corresponds to fiber breakage, as shown in Figure 4.29. Fiber breaks were observed in both +45° plies near the impacted surface. This is in stark contrast to the other 16-ply layup in which fiber damage was not observed. The fiber damage took the form of lines of fiber breakage oriented in the -45° direction and extending radially outward from the center of impact. The lines of broken fibers ran perpendicular to the fiber direction of the ply, and they did not run completely through the center of impact. The fiber breaks started approximately 2 mm away from the center and extended radially outward approximately 10 mm on either side. Some delamination occurred at almost all of the interfaces, with the largest delamination occurring at the rearmost interface and aligned with the +45° fibers below it.

4.3.2 IM7G/X8553-50 Material System

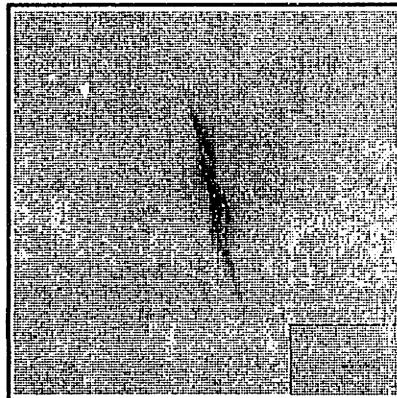
X-ray photographs of the $[\pm 15_2/0_2]_s$ layup of IM7G/X8553-50 impacted at 1.5, 4.0, and 5.0 m/s can be seen in Figure 4.30. As was the case with this same layup of AS4/3501-6, the incipient damage mode was matrix cracking in the +15° plies for this laminate. At an impact velocity of 1.5 m/s, a +15° crack 13 mm in overall length occurred. At an impact velocity of 4.0 m/s, this crack had a total length of 33 mm and at a velocity of 5.0 m/s, a delamination can be seen near the matrix crack (36 mm total length). The slender delamination is bounded by this matrix crack in places. This progression of damage is very similar to that of the $[\pm 15_2/0_2]_s$ layup of AS4/3501-6, but the impact velocities are higher in this case. Fiber damage, as well as delamination, can be seen in the deply transcription in Figure 4.31. A small line of broken fibers was found in



velocity = 1.5 m/s



velocity = 4.0 m/s



velocity = 5.0 m/s


1 cm

Figure 4.30 X-ray photographs of IM7G/X8553-50 $[\pm 15_2/0_2]_s$ specimens for impact velocities of (top) 1.5 m/s (incipient), (middle) 4.0 m/s, and (bottom) 5.0 m/s.

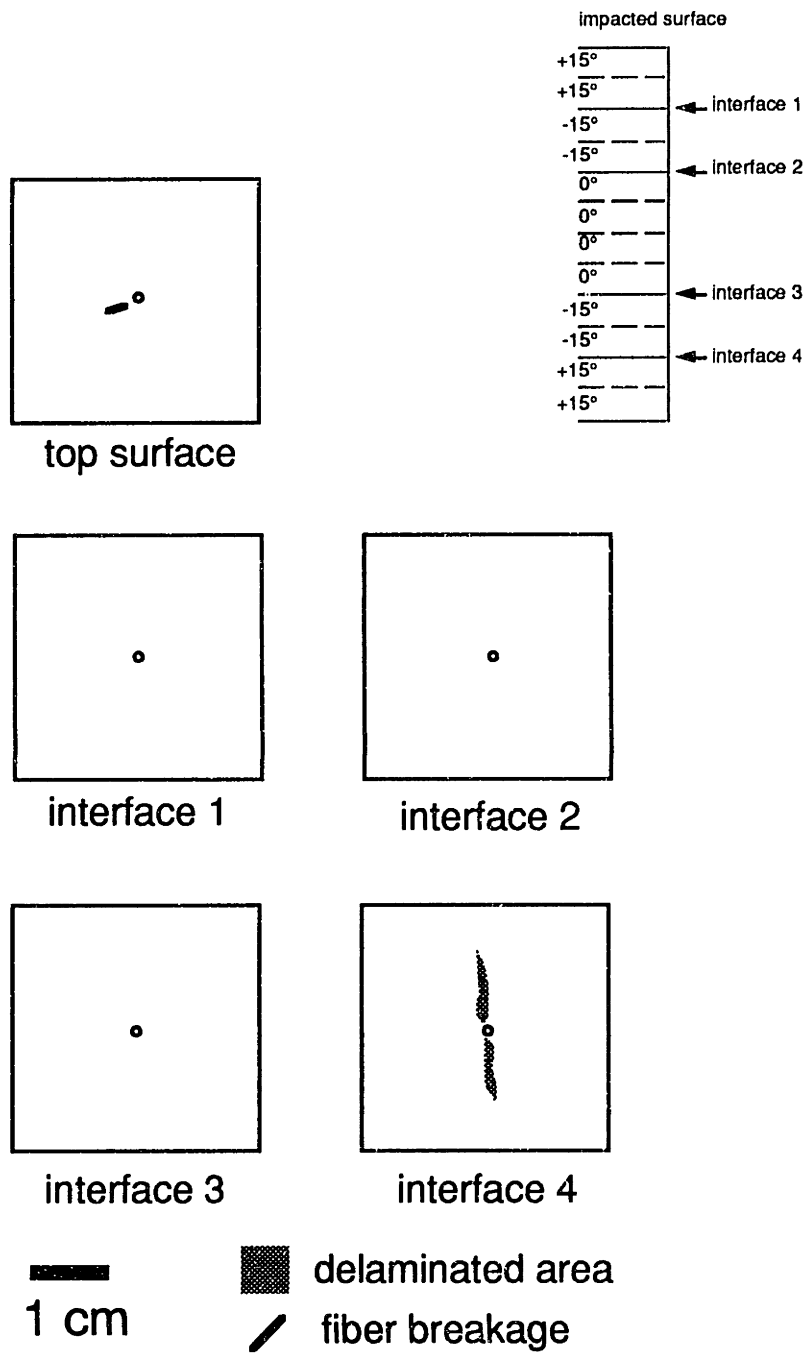
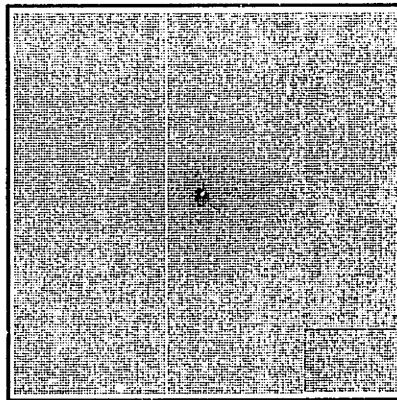


Figure 4.31 Delply transcription of IM7G/X8553-50 $[\pm 15_2/0_2]_s$ specimen impacted at 5.0 m/s.

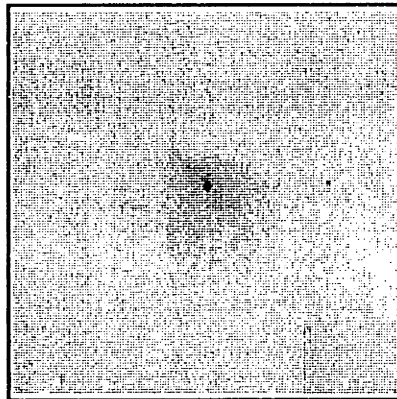
the top ply. This line is perpendicular to the fiber direction of the ply (+15°) and its total length is approximately 3 mm. A slender delamination of approximately 18 mm in length can be seen at the rearmost interface of the laminate, where a similar delamination was observed in the same layup of AS4/3501-6.

Matrix cracking of the +45° plies was the incipient damage mode for the $[\pm 45_2/0_2]_s$ layup, as shown in Figure 4.32. An impact of 2.5 m/s caused a matrix crack approximately 10 mm in length in the +45° direction. A similar crack of length 14 mm was caused by the 4.0 m/s impact and a small circular delamination (2 mm diameter) can be seen to one side of the impact center. This delamination is bisected by the +45° crack. An impact of 5.0 m/s caused a delamination which extends approximately 7 mm on either side of the impact center and is aligned with and bisected by a +45° matrix crack (23 mm total length). Small matrix cracks (less than 7 mm total length) in the -45° direction can also be observed. The delamination has the shape of a "figure 8" and is similar in appearance to that observed in the AS4/3501-6 laminate of the same layup. This delamination is located at the rearmost interface of the laminate, as shown by the deply transcription in Figure 4.33. The damage mode is very similar to that of the same layup of AS4/3501-6 material, but the impact velocities here are higher to cause the same damage state.

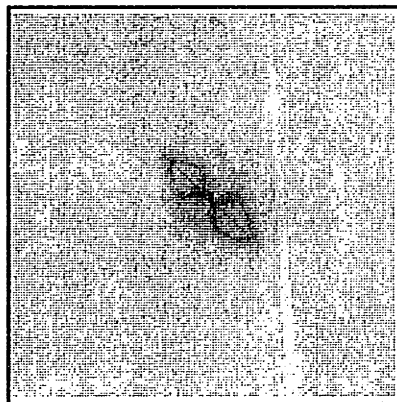
Matrix cracking in the +60° direction is the incipient damage mode in the $[\pm 60_2/0_2]_s$ layup as well, as shown in Figure 4.34. Two matrix cracks, each approximately 12 mm in total length, resulted from the 2.2 m/s impact. Two +60° matrix cracks (each of 25 mm total length) can be observed from the 4.0 m/s impact, as well. The 4.0 m/s impact also caused matrix cracking in the -60° and 0° directions. More intense matrix cracking in the +60°, -60° and 0° directions are caused by the 5.0 m/s impact, and from the deply in Figure 3.35



velocity = 2.5 m/s



velocity = 4.0 m/s



velocity = 5.0 m/s



1 cm

Figure 4.32 X-ray photographs of IM7G/X8553-50 $[\pm 45_2/0_2]_s$ specimens for impact velocities of (top) 2.5 m/s (incipient), (middle) 4.0 m/s, and (bottom) 5.0 m/s.

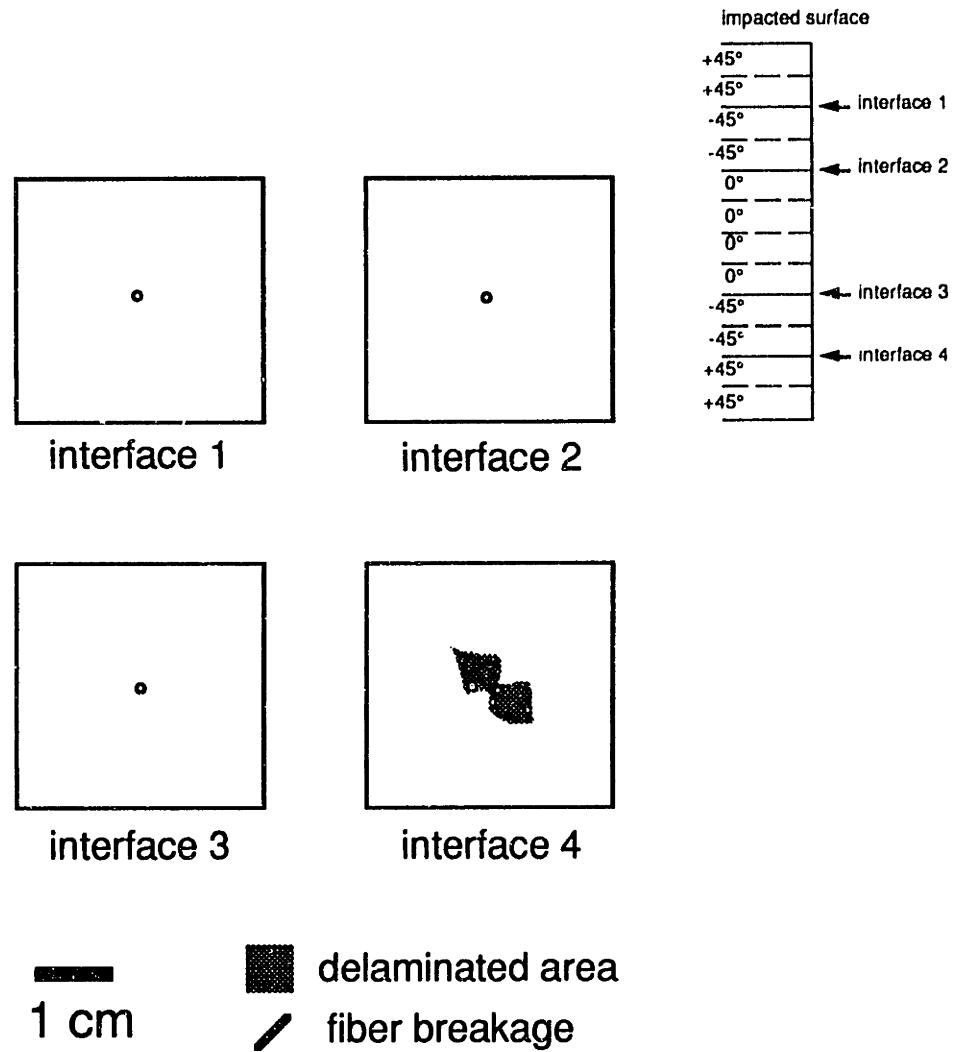
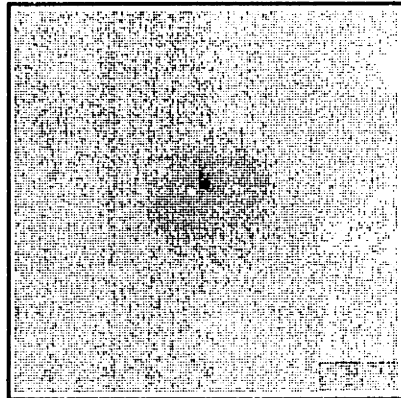
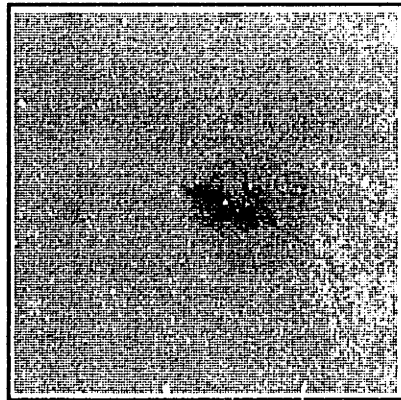


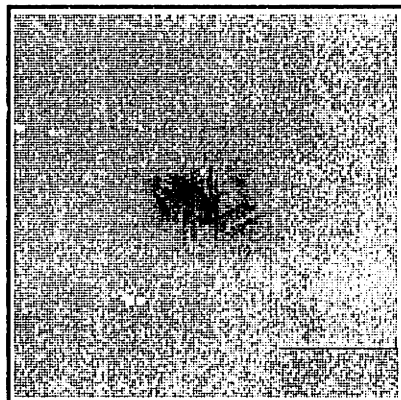
Figure 4.33 Deply transcription of IM7G/X8553-50 $[\pm 45_2/0_2]_8$ specimen impacted at 5.0 m/s.



velocity = 2.2 m/s



velocity = 4.0 m/s



velocity = 5.0 m/s

1 cm

Figure 4.34 X-ray photographs of IM7G/X8553-50 $[\pm 60_2/0_2]_s$ specimens for impact velocities of (top) 2.2 m/s (incipient), (middle) 4.0 m/s, and (bottom) 5.0 m/s.

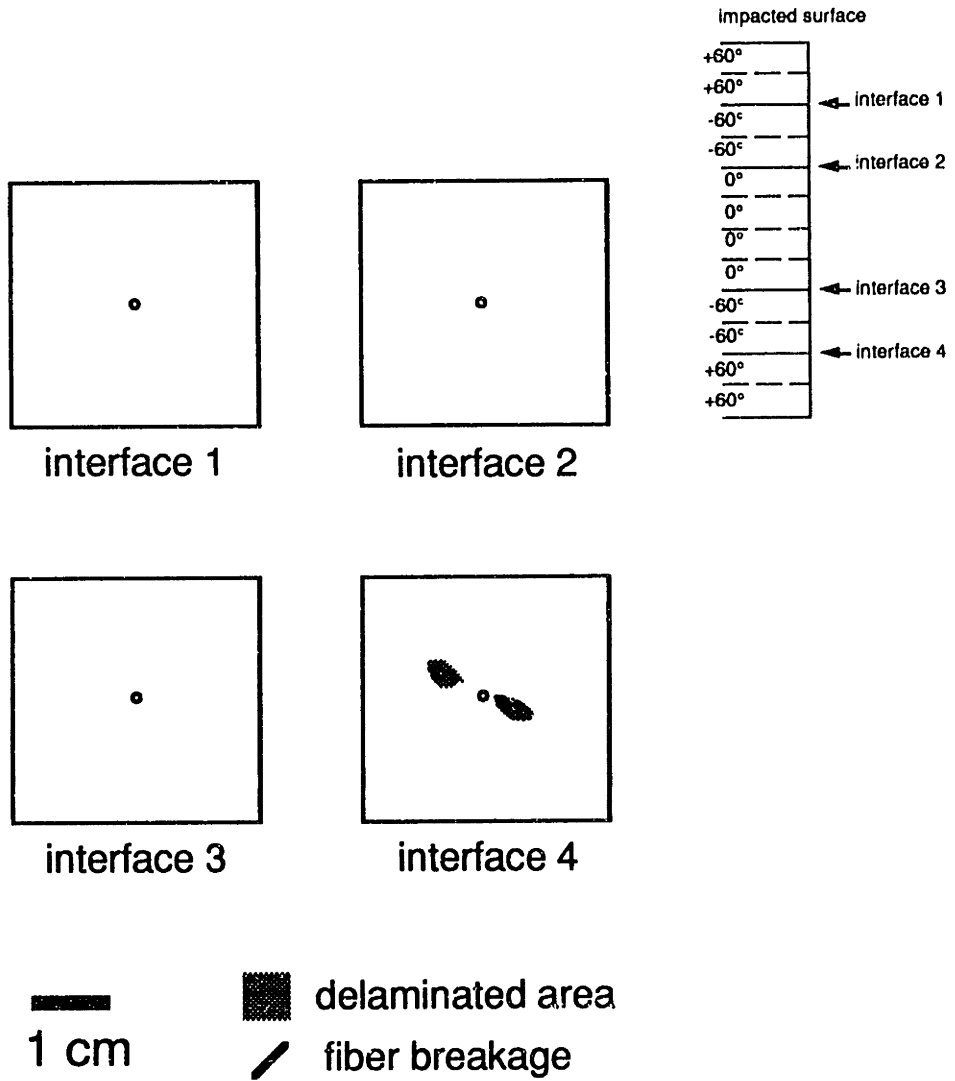
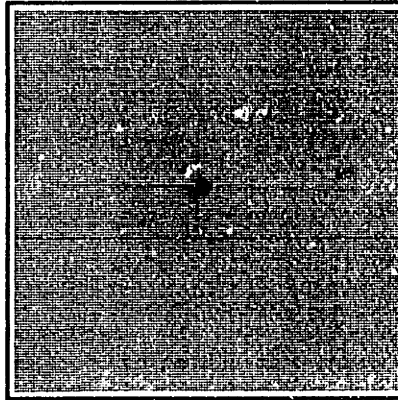


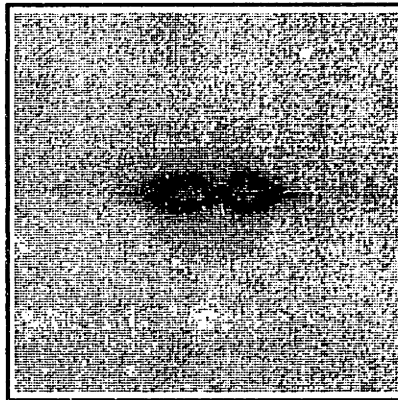
Figure 4.35 Deply transcription of IM7G/X8553-50 $[\pm 60_2/0_2]_8$ specimen impacted at 5.0 m/s.

it is observed that delamination was caused only at the rearmost interface from the 5.0 m/s impact. This delamination has a "figure 8" shape and is oriented in the +60° direction. The delamination extends approximately 9 mm on either side of the impact center. In contrast to the delamination observed in the same layup of AS4/3501-6, this delamination appears to be symmetric about a line in the +60° direction, and no delamination is observed at either interface 2 or 3, where delamination occurred in the AS4/3501-6 $[\pm 60_2/0_2]_s$ laminate.

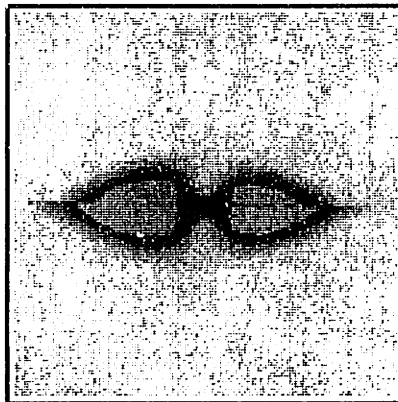
As was shown for the $[90_4/0_2]_s$ layup of AS4/3501-6, matrix cracking in the 90° direction is the incipient damage mode for the $[90_4/0_2]_s$ laminate of IM7G/X8553-50, as shown in Figure 4.36. At an impact velocity of 1.5 m/s, a matrix crack in the 90° direction can be observed extending approximately 21 mm on either side of the impact center. With the same layup of AS4/3501-6, the 90° crack extended across the entire width of the specimen, while here it did not. At 4.0 m/s, a delamination shaped like a "figure 8" and bisected by a crack (78 mm total length) in the 90° direction can be seen. This delamination is symmetric about the impact center and its overall length is approximately 16 mm. A similar delamination (32 mm overall length) is caused by the 5.0 m/s impact. In this case, the 90° matrix crack extends to the edges of the specimen, as was observed with the AS4/3501-6 $[90_4/0_2]_s$ laminates. The delamination is bounded by the 90° matrix crack near the tips of the delamination. The delamination is not quite symmetric about the 90° crack, and borders the matrix crack for approximately 2 mm at each end. This delamination is shown in Figure 4.37 to occur at the lower interface of the laminate, where a similar delamination was observed in the AS4/3501-6 specimen of this layup. The major axis of the delamination follows the fiber direction of the 90° plies below it. In contrast to the impact damage in the



velocity = 1.5 m/s



velocity = 4.0 m/s



velocity = 5.0 m/s



1 cm

Figure 4.36 X-ray photographs of IM7G/X8553-50 $[90_4/0_2]_8$ specimens for impact velocities of (top) 1.5 m/s (incipient), (middle) 4.0 m/s, and (bottom) 5.0 m/s.

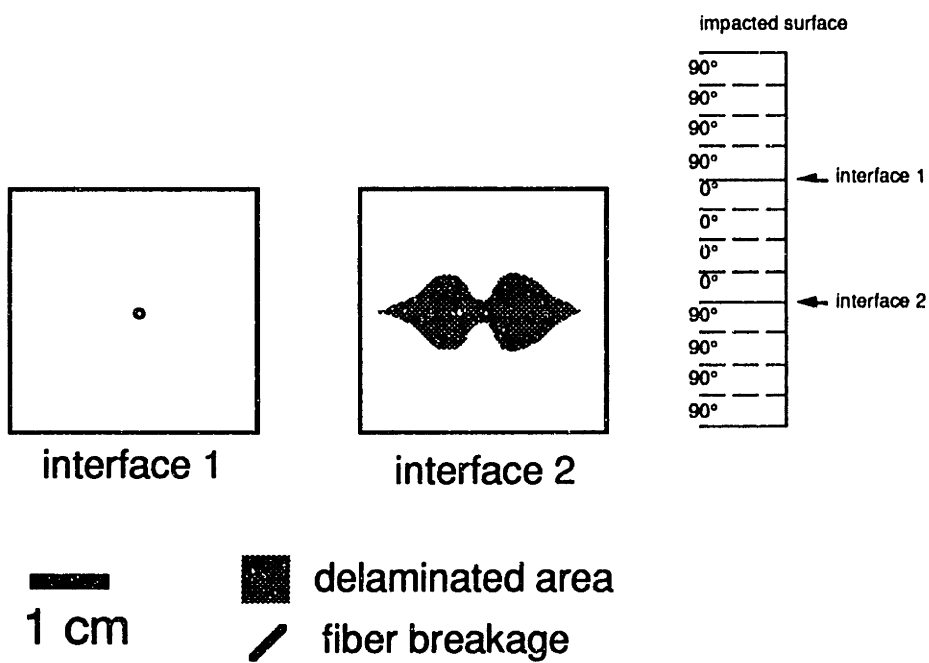
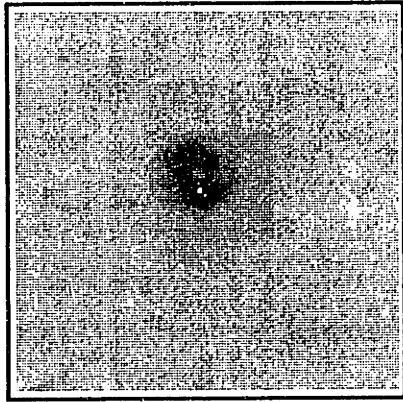


Figure 4.37 Deply transcription of IM7G/X8553-50 $[90_4/0_2]_s$ specimen impacted at 3.0 m/s.

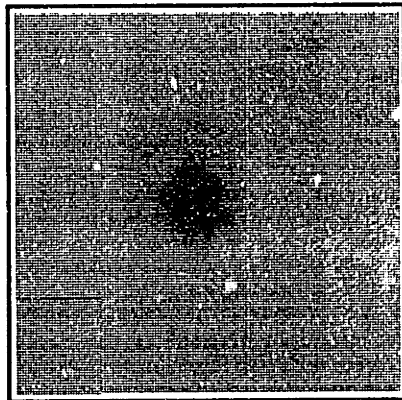
same layup of AS4/3501-6 where delamination occurred at both interfaces, delamination is observed only at the lower interface of this laminate.

4.3.3 A370-5H/3501-6S Material System

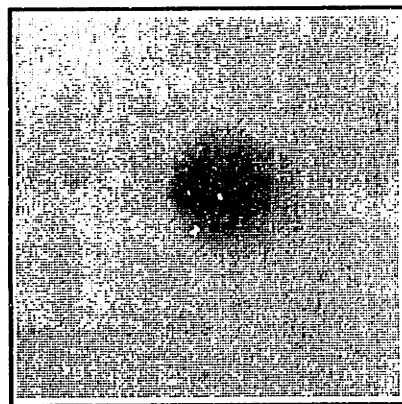
X-ray photographs of damaged $(45_2/0_2)_s$ specimens of A370-5H/3501-6S fabric are presented in Figure 4.38. The incipient damage velocity is 4.1 m/s, but the incipient damage mode is not easily identified. What appear to be many small cracks can be seen near the center of impact in the X-ray photographs. The damage from the 4.1 and 4.5 m/s impacts is confined to a circular region of approximately 10 mm diameter. No areas of delamination like those observed with the 16-ply tape laminates are readily identified. The damage from the 5.0 m/s impact is confined to a circular region of 13 mm diameter, and a dark line can be seen within this region. This line is approximately 5 mm in length and runs in the -45° direction. This is identified as fiber damage from the deply transcription in Figure 4.39. An additional broken tow, which could not be seen in the X-ray photograph, was found via deply in the upper ply of the laminate. A total of three broken tows of fibers were found in the upper two plies of the specimen. The broken tows ran in the $+45^\circ$ direction in these plies. This fiber damage pattern is very similar to that observed in the $[(\pm 45)_2/(0/90)_2]_s$ layup of AS4/3501-6 impacted at 5.0 m/s, but no delamination was observed here. In both cases, broken $+45^\circ$ fibers were noted near, but not directly under, the center of the impact. No other damage was observed from the deply of the fabric specimen. Because of the woven nature of the fabric plies, the surfaces of the plies were not as smooth as the tape plies when separated during deply. With the deply technique, the traces of gold chloride often could only be observed by holding the ply at a certain angle to a light source and observing the reflected light. The uneven surface of the fabric



velocity = 4.1 m/s



velocity = 4.5 m/s



velocity = 5.0 m/s



1 cm

Figure 4.38 X-ray photographs of A370-5H/3501-6S $(45_2/0_2)_S$ specimens for impact velocities of (top) 4.1 m/s (incipient), (middle) 4.5 m/s, and (bottom) 5.0 m/s.

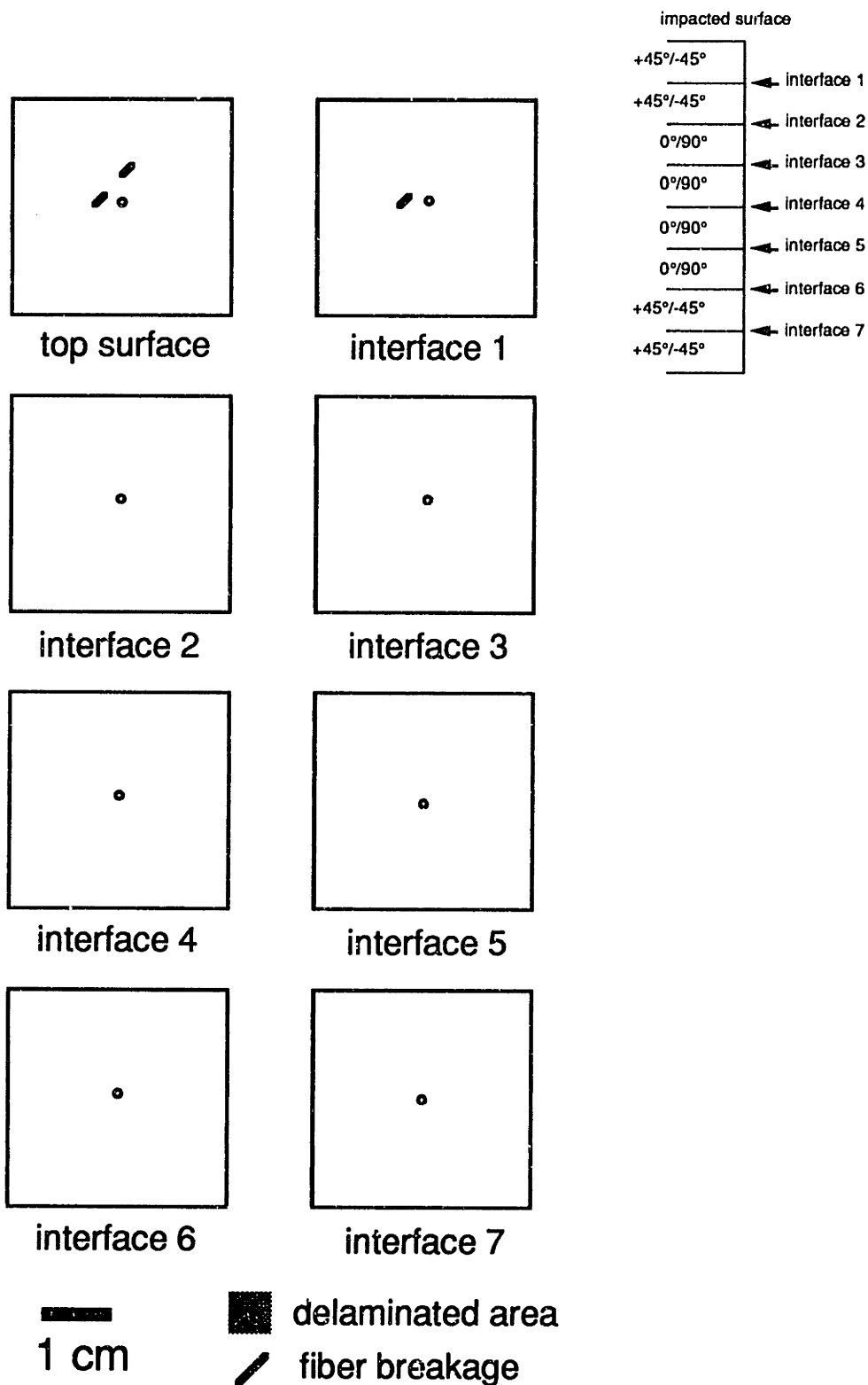


Figure 4.39 Deply transcription of A370-5H/3501-6S $(45_2/0_2)_s$ specimen impacted at 5.0 m/s.

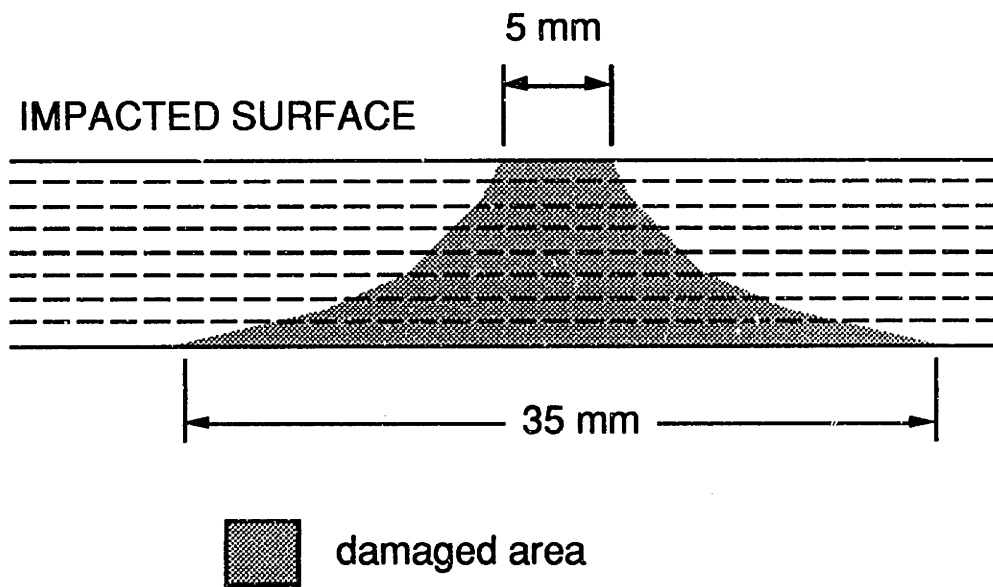
plies scattered light in many directions, and made detecting any traces of gold chloride very difficult. Hence, the deply technique would not be recommended for identifying interlaminar-type damage with woven materials.

4.3.4 Glass/Epoxy Material System

The damage states of the glass/epoxy specimens are presented in Figures 4.40 through 4.45. The specimens of this material system were transparent and the damage was such that the appearance of the damaged material became opaque. With this material system, visual inspections of the impacted specimens indicated that damage first occurred at the rear surface of the specimens. One specimen (impacted at 5.0 m/s) was cross-sectioned through the impact center, and the damage was found to expand radially as one travels through the thickness of the laminate, as shown in Figure 4.40. The diameter of the damaged area is approximately 5 mm at the impacted surface and flares out to a much larger diameter (approximately 35 mm) at the back surface.

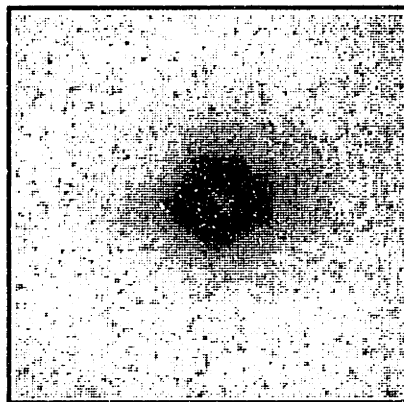
Photographs of the damage states from 3.0 and 5.0 m/s impacts are shown for the $(45_2/0_2)_s$ layup of glass/epoxy in Figure 4.41. The damage from a 3.0 m/s impact formed a ring of approximately 6 mm diameter around the center of impact. At the very center of this ring is an apparently undamaged circular region with a diameter of approximately 3 mm. The 5.0 m/s impact caused an elliptical region of damage which is longer in the 0° direction than in the 90° direction. The major and minor axes of the damaged area are approximately 10 and 7.5 mm, respectively. This damage appears consistent near the point of contact, such that no undamaged inner circle can be detected.

The damage states from 3.0 and 5.0 m/s impacts for the $(90_2/0_2)_s$ layup are presented in Figure 4.42. A ring of damage similar to that of the previous

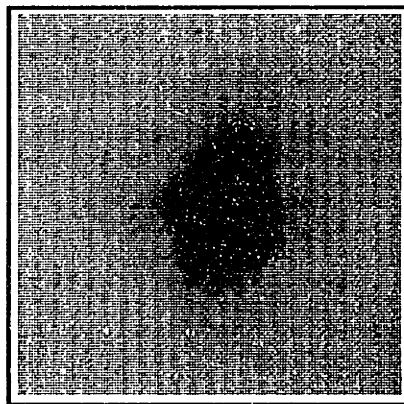


NOTE: Drawing not to scale.

Figure 4.40 Illustration of cross-section of glass/epoxy (45/0)_{2s} specimen impacted at 5.0 m/s.



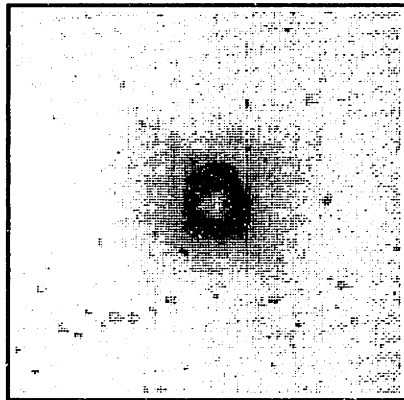
velocity = 3.0 m/s



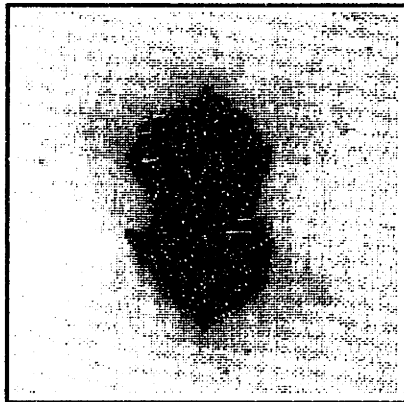
velocity = 5.0 m/s


1 cm

Figure 4.41 Photographs of glass/epoxy $(45_2/0_2)_s$ specimens impacted at (top) 3.0 m/s and (bottom) 5.0 m/s.



velocity = 3.0 m/s



velocity = 5.0 m/s


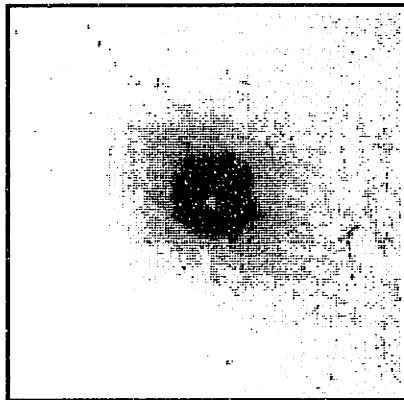
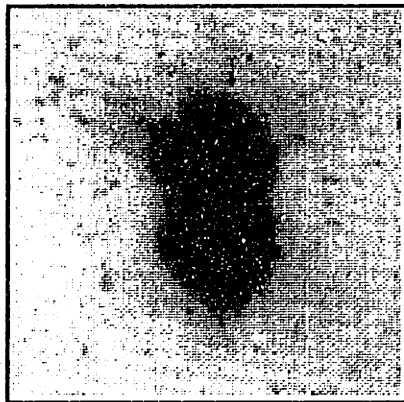

1 cm

Figure 4.42 Photographs of glass/epoxy $(90_2/0_2)_s$ specimens impacted at (*top*) 3.0 m/s and (*bottom*) 5.0 m/s.



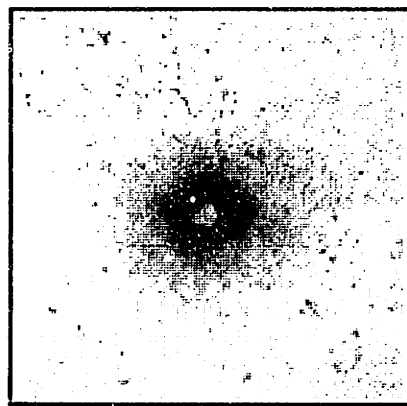
velocity = 3.0 m/s



velocity = 5.0 m/s


1 cm

Figure 4.43 Photographs of glass/epoxy $(0_2/45_2)_s$ specimens impacted at (*top*) 3.0 m/s and (*bottom*) 5.0 m/s.



velocity = 3.0 m/s


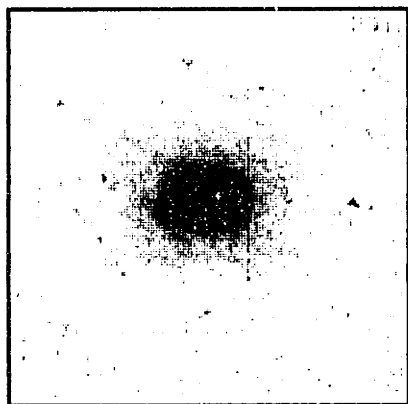
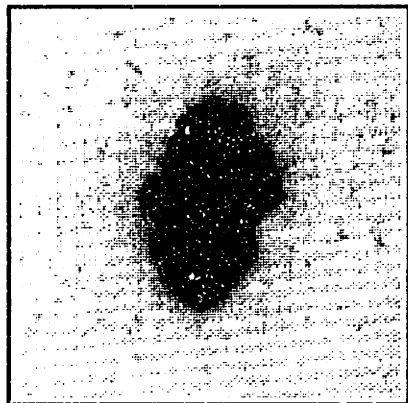

1 cm

Figure 4.44 Photograph of glass/epoxy $(45/0)_{2s}$ specimen impacted at 3.0 m/s.



velocity = 3.0 m/s



velocity = 5.0 m/s


1 cm

Figure 4.45 Photographs of glass/epoxy $(0/45)_{2S}$ specimens impacted at (*top*) 3.0 m/s and (*bottom*) 5.0 m/s.

layup resulted from the 3.0 m/s impact. The outer diameter of the ring is 5 mm and the diameter of the undamaged region in the center is approximately 2 mm. The damage resulting from the 5.0 m/s impact has the shape of a "figure 8" and is aligned with the 0° direction. Its longest dimension is approximately 18 mm. Again, no undamaged inner circle is visible from this impact velocity.

Similar damage states are observed for the $(0_2/45_2)_s$ layup, as shown in Figure 4.43. The 3.0 m/s impact caused a ring of damage with a diameter of approximately 5 mm, and the diameter of the undamaged region in the center is approximately 1.5 mm. The damaged region from the 5.0 m/s impact has a "figure 8" shape and it is aligned with the 0° direction. Its longest dimension is approximately 16 mm, and an undamaged inner region is not apparent.

The damage state from the 3.0 m/s impact is shown for the $(45/0)_{2s}$ layup in Figure 4.44. As with the three previous layups, a ring of damage is observed with a diameter of approximately 5 mm. The undamaged region within this ring has a diameter of approximately 2 mm. A 5.0 m/s impact was not performed for this laminate.

The damage from the 3.0 and 5.0 m/s impacts for the $(0/45)_{2s}$ layup are presented in Figure 4.45. The 3.0 m/s impact caused a ring of damage similar to those observed with the previous layups of this material system. The diameter of the ring is approximately 5 mm, and there appear to be undamaged areas within the ring. The 5.0 m/s impact created an elliptical damage area with its major axis aligned with the 0° direction. The dimensions of the major and minor axes of this area are approximately 15 mm and 10 mm, respectively, and there exists no undamaged inner circle.

4.3.5 General Characteristics

Matrix cracking was the incipient damage mode in the 12-ply laminates of both the AS4/3501-6 and the IM7G/X8553-50 material systems. Matrix cracks were generally accompanied by delaminations at the rearmost interface of the laminates at higher impact velocities. The delaminations in the $[\pm 45_2/0_2]_s$, $[\pm 60_2/0_2]_s$ and $[90_4/0_2]_s$ laminates generally had a "figure 8" shape, and were aligned with the fiber direction of the ply at the interface further away from the impacted surface. The delaminations in the $[\pm 15_2/0_2]_s$ laminates had an "S" shape, and were anti-symmetric about the impact center.

The incipient damage data are summarized in Table 4.1. In all cases, the incipient damage velocities and forces were lower for the AS4/3501-6 laminates than for laminates of IM7G/X8553-50 of the same layup. All four of the 12-ply AS4/3501-6 laminates were penetrated by the 5.0 m/s impact, and the peak forces before penetration are shown in Table 4.1. The force needed to penetrate the AS4/3501-6 $[90_4/0_2]_s$ laminate (1700 N) was significantly lower than that for the other three AS4/3501-6 laminates (typically 2300 N).

The $[\pm 45_2/0_2/90_2]_s$ laminate was more easily damaged than the $[(\pm 45)_2/(0/90)_2]_s$ laminate, and both of these were more easily damaged than the A370-5H/3501-6S fabric laminate, in terms of incipient damage force. The incipient damage mode in the 16-ply tape laminates appeared to be matrix cracking. Large delaminations were observed from the 5.0 m/s impact in the $[\pm 45_2/0_2/90_2]_s$ laminate, while smaller, more numerous delaminations occurred in the $[(\pm 45)_2/(0/90)_2]_s$ laminate, which has more ply interfaces. In addition, fiber damage occurred in the $[(\pm 45)_2/(0/90)_2]_s$ laminate which was not observed in the $[\pm 45_2/0_2/90_2]_s$ laminate impacted at the same velocity. Of the

Table 4.1 Summary of Incipient Damage Forces and Velocities

Layup	Material System	Incipient Damage Velocity (m/s)	Incipient Damage Force (N)	Penetration Force (N)
[±15 ₂ /0 ₂] _s	AS4/3501-6	1.1	400	2400
	IM7G/X8553-50	1.3	500	--
[±45 ₂ /0 ₂] _s	AS4/3501-6	1.2	450	2300
	IM7G/X8553-50	2.2	1000	--
[±60 ₂ /0 ₂] _s	AS4/3501-6	0.9	275	2250
	IM7G/X8553-50	2.2	950	--
[90 ₄ /0 ₂] _s	AS4/3501-6	0.9	300	1700
	IM7G/X8553-50	1.5	650	--
[±45 ₂ /0 ₂ /90 ₂] _s	AS4/3501-6	2.1	1000	--
[(+45) ₂ /(0/90) ₂] _s	AS4/3501-6	3.0	1550	--
(45 ₂ /0 ₂) _s	A370-5H/3501-6S	4.1	2400	--
	Glass/Epoxy	1.5	600	--
(90 ₂ /0 ₂) _s	Glass/Epoxy	1.5	600	--
(0 ₂ /45 ₂) _s	Glass/Epoxy	1.5	550	--
(45/0) _{2s}	Glass/Epoxy	1.5	550	--
(0/45) _{2s}	Glass/Epoxy	1.5	550	--

two tape laminates, the damaged region (as viewed via X-ray) was larger with the $[\pm 45_2/0_2/90_2]_s$ layup. The 5.0 m/s impact caused fiber damage in the A370-5H/3501-6S fabric laminate, but without any observable interlaminar failure. The damage was confined to a smaller region in the fabric laminate than in either of the 16-ply tape laminates.

The damage behavior of all of the glass/epoxy laminates was very similar, regardless of layup. It is difficult to determine the incipient damage mode in these laminates, although the damage was detected visually and appeared to be matrix crazing. Neither the X-ray dye nor the gold chloride penetrated into this damage, so it is likely that the matrix damage here was different from the matrix cracking encountered in the graphite/epoxy laminates. The incipient damage velocity of all of the glass/epoxy laminates was the same, and the damage states observed were also similar. A characteristic ring of damage around the center of impact resulted from the 3.0 m/s impacts in all five layups. The glass/epoxy $(45_2/0_2)_s$ laminate was damaged by a much lower force than the same layup of A370-5H/3501-6S.

Chapter 5

DISCUSSION

5.1 Force-Time Signatures

Several important observations can be made from the force data taken during the impact experiments. Specifically, it is of interest to note how the force history is affected by layup, material system, damage to the laminate, and impact velocity. Selected force-time signatures were presented in the previous chapter, and all of the force-time data obtained during this investigation can be found in Appendix A.

5.1.1 Effect of Layup

The 12-ply laminates of AS4/3501-6 and IM7G/X8553-50 were constructed in a $[\pm\theta_2/0_2]_s$ layup format with θ taking on the values 15° , 45° , 60° and 90° . Hence, the effect of the angle θ can be observed on the impact signatures in these laminates. It was found that this angle had very little effect on the impact signatures when penetration did not occur. Although the laminate bending stiffnesses were affected dramatically by this angle (see Table 5.1), the peak force and duration of impact were virtually unaffected by the layup angle. The peak impact force is plotted versus impact velocity for the AS4/3501-6 and IM7G/X8553-50 laminates in Figures 5.1 and 5.2. It can be seen from these figures that the peak force was not influenced by layup angle. For the 12-ply layups of AS4/3501-6, the peak contact force for a given impact velocity is independent of layup for impact velocities below 3.0 m/s. Laminates of all four layups were penetrated by the 5.0 m/s impact, and some deviation of the peak force can be seen. Most notably, the peak force before penetration of the

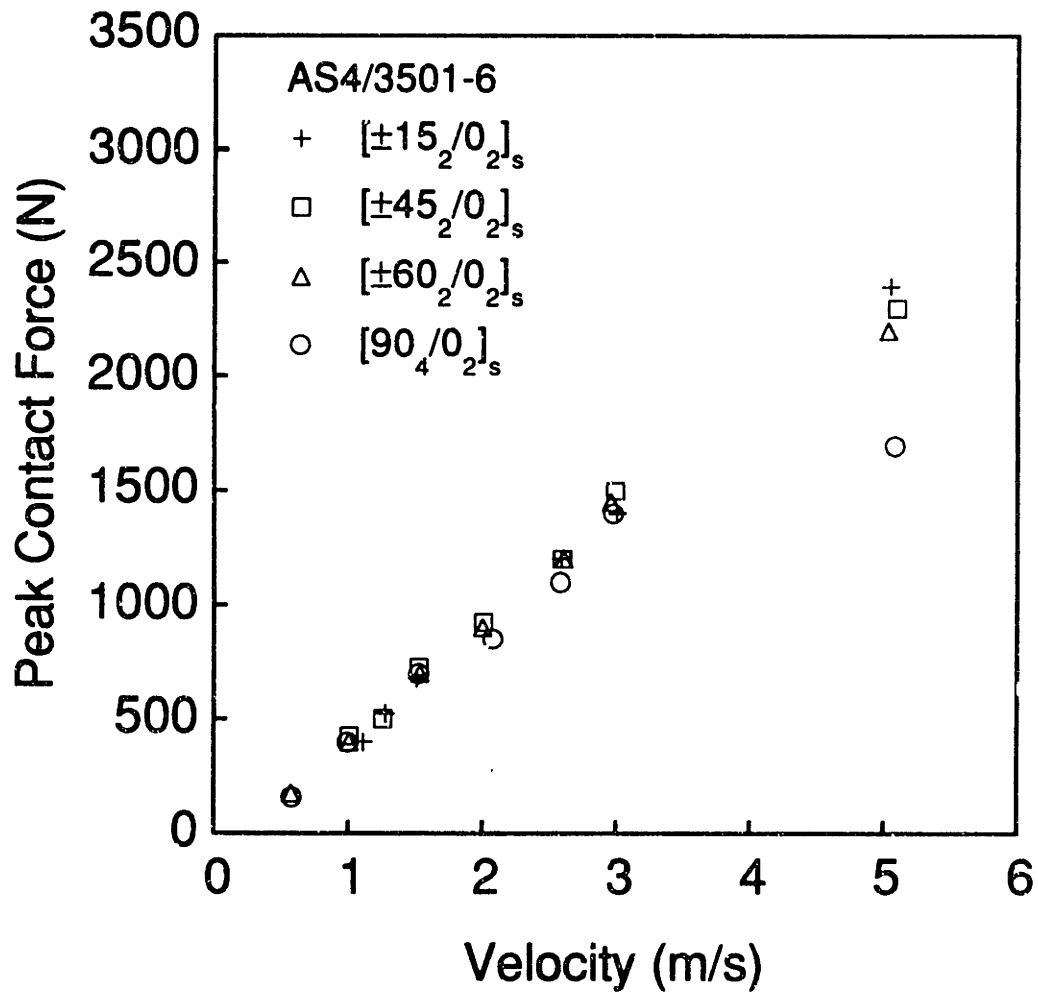


Figure 5.1 Peak force versus impact velocity for the 12-ply AS4/3501-6 layups.

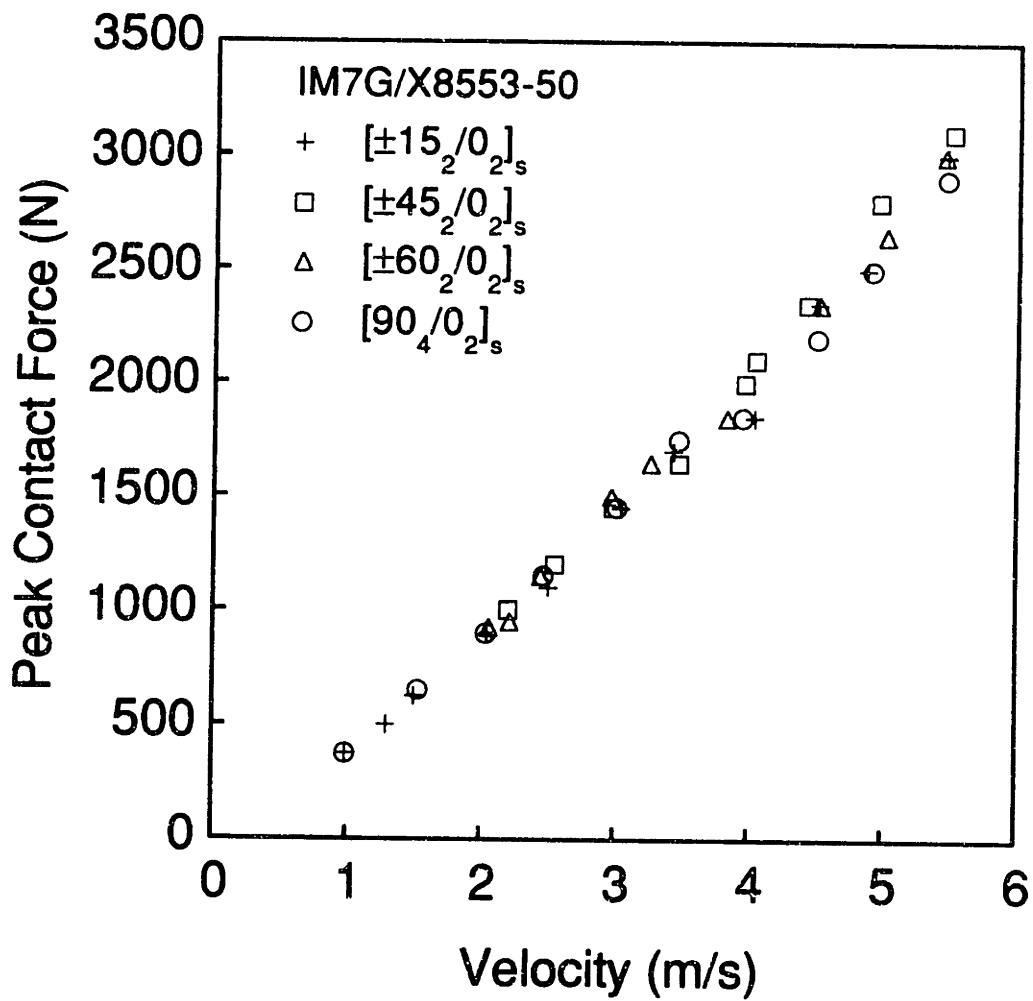


Figure 5.2 Peak force versus impact velocity for the 12-ply IM7G/X8553-50 layups.

$[90_4/0_2]_s$ layup was approximately 500 N lower than those of the other three layups. Penetration did not occur with any of the IM7G/X8553-50 layups, and peak force is shown to be virtually independent of layup for impact velocities through 5.5 m/s.

Impact duration is also not significantly affected by the layup angle θ . Impact duration is plotted versus impact velocity for the 12-ply layups of AS4/3501-6 and IM7G/X8553-50 in Figures 5.3 and 5.4. It can be seen in these graphs that the impact duration decreased with increasing impact velocity, but the impact duration does not appear to be affected by the layup.

Comparison of specific force versus time signatures gives further insight into the effect of layup. Although the bending stiffness in the x_1 direction (D_{1111}) of the AS4/3501-6 $[\pm 15_2/0_2]_s$ laminate is 8 times greater than that of the AS4/3501-6 $[90_4/0_2]_s$ laminate (see Table 5.1), the peak force and duration from a 3.0 m/s impact are nearly identical, as shown in Figure 5.5. This indicates that the major bending stiffness (D_{1111}) is not the dominant factor in shaping the force-time history of the impact. However, the secondary oscillations, and thus the overall signatures for these two cases, are somewhat different. The parameters which control the various aspects of the signature, such as the shape of the secondary oscillations, have not been identified. There is a need to better understand the relationship between individual factors (such as laminate properties or material properties) and the characteristics of the signature.

The differences in layup of the two 16-ply AS4/3501-6 laminates did not affect their force-time signatures, as can be seen in Figure 5.6. The signature for the 5.0 m/s impact of the laminate with ply grouping $[\pm 45_2/0_2/90_2]_s$ is virtually identical to that of the $[(\pm 45)_2/(0/90)_2]_s$ laminate. The peak forces are nearly the same (approximately 2700 N) and the secondary oscillations overlap.

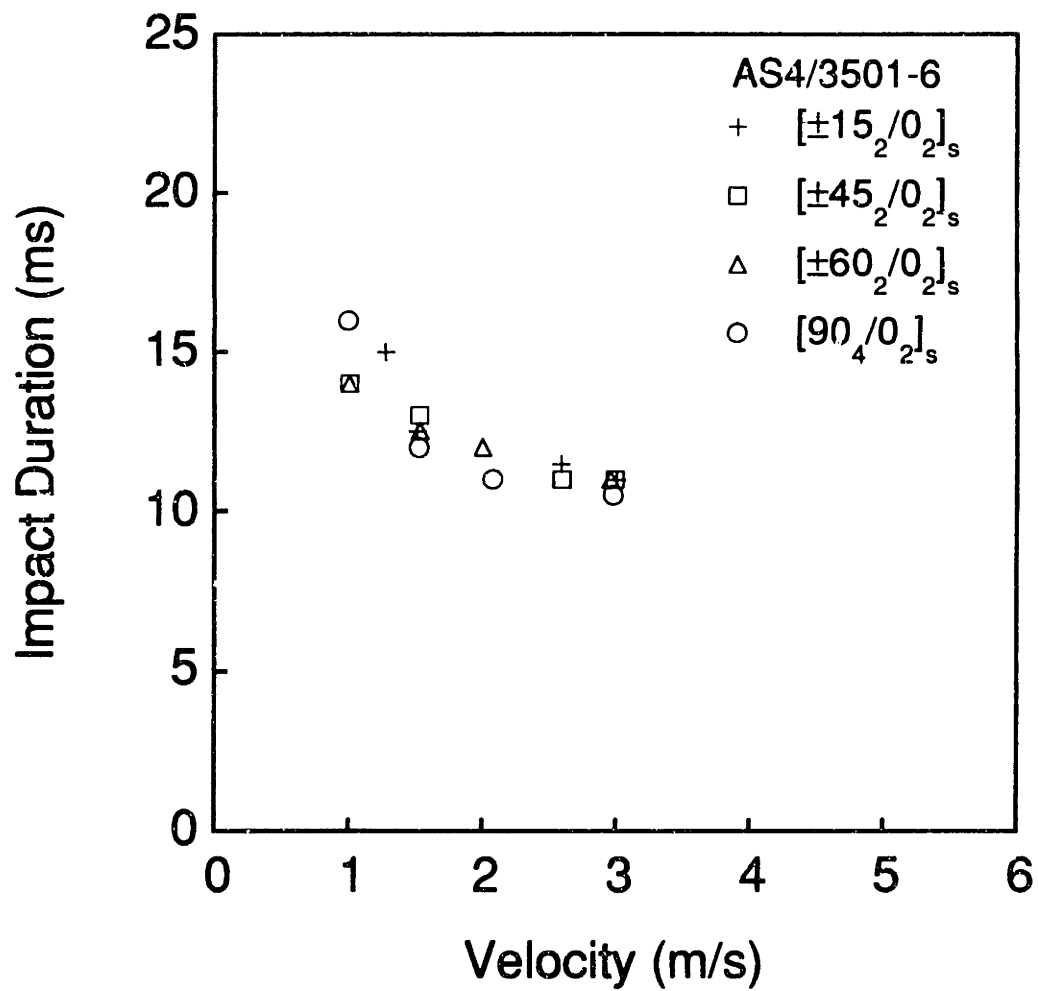


Figure 5.3 Impact duration versus impact velocity for the 12-ply AS4/3501-6 layups.

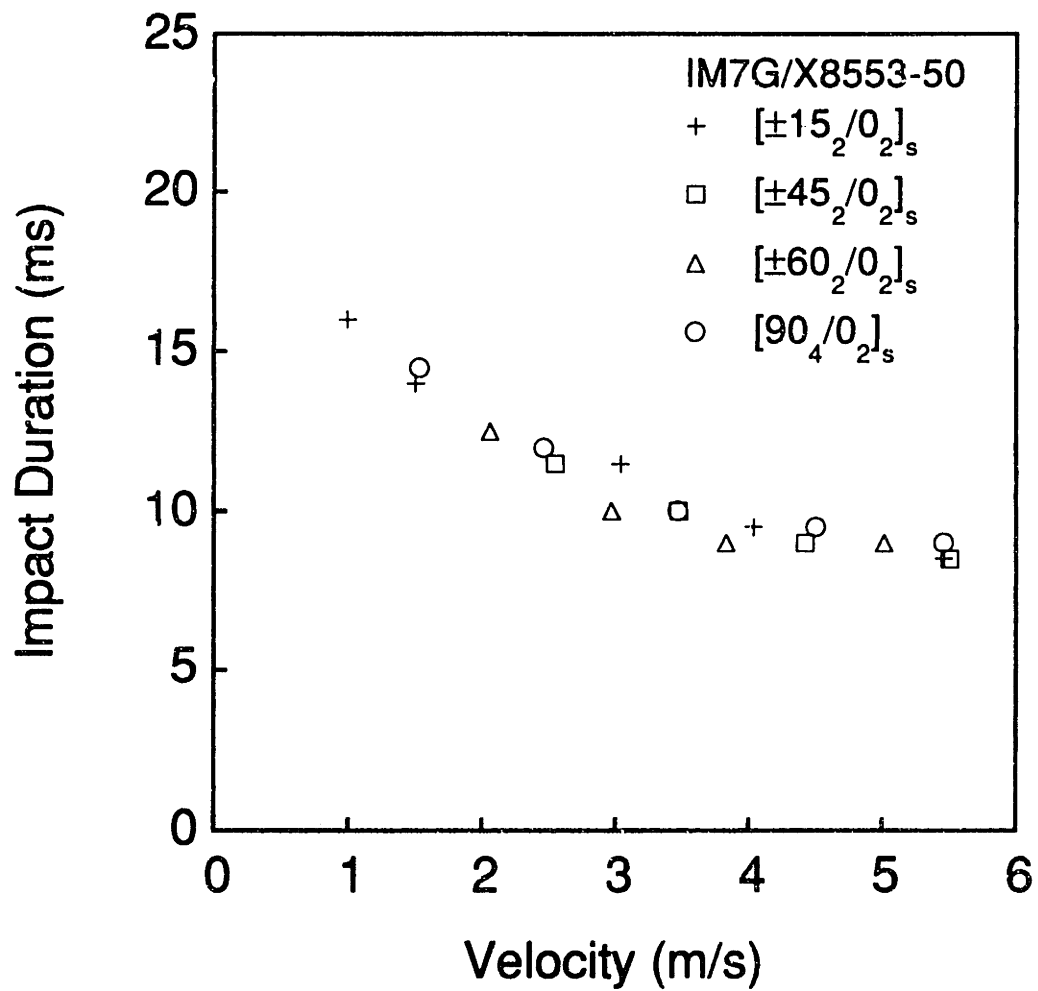


Figure 5.4 Impact duration versus impact velocity for the 12-ply IM7G/X8553-50 layups.

Table 5.1 Laminate Properties of the $[\pm\theta_2/0_2]_s$ Layups of AS4/3501-6 and IM7G/X8553-50

Layup	Material System	D_{1111} [N·m]	D_{2222} [N·m]	A_{1111} [MN/m]	A_{2222} [MN/m]
$[\pm 15_2/0_2]_s$	AS4/3501-6	44.0	3.83	212	17.2
	IM7G/X8553-50	59.5	4.24	245	16.1
$[\pm 45_2/0_2]_s$	AS4/3501-6	17.1	15.4	126	54.2
	IM7G/X8553-50	22.5	20.2	144	59.8
$[\pm 60_2/0_2]_s$	AS4/3501-6	8.54	29.0	98.1	98.1
	IM7G/X8553-50	10.8	38.9	111	111
$[90_4/0_2]_s$	AS4/3501-6	5.13	47.8	87.2	158
	IM7G/X8553-50	6.00	64.7	98.2	182

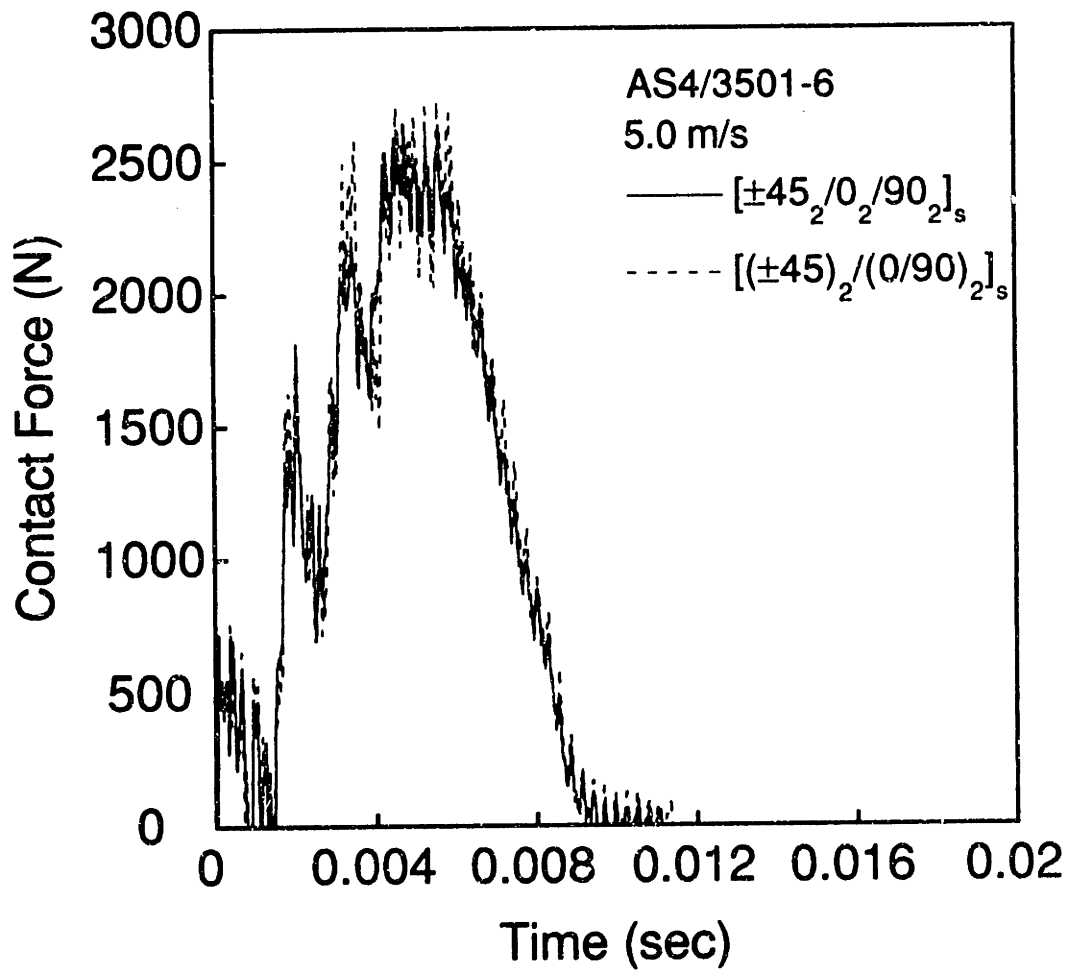


Figure 5.6 Signatures of AS4/3501-6 $[\pm 45_2/0_2/90_2]_s$ and $[(\pm 45)_2/(0/90)_2]_s$ laminates impacted at 5.0 m/s.

The laminate stiffnesses of these two layups were nearly the same, as shown in Table 5.2. The extensional properties (A_{1111} and A_{2222}) are independent of stacking sequence by definition, and the bending stiffnesses are nearly the same for the two layups. In addition, the signatures of the 16-ply layups were nearly the same, in terms of peak force and duration, as the signatures of the 12-ply layups. A comparison between the 3.0 m/s signatures of the $[\pm 45_2/0_2/90_2]_s$ laminate and the $[\pm 15_2/0_2]_s$ laminate, which is typical of the 3.0 m/s signatures of all of the 12-ply layups, is shown in Figure 5.7. It can be seen here that the peak force and impact duration of the 16-ply laminates are not significantly different than those of the 12-ply laminates.

The signatures of the glass/epoxy laminates were not affected significantly by layup. The 3.0 m/s signatures are virtually identical for all five layups used, and a typical comparison is shown in Figure 5.8.

5.1.2 Effect of Material System

The material system was found to have no effect on the signatures of the 12-ply laminates of AS4/3501-6 and IM7G/X8553-50 when penetration did not occur. The 3.0 m/s impact signatures of the four 12-ply laminates of AS4/3501-6 and IM7G/X8553-50 material systems are compared in Figures 5.9 through 5.12. The signatures of the laminates of these two material systems with the same layup are nearly identical despite the fact that the ply elastic properties of these material systems are not the same, as shown in Table 5.3. The longitudinal ply modulus (E_L) of AS4/3501-6 is 142 GPa, while that of the IM7G/X8553-50 ply is 152 GPa, which is a 7% difference. The ply thicknesses of these material systems are also different. The nominal ply thickness is 0.134 mm for AS4/3501-6 compared to 0.144 mm for IM7G/X8553-50. This amounts to a significant difference in the bending stiffnesses, as shown in Table 5.1. For

Table 5.2 Laminate Properties of the 16-Ply AS4/3501-6 Laminates and 8-Ply Fabric Laminates of A370-5H/3501-6S and Glass/Epoxy

Laminate	Material System	D_{1111} [N·m]	D_{2222} [N·m]	A_{1111} [MN/m]	A_{2222} [MN/m]
$[\pm 45_2/0_2/90_2]_s$	AS4/3501-6	45.8	35.5	131	131
$[(\pm 45)_2/(0/90)_2]_s$	AS4/3501-6	43.2	38.1	131	131
$(45_2/0_2)_s$	A370-5H/3501-6S	85.4	85.5	162	162
$(45_2/0_2)_s$	Glass/Epoxy	9.42	9.42	31.3	31.3

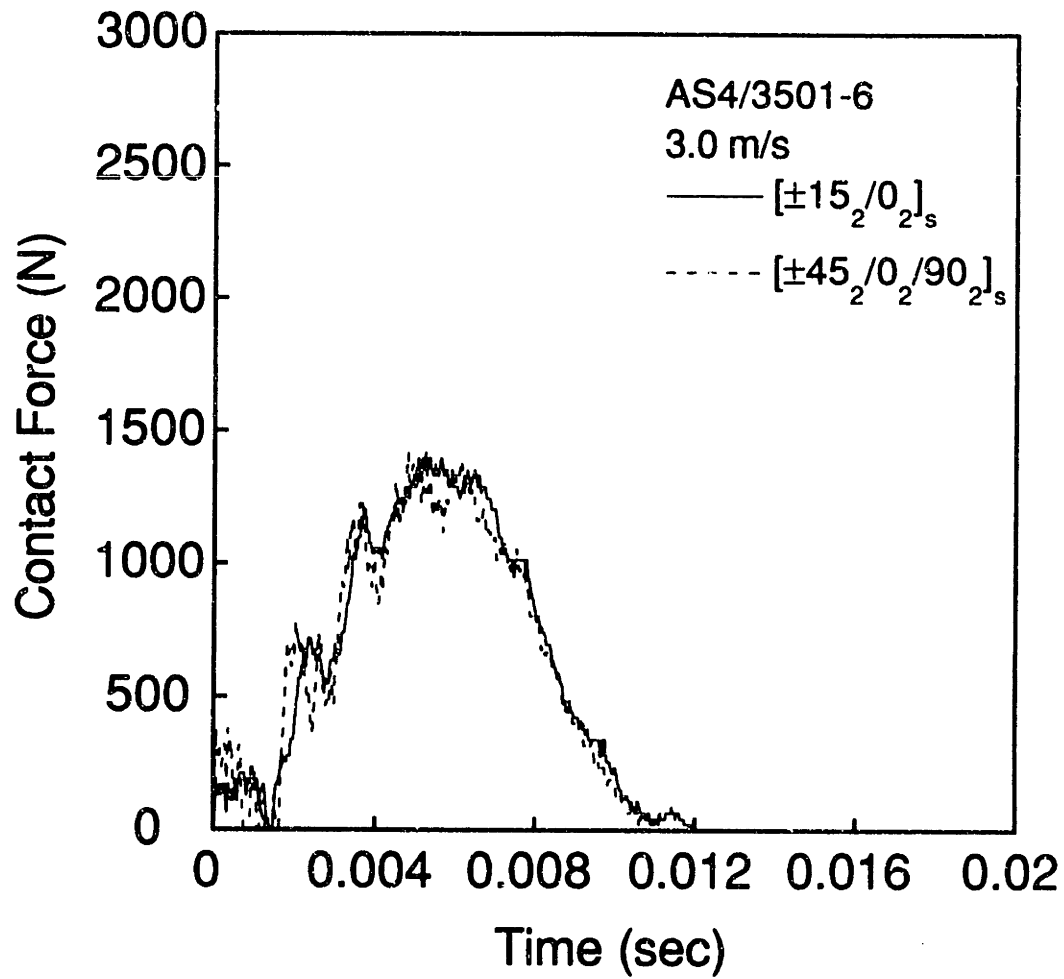


Figure 5.7 Signatures of AS4/3501-6 $[\pm 45_2/0_2/90_2]_s$ and $[\pm 15_2/0_2]_s$ laminates impacted at 3.0 m/s.

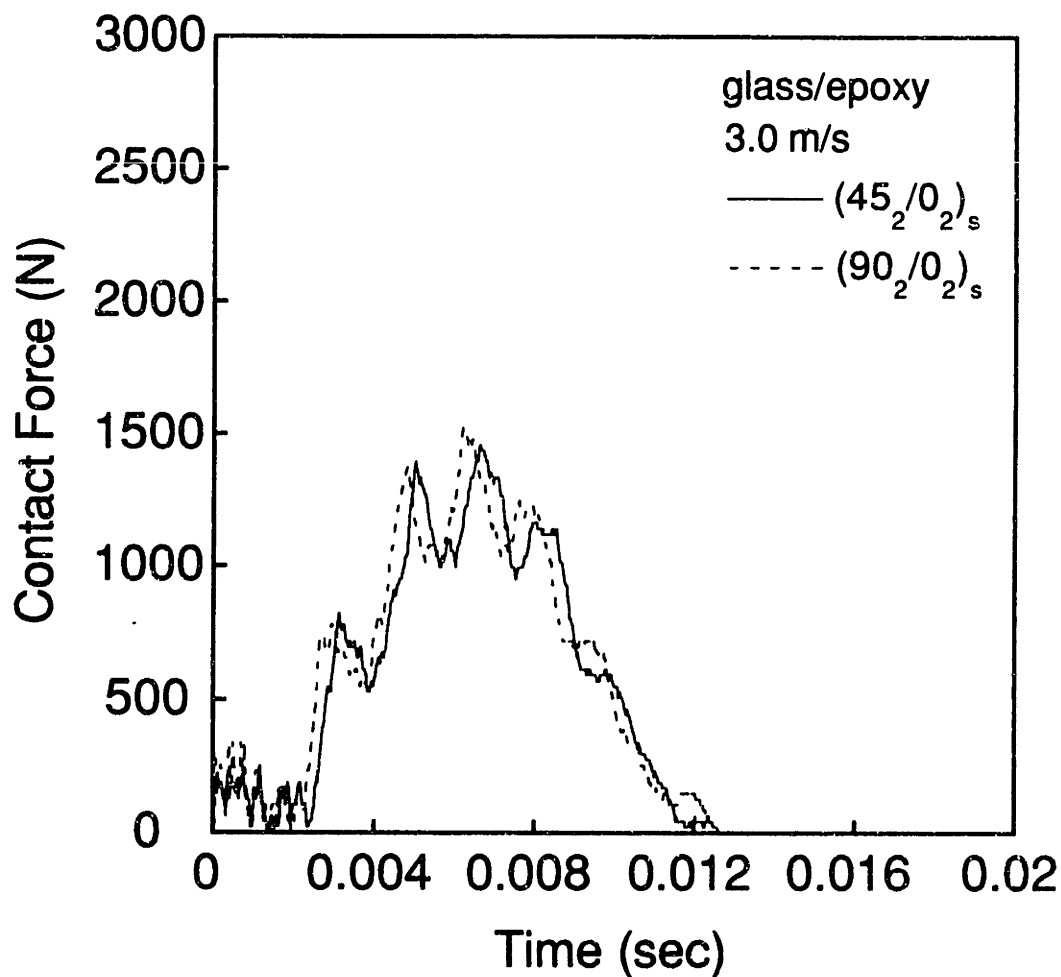


Figure 5.8 Force-time signatures of glass/epoxy $(45_2/0_2)_s$ and $(90_2/0_2)_s$ laminates impacted at 3.0 m/s.

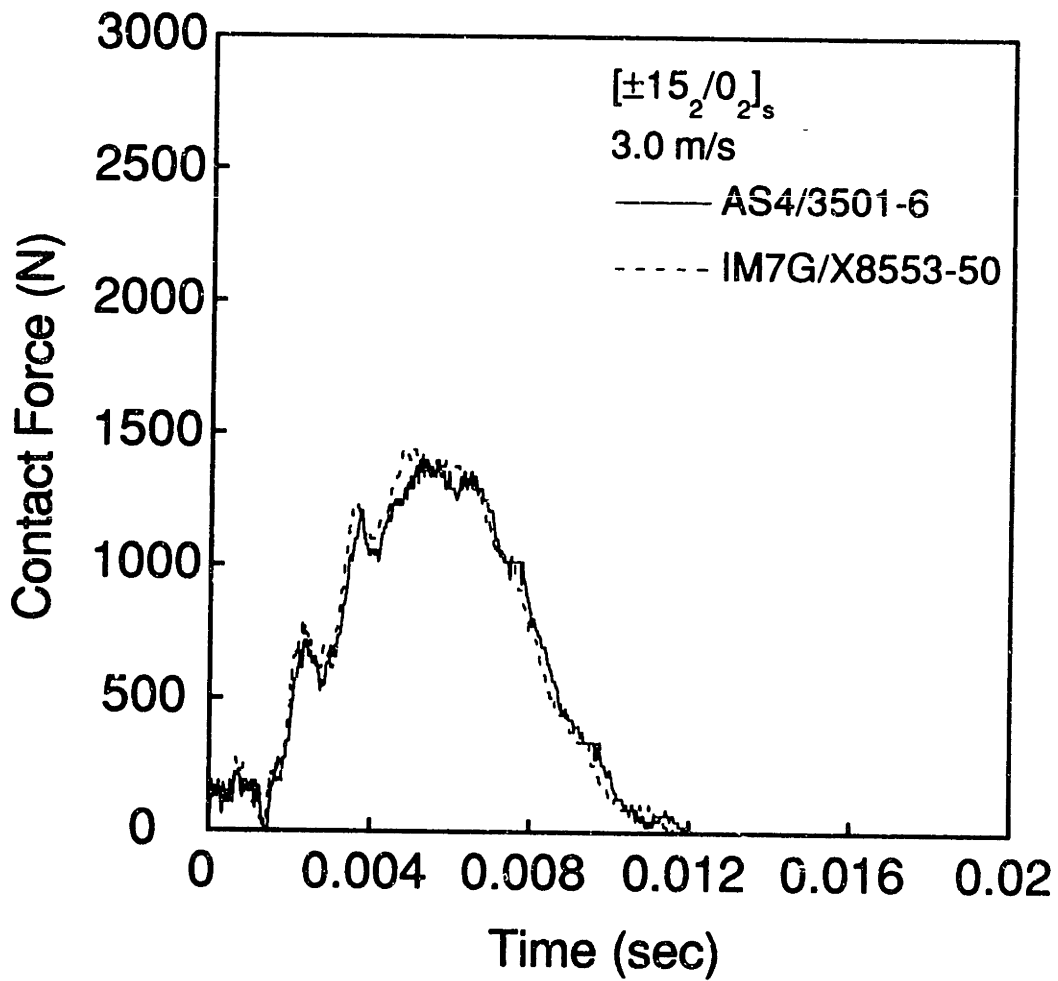


Figure 5.9 Signatures of $[\pm 15_2/0_2]_s$ laminates of AS4/3501-6 and IM7G/X8553-50 impacted at 3.0 m/s.

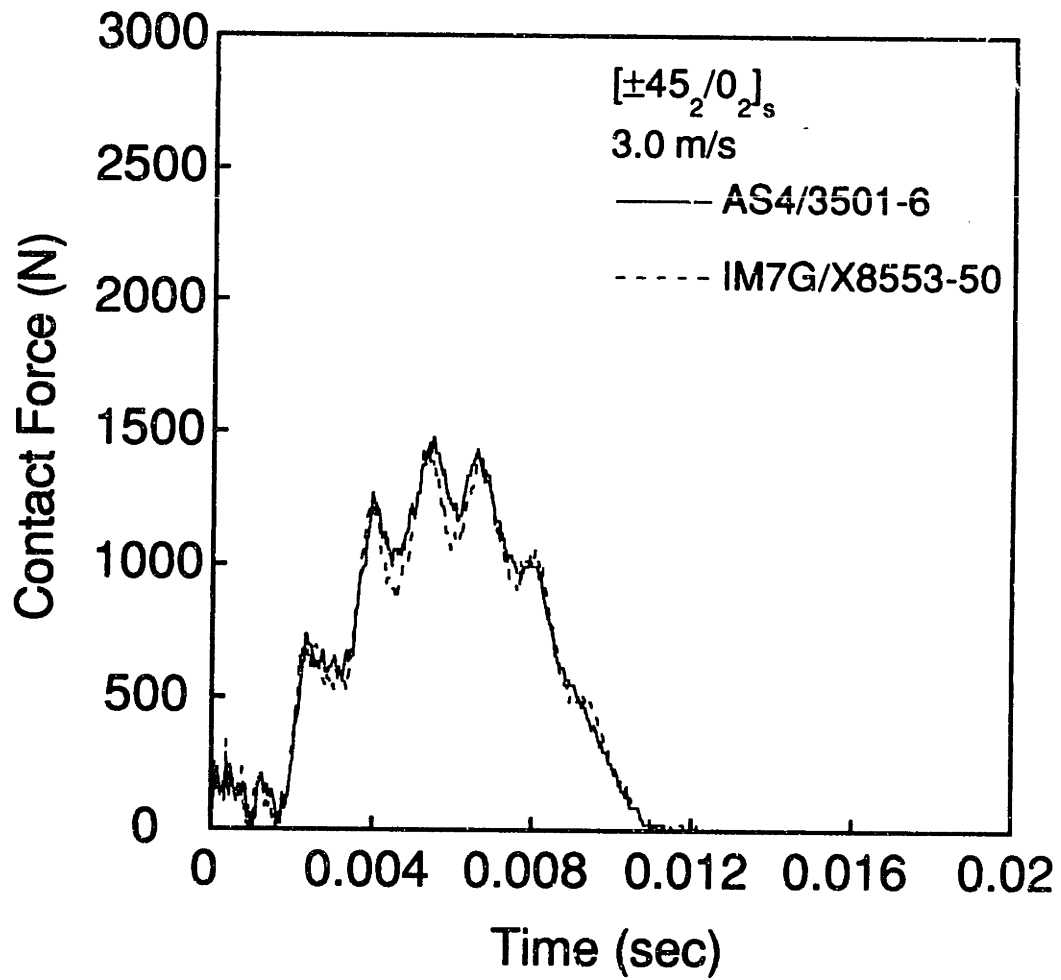


Figure 5.10 Signatures of $[\pm 45_2/0_2]_s$ laminates of AS4/3501-6 and IM7G/X8553-50 impacted at 3.0 m/s.

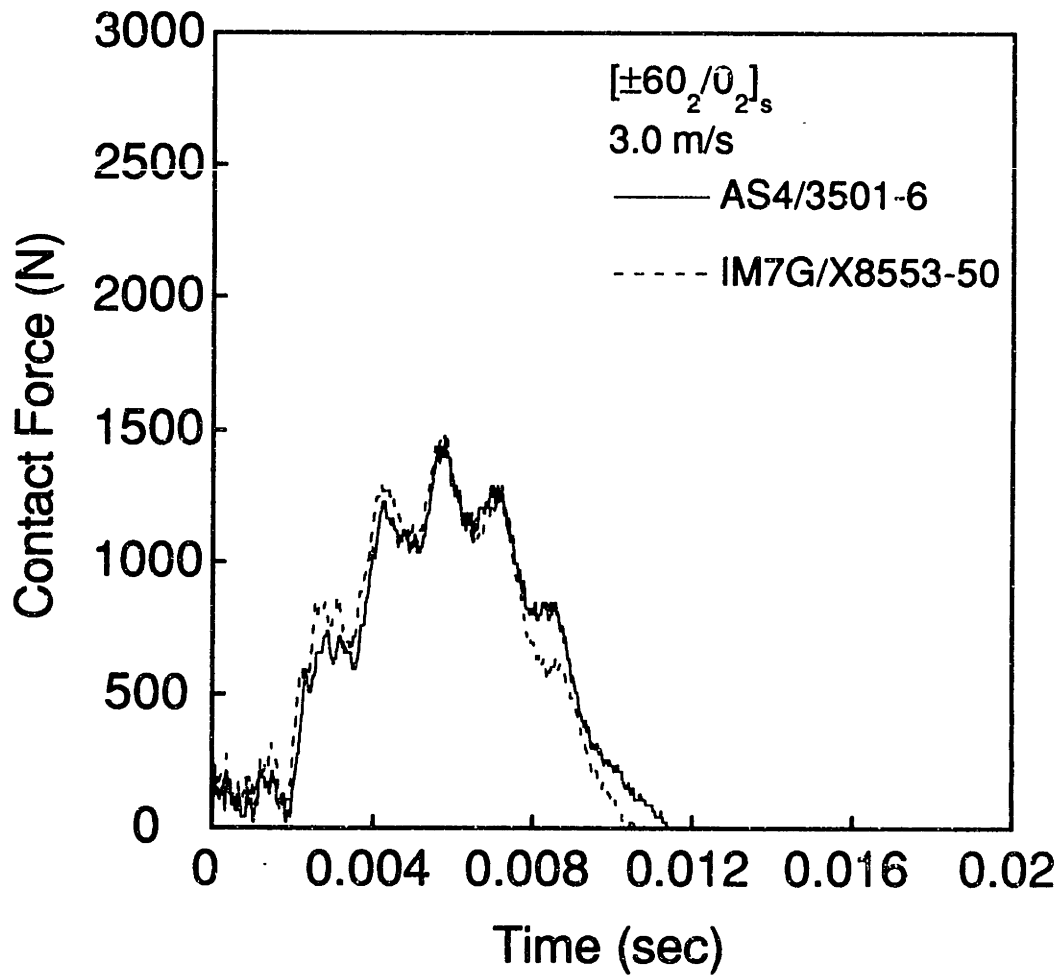


Figure 5.11 Signatures of $[\pm 60_2/0_2]_s$ laminates of AS4/3501-6 and IM7G/X8553-50 impacted at 3.0 m/s.

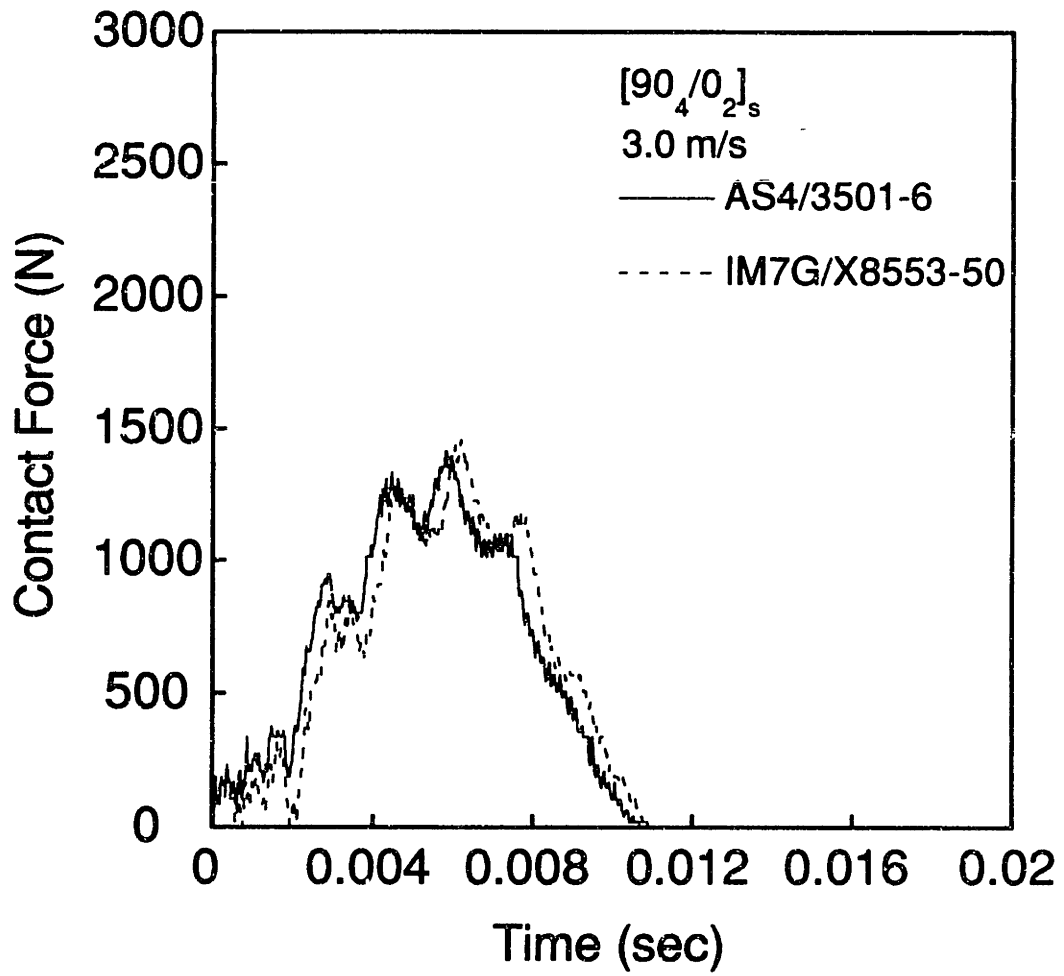


Figure 5.12 Signatures of $[90_4/0_2]_s$ laminates of AS4/3501-6 and IM7G/X8553-50 impacted at 3.0 m/s.

Table 5.3 Ply (Elastic) Properties of the Material Systems

Material System	E_L [GPa]	E_T [GPa]	ν_{LT}	G_{LT} [GPa]	t_{ply} [mm]
AS4/3501-6	142	9.81	0.30	6.0	0.134
IM7G/X8553-50	152	8.27	0.30	5.9	0.144
A370-5H/3501-6S	72.5	72.6	0.06	4.4	0.350
Glass/Epoxy	18.6	18.6	0.06	1.0	0.260

example, the bending stiffness in the x_1 direction (D_{1111}) for the IM7G/X8553-50 $[\pm 15_2/0_2]_s$ laminate is 34% higher than that for the same layup of AS4/3501-6. Also, the extensional stiffness (A_{1111}) of the same IM7G/X8553-50 laminate is higher than that of the AS4/3501-6 laminate by 15%. However, these differences do not seem to have a discernible effect on the signatures of the laminates, indicating that neither the bending nor extensional stiffnesses are the only controlling factors in shaping the signatures of these impacts.

However, the signatures are affected greatly when penetration occurs. All of the 12-ply laminates of the AS4/3501-6 material system were penetrated from the 5.0 m/s impact, while the laminates of IM7G/X8553-50 sustained only internal damage. A typical example of the differences in the signatures is shown in Figure 5.13. Because penetration occurs, the contact forces on the AS4/3501-6 laminates do not reach the levels that they do in the IM7G/X8553-50 laminates. This behavior is further discussed in the next section.

The material system has an effect on the signatures of the fabric A370-5H/3501-6S laminate as compared to the 16-ply AS4/3501-6 laminates. A comparison of the signatures of the tape and fabric laminates is shown in Figure 5.14. The basic shapes of these signatures is the same, in terms of the primary and secondary oscillation patterns, but the amplitudes of the secondary oscillations are much greater with the fabric laminate. The bending and extensional stiffnesses of the A370-5H/3501-6S $(45_2/0_2)_s$ laminate are shown in Table 5.2. The bending stiffnesses for this laminate are typically twice those for either of the 16-ply AS4/3501-6 tape laminates and the extensional stiffness of the fabric laminate is 26% higher, as well. These differences in the bending and extensional stiffnesses may account for the difference in amplitudes of the secondary oscillations, but the individual contribution of each of the laminate properties remains unclear.

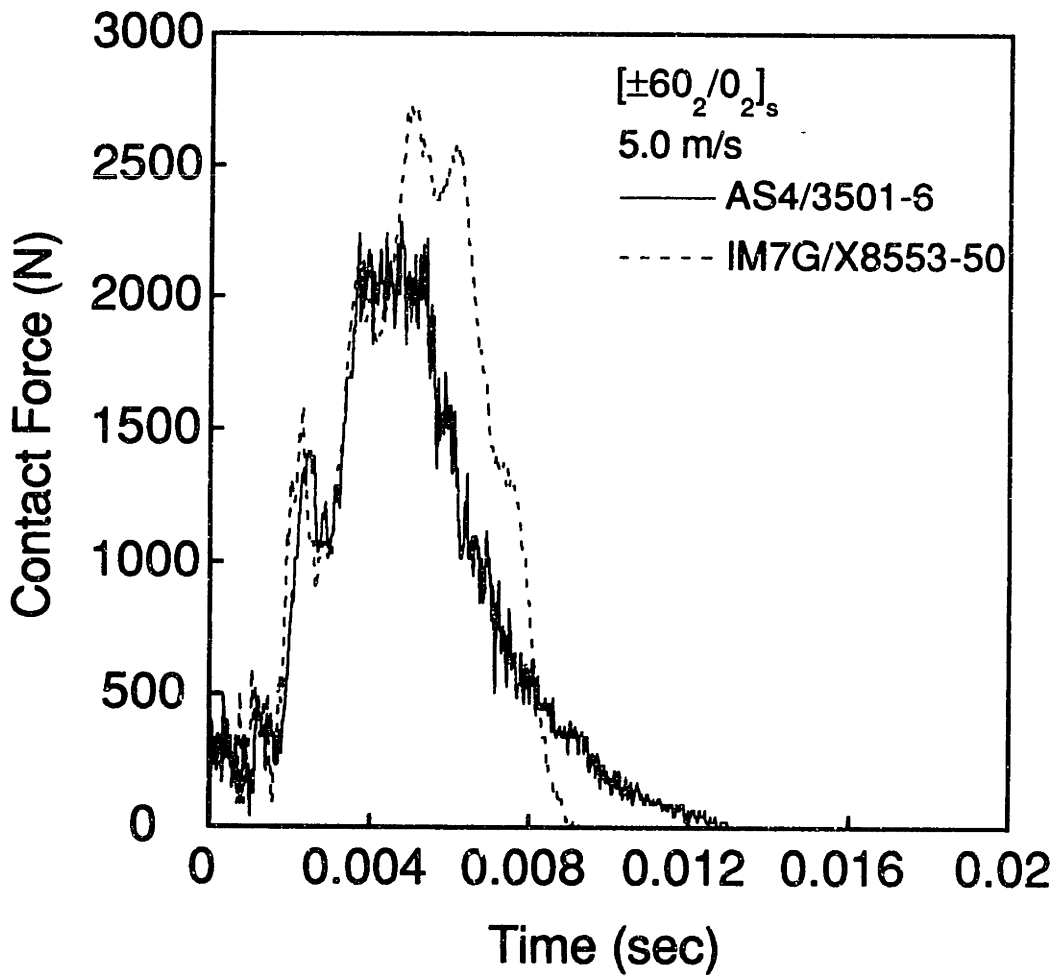


Figure 5.13 Signatures of $[\pm 60_2/0_2]_s$ laminates of AS4/3501-6 and IM7G/X8553-50 impacted at 5.0 m/s.

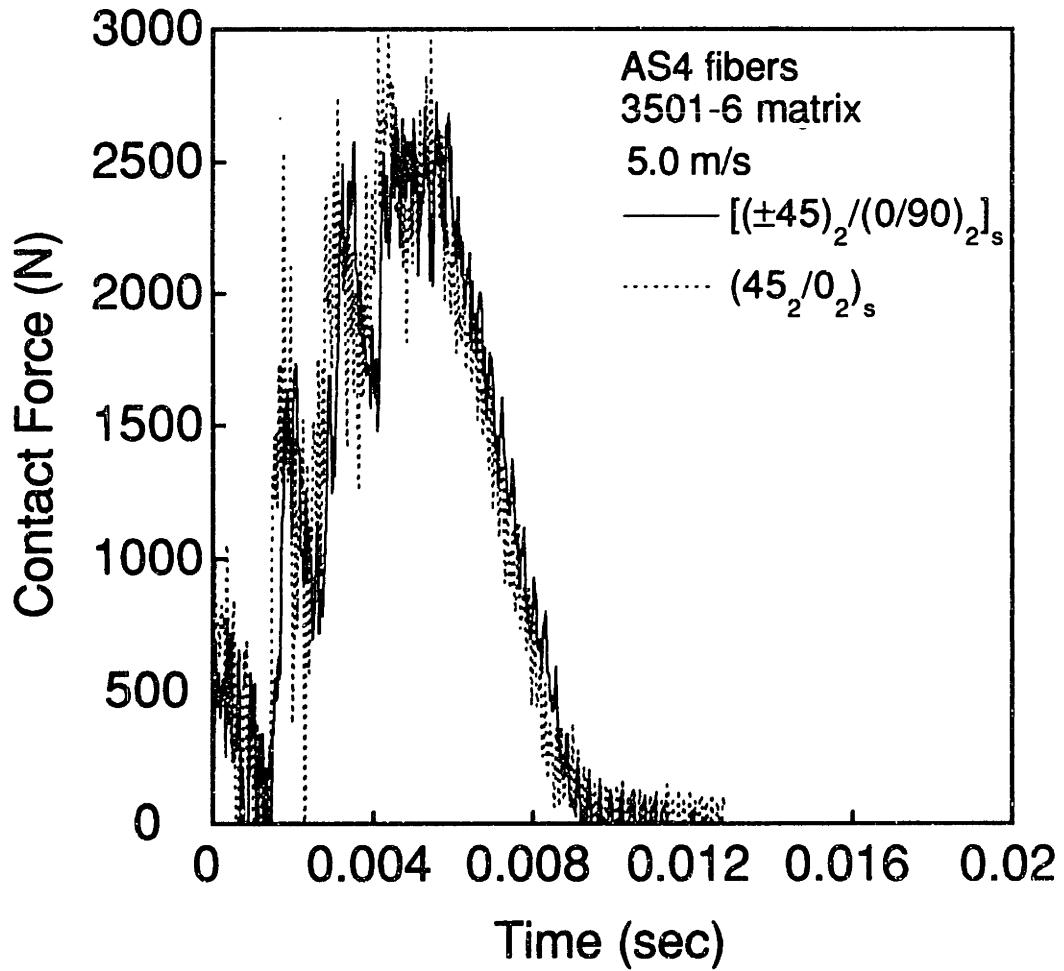


Figure 5.14 Signatures of AS4/3501-6 $[(\pm 45)_2 / (0/90)_2]_s$ and A370-5H/3501-6S $(45_2 / 0_2)_s$ laminates impacted at 5.0 m/s.

Differences can be noted in the signatures of the $(45_2/0_2)_s$ layup of glass/epoxy and A370-5H/3501-6S, as shown in Figure 5.15. The primary and secondary oscillations of the 5.0 m/s signatures of these $(45_2/0_2)_s$ laminates are clearly different. The graphite/epoxy signature has a higher peak (3000 N as compared to 2350 N) and a shorter duration (9 ms as compared to 10 ms). In addition, the amplitude of the secondary oscillations in the graphite/epoxy signature is much larger than in the glass/epoxy signature, and the frequency of the secondary oscillations in the graphite/epoxy signature appears to be higher. The differences in the appearance of these signatures should not be surprising in light of the differences in the bending and extensional stiffnesses of the two laminates (see Table 5.2). The bending stiffnesses (D_{1111} and D_{2222}) of the A370-5H/3501-6S laminate are typically 9 times those of the glass/epoxy laminate. The extensional stiffness (A_{1111}) of the graphite/epoxy laminate is 5 times that of the glass/epoxy laminate.

The peak forces in the signatures of the glass/epoxy specimens are comparable to those of the graphite/epoxy tape specimens at the same impact velocity. This can be seen for an impact velocity of 3.0 m/s in Figure 5.16. Despite the higher bending stiffnesses (D_{1111} and D_{2222}) of the graphite/epoxy laminate (see Tables 5.1 and 5.2), the peak impact force is virtually the same. The secondary oscillations differ somewhat, and the impact durations are typically slightly longer for the glass/epoxy specimens. The signatures shown here are typical for both the graphite/epoxy tape laminates and the glass/epoxy laminates.

5.1.3 Effect of Damage

One of the objectives of this investigation was to observe the force-time responses of impacted laminates and the relationship between impact damage

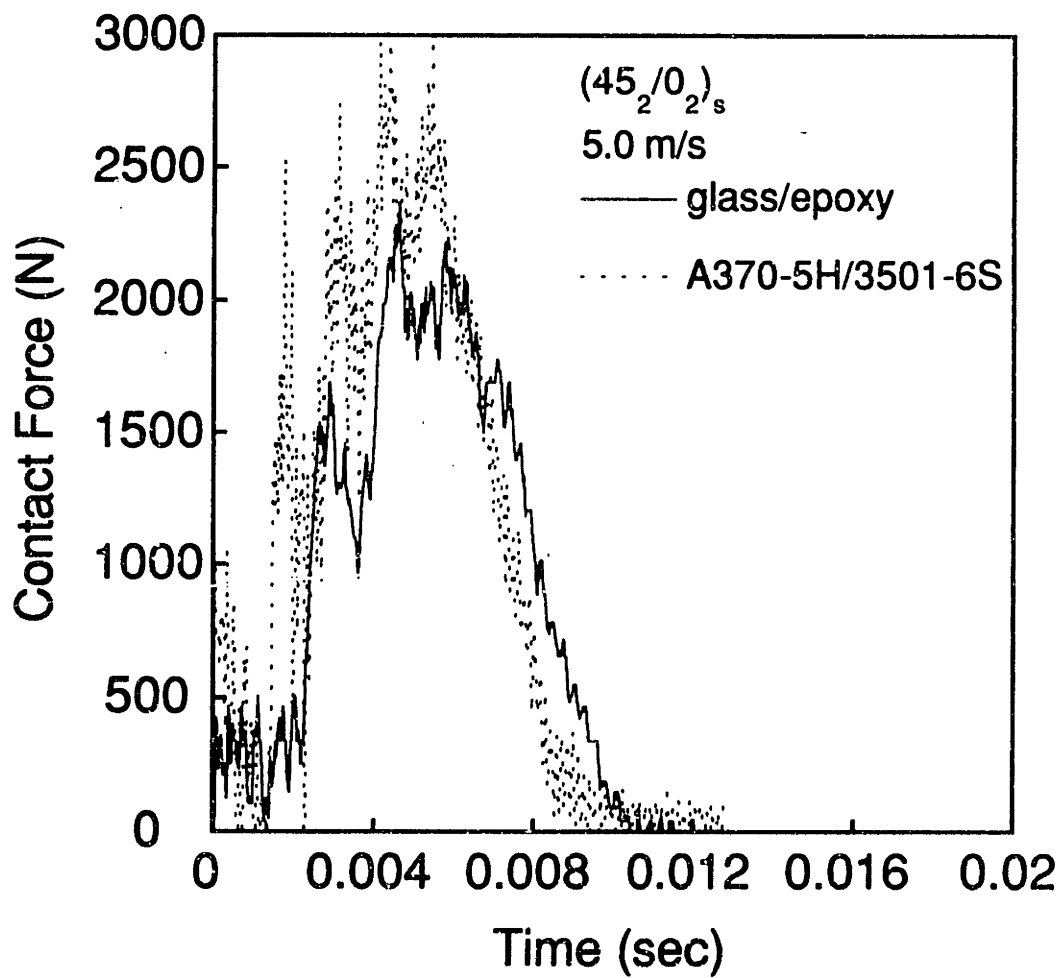


Figure 5.15 Signatures of A370-5H/3501-6S and glass/epoxy $(45_2/0_2)_s$ laminates impacted at 5.0 m/s.

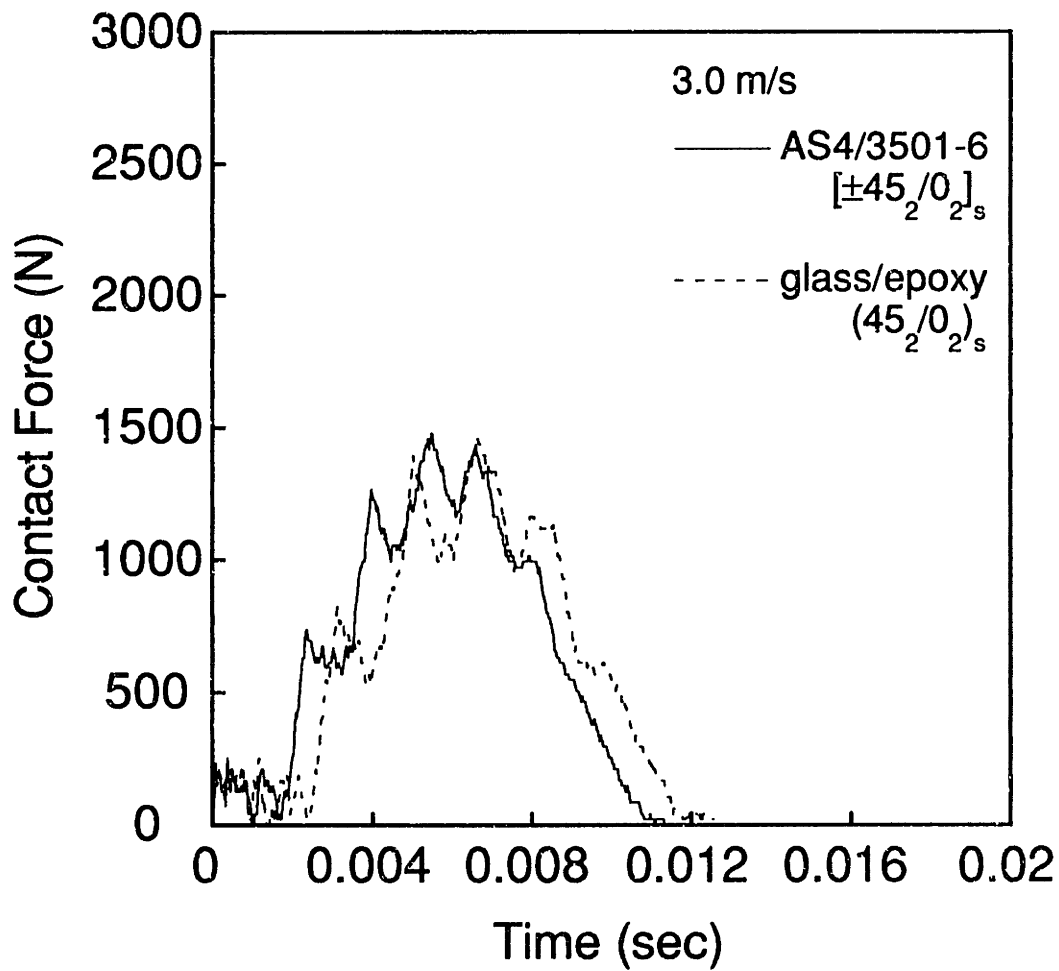


Figure 5.16 Signatures of AS4/3501-6 [±45₂/0₂]_s and glass/epoxy (45₂/0₂)_s laminates impacted at 3.0 m/s.

and the force-time signature. It was found that up until very heavy damage occurred within the laminate (i.e. penetration), the presence or formation of damage was found to have no apparent effect on the force-time history of the impact. At impact velocities which caused penetration of the laminates, a drop in the contact force occurs as the impactor penetrates the laminate, but up until very near this load drop, the presence of damage cannot be observed to have an effect on the signature.

The occurrence of incipient damage cannot be detected on the force-time histories of the impacts. A typical example of this is presented in Figure 5.17, where the signatures are shown for the IM7G/X8553-50 $[\pm 60_2/0_2]_s$ laminate impacted at 2.0 and 3.0 m/s. No damage was caused by the 2.0 m/s impact, but matrix cracking resulted from the 3.0 m/s impact. The signatures differ in duration and amplitude, but there is no characteristic difference in the shapes of the signatures which can be attributed to the formation of this incipient crack. This is a general result and applies to all of the laminates tested.

A change in the shape of the force-time signature cannot be observed from damage which is progressed well beyond the incipient stage, either. The force-time signature is unaffected by the presence of delaminations in addition to matrix cracks. This is a general result and is demonstrated for the $[\pm 45_2/0_2]_s$ layup in Figure 5.18. The force-time signatures of these $[\pm 45_2/0_2]_s$ laminates of AS4/3501-6 and IM7G/X8553-50 impacted at 3.0 m/s are nearly identical, yet very different damage states result in these specimens from this impact (see Figure 5.19). A single matrix crack exists in the IM7G/X8553-50 specimen, while matrix cracking and delamination are present in the AS4/3501-6 specimen. If the damage were to influence the force-time signature, differences would be expected in the signatures of these two

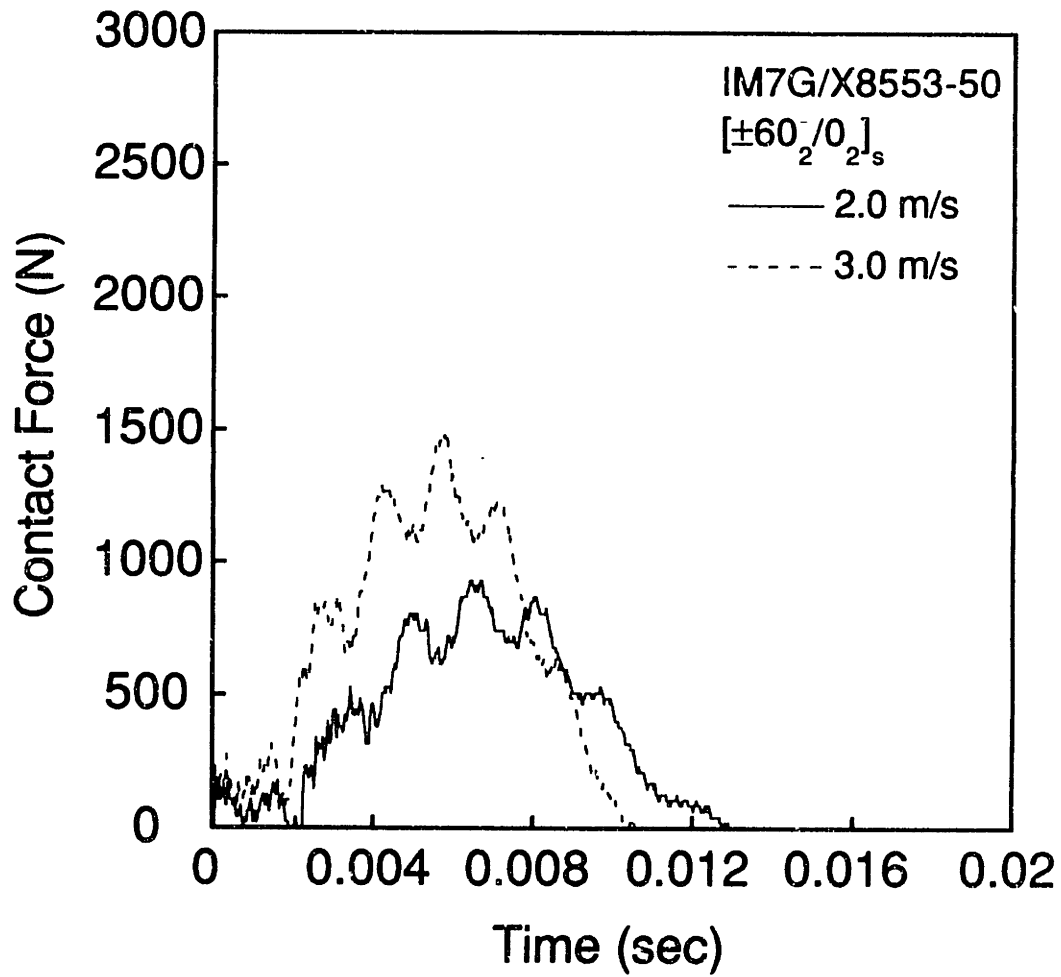


Figure 5.17 Signatures of IM7G/X8553-50 $[\pm 60_2/0_2]_s$ laminates for impact velocities of 2.0 m/s (undamaged) and 3.0 m/s (damaged).

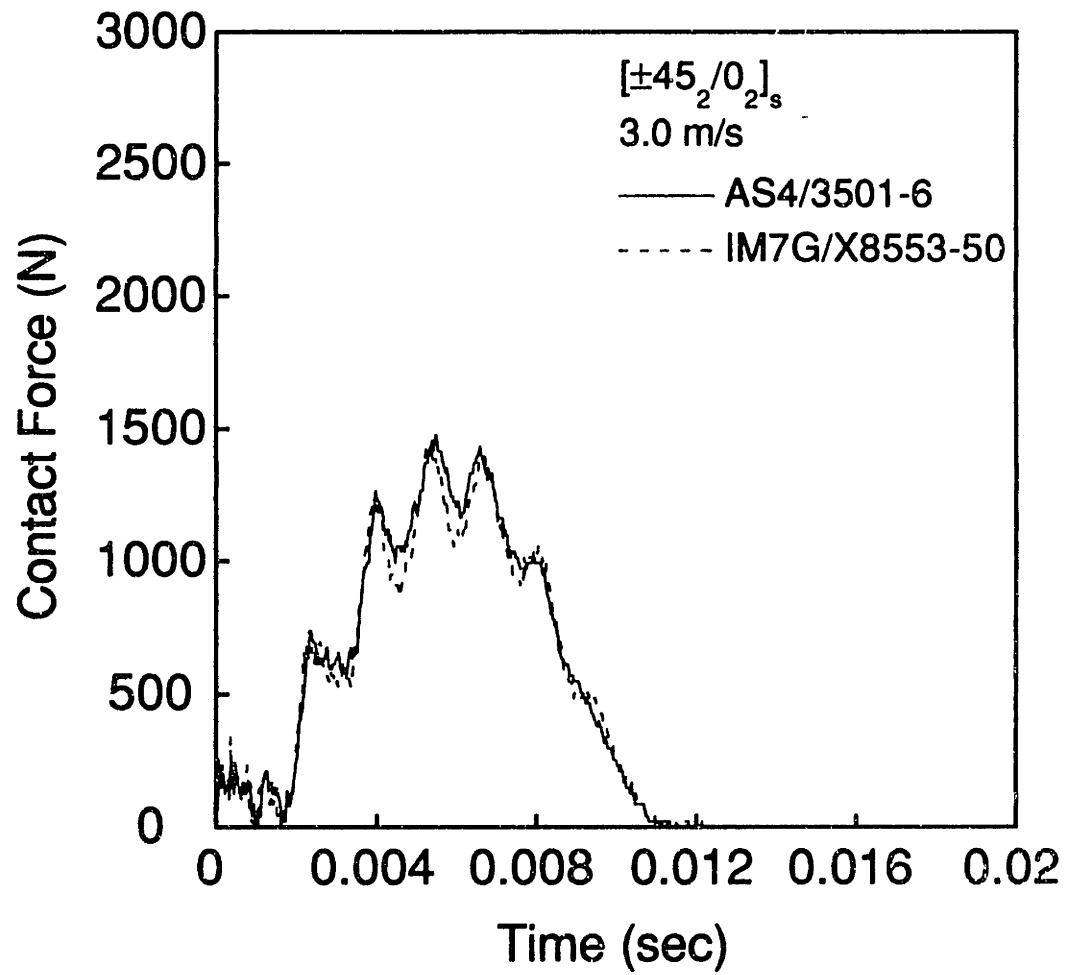
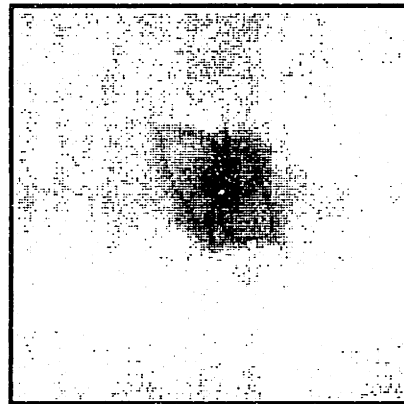
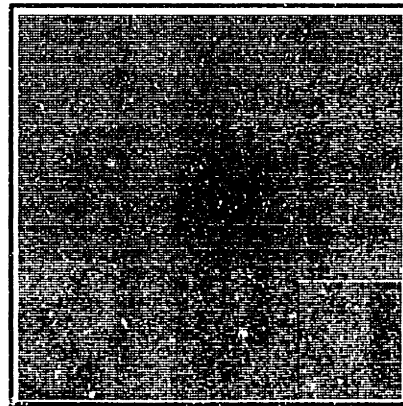


Figure 5.18 Signatures of $[\pm 45_2/0_2]_s$ laminates of AS4/3501-6 and IM7G/X8553-50 impacted at 3.0 m/s.



AS4/3501-6



IM7G/X8553-50

1 cm

Figure 5.19 X-ray photographs of $[\pm 45_2/0_2]_s$ laminates of (*upper*) AS4/3501-6 and (*lower*) IM7G/X8553-50 impacted at 3.0 m/s.

laminates with dissimilar damage states. However, this is clearly not the case here.

Penetration of the laminate by the impactor rod, however, can be seen on the force-time signature as a sharp drop in contact force. Up until the point of penetration, the signature is not visibly altered, as shown for the $[90_4/0_2]_s$ laminates of AS4/3501-6 and IM7G/X8553-50 in Figure 5.20. After approximately 4 ms, the contact force falls sharply in the signature of the AS4/3501-6 laminate as penetration occurs. Up until this point, the signatures of the IM7G/X8553-50 and AS4/3501-6 laminates nearly coincide. As the contact force of the penetrated AS4/3501-6 laminate trails off, the contact force in the unpenetrated laminate continues to rise to reach a peak (2600 N) which is much higher than the force (1700 N) which penetrated the AS4/3501-6 laminate. In this way, penetration of the impactor is observed to limit the peak force in the impacts of the 12-ply AS4/3501-6 laminates.

5.1.4 Effect of Impact Velocity

Several observations can be made regarding the effect of impact velocity on the force-time signatures of the laminates. First, it can be seen (see Figures 5.1 and 5.2) that the peak force scales approximately linearly with impact velocity for the 12-ply graphite/epoxy laminates (excluding those impacts which caused penetration). Second, it can be observed (see Figures 5.3 and 5.4) that impact duration decreases with increasing impact velocity in a nonlinear way. Finally, it can be seen that as the impact velocity increases, the secondary oscillations become less pronounced in the signature after the peak force. This can be seen in Figure 5.21. In the 2.0 and 3.0 m/s signatures, the secondary oscillations occur both before and after the peak force of the impact. In the 5.0 m/s signature, however, the secondary oscillations are much more

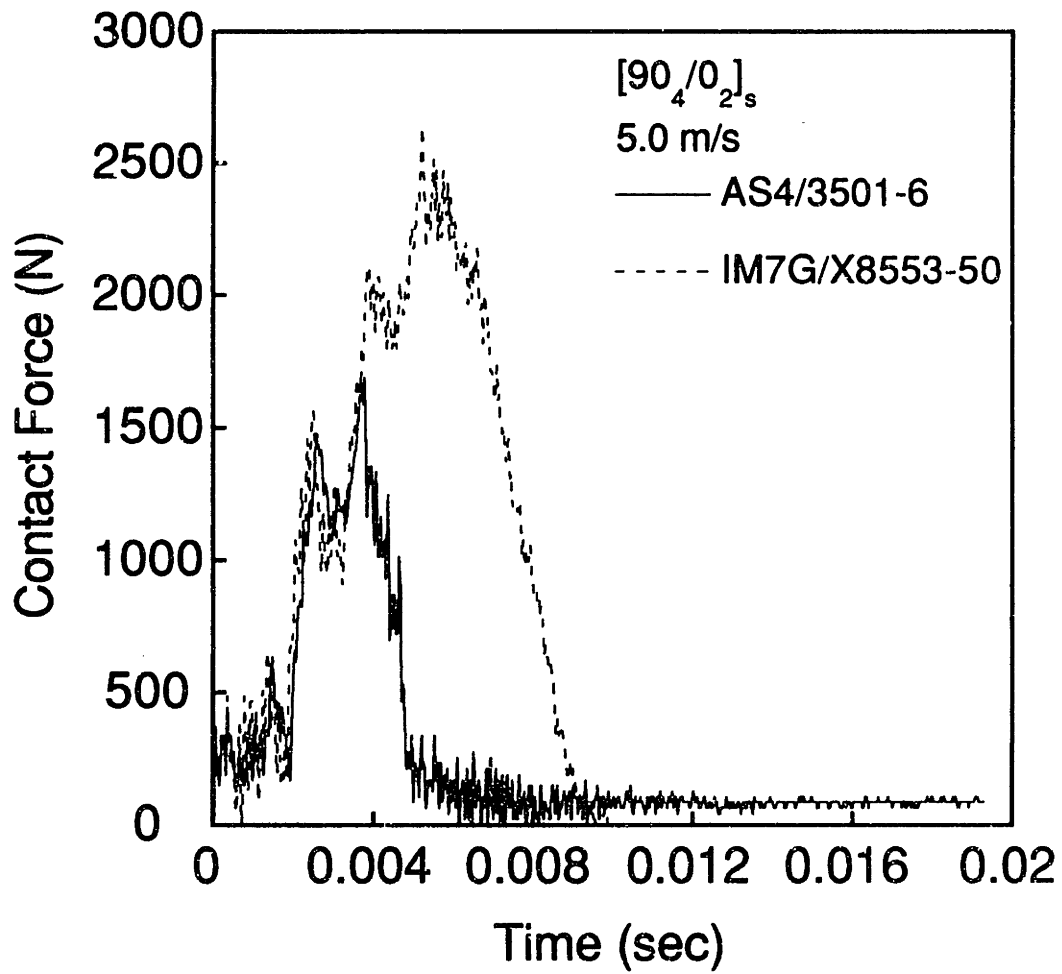


Figure 5.20 Signatures of $[90_4/0_2]_s$ laminates of AS4/3501-6 (penetrated) and IM7G/X8553-50 (no penetration) impacted at 5.0 m/s.

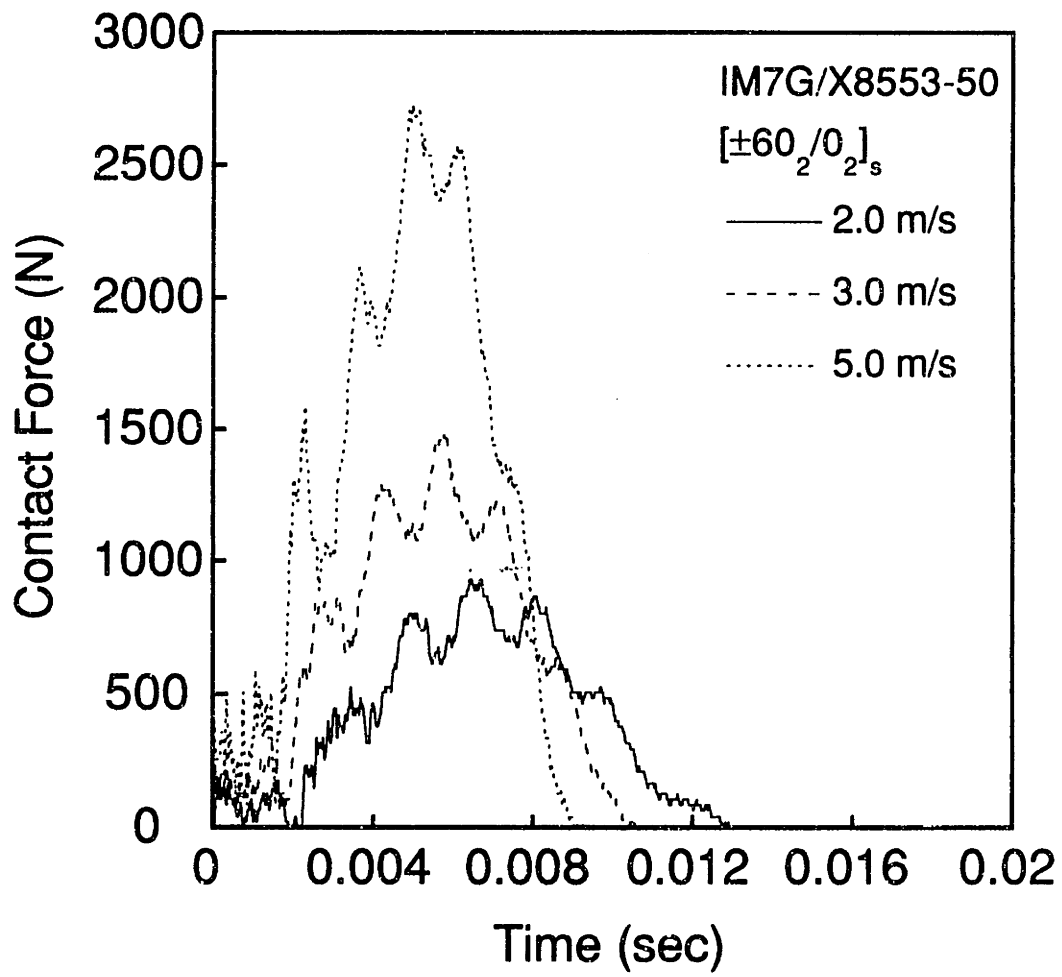


Figure 5.21 Force-time signatures of IM7G/X8553-50 $[\pm 60_2/0_2]_s$ laminate impacted at 2.0 m/s (undamaged), 3.0 m/s, and 5.0 m/s.

apparent in the signature before the peak force, than after. This behavior is common to all of the laminates tested here.

Also, it should be pointed out that the center plate deflections during these impacts were typically on the order of 5 to 10 laminate thicknesses. This information may be useful in trying to account for the behavior mentioned above. The laminate center deflections are obtained by integrating the force-time data obtained during impact. The force-time data are integrated, using the mass of the impactor rod and the impact velocity, to obtain the displacement of the impactor during the impact. This displacement corresponds to the center deflection of the plate plus the local indentation of the specimen. From similar impacts in a previous study [30], it was found that the local indentation is typically less than 1.0% of the center deflection. Thus, ignoring the local indentation, the following method can be used to obtain an approximation of the center deflection of the plate: The acceleration history, $a(t)$, of the impactor rod is obtained from the force history, $F(t)$, by dividing by the impactor mass, M , (1.53 kg):

$$a(t) = \frac{F(t)}{M} \quad (5.1)$$

The velocity history, $v(t)$, can be obtained by integrating the acceleration history and adding the initial velocity, v_0 :

$$v(t) = \int_0^t a(t) dt + v_0 \quad (5.2)$$

The displacement history, $w(t)$, can be obtained by integrating the velocity history, $v(t)$:

$$w(t) = \int_0^t v(t) dt \quad (5.3)$$

where the initial displacement is zero. This method was verified by comparing measured center deflection data with center deflection results derived from measured force versus time histories as obtained by Ryan [30]. These impacts are similar to the ones performed in this study.

Displacement curves normalized by the plate thickness for 1.0 and 3.0 m/s impacts can be seen in Figure 5.22 for the AS4/3501-6 $[\pm 15_2/0_2]_s$ laminate. The magnitudes of the deflections shown here are typical. The center deflection caused by the 1.0 m/s impact was greater than 3 laminate thicknesses, while the deflection from the 3.0 m/s impact was nearly 8 laminate thicknesses. Deflections this large may be sufficient to cause a significant amount of membrane stretching in the laminates [4].

In summary, it is not clear what factors control certain aspects of the impact signature. The peak force and duration of the impact were found to depend upon impact velocity, but were not primarily controlled by the major laminate bending stiffness (D_{1111}), or the laminate extensional stiffness (A_{1111}). The secondary oscillations of the signatures do vary somewhat from laminate to laminate, but the parameters which control their amplitudes and frequencies are not immediately obvious. So, there is a need to identify the factors which control this aspect of the signature. The occurrence of incipient damage does not affect the signature in any characteristic way, but penetration can be seen as a sharp drop in the contact force in the impact signature, and prevents the contact force from rising further.

5.2 Incipient Damage Characteristics

One objective of this study is to identify the type of damage which first occurs in each laminate from impact. It is desired to observe any effect of

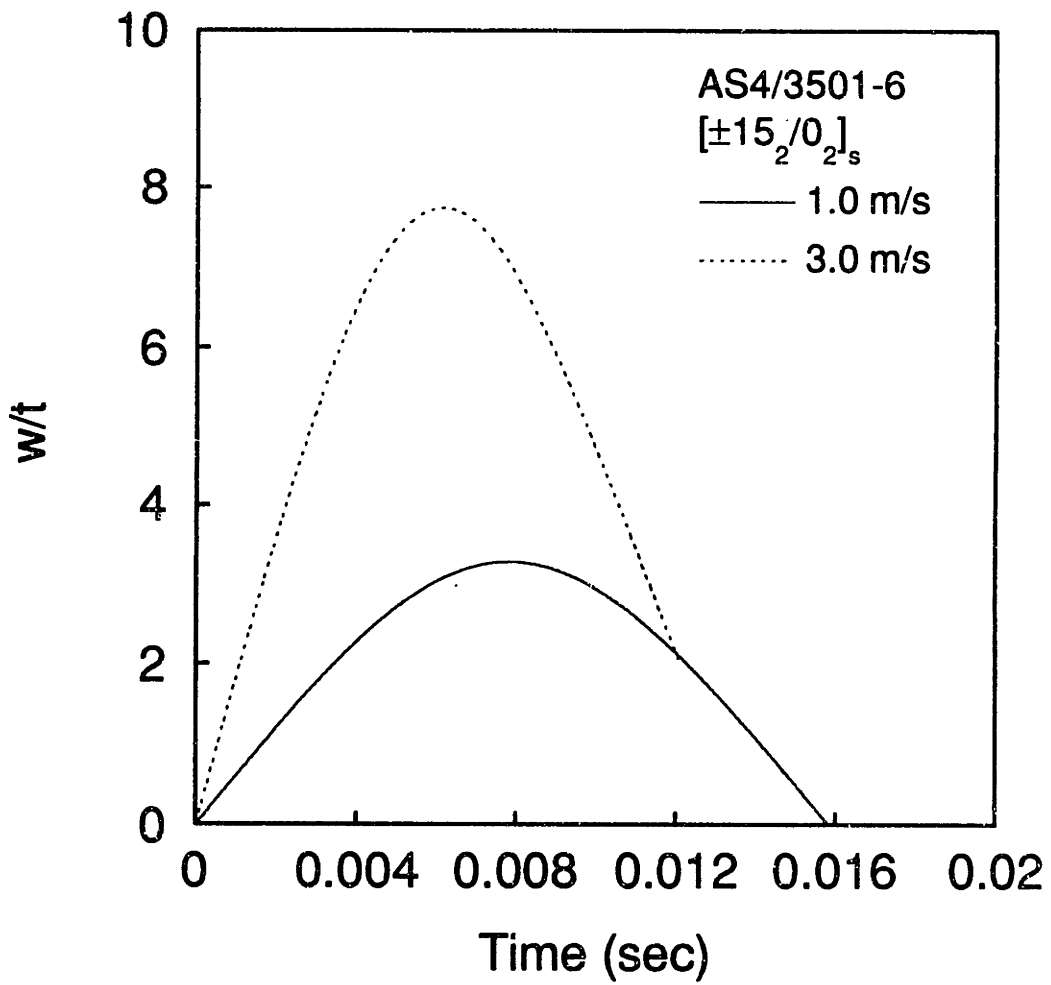


Figure 5.22 Derived center deflection curves (normalized by thickness) for AS4/3501-6 $[\pm 15_2/0_2]_s$ laminates impacted at 1.0 m/s and 3.0 m/s.

layup or material system on this incipient damage mode, or the force required to cause such damage.

5.2.1 Effect of Layup

The incipient damage mode in all of the 12-ply $[\pm\theta_2/0_2]_s$ laminates was matrix cracking in the two $+\theta^\circ$ plies at the rear of the laminate. This can be inferred from the X-ray photographs of more heavily damaged specimens in which delaminations were bounded in certain places by matrix cracks. These matrix cracks were enlarged versions of the incipient cracks and were oriented in the $+\theta^\circ$ direction. The deply results indicate that the delamination occurred at the ply interface furthest from the impacted surface, and the $+\theta^\circ$ plies at this interface are those at the rear of the laminate. This implies that the incipient matrix cracks occur in the $+\theta^\circ$ plies at the rear of the laminate, and not in the $+\theta^\circ$ plies at the impacted surface.

In these laminates it can be hypothesized that large tensile stresses from bending and stretching were the cause of the incipient matrix cracks. It has been pointed out previously that the deflections during these impacts were typically on the order of several laminate thicknesses. Deflections of this sort in conjunction with non-slipping clamped boundary conditions could cause a great deal of in-plane stretching in the laminate during impact [4]. It is at the back surface of the laminate where the tensile stresses of bending and tensile stresses of stretching would add together. On the impacted surface, tensile stresses of stretching would be mitigated by compressive bending stresses. Hence, it makes sense that the matrix cracking first occurred at the back surface.

The effect of the layup angle θ on the incipient damage force for the $[\pm\theta_2/0_2]_s$ laminates can be seen in Figure 5.23. For the AS4/3501-6 material system, the $[\pm60_2/0_2]_s$ laminate is the most easily damaged, in terms of

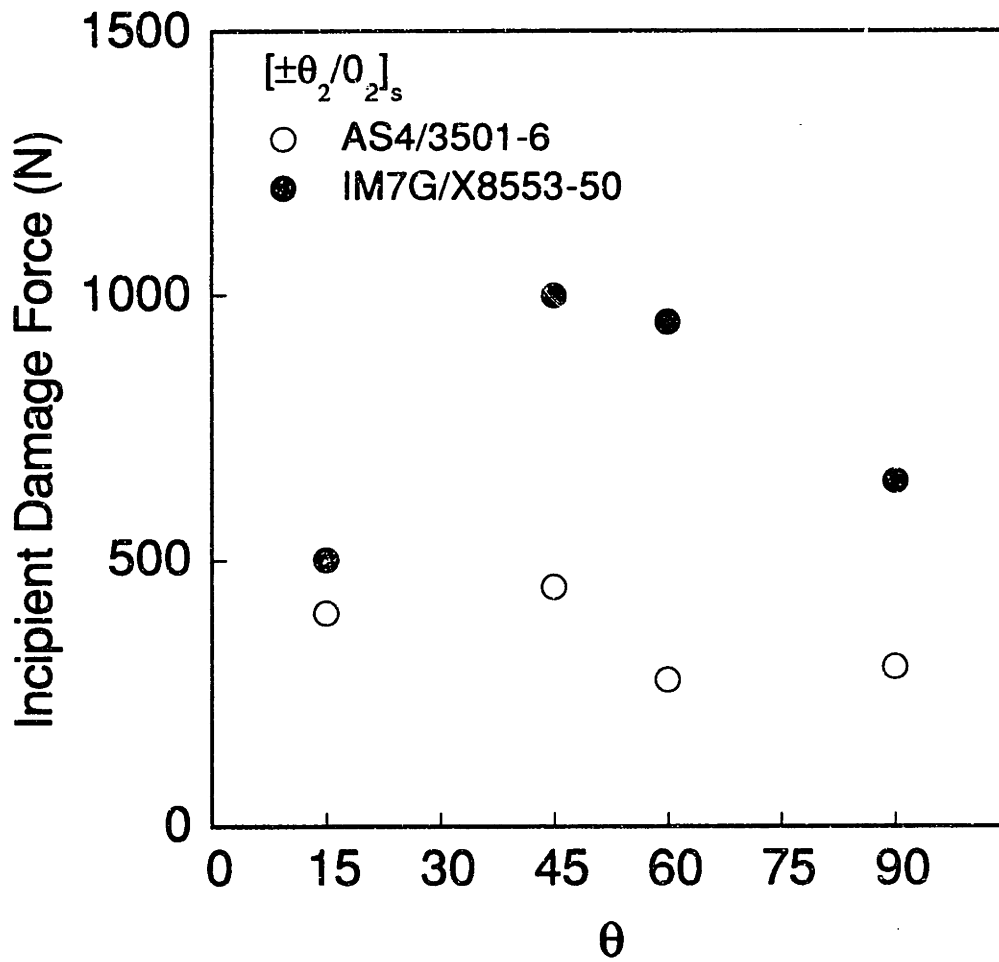


Figure 5.23 Incipient damage force versus layup angle for 12-ply laminates of AS4/3501-6 and IM7G/X8553-50.

incipient damage force, and the $[\pm 45_2/0_2]_s$ laminate is the least easily damaged. The incipient damage force for the $[\pm 15_2/0_2]_s$ laminate is nearly as high as that for the $[\pm 45_2/0_2]_s$ laminate, and that for the $[90_2/0_2]_s$ is nearly as low as that for the $[\pm 60_2/0_2]_s$ laminate. Overall, a strong trend cannot be seen in layup angle.

For the IM7G/X8553-50 material system, the incipient damage force is greatest for the $[\pm 45_2/0_2]_s$ laminate, as was the case with the AS4/3501-6. For this material system, the incipient damage force for the $[\pm 60_2/0_2]_s$ laminate is nearly as high as that for the $[\pm 45_2/0_2]_s$ laminate. The $[\pm 15_2/0_2]_s$ and $[90_2/0_2]_s$ laminates are damaged at a much lower force.

The stacking sequence affected the incipient damage force (and velocity) for the two 16-ply quasi-isotropic AS4/3501-6 laminates. The incipient damage force of the $[\pm 45_2/0_2/90_2]_s$ laminate (1000 N) was significantly lower than that of the $[(\pm 45)_2/(0/90)_2]_s$ laminate (1550 N). The grouping of the plies in the $[\pm 45_2/0_2/90_2]_s$ laminate allowed matrix cracking to occur in the rear plies due to impact forces which did not damage the $[(\pm 45)_2/(0/90)_2]_s$ laminate. A result similar to this was reported by Flaggs and Kural [32] with regard to matrix cracking in the 90° plies of a laminate resulting from tensile stresses. The grouping of several plies of the same orientation into one "effective ply" of several ply thicknesses lowers the transverse failure stress of the individual plies. This "ply grouping effect" allows matrix cracking at a lower stress level than would be the case were the plies interspersed with plies of other orientations. In this way, a laminate with double "effective plies" can be damaged from a lower contact force than a laminate without ply grouping.

The incipient damage mode of the $[(\pm 45)_2/(0/90)_2]_s$ laminate was not clearly identified. A circular region of intense matrix cracking in many different directions and what appeared to be delamination occurred at the

incipient damage velocity. However, the incipient damage mode of the $[\pm 45_2/0_2/90_2]_s$ laminate was clearly different (a single matrix crack in the rear plies). Thus, the stacking sequence of the plies affected not only the incipient damage force, but also the incipient damage mode.

In the glass/epoxy material system, the incipient damage mode was the same, regardless of layup. Crazeing, or very fine cracking of the matrix in many directions, on the rear surface of the laminates was the observed incipient damage mode. Also, the incipient damage force in all of the laminates was nearly the same (approximately 550 N). This indicates that the incipient damage mode was matrix controlled, since the fiber direction did not appear to have an effect on the damage mode.

5.2.2 Effect of Material System

All of the 12-ply laminates of AS4/3501-6 and IM7G/X8553-50 had the same incipient damage mode: matrix cracking of the rear plies. The material system did not have an effect on the damage mode, but did have an effect on the force at which damage first occurred in these laminates.

For the $[\pm\theta_2/0_2]_s$ laminates, the effect of material system on incipient damage force is shown in Figure 5.23. It is observed that all of the AS4/3501-6 laminates are more easily damaged than any of the IM7G/X8553-50 laminates. The most easily damaged laminate of IM7G/X8553-50, the $[\pm 15_2/0_2]_s$ laminate, has a higher incipient damage force than the least easily damaged laminate of AS4/3501-6, the $[\pm 45_2/0_2]_s$ laminate. This can be explained by the higher ply transverse failure strain for the IM7G/X8553-50 material, as shown in Table 5.4. The tensile transverse failure strain of the IM7G/X8553-50 ply is twice that of the AS4/3501-6 ply. This higher strain capability allows the IM7G/X8553-50

Table 5.4 Ply Failure Strains for AS4/3501-6 and IM7G/X8553-50

Material System	Tensile Failure Strain		
	ϵ_{11}	ϵ_{22}	γ_{12}
AS4/3501-6	1.5%	0.5%	1.75%
IM7G/X8553-50	1.6%	1.0%	2.0 %

laminates to withstand higher contact forces before the appearance of the incipient matrix crack in the rear plies.

Both of the 16-ply laminates of AS4/3501-6 were damaged more easily, in terms of incipient damage force, than the 8-ply fabric laminate of A370-5H/3501-6S. A force of 2400 N was required to damage the $(45_2/0_2)_s$ laminate, while the incipient damage forces of the $[\pm 45_2/0_2/90_2]_s$ laminate (1000 N) and the $[(\pm 45)_2/(0/90)_2]_s$ laminate (1550 N) were considerably lower.

It is noted, however, that the incipient damage modes were different among these three laminates. The incipient damage state of the A370-5H/3501-6S $(45_2/0_2)_s$ laminate was a circular region of what appeared to be fine cracks in several directions, much like the incipient damage state of the $[(\pm 45)_2/(0/90)_2]_s$ tape laminate, although delamination occurred in the tape laminate. The damage in the fabric may be the same as the matrix damage described by Kraft [33] in which a complex state of micro-cracking was observed in the matrix, but further investigation is needed to be certain. In the fabric and $[(\pm 45)_2/(0/90)_2]_s$ laminates, significant damage occurred suddenly over an entire area, in contrast to the single matrix crack in the AS4/3501-6 $[\pm 45_2/0_2/90_2]_s$ laminate. This difference in damage modes may be due to the ability of the fabric plies (and, to a certain extent, tape plies of single thickness) to inhibit the formation of long matrix cracks, which can propagate easily in a tape ply of double effective thickness. This may give the A370-5H/3501-6S $(45_2/0_2)_s$ and AS4/3501-6 $[(\pm 45)_2/(0/90)_2]_s$ laminates an advantage in preventing the formation of a large incipient matrix crack.

For the $(45_2/0_2)_s$ fabric laminates, the incipient damage force was dramatically different for the A370-5H/3501-6S and glass/epoxy material systems. The glass/epoxy $(45_2/0_2)_s$ laminate was damaged by a contact force of 600 N, while a contact force of 2400 N was necessary to cause damage to the

A370-5H/3501-6S $(45_2/0_2)_s$ laminate. The incipient damage mode in the glass/epoxy laminates was crazing of the matrix on the rear surface of the laminate. The incipient damage mode with the A370-5H/3501-6S system was identified only as matrix damage in a circular area at the impact center. The through-thickness location of these cracks was not identified, so a comparison with the glass/epoxy incipient damage mode cannot be made.

In summary, the incipient damage mode of the 12-ply laminates is matrix cracking in the rearmost plies, regardless of layup or material system. The IM7G/X8553-50 laminates are more damage resistant, in terms of incipient damage force and velocity, than the AS4/3501-6 laminates. Ply grouping in the 16-ply tape laminates allowed incipient damage to occur at a lower force. Both 16-ply tape laminates are damaged at a lower force than the graphite/epoxy fabric laminate. In the 16-ply tape layups, the stacking sequence affected the incipient damage mode, and the incipient damage state of the graphite/epoxy fabric laminate more closely resembled that of the $[(\pm 45)_2/(0/90)_2]_s$ laminate. In all of the glass/epoxy laminates, the incipient damage mode is crazing of the matrix at the rear surface, and the incipient damage force is not affected by layup.

5.3 General Damage Characteristics

It is of interest to investigate the progression of damage beyond the incipient damage mode in the laminates used in this study. It is desired to expose the roles of layup and material system in the development of higher states of damage, and ultimately, penetration of the specimen.

5.3.1 Effect of Layup

In the $[\pm 6_2/0_2]_s$ laminates of both the AS4/3501-6 and IM7G/X8553-50 material systems, the incipient damage mode (matrix cracking of the rearmost $+0^\circ$ plies) is accompanied by a delamination at the rearmost interface at higher impact velocities. This delamination typically has a "figure 8" shape and is oriented in the direction of the fibers of the bottom ply at the interface (the $+0^\circ$ direction). The smallest delaminations occur in the $[\pm 15_2/0_2]_s$ laminates. Long, slender "S"-shaped delaminations are observed and they are typically bounded by the $+15^\circ$ and -15° directions. Delaminations with a "figure 8" shape are observed in the $[\pm 45_2/0_2]_s$, $[\pm 60_2/0_2]_s$ and $[90_4/0_2]_s$ laminates. The largest delaminations occur in the $[90_4/0_2]_s$ laminates. Presently, a good metric does not exist for comparing the delaminations in these different laminates. Since the shapes of the delaminations vary somewhat from layup to layup, it is not particularly useful to compare the delaminations by using some measurement such as overall length, for example.

In the IM7G/X8553-50 material system, the layup angle was found to influence the onset of fiber damage. The 5.0 m/s impacts only caused fiber damage to the $[\pm 15_2/0_2]_s$ laminate. Matrix cracking and delamination occurred in all four layups at this impact velocity, but a limited amount of fiber damage was observed in the $[\pm 15_2/0_2]_s$ laminate. It is interesting to note that this laminate also had the least amount of delamination, in terms of total delamination area, of the 12-ply layups. The formation of delamination absorbs energy, and it is probable that laminates which delaminate less are more likely to find other ways to dissipate energy, such as in the breaking of fibers [12]. During an impact event, the initial kinetic energy of the impactor is stored elastically within the laminate. During this process, the laminate may

reach its limit in terms of how much energy it can store elastically, and energy is dissipated in the creation of damage. Energy which is not dissipated through delamination, will be dissipated in other ways. The layup influences the sizes and shapes of the delaminations which will occur. If the layup is such that relatively little delamination is permitted, then fiber damage may occur at a lower force than if more delamination occurred.

Penetration data were obtained for the 12-ply AS4/3501-6 laminates and are presented in Figure 5.24. It is noteworthy that the only fiber damage observed in the 12-ply AS4/3501-6 laminates occurred in the penetrated specimens. This is in contrast to the IM7G/X8553-50 specimens in which fiber damage occurred without penetration. The $[\pm 15_2/0_2]_s$ laminate has the highest penetration force (2400 N), followed by the $[\pm 45_2/0_2]_s$ and $[\pm 60_2/0_2]_s$ laminates (both approximately 2300 N) and the $[90_4/0_2]_s$ is the most easily penetrated (1700 N). It is obvious that this last laminate is much more easily penetrated than the other three. One explanation of this might be the number of ply interfaces within the laminate. There are only two interfaces in the $[90_4/0_2]_s$ laminate at which the ply angle changes, while the other laminates each have four interfaces. The $[90_4/0_2]_s$ laminate is essentially three unidirectional "sublaminates" of four plies each. This configuration allows matrix cracks to propagate through four plies at a time. In the other laminates, the outer four plies on each side of the laminate do not all have the same fiber direction, allowing matrix cracks in them to traverse only two plies before encountering an interface where the ply direction changes. Matrix cracking may lead to laminate penetration by allowing the impactor to penetrate each sublaminate by "wedging" it apart. This lack of inhibition to matrix cracking could be the reason that the penetration force was much lower in the $[90_4/0_2]_s$ laminate than in the other three laminates.

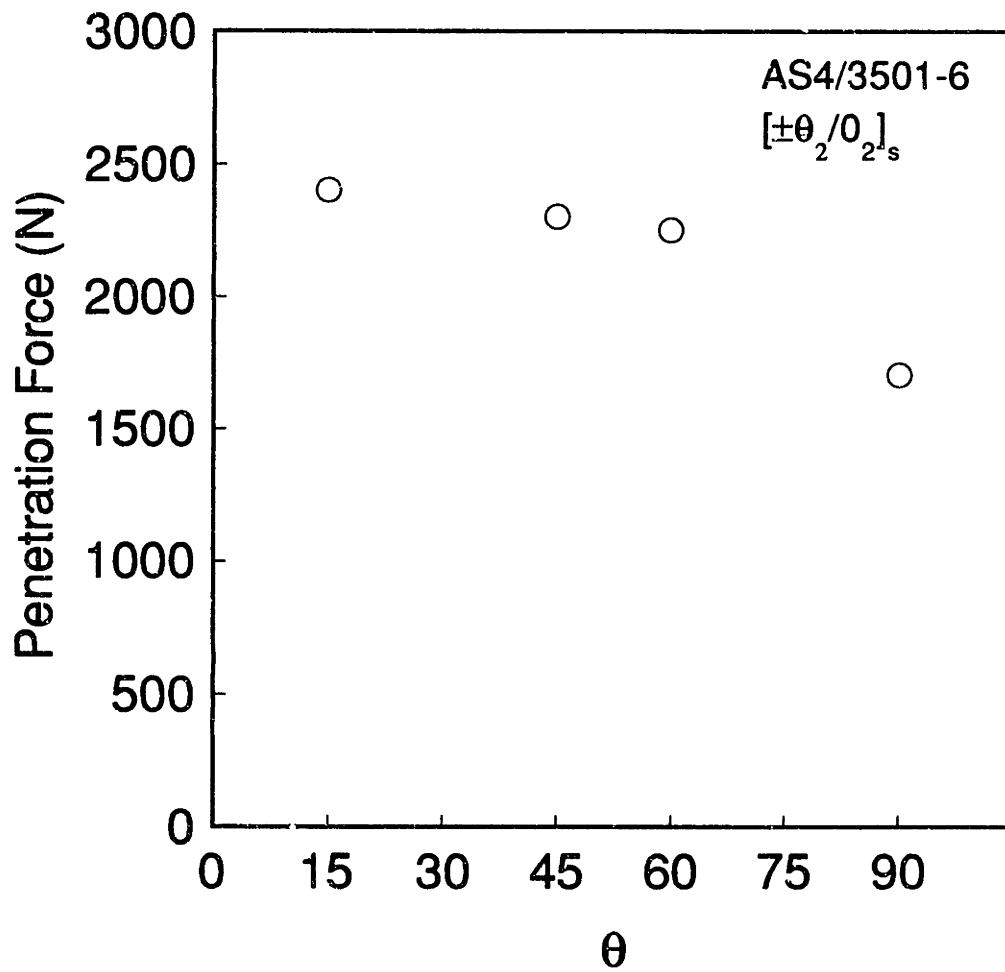


Figure 5.24 Penetration force versus layup angle for the 12-ply laminates of AS4/3501-6.

The ply stacking arrangement in the 16-ply AS4/3501-6 laminates has a definite effect on their damage characteristics. The ply grouping in the $[\pm 45_2/0_2/90_2]_s$ laminate allows matrix cracking to occur in the rear plies, followed by a large "figure 8" delamination at the rearmost interface and other smaller "figure 8" delaminations at the other interfaces, as well. The delaminations in the $[(\pm 45)_2/(0/90)_2]_s$ laminate also have a "figure 8" shape, but are typically much smaller and there are many more ply interfaces at which delamination can occur. The $[\pm 45_2/0_2/90_2]_s$ laminate has six interfaces at which the ply angle changes, compared to fourteen interfaces in the $[(\pm 45)_2/(0/90)_2]_s$ laminate. The individual delaminations are smaller in the laminate with more ply interfaces, but the total delaminated area may be a key parameter here. A comparison of the total delaminated areas in these two laminates may reveal important information regarding energy dissipation during impact. The smaller delaminations in the $[(\pm 45)_2/(0/90)_2]_s$ laminate cause a smaller overall damage region (as viewed via X-ray) than in the $[\pm 45_2/0_2/90_2]_s$ laminate. In addition, fiber damage occurs in the $[(\pm 45)_2/(0/90)_2]_s$ laminate which is not observed in the laminate with grouped plies. Lines of broken fibers were found in the two $+45^\circ$ plies near the impacted surface (the first and third plies) of the $[(\pm 45)_2/(0/90)_2]_s$ laminate. The fiber damage was observed to occur on either side of the impact center, but did not occur directly beneath the point of contact. This could indicate that the fibers were broken from excessively high stresses due to "local bending". By "local bending" it is meant the bending of the laminate near the point of contact to conform to the shape of the impactor.

The layup did not significantly affect the damage characteristics in the glass/epoxy material system. The same "ring" of damage was observed in all five layups at the 3.0 m/s impact velocity. At 5.0 m/s, the damage area had a

"figure 8" shape aligned with the 0° direction for the $(90_2/0_2)_s$ and $(0_2/45_2)_s$ laminates, and an elliptical shape for the $(45_2/0_2)_s$ and $(0/45)_{2s}$ laminates. The major axis of the ellipses in the last two laminates were aligned with the 0° direction.

5.3.2 Effect of Material System

The general damage characteristics were basically the same in the 12-ply laminates of AS4/3501-6 and IM7G/X8553-50. The incipient damage mode was matrix cracking of the rearmost plies of the laminate, followed by delamination at the rearmost interface. It has already been shown that the force-time histories of the impacts were essentially the same with both material systems (for the same layup and impact velocity). This fact allows an evenhanded comparison, based on impact velocity, of the damage characteristics of the two material systems. Since the force history was independent of the material system, any differences in the damage states (in laminates with the same layup) resulting from impacts of the same velocity must be attributed to differences in material properties in the local region of contact.

The laminates of IM7G/X8553-50 consistently had less damage than their AS4/3501-6 counterparts for the same impact velocity. The damage modes were the same, but the incipient damage velocity was consistently higher for the IM7G/X8553-50 laminates. Also, the IM7G/X8553-50 laminates were more reluctant to delaminate with the presence of the matrix crack in the rear plies. This can be seen in the case of the $[90_4/0_2]_s$ layup. The AS4/3501-6 laminate developed an incipient matrix crack at an impact velocity of 0.9 m/s (peak force of 300 N) and suffered significant delamination from an impact of 2.1 m/s (850 N). The same layup of IM7G/X8553-50 developed an incipient

crack at an impact velocity of 1.5 m/s (650 N), but an impact velocity of 4.0 m/s (1900 N) was required to produce a similar delamination to that of the AS4/3501-6 impacted at 2.0 m/s. Thus, an increase in velocity of 1.2 m/s (550 N) was required to create a delamination in the AS4/3501-6 laminate, while an increase of 2.5 m/s (1250 N) was required to create a similar delamination in the IM7G/X8553-50 laminate. Hence, it can be said that IM7G/X8553-50 is superior to the AS4/3501-6 material system in resisting initial damage, and also in preventing the progression of damage into higher states.

In terms of penetration, the IM7G/X8553-50 laminates were more damage resistant than the AS4/3501-6 laminates. The 5.0 m/s impact was sufficient to penetrate every one of the 12-ply AS4/3501-6 laminates, while only internal damage occurred in the IM7G/X8553-50 laminates at this impact velocity. The penetration force for each of the AS4/3501-6 laminates is below 2500 N. In contrast, all four of the IM7G/X8553-50 layups were able to withstand forces higher than 2500 N without penetration.

Different damage characteristics are observed in the fabric and tape graphite/epoxy laminates. The damage characteristics of the $(45_2/0_2)_s$ A370-5H/3501-6S laminate are more similar to those of the $[(\pm 45)_2/(0/90)_2]_s$ laminate than the $[\pm 45_2/0_2/90_2]_s$ laminate. Damage occurred to $+45^\circ$ fibers near the impacted surface in the fabric laminate, as was the case in the AS4/3501-6 $[(\pm 45)_2/(0/90)_2]_s$ tape laminate. In this case, the difference between the tape layup and the fabric layup is the presence of delamination. Delamination was observed in both tape laminates, while no damage could be identified between the plies of the fabric layup. In comparison with the tape layups, the fabric layup confined the damage to a much smaller area (as viewed via X-ray) than either of the tape layups. The woven nature of the fabric plies does not allow the matrix cracking that was observed in the tape

laminates, especially in the laminate with the grouped plies. The $[(\pm 45)_2/(0/90)_2]_s$ laminate controlled the matrix cracking better than the $[\pm 45_2/0_2/90_2]_s$ laminate, and the fabric was better in this respect than either of the tape laminates.

The damage characteristics of the graphite/epoxy and glass/epoxy $(45_2/0_2)_s$ laminates are not easily compared for two reasons. First, the damage states in either of these two material systems were not clearly identified. Secondly, the force-time signatures of these laminates were very different, making a comparison based on impact velocity very difficult. It is suggested that a comparison can be made between the damage characteristics of these two material systems based on peak impact force. For such a comparison, impacts causing the same peak force would have to be performed on these laminates. There is insufficient data for these two laminates to perform such a comparison here.

In summary, the incipient matrix cracks in the rear plies of the 12-ply laminates are accompanied by delamination at the rearmost interface at higher impact velocities. The shape and size of this delamination is strongly dependent upon layup. The AS4/3501-6 laminates are more easily penetrated, in terms of penetration force and velocity, than the IM7G/X8553-50 laminates. In the IM7G/X8553-50 laminates, fiber damage is only observed in the $[\pm 15_2/0_2]_s$ layup, which is also the layup in which the smallest delaminations are observed. The stacking sequence of the 16-ply laminates affects their damage states. The laminate with double effective ply thickness has fewer interfaces at which delamination can occur, but the delaminations are much larger than those in the laminate with single effective ply thickness. Fiber damage near the impacted surface is observed in the latter tape laminate and

also in the fabric laminate, but not in the tape laminate with double effective ply thickness. It is postulated that since delamination dissipates energy, laminates with significant delamination will have less energy to dissipate in the breaking of fibers (and will therefore have less fiber breakage) than laminates with less delamination.

Chapter 6

CONCLUSIONS AND RECOMMENDATIONS

In this investigation, the impact behavior of several laminated material systems was examined. Incipient damage modes were determined for laminates of various layup, and the force data from the impacts were obtained. The force-time histories were studied in order to develop an understanding of the relationship between damage within the specimen and the force-time signature. Also, the signatures of laminates of different layups and material systems were compared. The conclusions drawn from this endeavor with regard to the force-time data are:

1. The occurrence of incipient damage was not detected in the force-time signature. In addition, the presence of internal damage was found to have no discernible effect on the force-time signatures for non-penetrating impacts.
2. Penetration can be seen in the force-time signature as a sudden drop in the contact force.
3. The force-time signatures of identical layups of a traditional graphite/epoxy material system (AS4/3501-6) and a newer "toughened matrix" material system (IM7G/X8553-50) were virtually identical up until penetration of the AS4/3501-6 laminates.

4. For impact velocities which penetrated the AS4/3501-6 laminates, the same layups of IM7G/X8553-50 were subjected to higher contact forces because penetration did not occur.
5. An increase in impactor velocity causes an increase in peak force and a decrease in impact duration.
6. The force-time signature, in terms of peak force and duration, was not significantly affected by the layup angle θ in the $[\pm\theta_2/0_2]_s$ laminates. The major extensional and bending stiffnesses of the laminate (A_{1111} and D_{1111}) do not appear to be the factors controlling the shape of the signature.
7. The parameters controlling the secondary oscillations in the impact signature have not been identified.
8. The force-time signatures of a fabric layup and a tape layup, which imitates the fiber arrangement in the fabric, were nearly the same, except the amplitudes of the secondary oscillations were greater for the fabric laminate.
9. The force-time history of an impact can be integrated (with the use of the impactor mass and initial velocity) to obtain the center deflection history of the laminate, neglecting a small error due to indentation.

10. Derived center deflections for the impacts performed indicate deflections on the order of 5 to 10 laminate thicknesses. Thus, membrane stretching of the laminate may be significant.

The following conclusions can be made with regard to the observations made of the damage states resulting from impact:

1. The incipient damage mode in the $[\pm\theta_2/0_2]_s$ laminates was matrix cracking of the $+\theta^\circ$ plies at the back surface of the laminate. At higher impact velocities, this matrix crack was accompanied by a delamination at the rearmost interface of the laminate.
2. The incipient damage mode was not affected by ply layup angle θ or material system for the $[\pm\theta_2/0_2]_s$ layups of AS4/3501-6 and IM7G/X8553-50.
3. Higher contact forces were required to cause incipient damage to the laminates of IM7G/X8553-50 because of the higher transverse tensile ply failure strain of this material system as compared to AS4/3501-6.
4. The IM7G/X8553-50 laminates are more damage resistant, in terms of incipient damage force (and velocity) and penetration force (and velocity), than the AS4/3501-6 laminates.
5. Ply grouping reduces the number of ply interfaces in a laminate, and causes larger but fewer delaminations from impact than was the case in a laminate with interspersed plies. Thus, the integrated damage area

(as viewed via X-ray) is larger in the laminate with double effective ply thickness.

6. A laminate with double effective thickness plies develops transverse ply cracks at a considerably lower contact force than a laminate with interspersed plies due to the ply grouping effect.
7. Ply stacking sequence was observed to change the incipient damage mode in two 16-ply quasi-isotropic laminates.
8. The incipient damage mode was not clearly identified for the A370-5H/3501-6S laminate or the 16-ply AS4/3501-6 laminate with single effective ply thickness. In contrast to the single incipient matrix crack identified for each of the other graphite/epoxy laminates, a circular area of matrix damage (of slightly smaller diameter than the tup diameter) suddenly appeared at the incipient damage velocity for these two laminates.
9. Fiber damage was observed in the plies near the impacted surface of a graphite/epoxy fabric laminate, without the presence of interlaminar damage, while delamination preceded fiber damage in all of the tape laminates investigated here.
10. Delamination appears to be a method of energy dissipation which could delay (in terms of contact force) the onset of fiber breakage in laminates which are prone to delaminate, as compared to laminates which are not.

11. The incipient damage force was higher for a laminate with fabric plies than for a similar laminate with tape plies, possibly due to the ability of the fabric plies to inhibit the development of long matrix cracks.

Based on the work performed, the following recommendations for further research are presented:

1. Investigate the contributions of individual laminate and material properties toward the shape of the impact signature. An analytical tool, which can correctly predict the contact force history and displacement of an impacted laminate, should be used to perform a sensitivity study.
2. Develop standardized damage metrics to allow quantitative comparisons of damage states in different laminates.
3. Investigate the possible correlation of peak impact force to damage state. This could be done by repeating the tests performed here with different impactor masses and velocities (including quasi-static).
4. Provide an explanation for the observation that, as impact velocity increases, the secondary oscillations become more pronounced before the peak force in the impact signature than after the peak force.
5. Repeat some of the impact experiments performed here with clamped-slipping boundary conditions to observe the influence of this aspect of the boundary condition on the force-time history and the damage state.

6. Identify the specific nature of the matrix damage observed in the glass/epoxy and graphite/epoxy fabric laminates.
7. Investigate the possibility of increasing the incipient damage force of a tape laminate, such as $[\pm 45/0/\pm 15/0]_s$ by replacing the surface plies with fabric plies, such as $[45_f/0/\pm 15/0]_s$, in which matrix cracking of the rear plies would be repressed.
8. Explore the possibility of using selective delamination as a device for energy dissipation to prevent fiber damage from impact. This could possibly be done by making alterations to "encourage" delamination in one laminate and comparing the force required to cause fiber damage with that of an unaltered laminate.

REFERENCES

1. Abrate, S., "Impact on Laminated Composite Materials," Applied Mechanics Review, Vol. 44, No. 4, April 1991, pp. 155-190.
2. Morton, J., and Godwin, E. W., "Impact Response of Tough Carbon Fiber Composites," Composite Structures, 1989, pp. 1-19.
3. Gause, L. W., and Buckley, L. J., "Impact Characterization of New Composite Materials," Instrumented Impact Testing of Plastics and Composite Materials, ASTM STP 936, American Society for Testing and Materials, 1987, pp. 248-261.
4. Bowles, K. J., "The Correlation of Low-Velocity Impact Resistance of Graphite-Fiber-Reinforced Composites with Matrix Properties," Composite Materials: Testing and Design (Eighth Conference), ASTM STP 972, American Society for Testing and Materials, 1988, pp. 124-142.
5. Sjoblom, P. O., Hartness, J. T., and Cordell, T. M., "On Low-Velocity Impact Testing of Composite Materials," Journal of Composite Materials, Vol. 22, No. 1, January 1988, pp. 30-52.
6. Reed, P. E., and Turner, S., "Flexed Plate Impact, Part 7. Low Energy and Excess Energy Impacts on Fibre-Reinforced Polymer Composites," Composites, Vol. 19, No. 3, May 1988, pp. 193-203.
7. Lee, S. M., and Zahuta, P., "Instrumented Impact and Static Indentation of Composites," Journal of Composite Materials, Vol. 25, No. 2, February 1991, pp. 204-221.
8. Elber, W., "Failure Mechanics in Low-Velocity Impacts on Thin Composite Plates," NASA-TP 2152, April 1983.
9. Cantwell, W. J., and Morton, J., "Geometrical Effects in the Low Velocity Impact Response of CFRP," Composite Structures, Vol 12, 1989, pp. 39-59.
10. Boll, D. J., Bascom, W. D., Weidner, J. C., and Murri, W. J., "A Microscopy Study of Impact Damage of Epoxy-Matrix Carbon-Fiber Composites," Journal of Material Science, Vol. 21, 1986, pp. 2667-2677.
11. Kumar, P., and Rai, B., "Reduction of Impact Damage in KFRP through Replacement of Surface Plies with Glass Fabric Plies," Journal of Composite Materials, Vol. 25, No. 6, June 1991, pp. 694-702.
12. Sun, C. T., and Rechak, S., "Effect of Adhesive Layers on Impact Damage in Composite Laminates," Composite Materials: Testing and Design (Eighth Conference), ASTM STP 972, American Society for Testing and Materials, 1988, pp. 97-123.

13. Greszczuk, L. B., "Response of Isotropic and Composite Materials to Particle Impact," Foreign Object Impact Damage to Composites, ASTM STP 568, American Society for Testing and Materials, 1975, pp. 183-211.
14. Aggour, H., and Sun, C. T., "Finite Element Analysis of a Laminated Composite Plate Subjected to Circularly Distributed Central Impact Loading," Computers and Structures, Vol. 28, No. 6, 1988, pp. 729-736.
15. Joshi, S. P., and Sun, C. T., "Impact Induced Fracture in a Laminated Composite," Journal of Composite Materials, Vol. 19, No. 1, January 1985, pp. 51-66.
16. Ross, C. A., Malvern, L. E., Sierakowski, R. L., and Takeda, N., "Finite-Element Analysis of Interlaminar Shear Stress Due to Local Impact," Recent Advances in Composites in the United States and Japan, ASTM STP 864, American Society for Testing and Materials, 1985, pp. 355-367.
17. Wu, H. T., and Springer, G. S., "Impact Induced Stresses, Strains, and Delaminations in Composite Plates," Journal of Composite Materials, Vol. 22, No. 6, June 1988, pp. 533-560.
18. Humphreys, E. A., and Goering, J., "Development of an Analytic Procedure to Calculate Damage Accumulation in Composites During Low Velocity Impact," NASA-CR-166086, 1983.
19. Ramkumar, R. L., and Chen, P. C., "Low-Velocity Impact Response of Laminated Plates," AIAA Journal, Vol. 21, 1983, pp. 1448-1452.
20. Cairns, D. S., and Lagace, P. A., "A Consistent Engineering Methodology for the Treatment of Impact in Composite Materials," Proceedings of the American Society for Composites, Fifth Technical Conference, East Lansing, Michigan, June, 1990, pp. 589-599.
21. Cairns, D. S., and Lagace, P. A., "Transient Response of Graphite/Epoxy and Kevlar/Epoxy Laminates Subjected to Impact," AIAA Journal, Vol. 27, No. 11, November, 1989, pp. 1590-1596.
22. Cairns, D. S., and Lagace, P. A., "Thick Composite Plates Subjected to Lateral Loadings," Journal of Applied Mechanics, Vol. 54, No. 3, September, 1987, pp. 611-616.
23. Chang, F., Choi, H. Y., and Jeng, S., "Characterization of Impact Damage in Laminated Composites," Proceeding of the 34th International SAMPE Symposium, May, 1989, pp. 702-713.
24. Gosse, J. H., and Mori, P. B. Y., "Impact Damage Characterization of Graphite/ Epoxy Laminates," Proceedings of the Third Technical Conference of the American Society for Composites, Seattle, 1988, pp. 344-353.

25. Clark, G., "Modeling of Impact Damage in Composite Laminates," Composites, Vol. 20, No. 3, 1989, pp. 209-214.
26. Guynn, E. G., and O'Brien, T. K., "The Influence of Lay-up and Thickness on Composite Impact Damage and Compression Strength," 26th AIAA Structures, Structural Dynamics and Materials Conference, 1985, pp. 187-196.
27. Takeda, N., Sierakowski, R. L., and Malvern, L. E., "Microscopic Observations of Cross Sections of Impacted Composite Laminates," Composite Technology Review, Vol. 4, 1982, pp. 40-44.
28. Liu, D., and Malvern, L. E., "Matrix Cracking in Impacted Glass/Epoxy Plates," Journal of Composite Materials, Vol. 21, 1987, pp. 594-609.
29. Guy, T. A., "Compressive Residual Strength of Graphite/Epoxy Laminates After Impact," TELAC Report No. 91-9, Massachusetts Institute of Technology, May 1991.
30. Ryan, K. F., "Dynamic Response of Graphite/Epoxy Plates Subjected to Impact Loading," TELAC Report No. 89-13, Massachusetts Institute of Technology, September, 1989.
31. Lagace, P. A., Brewer, J. C., and Varnerin, C. F., "TELAC Manufacturing Course Class Notes," TELAC Report No. 88-4, Massachusetts Institute of Technology, 1988.
32. Flagg, D. L., and Kural, M. H., "Experimental Determination of the In Situ Transverse Lamina Strength in Graphite/Epoxy Laminates," Journal of Composite Materials, Vol. 16, March 1982, pp. 103-115.
33. Kraft, M. J., "Impact Damage Response of Graphite/Epoxy Fabric Structures," TELAC Report 88-9, Massachusetts Institute of Technology, Cambridge, MA, July 1988.

APPENDIX A

All of the force-time data from this investigation are contained in this section. The force-time signature of each graphite/epoxy specimen is accompanied by an X-ray photograph of the damage state, or the words "NO DAMAGE", where damage could not be detected in the original X-ray photograph. The X-ray photographs shown here have been electronically scanned for reproduction purposes and some of the detail of the original photograph may be lost, especially in cases where the damage was very slight. The presence of an X-ray photograph (as opposed to the words "NO DAMAGE") indicates that damage was visible in the original X-ray photograph, even though it may not be apparent in the reproduction.

For the glass/epoxy specimens, each force-time signature is accompanied by a photograph of the damage state in the cases where the damage was extensive enough to be photographed. Where damage to the specimen was very slight, the damage was detected visually on the specimens, but was not easily photographed. Therefore, photographs of the damage states of these specimens are not provided. Instead, the words "SLIGHT DAMAGE" appear.

A quick reference to the contents of this appendix and the location of each figure is provided in Table A.1 on the following page.

Table A.1 Appendix Contents

Layup	Material System	Figure Numbers
$[\pm 15_2/0_2]_s$	AS4/3501-6	A.1 - A.10
	IM7G/X8553-50	A.62 - A.74
$[\pm 45_2/0_2]_s$	AS4/3501-6	A.11 - A.20
	IM7G/X8553-50	A.75 - A.84
$[\pm 60_2/0_2]_s$	AS4/3501-6	A.21 - A.31
	IM7G/X8553-50	A.85 - A.94
$[90_4/0_2]_s$	AS4/3501-6	A.32 - A.42
	IM7G/X8553-50	A.95 - A.104
$[\pm 45_2/0_2/90_2]_s$	AS4/3501-6	A.43 - A.52
$[(\pm 45)_2/(0/90)_2]_s$	AS4/3501-6	A.53 - A.61
$(45_2/0_2)_s$	A370-5H/3501-6S	A.105 - A.113
	Glass/Epoxy	A.114 - A.121
$(90_2/0_2)_s$	Glass/Epoxy	A.122 - A.127
$(0_2/45_2)_s$	Glass/Epoxy	A.128 - A.133
$(45/0)_{2s}$	Glass/Epoxy	A.134 - A.138
$(0/45)_{2s}$	Glass/Epoxy	A.139 - A.144

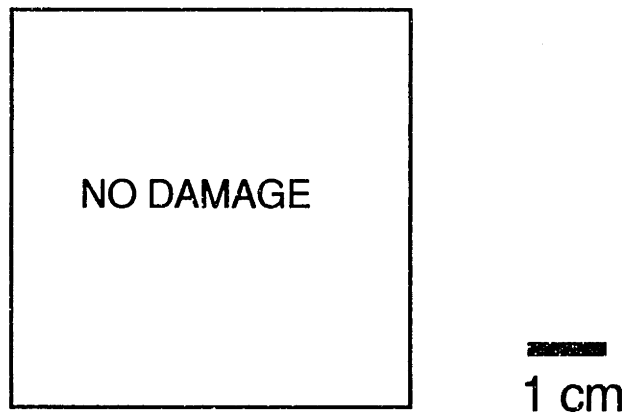
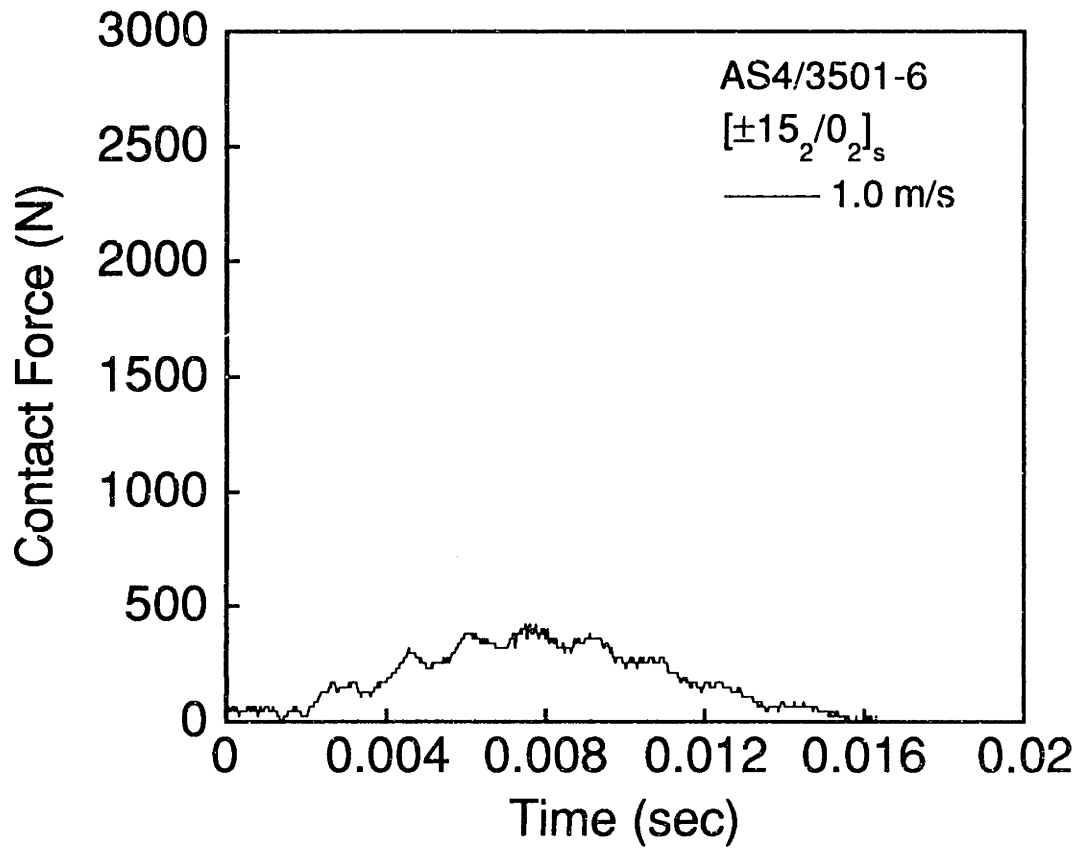
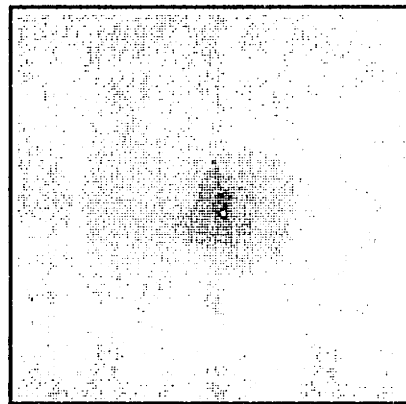
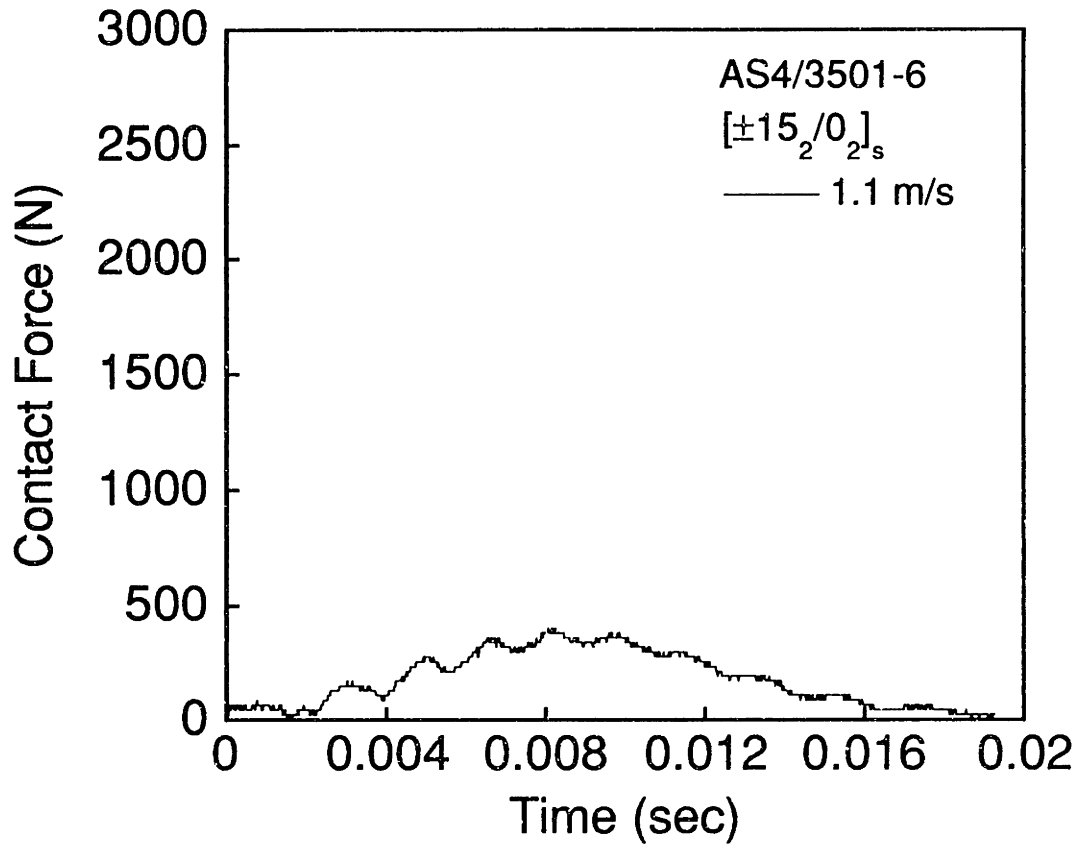
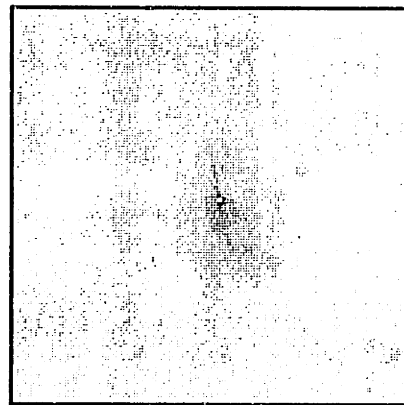
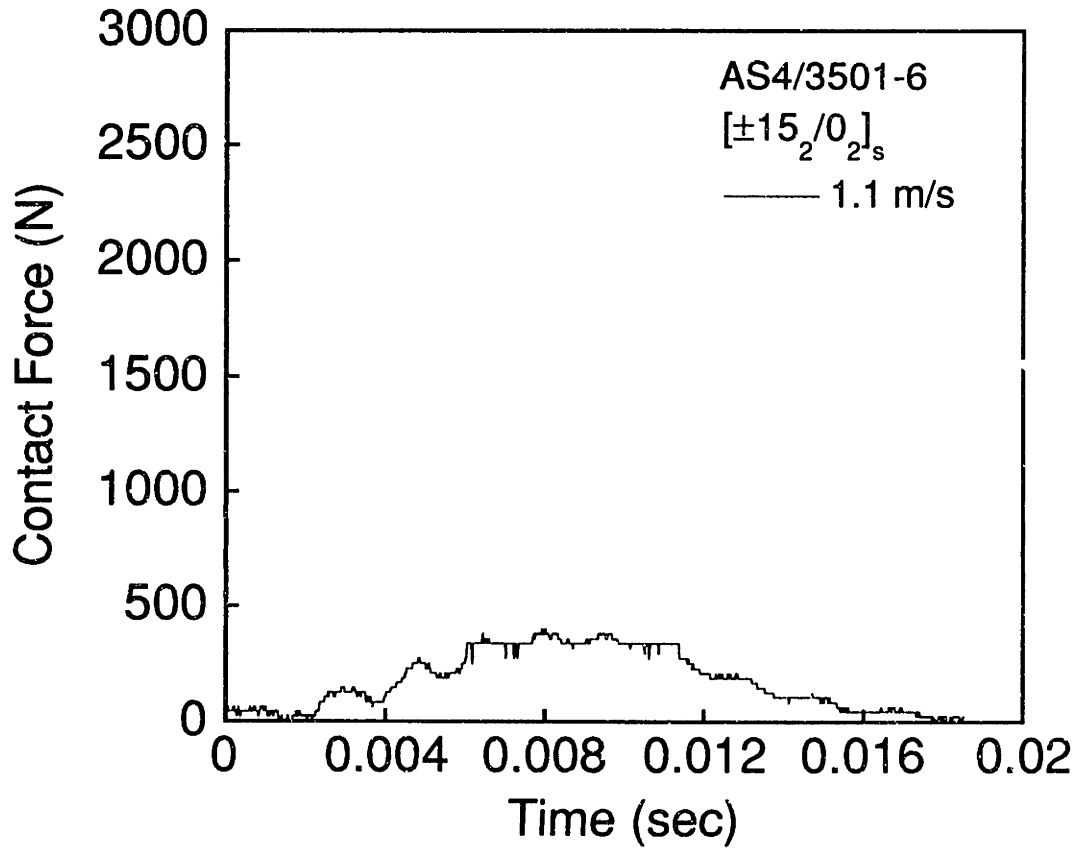


Figure A.1 (upper) Force versus time and (lower) X-ray photograph for AS4/3501-6 [±15₂/0₂]_s specimen impacted at 1.0 m/s.



1 cm

Figure A.2 (upper) Force versus time and (lower) X-ray photograph for AS4/3501-6 [±15₂/0₂]_s specimen impacted at 1.1 m/s.



1 cm

Figure A.3 (upper) Force versus time and (lower) X-ray photograph for AS4/3501-6 [±15₂/0₂]_s specimen impacted at 1.1 m/s.

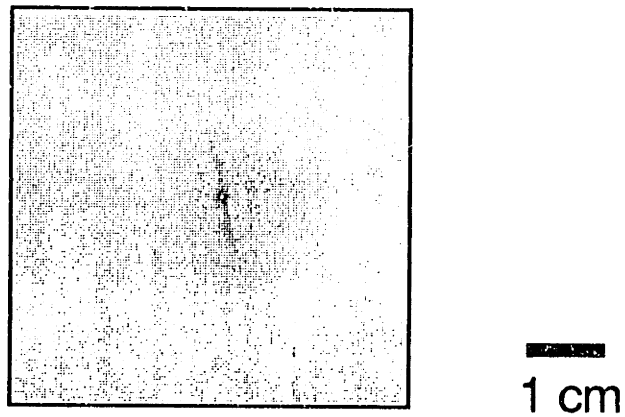
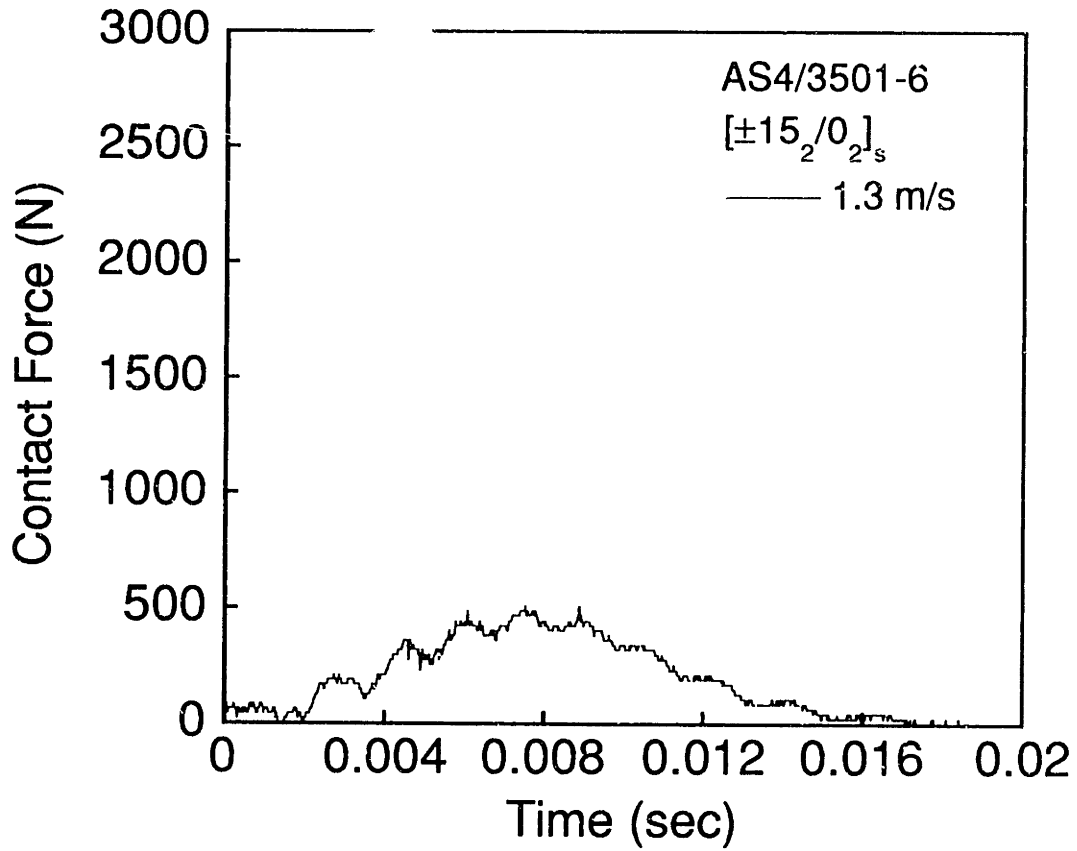


Figure A.4 (upper) Force versus time and (lower) X-ray photograph for AS4/3501-6 [±15₂/0₂]_s specimen impacted at 1.3 m/s.

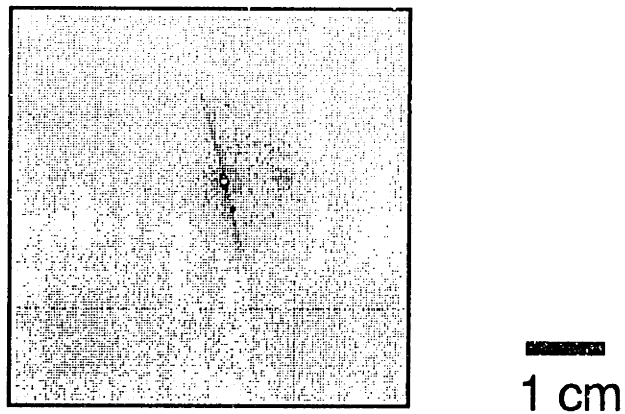
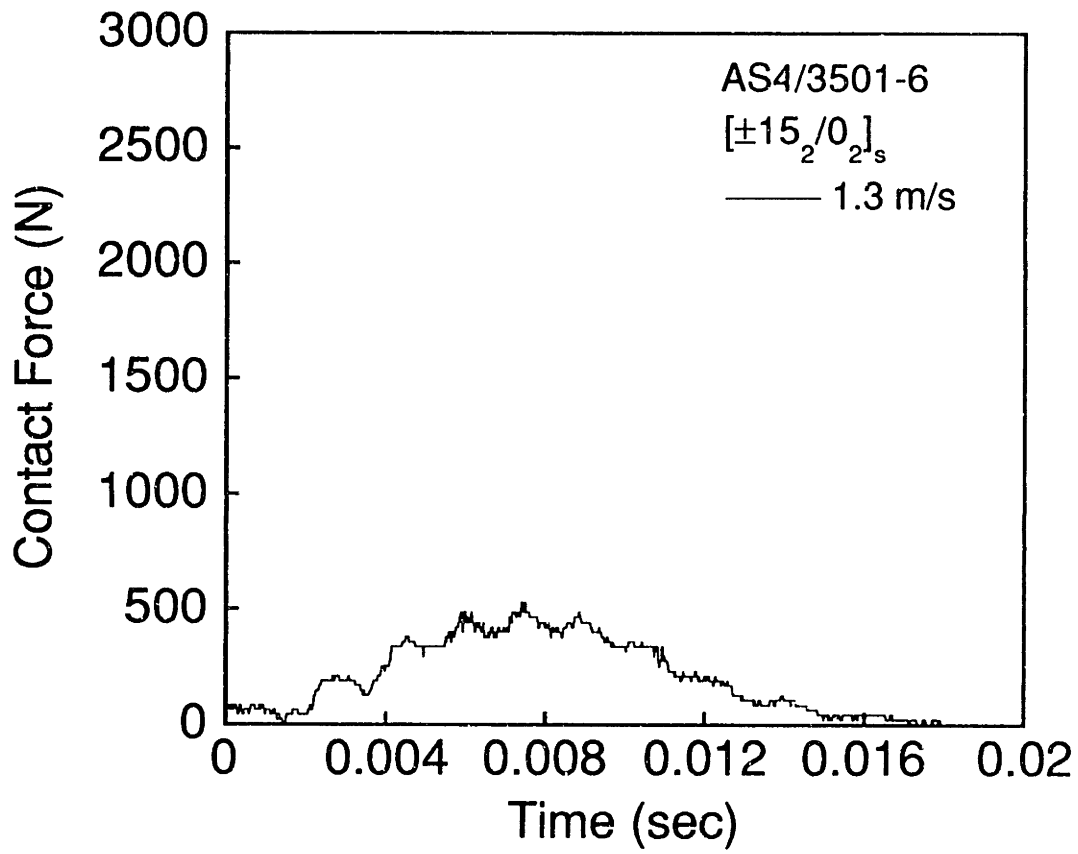
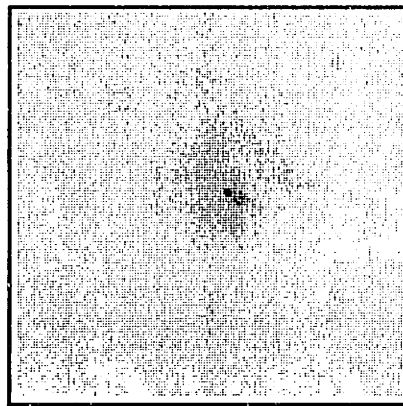
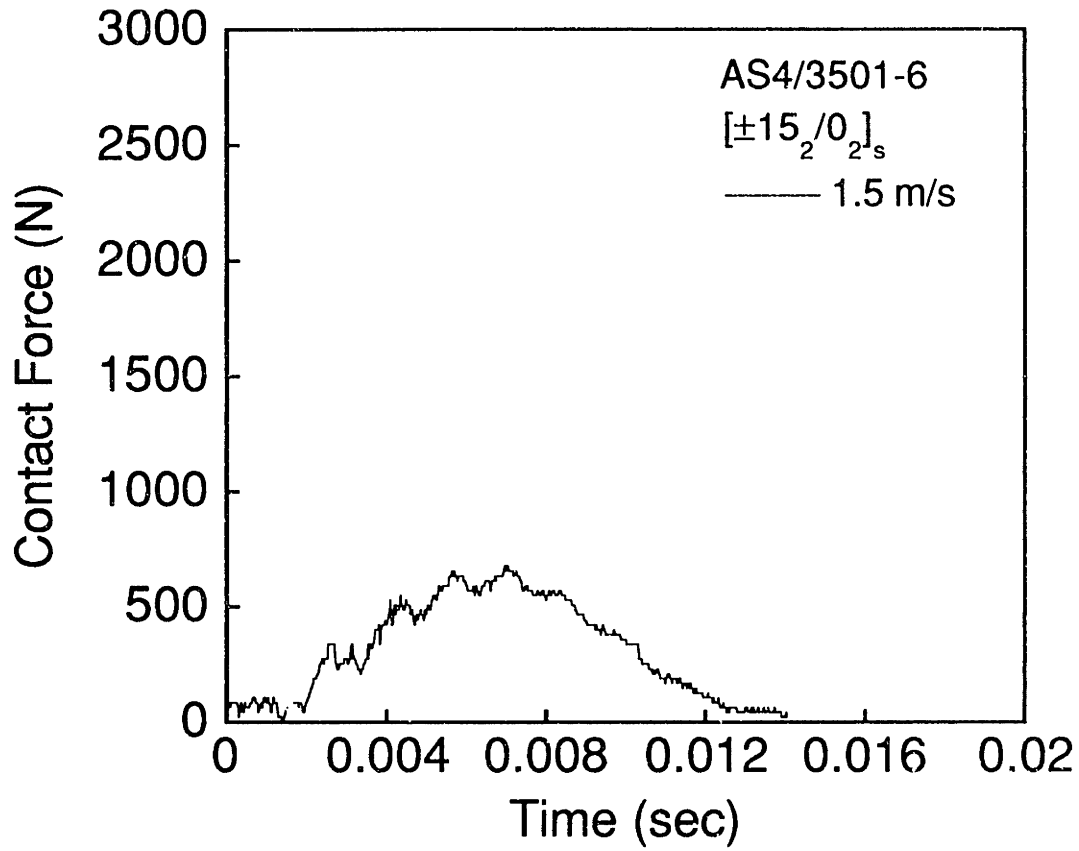
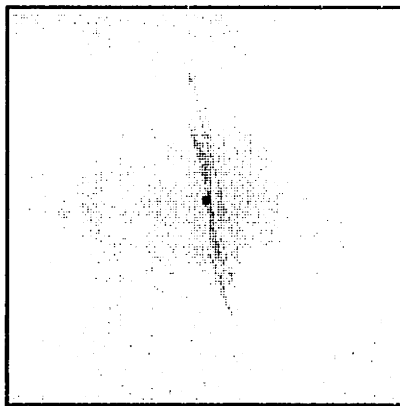
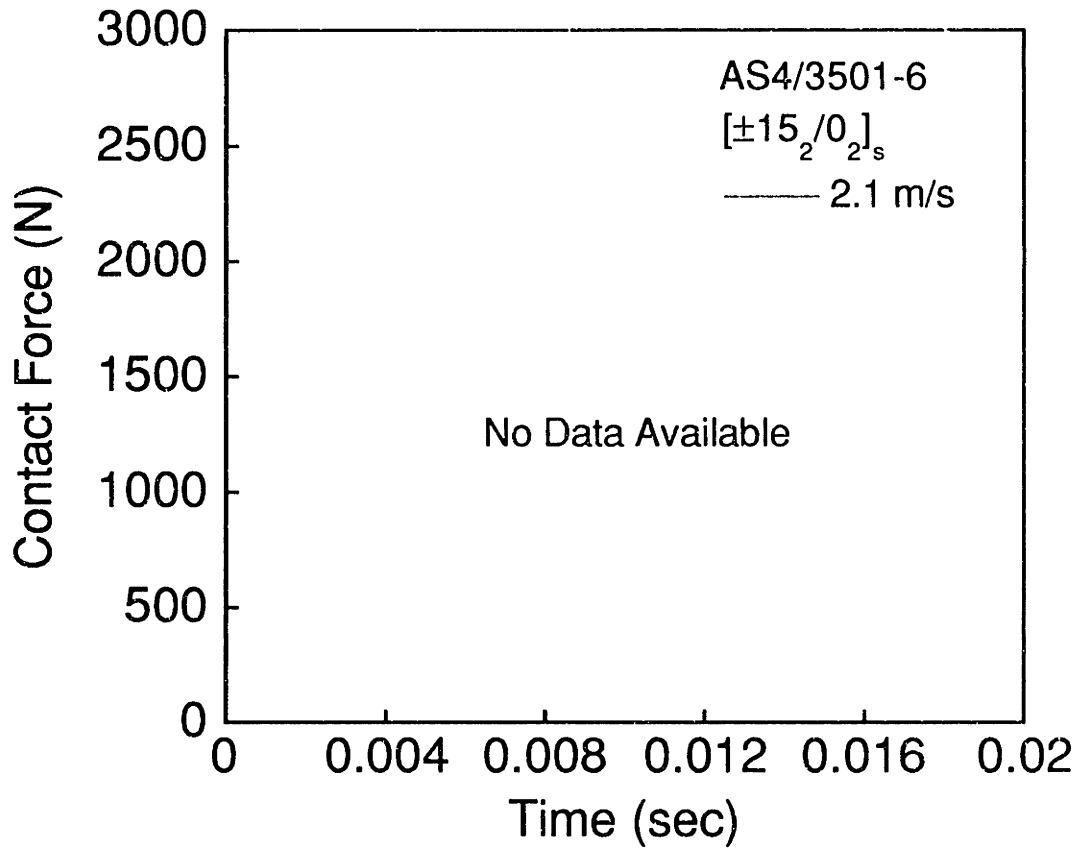


Figure A.5 (upper) Force versus time and (lower) X-ray photograph for AS4/3501-6 [±15₂/0₂]_s specimen impacted at 1.3 m/s.



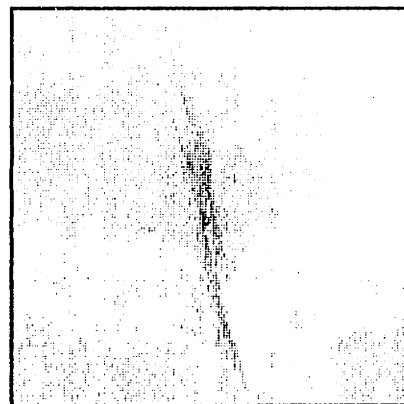
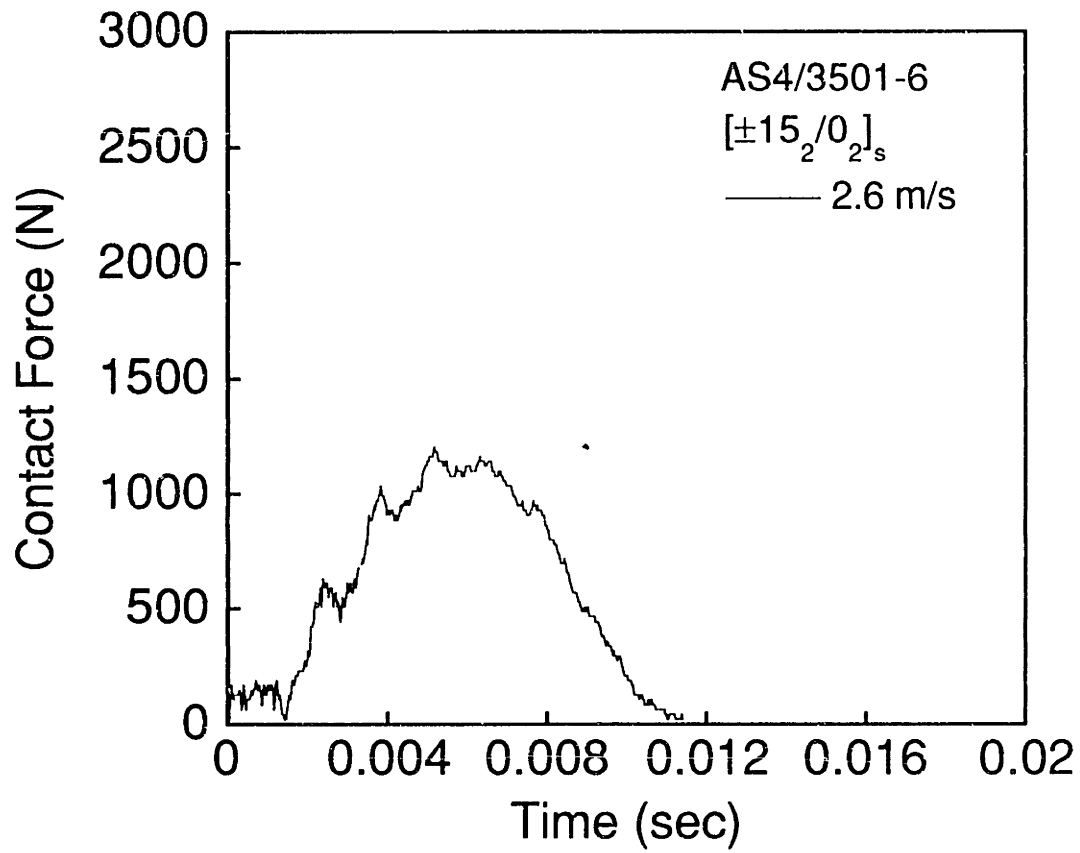
1 cm

Figure A.6 (upper) Force versus time and (lower) X-ray photograph for AS4/3501-6 [±15₂/0₂]_s specimen impacted at 1.5 m/s.



1 cm

Figure A.7 X-ray photograph for AS4/3501-6 [±15₂/0₂]_s specimen impacted at 2.1 m/s.



1 cm

Figure A.8 (upper) Force versus time and (lower) X-ray photograph for AS4/3501-6 [±15₂/0₂]_s specimen impacted at 2.6 m/s.

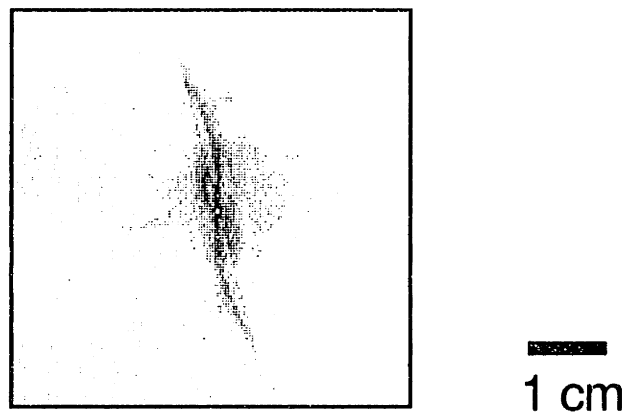
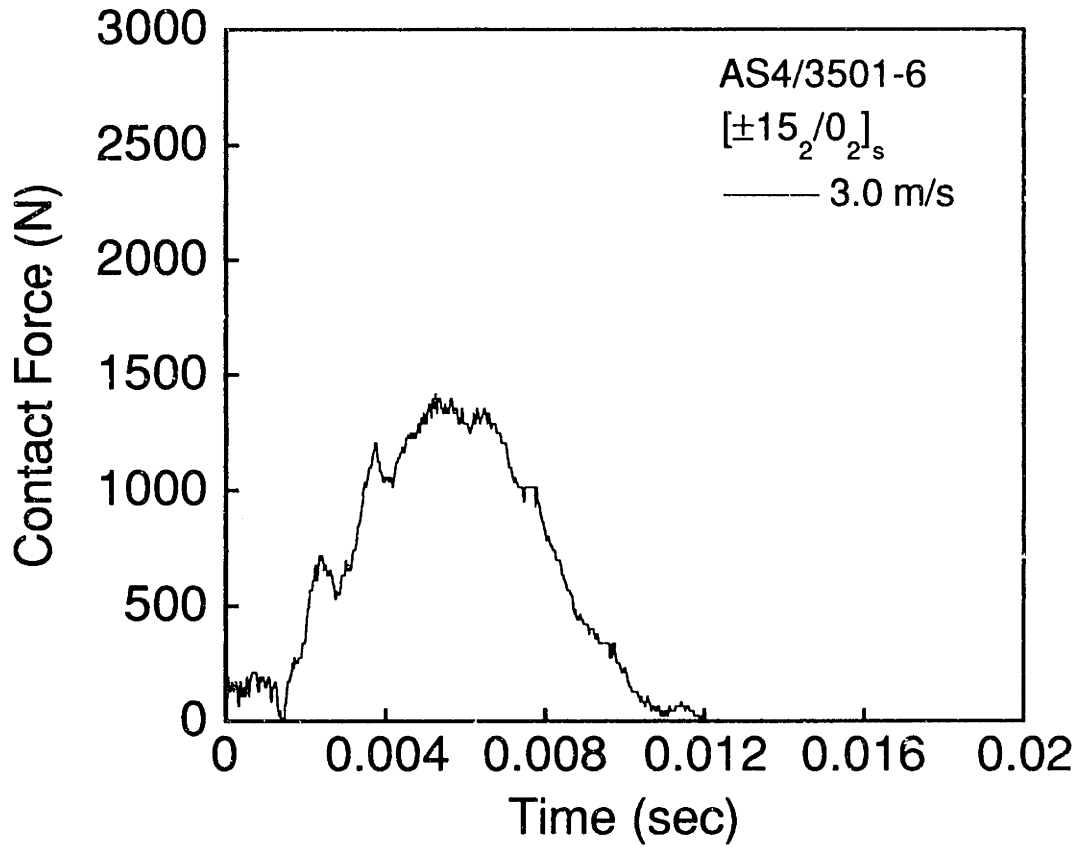


Figure A.9 (upper) Force versus time and (lower) X-ray photograph for AS4/3501-6 [±15₂/0₂]_s specimen impacted at 3.0 m/s.

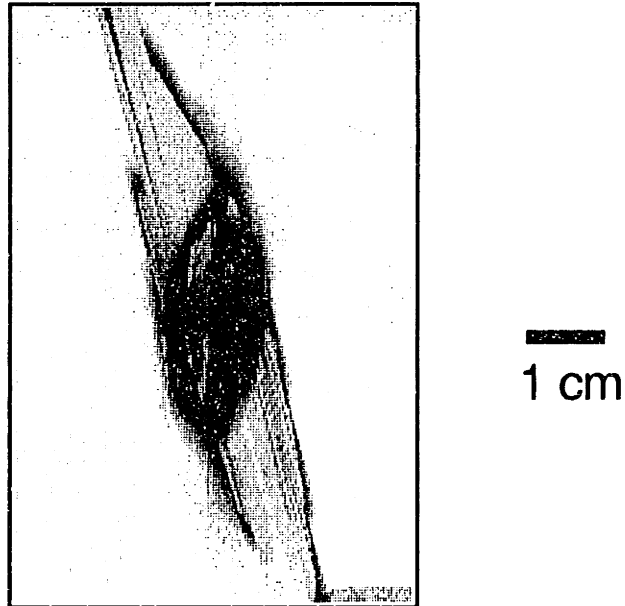
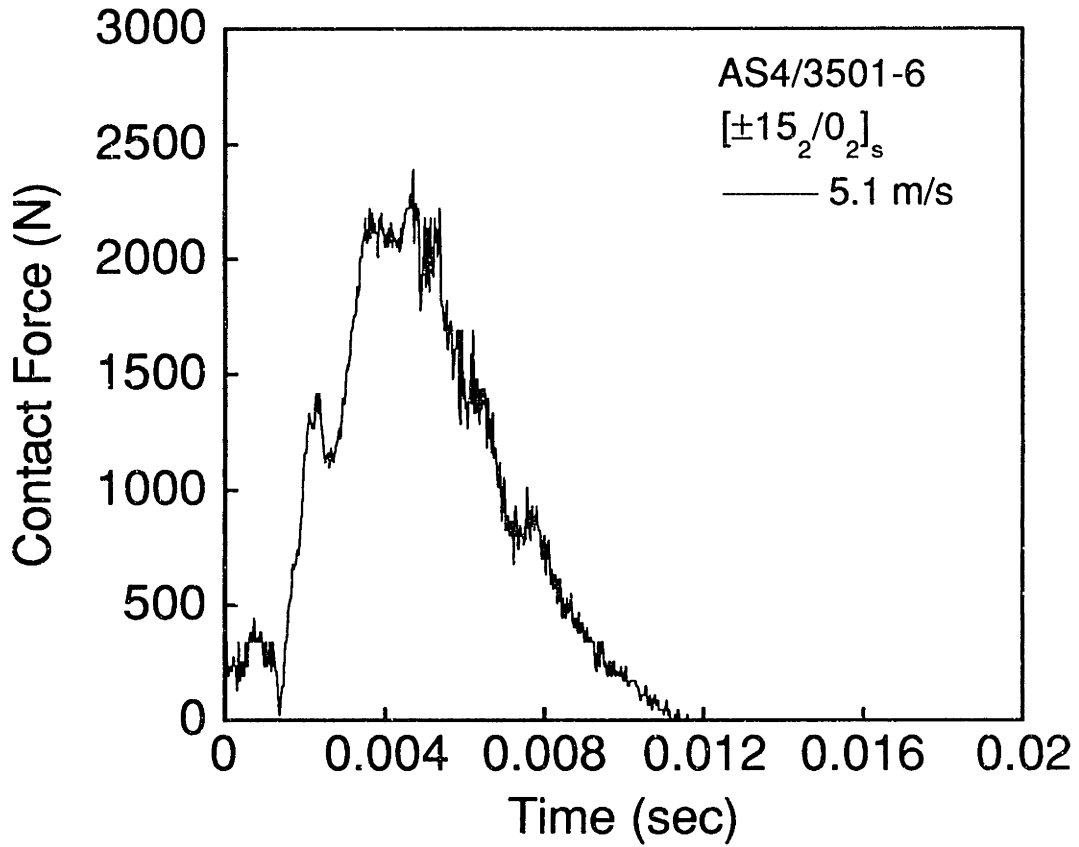


Figure A.10 (upper) Force versus time and (lower) X-ray photograph for AS4/3501-6 [±15₂/0₂]_s specimen impacted at 5.1 m/s.

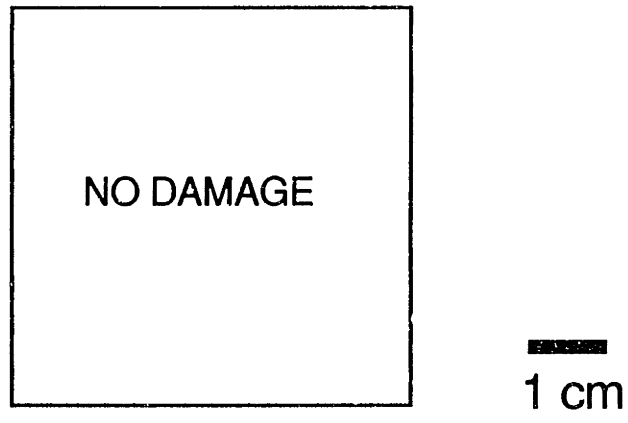
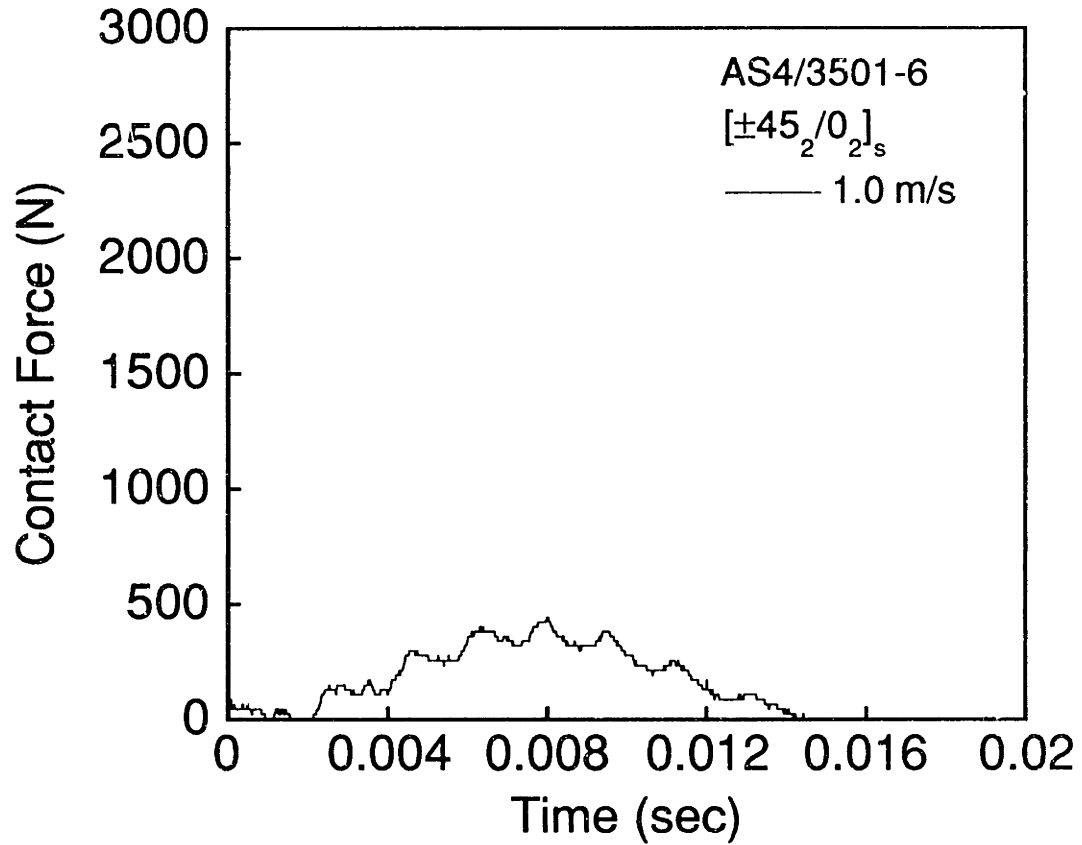
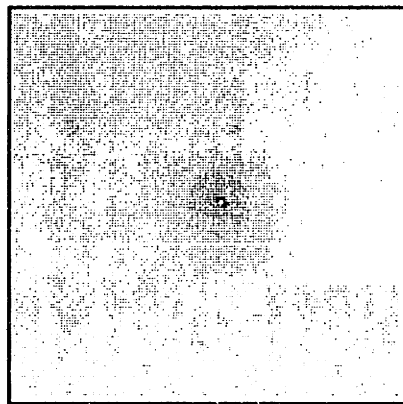
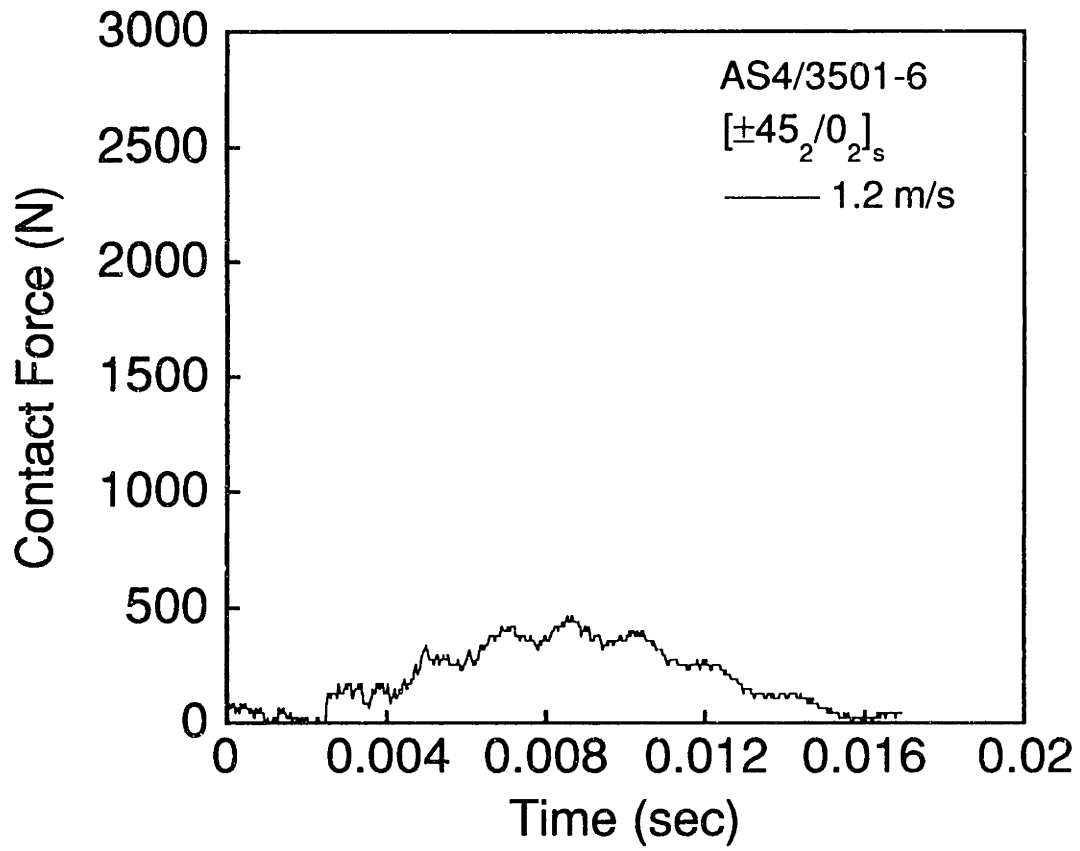


Figure A.11 (upper) Force versus time and (lower) X-ray photograph for AS4/3501-6 [±45₂/0₂]_s specimen impacted at 1.0 m/s.



1 cm

Figure A.12 (upper) Force versus time and (lower) X-ray photograph for AS4/3501-6 [±45₂/0₂]_s specimen impacted at 1.2 m/s.

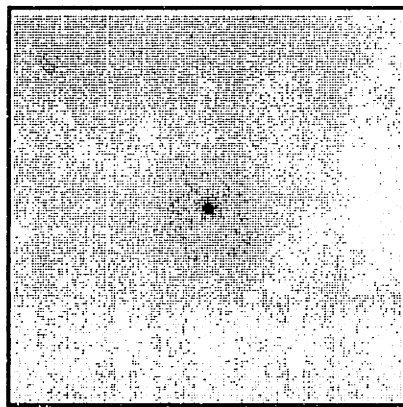
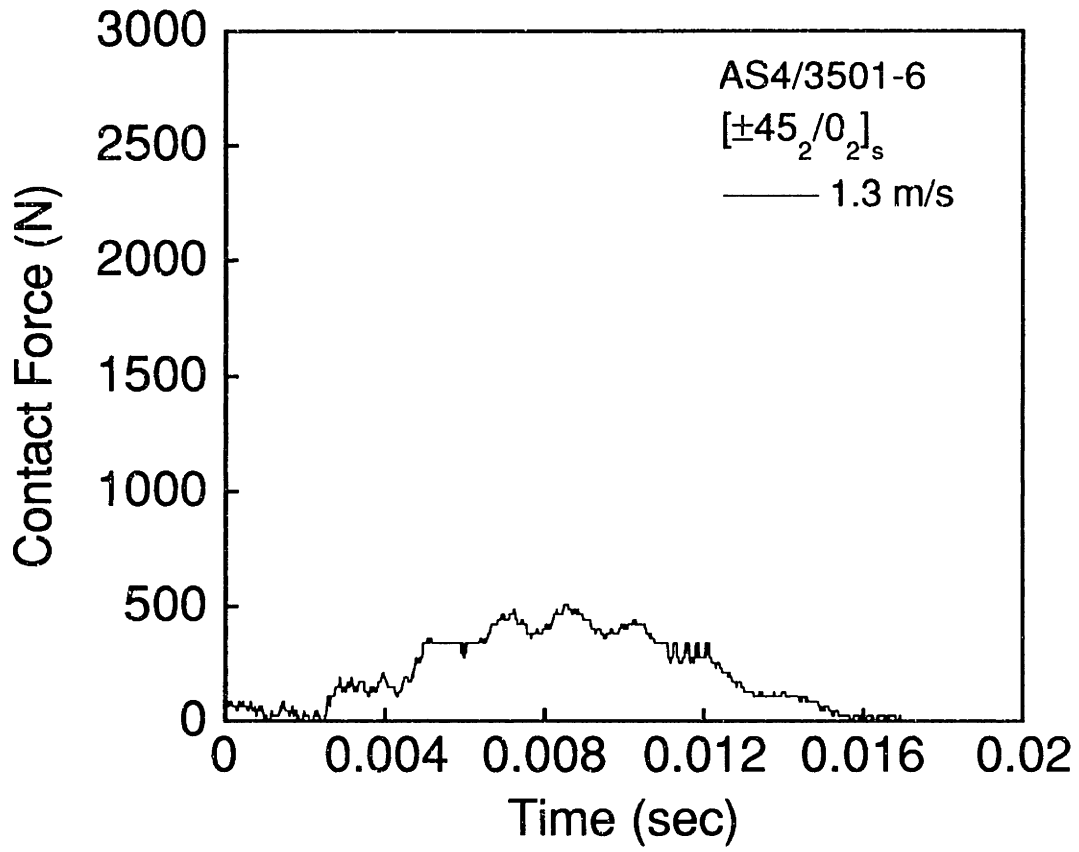
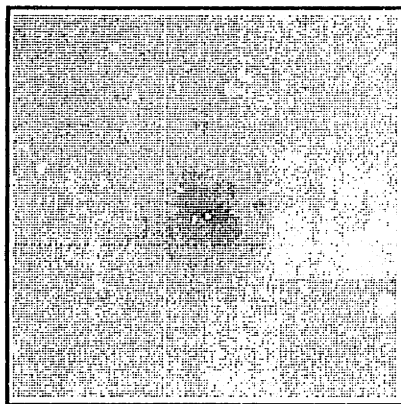
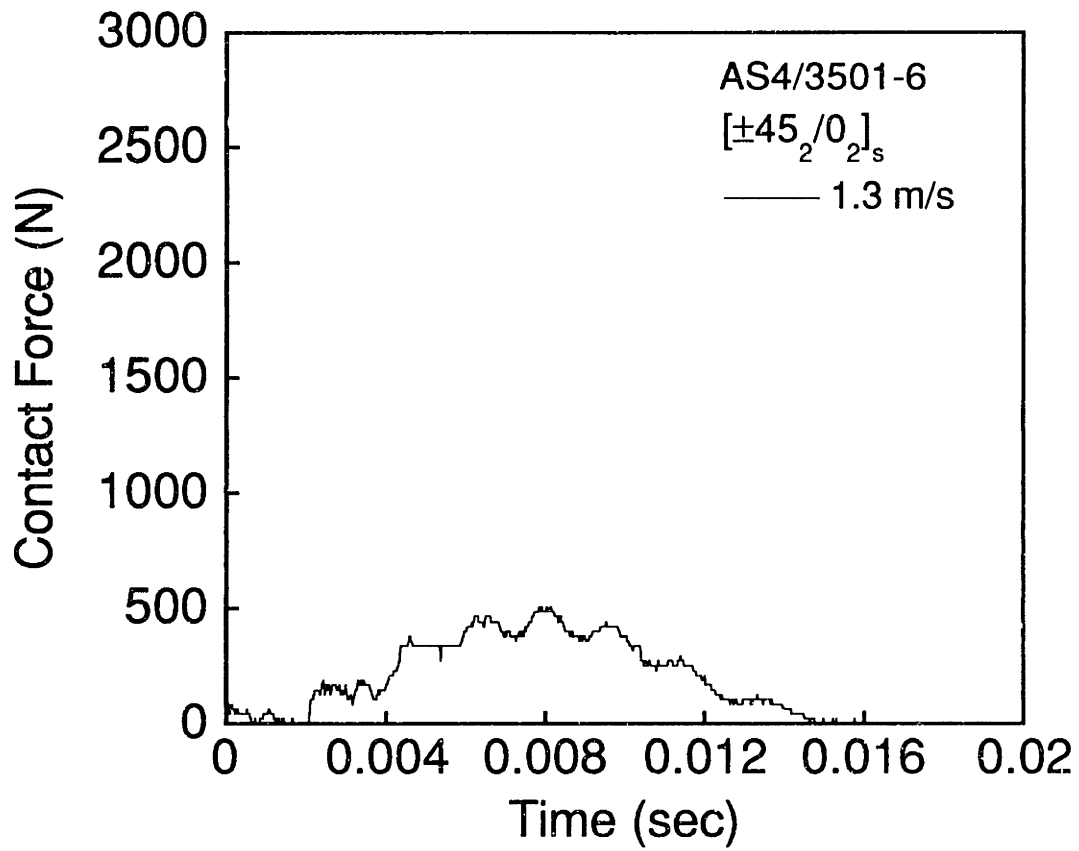
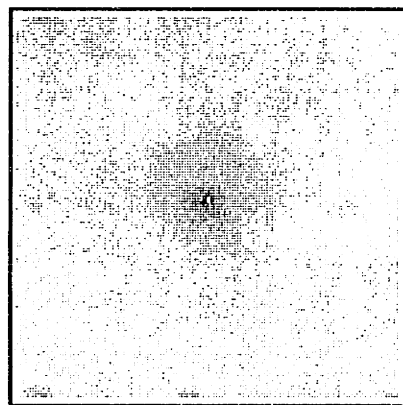
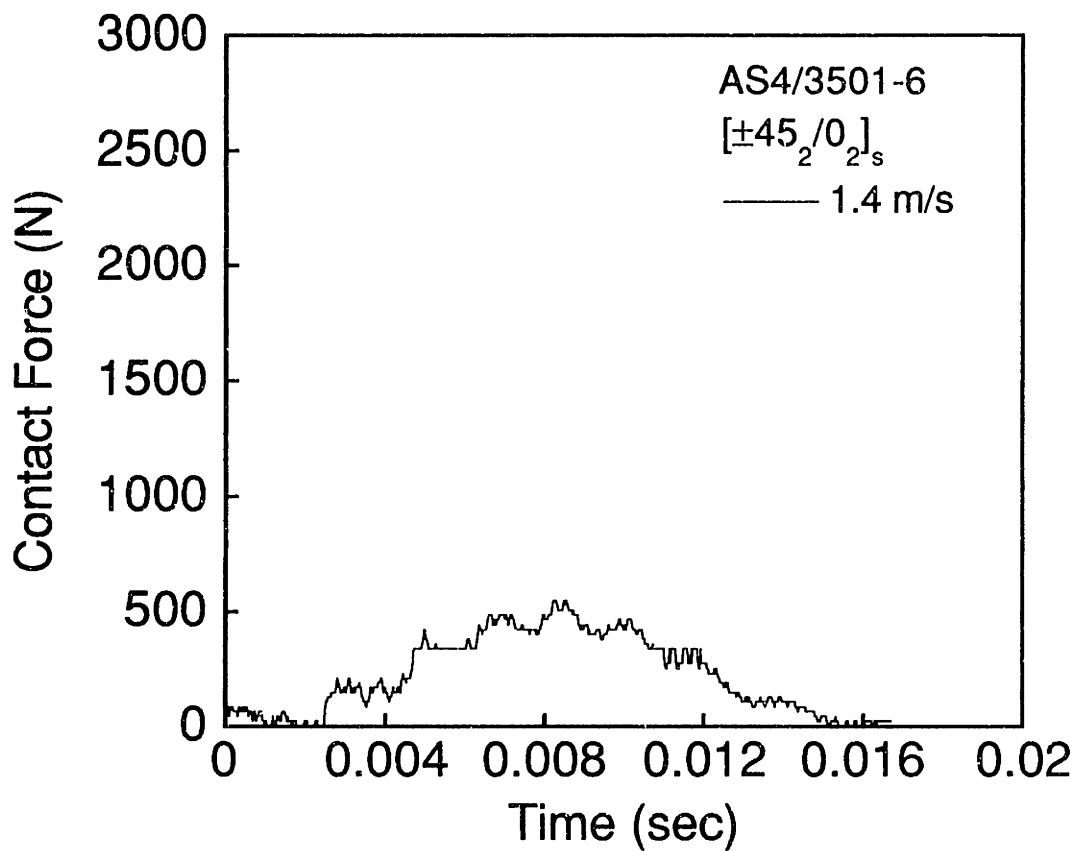


Figure A.13 (upper) Force versus time and (lower) X-ray photograph for AS4/3501-6 [±45₂/0₂]_s specimen impacted at 1.3 m/s.



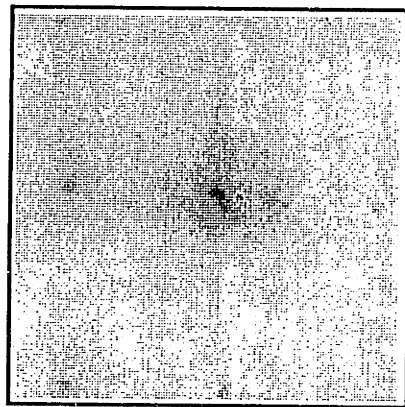
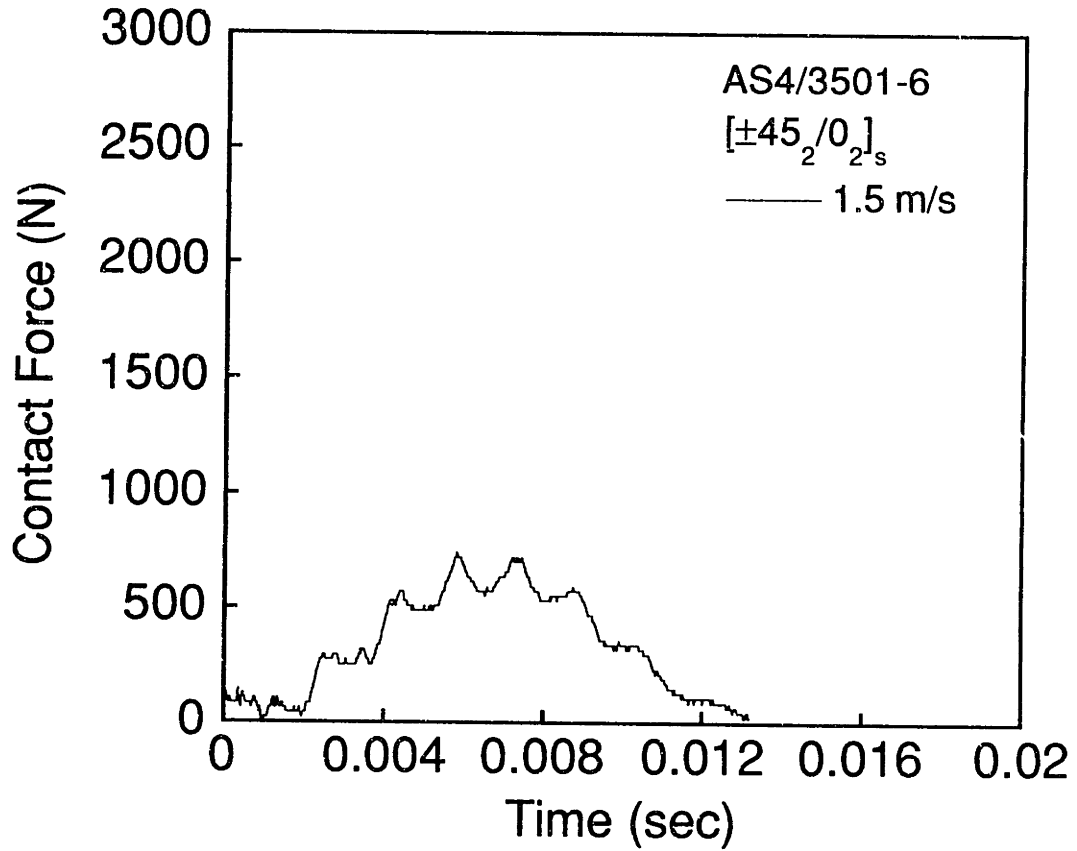
1 cm

Figure A.14 (upper) Force versus time and (lower) X-ray photograph for AS4/3501-6 [±45₂/0₂]_s specimen impacted at 1.3 m/s.



1 cm

Figure A.15 (upper) Force versus time and (lower) X-ray photograph for AS4/3501-6 [±45₂/0₂]_s specimen impacted at 1.4 m/s.



1 cm

Figure A.16 (upper) Force versus time and (lower) X-ray photograph for AS4/3501-6 [±45₂/0₂]_s specimen impacted at 1.5 m/s.

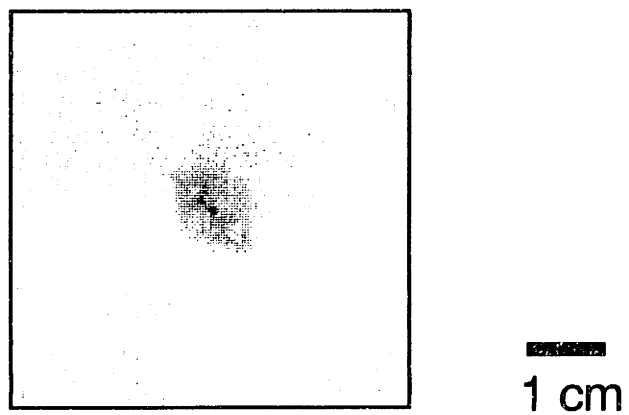
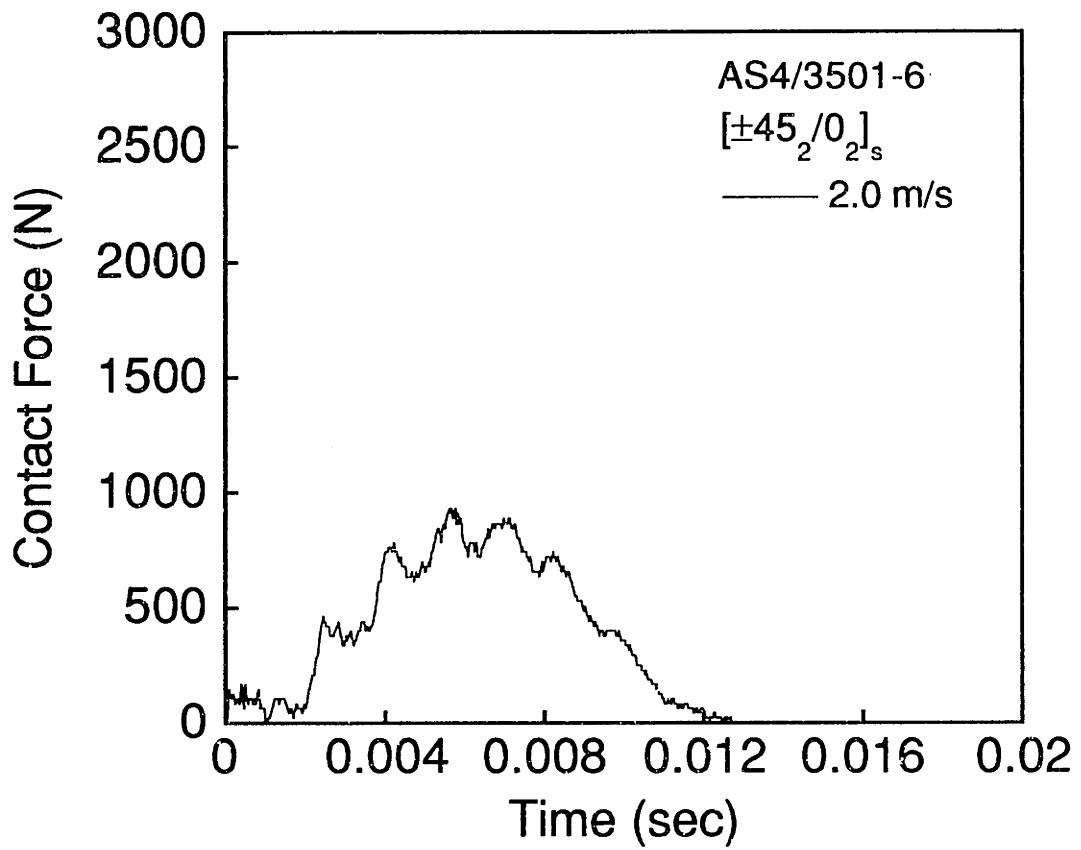


Figure A.17 (upper) Force versus time and (lower) X-ray photograph for AS4/3501-6 [±45₂/0₂]_s specimen impacted at 2.0 m/s.

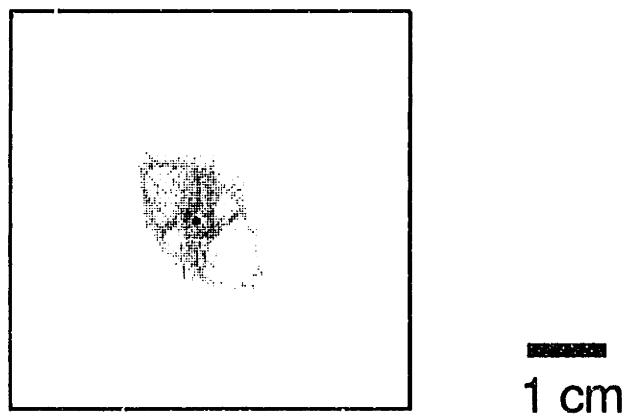
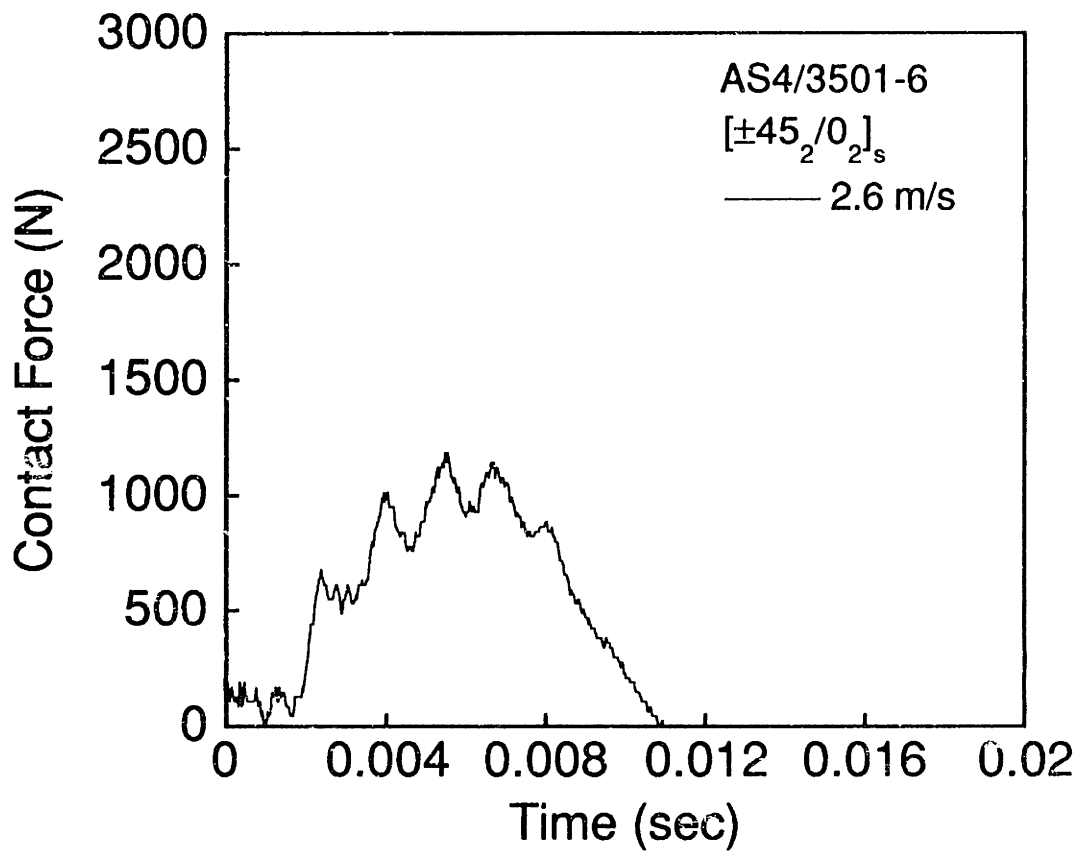


Figure A.18 (upper) Force versus time and (lower) X-ray photograph for AS4/3501-6 [±45₂/0₂]_s specimen impacted at 2.6 m/s.

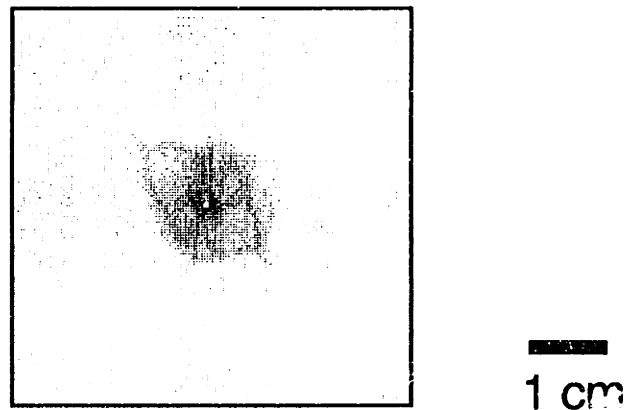
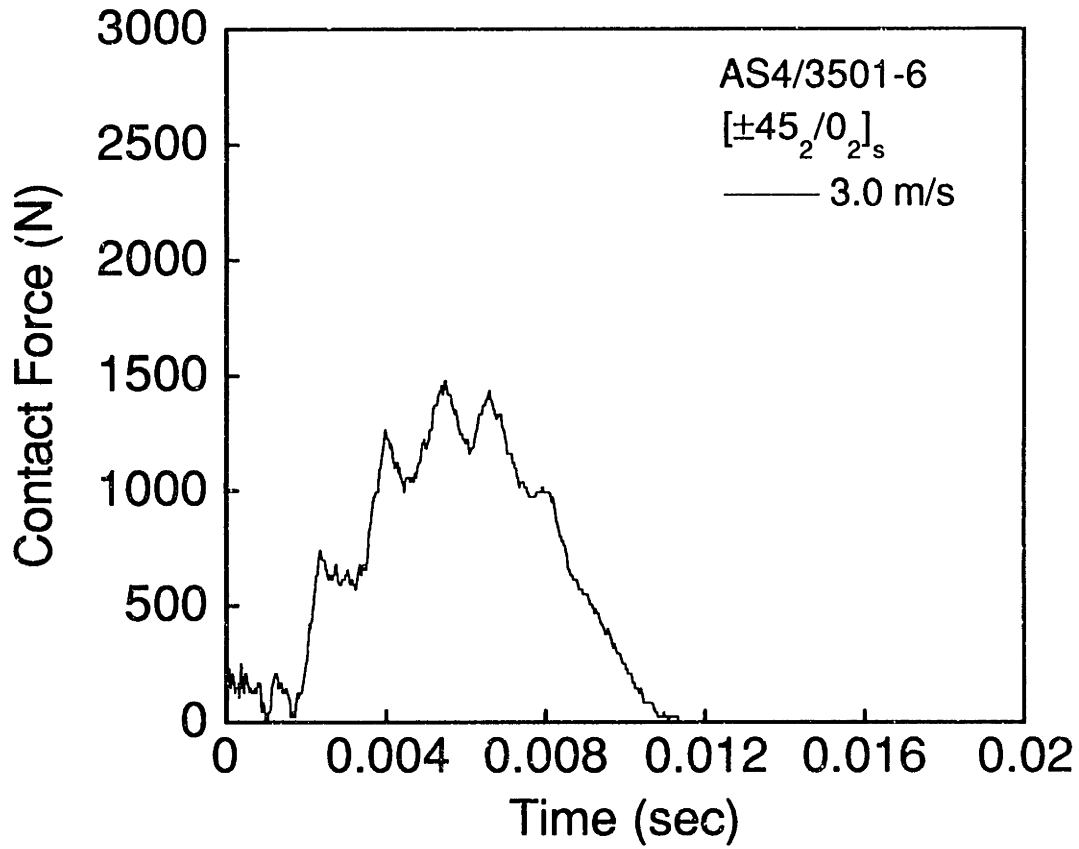
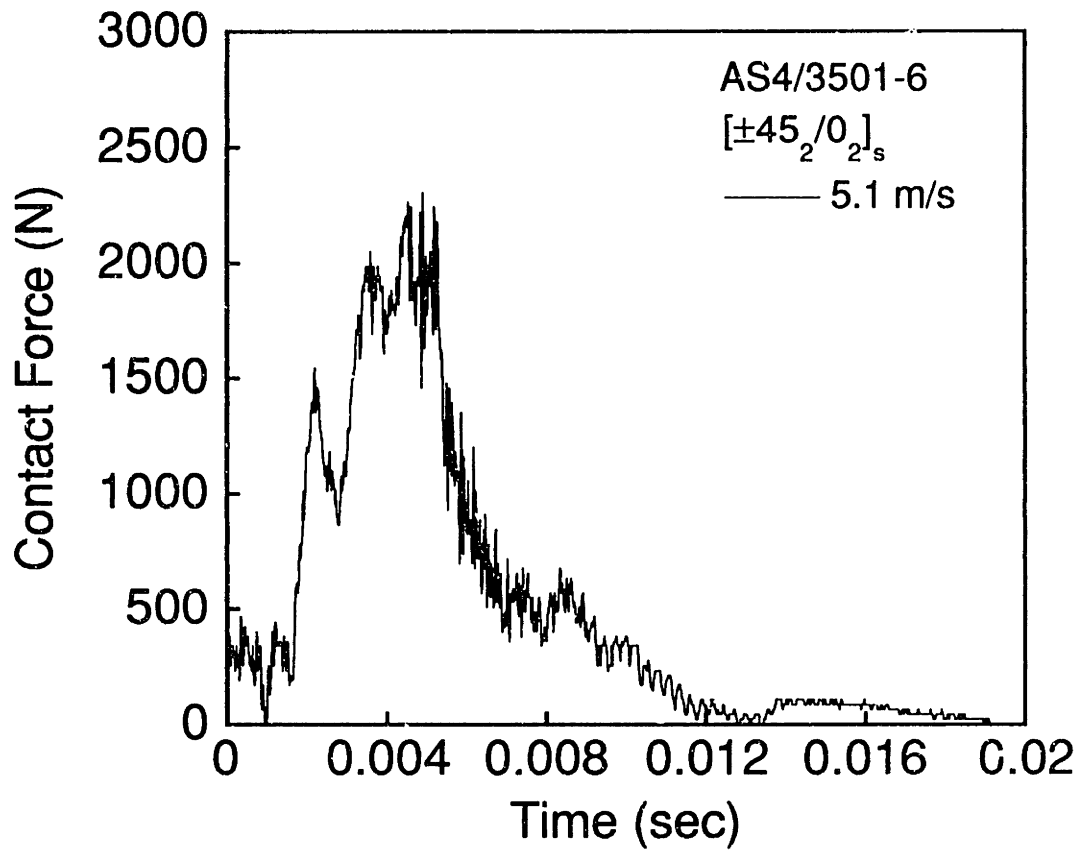


Figure A.19 (upper) Force versus time and (lower) X-ray photograph for AS4/3501-6 [±45₂/0₂]_s specimen impacted at 3.0 m/s.



1 cm

Figure A.20 (upper) Force versus time and (lower) X-ray photograph for AS4/3501-6 [±45₂/0₂]₈ specimen impacted at 5.1 m/s.

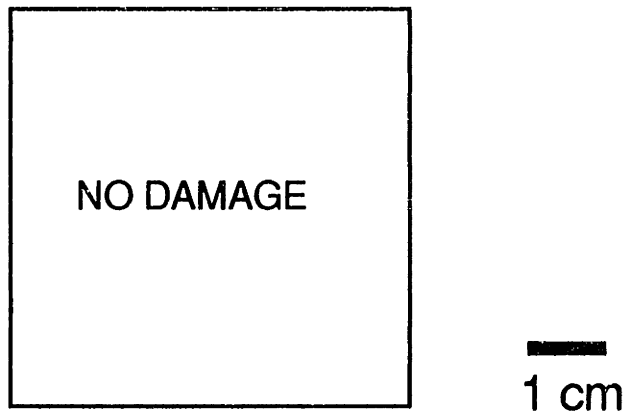
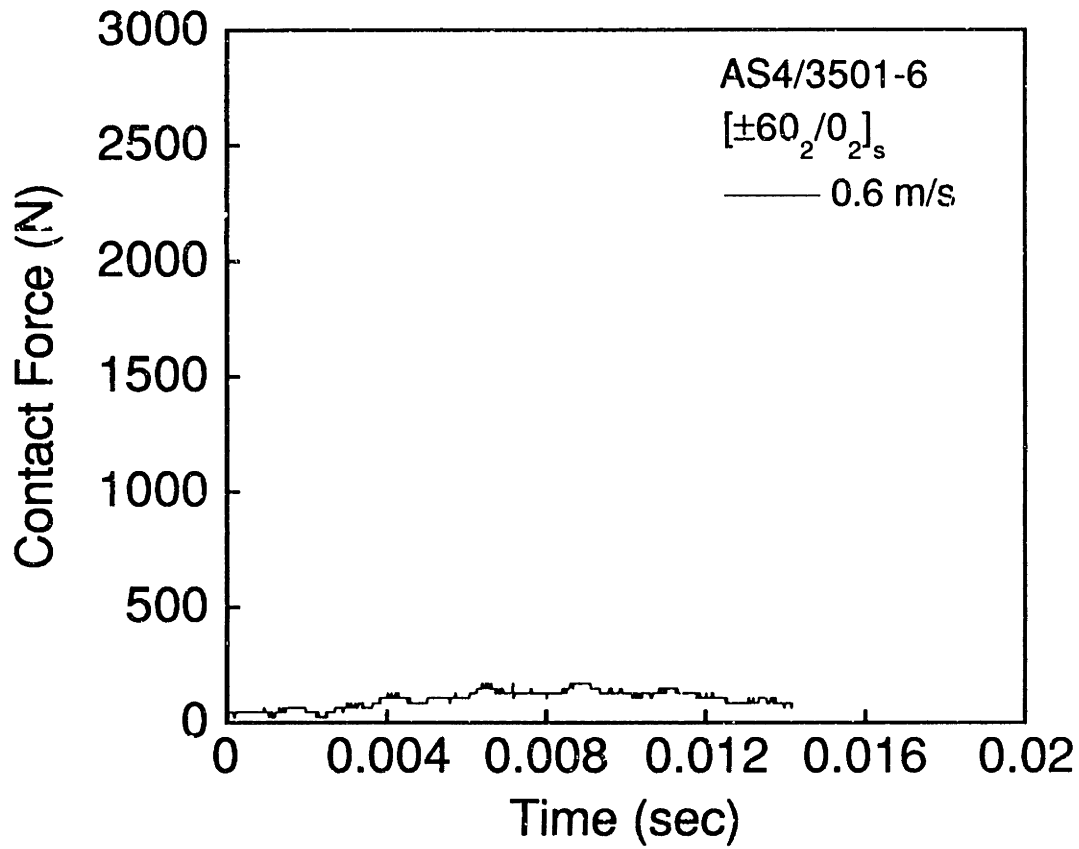


Figure A.21 (upper) Force versus time and (lower) X-ray photograph for AS4/3501-6 [±60₂/0₂]_s specimen impacted at 0.6 m/s.

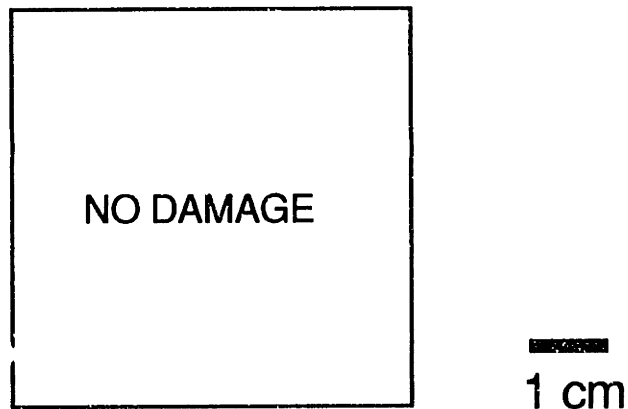
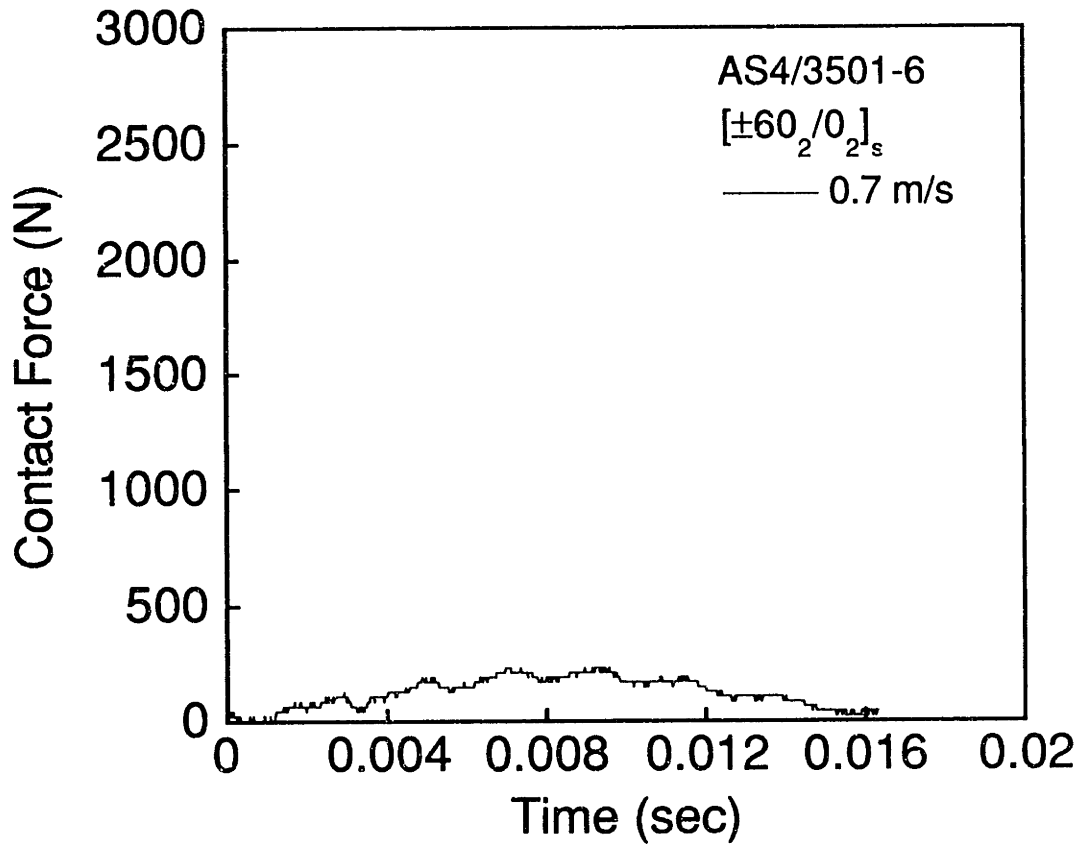


Figure A.22 (upper) Force versus time and (lower) X-ray photograph for AS4/3501-6 [±60₂/0₂]_s specimen impacted at 0.7 m/s.

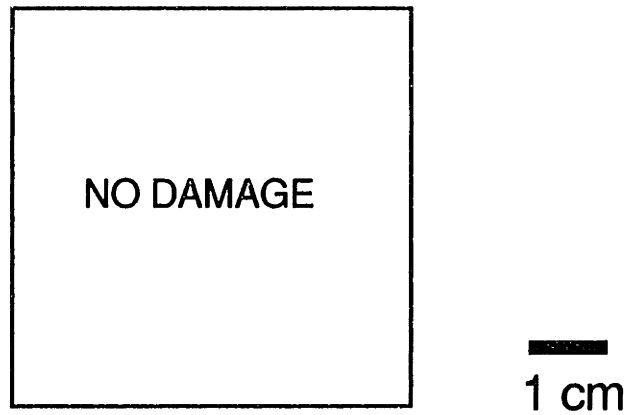
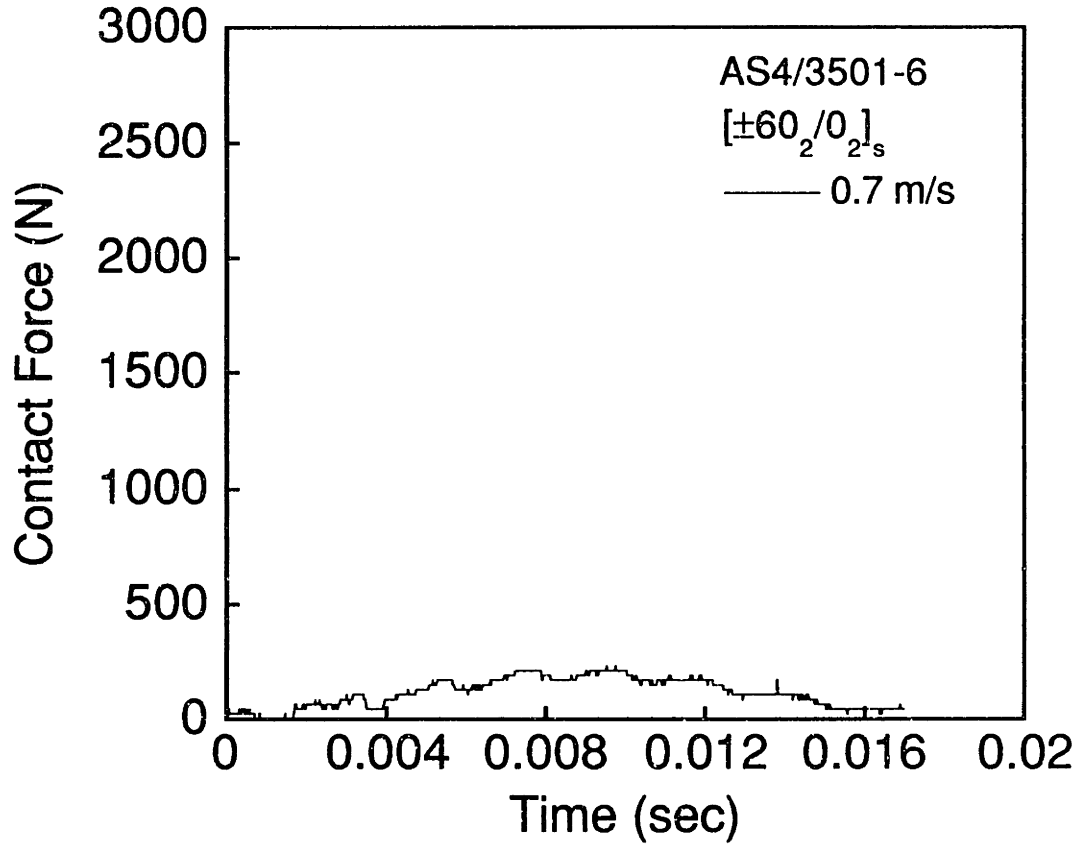
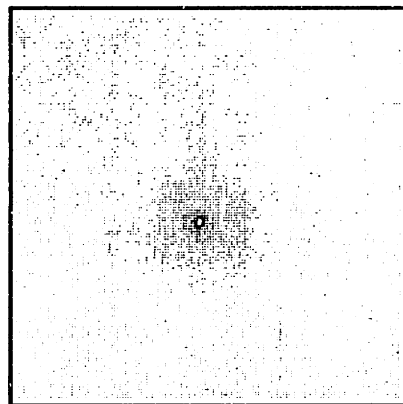
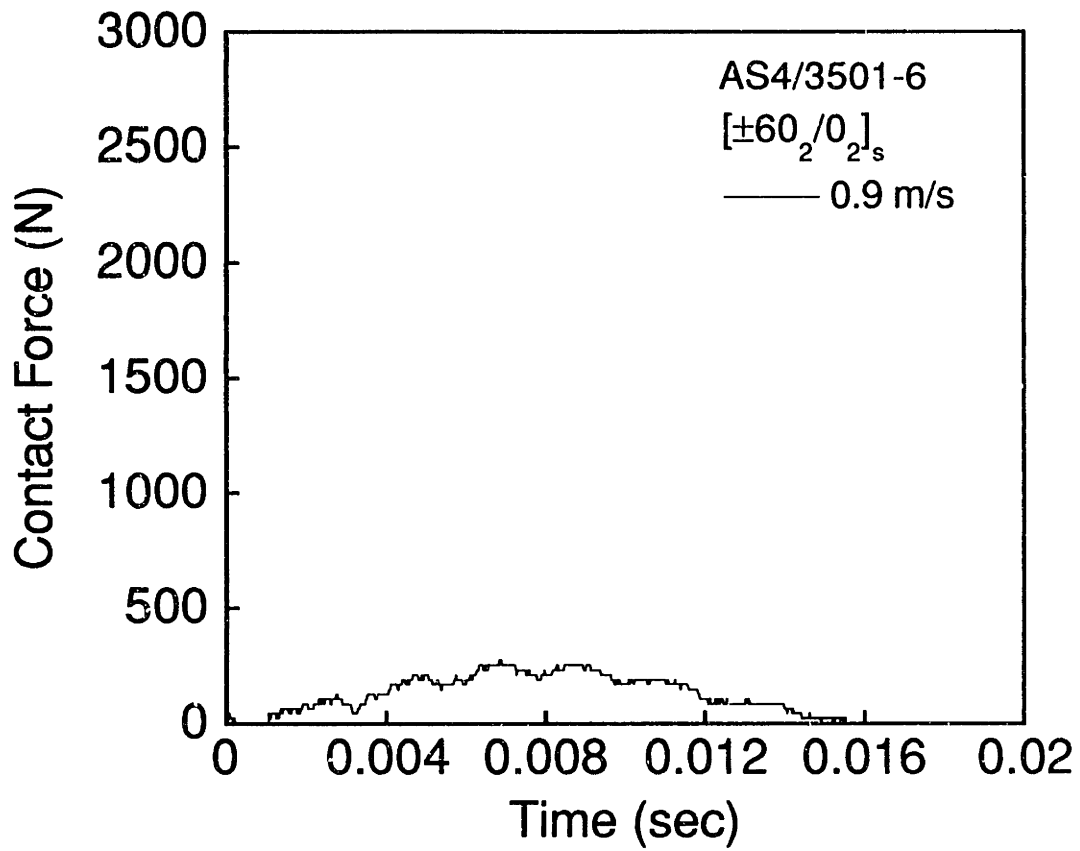


Figure A.23 (upper) Force versus time and (lower) X-ray photograph for AS4/3501-6 [±60₂/0₂]_s specimen impacted at 0.7 m/s.



1 cm

Figure A.24 (upper) Force versus time and (lower) X-ray photograph for AS4/3501-6 [±60₂/0₂]_s specimen impacted at 0.9 m/s.

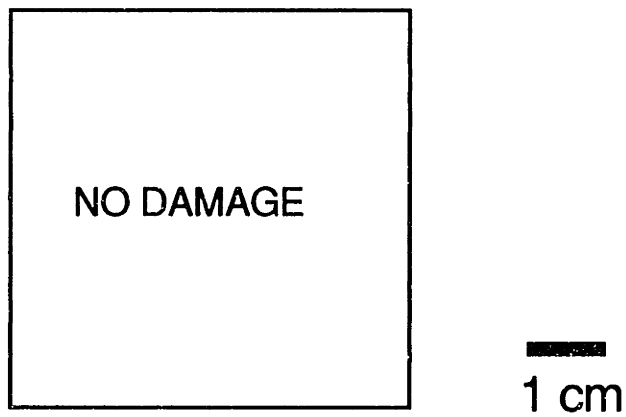
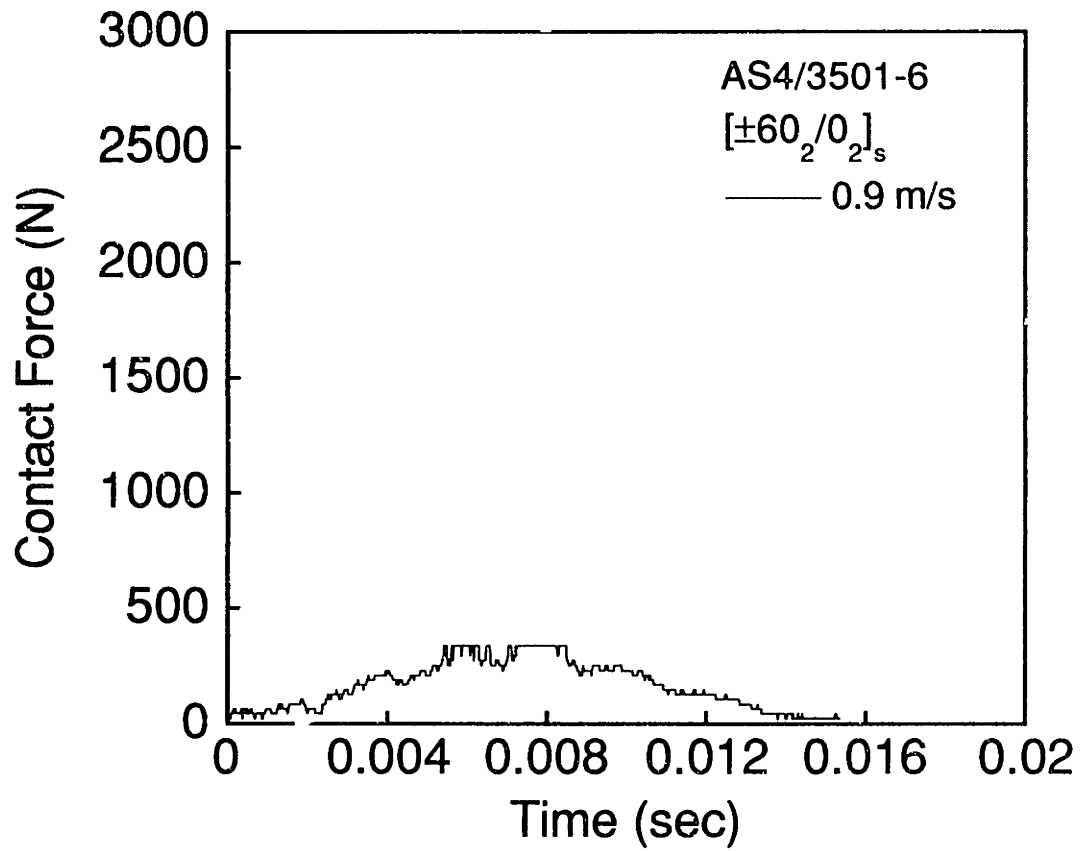


Figure A.25 (upper) Force versus time and (lower) X-ray photograph for AS4/3501-6 [±60₂/0₂]_s specimen impacted at 0.9 m/s.

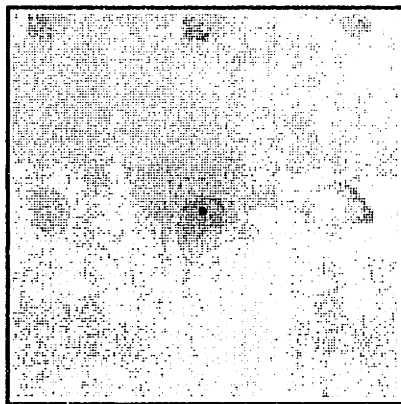
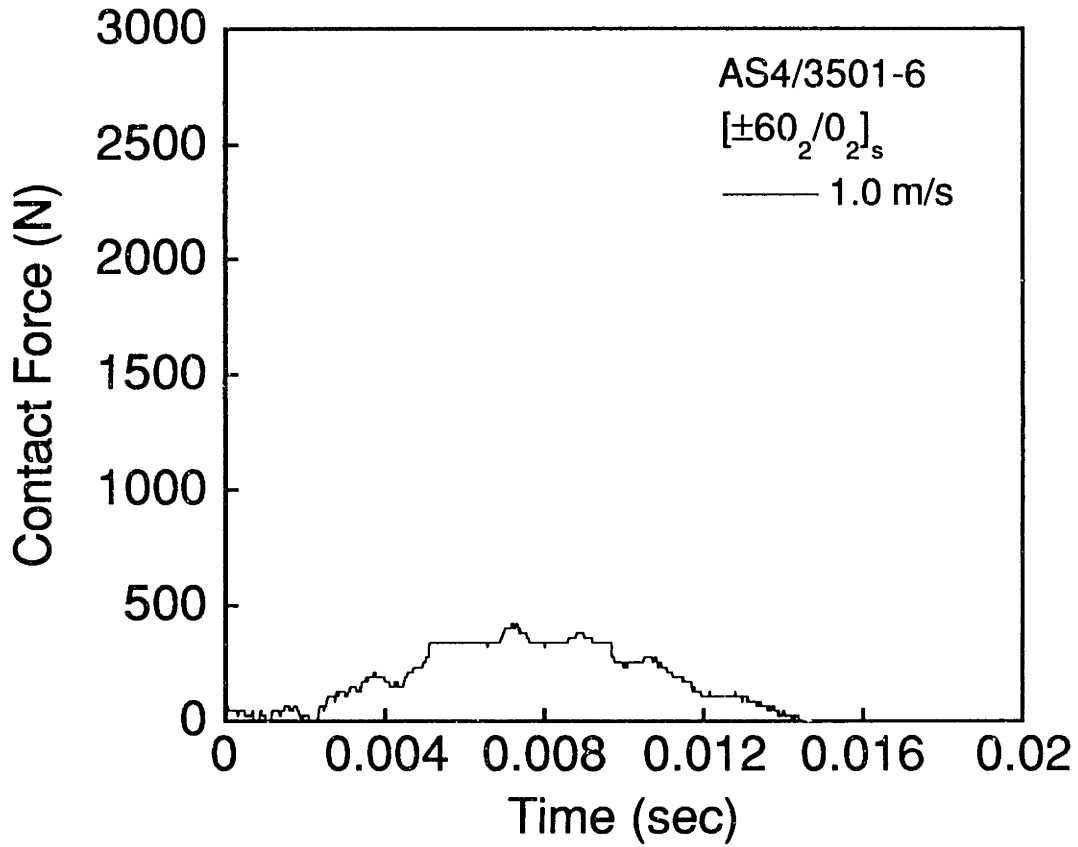
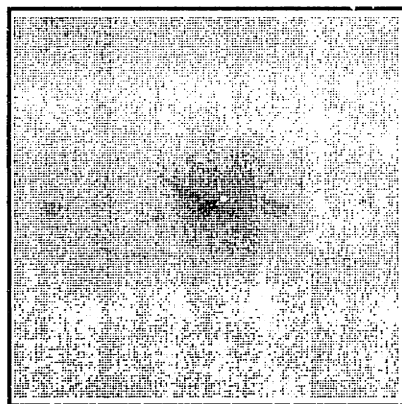
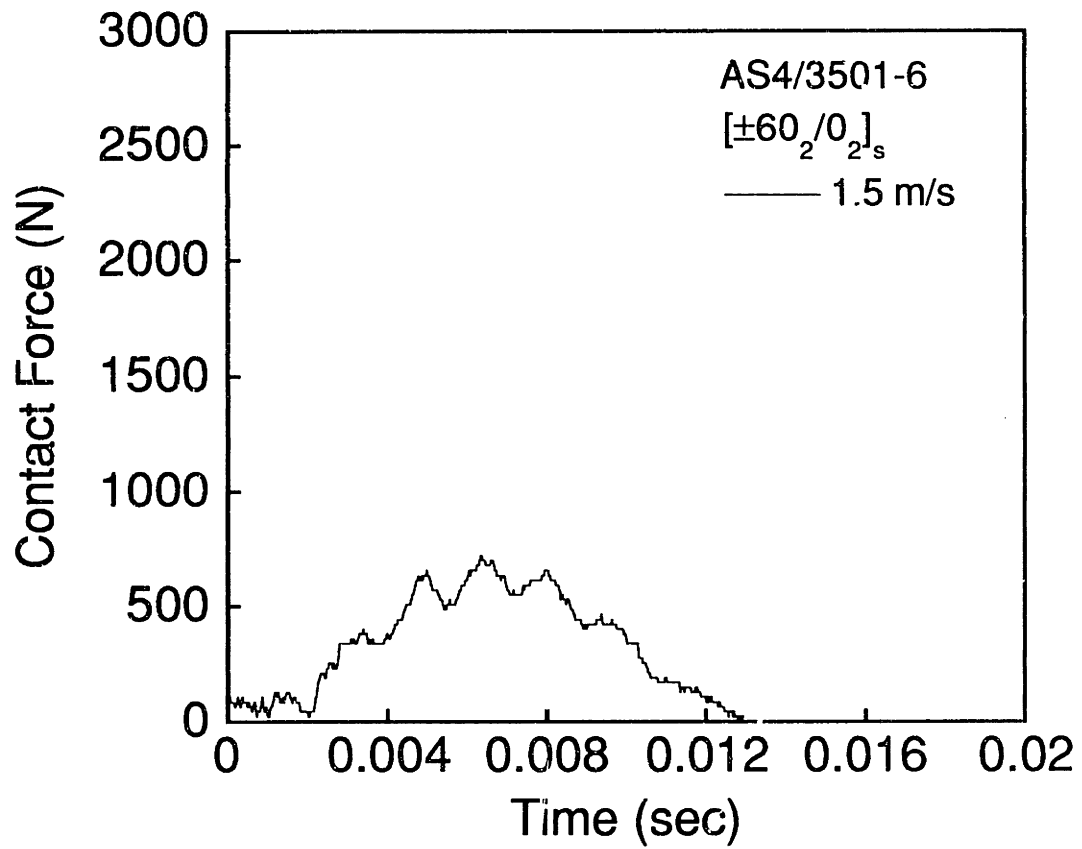


Figure A.26 (upper) Force versus time and (lower) X-ray photograph for AS4/3501-6 [±60₂/0₂]_s specimen impacted at 1.0 m/s.



1 cm

Figure A.27 (upper) Force versus time and (lower) X-ray photograph for AS4/3501-6 [±60₂/0₂]_s specimen impacted at 1.5 m/s.

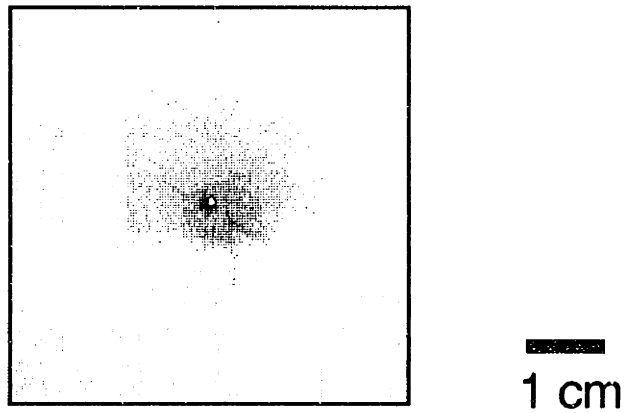
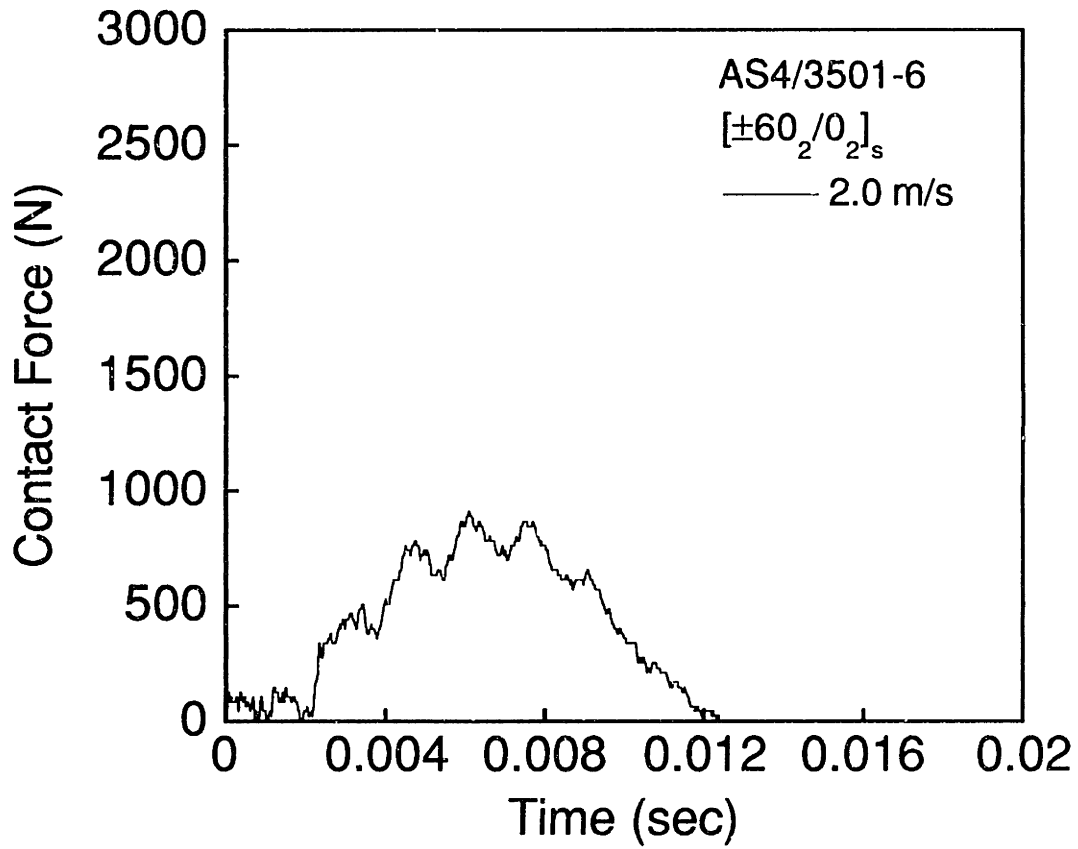


Figure A.28 (upper) Force versus time and (lower) X-ray photograph for AS4/3501-6 [±60₂/0₂]_s specimen impacted at 2.0 m/s.

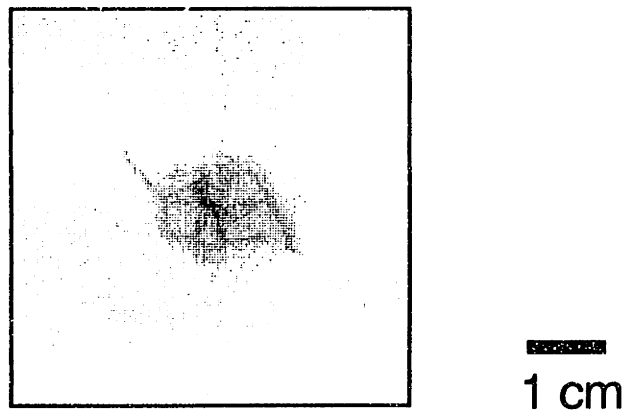
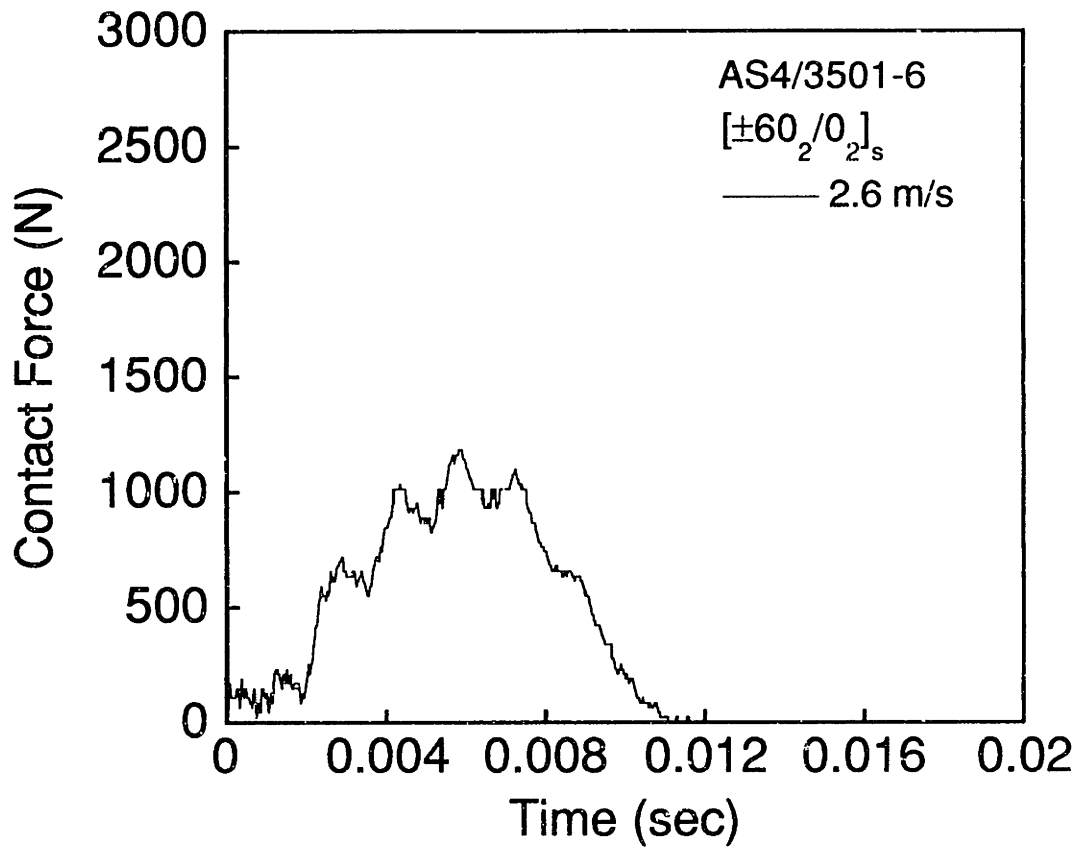
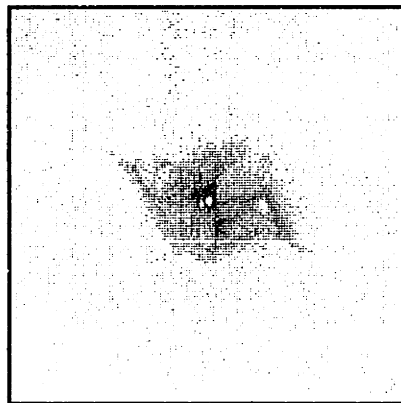
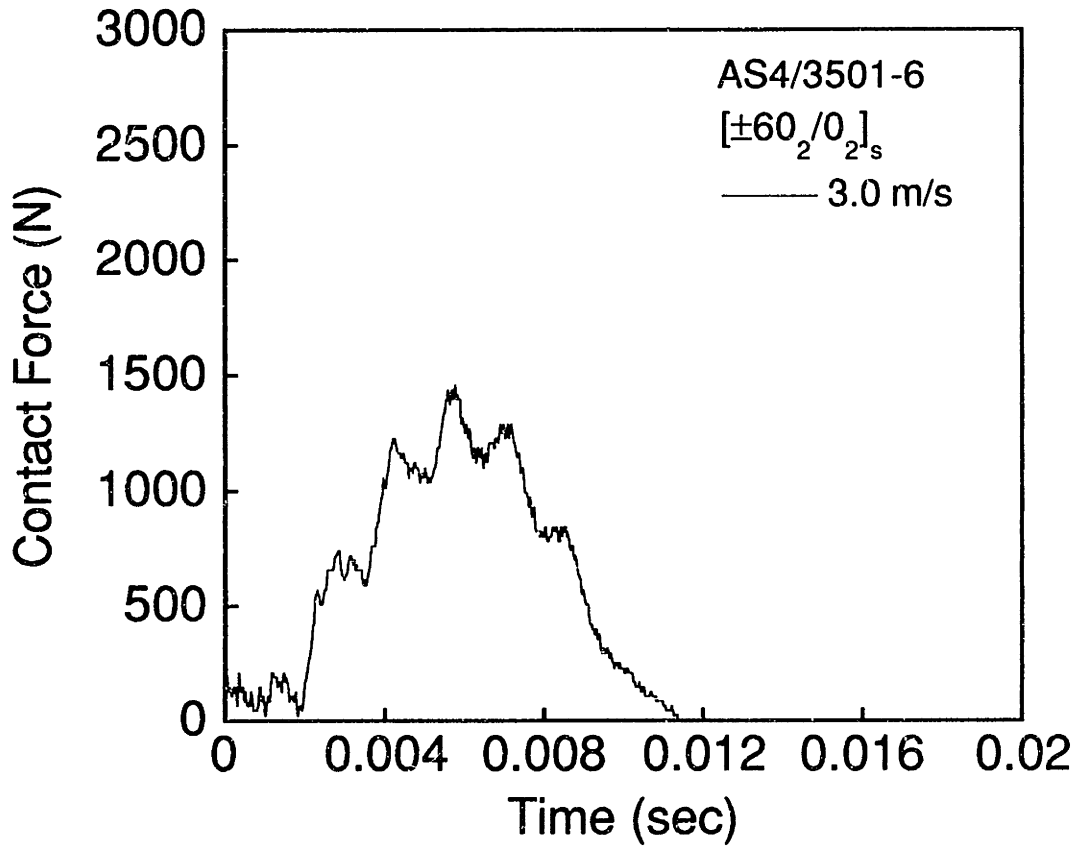
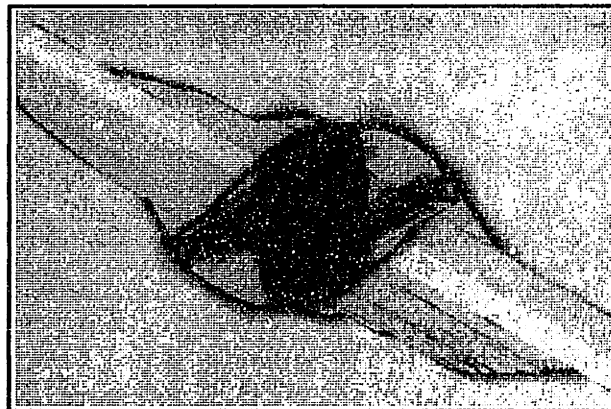
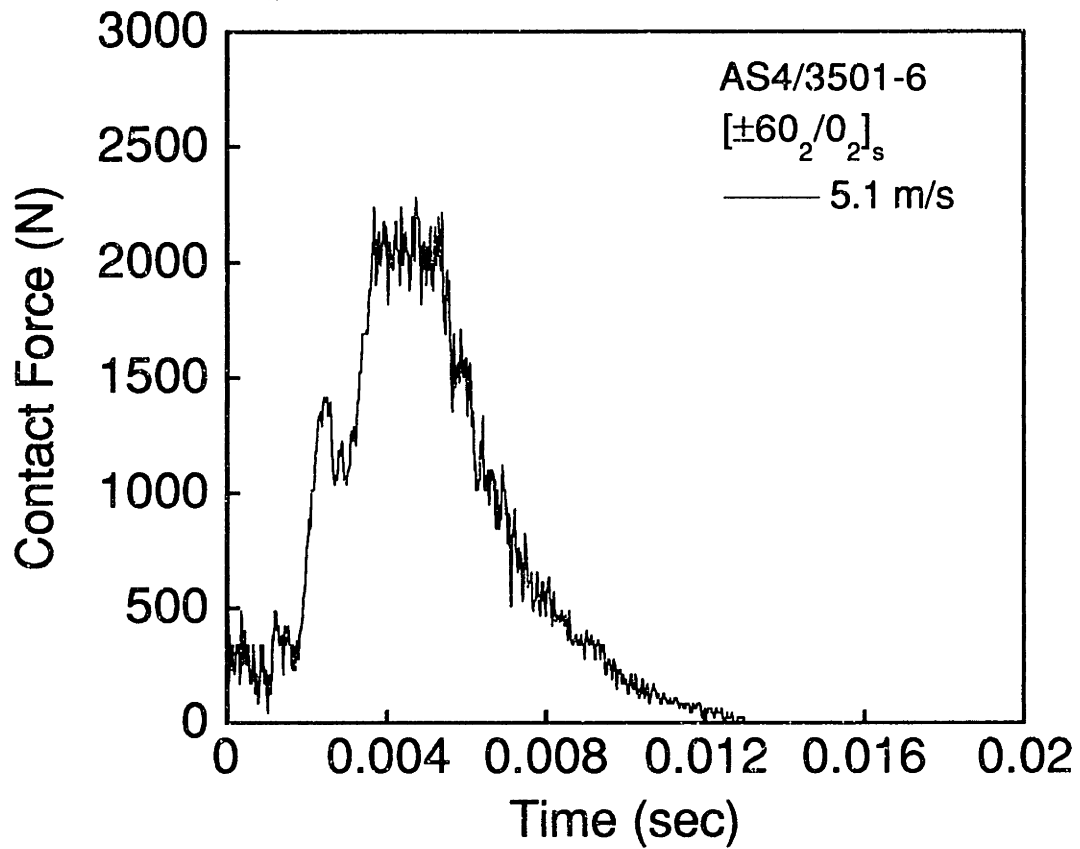


Figure A.29 (upper) Force versus time and (lower) X-ray photograph for AS4/3501-6 [±60₂/0₂]_s specimen impacted at 2.6 m/s.



1 cm

Figure A.30 (upper) Force versus time and (lower) X-ray photograph for AS4/3501-6 [±60₂/0₂]_s specimen impacted at 3.0 m/s.



1 cm

Figure A.31 (upper) Force versus time and (lower) X-ray photograph for AS4/3501-6 [±60₂/0₂]_s specimen impacted at 5.1 m/s.

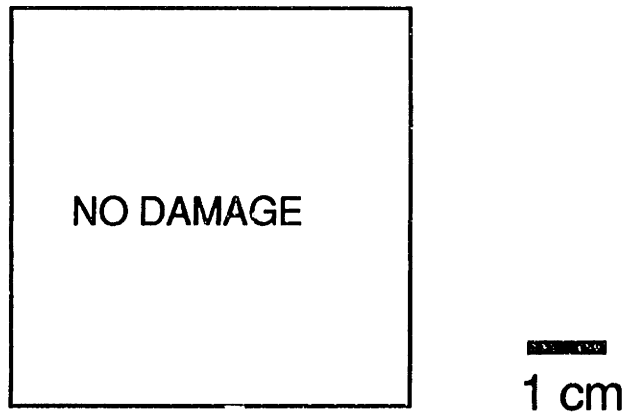
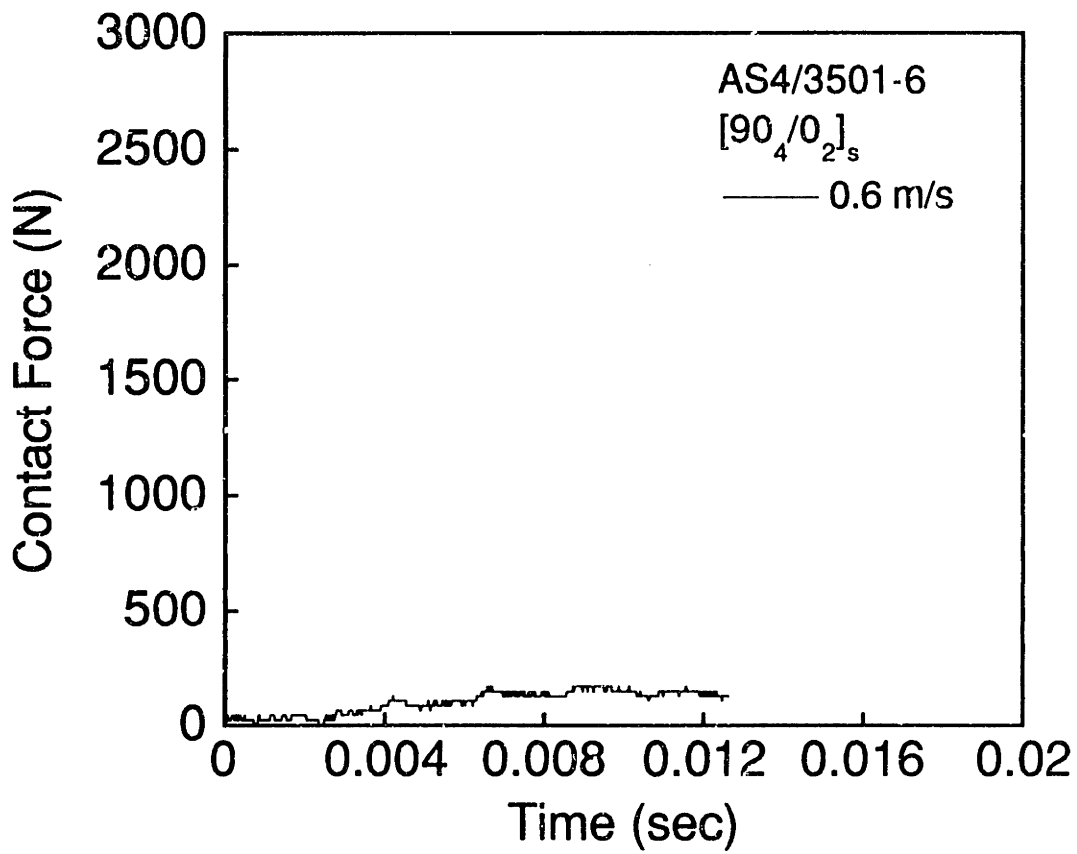


Figure A.32 (upper) Force versus time and (lower) X-ray photograph for AS4/3501-6 [90₄/0₂]_s specimen impacted at 0.6 m/s.

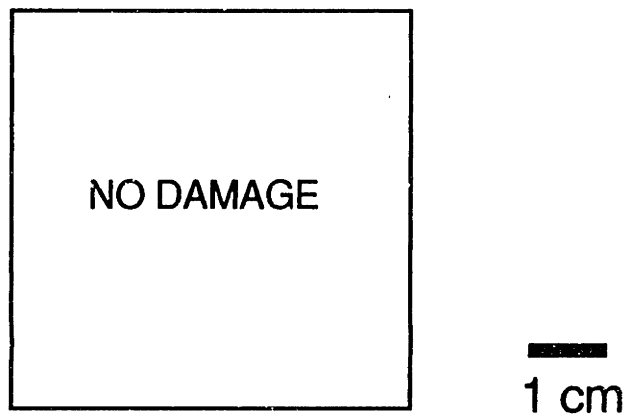
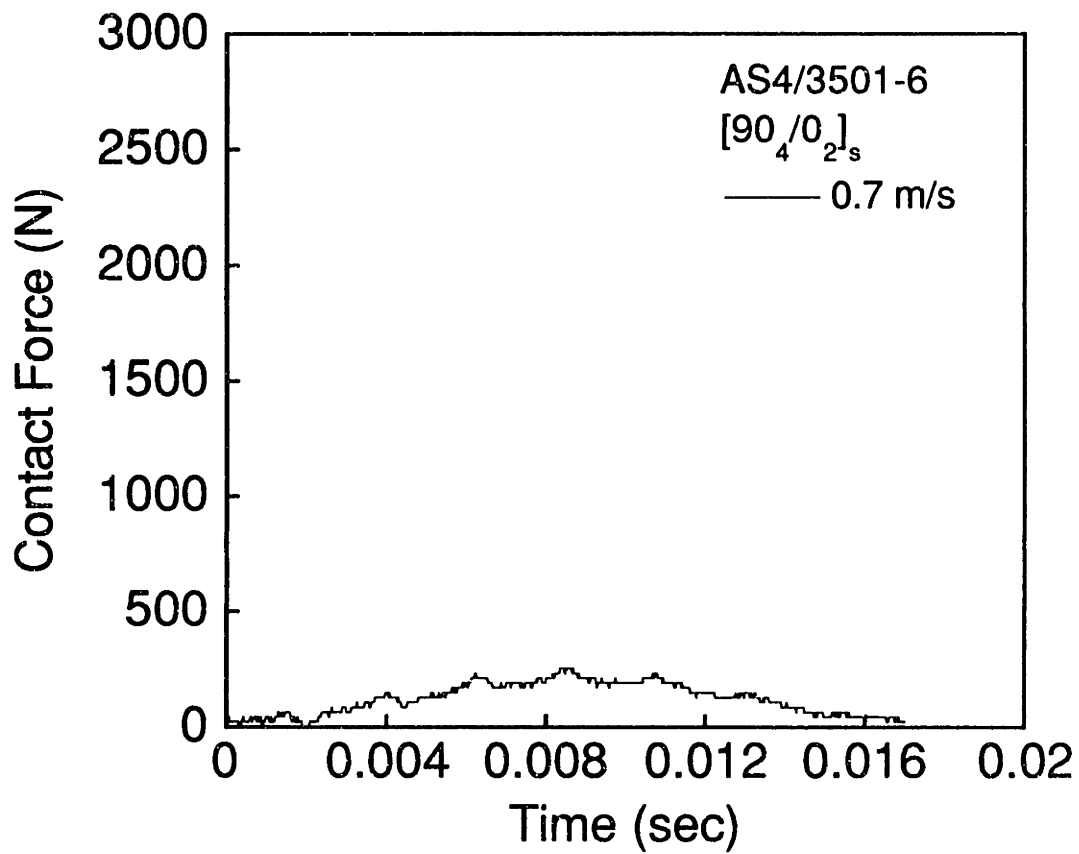
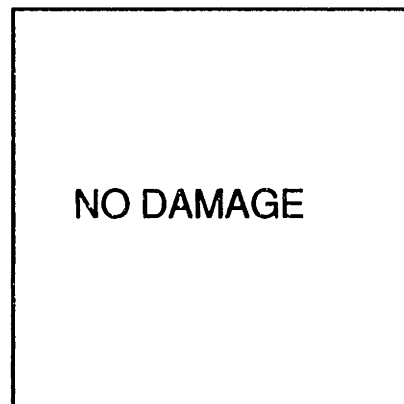
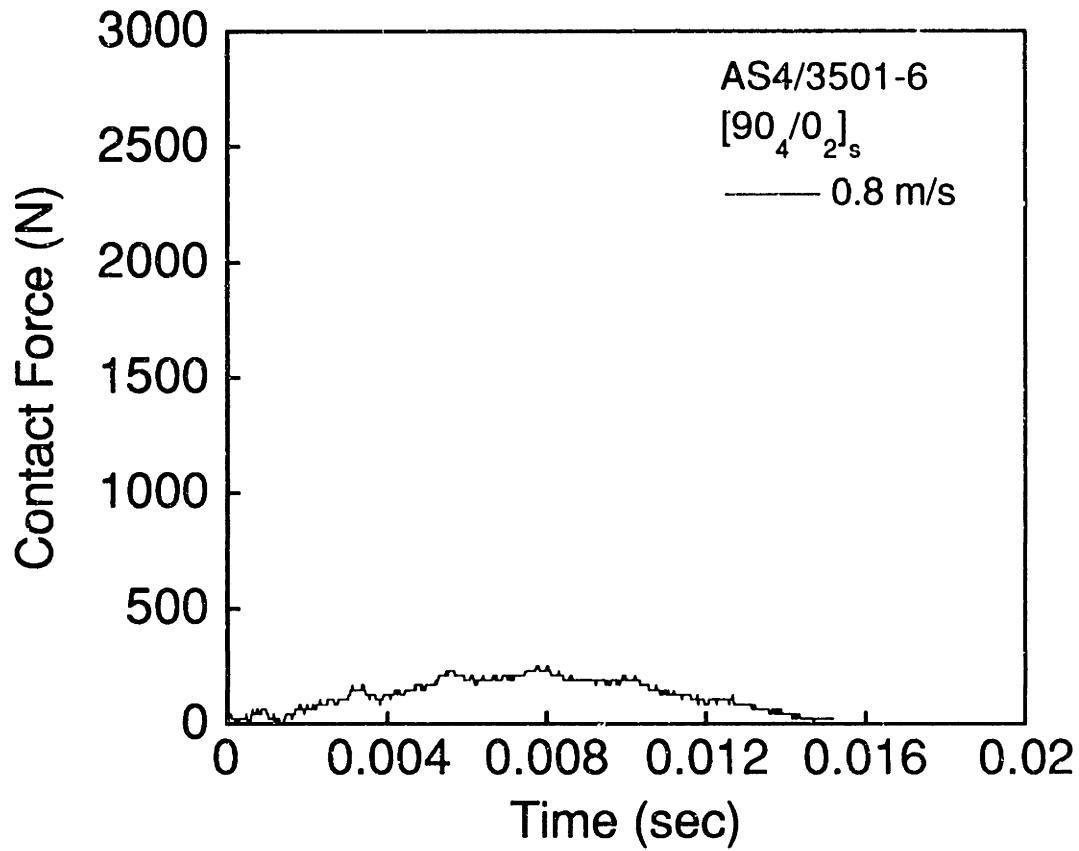


Figure A.33 (upper) Force versus time and (lower) X-ray photograph for AS4/3501-6 [90₄/0₂]_s specimen impacted at 0.7 m/s.



1 cm

Figure A.34 (upper) Force versus time and (lower) X-ray photograph for AS4/3501-6 [90₄/0₂]_s specimen impacted at 0.8 m/s.

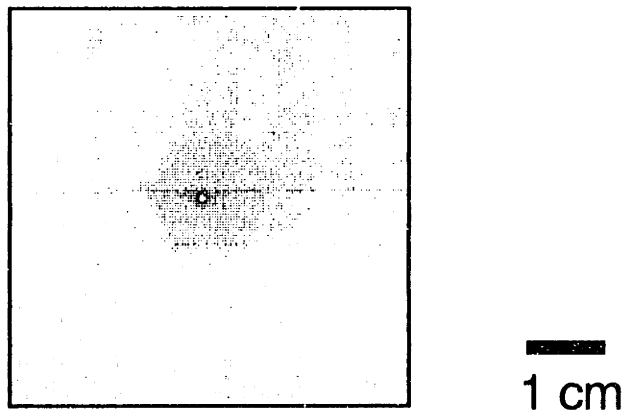
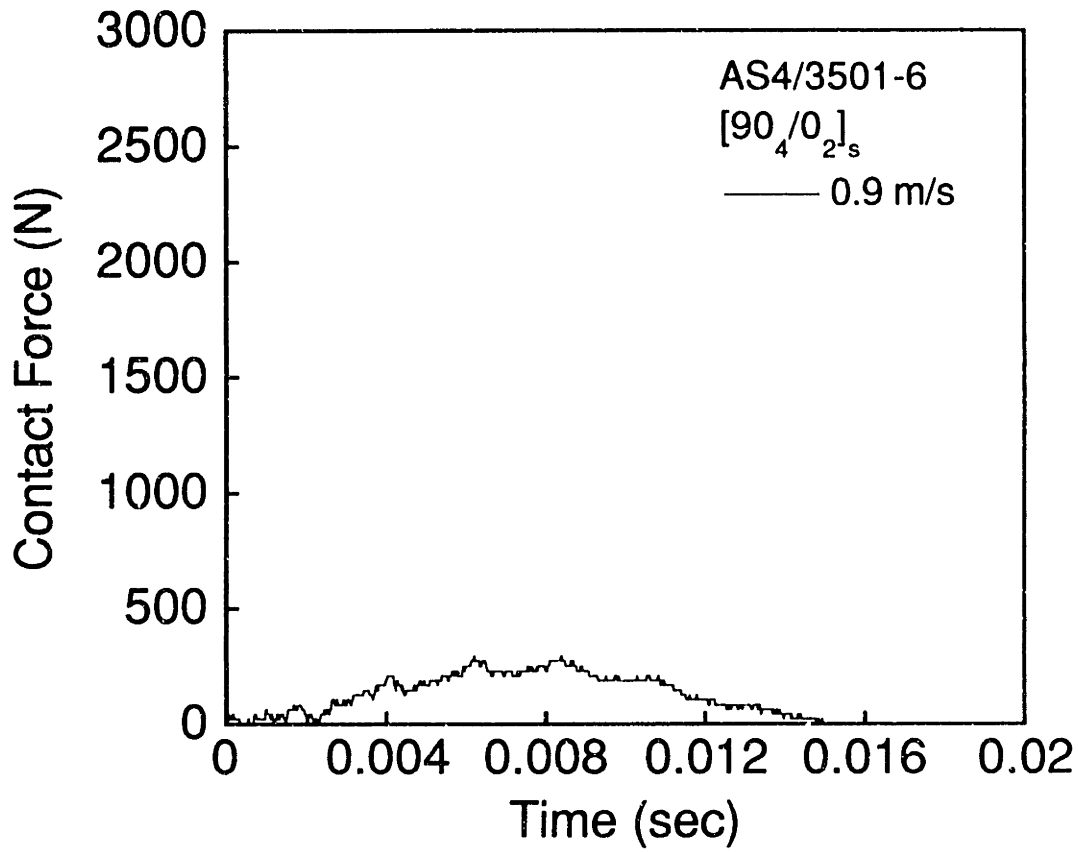


Figure A.35 (upper) Force versus time and (lower) X-ray photograph for AS4/3501-6 [90₄/0₂]_s specimen impacted at 0.9 m/s.

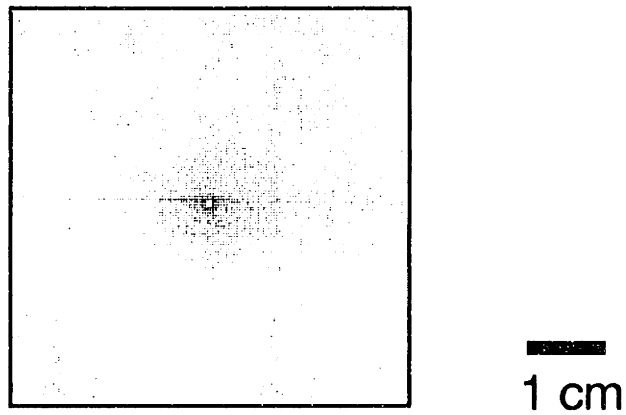
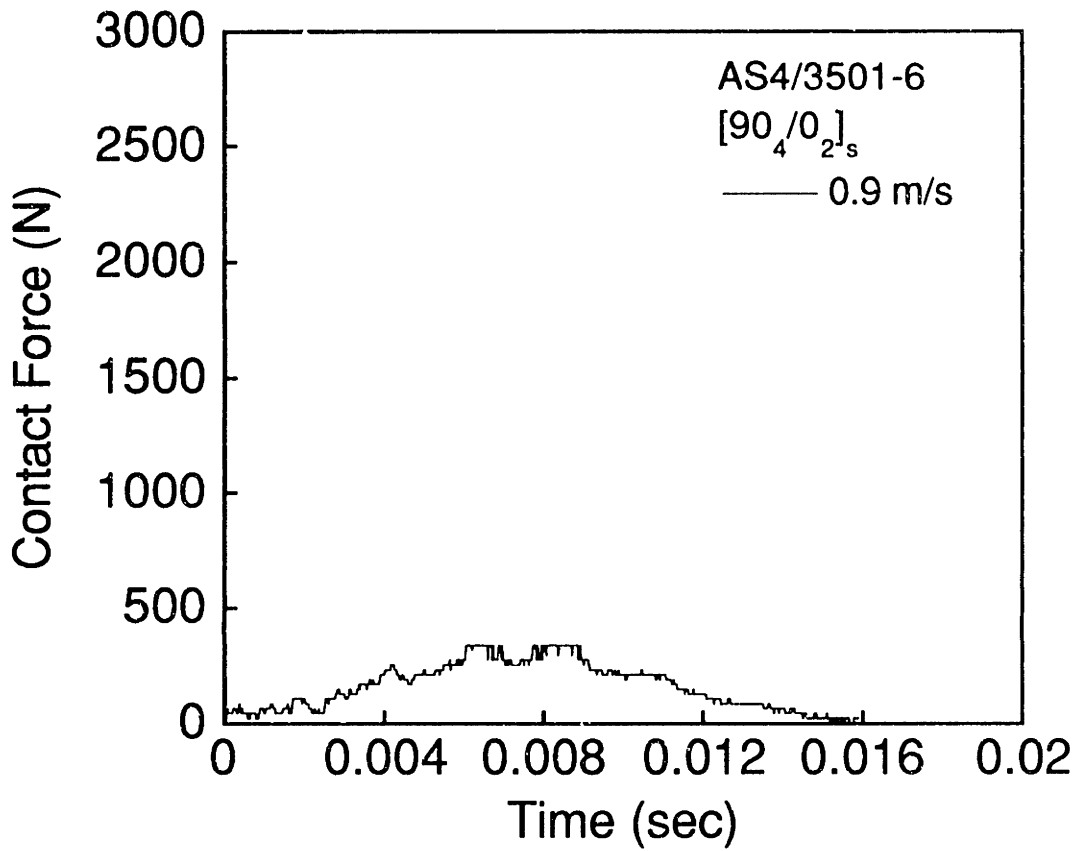


Figure A.36 (upper) Force versus time and (lower) X-ray photograph for AS4/3501-6 [90₄/0₂]_s specimen impacted at 0.9 m/s.

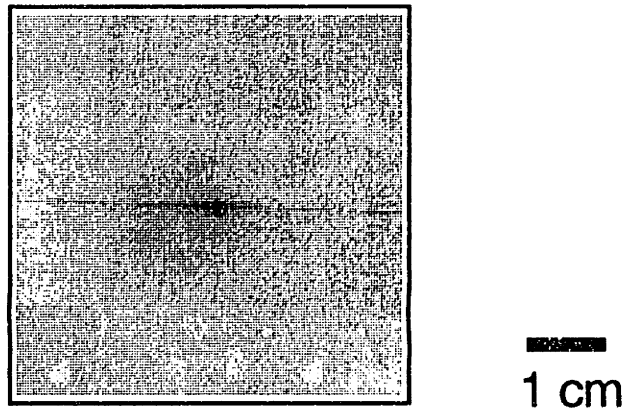
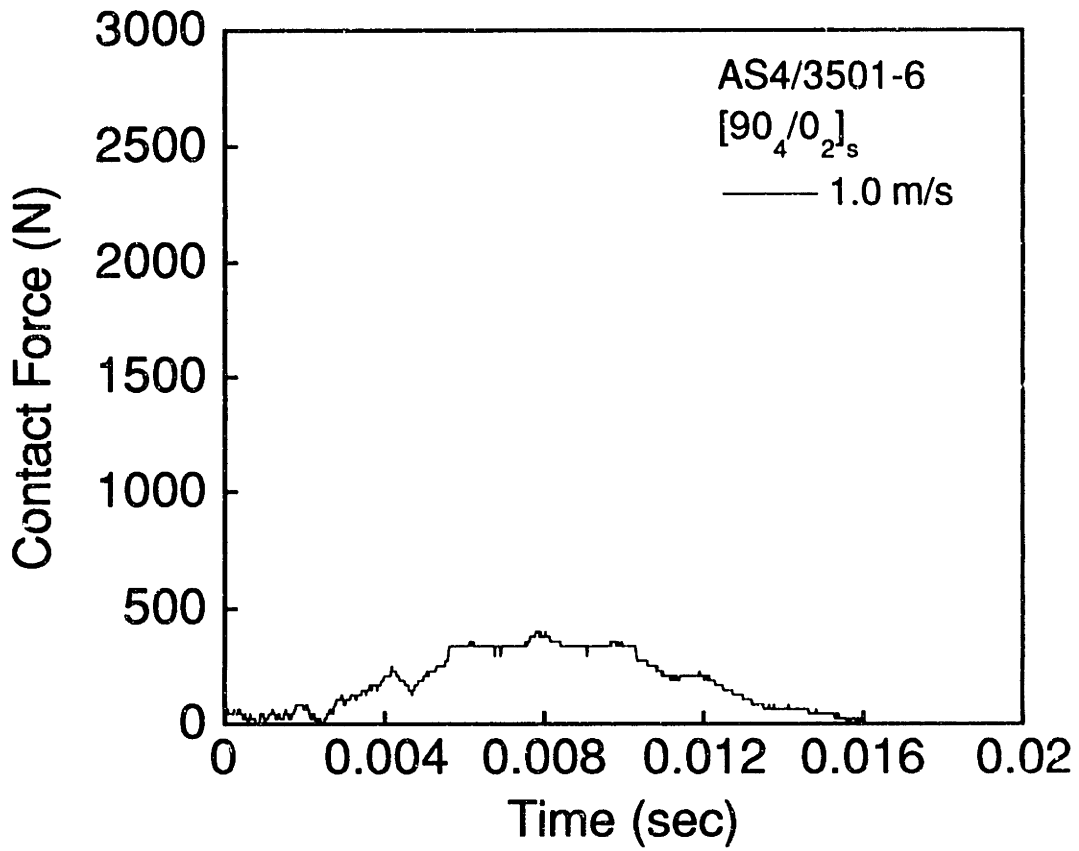
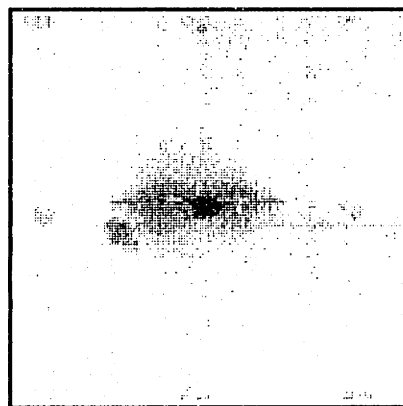
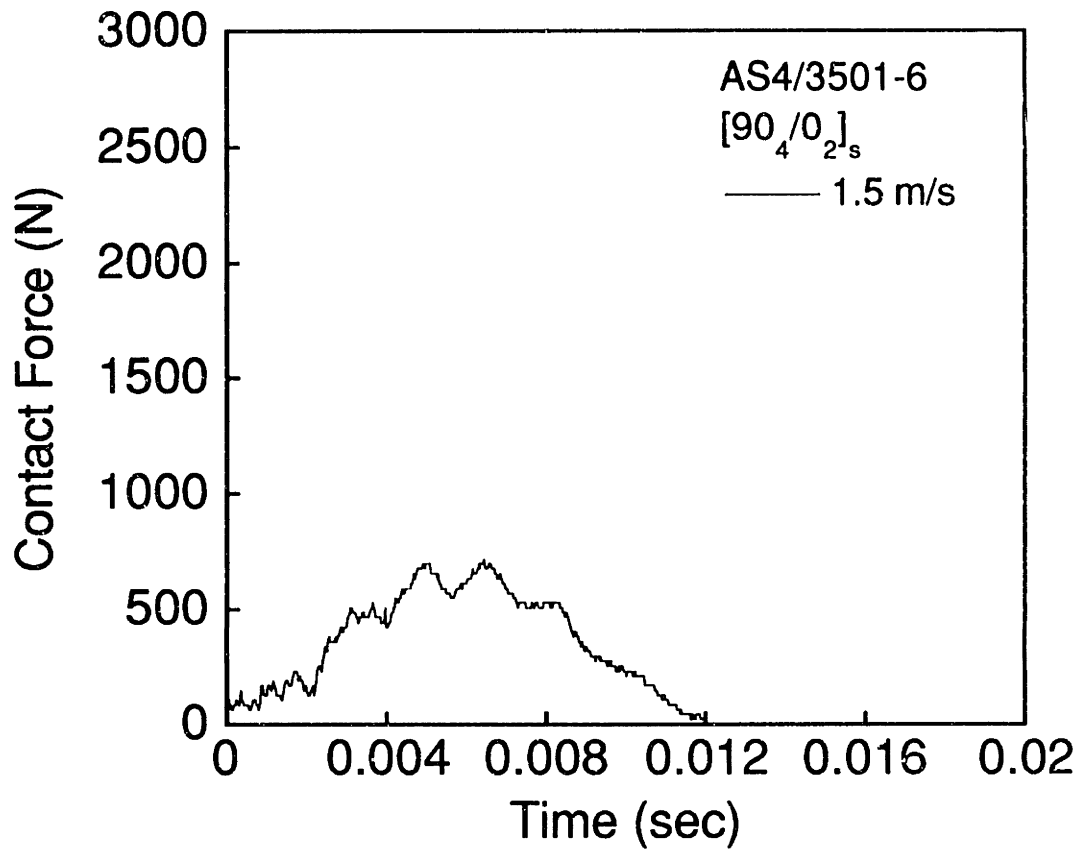


Figure A.37 (upper) Force versus time and (lower) X-ray photograph for AS4/3501-6 [90₄/0₂]_s specimen impacted at 1.0 m/s.



1 cm

Figure A.38 (upper) Force versus time and (lower) X-ray photograph for AS4/3501-6 [90₄/0₂]_s specimen impacted at 1.5 m/s.

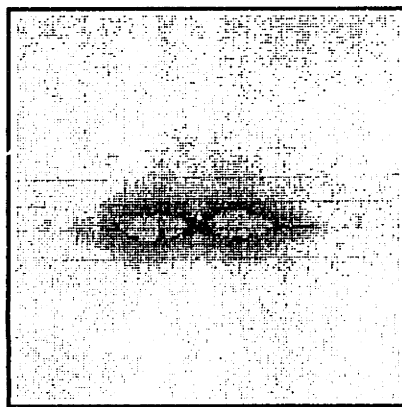
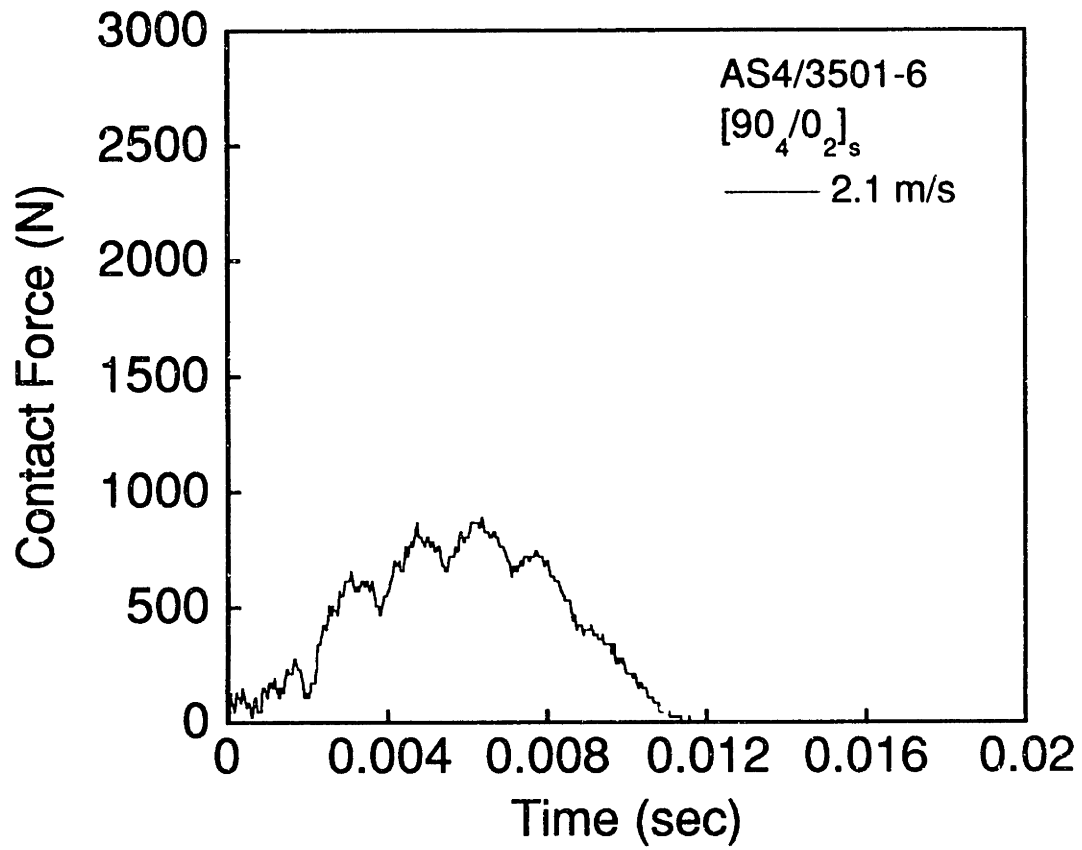


Figure A.39 (upper) Force versus time and (lower) X-ray photograph for AS4/3501-6 [90₄/0₂]_s specimen impacted at 2.1 m/s.

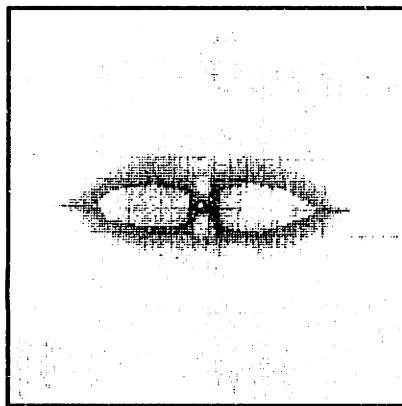
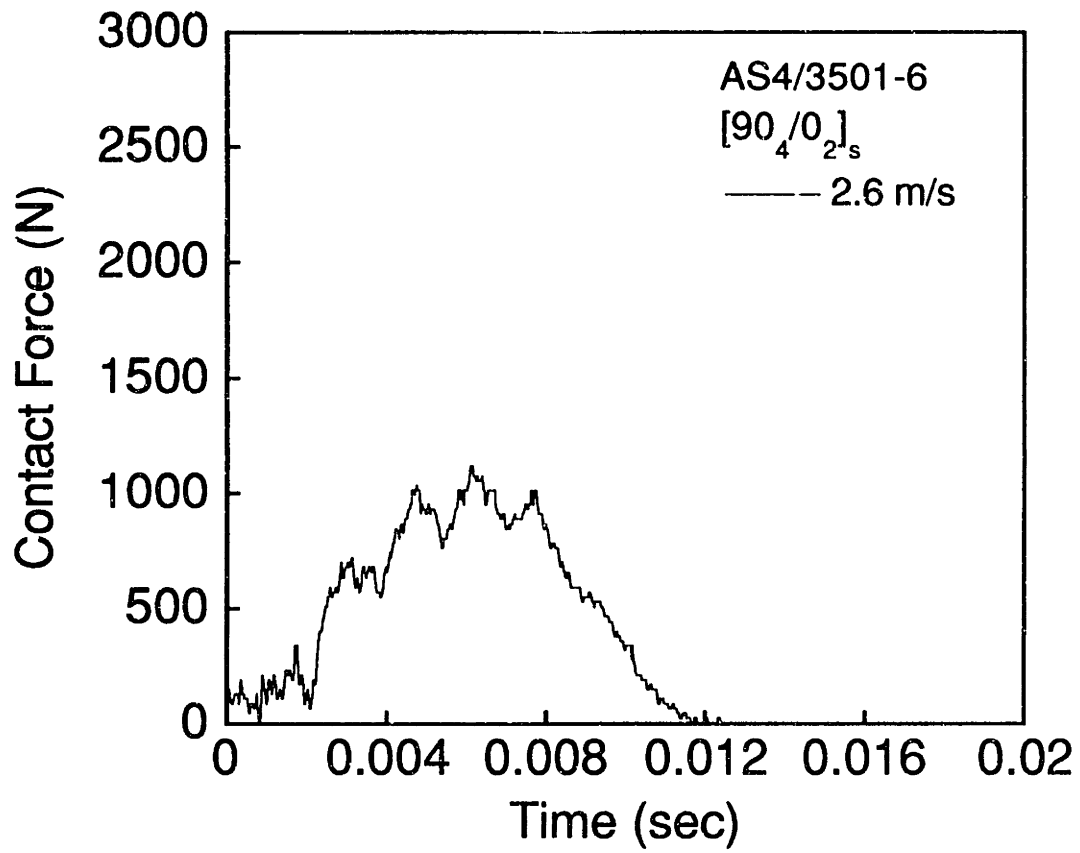
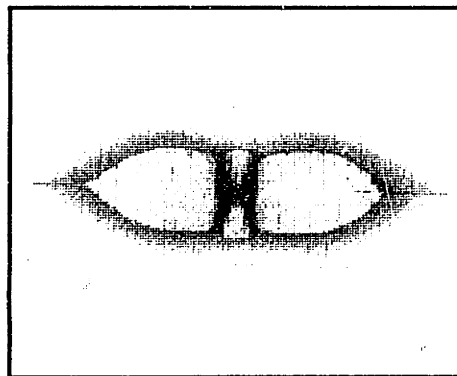
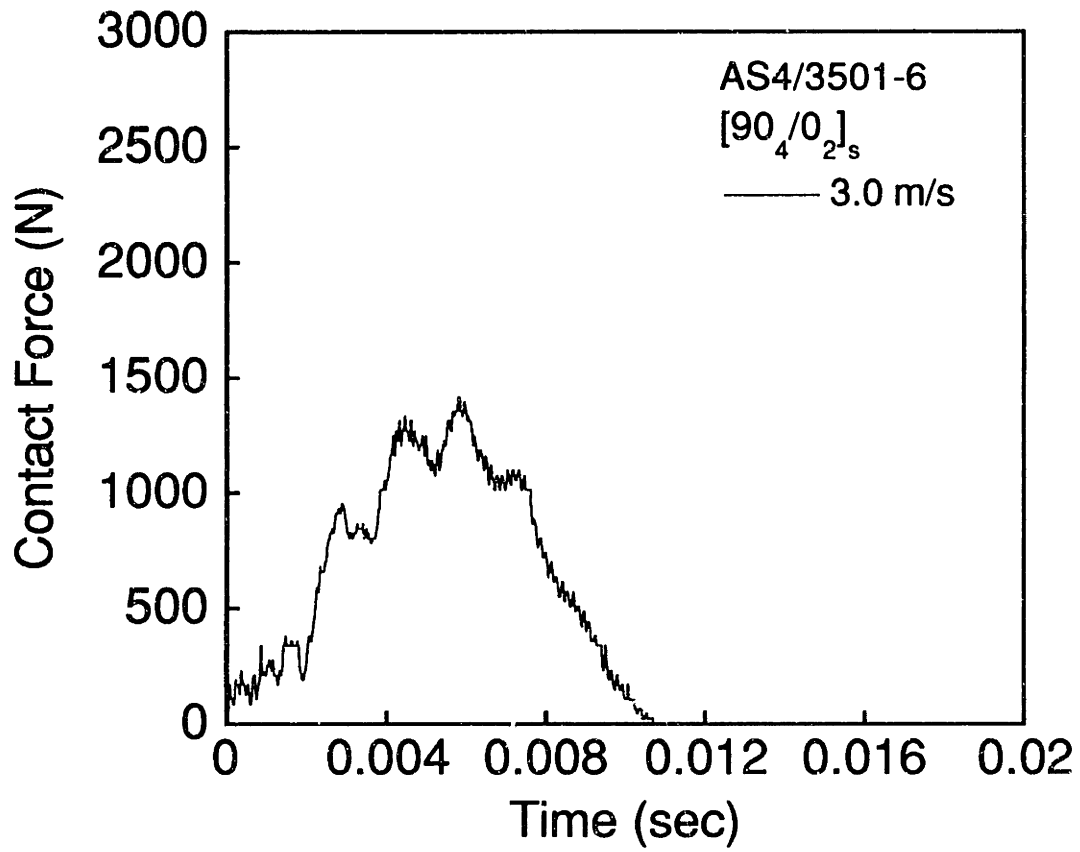


Figure A.40 (upper) Force versus time and (lower) X-ray photograph for AS4/3501-6 [90₄/0₂]_s specimen impacted at 2.6 m/s.



1 cm

Figure A.41 (upper) Force versus time and (lower) X-ray photograph for AS4/3501-6 [90₄/0₂]_s specimen impacted at 3.0 m/s.

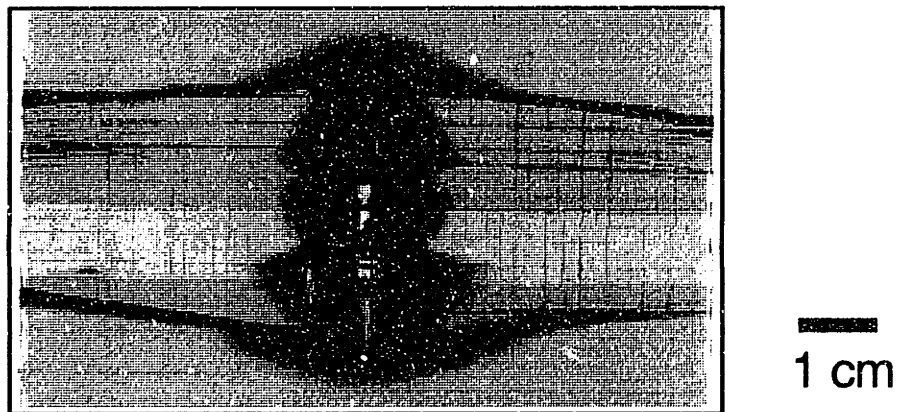
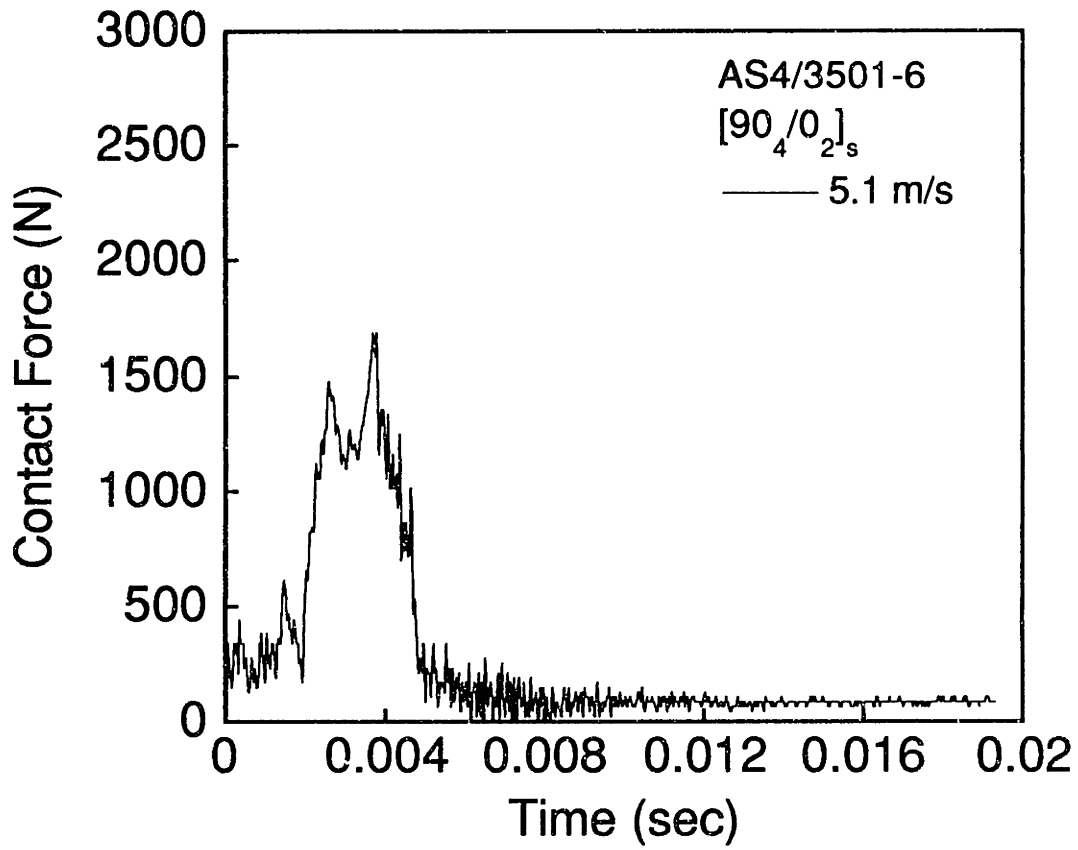
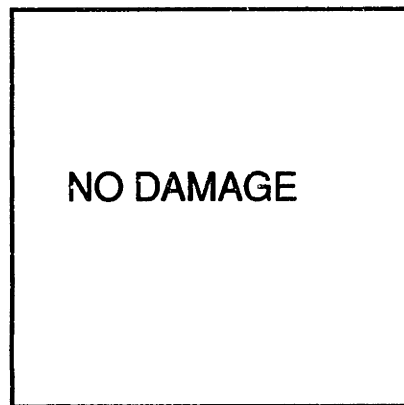
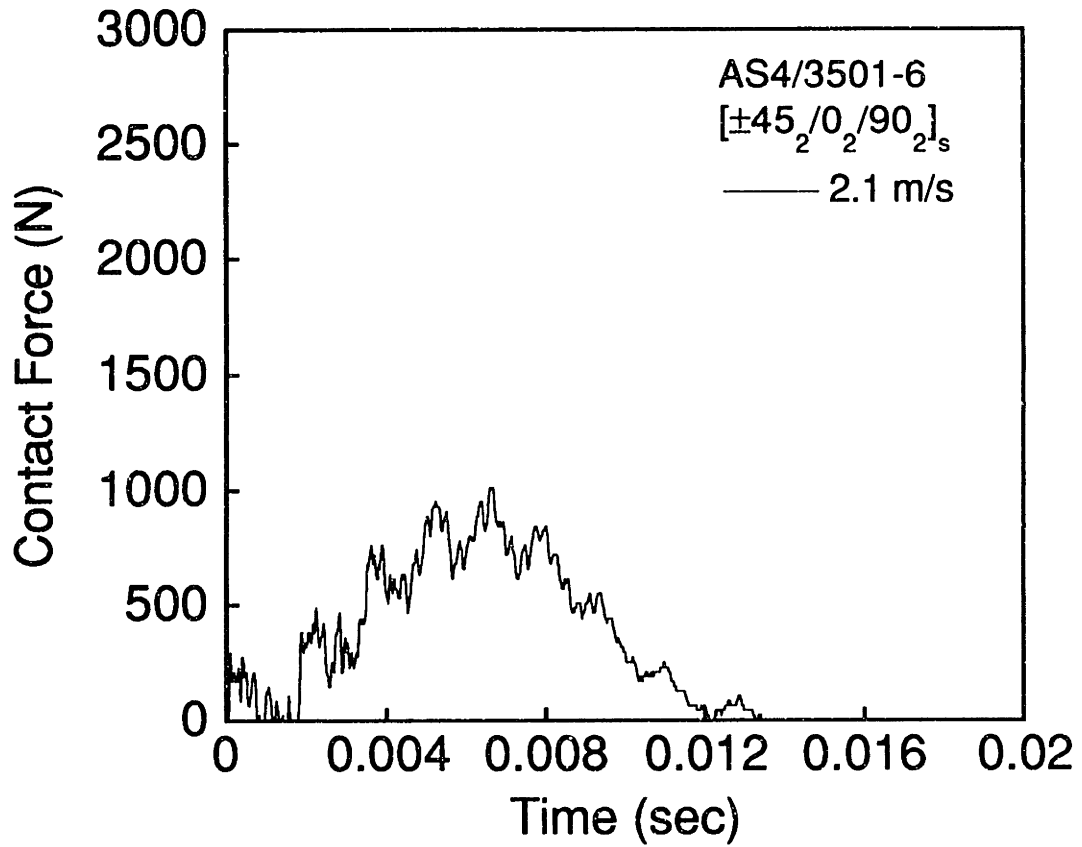
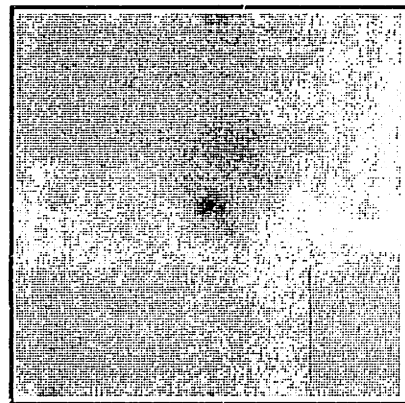
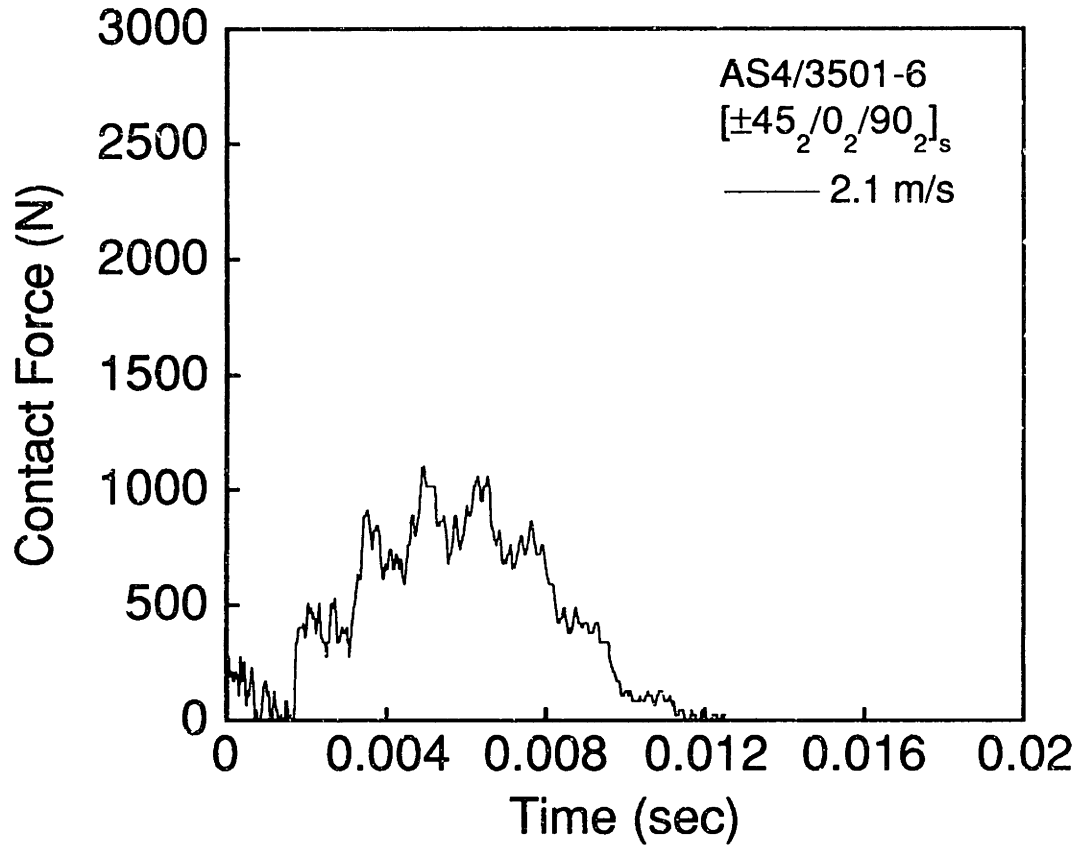


Figure A.42 (upper) Force versus time and (lower) X-ray photograph for AS4/3501-6 [90₄/0₂]_s specimen impacted at 5.1 m/s.



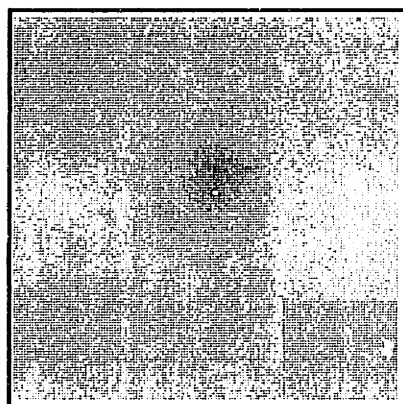
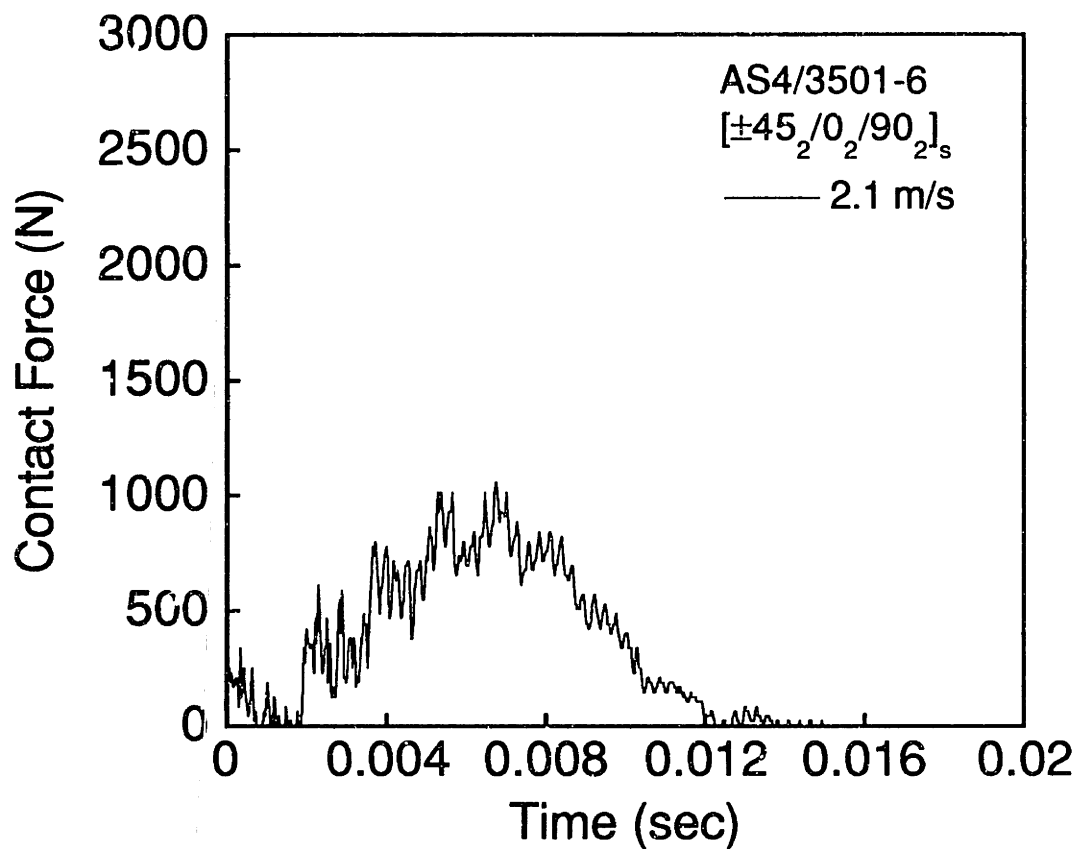
1 cm

Figure A.43 (upper) Force versus time and (lower) X-ray photograph for AS4/3501-6 [±45₂/0₂/90₂]_s specimen impacted at 2.1 m/s.



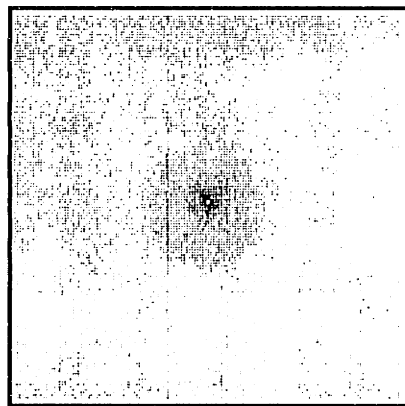
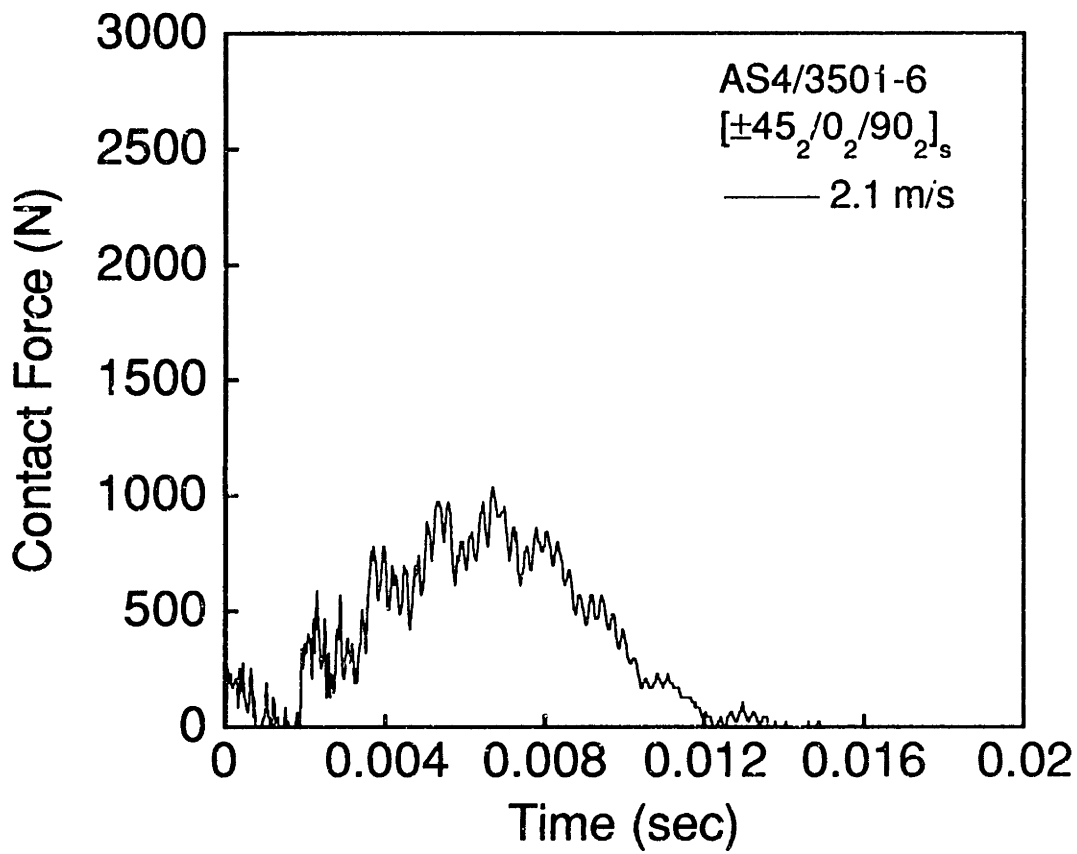
1 cm

Figure A.44 (upper) Force versus time and (lower) X-ray photograph for AS4/3501-6 [±45₂/0₂/90₂]_s specimen impacted at 2.1 m/s.



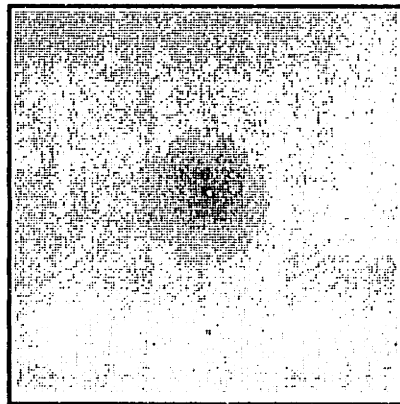
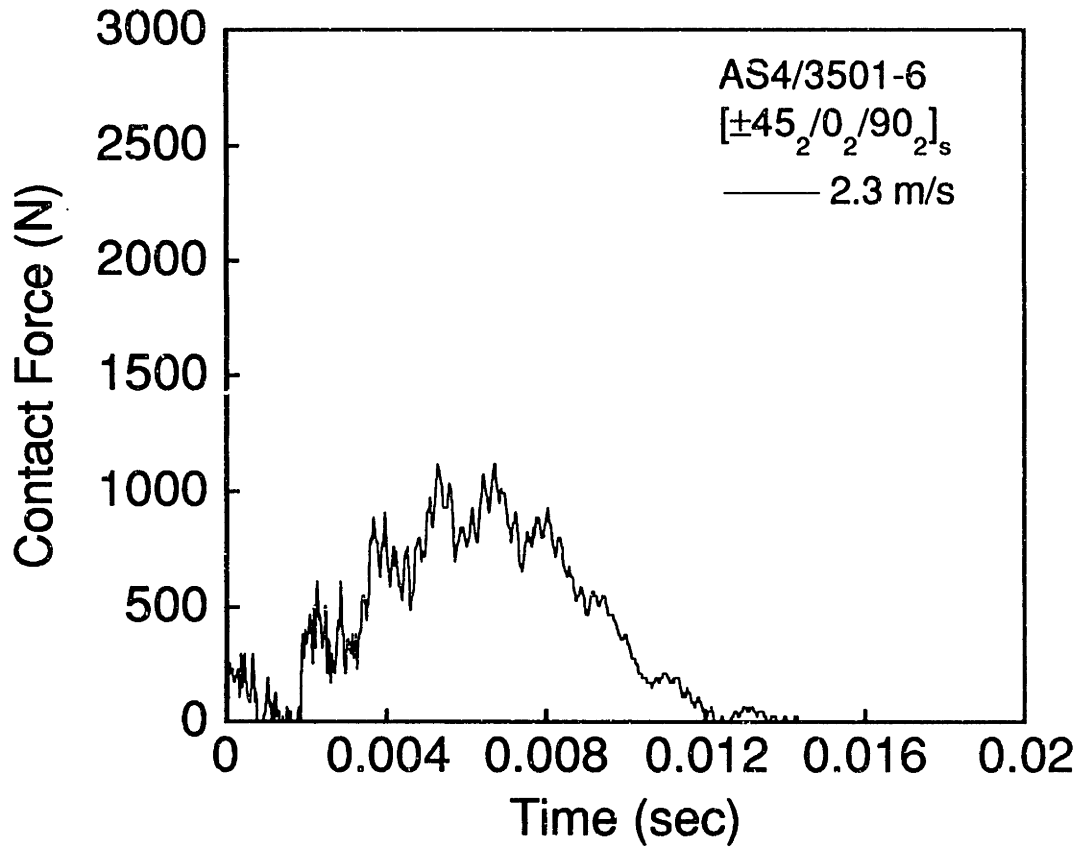
1 cm

Figure A.45 (upper) Force versus time and (lower) X-ray photograph for AS4/3501-6 [±45₂/0₂/90₂]_s specimen impacted at 2.1 m/s.



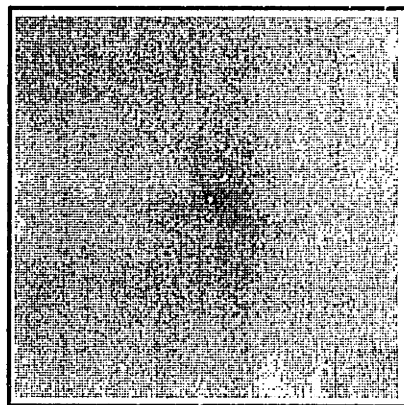
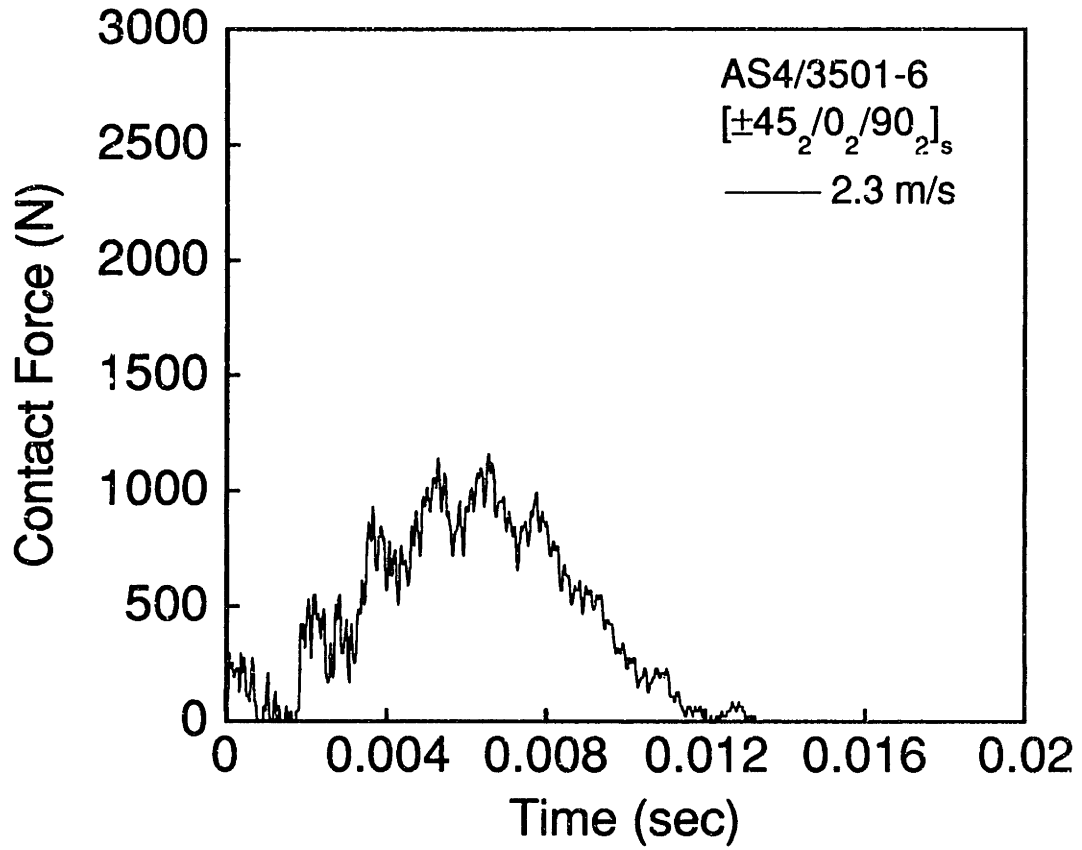
1 cm

Figure A.46 (upper) Force versus time and (lower) X-ray photograph for AS4/3501-6 [±45₂/0₂/90₂]_s specimen impacted at 2.1 m/s.



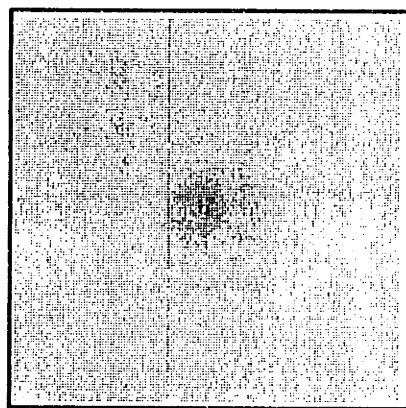
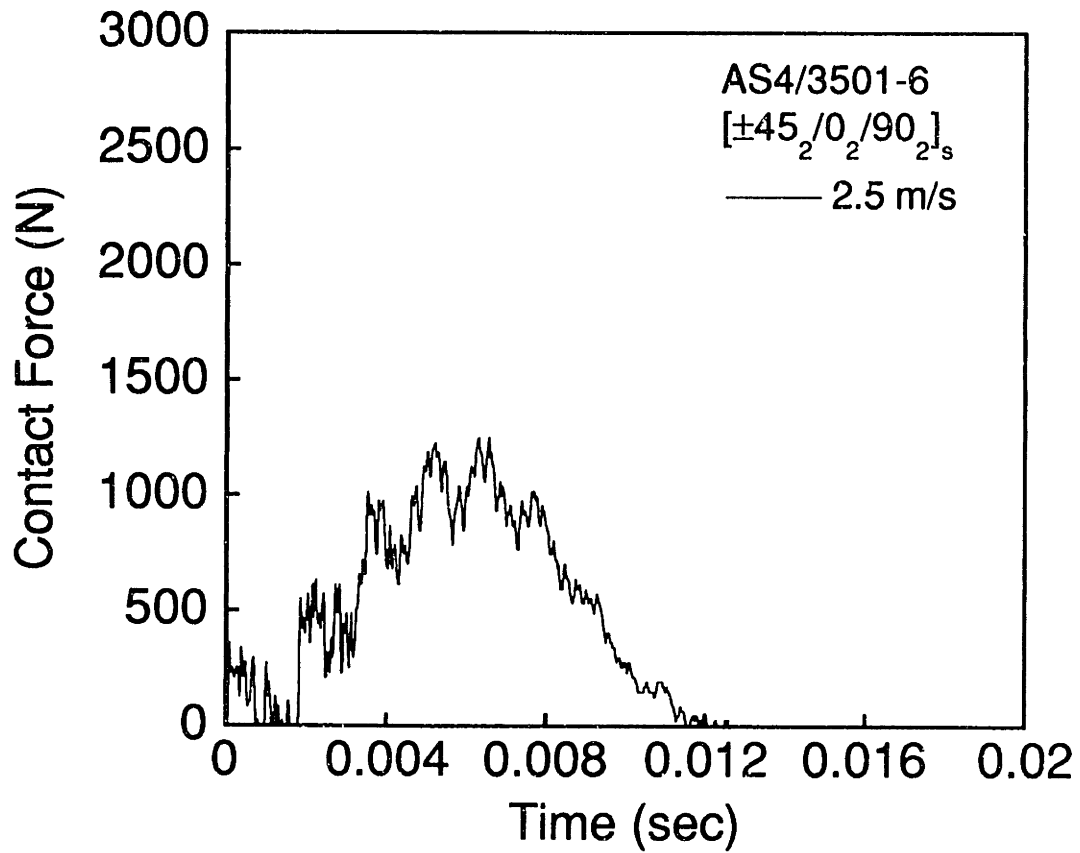
1 cm

Figure A.47 (upper) Force versus time and (lower) X-ray photograph for AS4/3501-6 [±45₂/0₂/90₂]_s specimen impacted at 2.3 m/s.



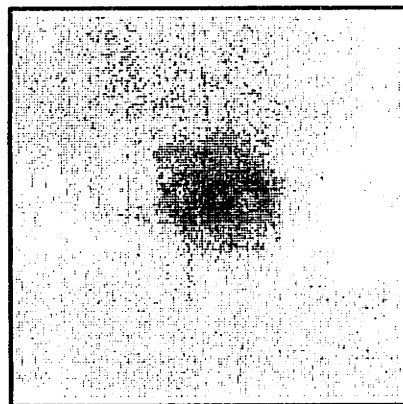
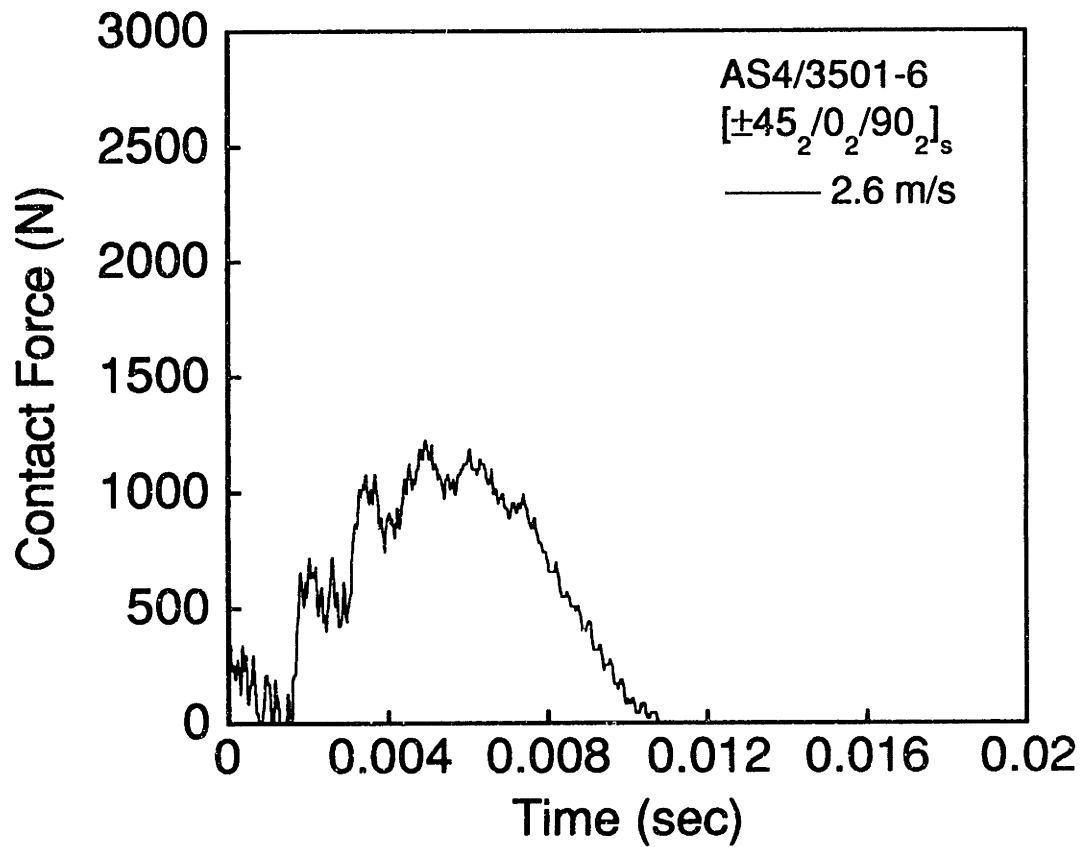
1 cm

Figure A.48 (upper) Force versus time and (lower) X-ray photograph for AS4/3501-6 [±45₂/0₂/90₂]_s specimen impacted at 2.3 m/s.



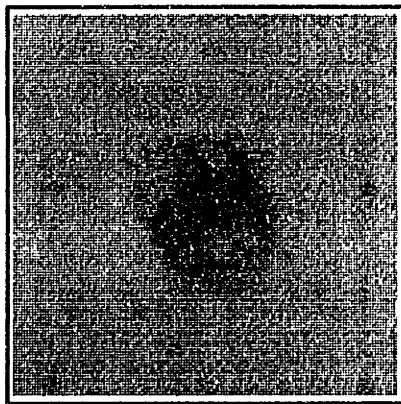
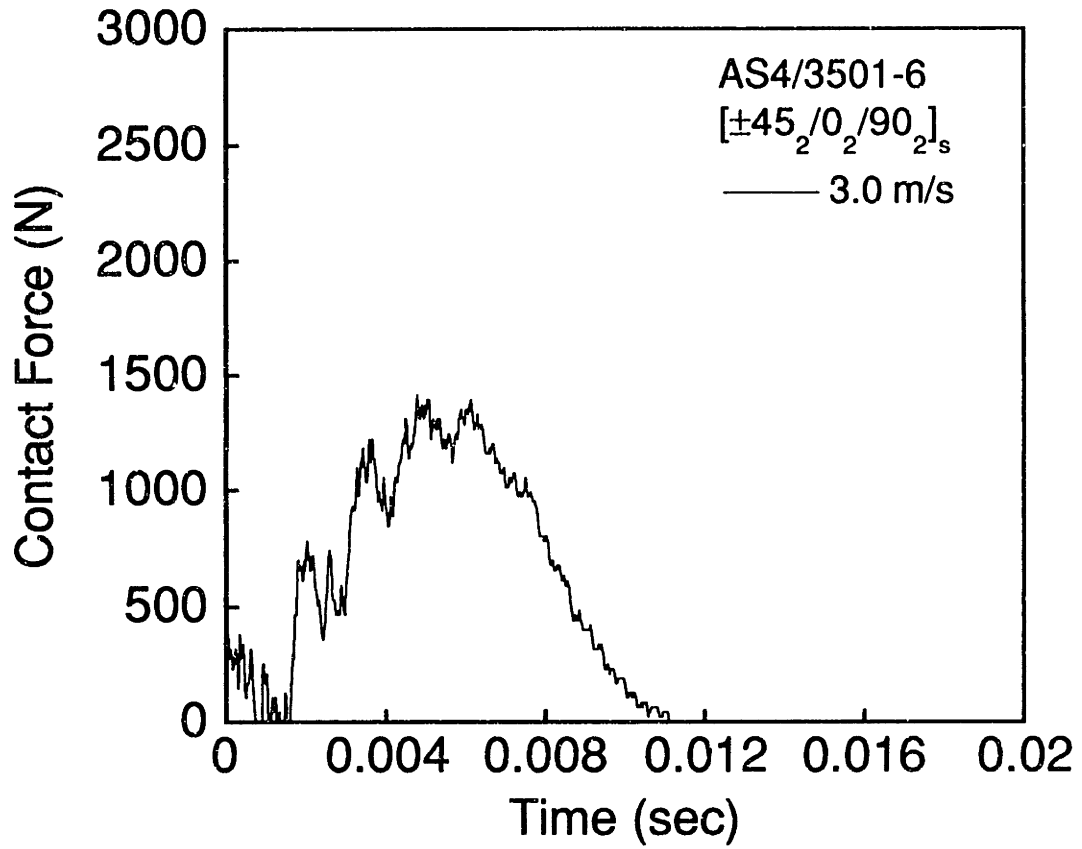
1 cm

Figure A.49 (upper) Force versus time and (lower) X-ray photograph for AS4/3501-6 [±45₂/0₂/90₂]_s specimen impacted at 2.5 m/s.



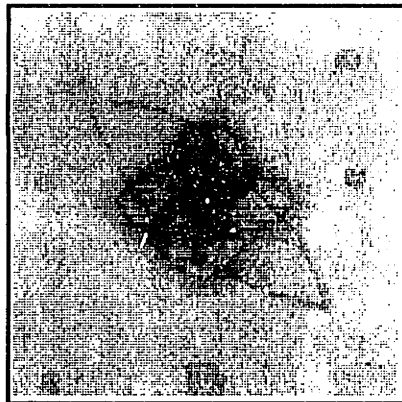
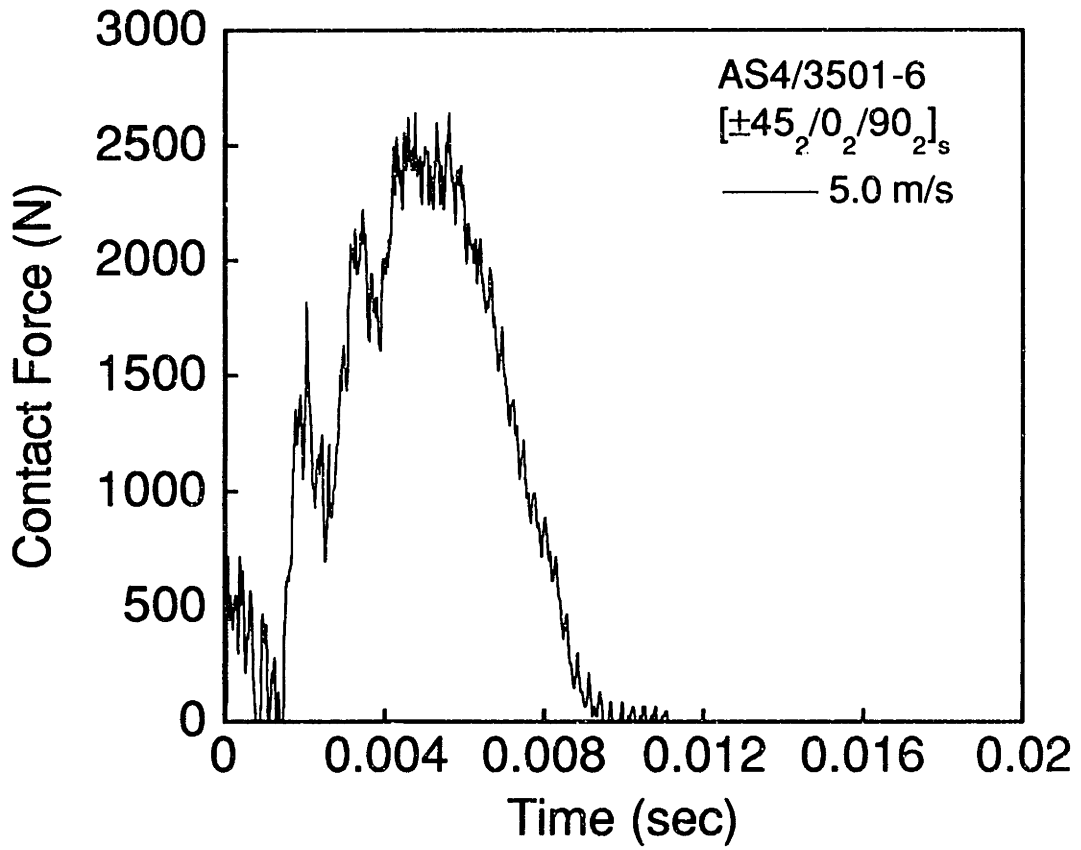
1 cm

Figure A.50 (upper) Force versus time and (lower) X-ray photograph for AS4/3501-6 [±45₂/0₂/90₂]_s specimen impacted at 2.6 m/s.



1 cm

Figure A.51 (upper) Force versus time and (lower) X-ray photograph for AS4/3501-6 [±45₂/0₂/90₂]_s specimen impacted at 3.0 m/s.



1 cm

Figure A.52 (upper) Force versus time and (lower) X-ray photograph for AS4/3501-6 [±45₂/0₂/90₂]_s specimen impacted at 5.0 m/s.

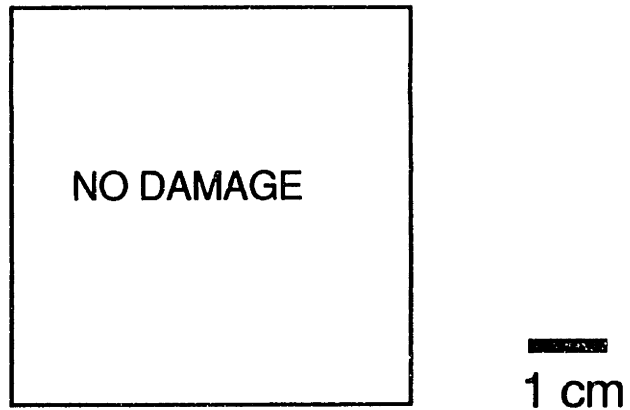
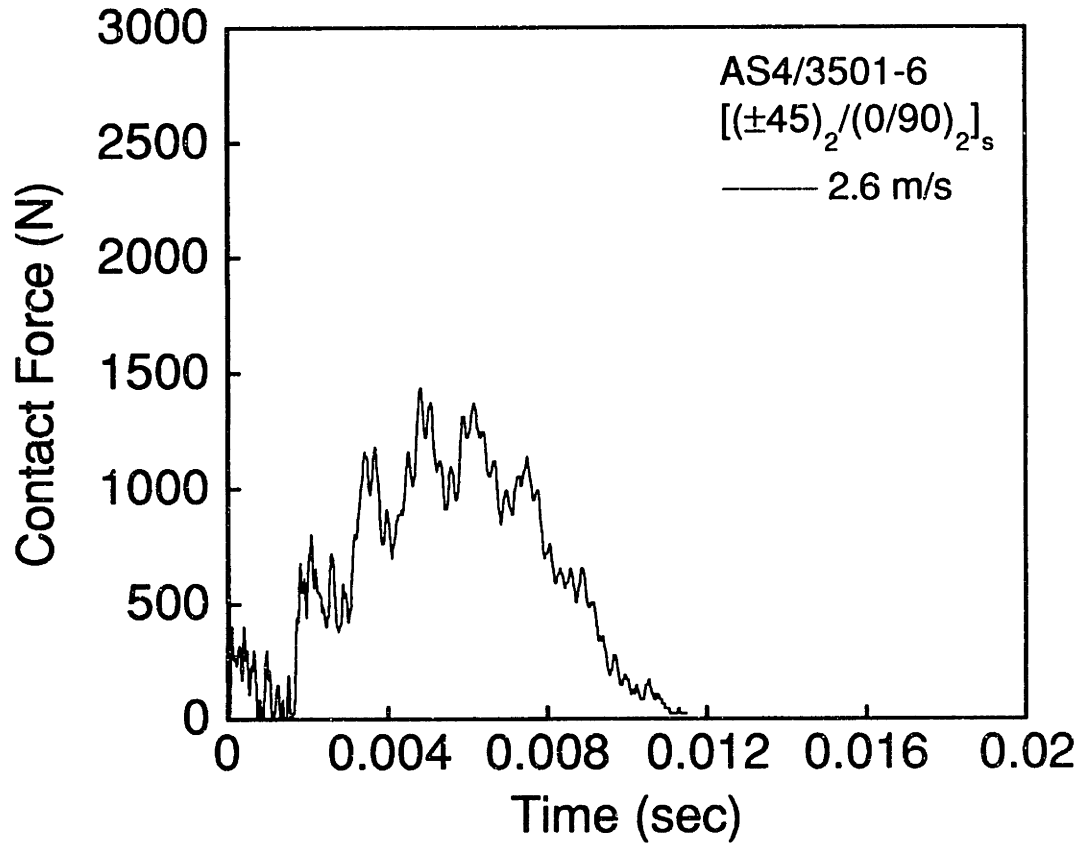
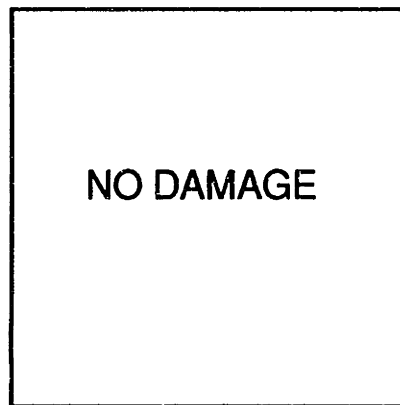
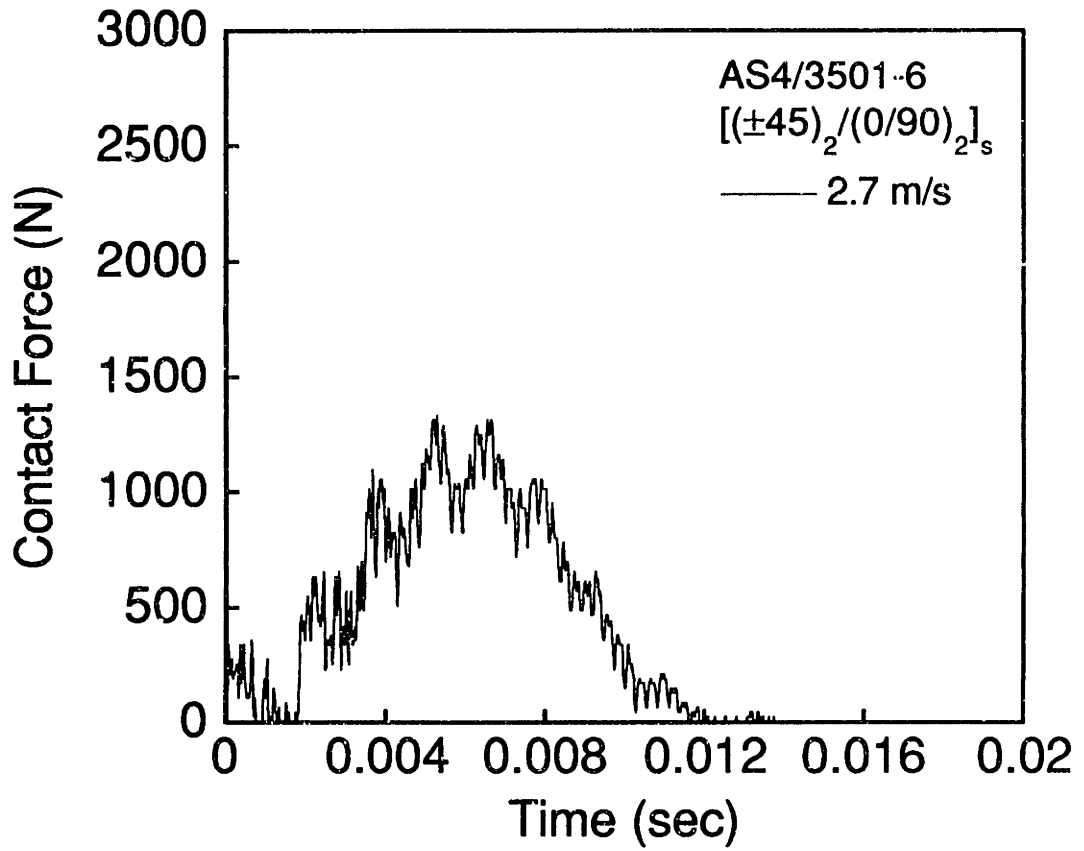
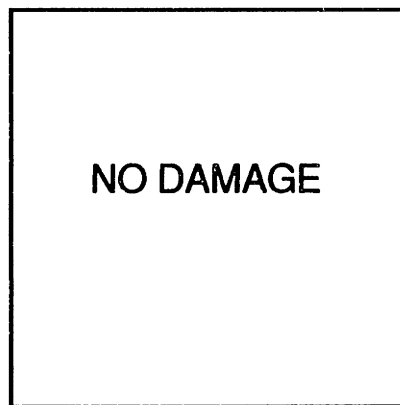
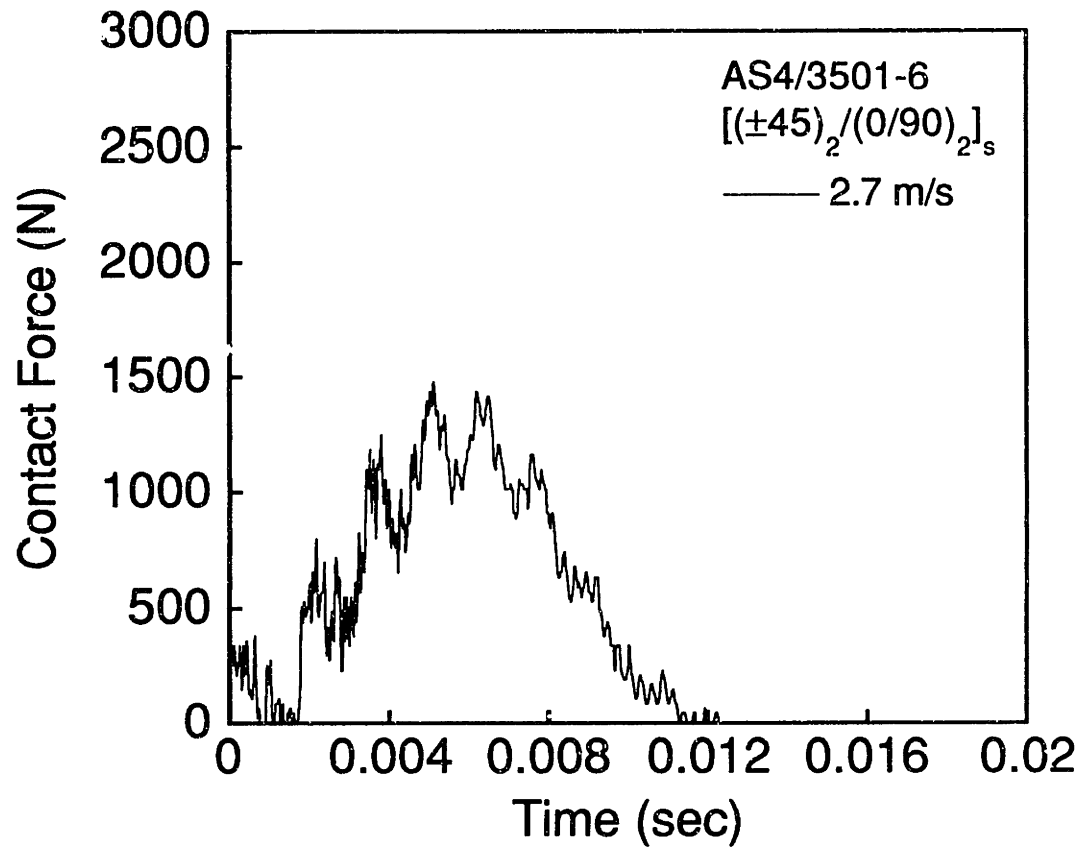


Figure A.53 (upper) Force versus time and (lower) X-ray photograph for AS4/3501-6 [(±45)₂/(0/90)₂]_s specimen impacted at 2.6 m/s.



1 cm

Figure A.54 (upper) Force versus time and (lower) X-ray photograph for AS4/3501-6 [(±45)₂/(0/90)₂]_s specimen impacted at 2.7 m/s.



1 cm

Figure A.55 (upper) Force versus time and (lower) X-ray photograph for AS4/3501-6 [(±45)₂/(0/90)₂]_s specimen impacted at 2.7 m/s.

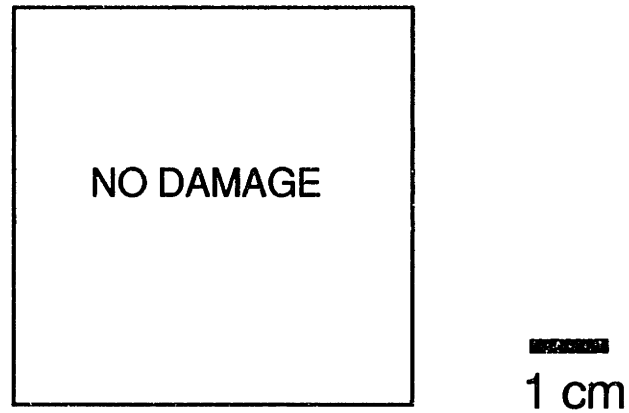
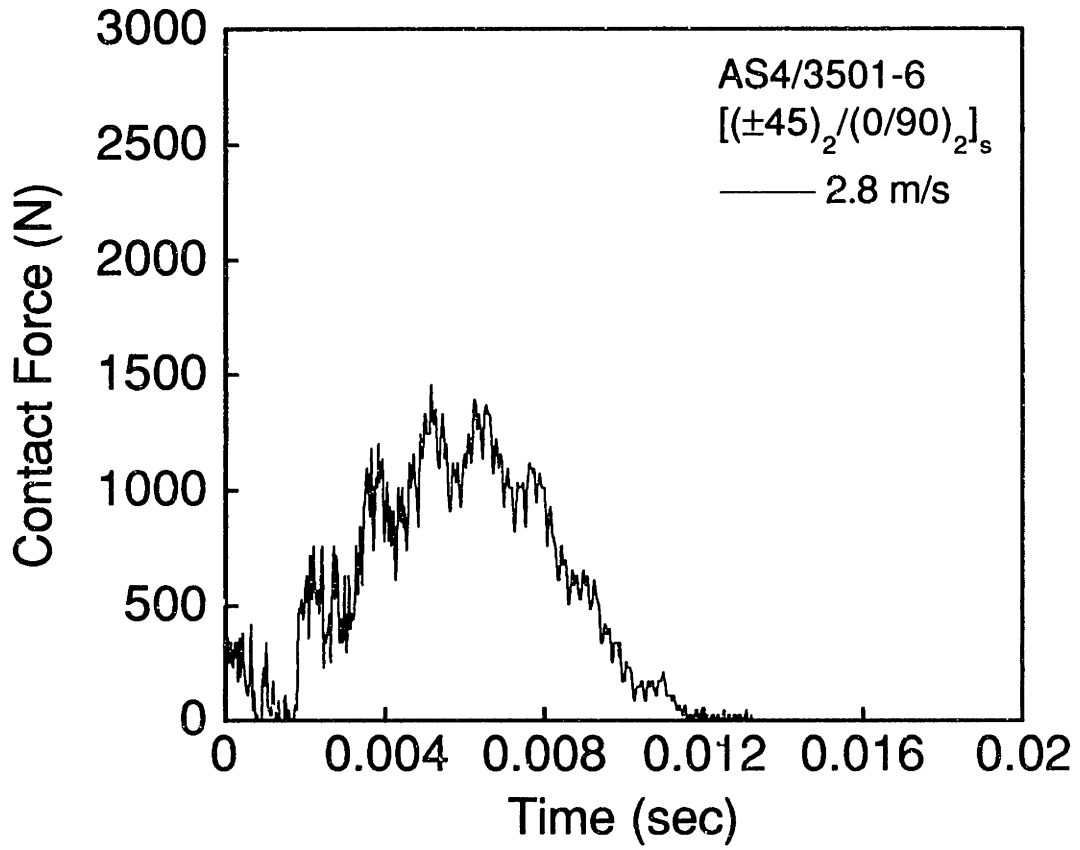
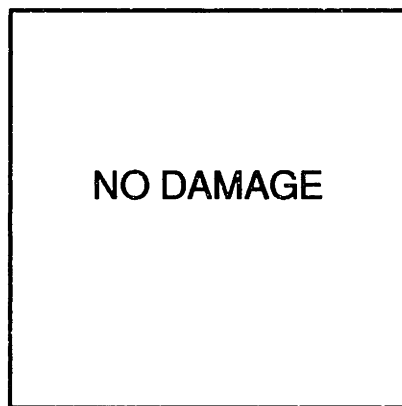
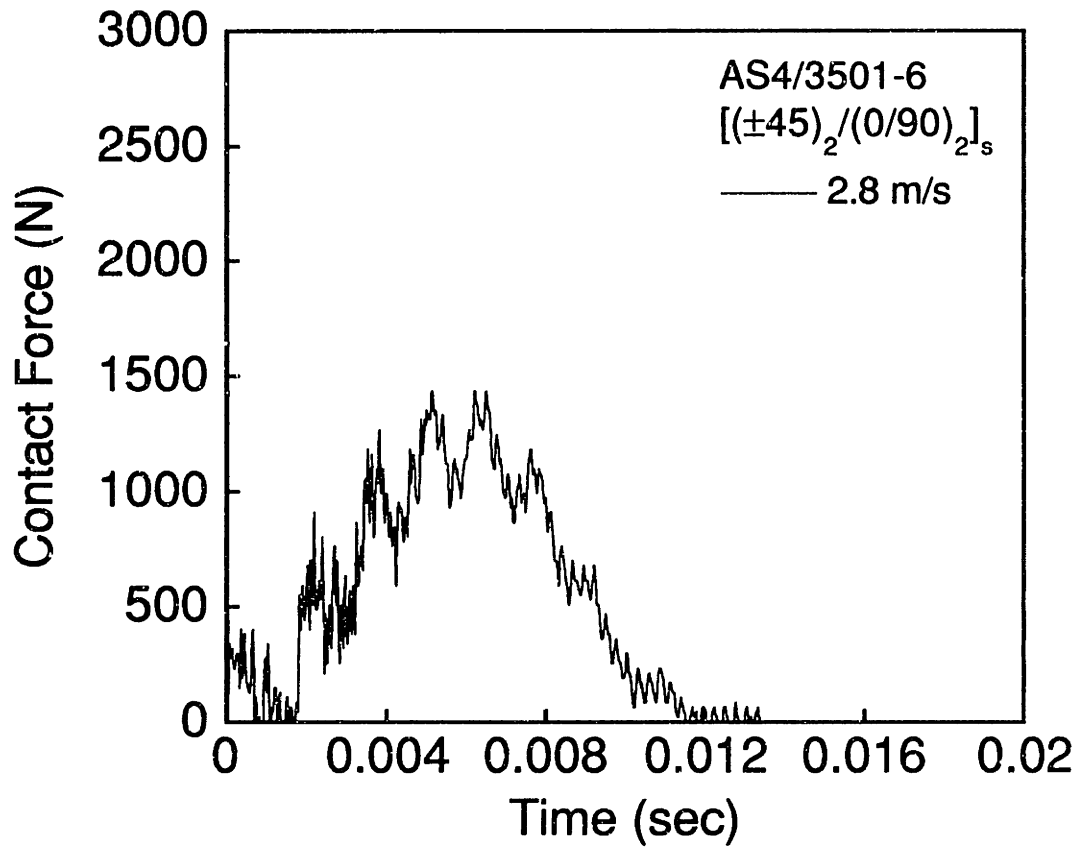
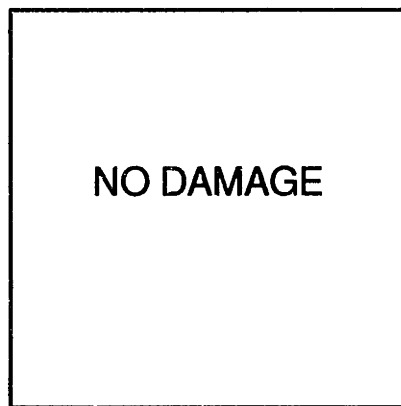
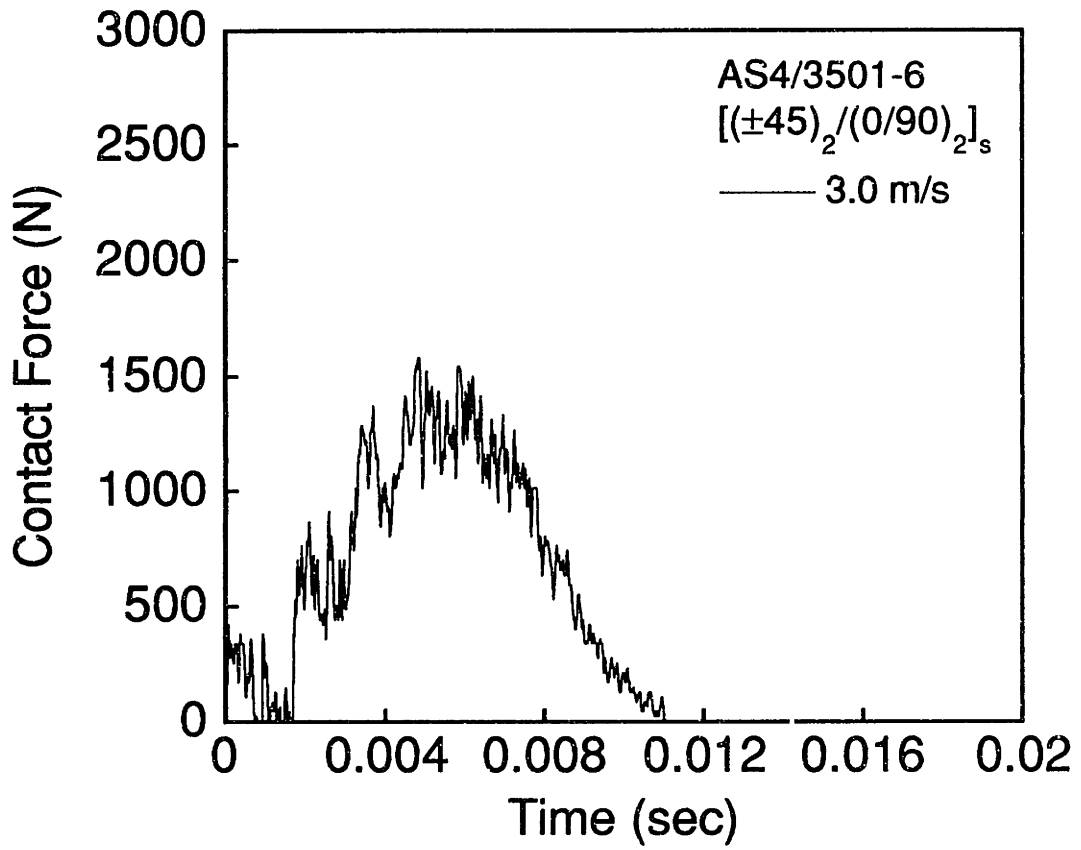


Figure A.56 (upper) Force versus time and (lower) X-ray photograph for AS4/3501-6 [(±45)₂/(0/90)₂]_s specimen impacted at 2.8 m/s.



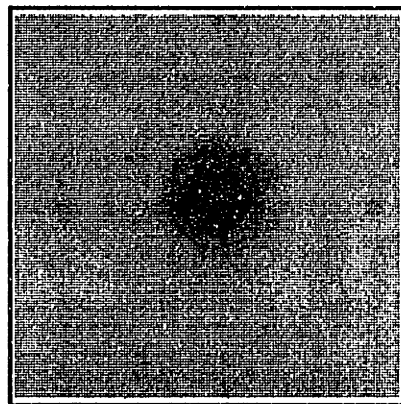
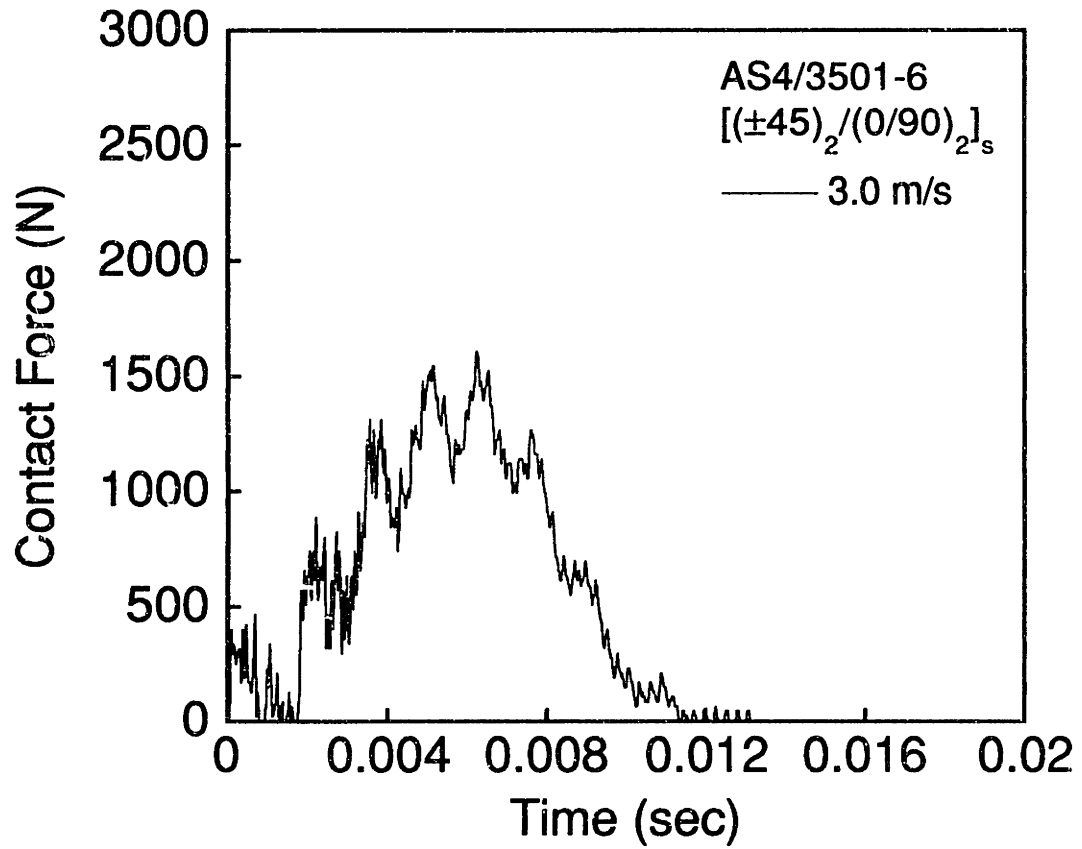
1 cm

Figure A.57 (upper) Force versus time and (lower) X-ray photograph for AS4/3501-6 [(±45)₂/(0/90)₂]_s specimen impacted at 2.8 m/s.



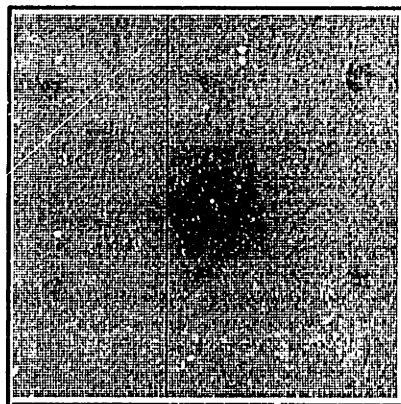
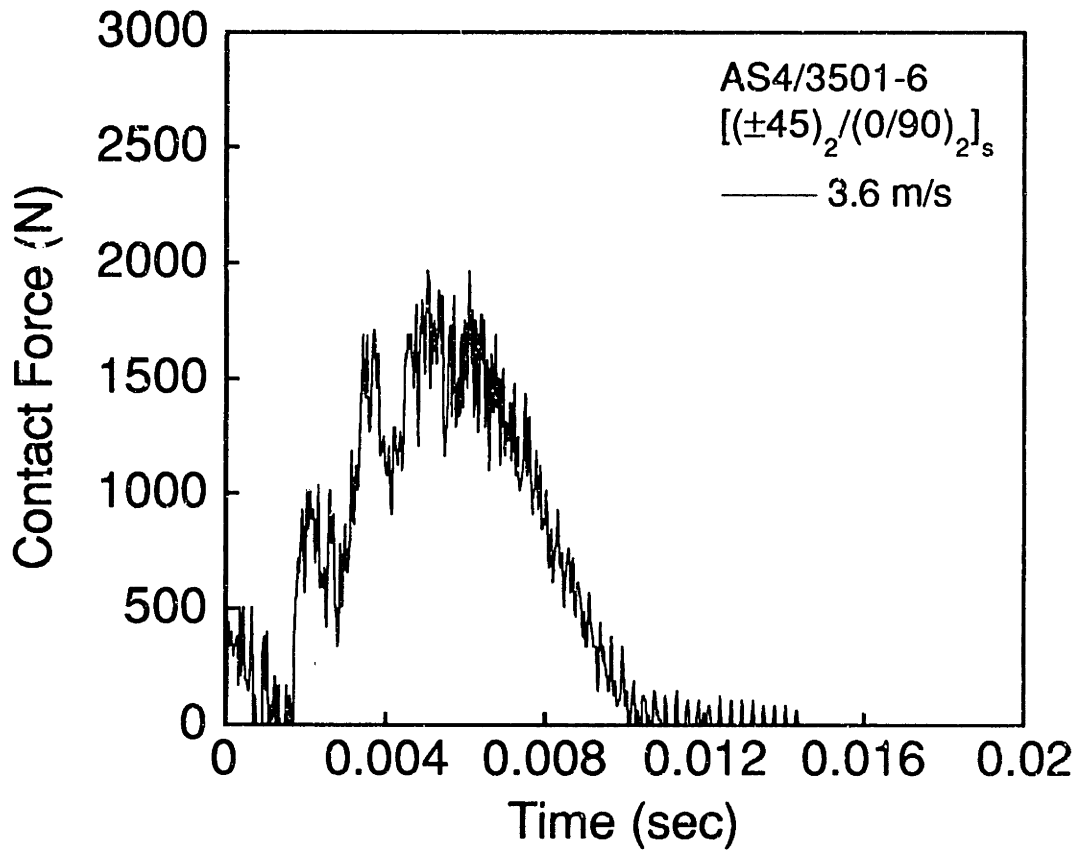
1 cm

Figure A.58 (upper) Force versus time and (lower) X-ray photograph for AS4/3501-6 [(±45)₂/(0/90)₂]_s specimen impacted at 3.0 m/s.



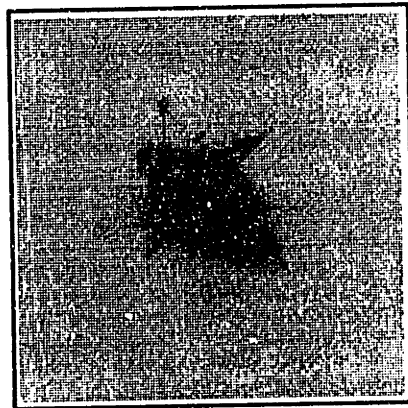
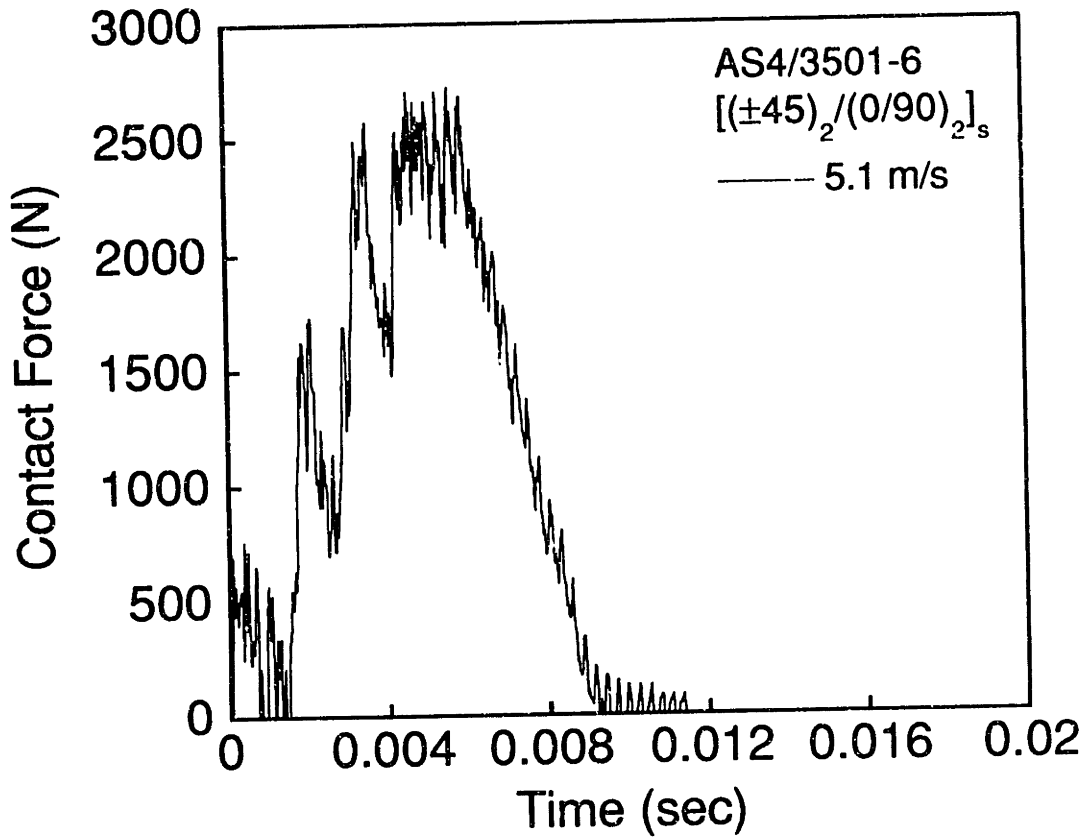
1 cm

Figure A.59 (upper) Force versus time and (lower) X-ray photograph for AS4/3501-6 [(±45)₂/(0/90)₂]_s specimen impacted at 3.0 m/s.



1 cm

Figure A.60 (upper) Force versus time and (lower) X-ray photograph for AS4/3501-6 [(±45)₂/(0/90)₂]_s specimen impacted at 3.6 m/s.



1 cm

Figure A.61 (upper) Force versus time and (lower) X-ray photograph for AS4/3501-6 [(±45)₂/(0/90)₂]_s specimen impacted at 5.1 m/s.

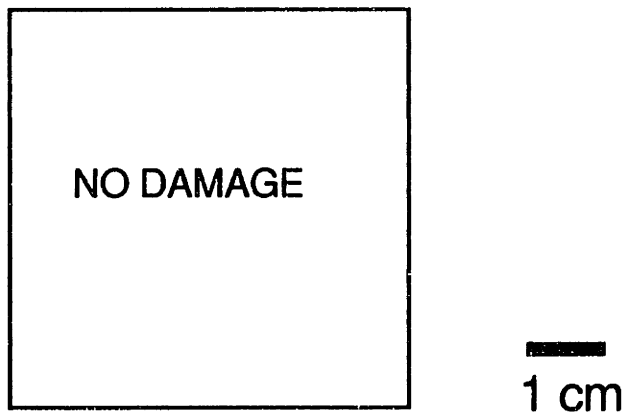
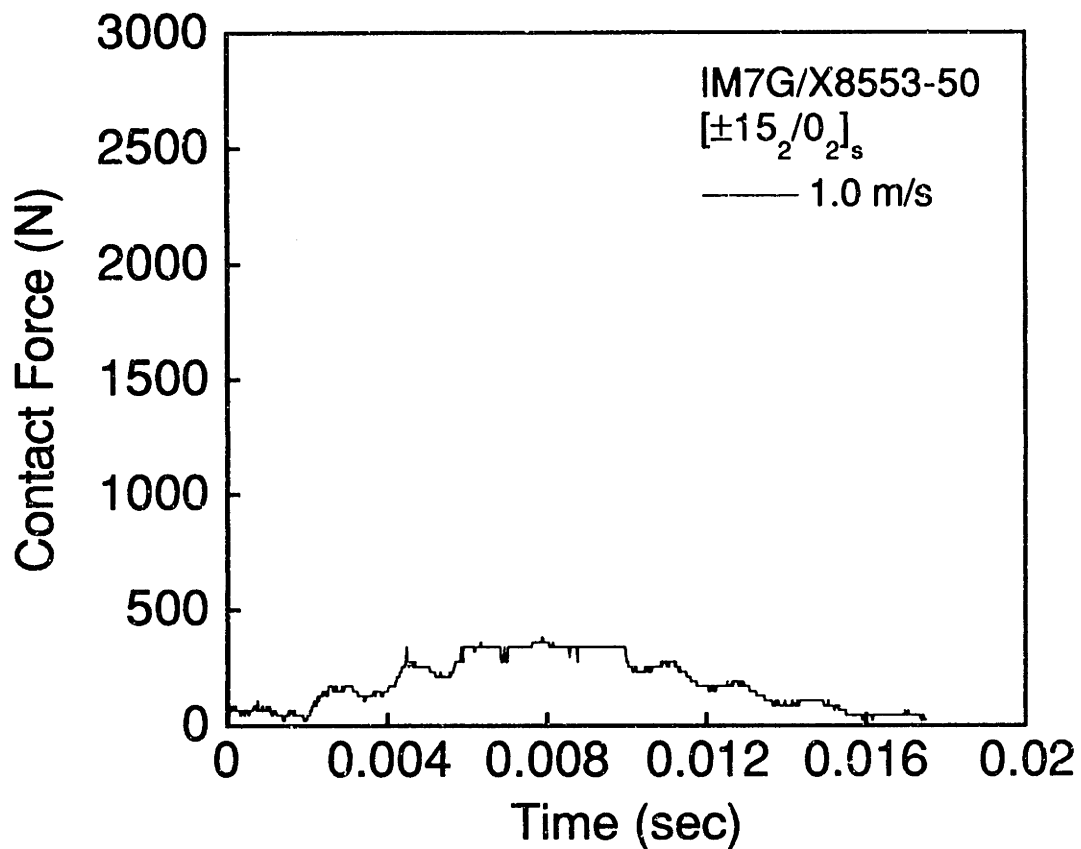


Figure A.62 (upper) Force versus time and (lower) X-ray photograph for IM7G/X8553-50 [±15₂/0₂]_s specimen impacted at 1.0 m/s.

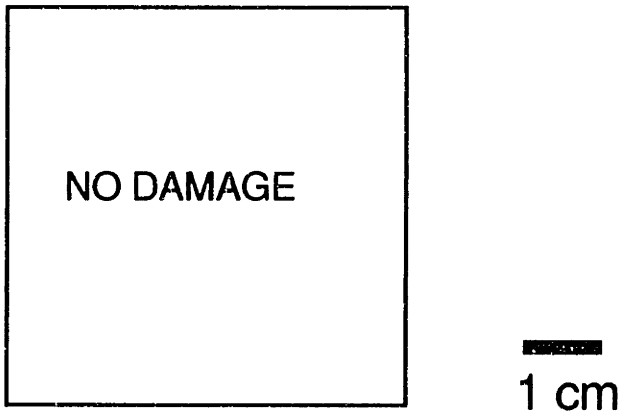
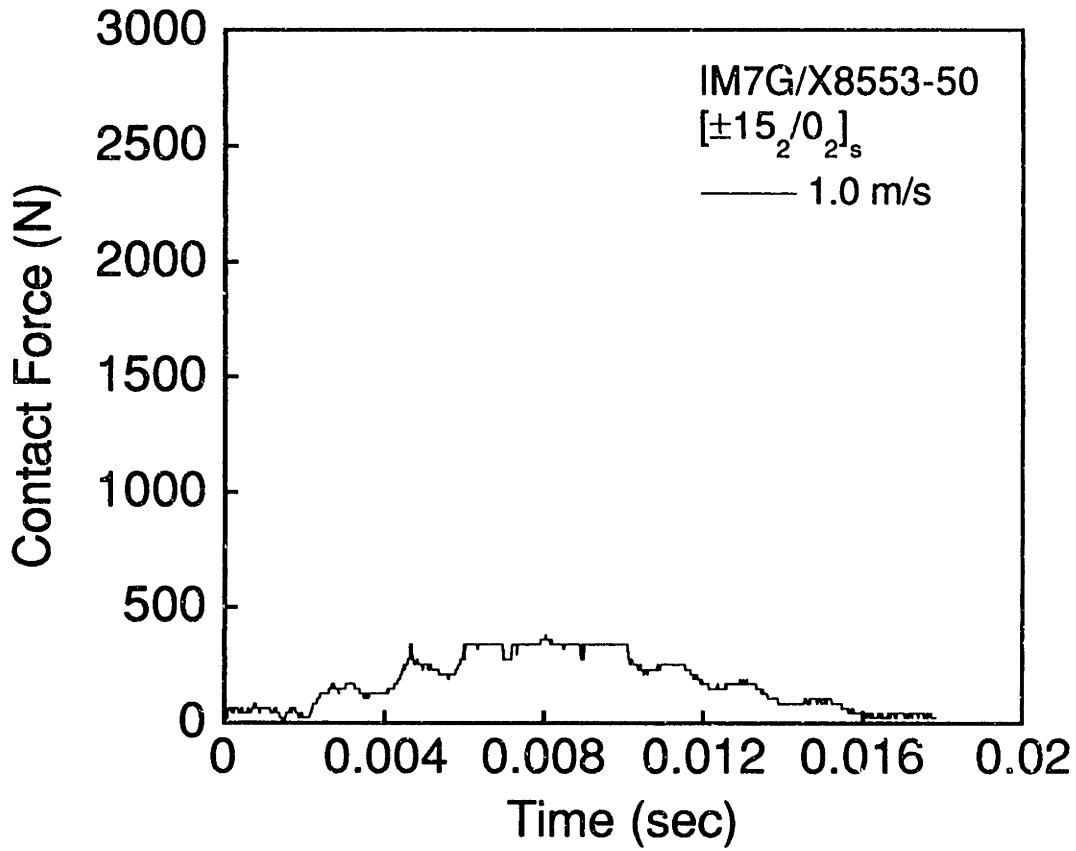


Figure A.63 (upper) Force versus time and (lower) X-ray photograph for IM7G/X8553-50 [±15₂/0₂]_s specimen impacted at 1.0 m/s.

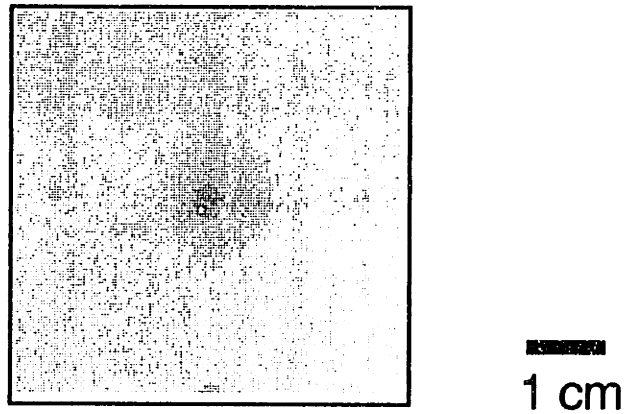
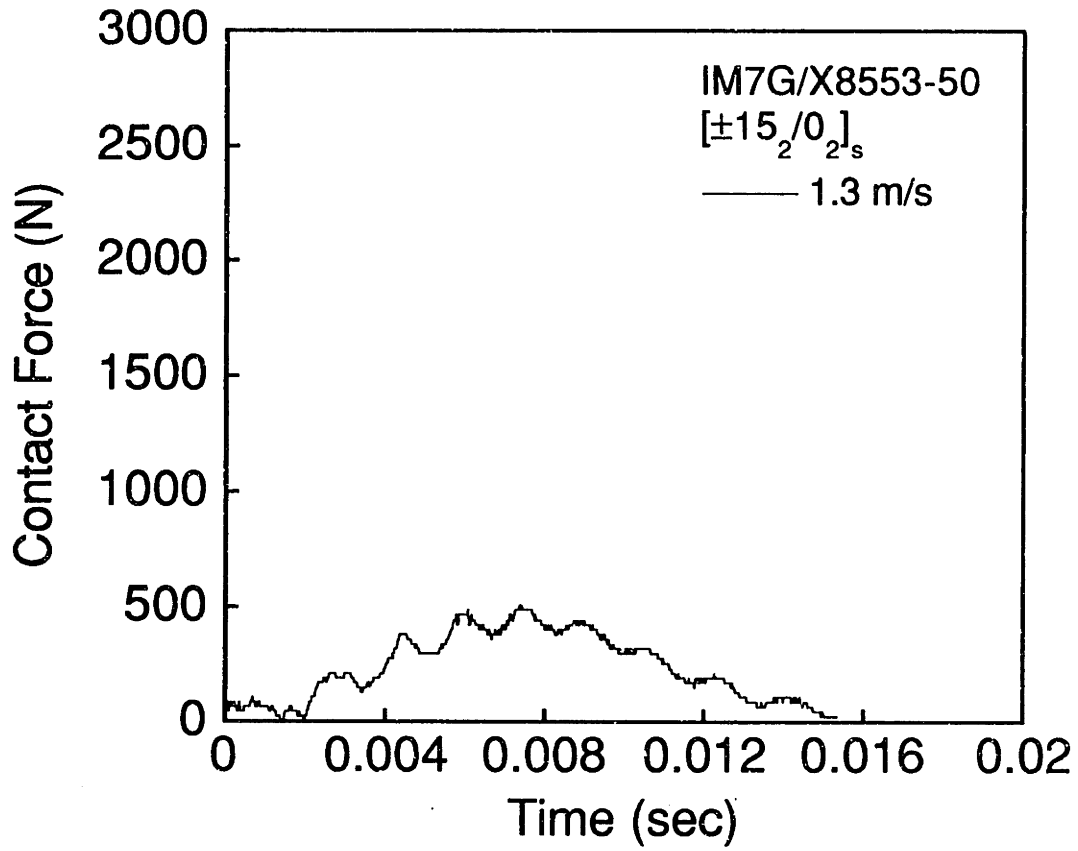
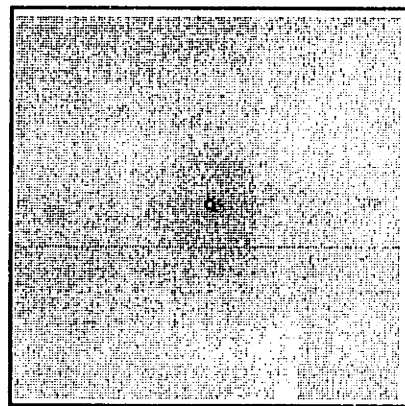
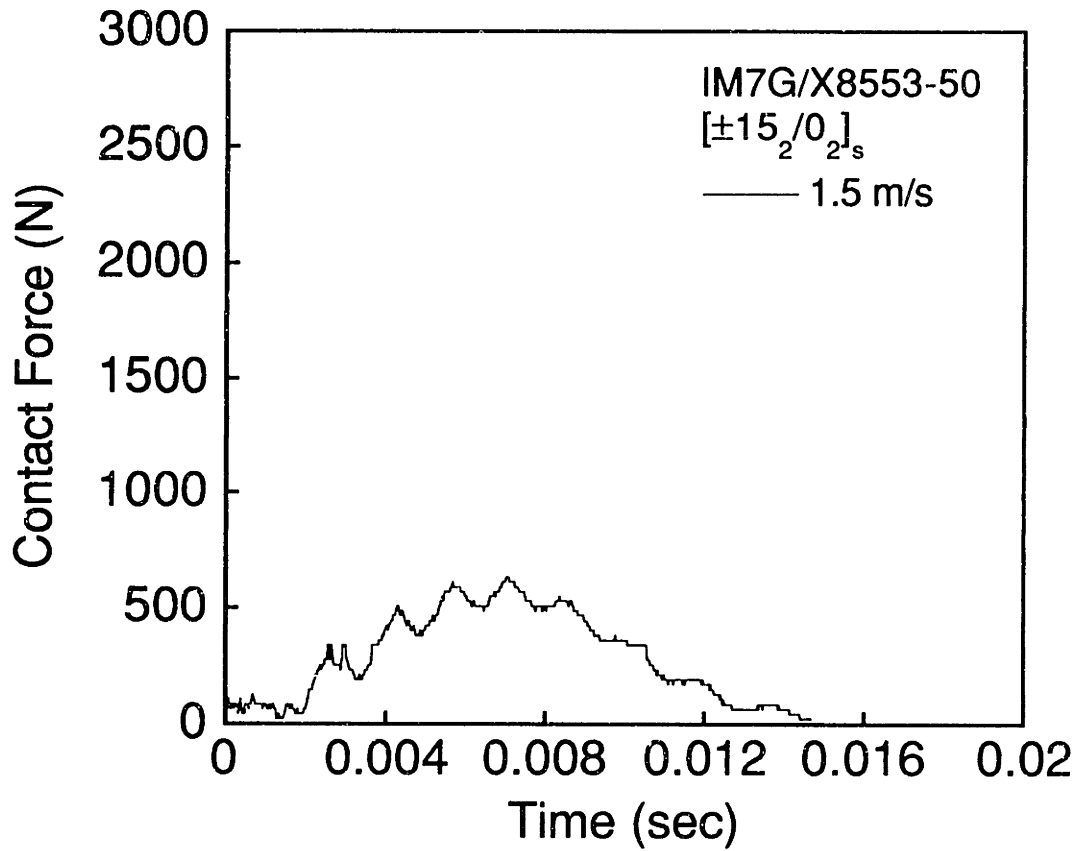
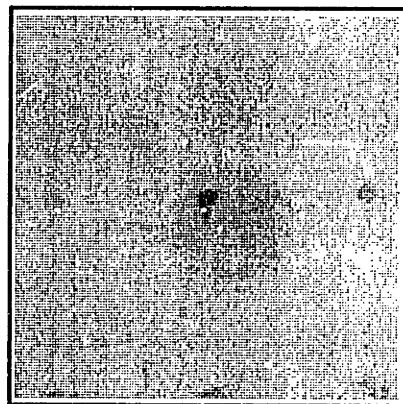
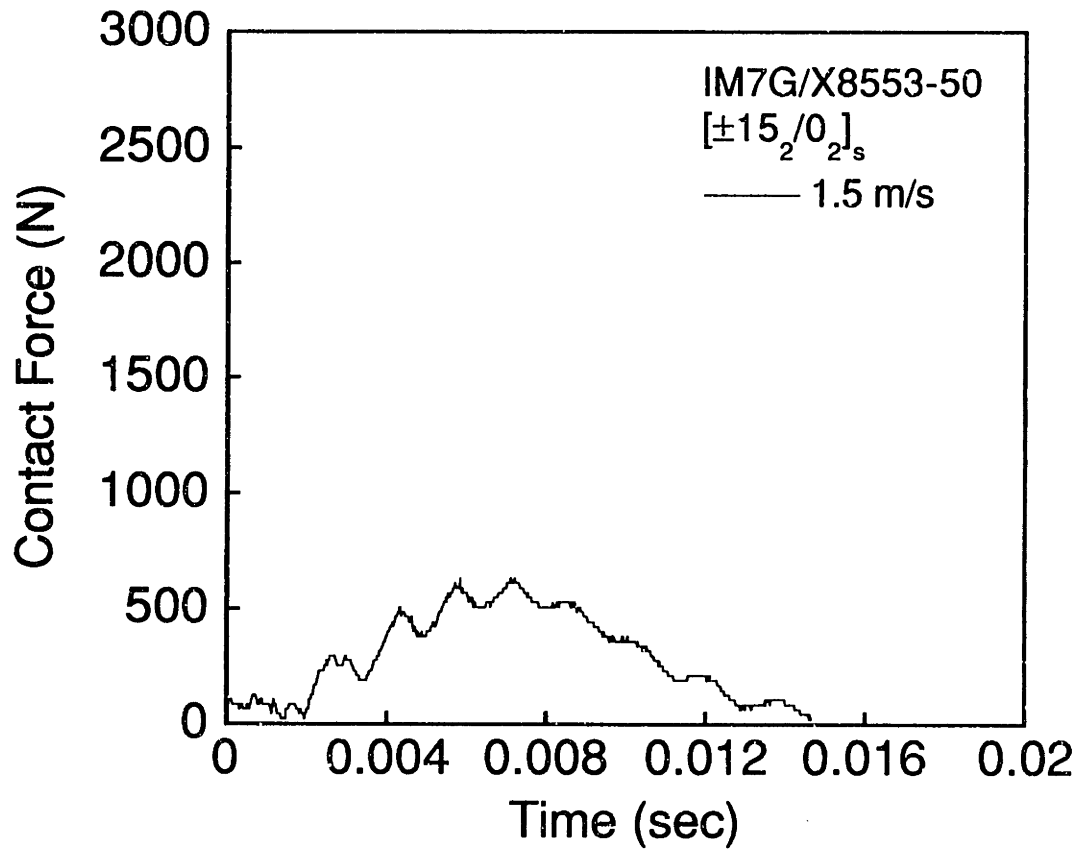


Figure A.64 (upper) Force versus time and (lower) X-ray photograph for IM7G/X8553-50 $[\pm 15_2/0_2]_s$ specimen impacted at 1.3 m/s.



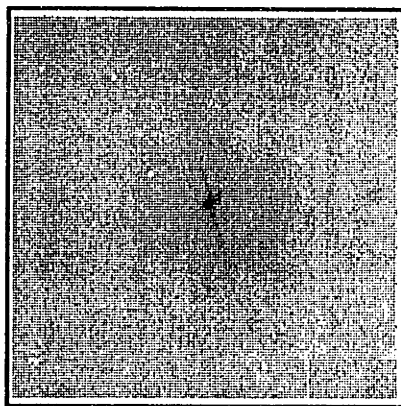
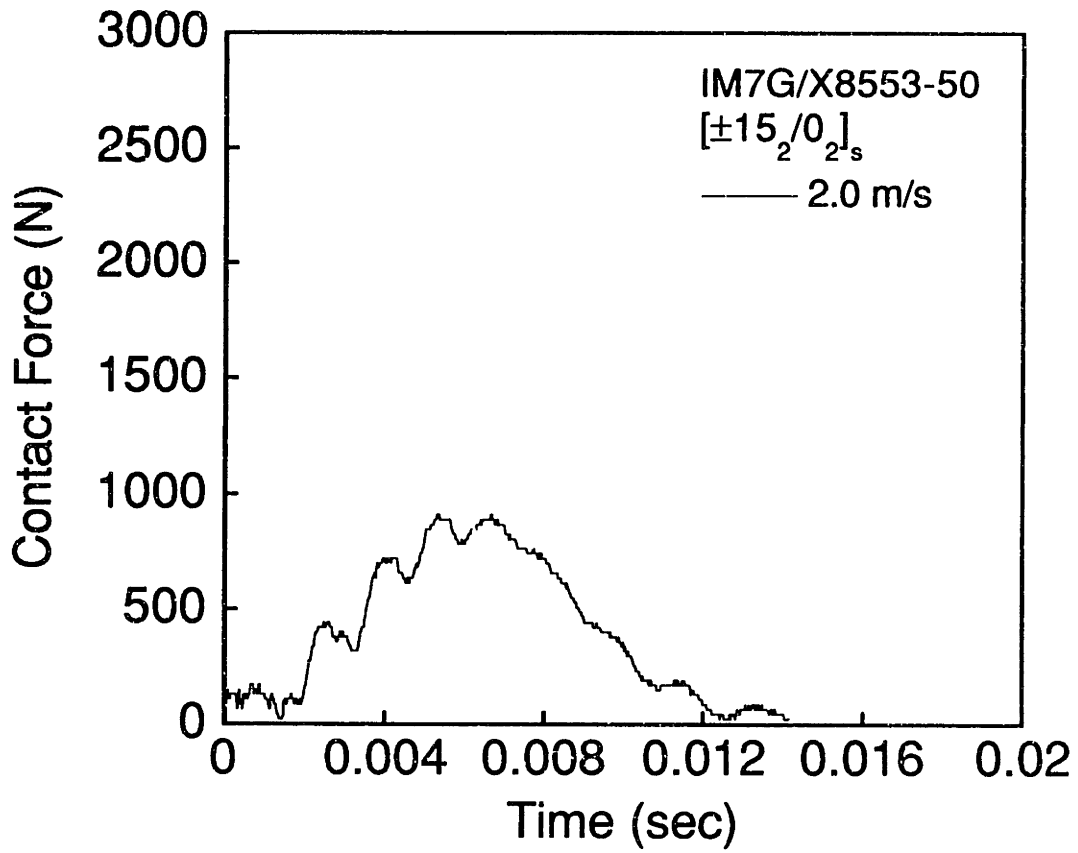
1 cm

Figure A.65 (upper) Force versus time and (lower) X-ray photograph for IM7G/X8553-50 [±15₂/0₂]_s specimen impacted at 1.5 m/s.



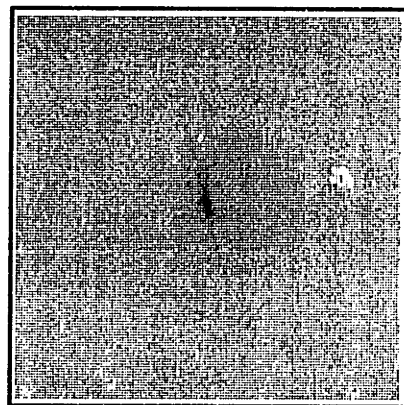
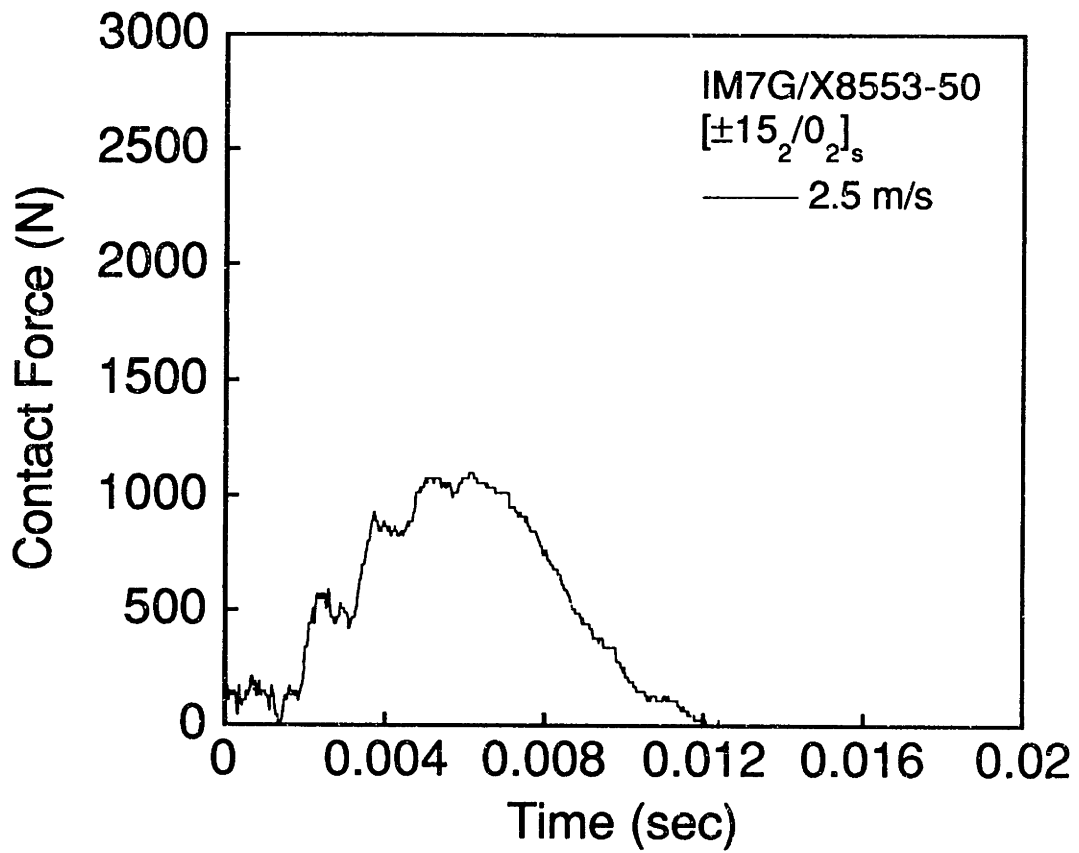
1 cm

Figure A.66 (upper) Force versus time and (lower) X-ray photograph for IM7G/X8553-50 [±15₂/0₂]_s specimen impacted at 1.5 m/s.



1 cm

Figure A.67 (upper) Force versus time and (lower) X-ray photograph for IM7G/X8553-50 [±15₂/0₂]_s specimen impacted at 2.0 m/s.



1 cm

Figure A.68 (upper) Force versus time and (lower) X-ray photograph for IM7G/X8553-50 [±15₂/0₂]_s specimen impacted at 2.5 m/s.

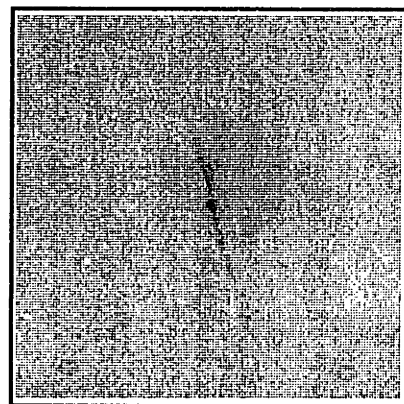
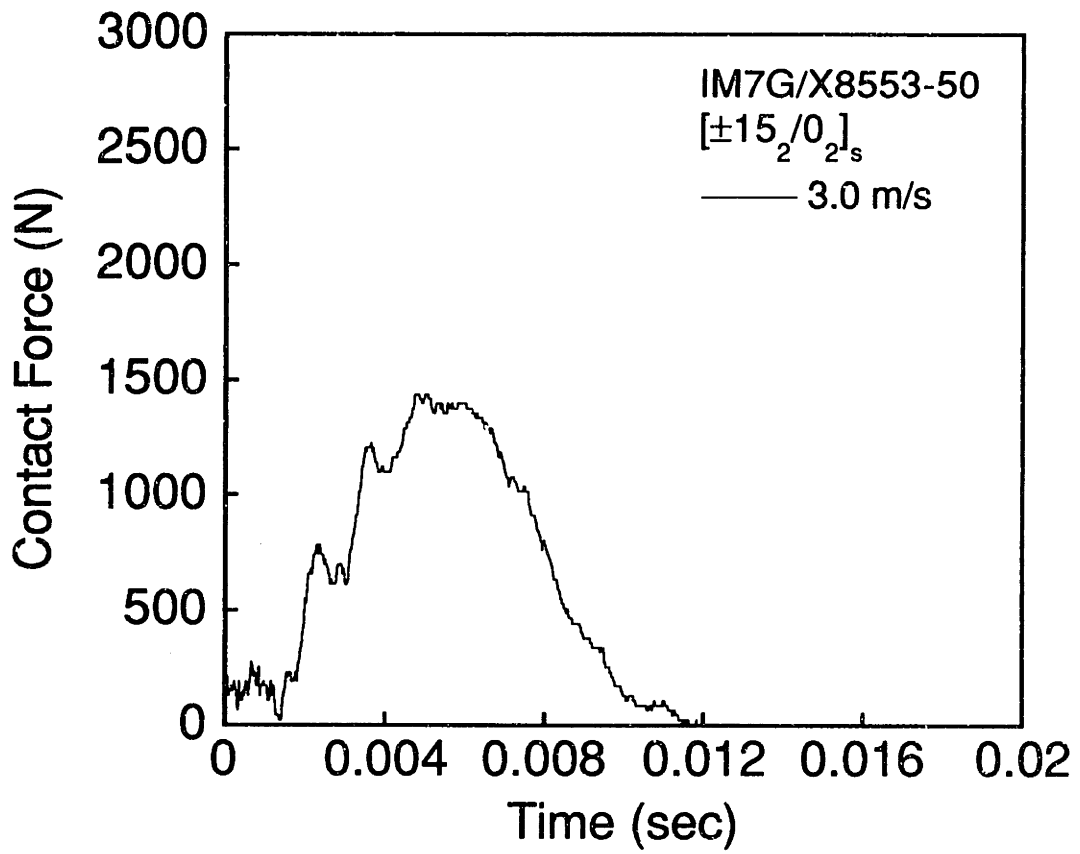
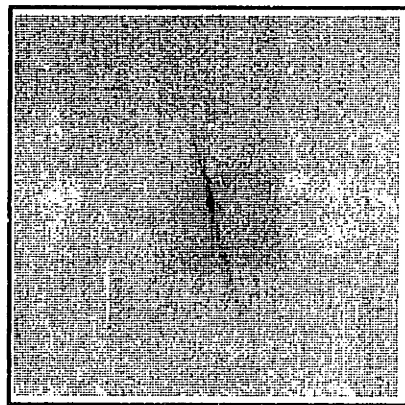
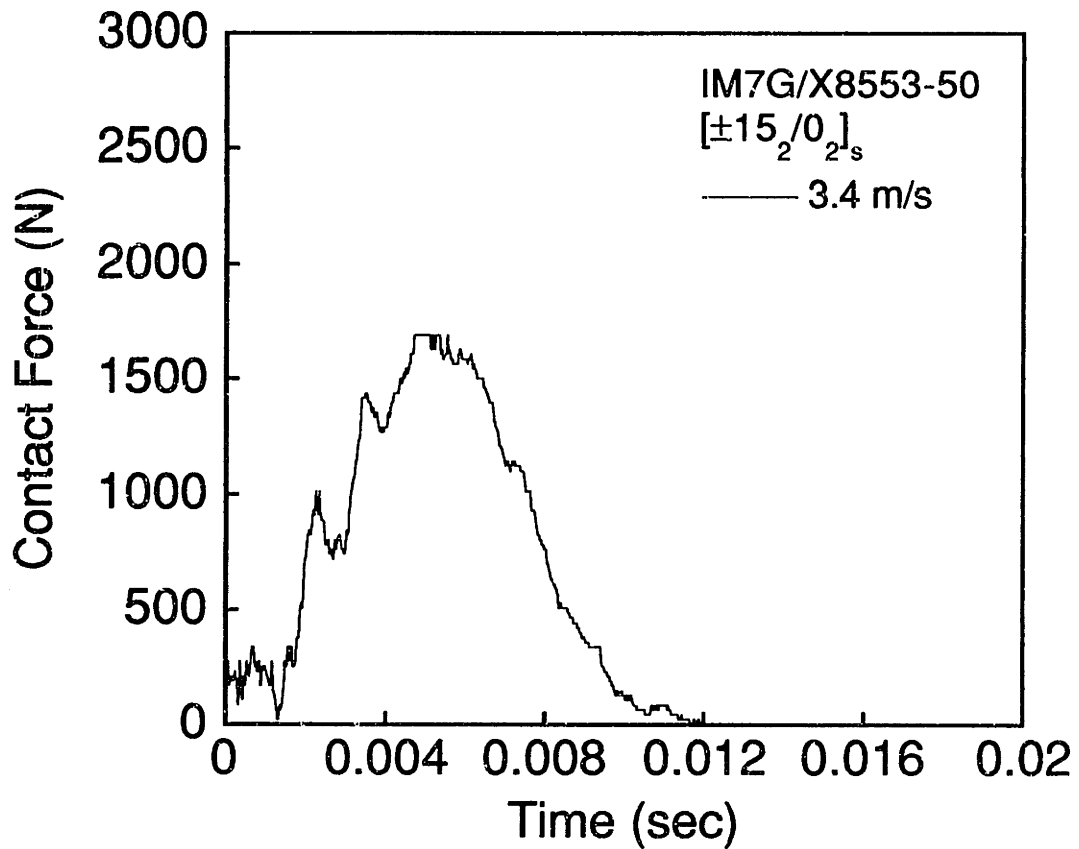
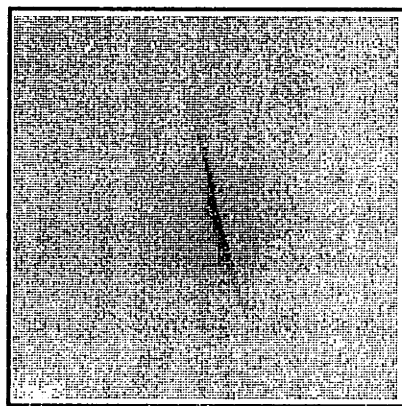
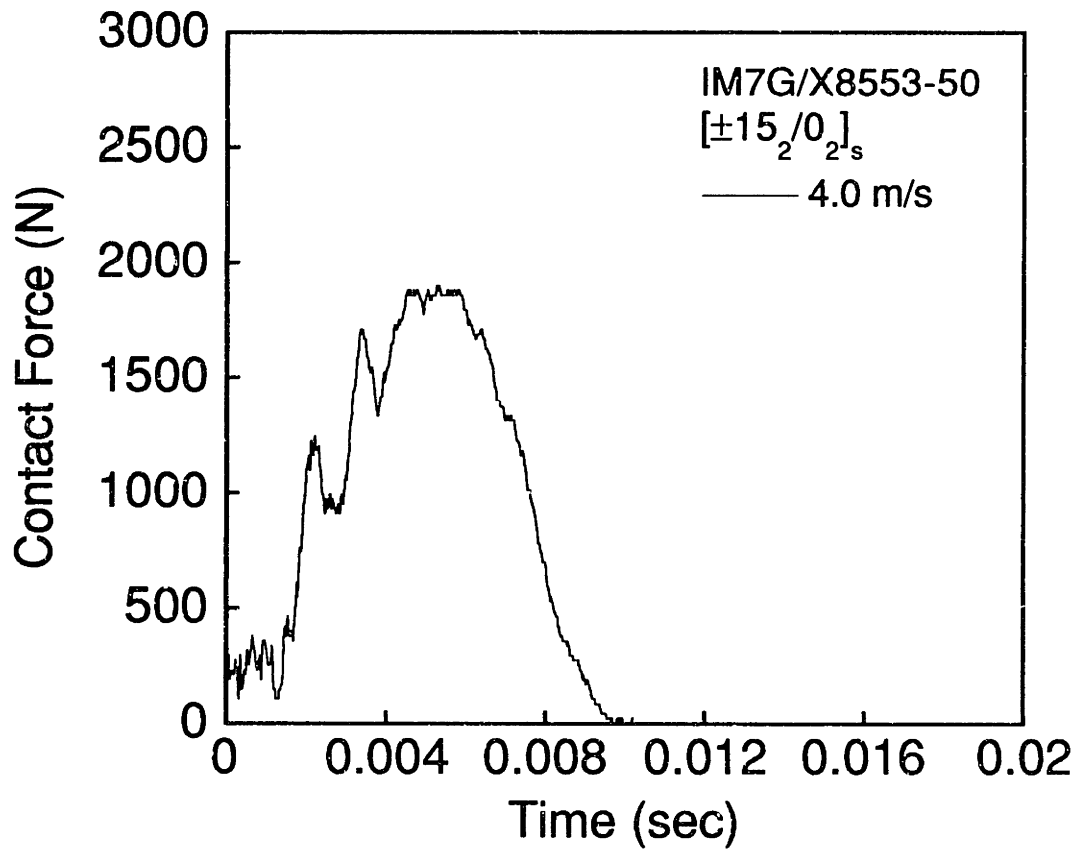


Figure A.69 (upper) Force versus time and (lower) X-ray photograph for IM7G/X8553-50 [±15₂/0₂]_s specimen impacted at 3.0 m/s.



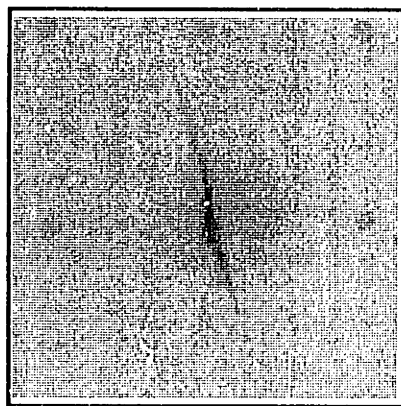
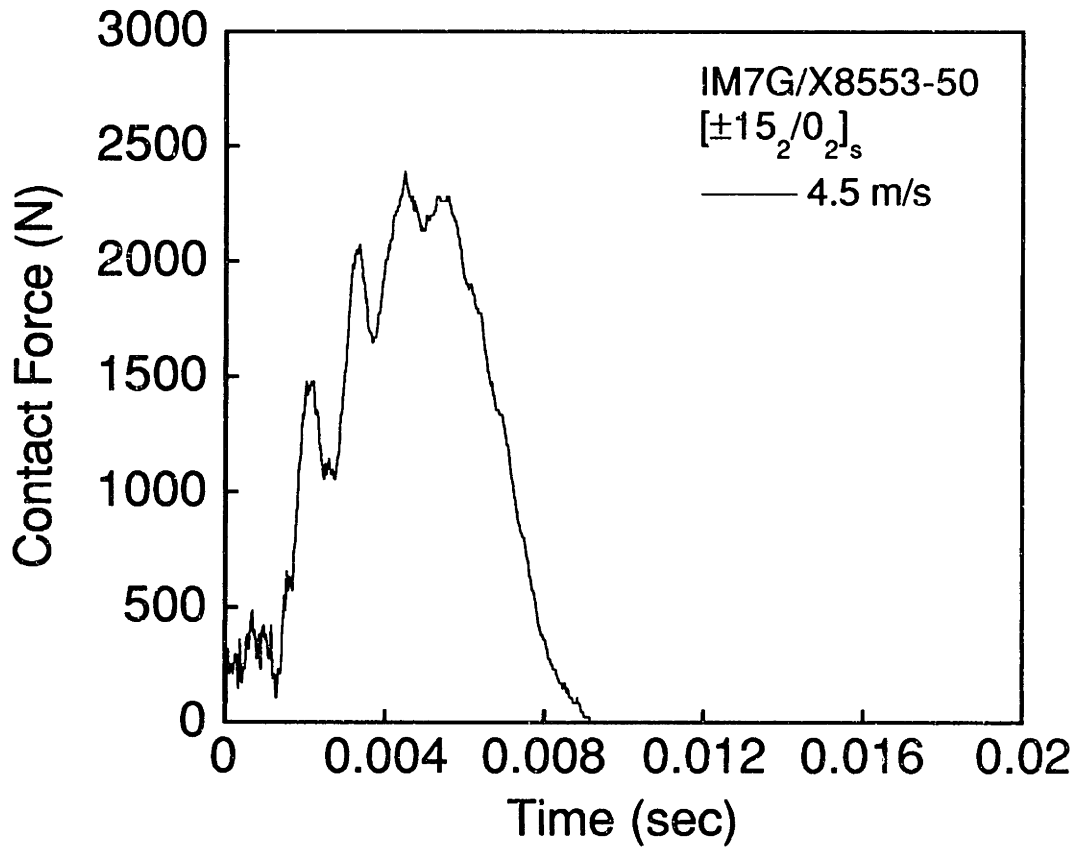
1 cm

Figure A.70 (upper) Force versus time and (lower) X-ray photograph for IM7G/X8553-50 [±15₂/0₂]_s specimen impacted at 3.4 m/s.



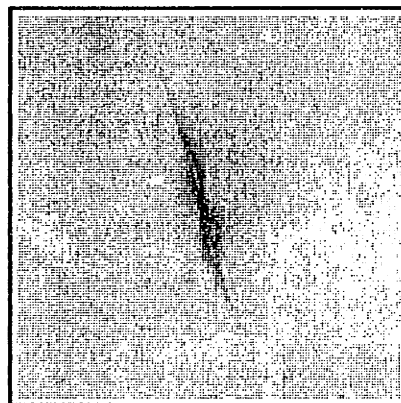
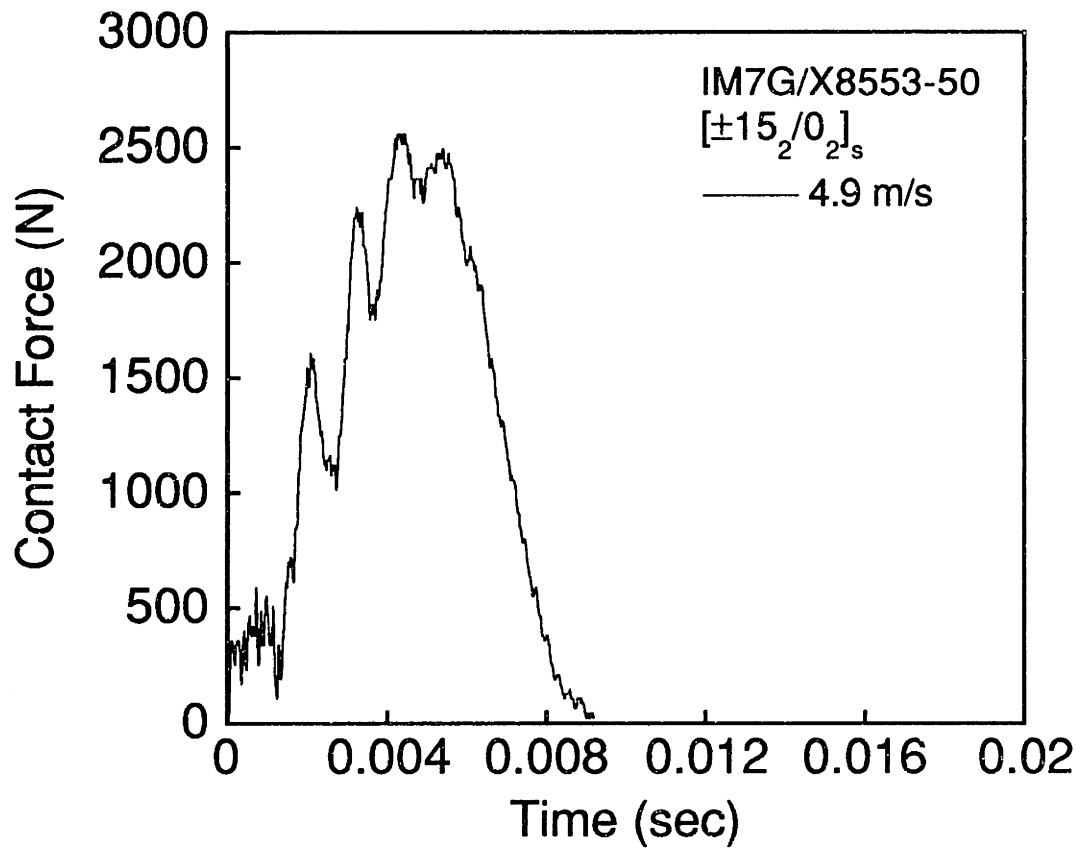
1 cm

Figure A.71 (upper) Force versus time and (lower) X-ray photograph for IM7G/X8553-50 [±15₂/0₂]_s specimen impacted at 4.0 m/s.



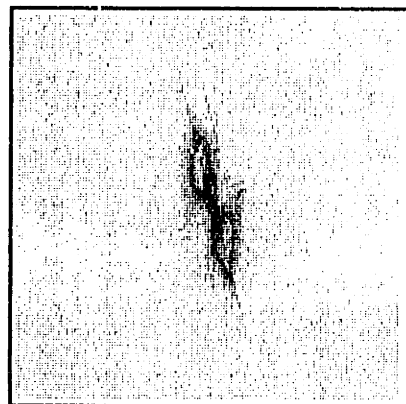
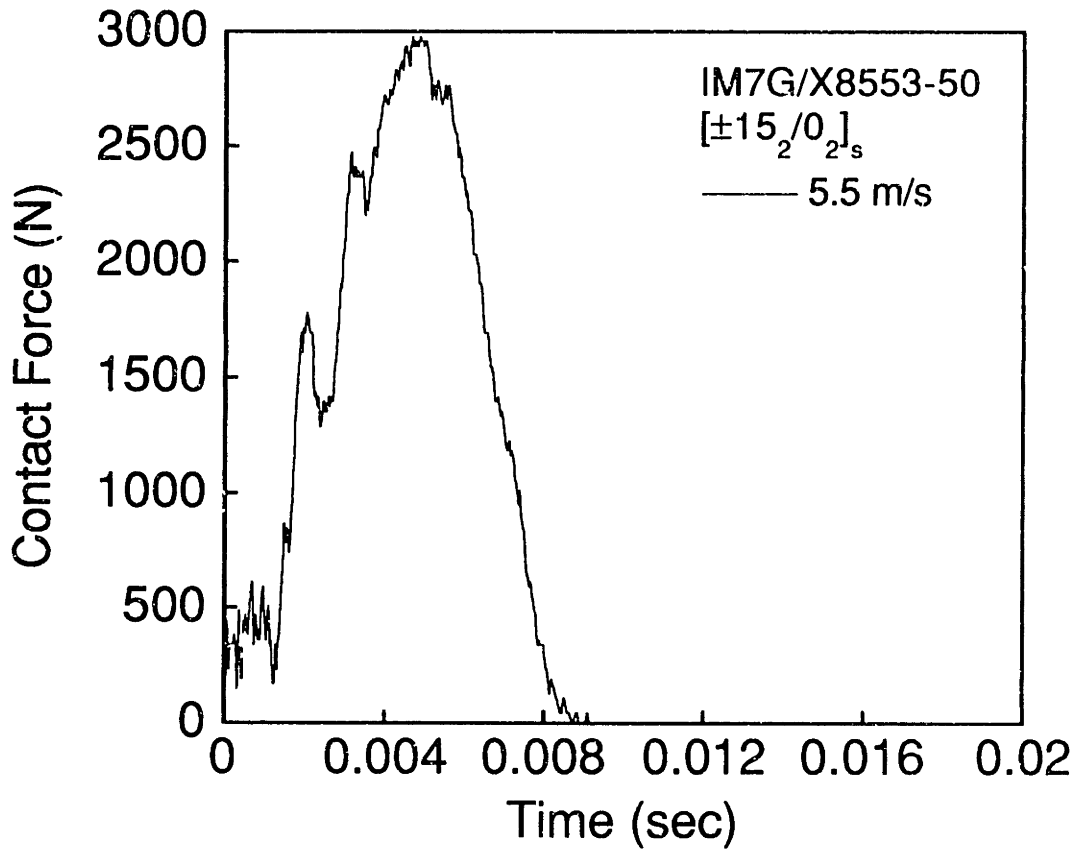
1 cm

Figure A.72 (upper) Force versus time and (lower) X-ray photograph for IM7G/X8553-50 [±15₂/0₂]_s specimen impacted at 4.5 m/s.



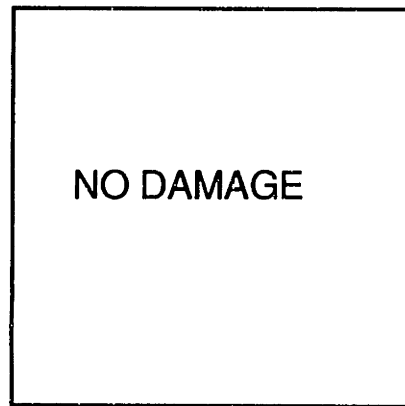
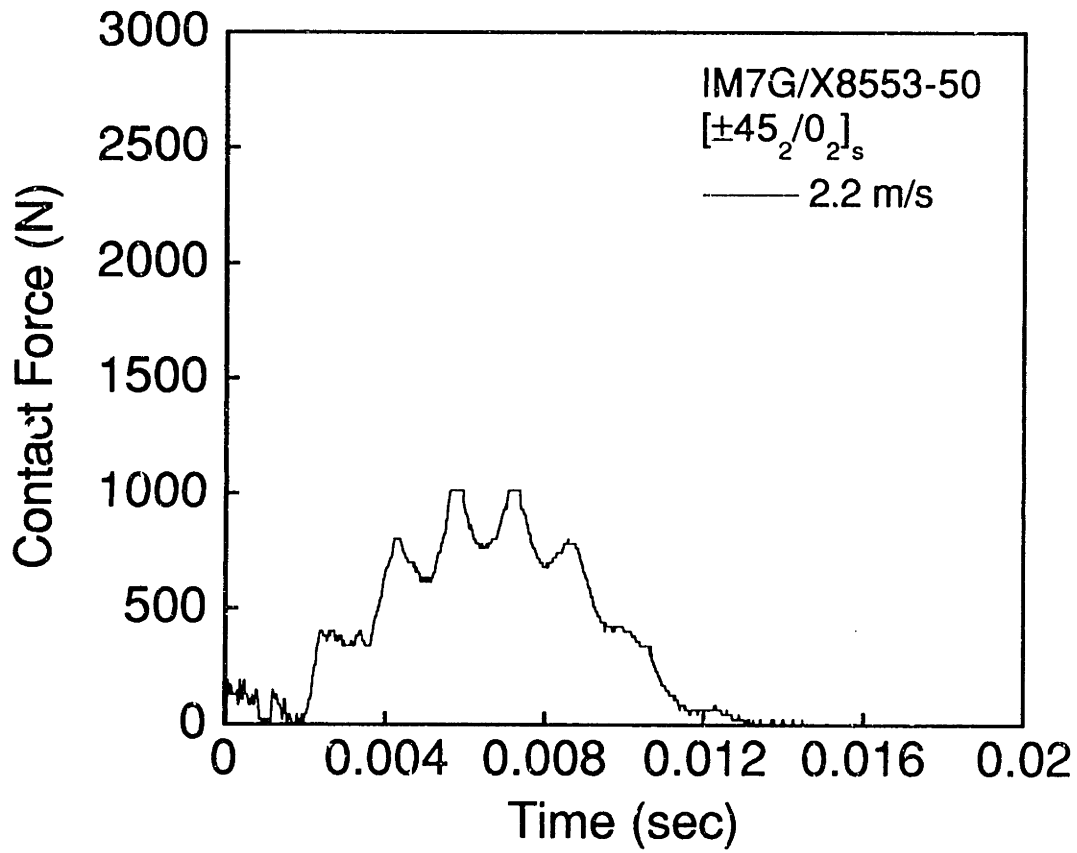
1 cm

Figure A.73 (upper) Force versus time and (lower) X-ray photograph for IM7G/X8553-50 [±15₂/0₂]_s specimen impacted at 4.9 m/s.



1 cm

Figure A.74 (upper) Force versus time and (lower) X-ray photograph for IM7G/X8553-50 [±15₂/0₂]_s specimen impacted at 5.5 m/s.



1 cm

Figure A.75 (upper) Force versus time and (lower) X-ray photograph for IM7G/X8553-50 [±45₂/0₂]_s specimen impacted at 2.2 m/s.

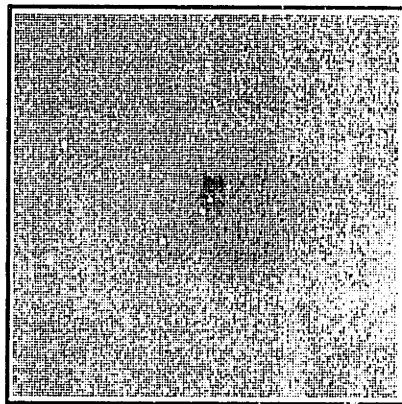
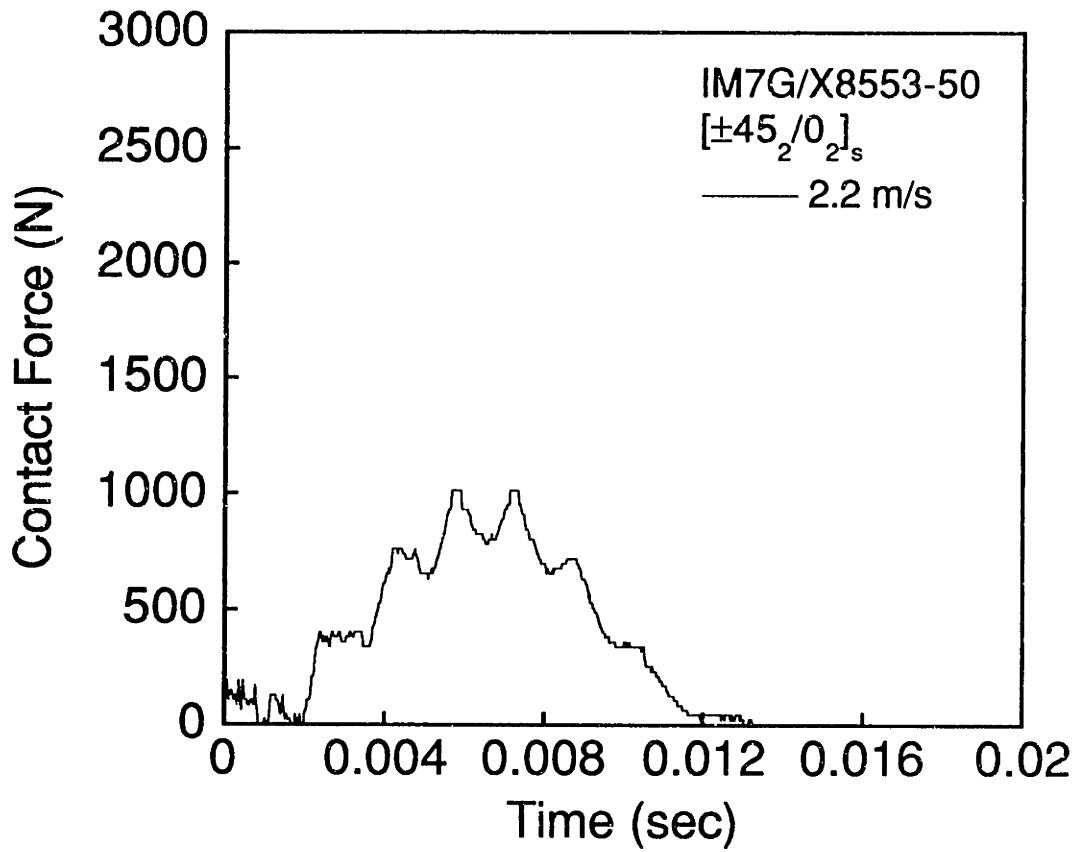
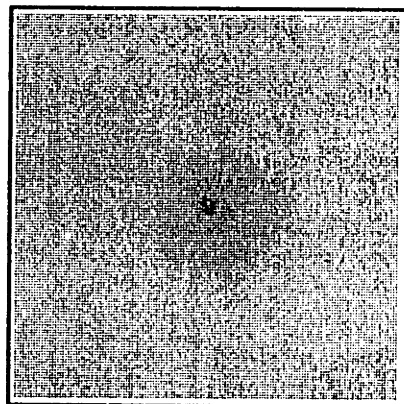
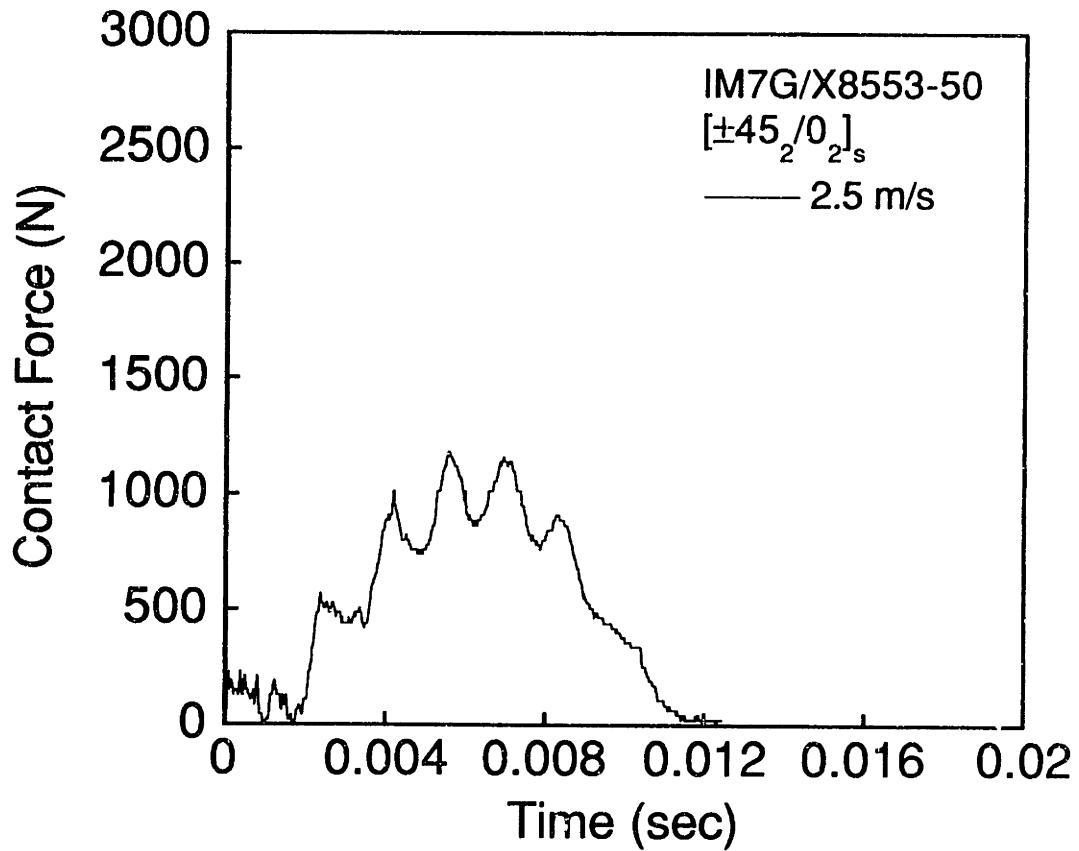
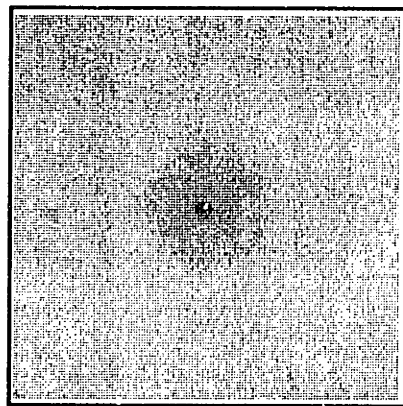
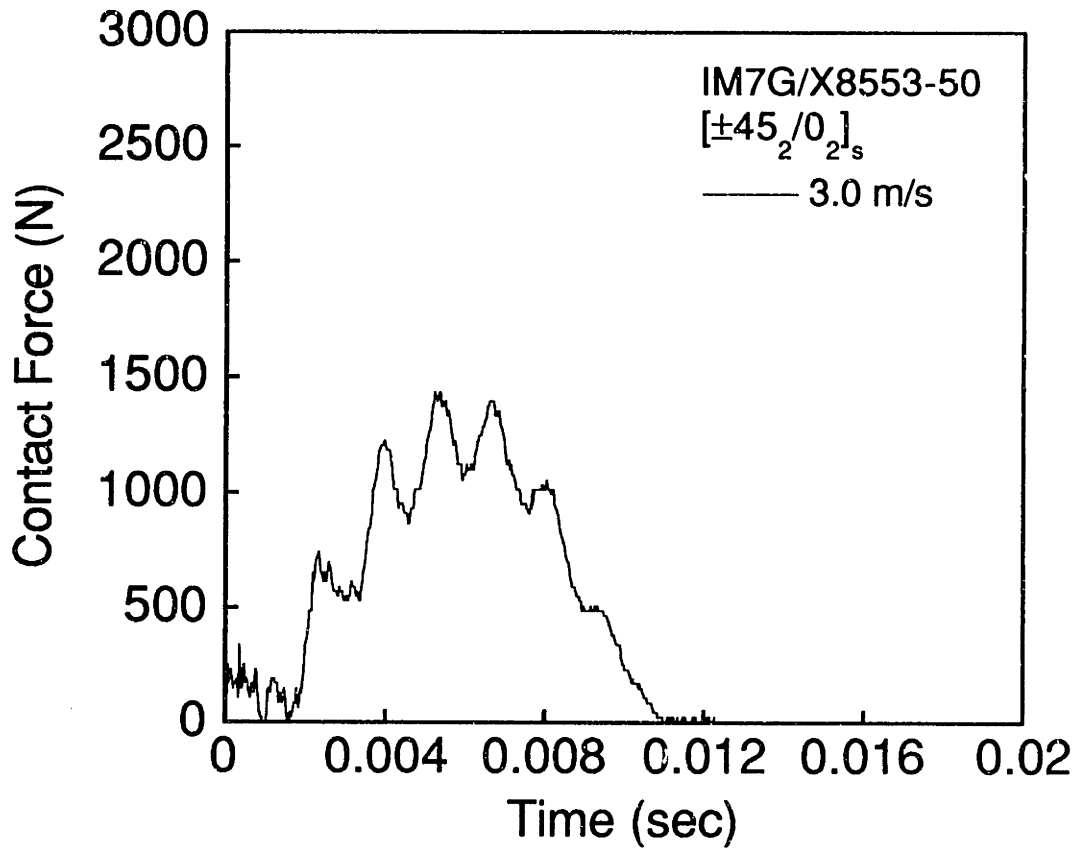


Figure A.76 (upper) Force versus time and (lower) X-ray photograph for IM7G/X8553-50 [±45₂/0₂]_s specimen impacted at 2.2 m/s.



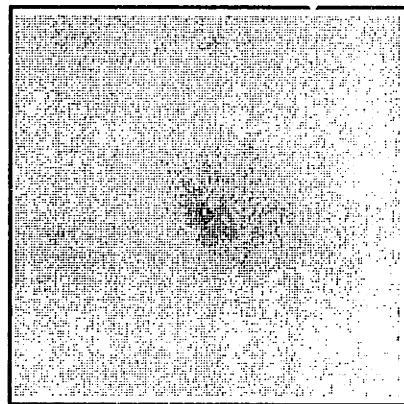
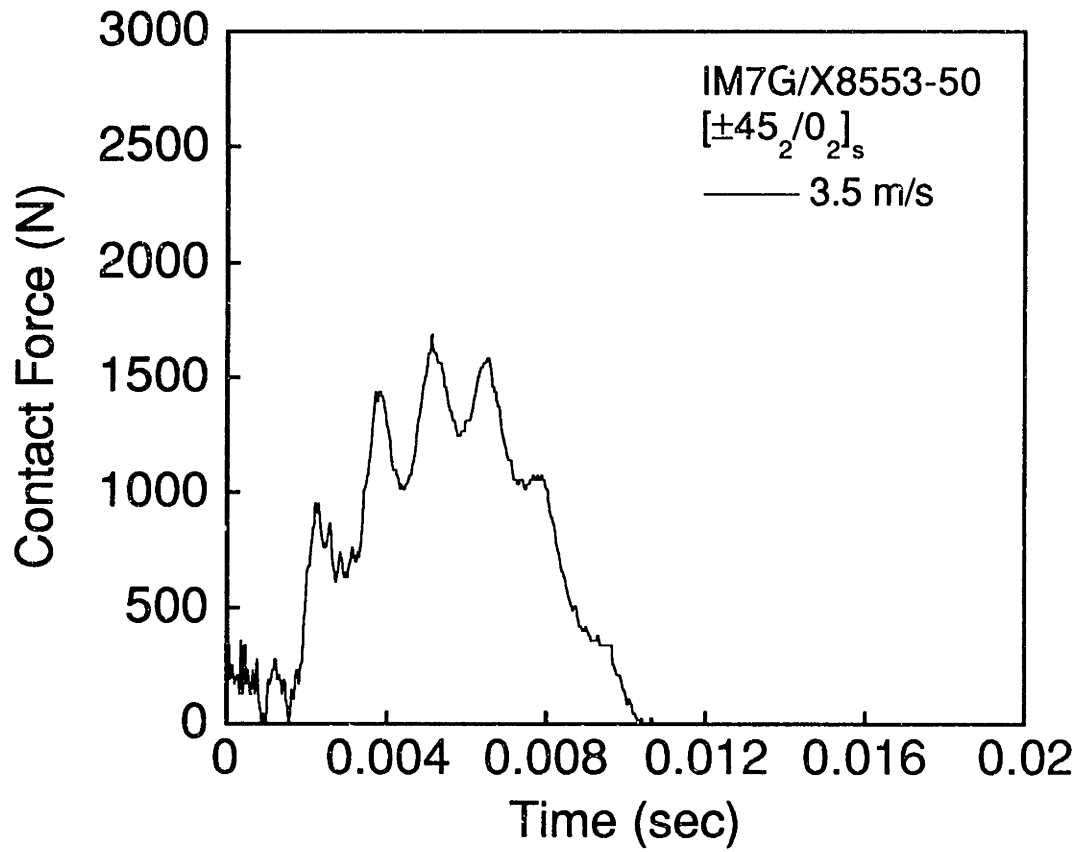
1 cm

Figure A.77 (upper) Force versus time and (lower) X-ray photograph for IM7G/X8553-50 [±45₂/0₂]_s specimen impacted at 2.5 m/s.



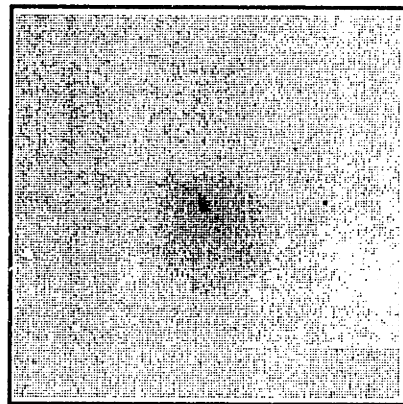
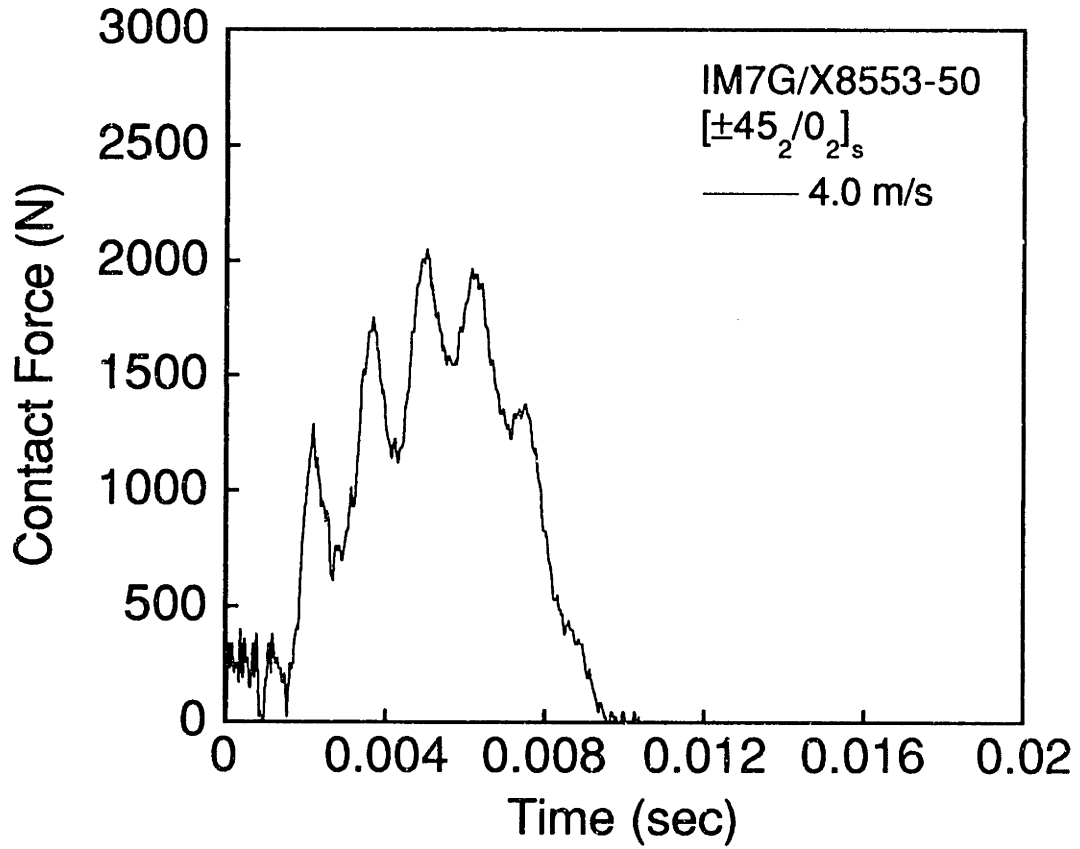
1 cm

Figure A.78 (upper) Force versus time and (lower) X-ray photograph for IM7G/X8553-50 [±45₂/0₂]_s specimen impacted at 3.0 m/s.



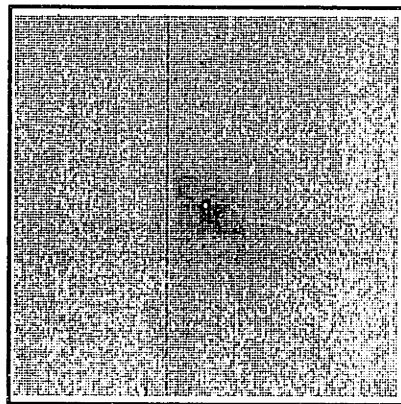
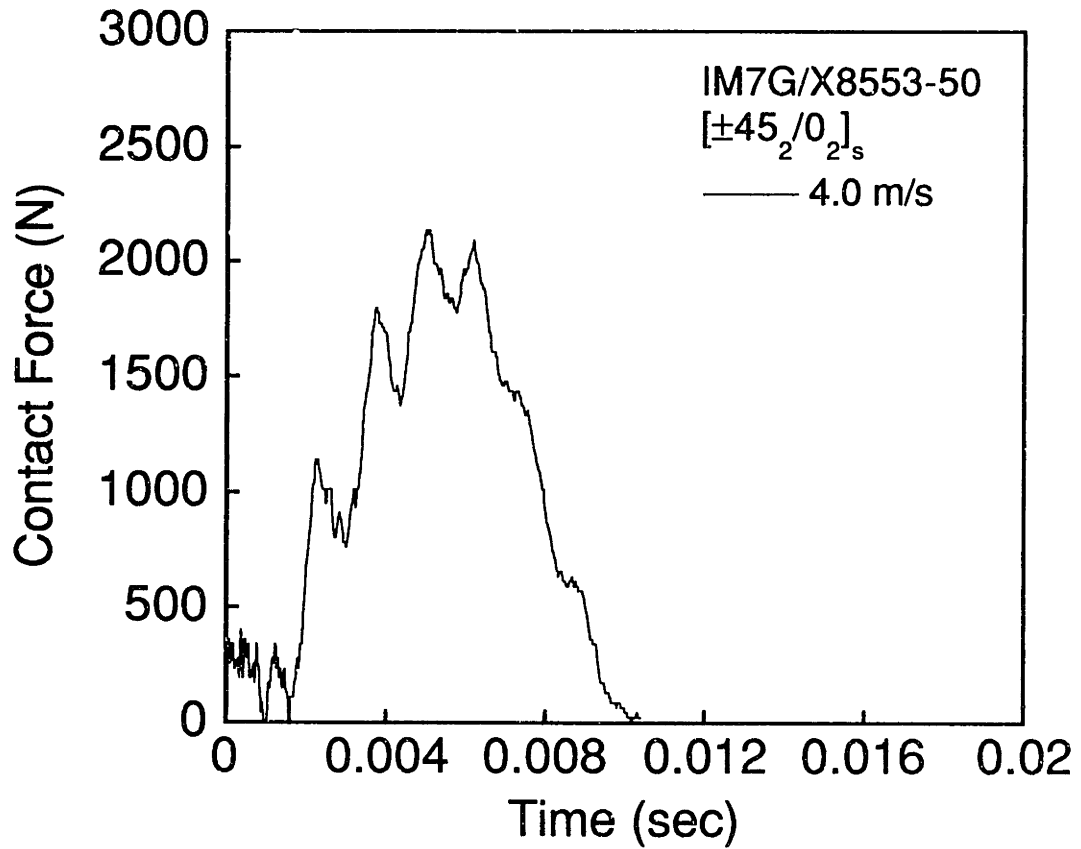
1 cm

Figure A.79 (upper) Force versus time and (lower) X-ray photograph for IM7G/X8553-50 [±45₂/0₂]_s specimen impacted at 3.5 m/s.



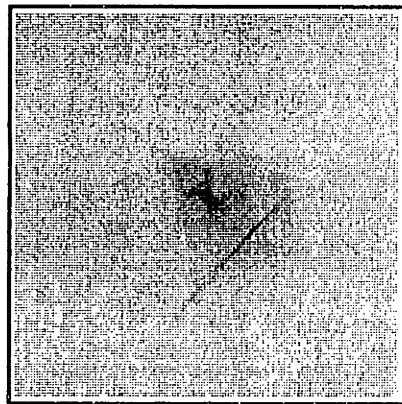
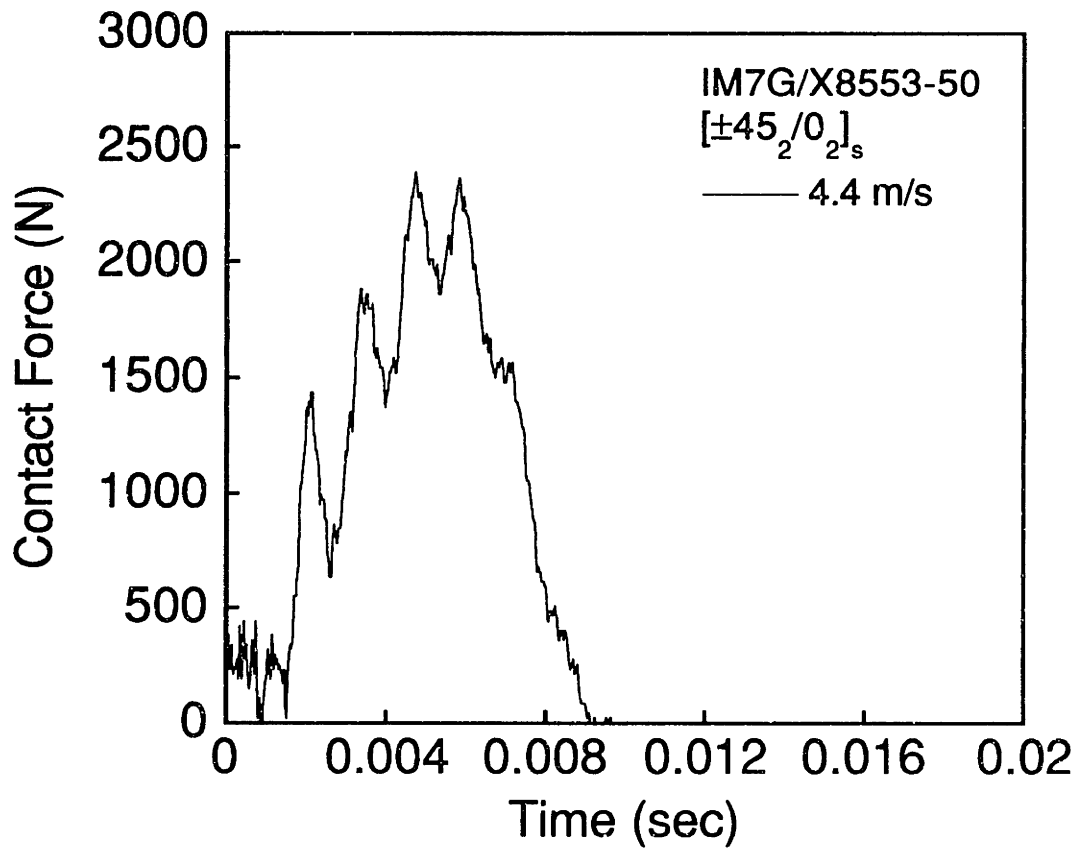
1 cm

Figure A.80 (upper) Force versus time and (lower) X-ray photograph for IM7G/X8553-50 [±45₂/0₂]_s specimen impacted at 4.0 m/s.



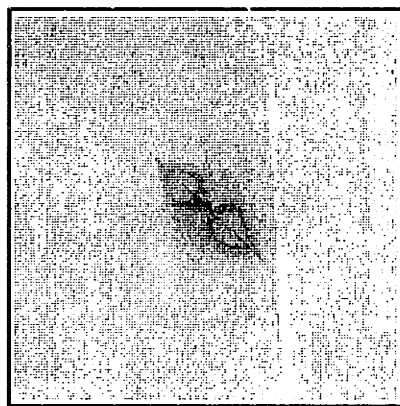
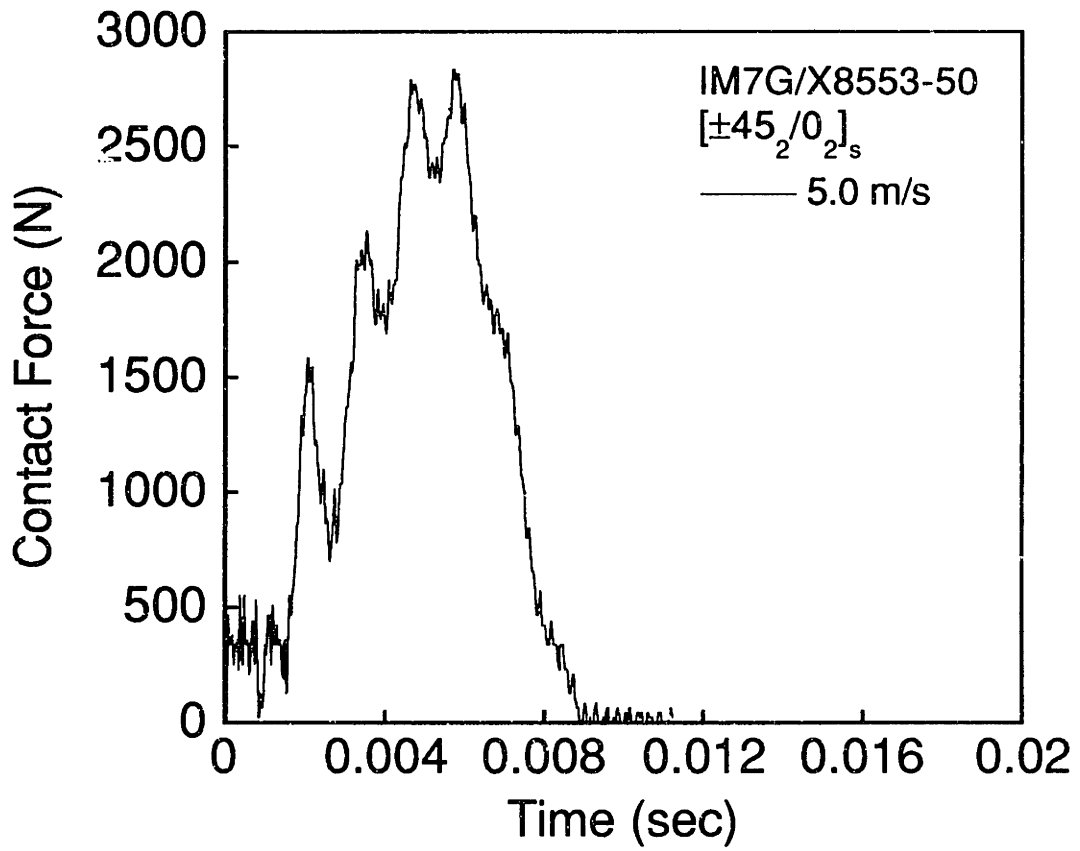
1 cm

Figure A.81 (upper) Force versus time and (lower) X-ray photograph for IM7G/X8553-50 [±45₂/0₂]_s specimen impacted at 4.0 m/s.



1 cm

Figure A.82 (upper) Force versus time and (lower) X-ray photograph for IM7G/X8553-50 $[\pm 45_2/0_2]_s$ specimen impacted at 4.4 m/s.



1 cm

Figure A.83 (upper) Force versus time and (lower) X-ray photograph for IM7G/X8553-50 [±45₂/0₂]_s specimen impacted at 5.0 m/s.

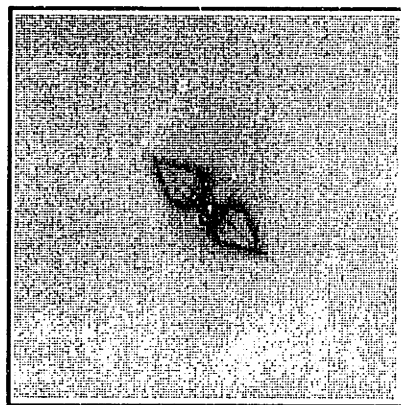
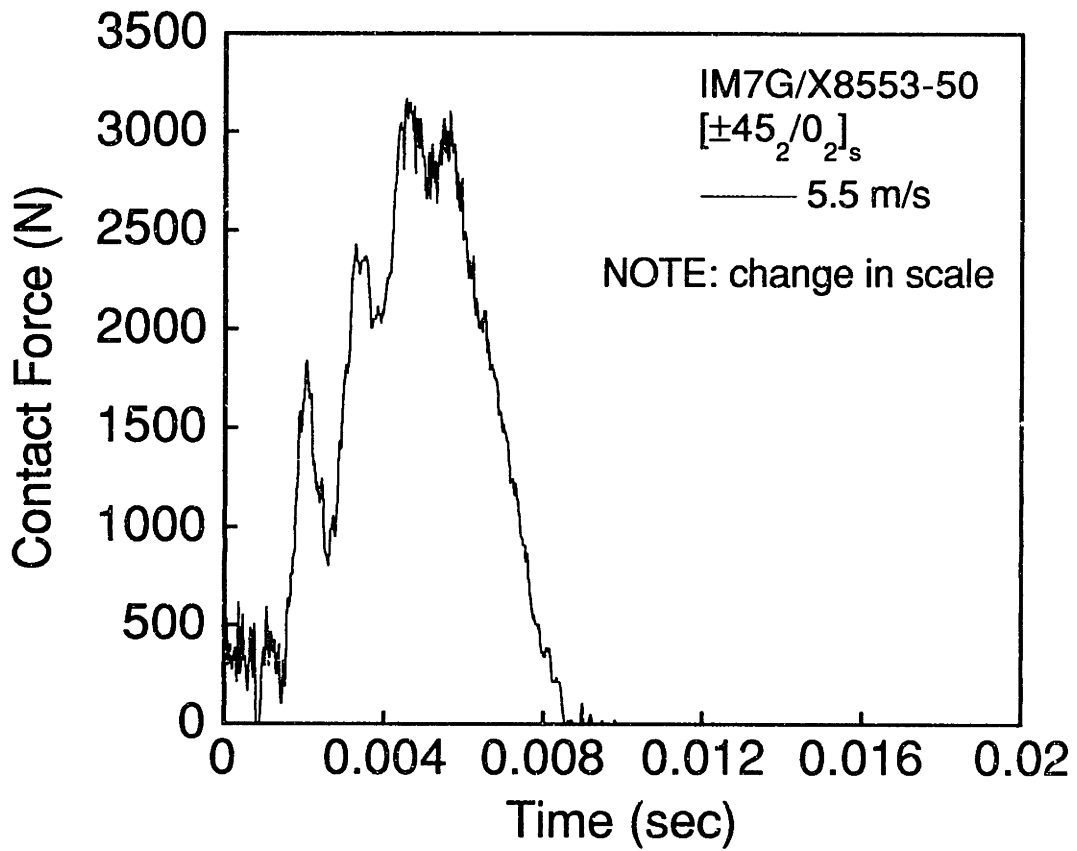


Figure A.84 (upper) Force versus time and (lower) X-ray photograph for IM7G/X8553-50 [±45₂/0₂]_s specimen impacted at 5.5 m/s.

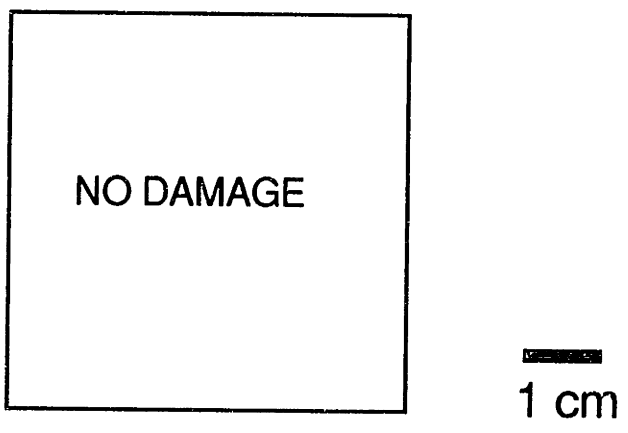
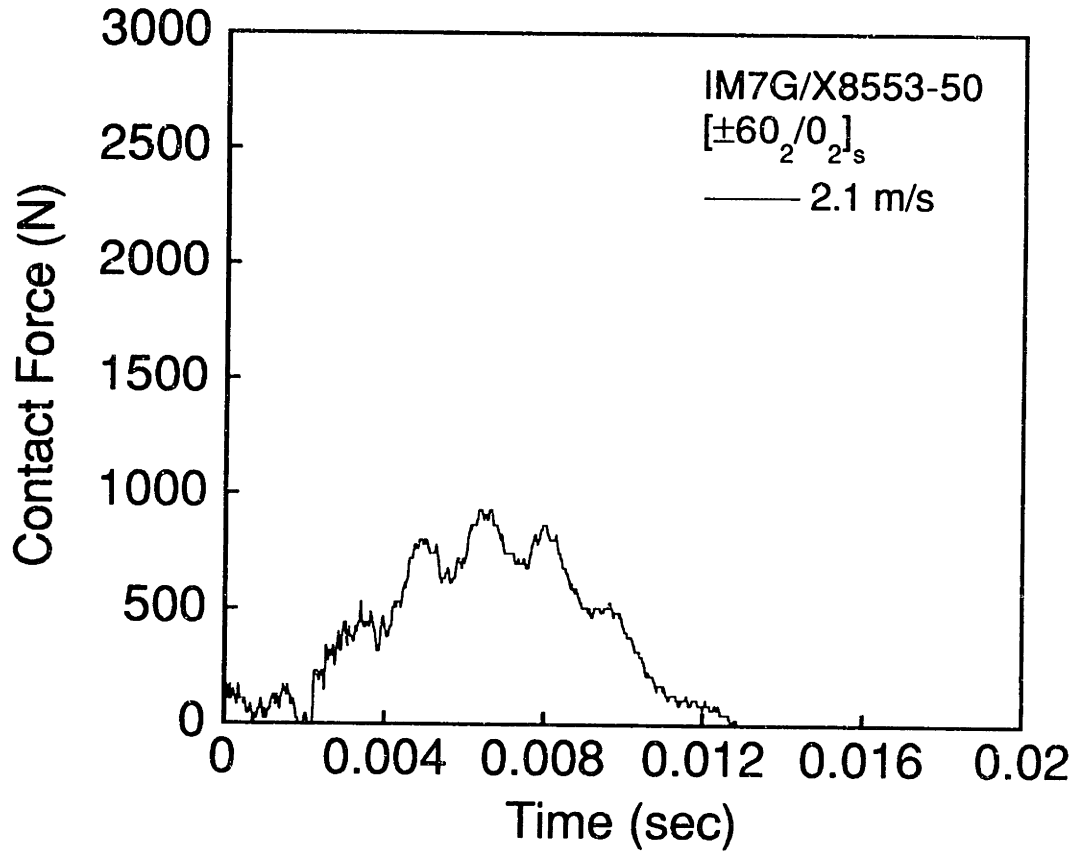
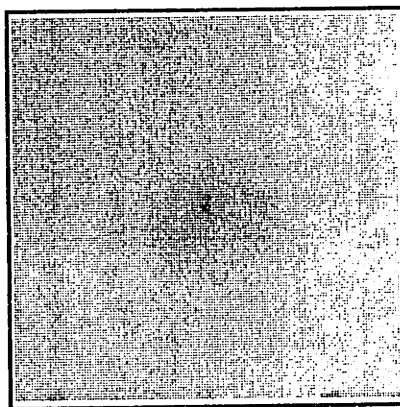
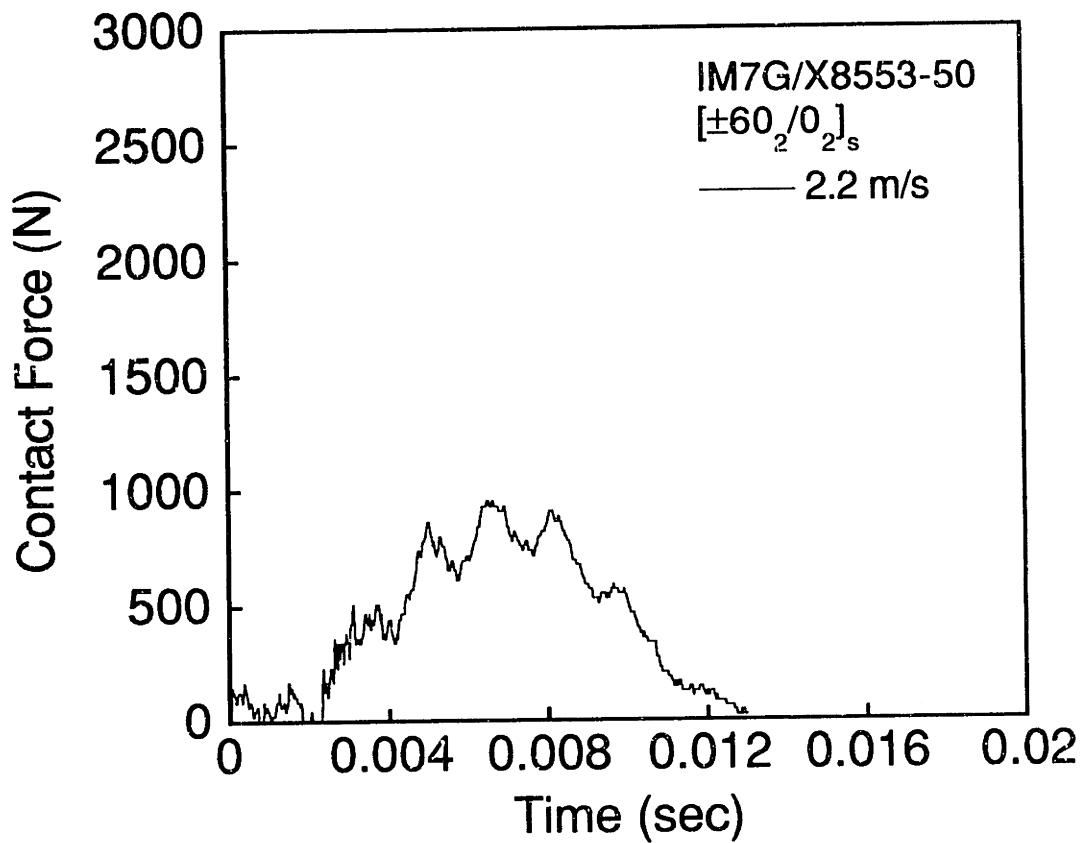
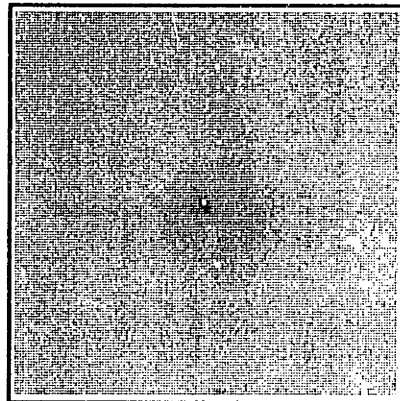
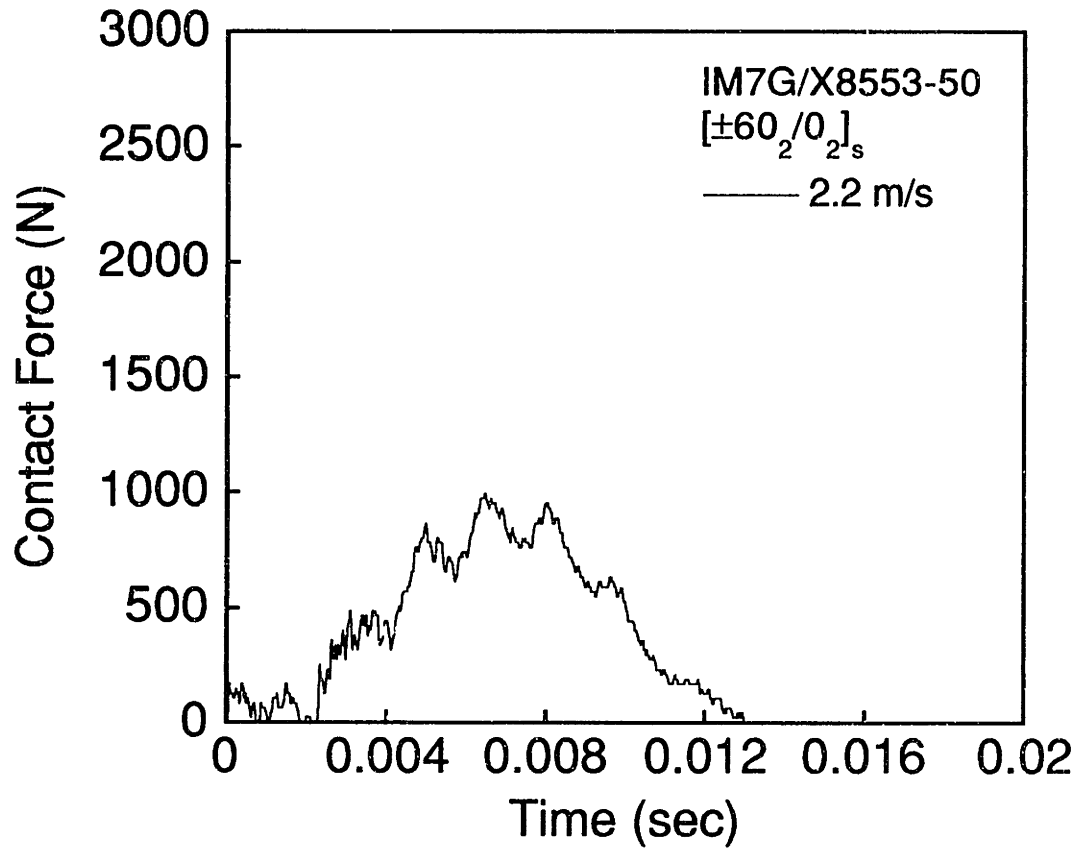


Figure A.85 (upper) Force versus time and (lower) X-ray photograph for IM7G/X8553-50 [±60₂/0₂]_s specimen impacted at 2.1 m/s.



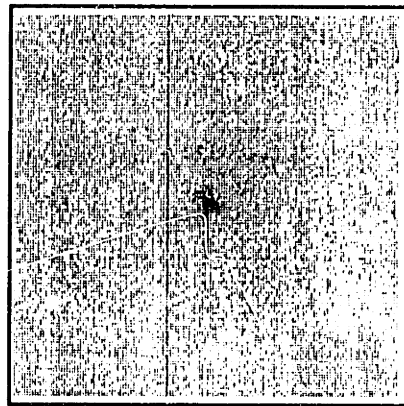
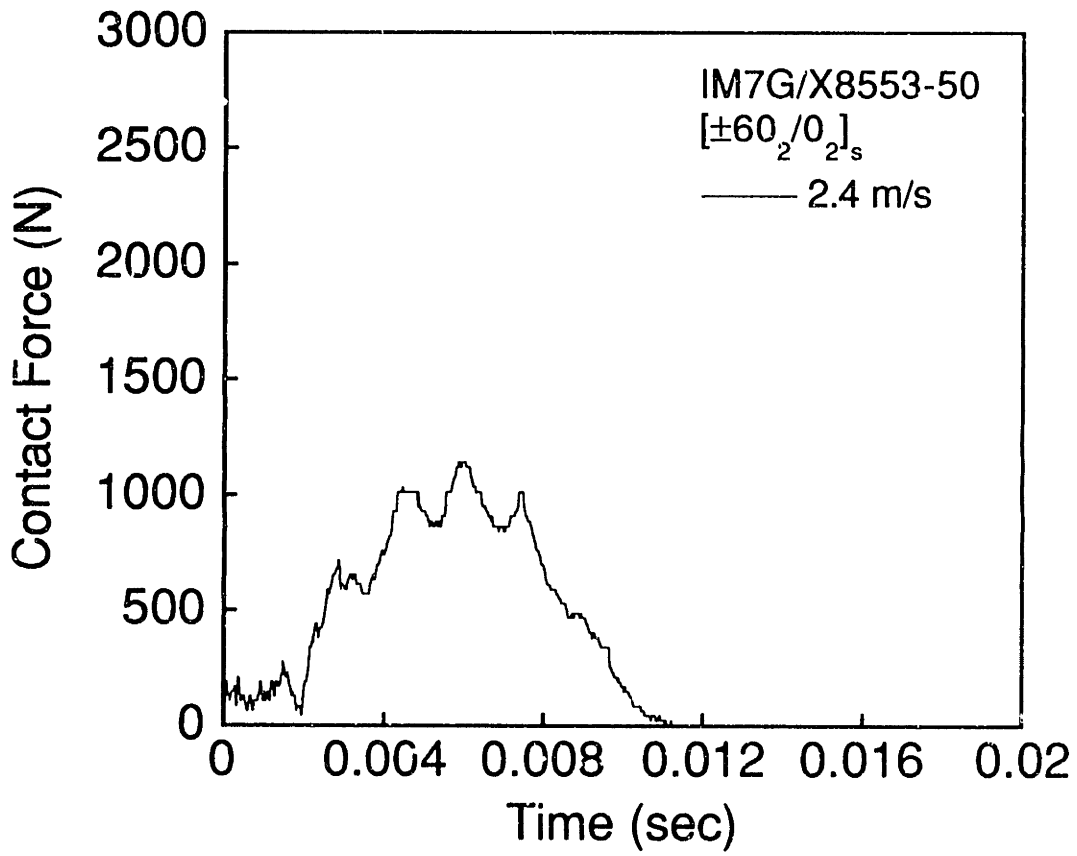
1 cm

Figure A.86 (upper) Force versus time and (lower) X-ray photograph for IM7G/X8553-50 [±60₂/0₂]_s specimen impacted at 2.2 m/s.



1 cm

Figure A.87 (upper) Force versus time and (lower) X-ray photograph for IM7G/X8553-50 [±60₂/0₂]_s specimen impacted at 2.2 m/s.



1 cm

Figure A.88 (upper) Force versus time and (lower) X-ray photograph for IM7G/X8553-50 [±60₂/0₂]_s specimen impacted at 2.4 m/s.

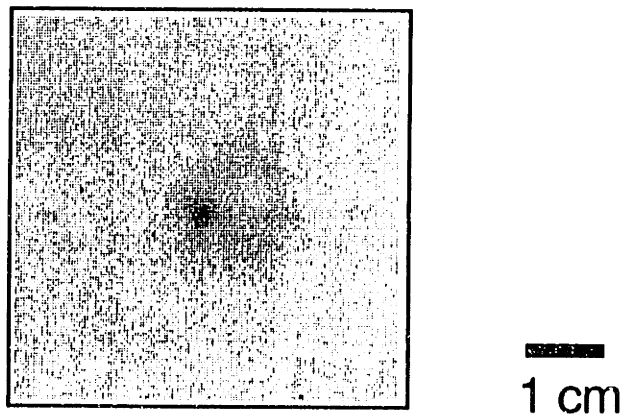
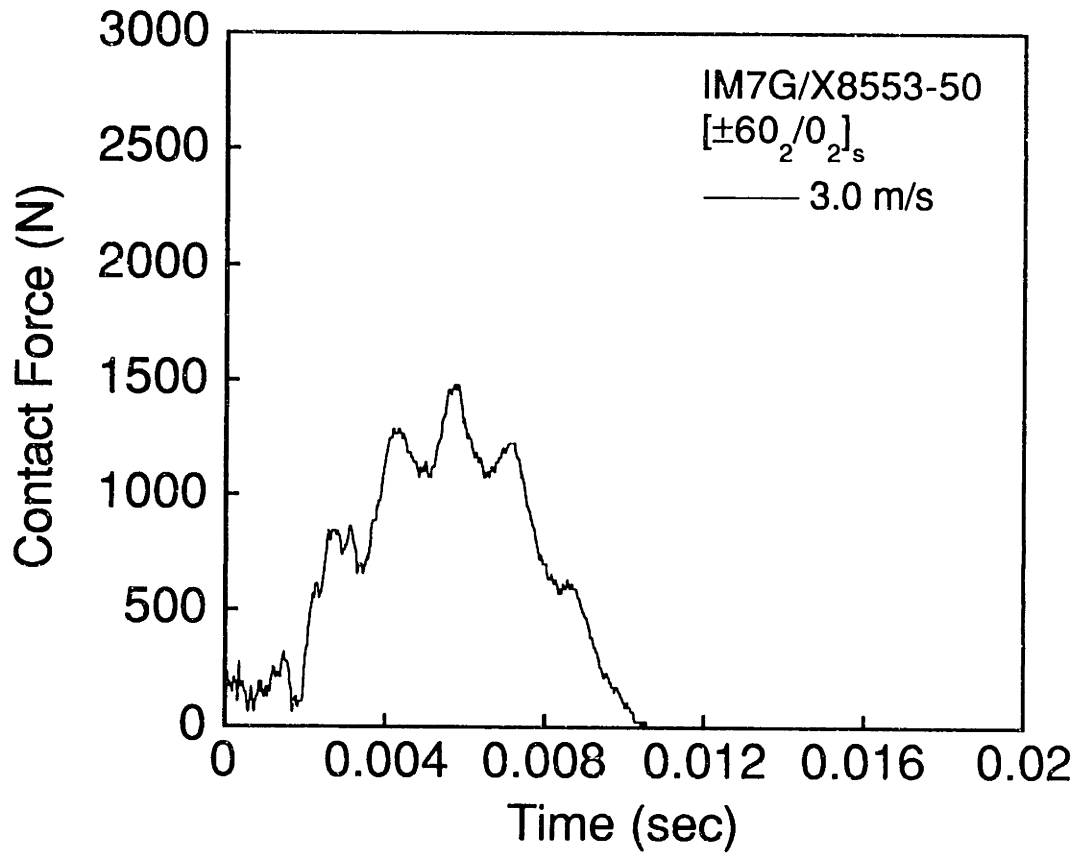
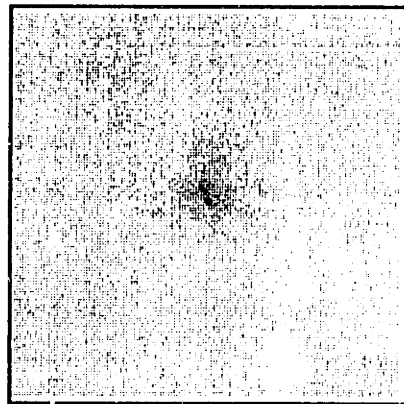
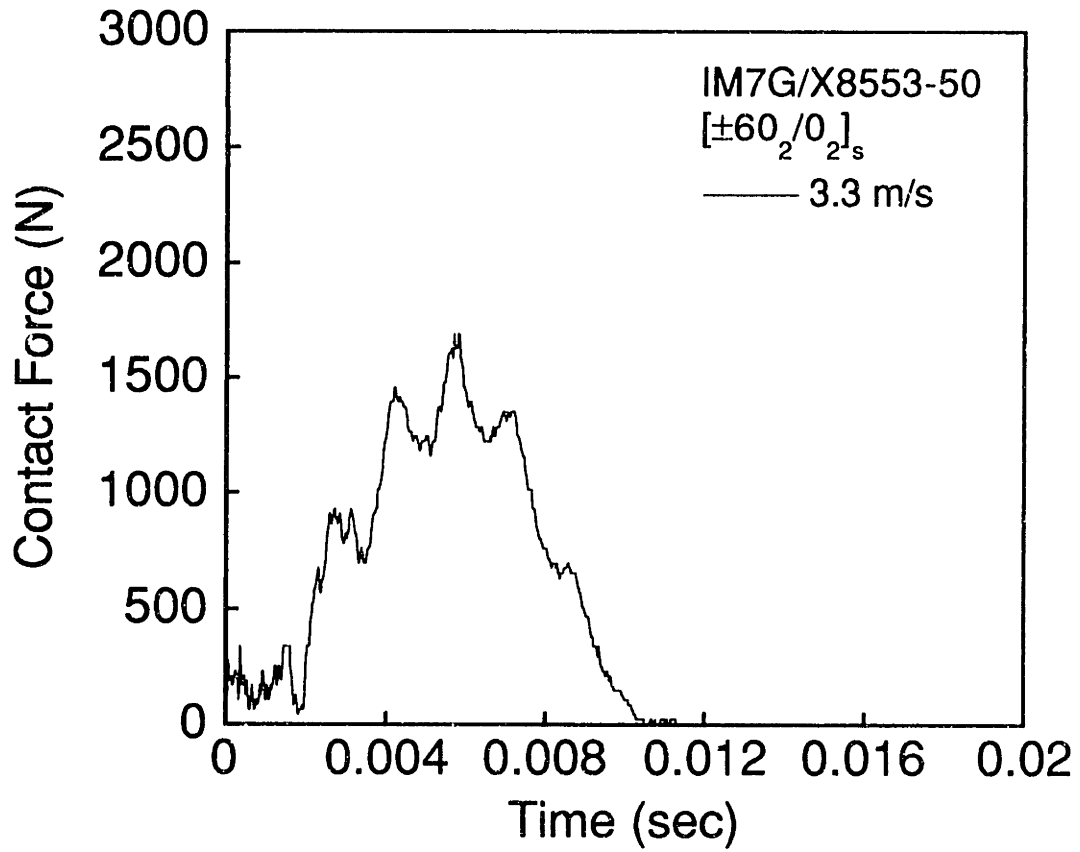
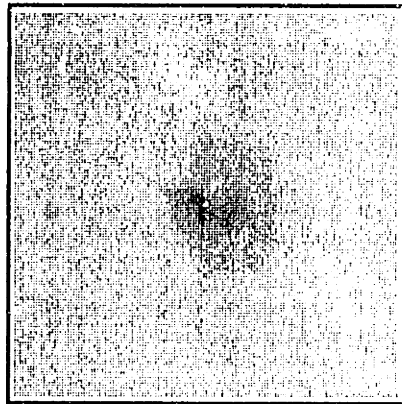
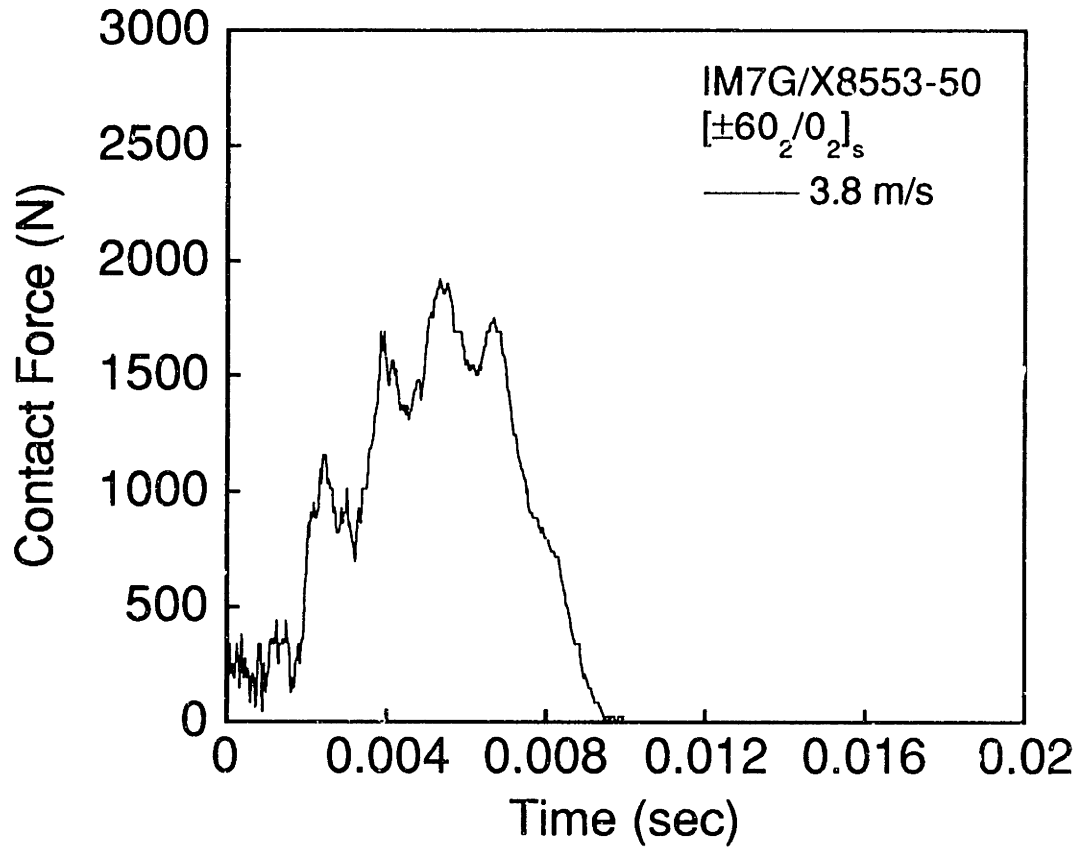


Figure A.89 (upper) Force versus time and (lower) X-ray photograph for IM7G/X8553-50 [±60₂/0₂]_s specimen impacted at 3.0 m/s.



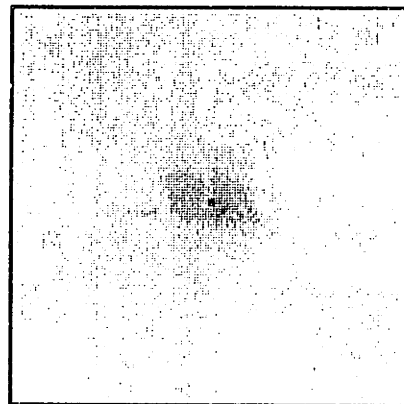
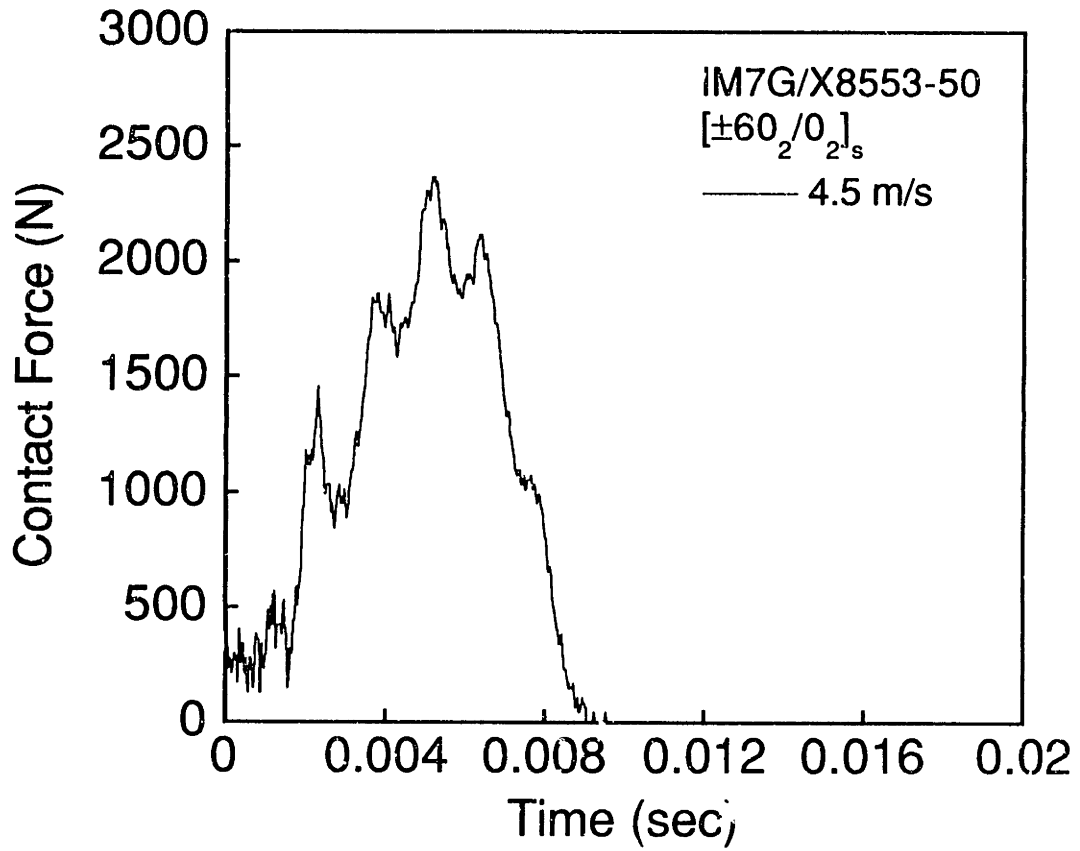
1 cm

Figure A.90 (upper) Force versus time and (lower) X-ray photograph for IM7G/X8553-50 [±60₂/0₂]_s specimen impacted at 3.3 m/s.



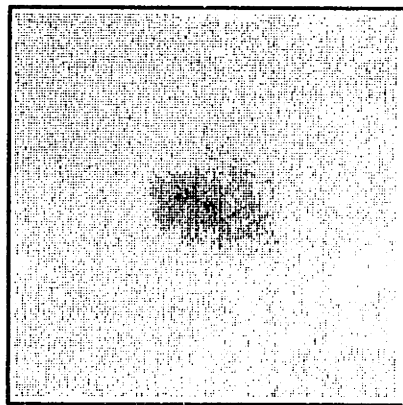
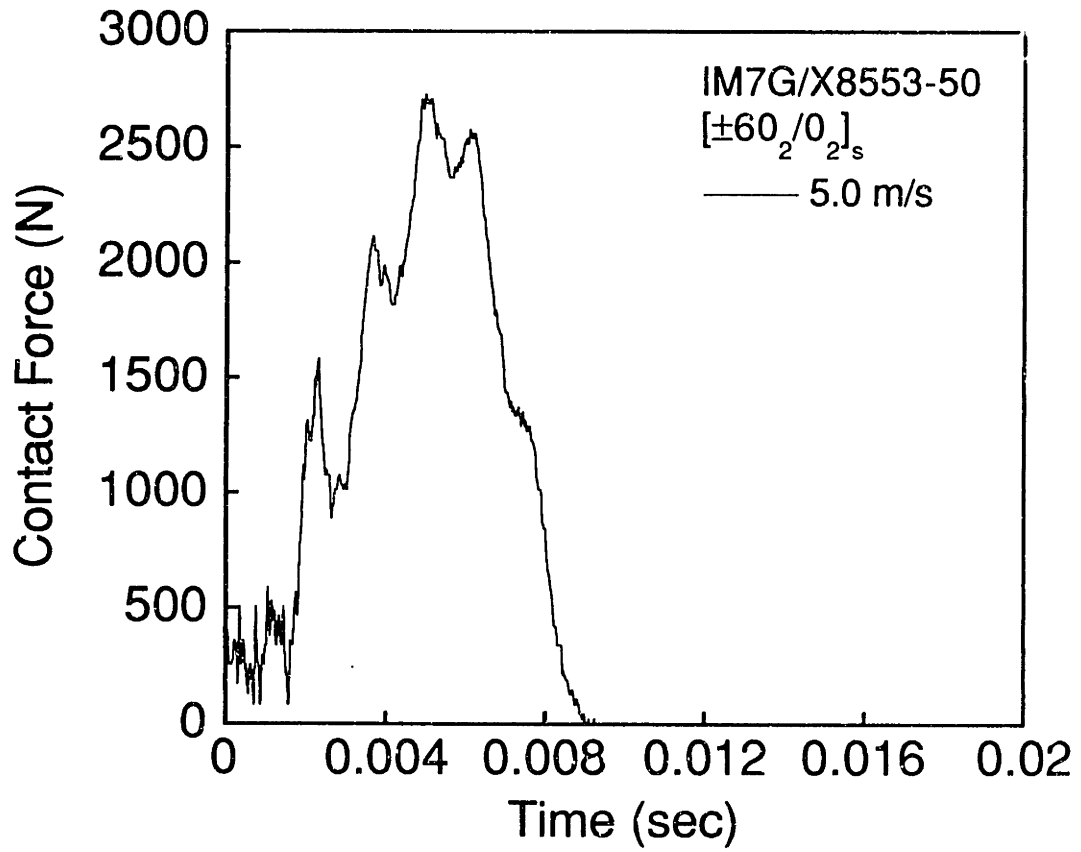
1 cm

Figure A.91 (upper) Force versus time and (lower) X-ray photograph for IM7G/X8553-50 [±60₂/0₂]_s specimen impacted at 3.8 m/s.



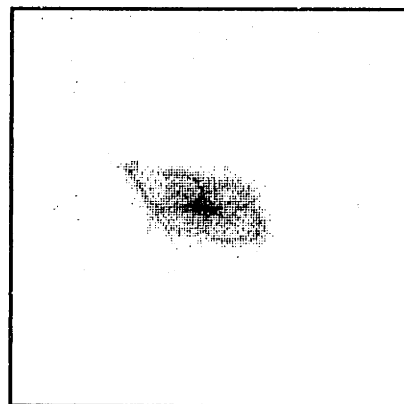
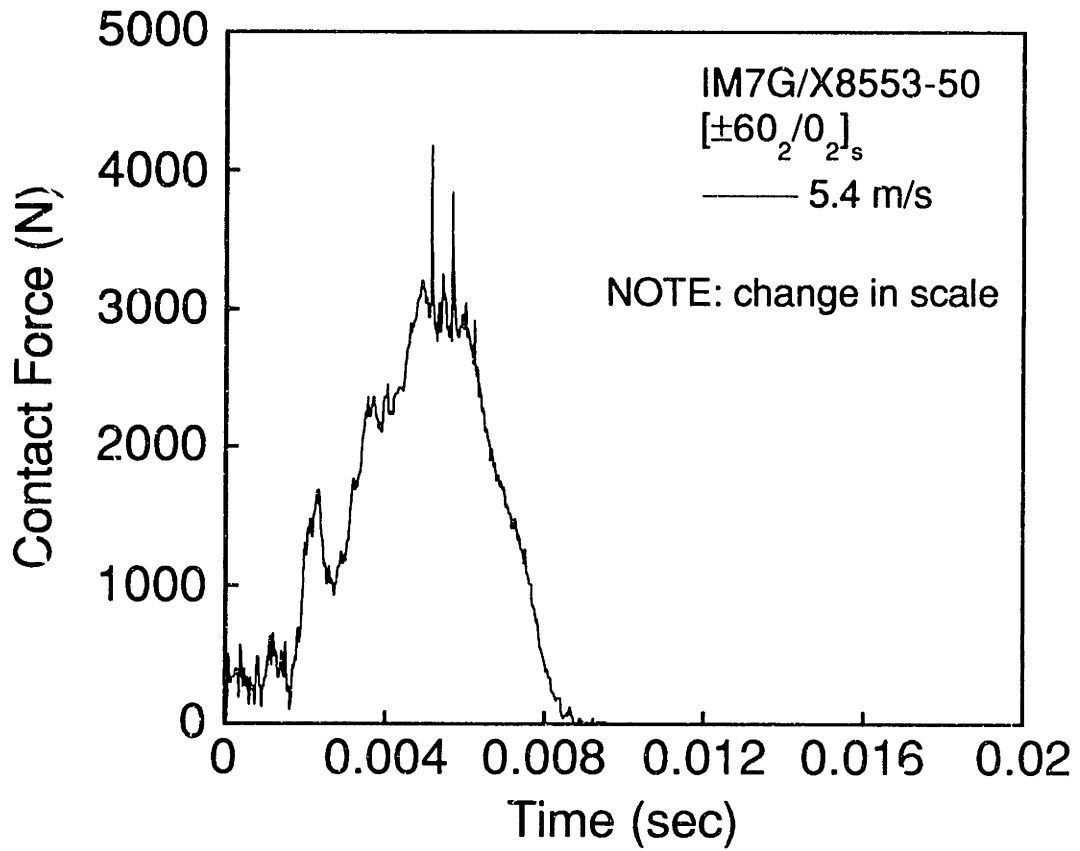
1 cm

Figure A.92 (upper) Force versus time and (lower) X-ray photograph for IM7G/X8553-50 [±60₂/0₂]_s specimen impacted at 4.5 m/s.



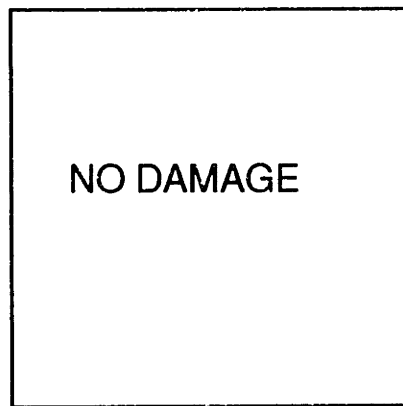
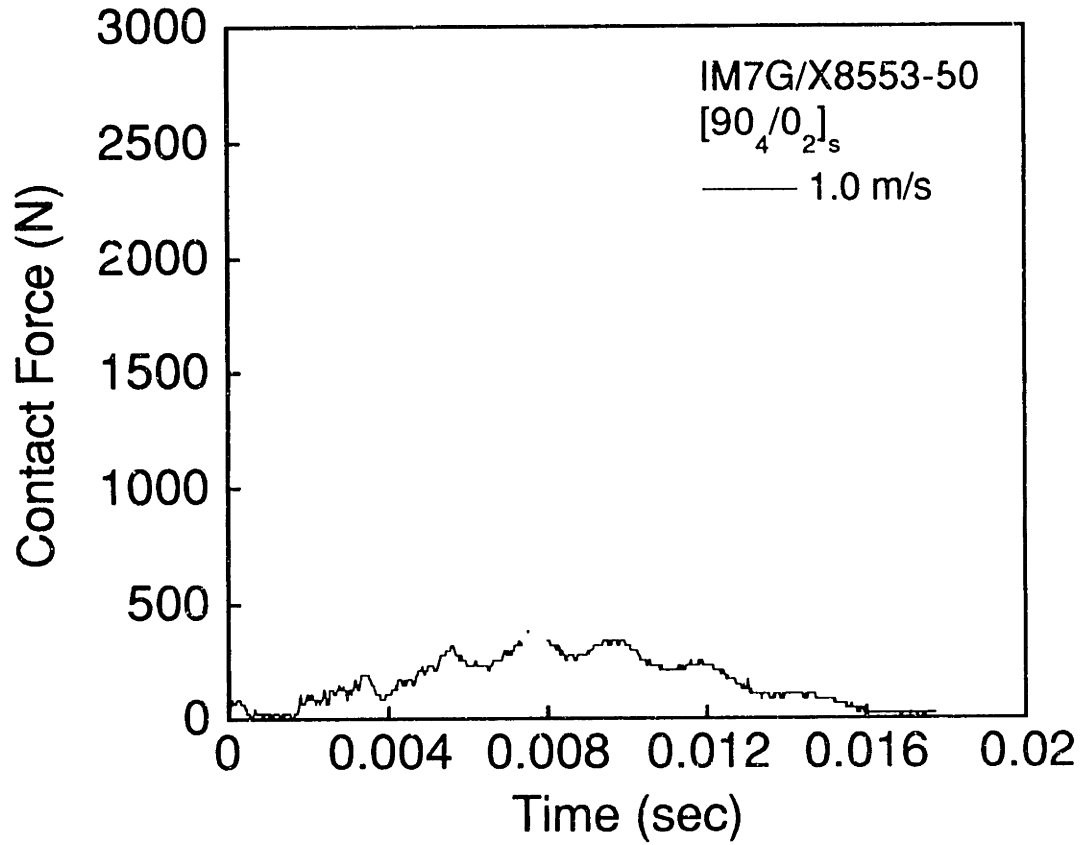
1 cm

Figure A.93 (upper) Force versus time and (lower) X-ray photograph for IM7G/X8553-50 [±60₂/0₂]_s specimen impacted at 5.0 m/s.



1 cm

Figure A.94 (upper) Force versus time and (lower) X-ray photograph for IM7G/X8553-50 [±60₂/0₂]_s specimen impacted at 5.4 m/s.



1 cm

Figure A.95 (upper) Force versus time and (lower) X-ray photograph for IM7G/X8553-50 [90₄/0₂]_s specimen impacted at 1.0 m/s.

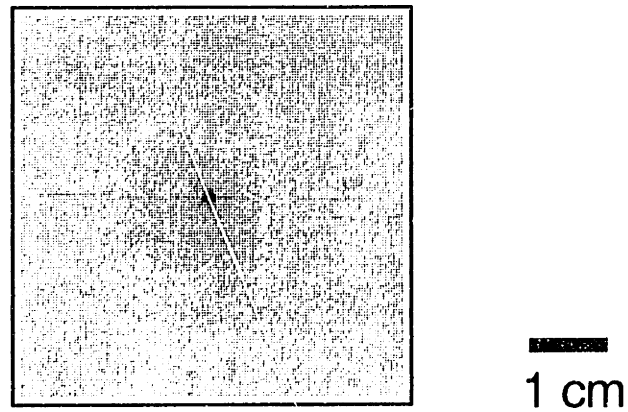
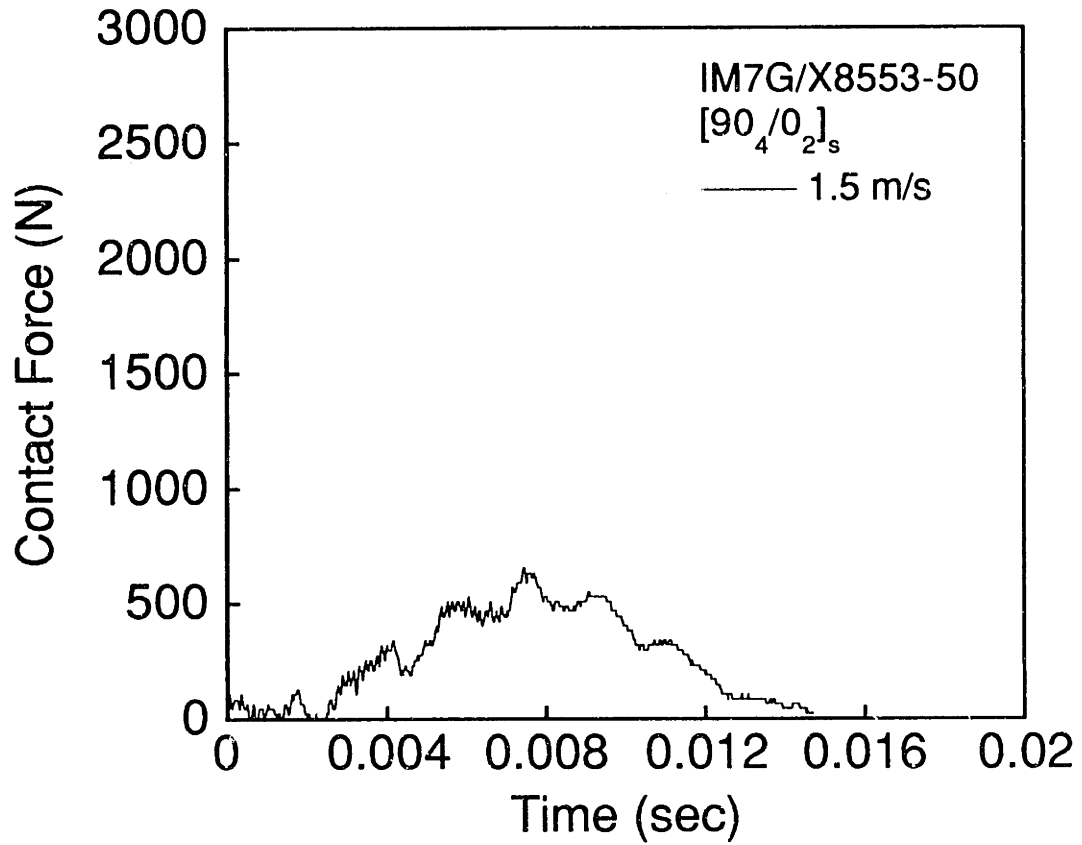
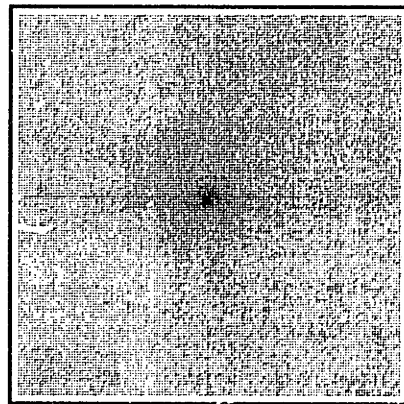
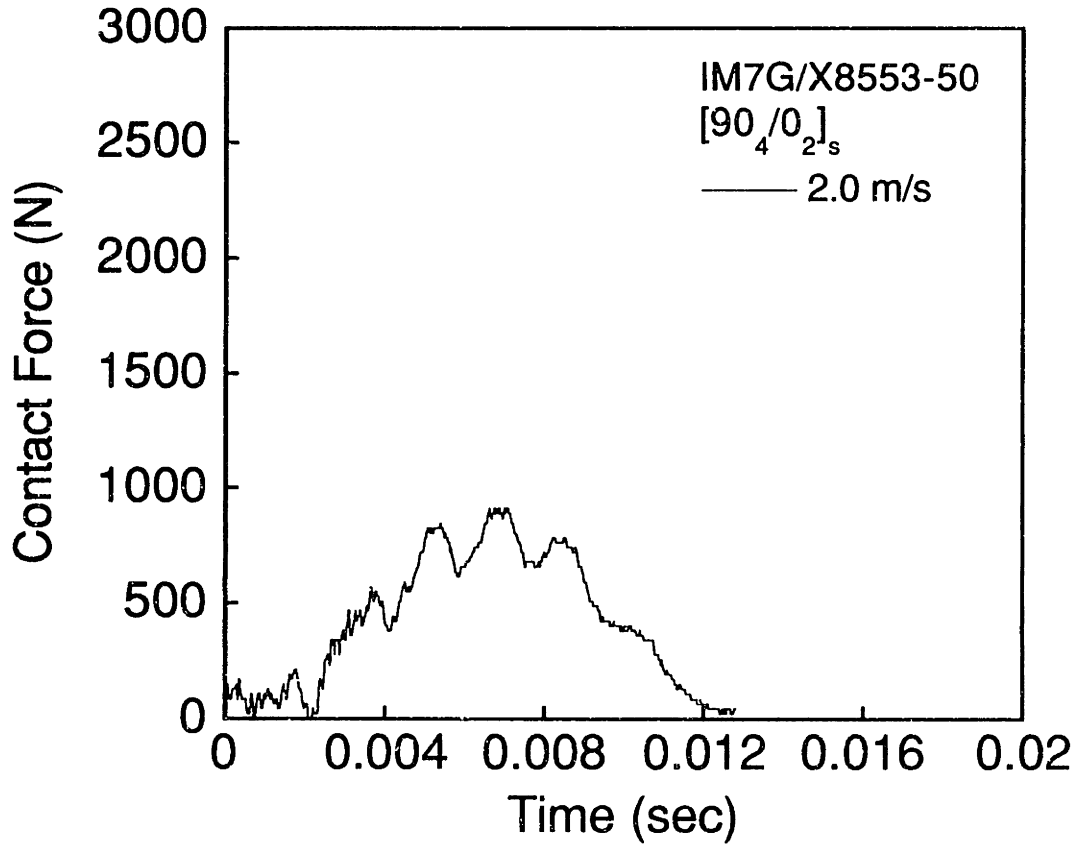


Figure A.96 (upper) Force versus time and (lower) X-ray photograph for IM7G/X8553-50 $[90_4/0_2]_s$ specimen impacted at 1.5 m/s.



1 cm

Figure A.97 (upper) Force versus time and (lower) X-ray photograph for IM7G/X8553-50 $[90_4/0_2]_s$ specimen impacted at 2.0 m/s.

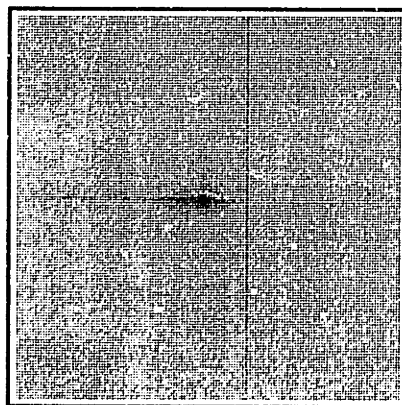
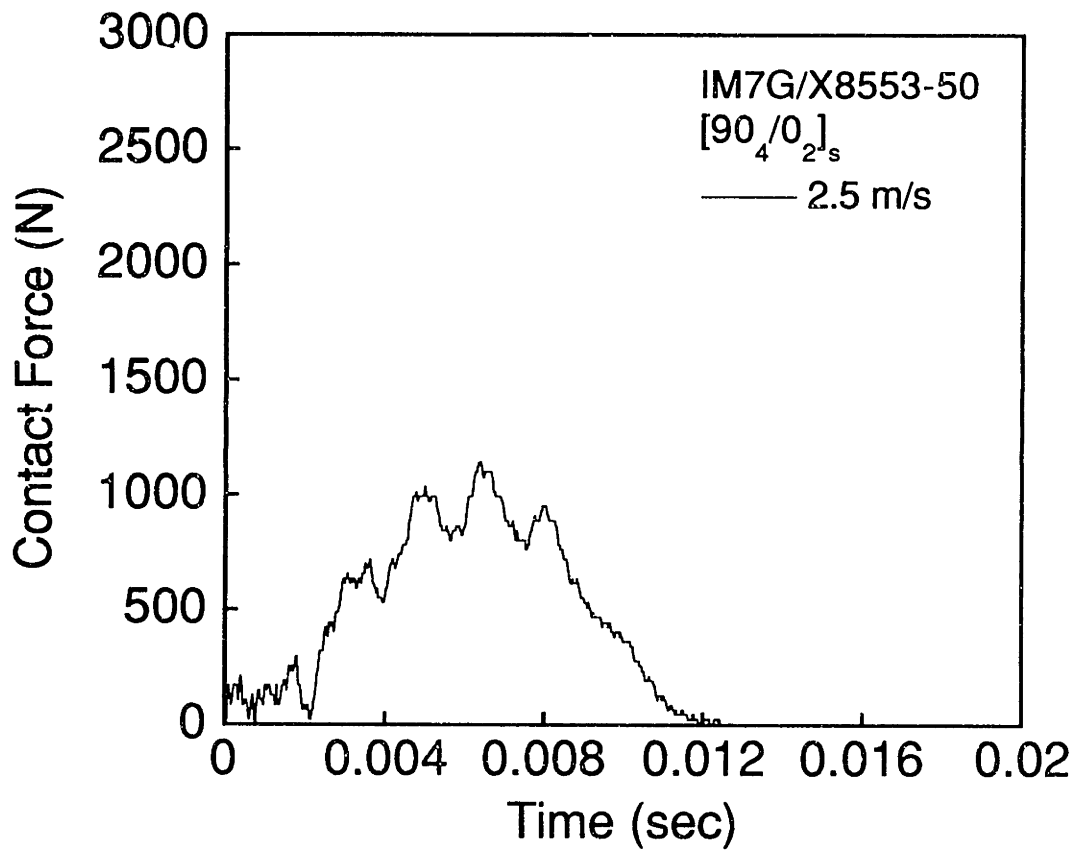


Figure A.98 (upper) Force versus time and (lower) X-ray photograph for IM7G/X8553-50 [90₄/0₂]_s specimen impacted at 2.5 m/s.

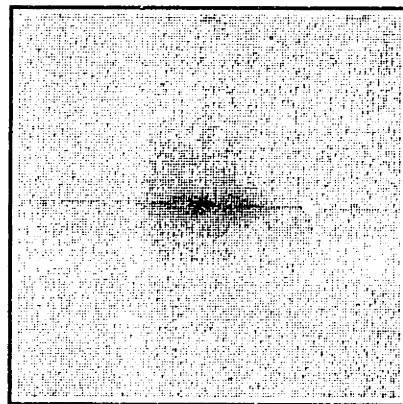
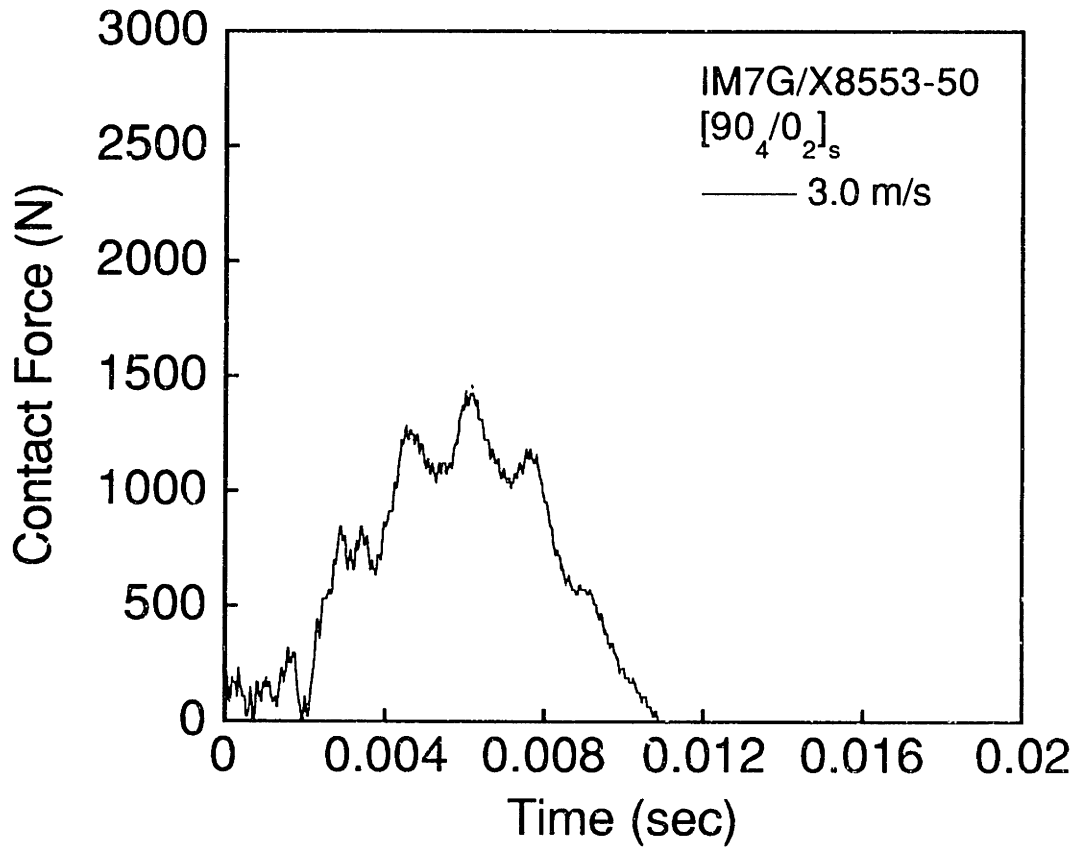
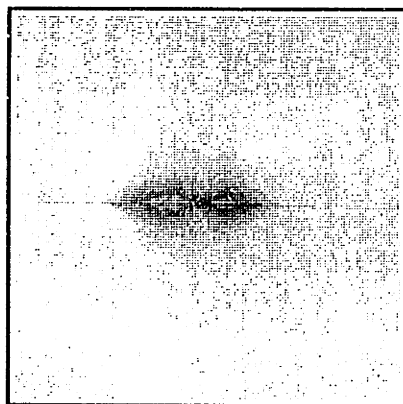
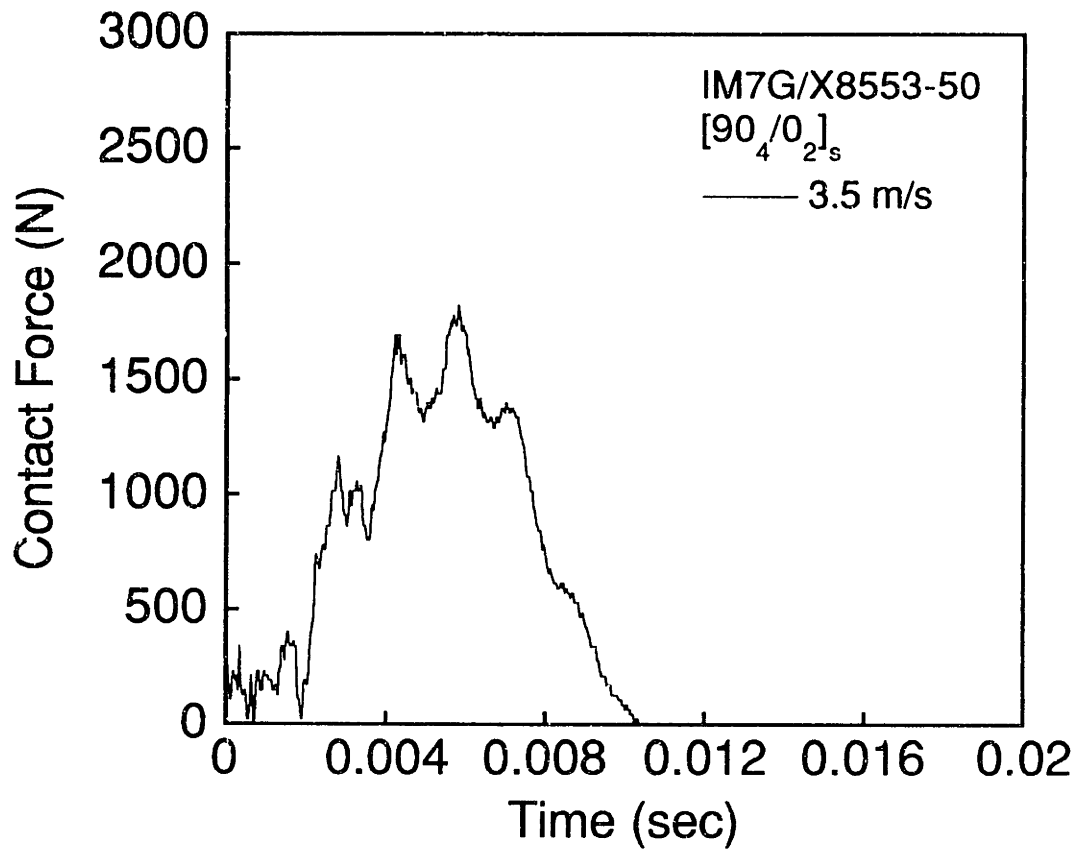
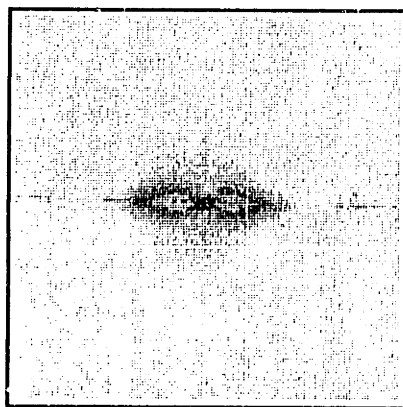
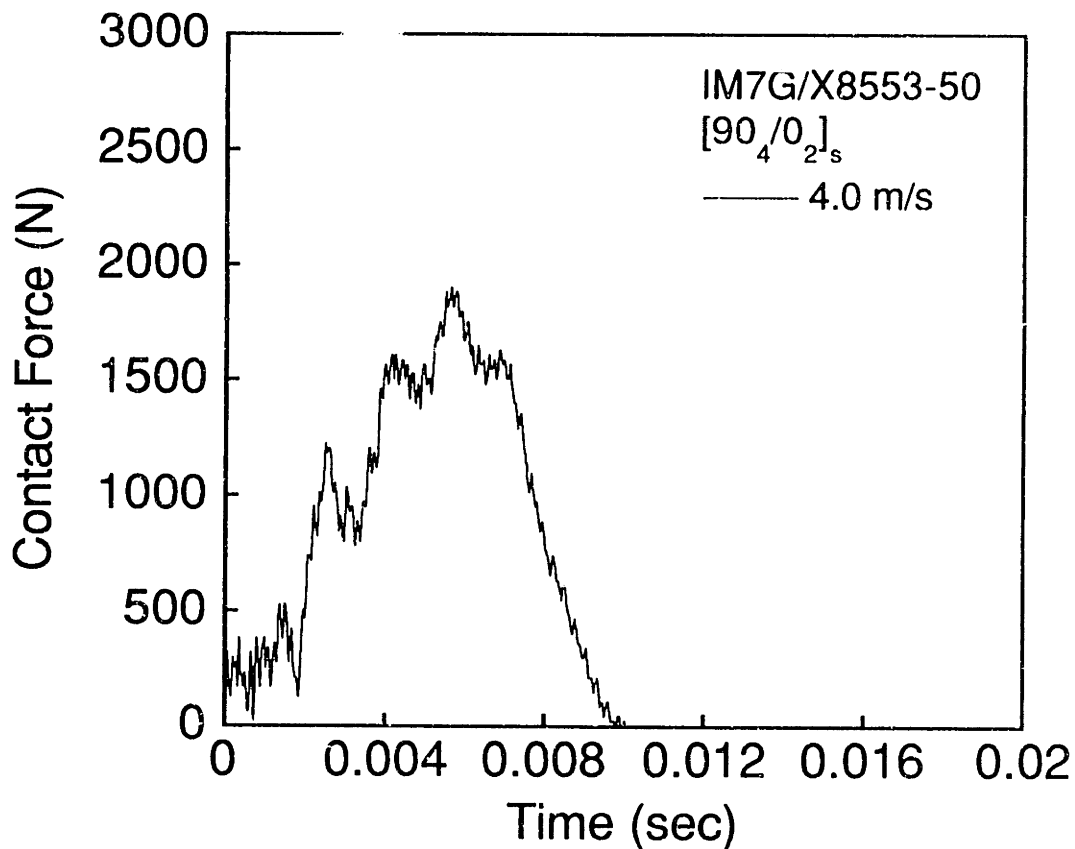


Figure A.99 (upper) Force versus time and (lower) X-ray photograph for IM7G/X8553-50 [90₄/0₂]_s specimen impacted at 3.0 m/s.



1 cm

Figure A.100 (upper) Force versus time and (lower) X-ray photograph for IM7G/X8553-50 [90₄/0₂]_s specimen impacted at 3.5 m/s.



1 cm

Figure A.101 (upper) Force versus time and (lower) X-ray photograph for IM7G/X8553-50 [90₄/0₂]_s specimen impacted at 4.0 m/s.

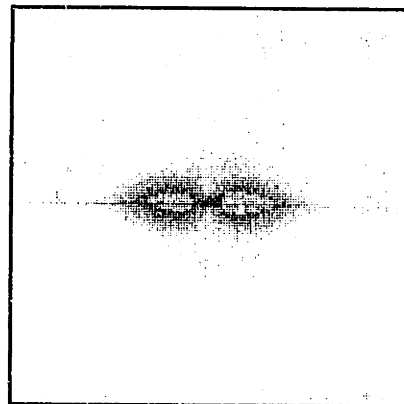
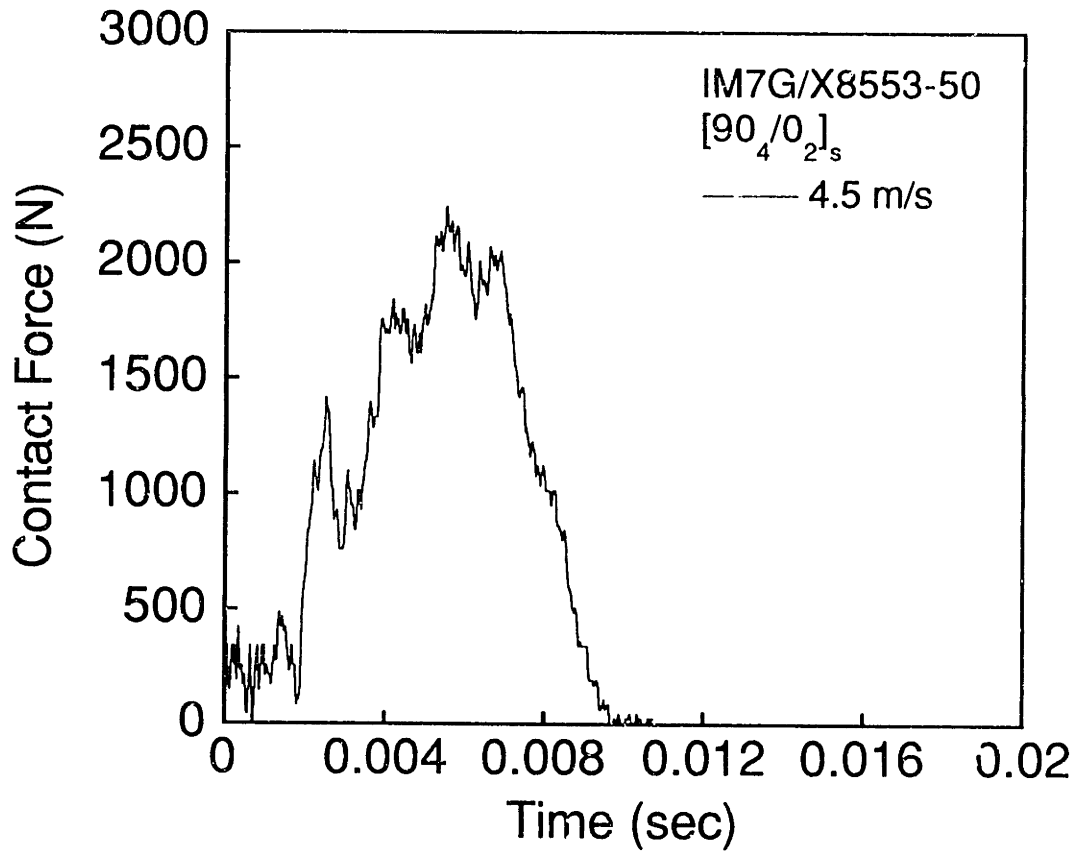
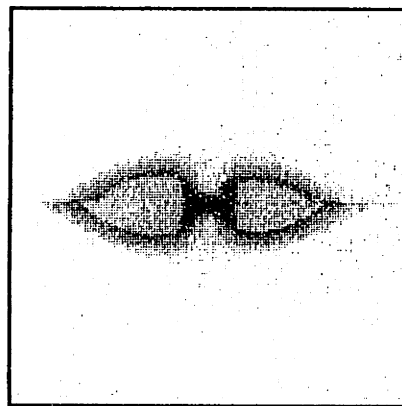
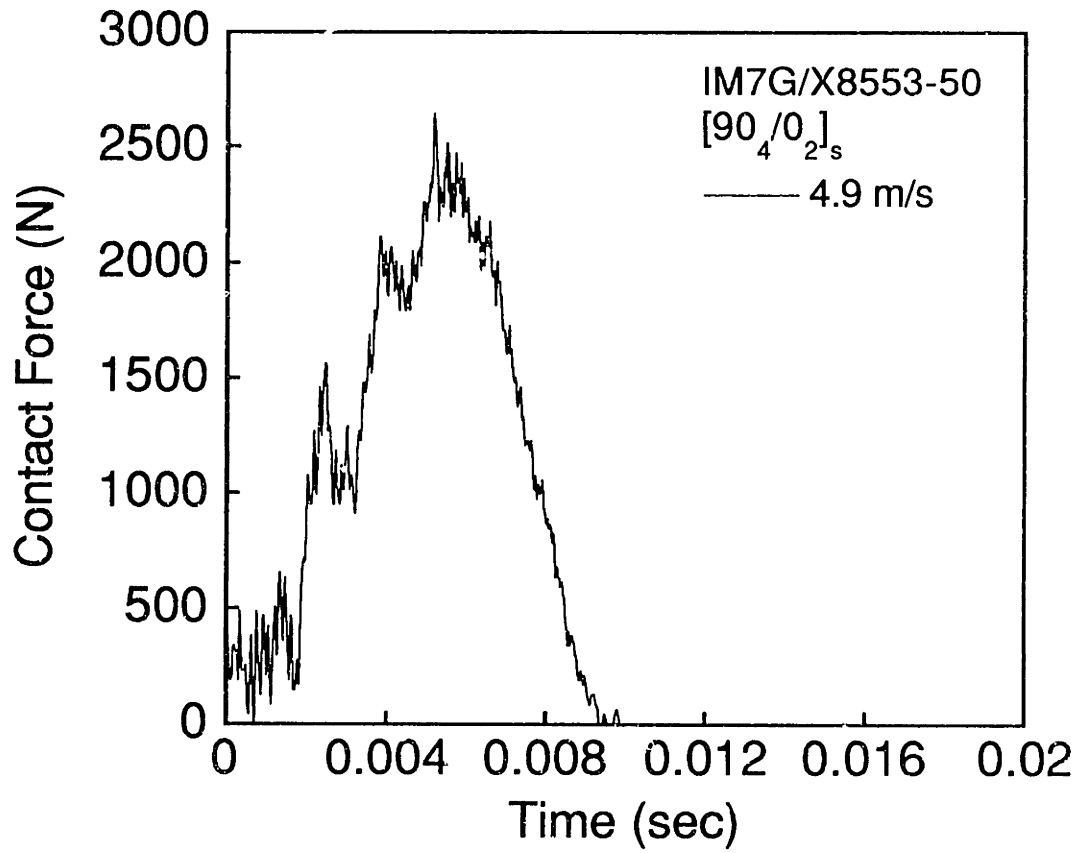


Figure A.102 (upper) Force versus time and (lower) X-ray photograph for IM7G/X8553-50 [90₄/0₂]_s specimen impacted at 4.5 m/s.



1 cm

Figure A.103 (upper) Force versus time and (lower) X-ray photograph for IM7G/X8553-50 [90₄/0₂]_s specimen impacted at 4.9 m/s.

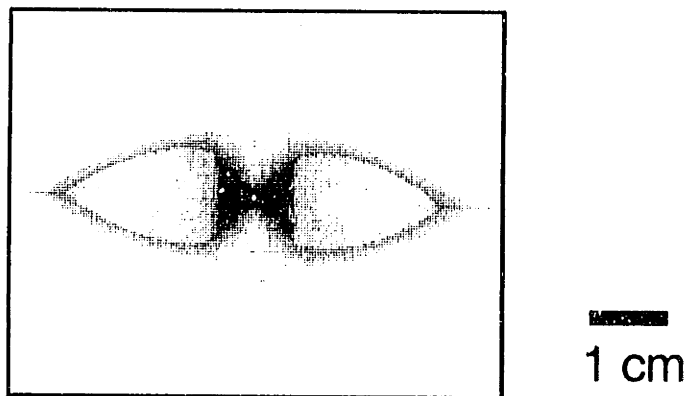
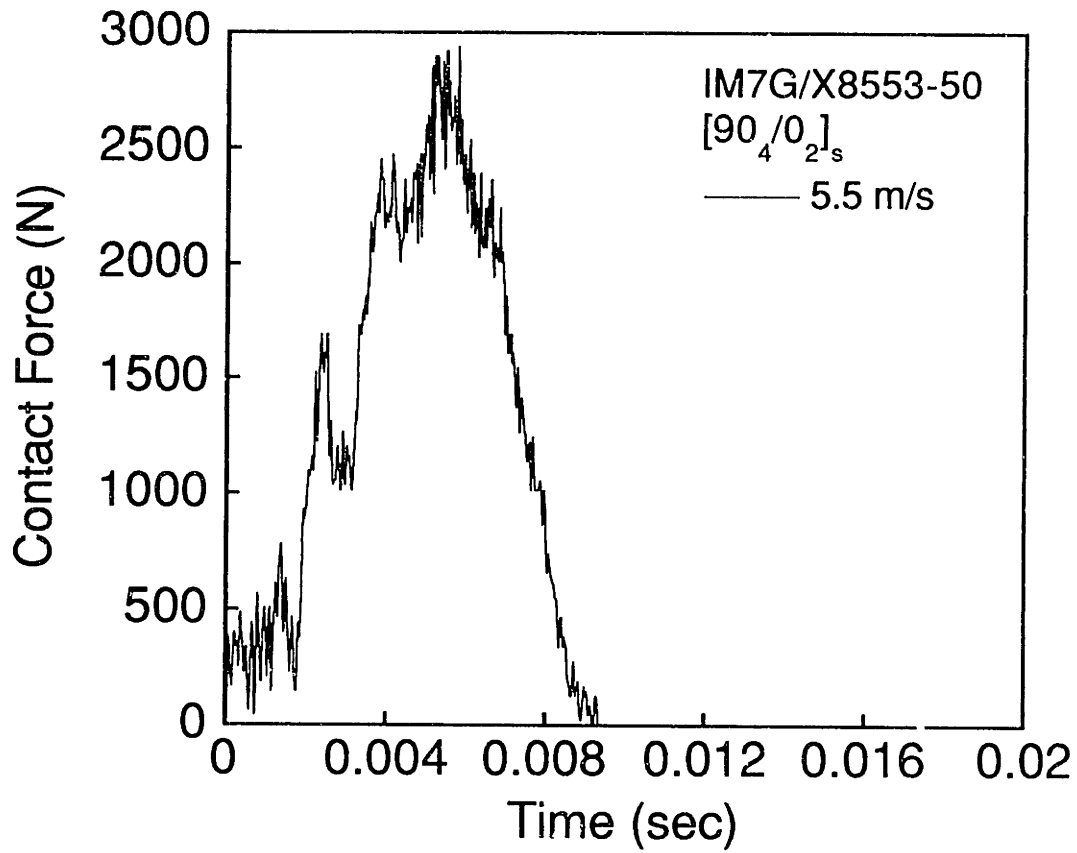
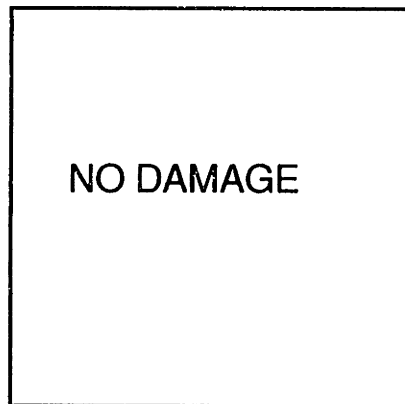
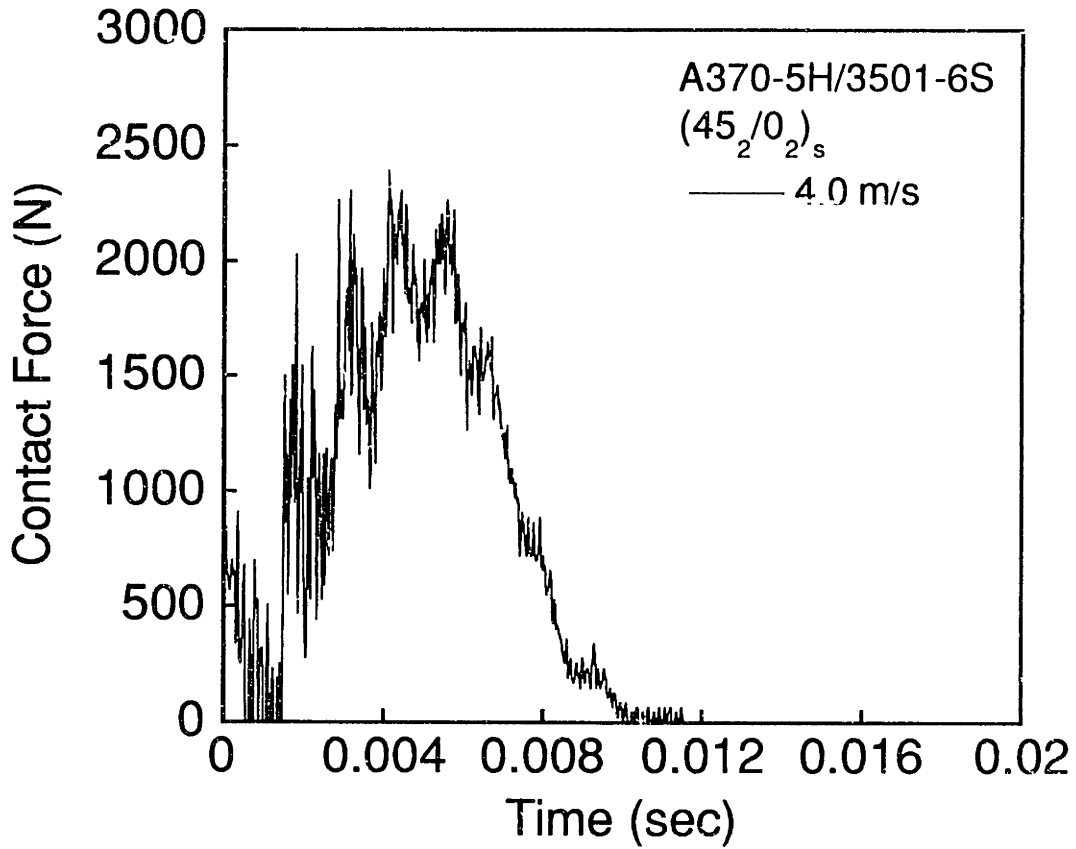


Figure A.104 (upper) Force versus time and (lower) X-ray photograph for IM7G/X8553-50 [90₄/0₂]_s specimen impacted at 5.5 m/s.



1 cm

Figure A.105 (upper) Force versus time and (lower) X-ray photograph for A370-5H/3501-6S (45₂/0₂)_s specimen impacted at 4.0 m/s.

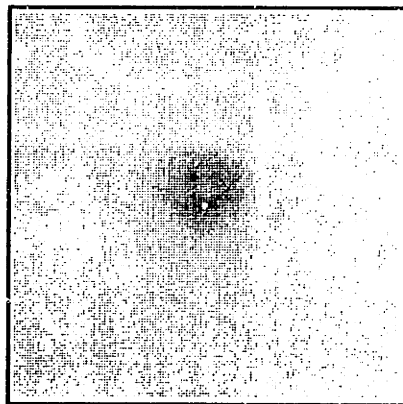
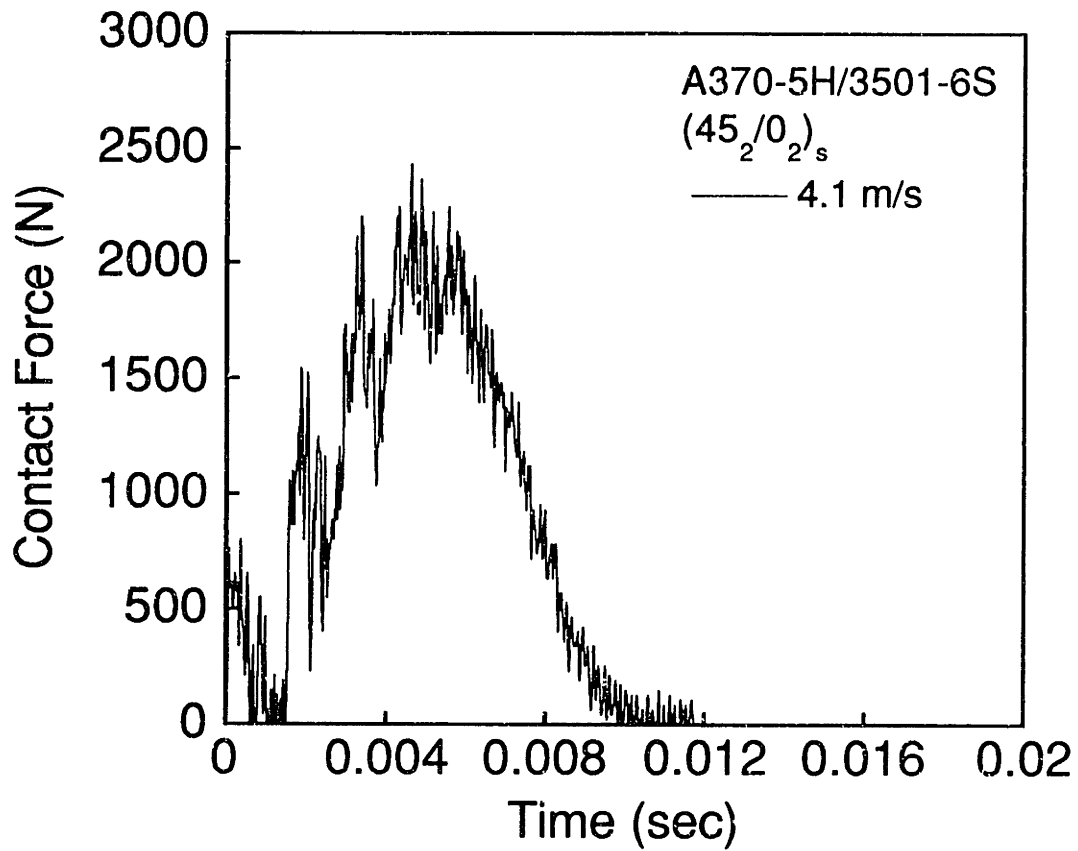


Figure A.106 (upper) Force versus time and (lower) X-ray photograph for A370-5H/3501-6S (45₂/0₂)_s specimen impacted at 4.1 m/s.

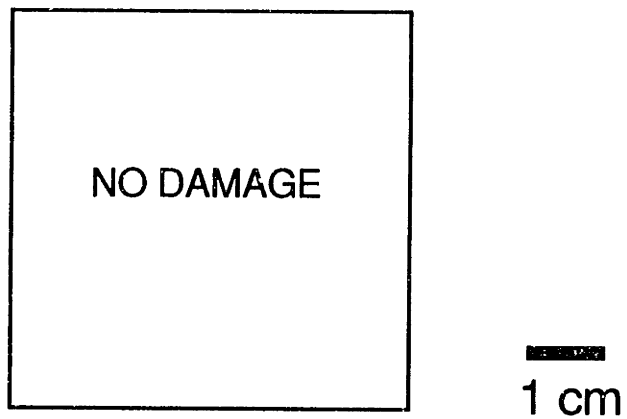
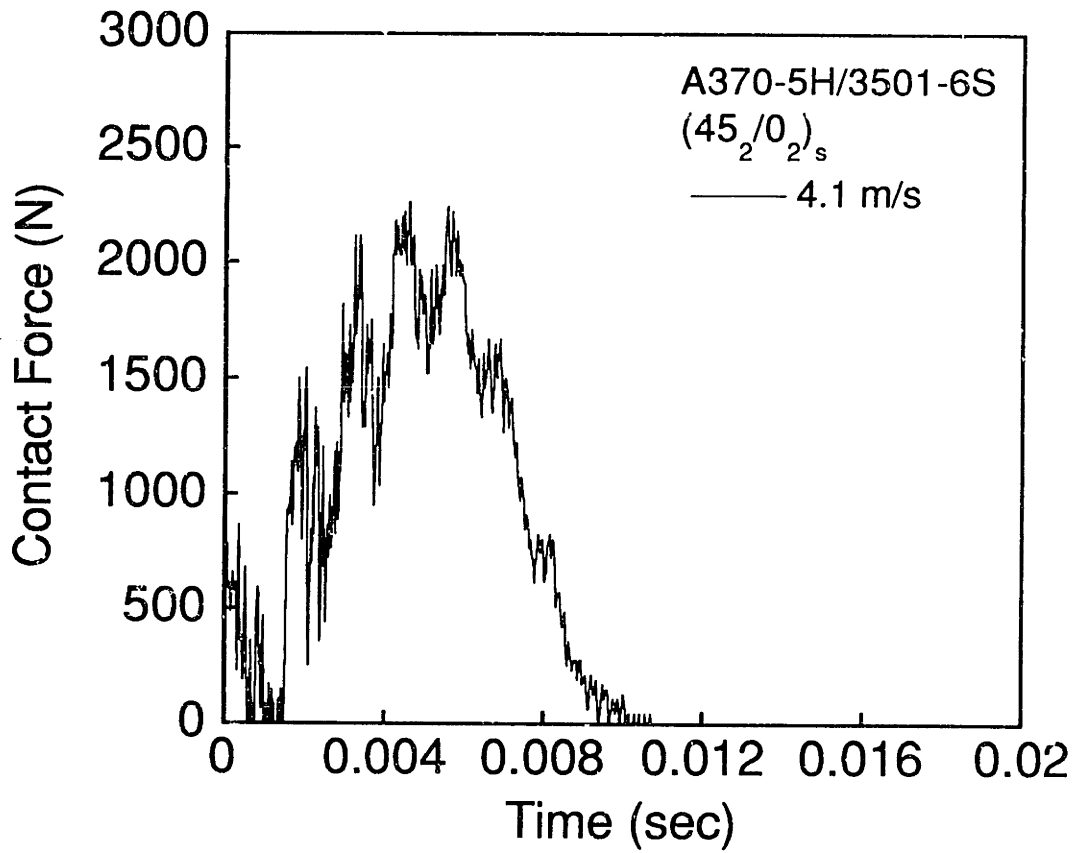
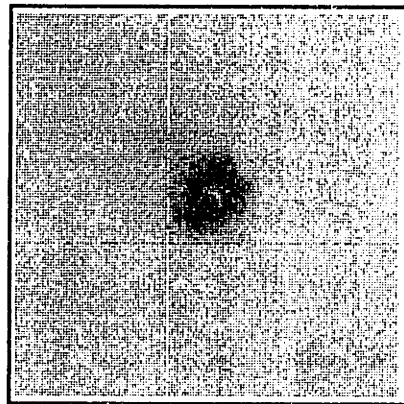
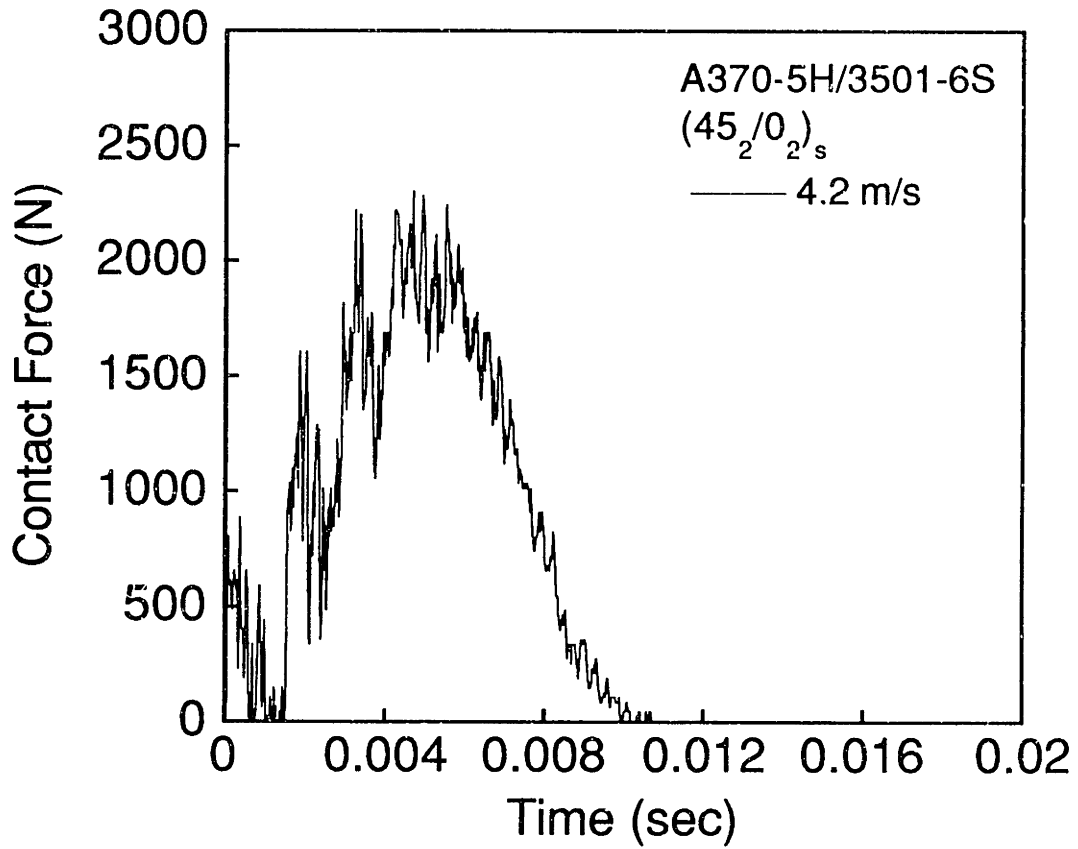
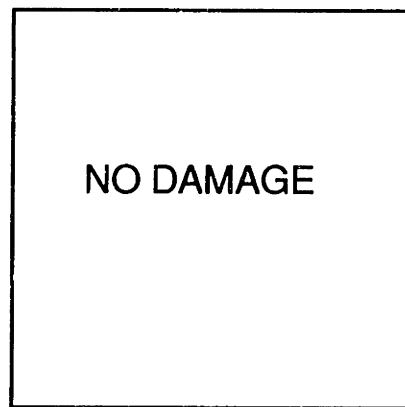
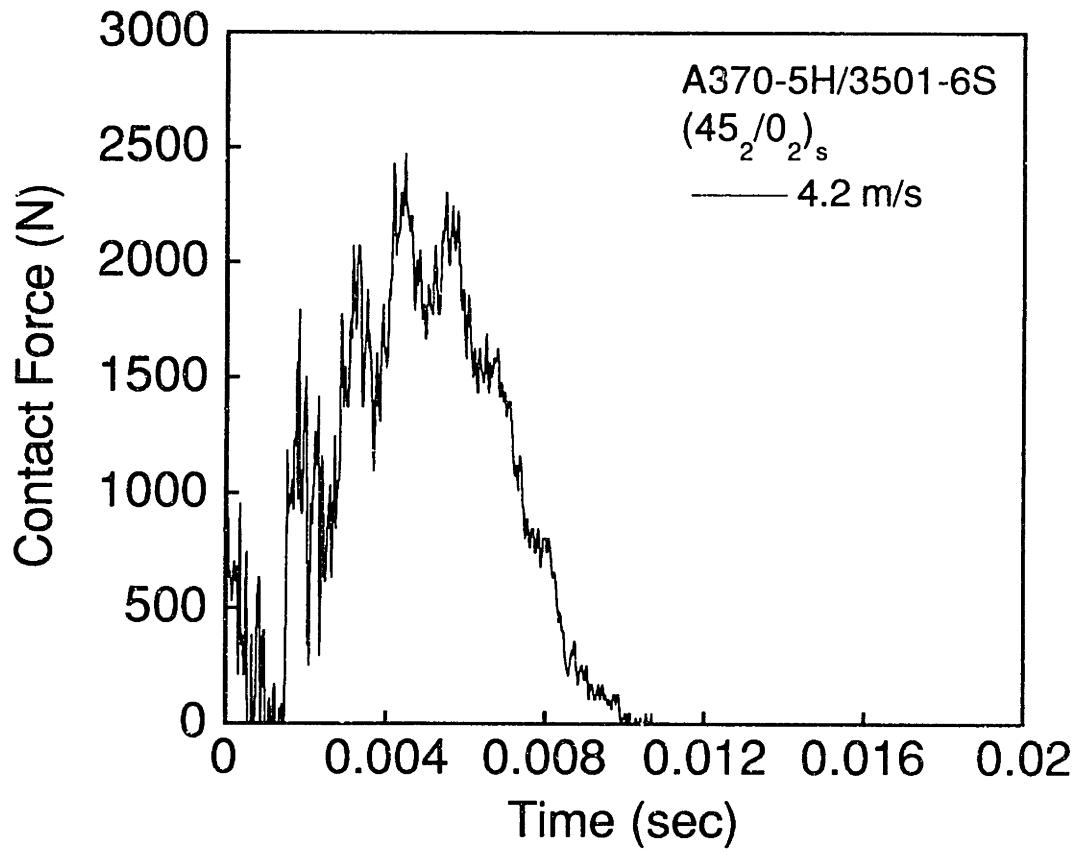


Figure A.107 (upper) Force versus time and (lower) X-ray photograph for A370-5H/3501-6S (45₂/0₂)_s specimen impacted at 4.1 m/s.



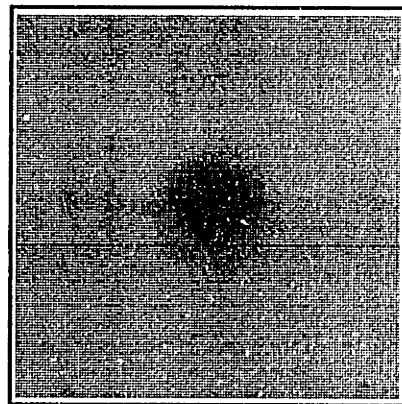
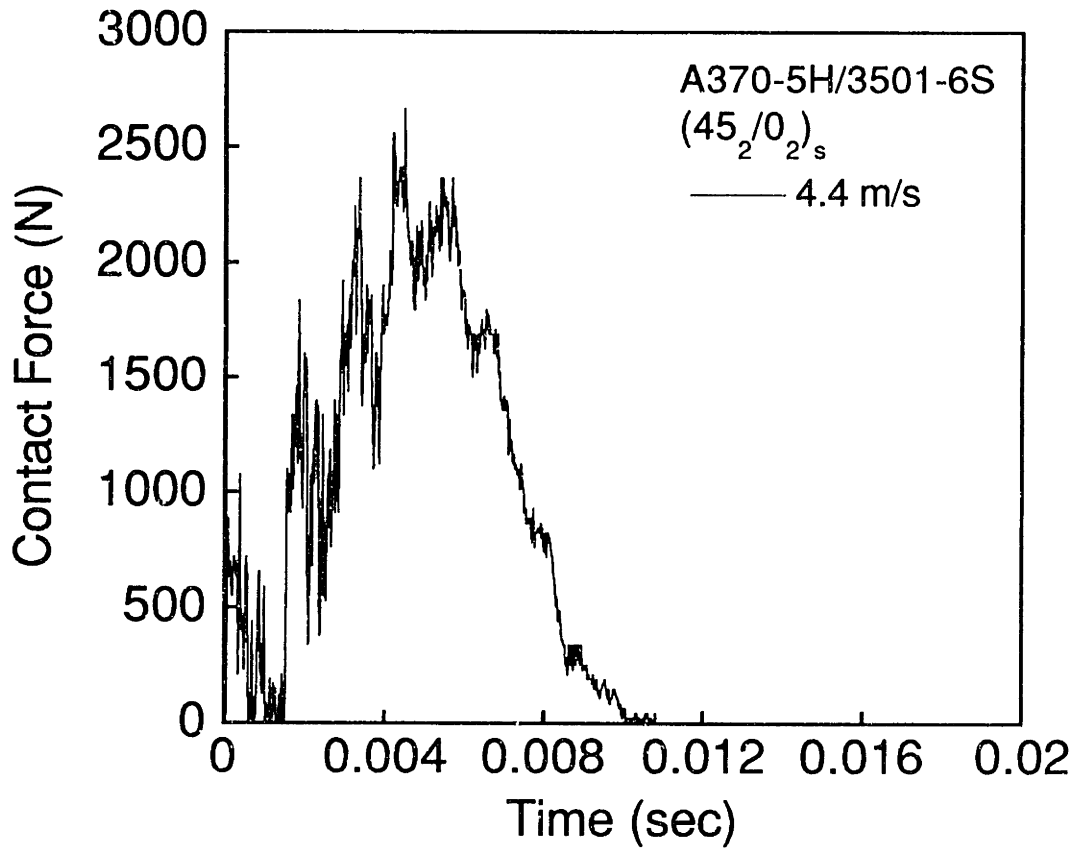
1 cm

Figure A.108 (upper) Force versus time and (lower) X-ray photograph for A370-5H/3501-6S (45₂/0₂)_s specimen impacted at 4.2 m/s.



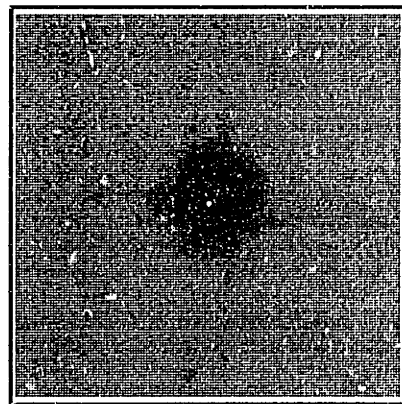
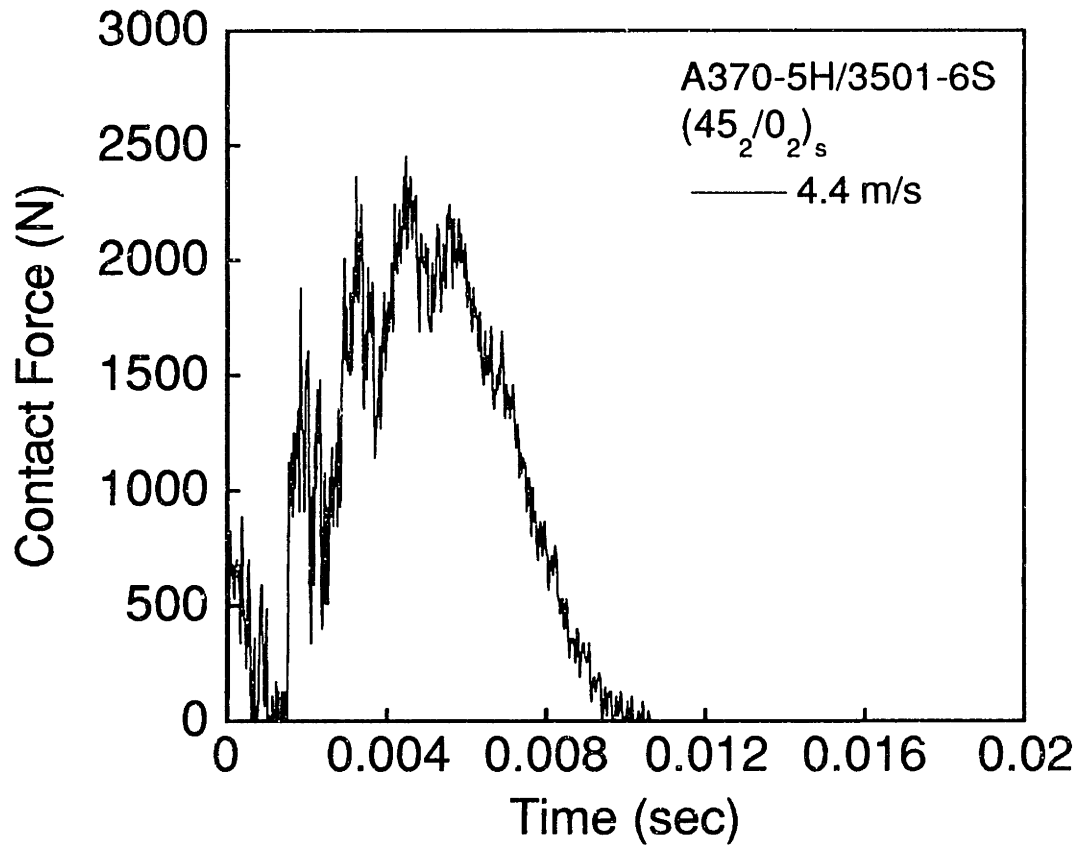
1 cm

Figure A.109 (upper) Force versus time and (lower) X-ray photograph for A370-5H/3501-6S (45₂/0₂)_s specimen impacted at 4.2 m/s.



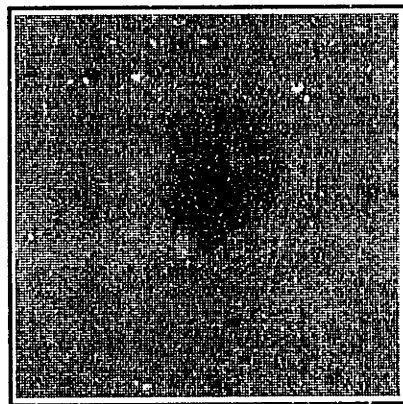
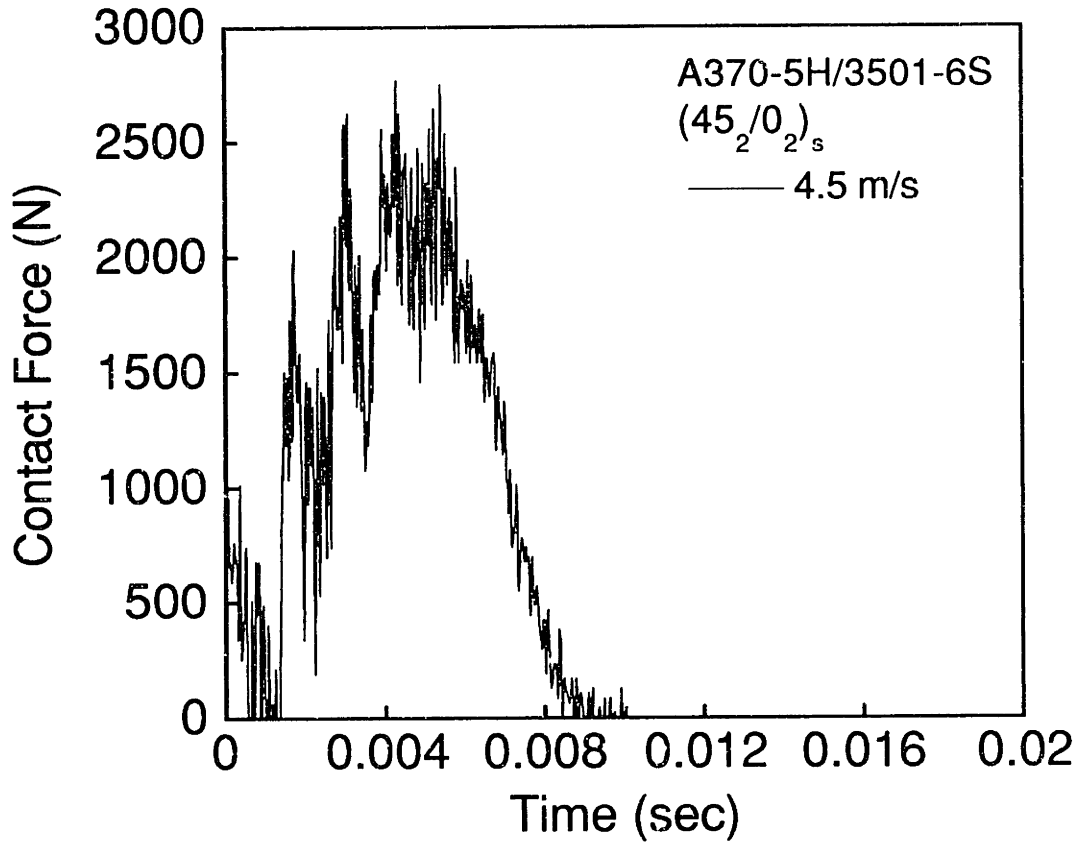
1 cm

Figure A.110 (upper) Force versus time and (lower) X-ray photograph for A370-5H/3501-6S (45₂/0₂)_s specimen impacted at 4.4 m/s.



1 cm

Figure A.111 (upper) Force versus time and (lower) X-ray photograph for A370-5H/3501-6S (45₂/0₂)_s specimen impacted at 4.4 m/s.



1 cm

Figure A.112 (upper) Force versus time and (lower) X-ray photograph for A370-5H/3501-6S (45₂/0₂)_s specimen impacted at 4.5 m/s.

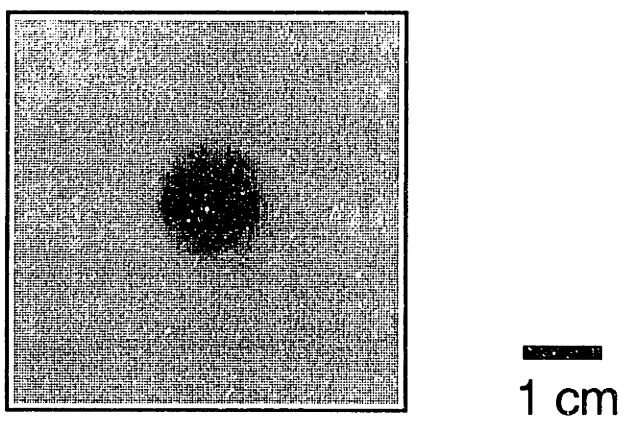
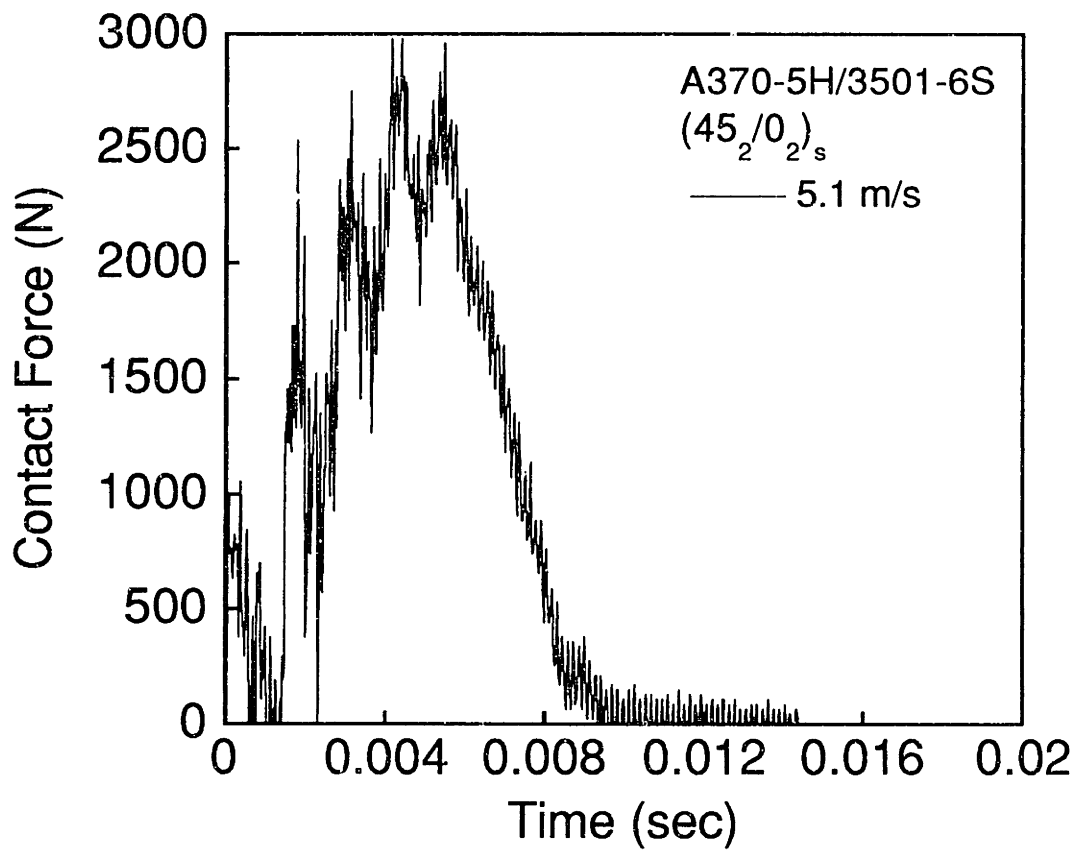


Figure A.113 (upper) Force versus time and (lower) X-ray photograph for A370-5H/3501-6S (45₂/0₂)_s specimen impacted at 5.1 m/s.

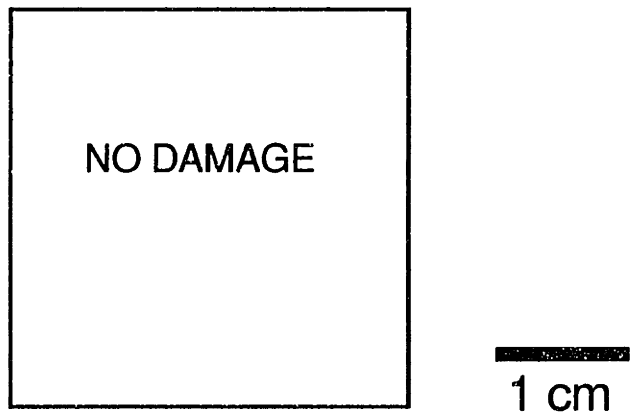
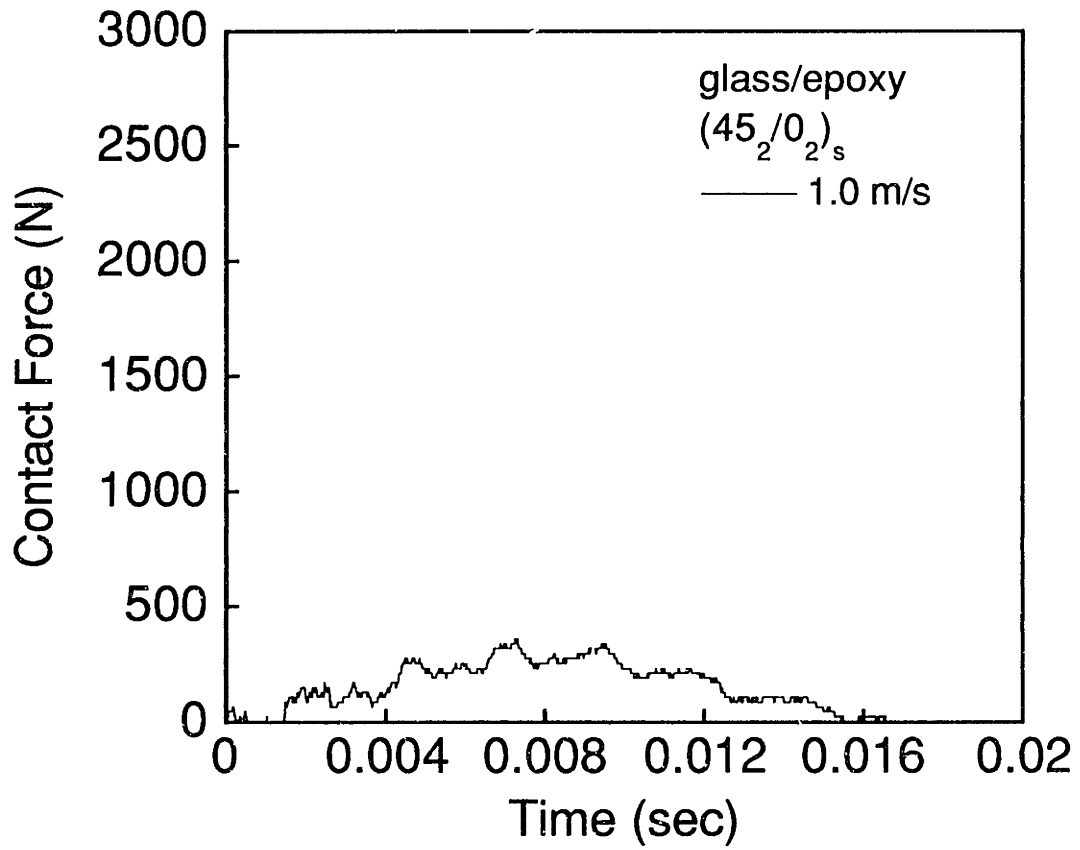


Figure A.114 (upper) Force versus time and (lower) photograph for glass/epoxy (45₂/0₂)_s specimen impacted at 1.0 m/s.

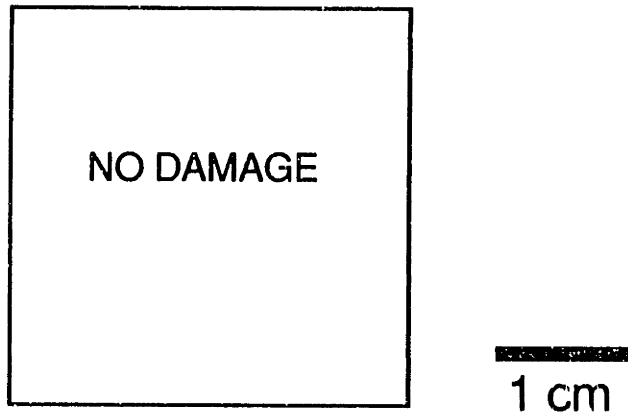
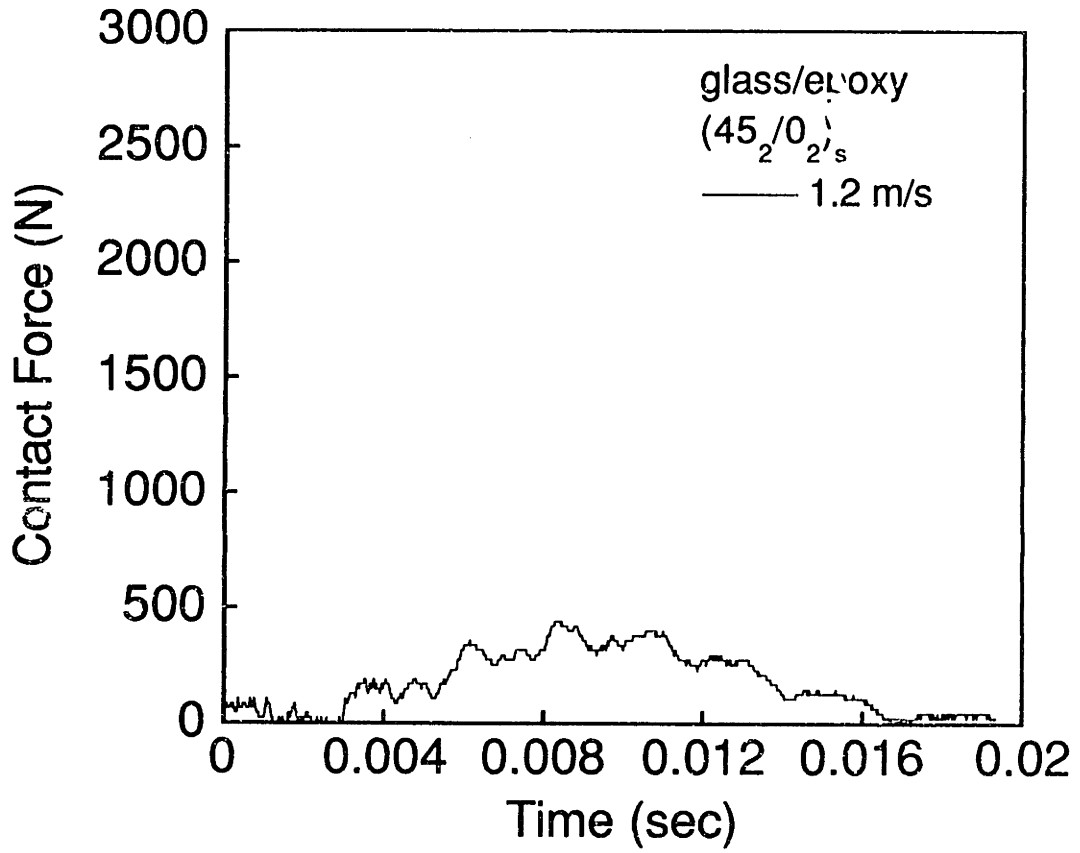


Figure A.115 (upper) Force versus time and (lower) photograph for glass/epoxy (45₂/0₂)_s specimen impacted at 1.2 m/s.

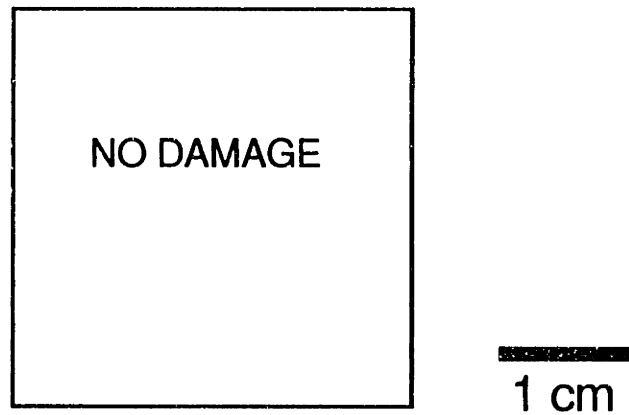
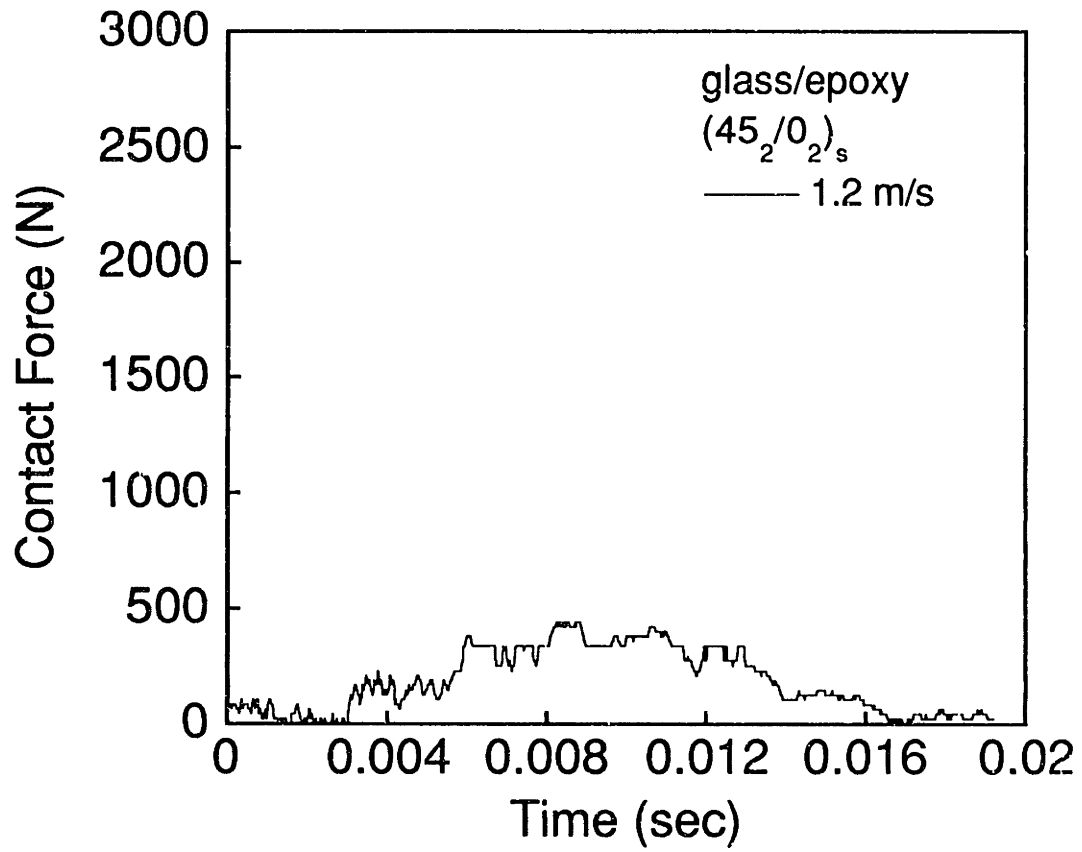


Figure A.116 (upper) Force versus time and (lower) photograph for glass/epoxy (45₂/0₂)_s specimen impacted at 1.2 m/s.

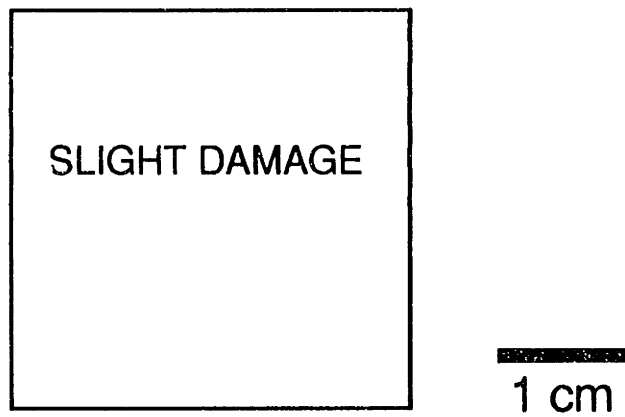
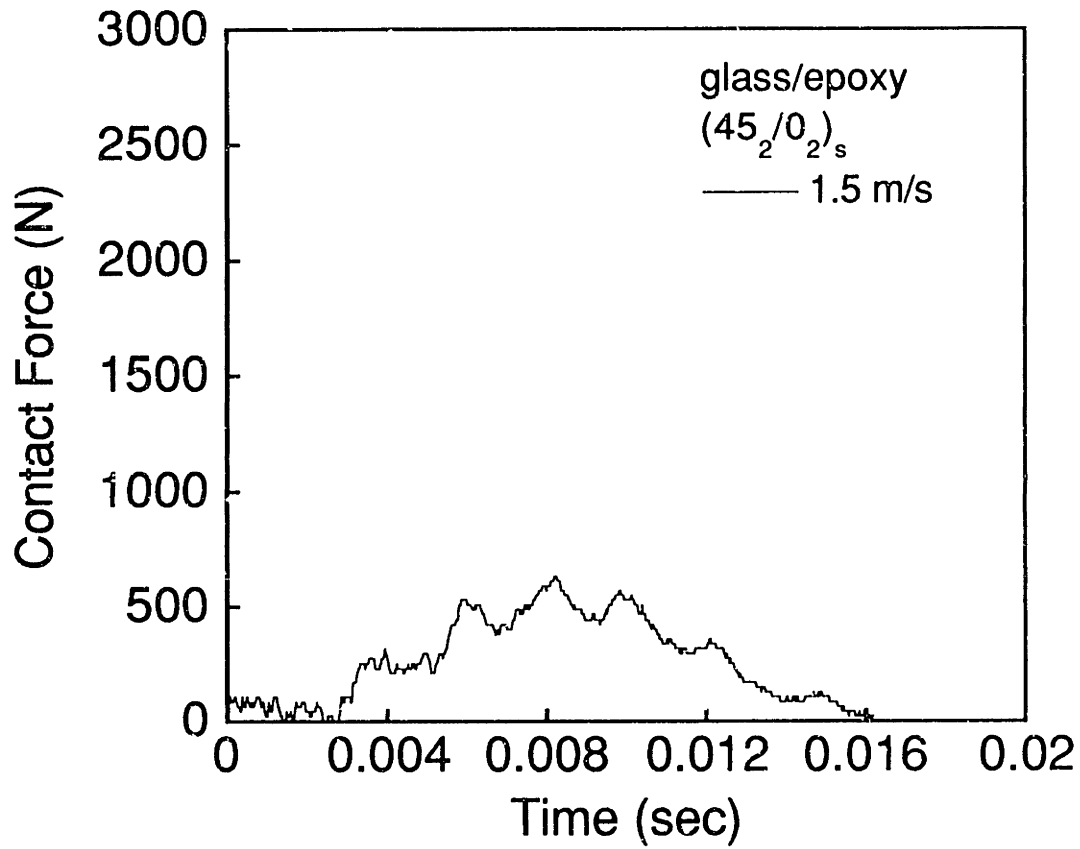


Figure A.117 (upper) Force versus time and (lower) photograph for glass/epoxy (45₂/0₂)_s specimen impacted at 1.5 m/s.

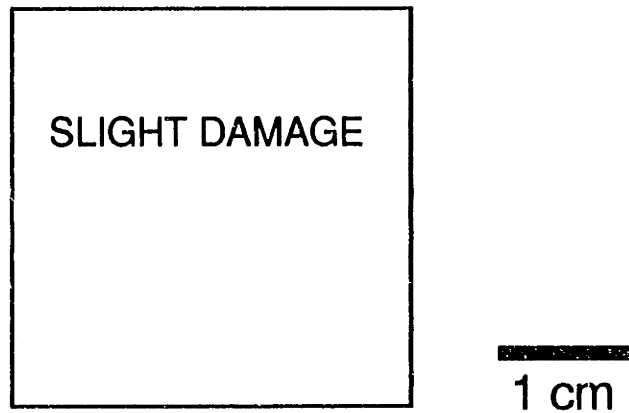
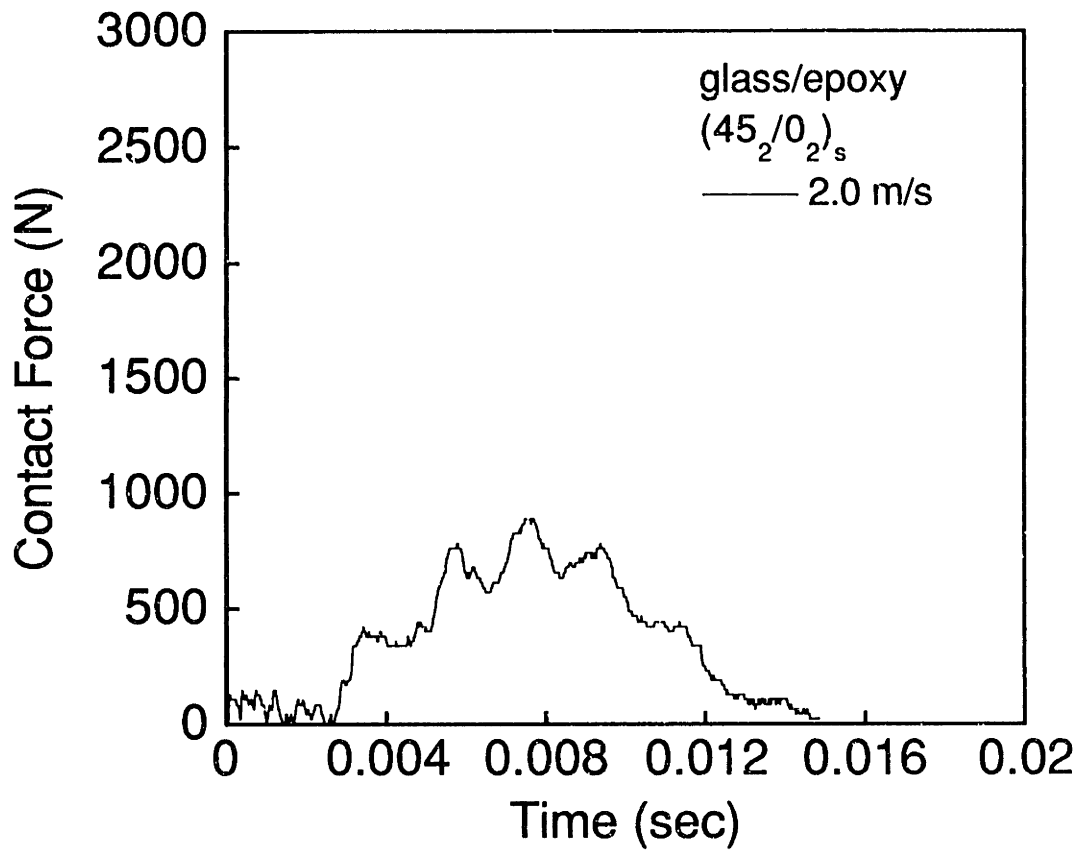


Figure A.118 (upper) Force versus time and (lower) photograph for glass/epoxy (45₂/0₂)_s specimen impacted at 2.0 m/s.

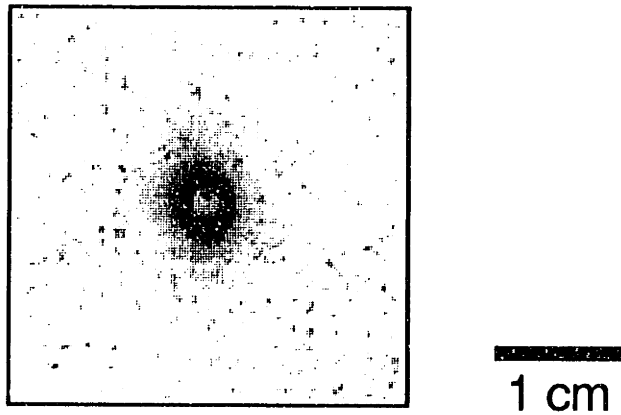
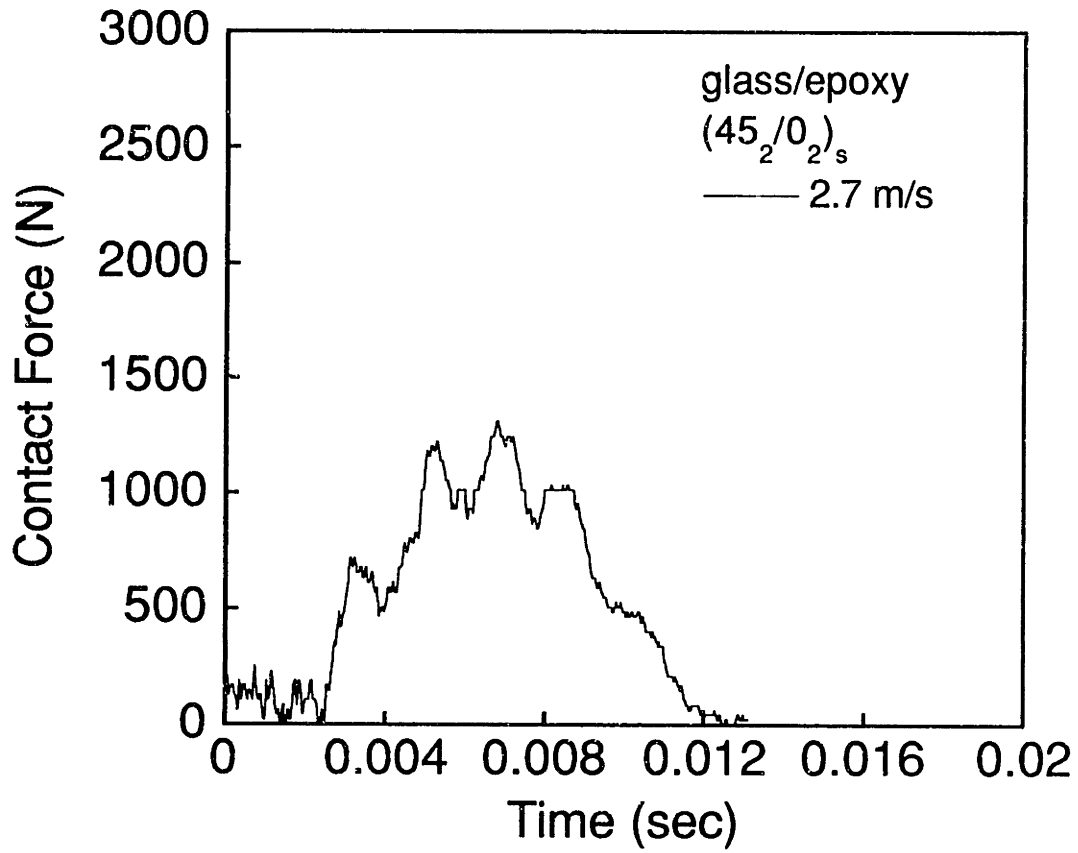


Figure A.119 (upper) Force versus time and (lower) photograph for glass/epoxy (45₂/0₂)_s specimen impacted at 2.7 m/s.

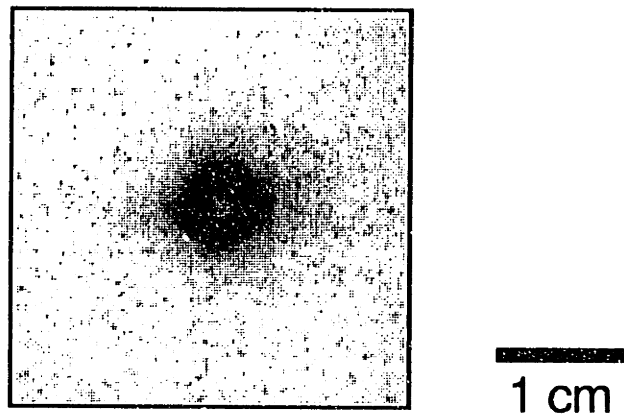
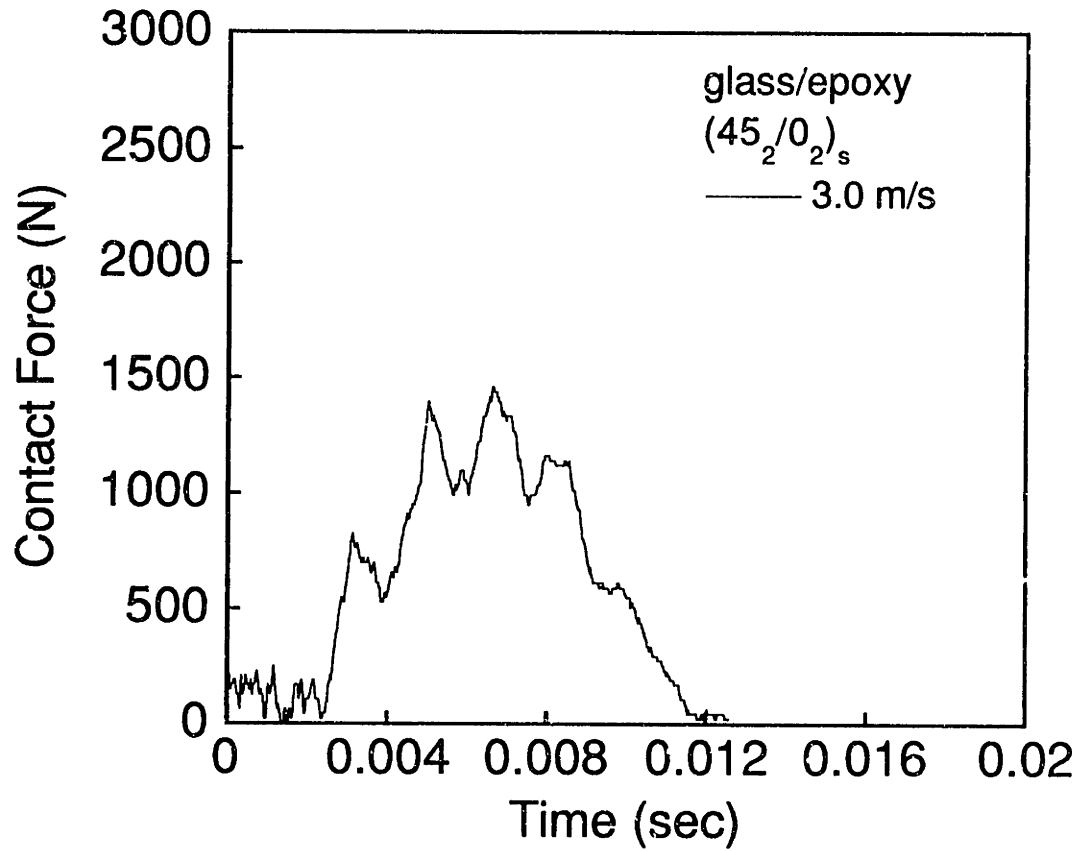


Figure A.120 (upper) Force versus time and (lower) photograph for glass/epoxy (45₂/0₂)_s specimen impacted at 3.0 m/s.

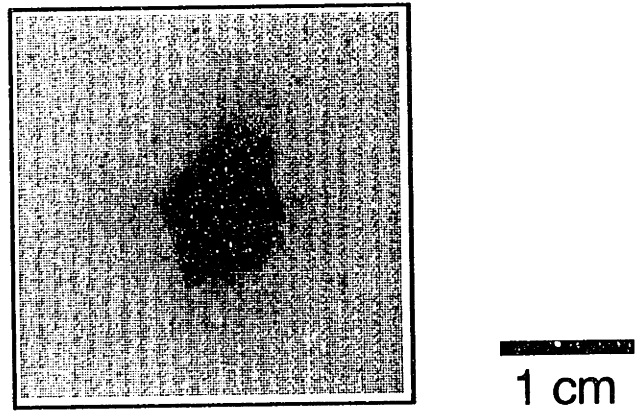
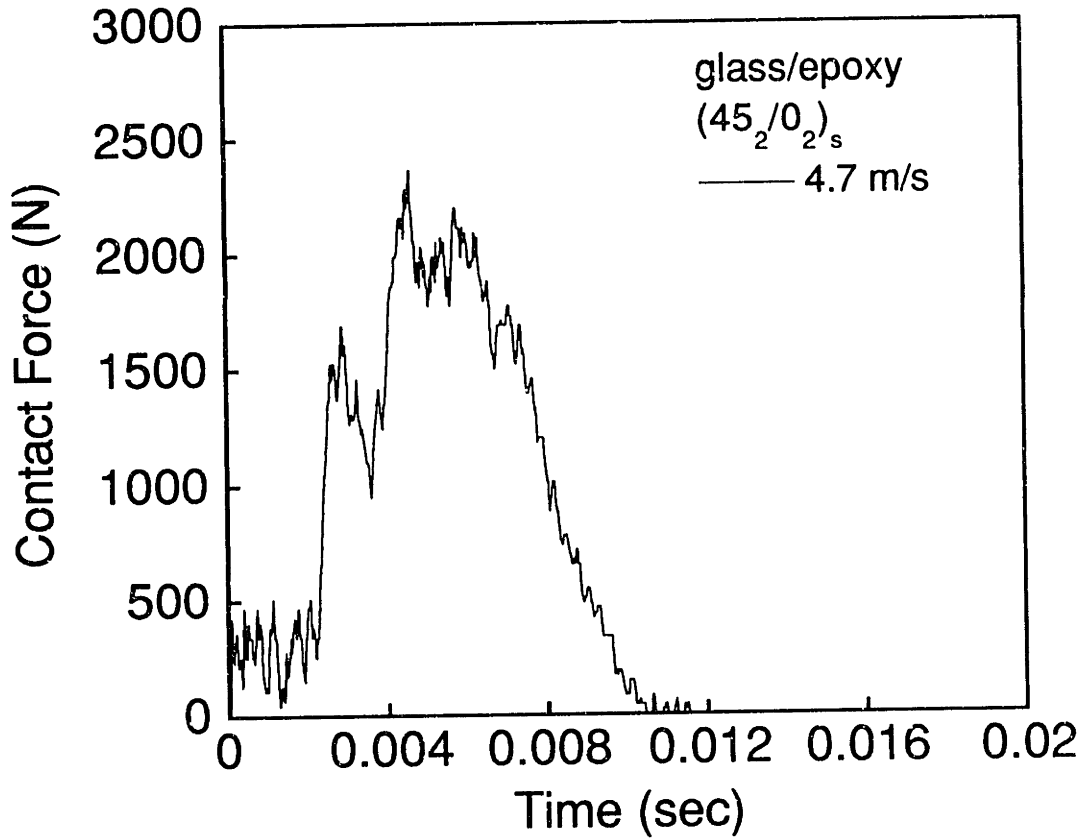


Figure A.121 (upper) Force versus time and (lower) photograph for glass/epoxy (45₂/0₂)_s specimen impacted at 4.7 m/s.

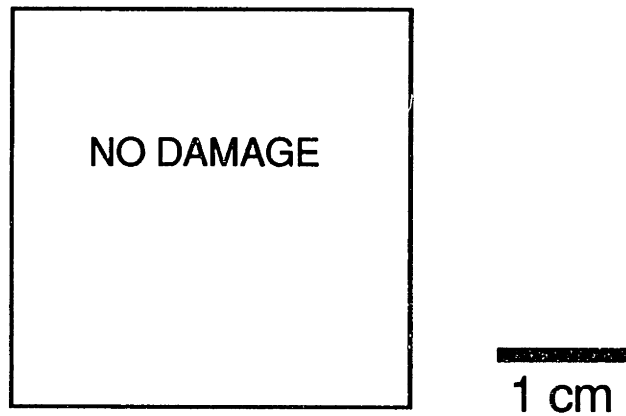
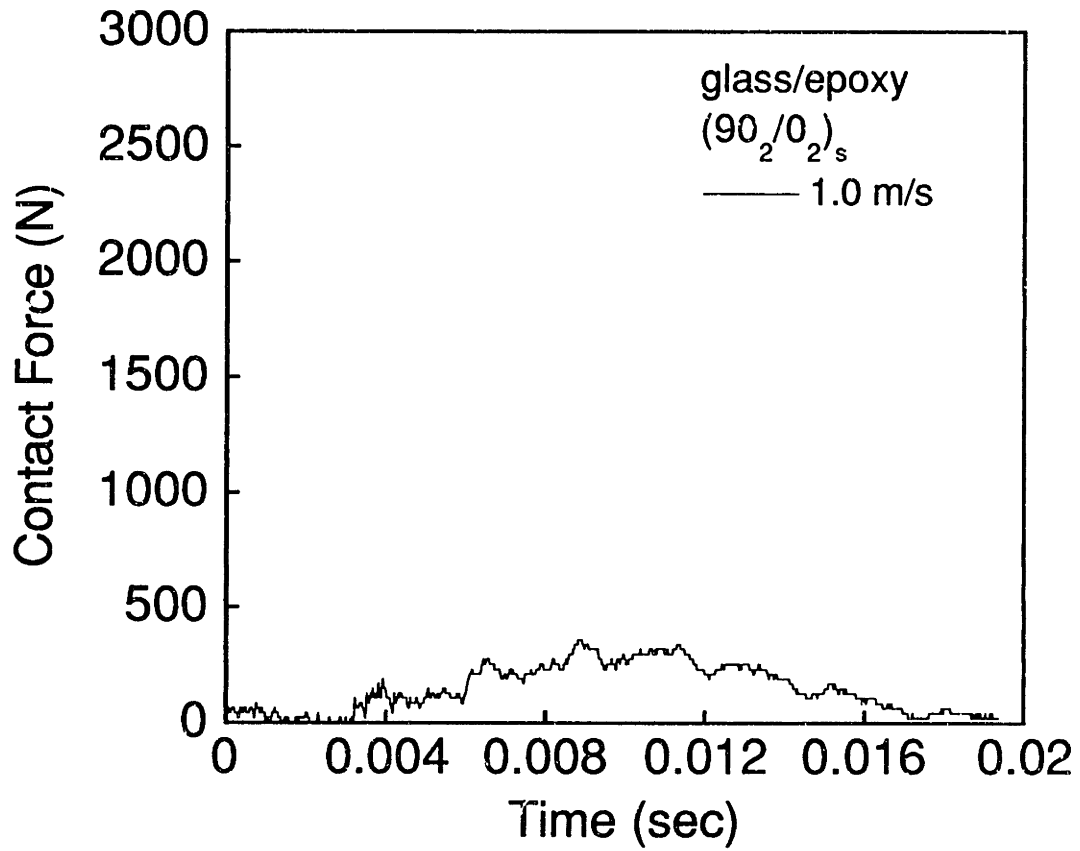


Figure A.122 (upper) Force versus time and (lower) photograph for glass/epoxy (90₂/0₂)_s specimen impacted at 1.0 m/s.

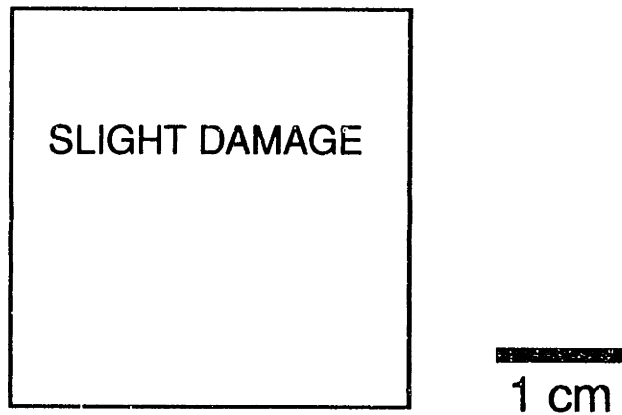
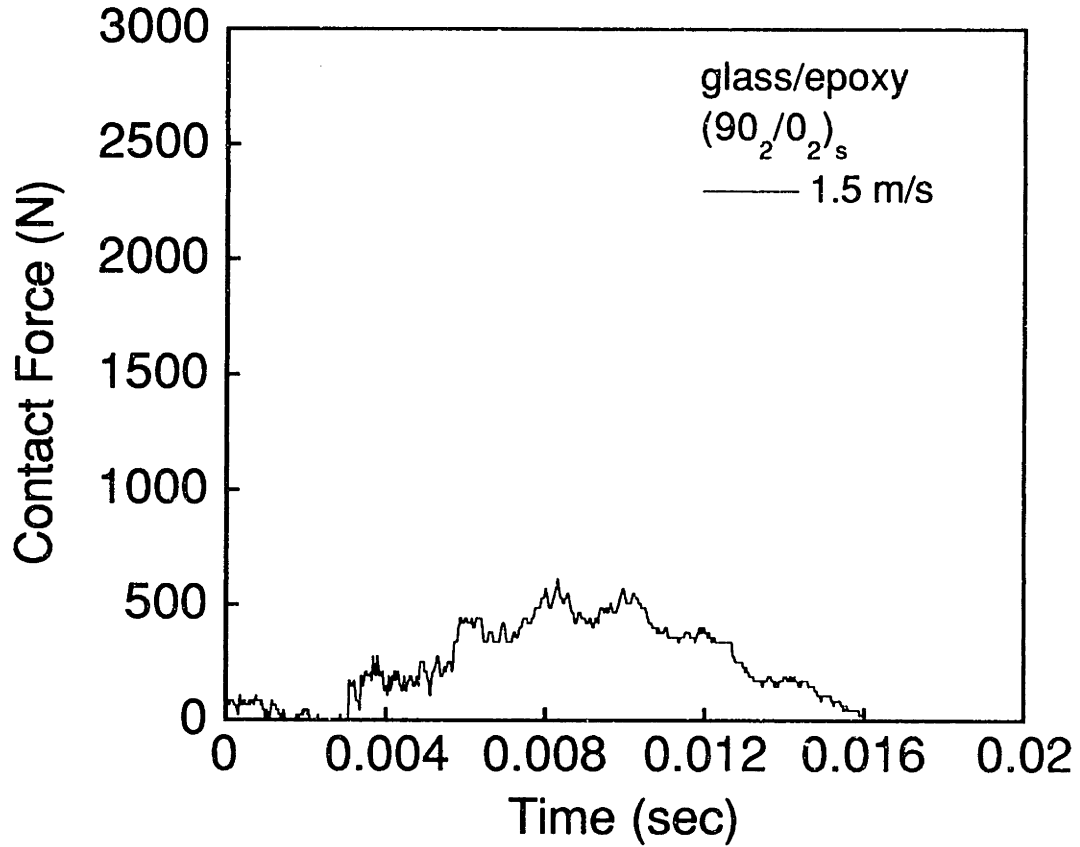


Figure A.123 (upper) Force versus time and (lower) photograph for glass/epoxy (90₂/0₂)_s specimen impacted at 1.5 m/s.

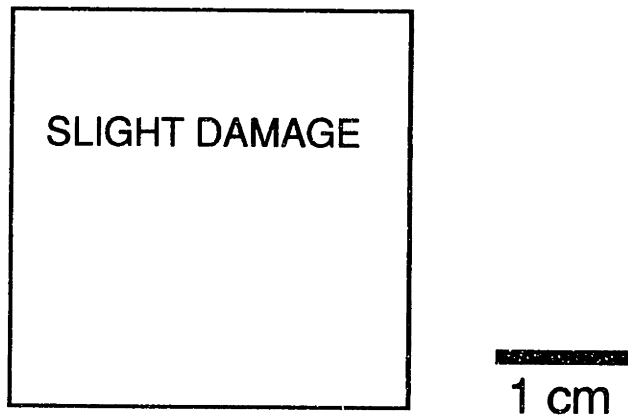
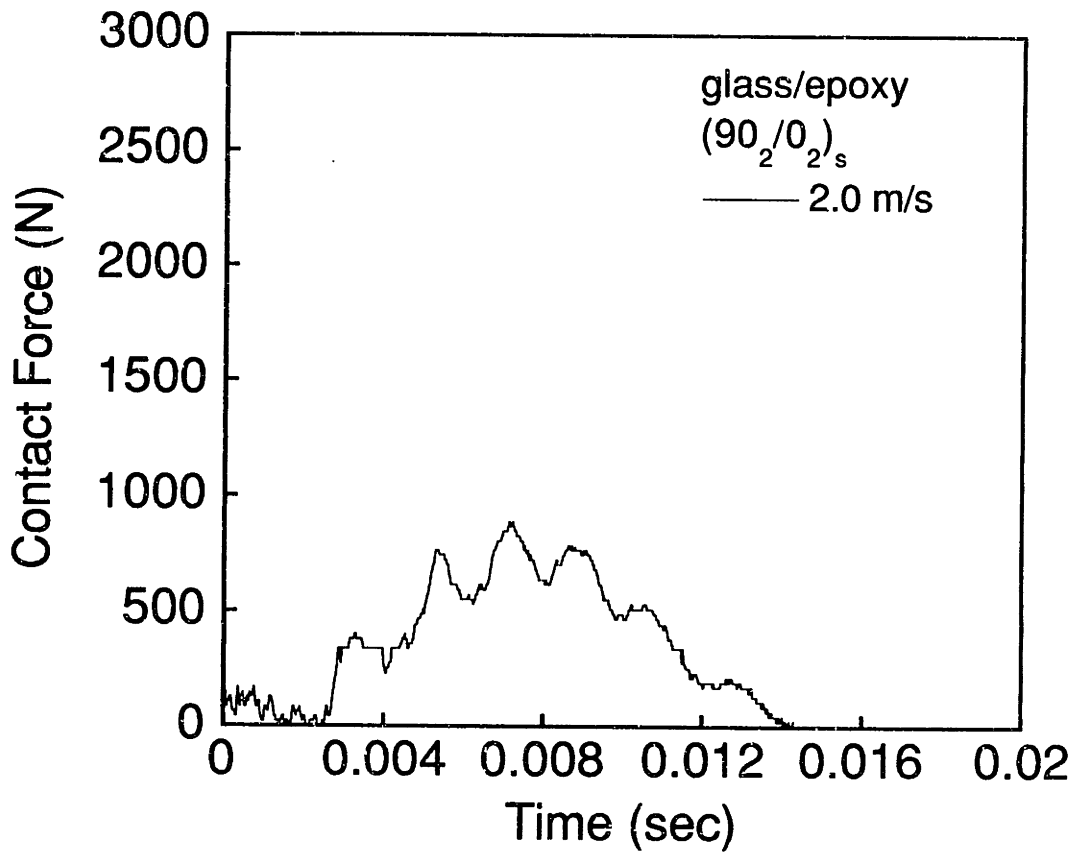


Figure A.124 (upper) Force versus time and (lower) photograph for glass/epoxy (90₂/0₂)_s specimen impacted at 2.0 m/s.

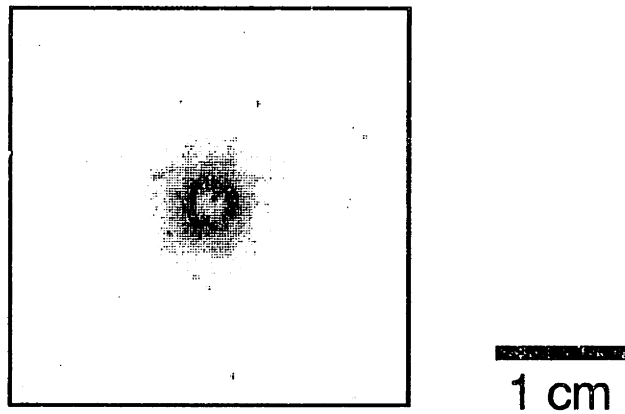
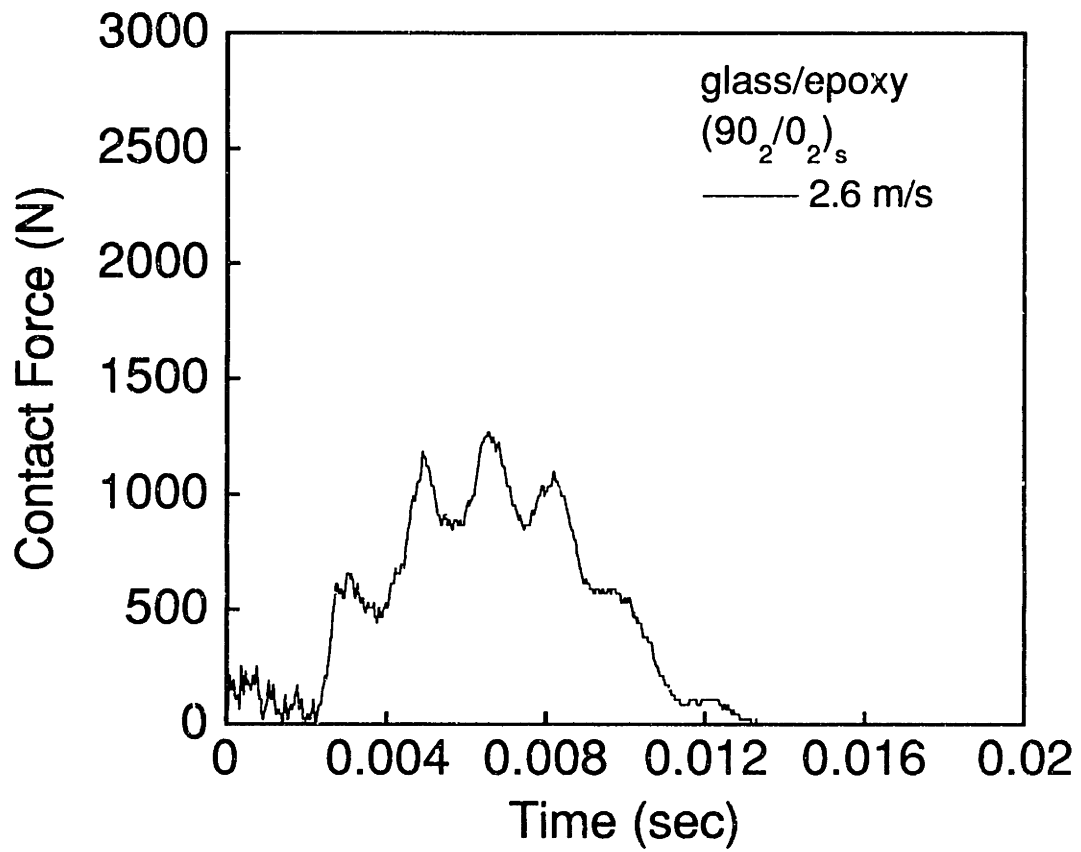


Figure A.125 (upper) Force versus time and (lower) photograph for glass/epoxy (90₂/0₂)_s specimen impacted at 2.6 m/s.

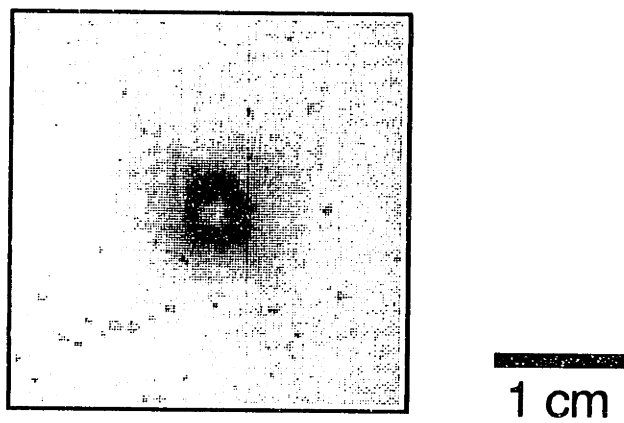
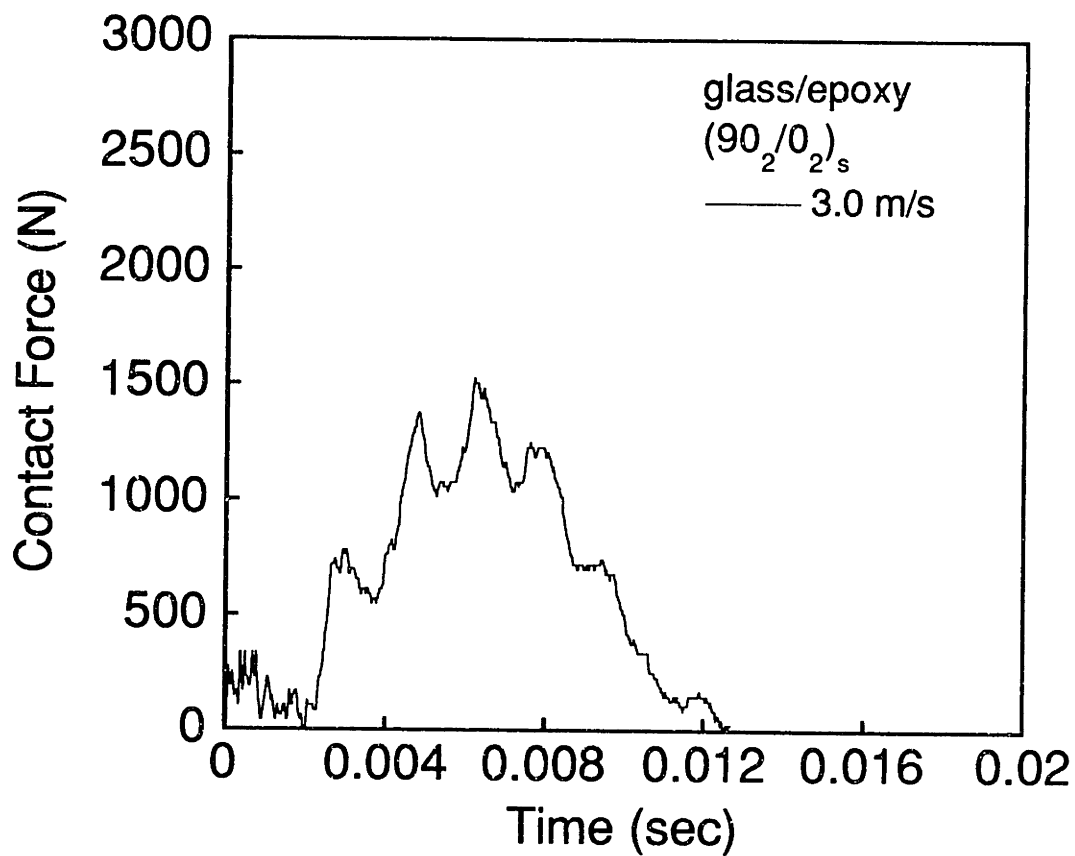


Figure A.126 (upper) Force versus time and (lower) photograph for glass/epoxy (90₂/0₂)_s specimen impacted at 3.0 m/s.

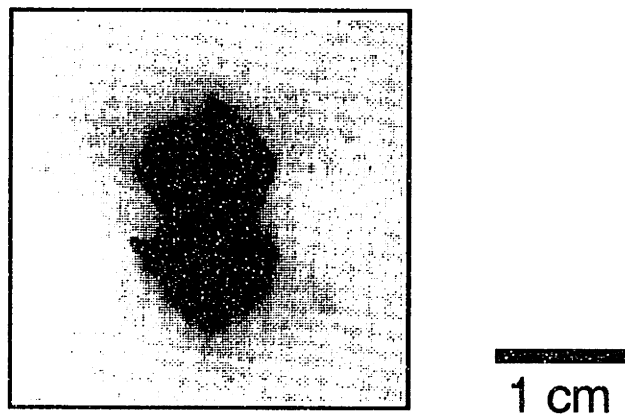
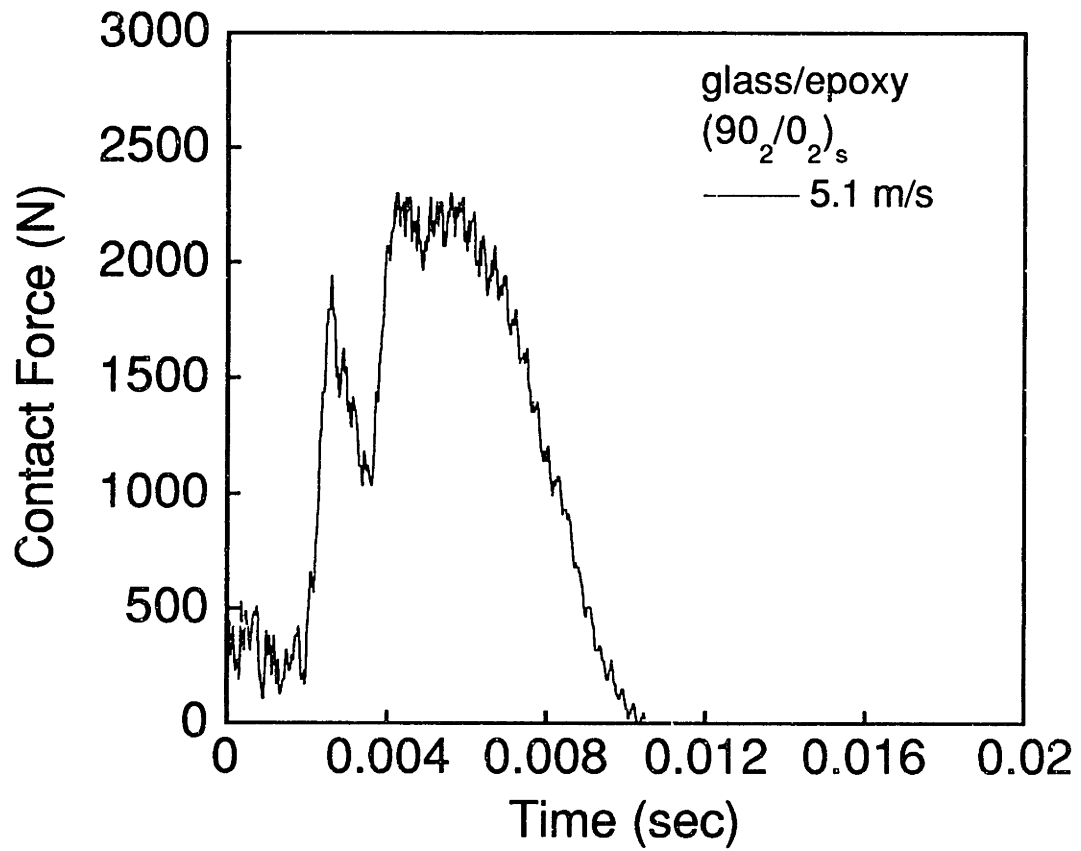


Figure A.127 (upper) Force versus time and (lower) photograph for glass/epoxy (90₂/0₂)_s specimen impacted at 5.1 m/s.

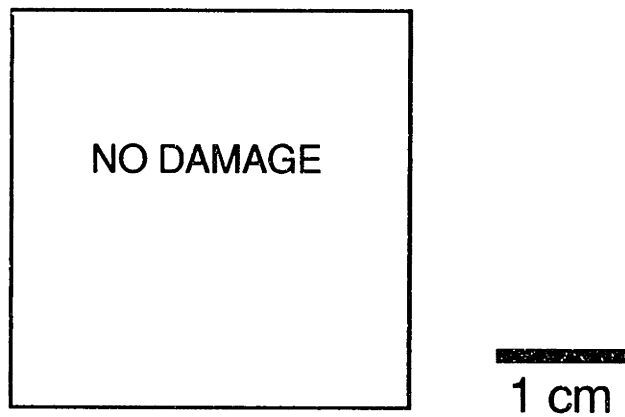
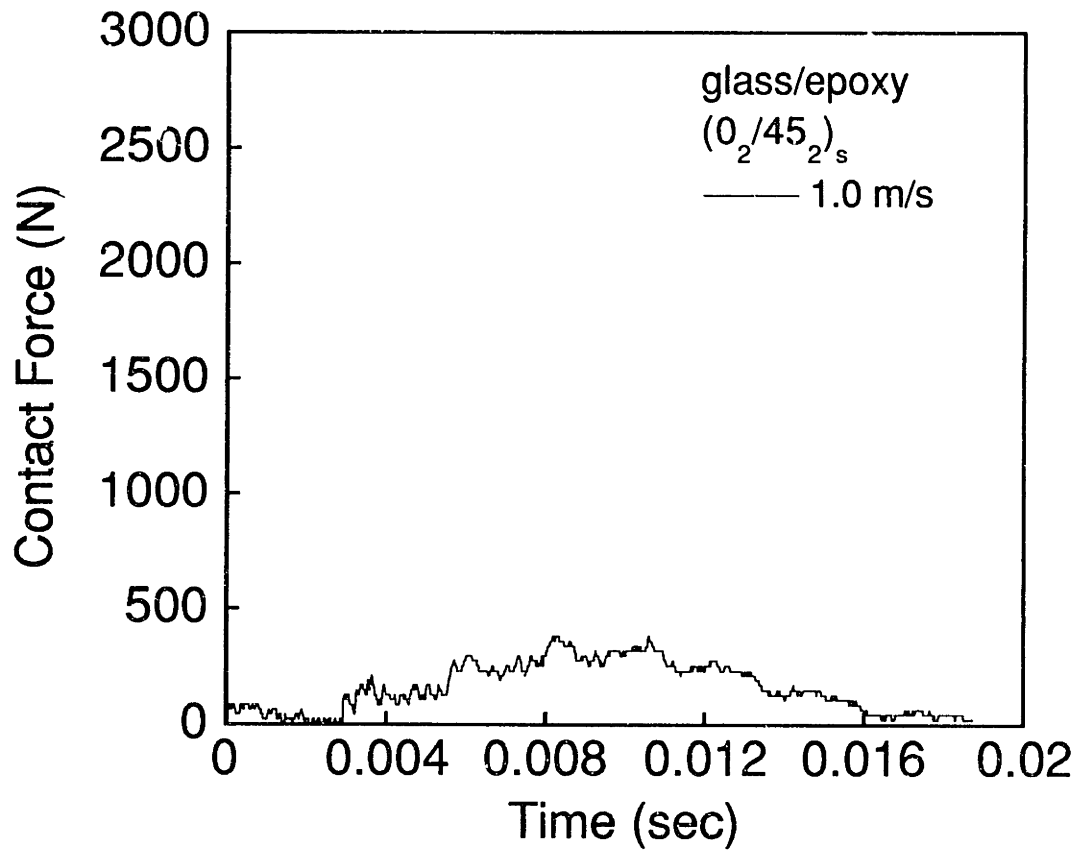


Figure A.128 (upper) Force versus time and (lower) photograph for glass/epoxy (0₂/45₂)_s specimen impacted at 1.0 m/s.

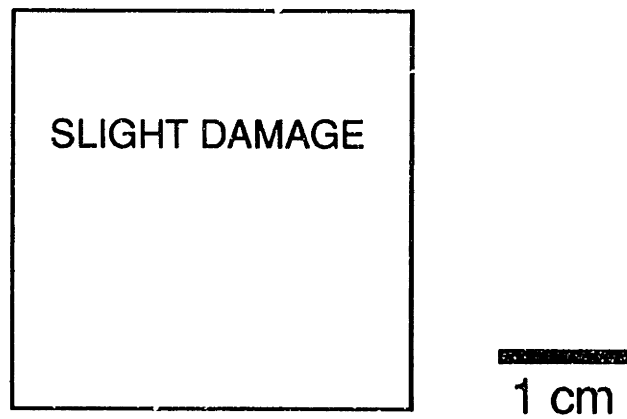
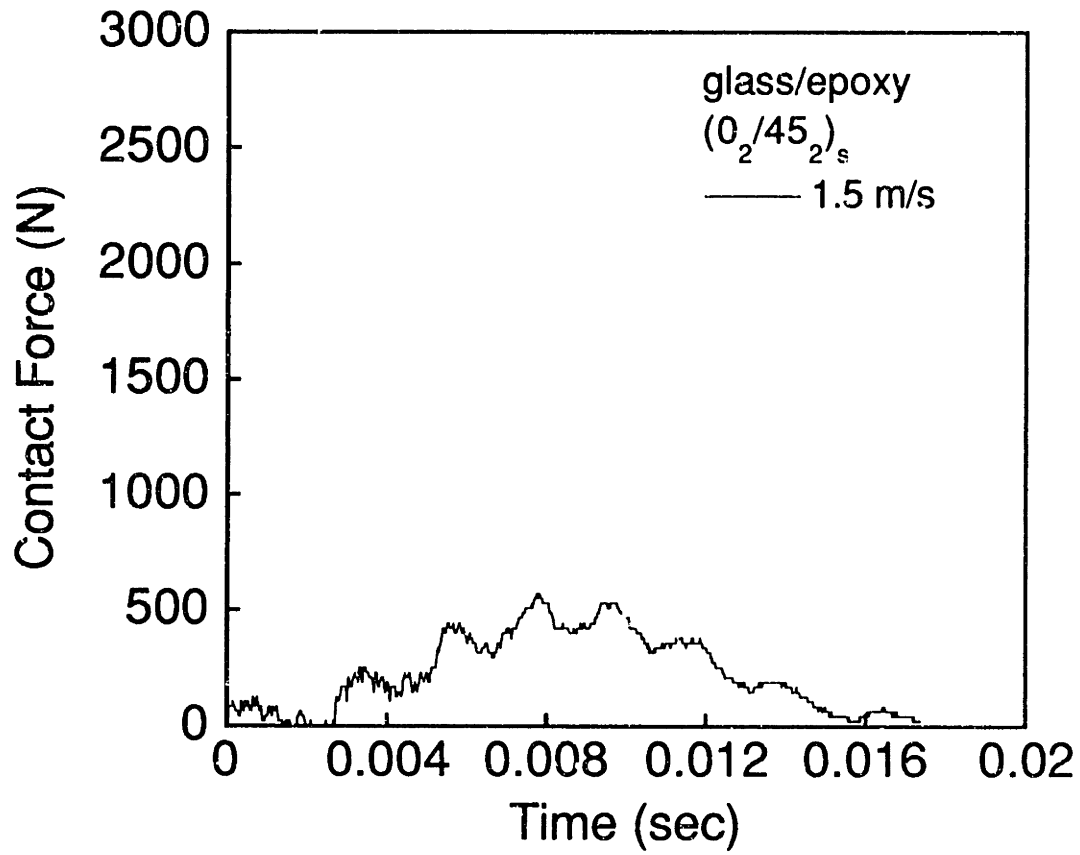


Figure A.129 (upper) Force versus time and (lower) photograph for glass/epoxy (0₂/45₂)_s specimen impacted at 1.5 m/s.

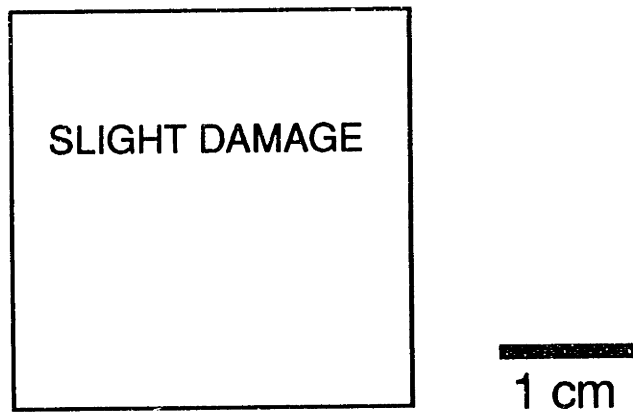
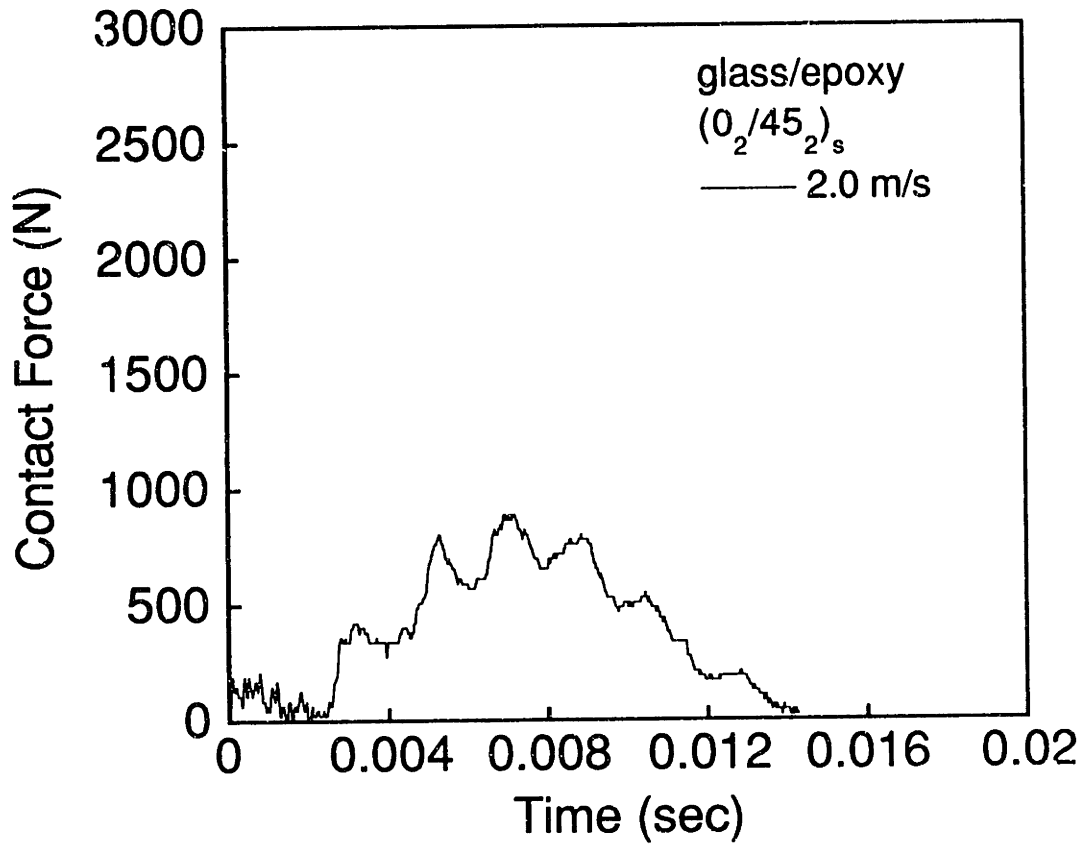


Figure A.130 (upper) Force versus time and (lower) photograph for glass/epoxy (0₂/45₂)_s specimen impacted at 2.0 m/s.

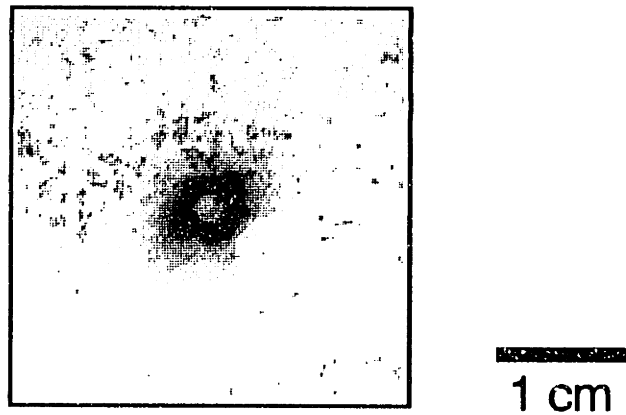
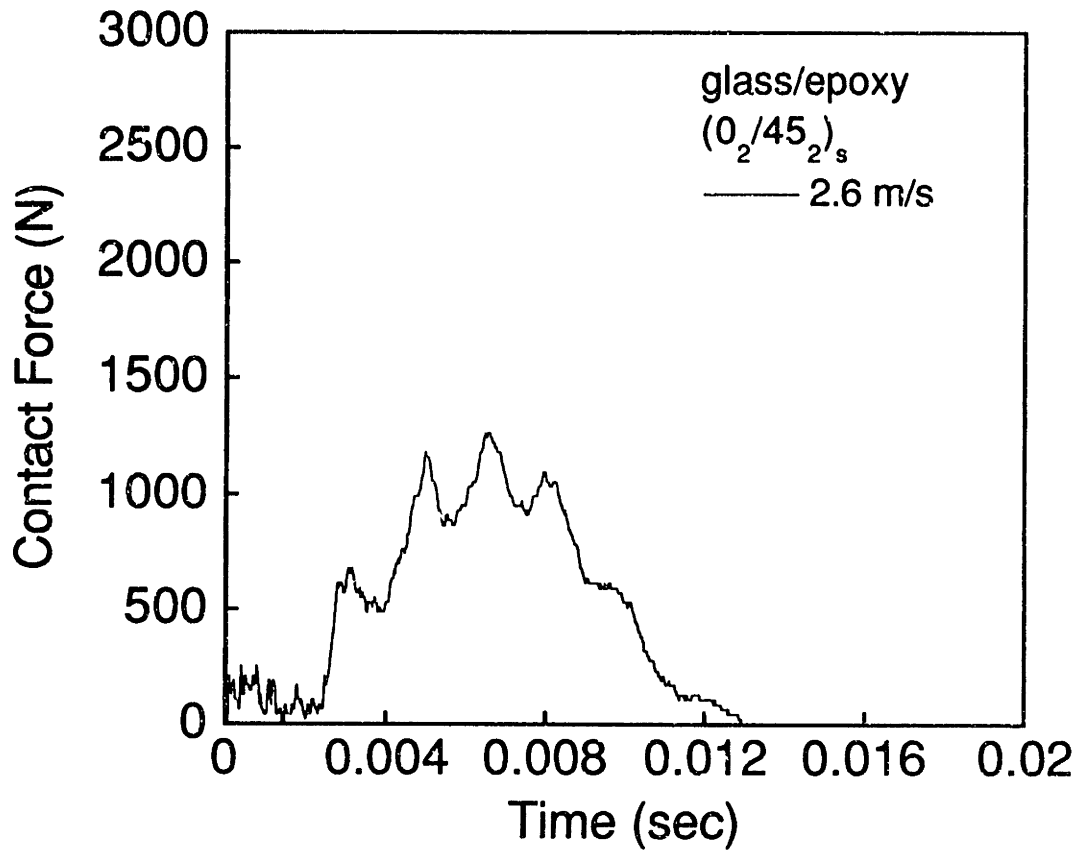


Figure A.131 (upper) Force versus time and (lower) photograph for glass/epoxy (0₂/45₂)_s specimen impacted at 2.6 m/s.

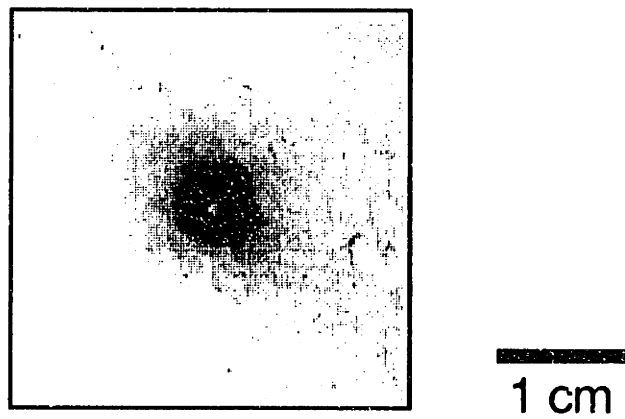
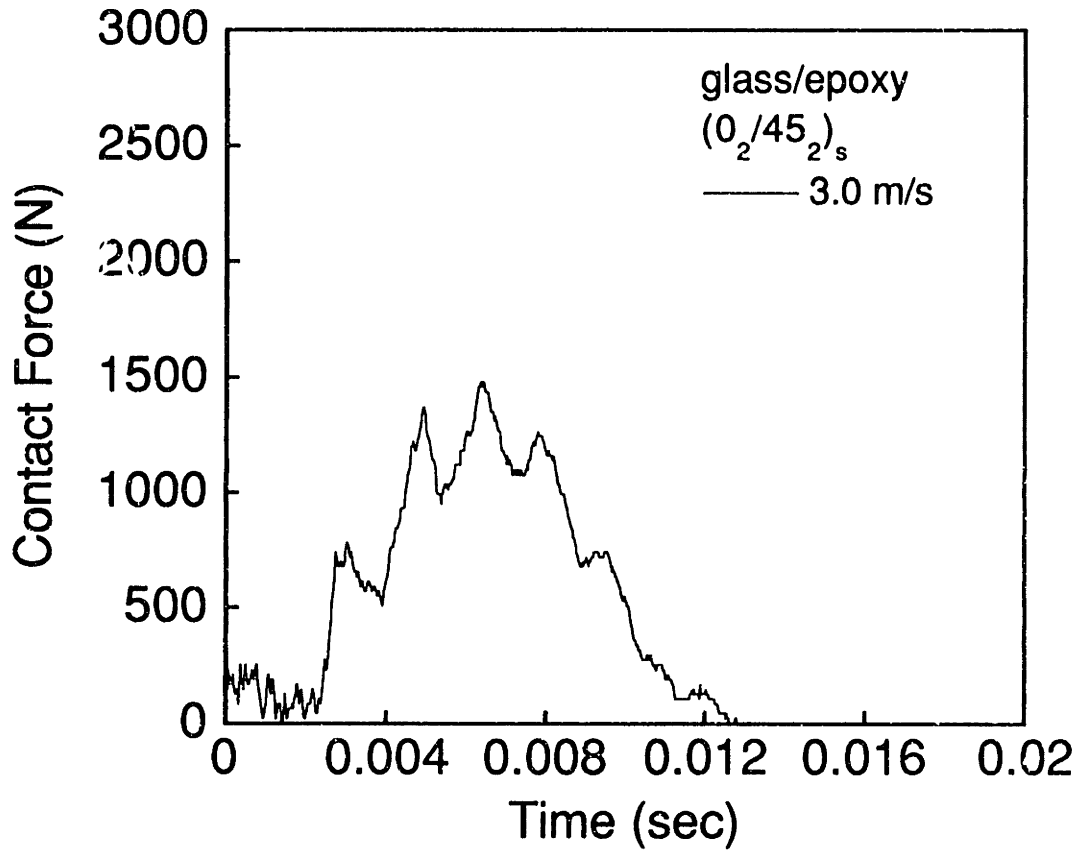


Figure A.132 (upper) Force versus time and (lower) photograph for glass/epoxy (0₂/45₂)_s specimen impacted at 3.0 m/s.

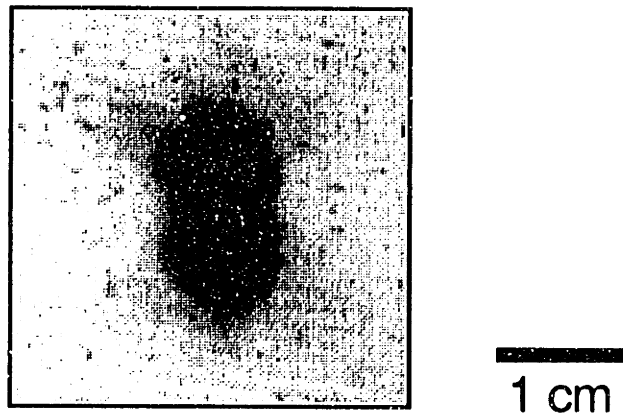
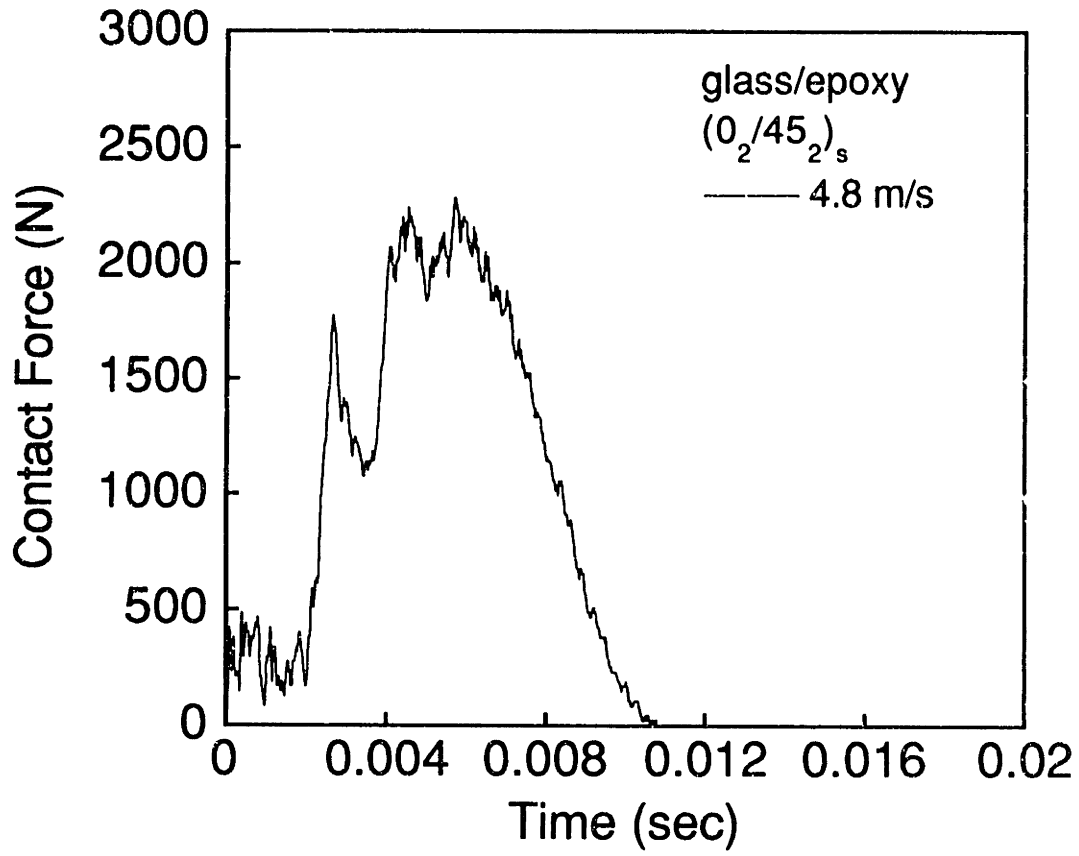


Figure A.133 (upper) Force versus time and (lower) photograph for glass/epoxy (O₂/45₂)_s specimen impacted at 4.8 m/s.

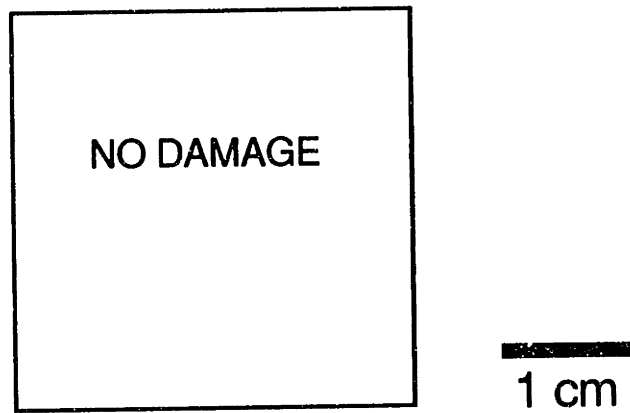
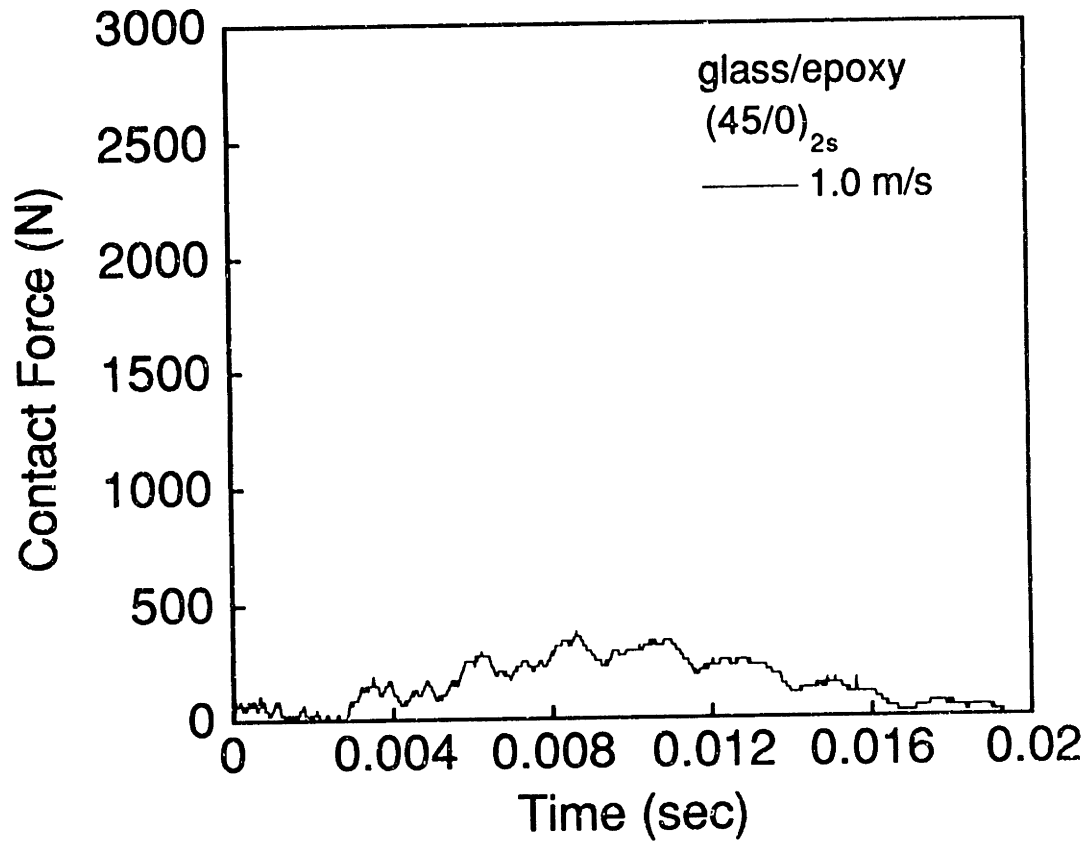


Figure A.134 (upper) Force versus time and (lower) photograph for glass/epoxy (45/0)_{2s} specimen impacted at 1.0 m/s.

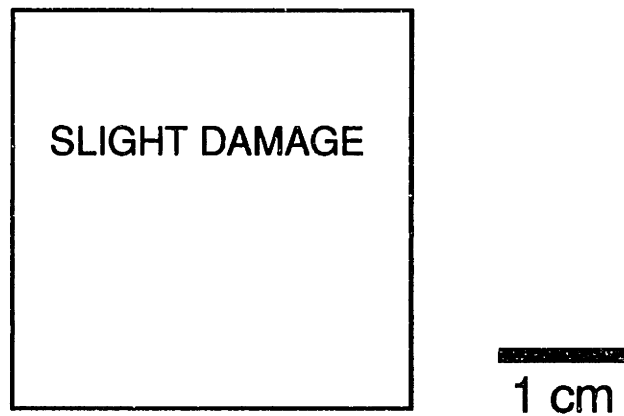
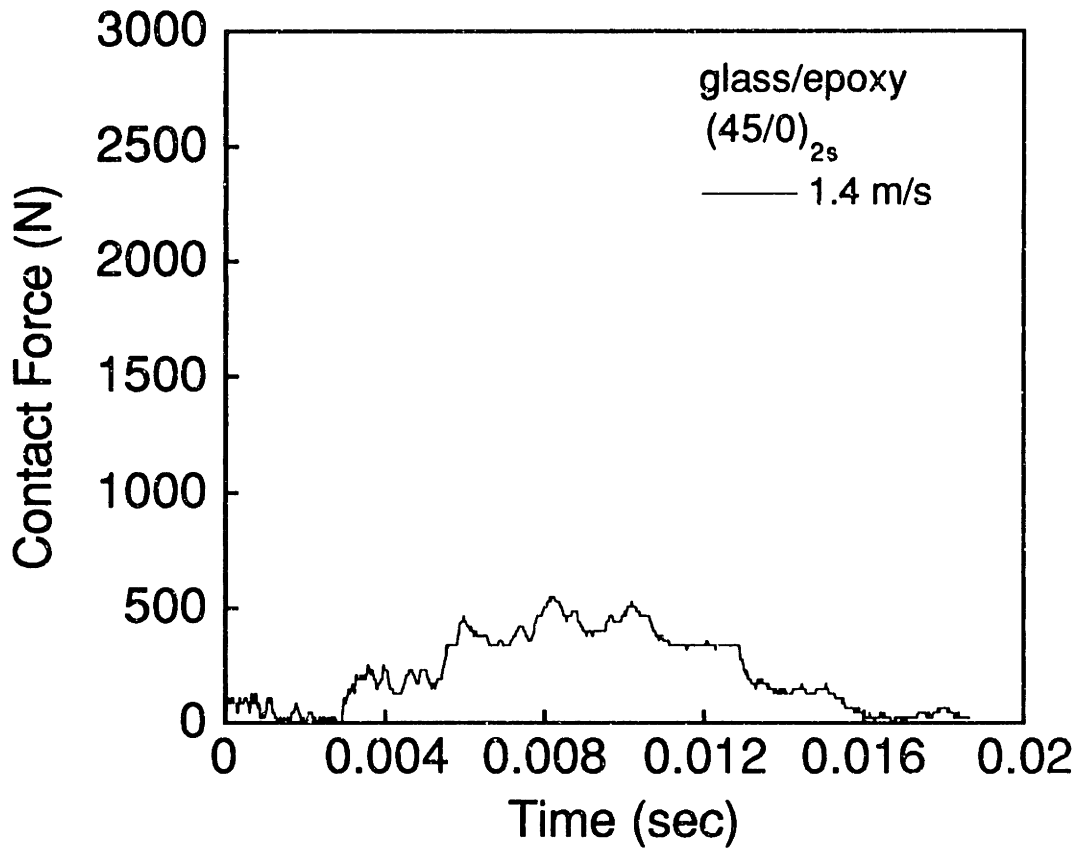


Figure A.135 (upper) Force versus time and (lower) photograph for glass/epoxy (45/0)_{2s} specimen impacted at 1.4 m/s.

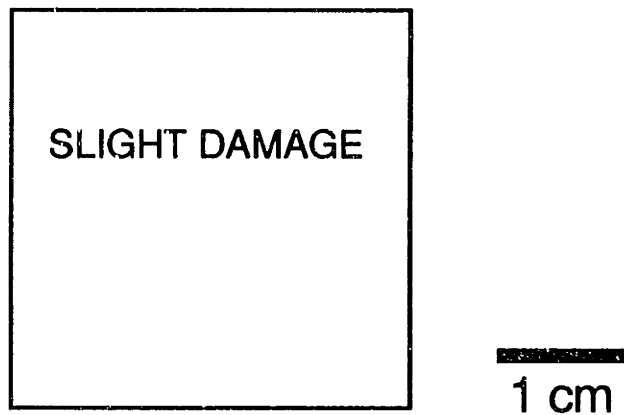
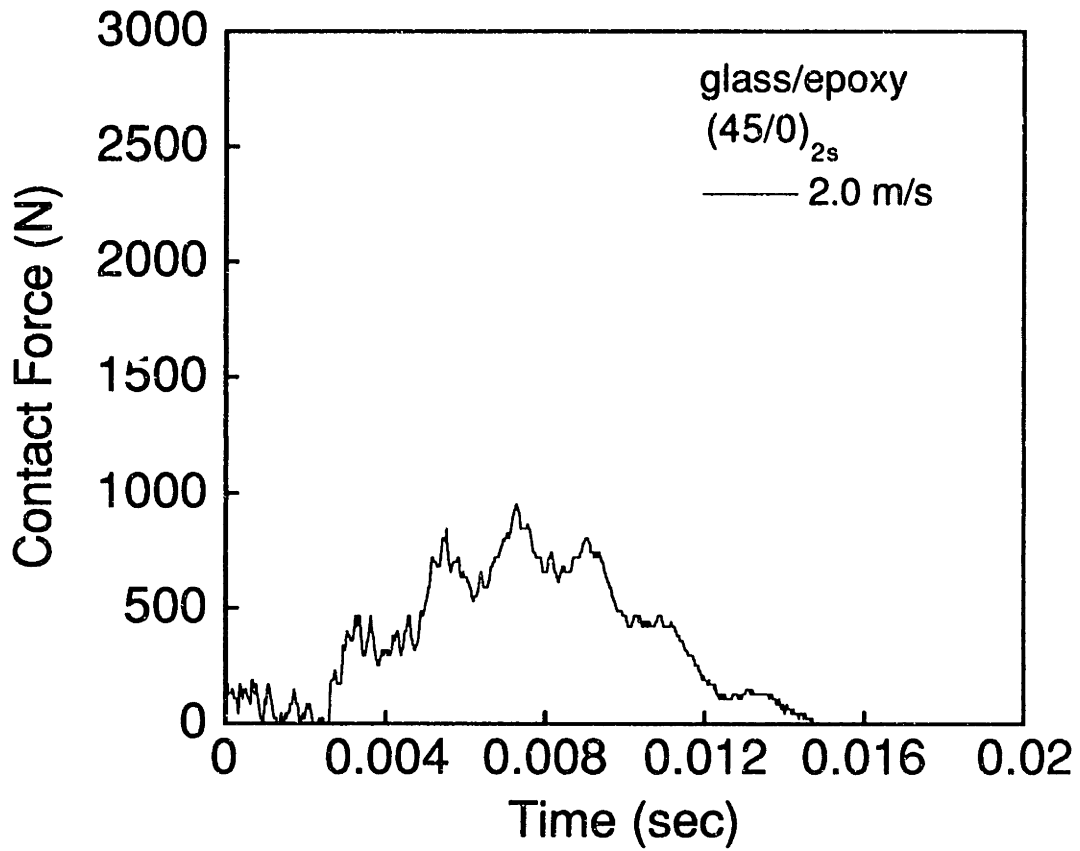


Figure A.136 (upper) Force versus time and (lower) photograph for glass/epoxy (45/0)_{2s} specimen impacted at 2.0 m/s.

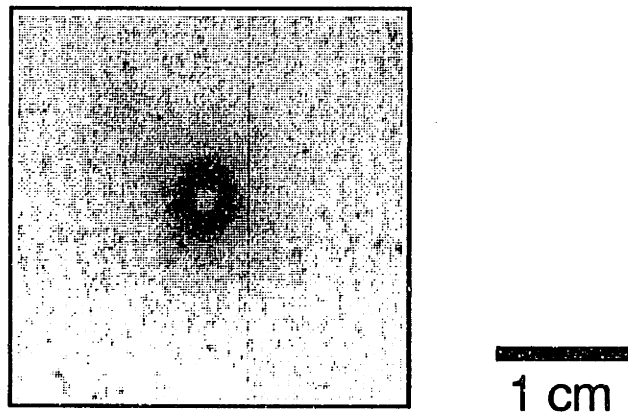
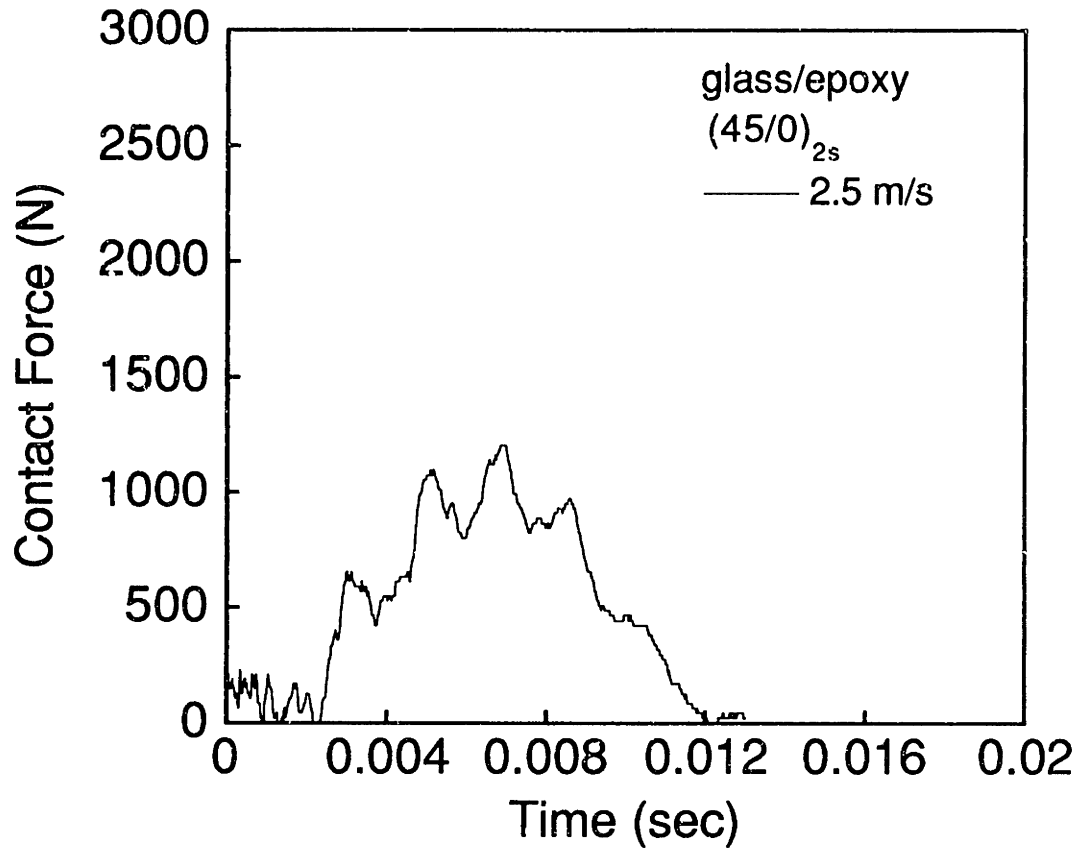


Figure A.137 (upper) Force versus time and (lower) photograph for glass/epoxy (45/0)_{2s} specimen impacted at 2.5 m/s.

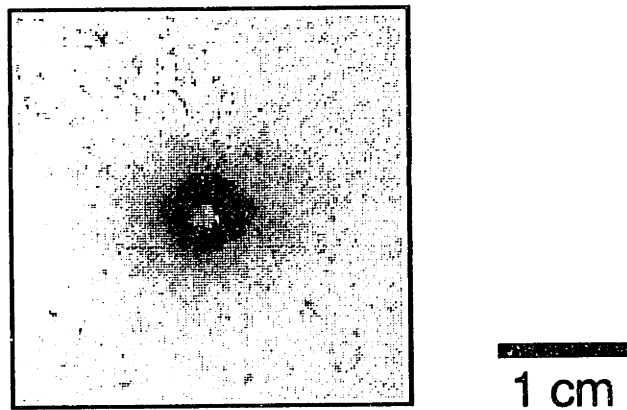
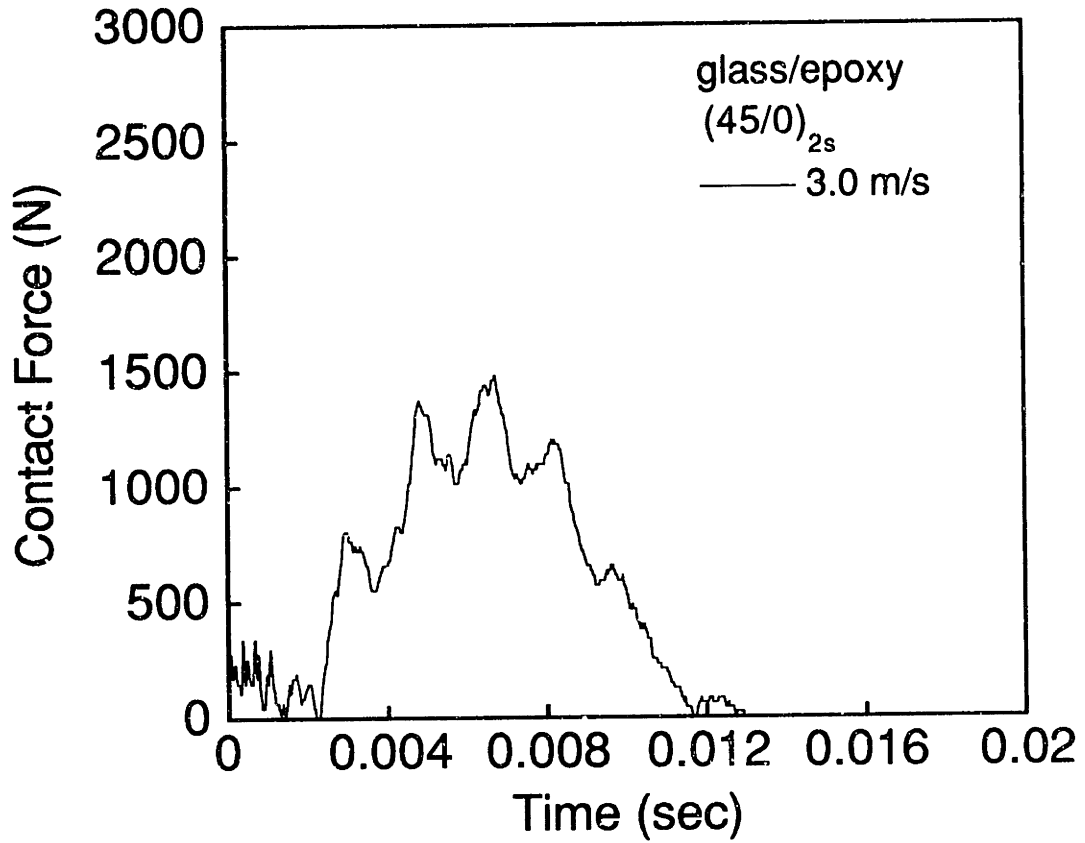


Figure A.138 (upper) Force versus time and (lower) photograph for glass/epoxy (45/0)_{2s} specimen impacted at 3.0 m/s.

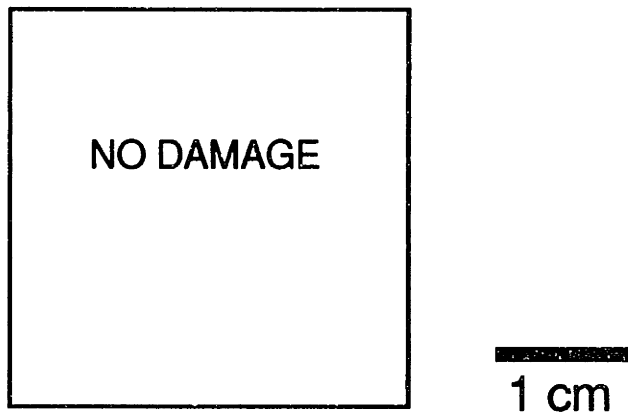
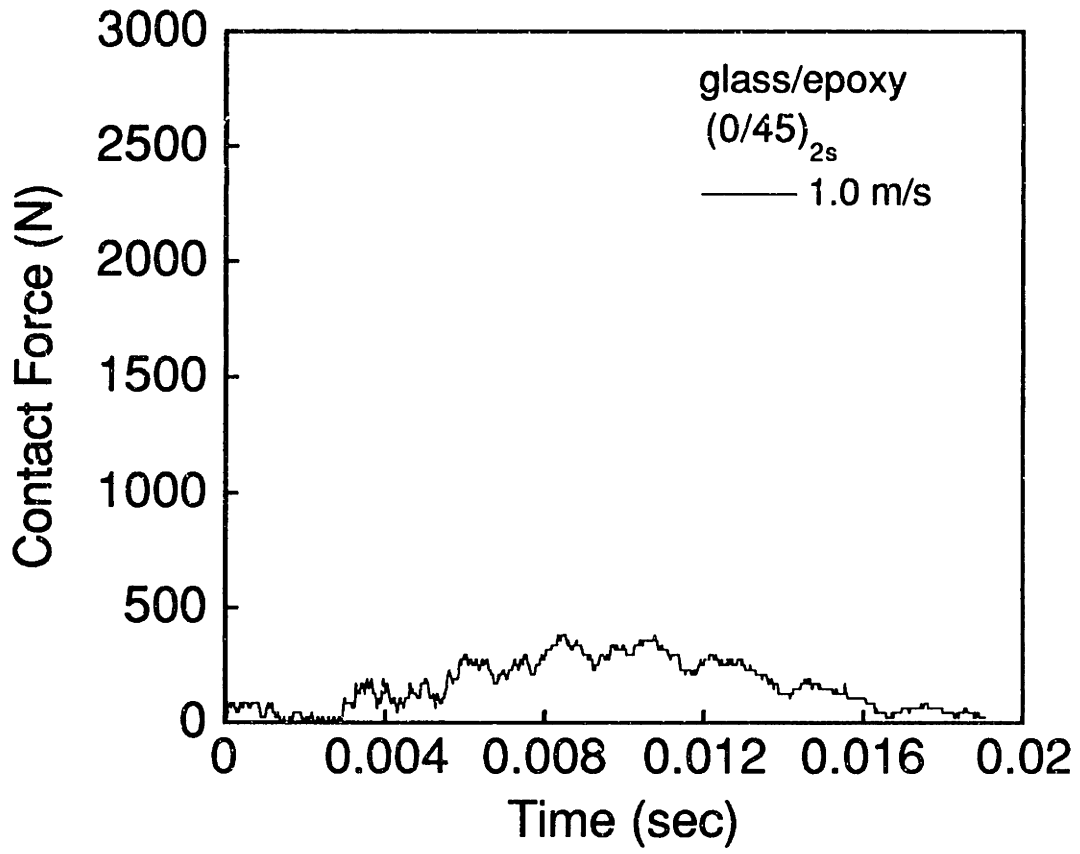


Figure A.139 (upper) Force versus time and (lower) photograph for glass/epoxy (0/45)_{2s} specimen impacted at 1.0 m/s.

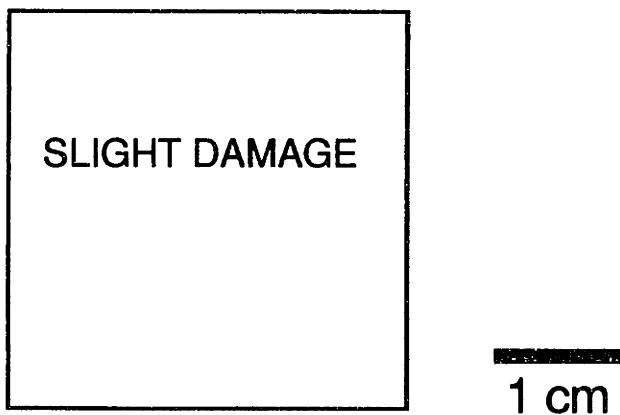
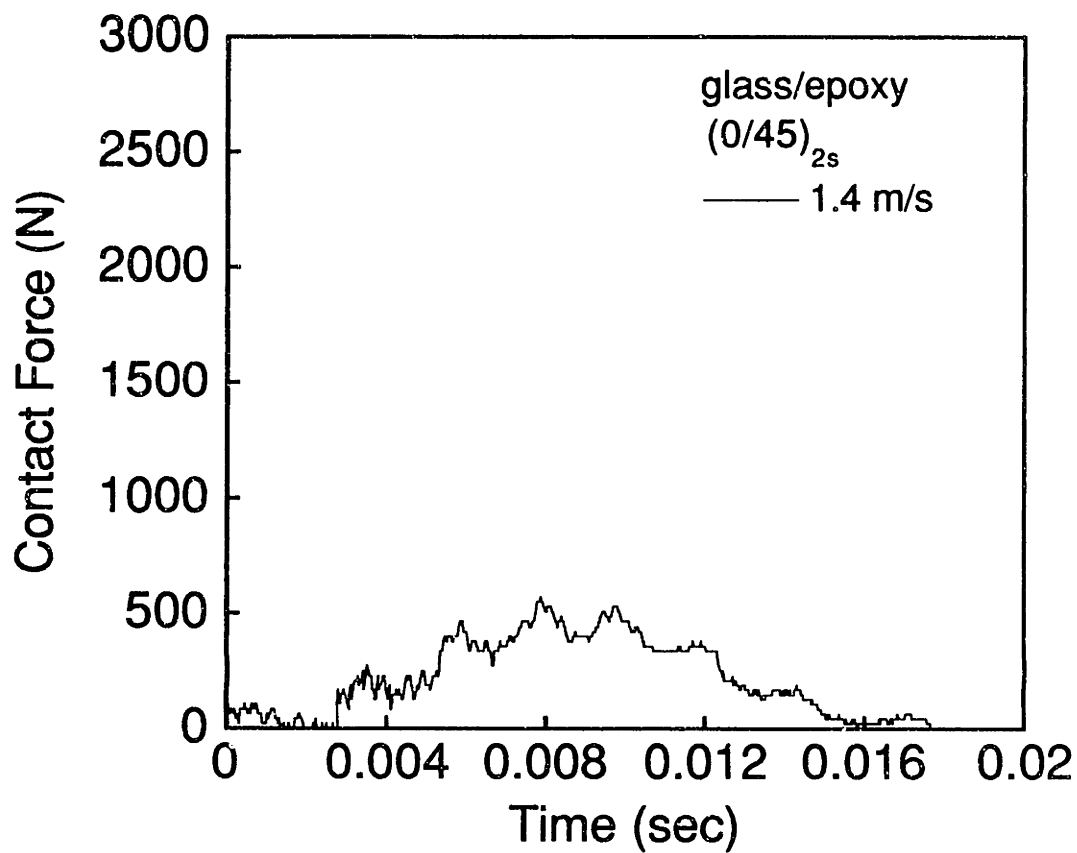


Figure A.140 (upper) Force versus time and (lower) photograph for glass/epoxy (0/45)_{2s} specimen impacted at 1.4 m/s.

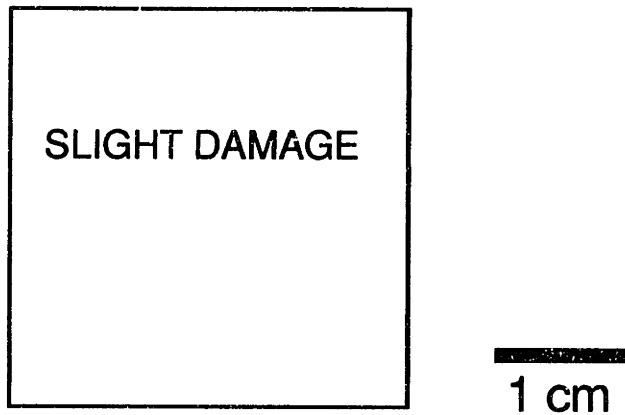
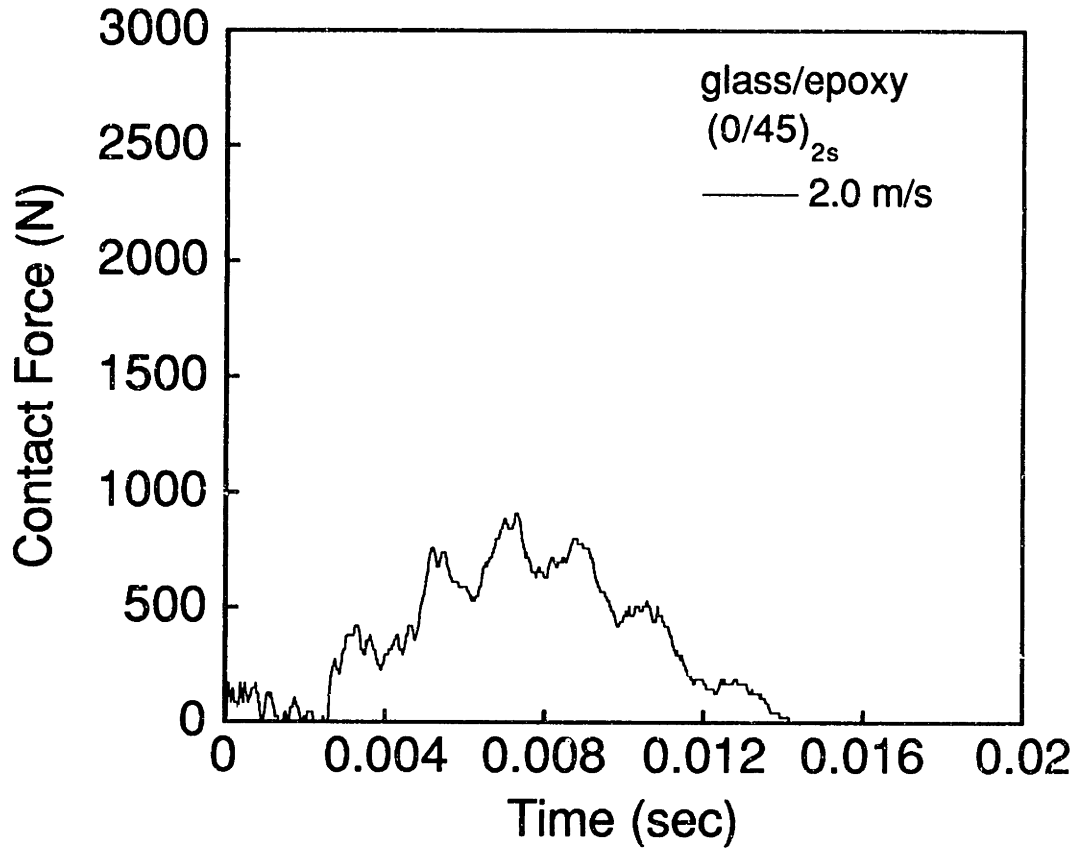


Figure A.141 (upper) Force versus time and (lower) photograph for glass/epoxy (0/45)_{2s} specimen impacted at 2.0 m/s.

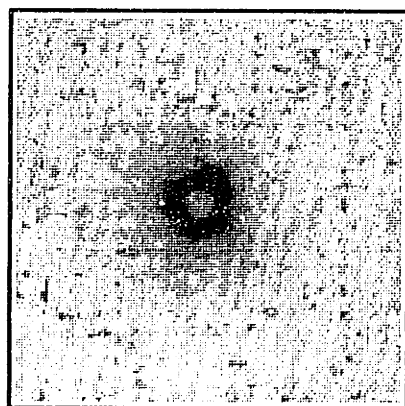
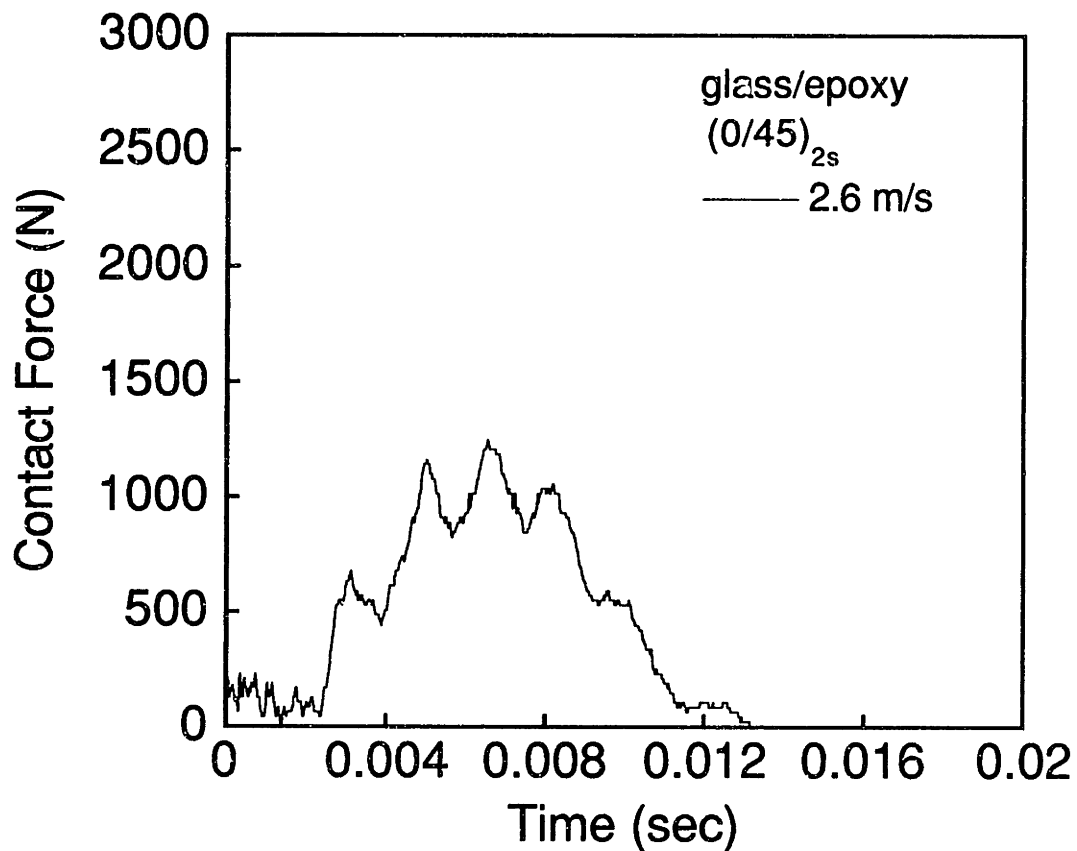


Figure A.142 (upper) Force versus time and (lower) photograph for glass/epoxy (0/45)_{2s} specimen impacted at 2.6 m/s.

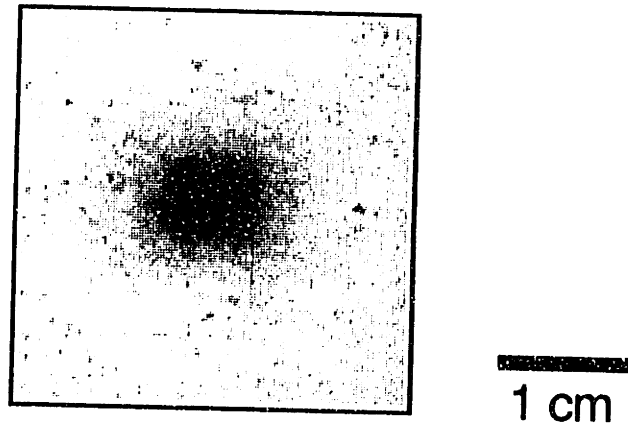
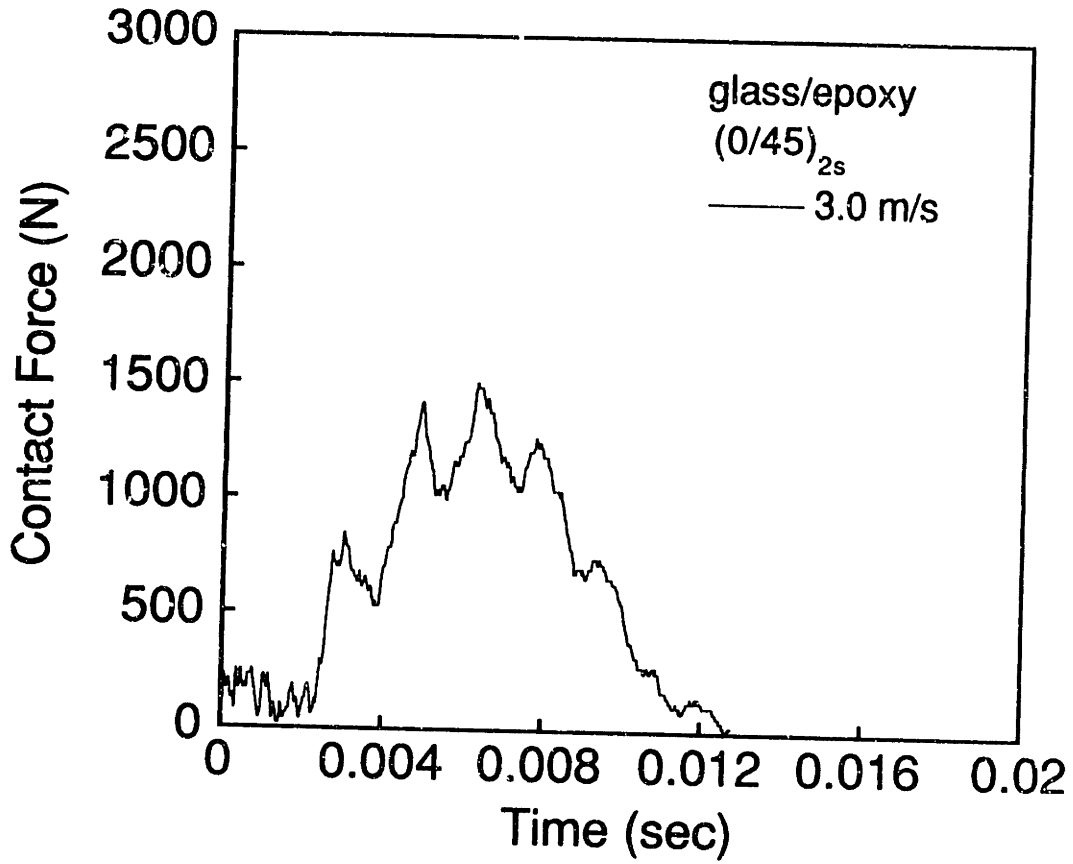


Figure A.143 (upper) Force versus time and (lower) photograph for glass/epoxy $(0/45)_{2s}$ specimen impacted at 3.0 m/s.

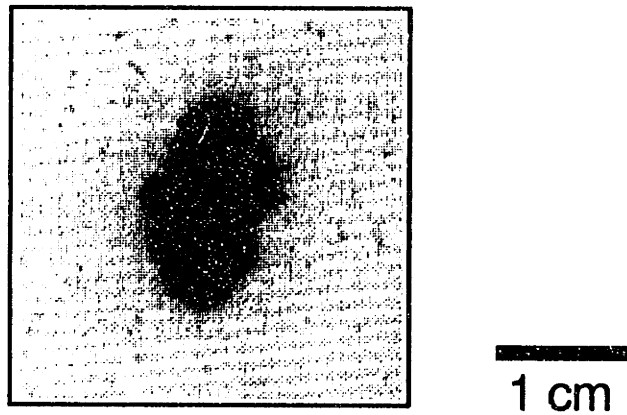
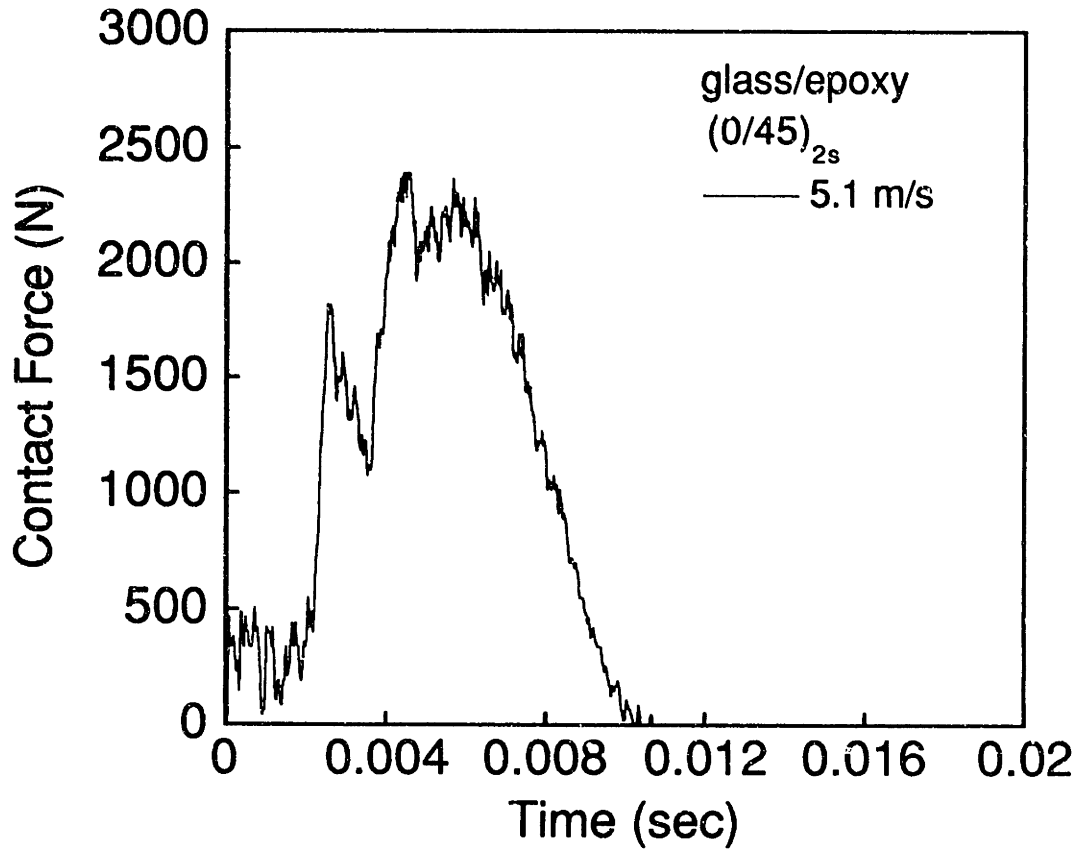


Figure A.144 (upper) Force versus time and (lower) photograph for glass/epoxy (0/45)_{2s} specimen impacted at 5.1 m/s.